

Miscellaneous Publication 144

# The 1989 Precipitation Augmentation for Crops Experiment (PACE) Data Book

by Robert R. Czys, Stanley A. Changnon,  
Mary Schoen Petersen, Nancy E. Westcott,  
and Robert W. Scott

April 1993



Illinois State Water Survey  
Champaign, Illinois

A Division of the Illinois Department of Energy and Natural Resources

**THE 1989 PRECIPITATION AUGMENTATION FOR  
CROPS EXPERIMENT (PACE) DATA BOOK**

by

Robert R. Czys,

Stanley A. Changnon,

Mary Schoen Petersen,

Nancy E. Westcott,

and

Robert W. Scott

Miscellaneous Publication 144

Atmospheric Sciences Division  
Illinois State Water Survey  
Champaign, Illinois

April 1993

## Table of Contents

Part A. Variable Abbreviations and Definitions.....	1
Part B. Cloud to Cloud Values.....	10
Part C. Distributions of Agl- and Sand-Treated Cloud Populations.....	77
Part D. Subpopulation Composite Diagrams and Comparisons.....	149
Part E. Review of the Experiment's Randomization Outcome.....	211
Part F. Rerandomization Procedures.....	223
Part G. Radar Cloud Description: Experimental Unit and Echo Core Histories.....	226
Part H. Daily Synoptic and Mesoscale Charts.....	285
Part I. Response Diagrams.....	330

**Part A**  
**Variable Abbreviations and Definitions**

**1. Synoptic Variables**

temp	Surface temperature (°C) (this and the following synoptic variables are all from 0700 CDT Peoria sounding).
dpt	Surface dew point temperature (°C).
ct	Convective temperature using average mixing ratio in lowest 100 mb (°C).
dbar	Average dew point temperature in lowest 100 mb layer (°C).
plcl	Pressure of lifting condensation level (LCL) using averaged data in lowest 100 mb (mb).
tlcl	Temperature of LCL using averaged data in lowest 100 mb (°C).
hlcl	Height of LCL using averaged data in lowest 100 mb (m).
pccl	Pressure of convective condensation level (CCL) using averaged data in lowest 100 mb (mb).
tccl	Temperature of CCL using averaged data in lowest 100 mb (°C).
hccl	Height of CCL using averaged data in lowest 100 mb (m).
pres0	Pressure of 0°C level (mb).
hgt0	Height of 0°C level (m).
pres10	Pressure of -10°C level (mb).
hgt10	Height of -10°C level (m).
dh38	Height difference between height of -3°C level and -8°C level (m).
pw	Precipitable water between the surface and 500 mb (cm).
dir85	850 mb wind direction (degrees).
spd85	850 mb wind speed (ms <sup>-1</sup> ).
dir50	500 mb wind direction (degrees).
spd50	500 mb wind speed (ms <sup>-1</sup> ).
L	Index of coalescence activity (raindrop size discriminant function based on tccl and pb).
cpe	Coalescence precipitation efficiency; relative size of L (%).
pb	Synoptic (parcel) potential buoyancy (°C).

li	Lifted index (measure of latent instability).
ki	K-index (heat differential and moisture depth in the lower levels of the atmosphere).
mki	Modified K-index.
jef	Jefferson index (measure of instability).
msh	Modified Showalter index (measure of instability).
swt	Sweat index (measure of instability).
pbot	Pressure at the bottom of "positive" area of rawinsonde (mb).
ptop	Pressure at the top of "positive" area of rawinsonde (mb).
CAPE	Convective available potential energy ( $m^2s^{-2}$ ).
vshr	Vector difference in wind at 4 km and average wind in lowest 500 m ( $ms^{-1}$ ).
Ri	Bulk Richardson number, calculated using CAPE and vshr.
m100	Tallest max radar echo top within 100 nm of CMI observed between 1130 and 2030 CDT at the NWS site (MMO, STL, EVV) closest to the echo (kft).
m80	Tallest max radar echo top within 80 nm of CMI observed between 1130 and 1830 CDT at the NWS site (MMO, STL, EVV) closest to the echo (kft).
An-targ	80 nm radius area (not including Indiana, centered on CMI) 24 hr (80-85% 7:00am obs) station averaged precipitation which fell on the day prior to the experimental unit (mm).
An-buff	80-100 nm radius area (not including Indiana, centered on CMI) 24 hr (80-85% 7:00am obs) station averaged precipitation which fell on the day prior to the experimental unit (mm).
EU-targ	80 nm radius area (not including Indiana, centered on CMI) 24 hr (80-85% 7:00am obs) station averaged precipitation which fell on the experimental unit day (mm).
EU-buff	80-100 nm radius area (not including Indiana, centered on CMI) 24 hr (80-85% 7:00am obs) station averaged precipitation which fell on the experimental unit day (mm).

## 2. Radar Variables

RFxtCPeu	Experimental unit rain flux at first treatment ( <u>C</u> loud <u>P</u> ass) ( $10^{10} \times cm^3 \text{ hr}^{-1}$ ).
RFxt-15eu	Experimental unit rain flux at 15 minutes prior to first treatment ( $10^{10} \times cm^3 \text{ hr}^{-1}$ ).
RFxDifeu	Change in experimental unit rain flux from a) 15 minutes prior to first treatment to b) at first treatment ( $10^{10} \times cm^3 \text{ hr}^{-1}$ ).

AtCPeu	Experimental unit echo areal coverage at first treatment (km <sup>2</sup> ).
At-15eu	Experimental unit echo areal coverage 15 minutes prior to first treatment (km <sup>2</sup> ).
ADifeu	Change in experimental unit echo areal coverage from a) 15 minutes prior to first treatment to b) at first treatment (km <sup>2</sup> ).
RFxtCPtn	Total network rain flux at first treatment (10 <sup>10</sup> x cm <sup>3</sup> hr <sup>-1</sup> ).
RFxt-15tn	Total network rain flux at 15 minutes prior to first treatment (10 <sup>10</sup> x cm <sup>3</sup> hr <sup>-1</sup> ).
RFxDiftn	Change in total network rain flux from a) 15 minutes prior to first treatment to b) at first treatment (10 <sup>10</sup> x cm <sup>3</sup> hr <sup>-1</sup> ).
AtCPtn	Total network echo areal coverage at first treatment (km <sup>2</sup> ).
At-15tn	Total network echo areal coverage 15 minutes prior to first treatment (km <sup>2</sup> ).
ADiftn	Change in total network echo areal coverage from a) 15 minutes prior to first treatment to b) at first treatment (km <sup>2</sup> ).
range	Distance from airport (radar site) to echo/treatment (km).
FeStat	Indicator of core merging at first echo (0 no echo at that time, 1 separate at all levels, 2 joined at some levels but can see base & top, 3 joined at lower levels but can see top, 4 no echo ever).
FEMndia	Mean diameter of echo at first echo, averaged in height (km).
FEHtp10	Top height of the 10 dBZ contour at first echo (km).
FEdpth10	Depth of the 10 dBZ contour at first echo (km).
FEA10	Max area of the 10 dBZ contour at first echo (km <sup>2</sup> ).
FEVollO	Volume of the 10 dBZ contour at first echo (km <sup>3</sup> ).
FEMxZ	Max reflectivity at first echo (dBZ).
FEHMxZ	Height of max reflectivity at first echo (km).
FEMxB	Max brightness at first echo (dBZ).
FEtpTmp	Top of echo temperature at first echo (°C).
FEmzTmp	Temperature at the height of the max reflectivity at first echo (°C).
CpStat	Indicator of core merging at treatment (0 no echo at that time, 1 isolated, 2 merged, 4 no echo ever).
CPmndia	Mean diameter of echo at treatment ( <u>C</u> loud <u>P</u> ass), averaged in height (km).
CPA.L1	Area at 1 km level at treatment (km <sup>2</sup> ).

CPZ.L1	Max reflectivity at 1 km level at treatment (dBZ).
CPA.L6	Area near flight level (6 km) at treatment (km <sup>2</sup> ).
CPZ.L6	Max reflectivity near flight level (6 km) at treatment (dBZ).
CPdia.L6	Diameter of echo near flight level (6 km) at treatment (km).
CPA56	Area at flight level at treatment (km <sup>2</sup> ).
CPZ56	Max reflectivity at flight level at treatment (dBZ).
CPdia56	Diameter of echo at flight level at treatment (km).
FltAltR	Radar (RATS) derived aircraft flight level at treatment (km).
FltAltA	Aircraft derived aircraft flight level at treatment (km).
CPHtp10	Top height of the 10 dBZ contour at treatment (km).
CPA10	Max area of the 10 dBZ contour at treatment (km <sup>2</sup> ).
CPMxZ	Max reflectivity at treatment (dBZ).
CPHMxZ	Height of max reflectivity at treatment (km).
CPMxB	Max brightness at treatment (dBZ).
FECpt	Time from first echo to treatment (min).
CPFEdH10	Change in top height of the 10 dBZ contour from first echo to treatment (km).
CPFEdA10	Change in area of the 10 dBZ contour from first echo to treatment (km <sup>2</sup> ).
CPFEdZ	Change in max reflectivity from first echo to treatment (dBZ).
CPFEdB	Change in max brightness from first echo to treatment (dBZ).
CPFEdH/dt	Rate of change of echo 10 dBZ top height from first echo to treatment (km min <sup>-1</sup> ).
CPFEdA/dt	Rate of change of 10 dBZ area from first echo to treatment (km <sup>2</sup> min <sup>-1</sup> ).
CPFEdZ/dt	Rate of change of max reflectivity from first echo to treatment (dBZ min <sup>-1</sup> ).
MaxH10*	Maximum top height of the 10 dBZ reflectivity contour (km).
MaxA10*	Maximum area of the 10 dBZ reflectivity contour (km <sup>2</sup> ).
MaxZ*	Maximum reflectivity (dBZ).
MaxB*	Maximum brightness (dBZ).

---

\* Response Variable

MxRFx\* Max rain flux of echo core ( $10^{10} \times \text{cm}^3 \text{ hr}^{-1}$ ).

TotRNVOL\* Total accumulated rain volume of echo core ( $10^{10} \times \text{cm}^3$ ).

FRtoMxRFx\* Time from first rain to max rain flux of echo core (min).

FEMXtMxH\* Time from first echo to max height (min).

FEMXtMxA\* Time from first echo to max area (min).

FEMXtMxZ\* Time from first echo to max reflectivity (min).

FEMXtMxB\* Time from first echo to max brightness (min).

MXFEdH10\* Change in the 10 dBZ top height from first echo to max height of core (km).

MXFEdA10\* Change in area of the 10 dBZ contour from first echo to max area ( $\text{km}^2$ ).

MXFEdZ\* Change in max reflectivity from first echo to max reflectivity (dBZ).

MXFEdH/dt\* Rate of change of echo top height from first echo to max height ( $\text{km min}^{-1}$ ).

MXFEdA/dt\* Rate of change of 10 dBZ echo area from first echo to max area ( $\text{km}^2 \text{ min}^{-1}$ ).

MXFEdZ/dt\* Rate of change of max reflectivity from first echo to max reflectivity ( $\text{dBZ min}^{-1}$ ).

CPMXtMxH\* Time from treatment to max 10 dBZ top height (min).

CPMXtMxA\* Time from treatment to max 10 dBZ area (min).

CPMXtMxZ\* Time from treatment to max reflectivity (min).

MXCPdH10\* Change in top height of the 10 dBZ contour from treatment to max height (km).

MXCPdA10\* Change in area of the 10 dBZ contour from treatment to max area ( $\text{km}^2$ ).

MXCPdZ\* Change in max reflectivity from treatment to max reflectivity (dBZ).

MXCPdB\* Change in max brightness from treatment to max brightness (dBZ).

MXCPdH/dt\* Rate of change of echo top height from treatment to max height ( $\text{km min}^{-1}$ ).

MXCPdA/dt\* Rate of change of echo area from treatment to max area ( $\text{km}^2 \text{ min}^{-1}$ ).

MXCPdZ/dt\* Rate of change of max reflectivity from treatment to max reflectivity ( $\text{dBZ min}^{-1}$ ).

FEtTerm\* Time from first echo to termination of echo core tracking (min).

pdeg Degree of polynomial used to determine velocities and accelerations of echo top before, at, and after treatment (the following 6 variables).

---

\* Response Variable

v_bef	Velocity of echo top 2 minutes before treatment (km min <sup>-1</sup> ).
v_cdp	Velocity of echo top at treatment (km min <sup>-1</sup> ).
v_aft*	Velocity of echo top 4 minutes after treatment (km min <sup>-1</sup> ).
a_bef	Acceleration of echo top 2 minutes before treatment (km min <sup>2</sup> ).
a_cdp	Acceleration of echo top at treatment (km min <sup>2</sup> ).
a_aft*	Acceleration of echo top 4 minutes after treatment (km min <sup>2</sup> ).
FEHbsLO	Base height of the 10 dBZ contour at first echo (km).
FEbsTmp	Temperature at base of echo at first echo (°C).
FEtoFR	Time from first echo to first rain (min).
CPtoFR*	Time from treatment to first rain (min).
dH/dt-PO/PR*	Ratio of rates of change of echo height from a) treatment to time of max height and b) first echo to treatment (a/b).
dA/dt-PO/PR*	Ratio of rates of change of echo area from a) treatment to time of max area and b) first echo to treatment (a/b).
dZ/dt-PO/PR*	Ratio of rates of change of max reflectivity from a) treatment to time of max reflectivity and b) first echo to treatment (a/b).
dH-PO/PR*	Ratio of changes of echo height from a) treatment to time of max height and b) first echo to treatment (a/b).
dA-PO/PR*	Ratio of changes of max area from a) treatment to time of max area and b) first echo to treatment (a/b).
dZ-PO/PR*	Ratio of changes of max reflectivity from a) treatment to time of max reflectivity and b) first echo to treatment (a/b).

### 3. Aircraft Variables

Cld_Dia	Diameter of cloud (m).
#_Ups	Number of updrafts in cloud (updraft = 1 ms <sup>-1</sup> for at least 3 consecutive seconds).
%_Updraft	Percent of cloud which is updraft.
C_flrs	Number of flares in the cloud.

---

\* Response Variable

%_in_Up	Percentage of flares released in any updraft.
Env_ThetaV	Mean virtual potential temperature of the environment (K) (i.e., 10 consecutive second mean within 1 minute prior to cloud).
Env_TC	Temperature of the environment (°C) (i.e., 10 consecutive second mean within 1 minute prior to cloud).
#_SECS	Number of seconds of the longest or broadest updraft.
UP_Dia	Diameter of the main (broadest or longest) updraft (m) ("the updraft" in the following variables refers to this main updraft).
Mean_VW	Mean vertical velocity (vertical wind) of the updraft ( $\text{ms}^{-1}$ ).
Max_VW	Maximum vertical velocity during the updraft ( $\text{ms}^{-1}$ ).
Mean_ThV	Mean virtual potential temperature of the updraft (K).
Max_ThV	Maximum virtual potential temperature during the updraft (K).
U_flrs	Number of flares in the updraft.
Mean_TBuoy	Mean thermal buoyancy (°C) (= Mean_ThV - Env_ThetaV).
Max_TBuoy	Maximum thermal buoyancy (°C) (= Max_ThV - Env_ThetaV).
Load_W	Loading from water (liquid) (°C) ( $1^\circ\text{C} / 2.5 \text{ gm}^{-3}$ ).
Load_I	Loading from ice (solid) (°C) ( $1^\circ\text{C} / 2.5 \text{ gnr}^{-3}$ ).
Buoy_Enh <sup>1</sup>	Buoyancy enhancement (°C).
NBuoy	Net buoyancy (°C) (= Mean_TBuoy - Load_W - Load_I)
PBuoy	Potential buoyancy (°C) (= NBuoy + Buoy_Enh).
SWC_frac	Fraction of solid water content [SWCd / (Mean_JWC + LWCd + SWCd)].
Mean_JWC	Mean liquid water content of the updraft from the JW probe (i.e., cloud droplets) ( $\text{gnr}^3$ ).
Max_JWC	Max liquid water content during updraft from the JW probe ( $\text{gm}^{-3}$ ).

---

<sup>1</sup>Orville, H.D., and K. Hubbard, 1973: On the freezing of liquid water in a cloud. *J. Appl. Met.*, 12, 671-676.

Mean_FWC	Mean liquid water content of the updraft from the FSSP probe (i.e., cloud droplets --> $D < 45 \mu\text{m}$ ) ( $\text{gmv}^3$ ).
Max_FWC	Max liquid water content during updraft from the FSSP probe ( $\text{gmv}^3$ ).
Mean_Dia	Mean diameter of cloud droplet particles (from FSSP data) ( $\mu\text{m}$ ).
Max_Dia	Max diameter of cloud droplet particles ( $\mu\text{m}$ ).
Ttres_Dia <sup>2</sup>	THreshold diameter --> defined such that the total concentration of droplets with diameters $\geq \text{Thres\_Dia}$ is $3 \text{ cm}^{-3}$ (as measured by the FSSP probe) ( $\mu\text{m}$ ).
Mean_Conc	Mean concentration of cloud droplets in the updraft ( $\text{cm}^{-3}$ ).
Max_Conc	Max concentration of cloud droplets in the updraft ( $\text{cm}^{-3}$ ).
Mean_Conc_D<13	Mean concentration of cloud droplets $< 13 \mu\text{m}$ in the updraft ( $\text{cm}^{-3}$ ).
Mean_Conc_D>=25	Mean concentration of cloud droplets $\geq 25 \mu\text{m}$ in the updraft ( $\text{cm}^{-3}$ ).
Dmax_W	Maximum diameter of supercooled liquid rain/drizzle drop particles (i.e., water, and $D > 150 \mu\text{m}$ ) in the updraft (mm).
Tconc_W	Total concentration of water particles ( $\text{L}^{-1}$ ).
2DWCnt	Total 2D probes particle count in Tconc_W.
Tconc_W3	Total concentration of water particles $> 300 \mu\text{m}$ ( $\text{L}^{-1}$ ).
2DW3Cnt	Total 2D probes particle count in Tconc_W3.
LWCd	Liquid water content by method I (i.e., discrete) ( $\text{gmv}^3$ ).
Dmax_I	Maximum diameter of ice particles ( $D > 150 \mu\text{m}$ ) in the updraft (mm).
Tconc_g	Concentration of graupel particles in the updraft ( $\text{L}^{-1}$ ).
2DgCnt	Total 2D probes particle count (of graupel) in Tconc_g.
Tconc_f	Concentration of ice fragment particles in the updraft ( $\text{L}^{-1}$ ).
2DfCnt	Total 2D probes particle count (of ice fragments) in Tconc_f.
Tconc_i	Concentration of ice crystal particles in the updraft ( $\text{L}^{-1}$ ).

---

<sup>2</sup> Hobbs, P.V., and A.L. Rangno, 1985: Ice particle concentrations in clouds. *J. Atmos. Sci.*, 43, 2523-2549.

2DiCnt	Total 2D probes particle count (of ice crystals) in Tconc_i.
Tconc_I	Total Concentration of ice particles in the updraft ( $L^{-1}$ ).
2DICnt	Total 2D probes particle count (of graupel, fragments and crystals) in TconcJ.
Tconc_Po	Concentration of particles with depolarization signal $> 0$ in the updraft ( $L^{-1}$ ).
2DPoCnt	Total 2D probes particle count (of particles with depolarization $> 0$ ) in Tconc_Po.
SWCd	Solid water content by method I (i.e., discrete) ( $gm^{-3}$ ).
NO_W	Water size distribution intercept ( $L^{-1}$ ).
lamda_W	Water size distribution slope ( $cm^{-1}$ ).
LWCc	Liquid water content by method II (i.e., continuous; area under the line defined by NO_W and lamda_W) ( $gm^{-3}$ ).
NO_I	Ice size distribution intercept ( $L^{-1}$ ).
lamda_I	Ice size distribution slope ( $cm^{-1}$ ).
SWCc	Solid water content by method II (i.e., continuous; area under the line defined by NO_I and lamda_I) ( $gm^{-3}$ ).

## **Part B**

### **Cloud to Cloud Values**

This Part presents figures of the cloud to cloud values of all 191 variables for the 71 "large" or " " clouds, plus some derived from them, such as two variables calculated using the number of flares fired into the cloud, showing the variability of the data through the operational period. Solid circles indicate clouds that received silver iodide (AgI) treatments, whereas open circles signify clouds which received sand treatments. Cloud 1 is the first ("large") cloud that was treated in the summer (on May 19), and cloud 71 is the last cloud treated (on July 25). The short double lines separate the experimental units, and the dates for each group of clouds are shown at the top of the graph.

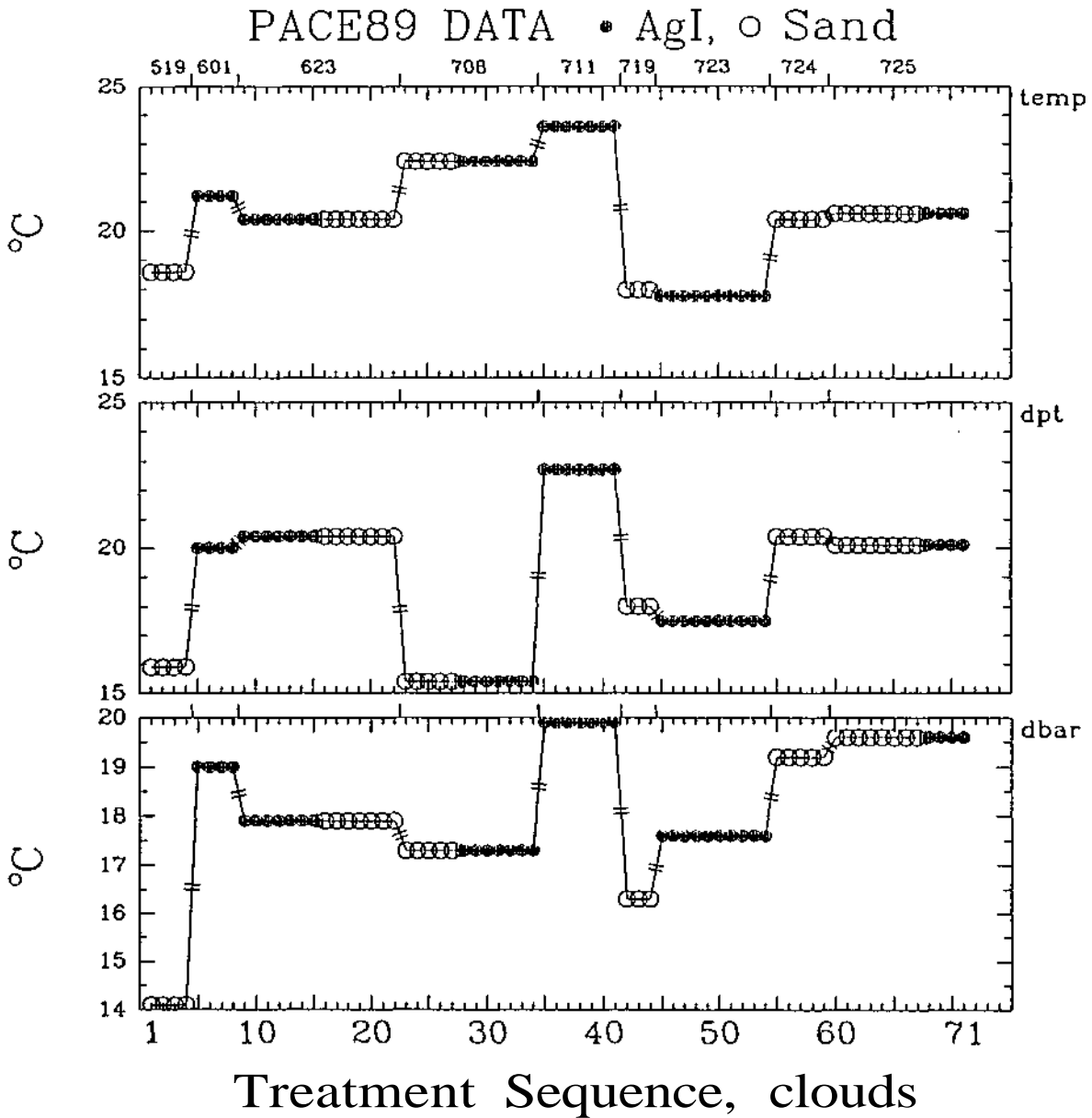


Figure B.1. Time history of the surface temperature (temp), the surface dew point temperature (dpt), and the average dew point temperature in lowest 100 mb layer (dbar) (these and the following synoptic variables are all from 0700 CDT Peoria sounding).

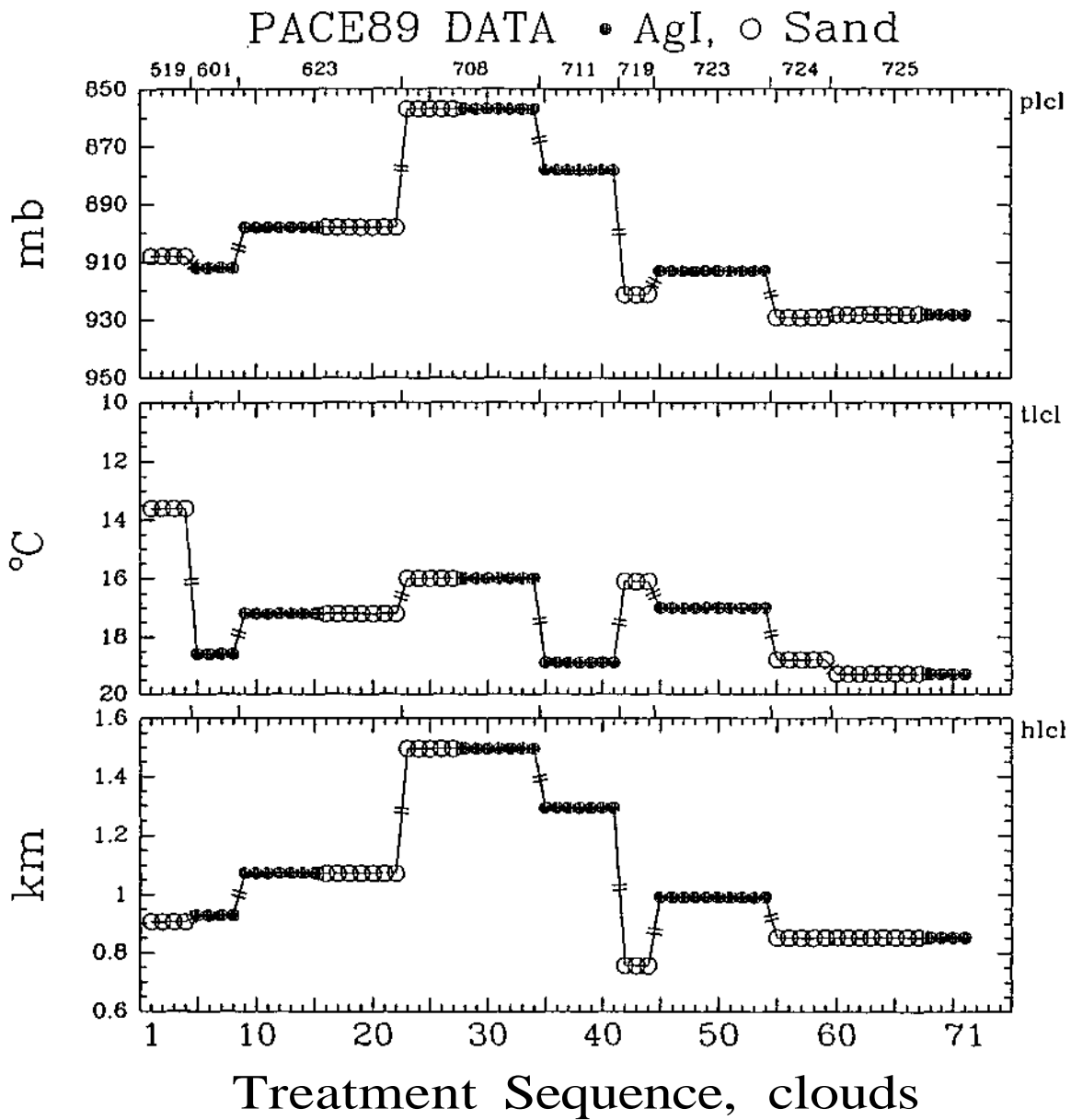


Figure B.2, Time history of the pressure (plcl), temperature (tlcl), and height (hlcl) of the lifting condensation level (LCL) using averaged data in lowest 100 mb.

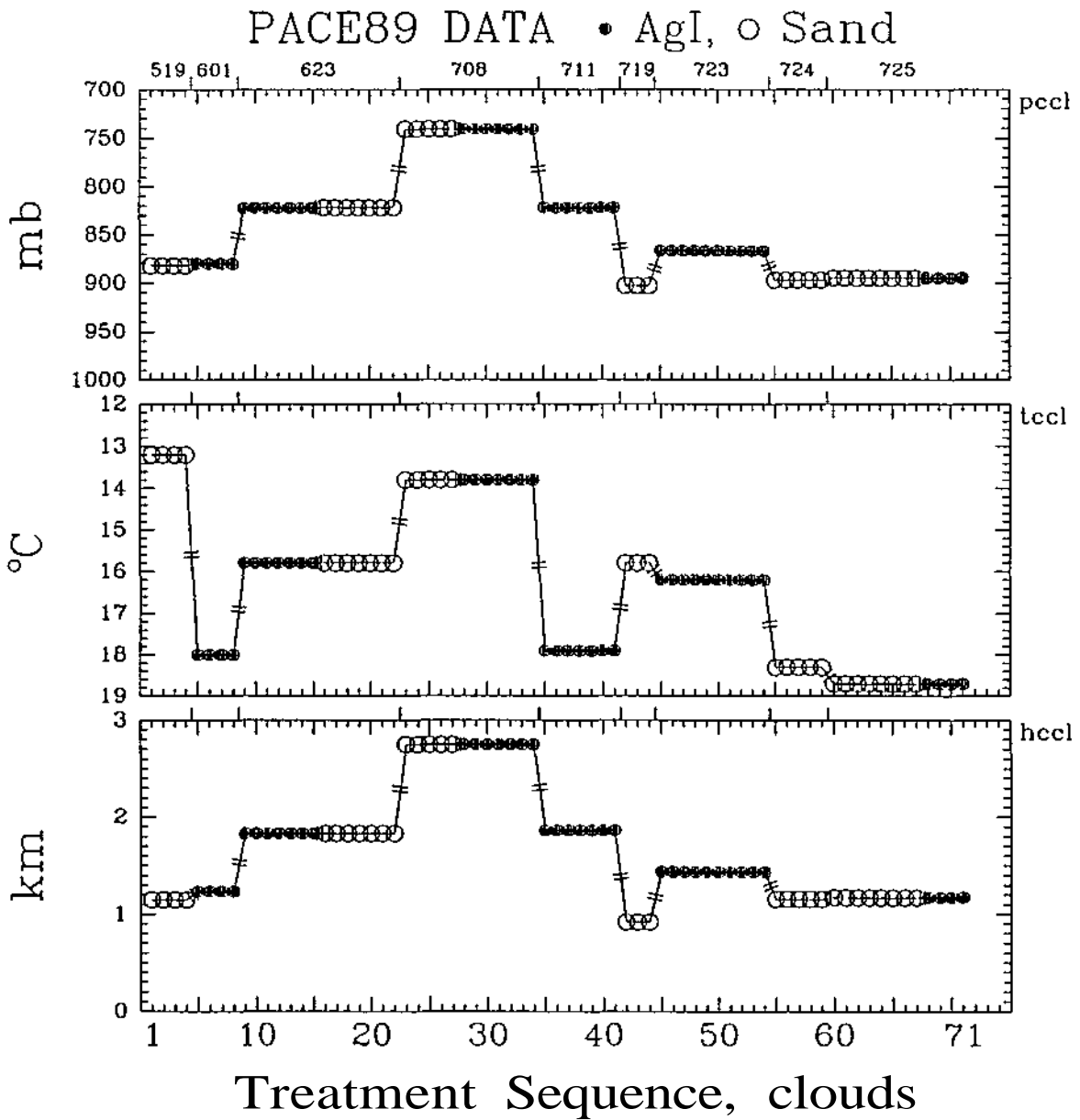


Figure B.3. Time history of the pressure (*ped*), temperature (*tecl*), and height (*heel*) of the convective condensation level (CCL) using averaged data in lowest 100 mb.

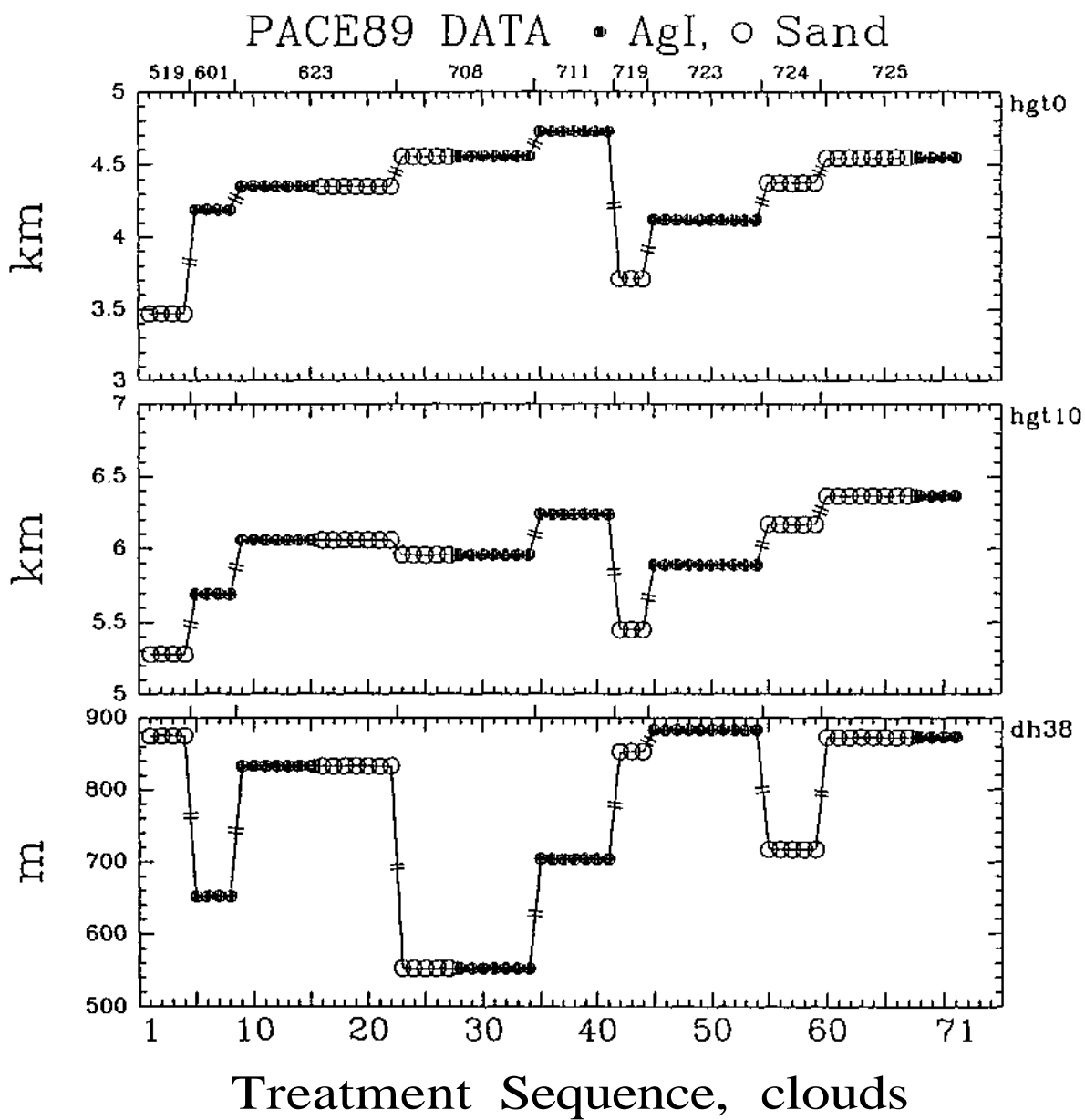


Figure B.4. Time history of the heights of the 0°C (hgt0) and -10°C (hgt10) levels, and the height difference between the heights of the -3°C and -8°C levels (dh38).

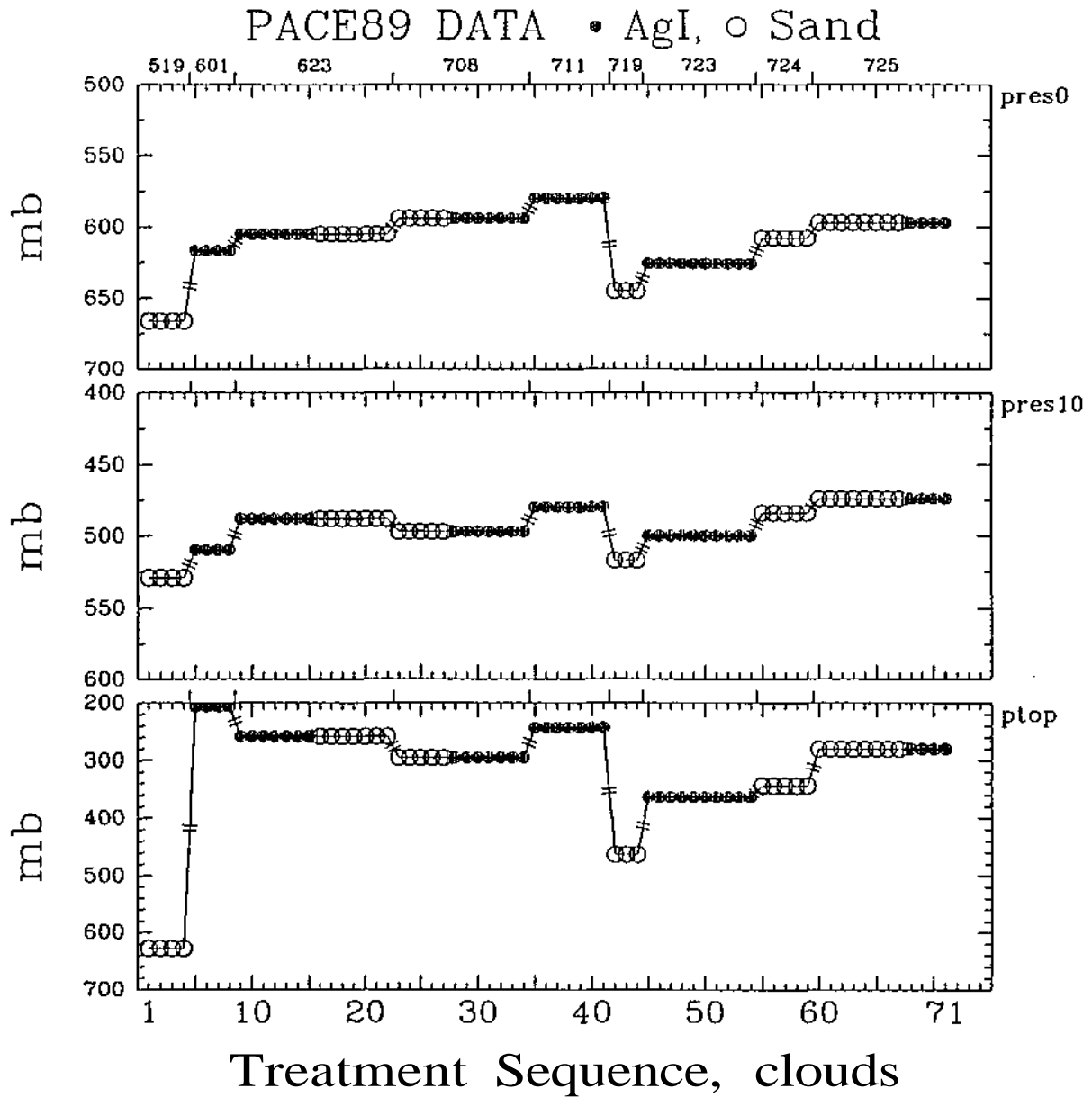


Figure B.5. Time history of the pressures of the 0°C (pres0) and -10°C (pres10) levels, and the pressure of the top of the "positive area" on the sounding (ptop).

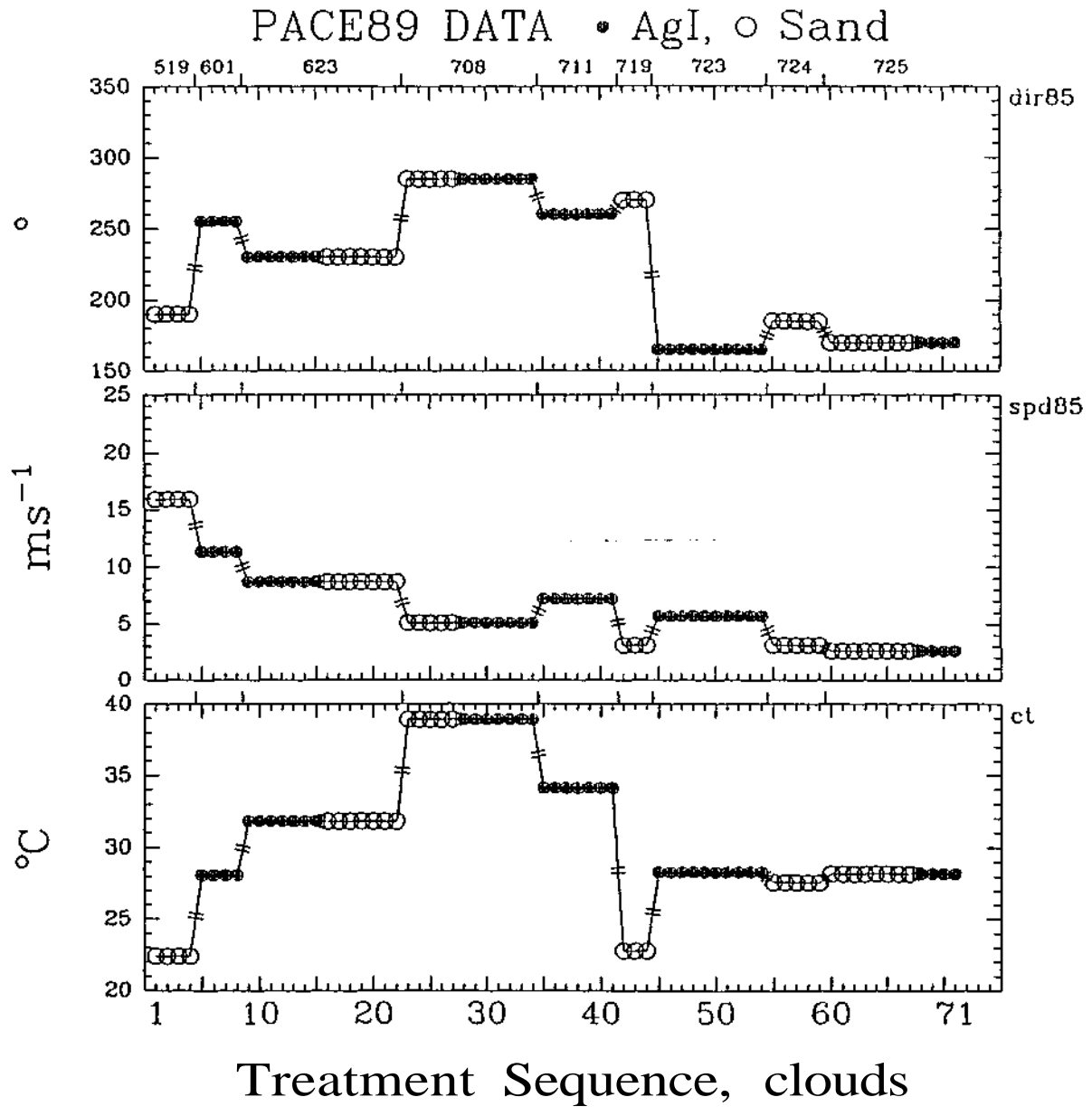


Figure B.6. Time history of the 850 mb wind direction (dir85) and speed (spd85), and the convective temperature using average mixing ratio in lowest 100 mb (ct).

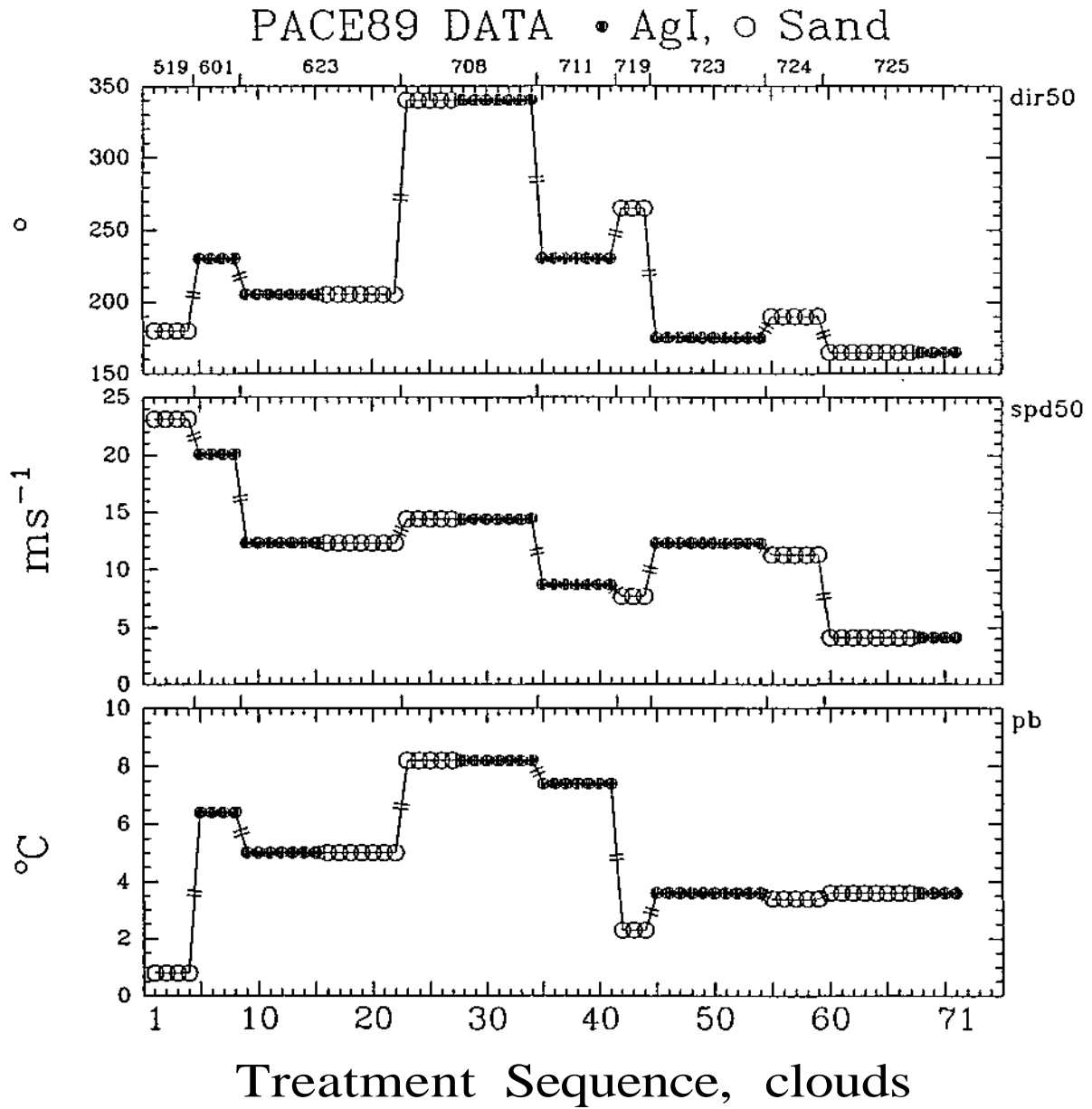


Figure B.7. Time history of the 500 mb wind direction (*dir50*) and speed (*spd50*), and the synoptic (parcel) potential buoyancy (*pb*).

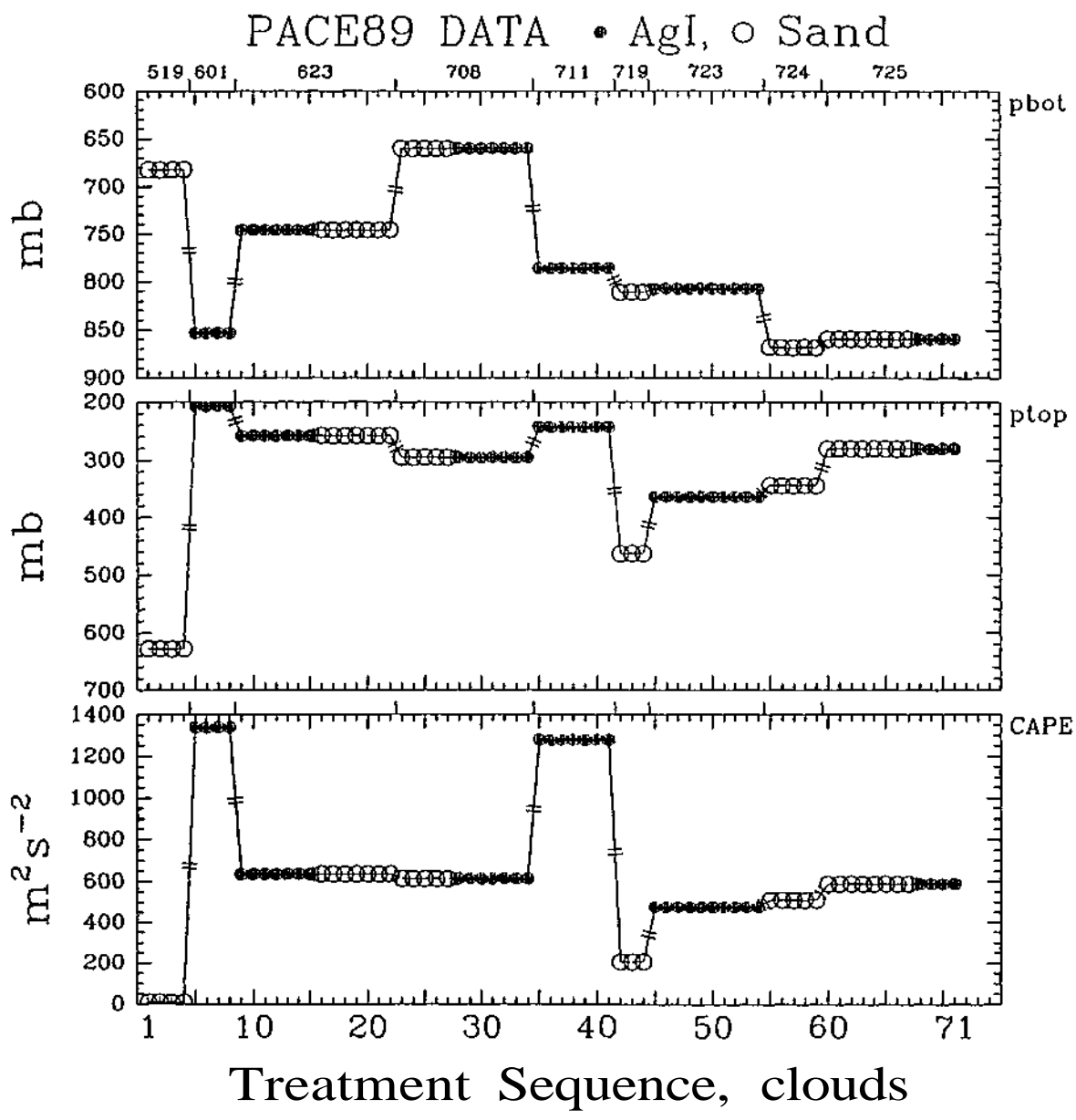


Figure B.8. Time history of the pressure at the bottom ( $p_{bot}$ ) and the top ( $p_{top}$ ) of the "positive area" of the rawinsonde, and the convective available potential energy (CAPE).

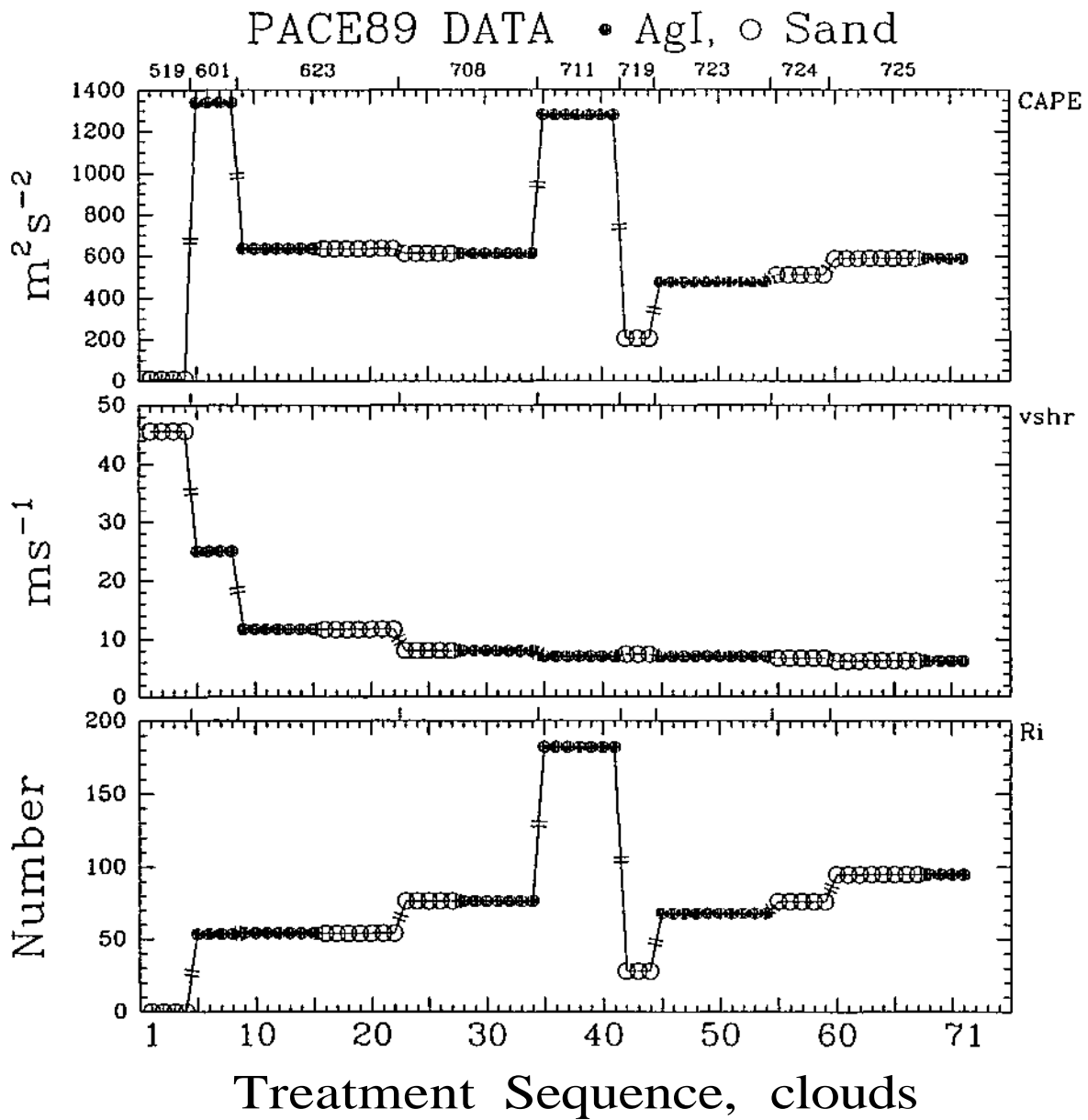


Figure B.9. Time history of the convective available potential energy (CAPE), the vector difference between the wind at 4 km and the average wind in lowest 500 m ( $v_{shr}$ ), and the Bulk Richardson number (Ri), calculated using CAPE and  $v_{shr}$ .

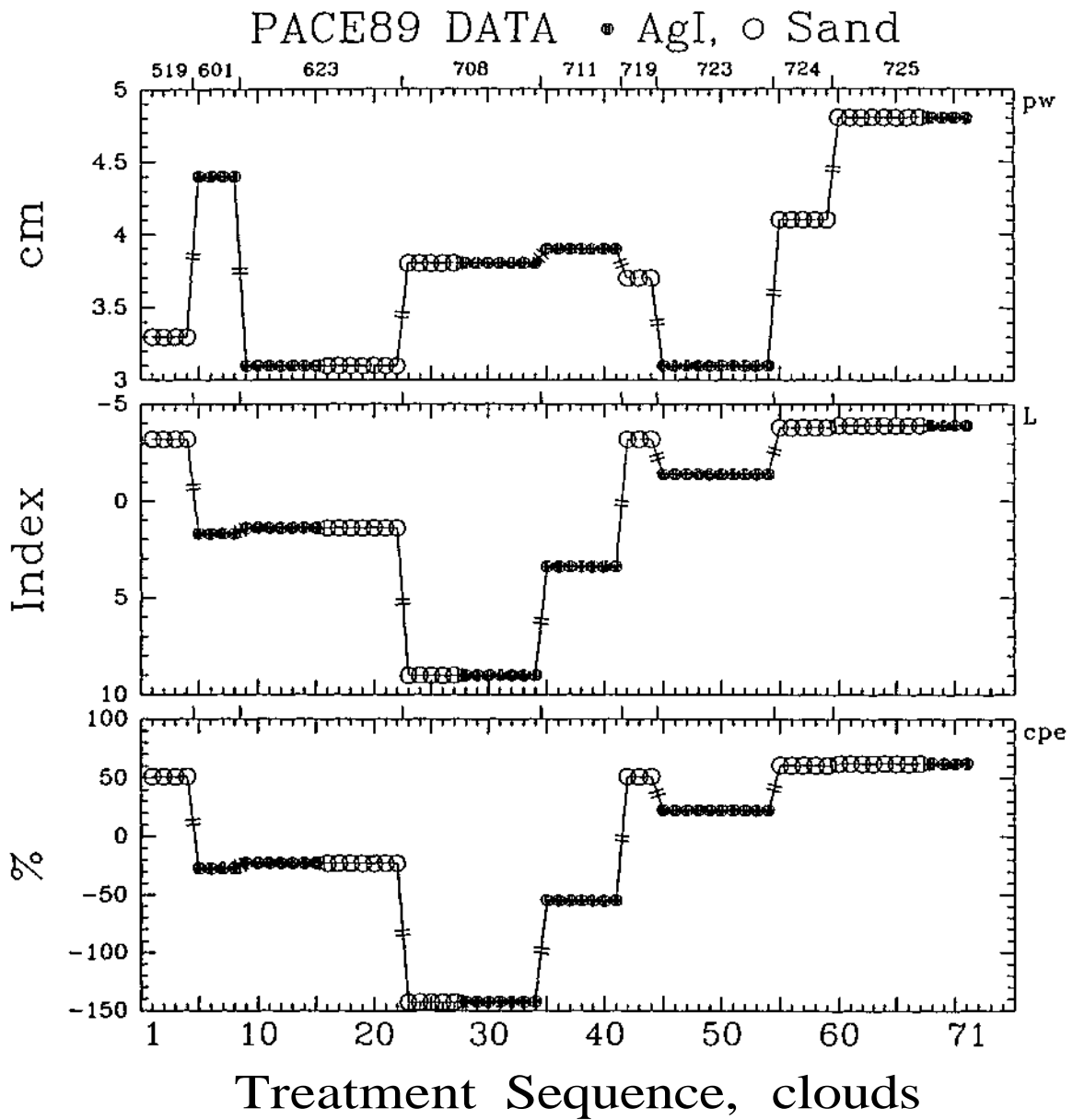


Figure B. 10. Time history of the precipitable water between the surface and 500 mb (pw), the index of coalescence activity (L) (i.e., a raindrop size discriminant function based on tccl and pb), and the coalescence precipitation efficiency (cpe) (i.e., relative size of L).

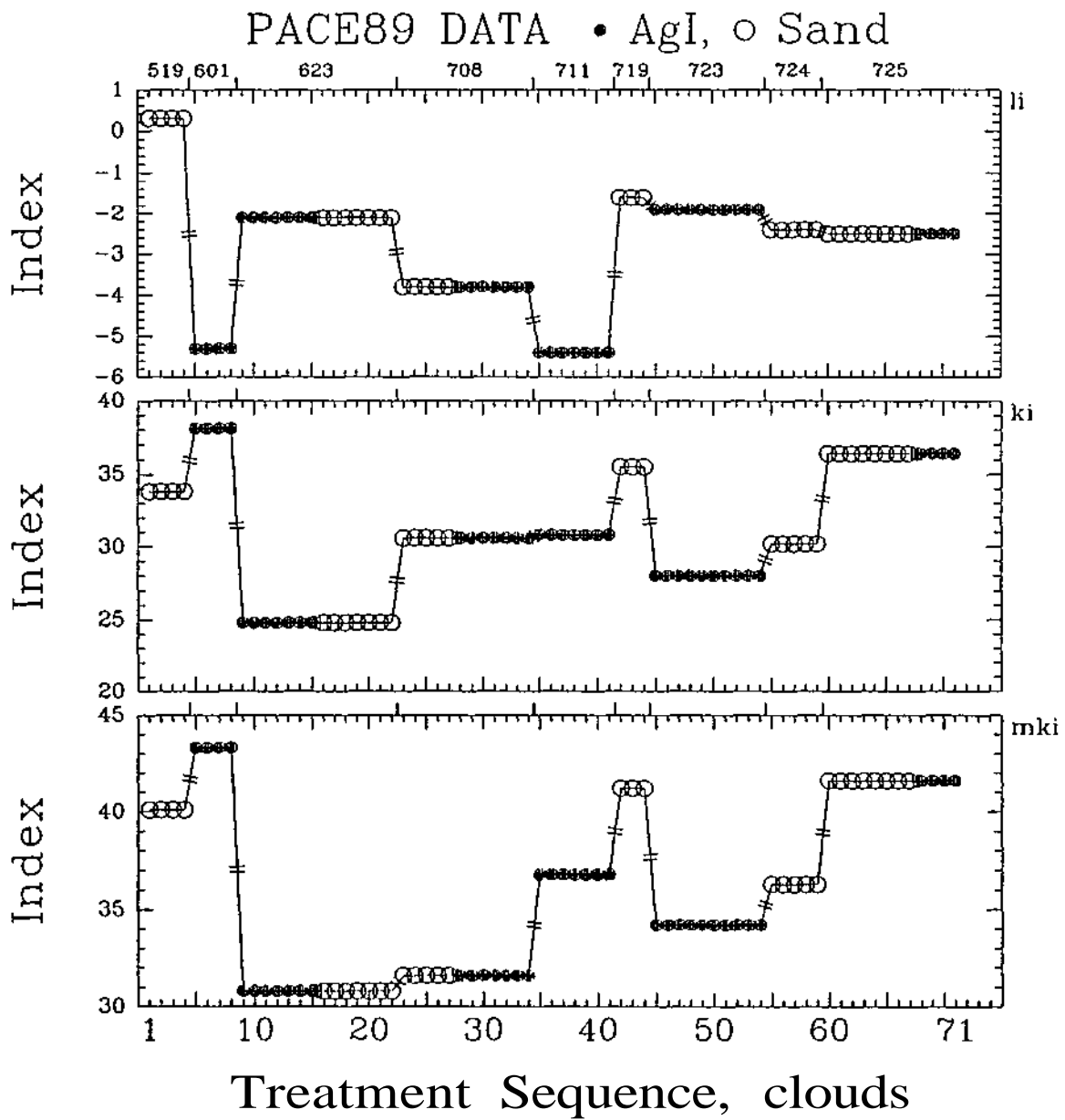


Figure B.11. Time history of the lifted index (li) (measure of latent instability), the K-index (ki) (heat differential and moisture depth in the lower levels of the atmosphere), and the Modified K-index (mki).

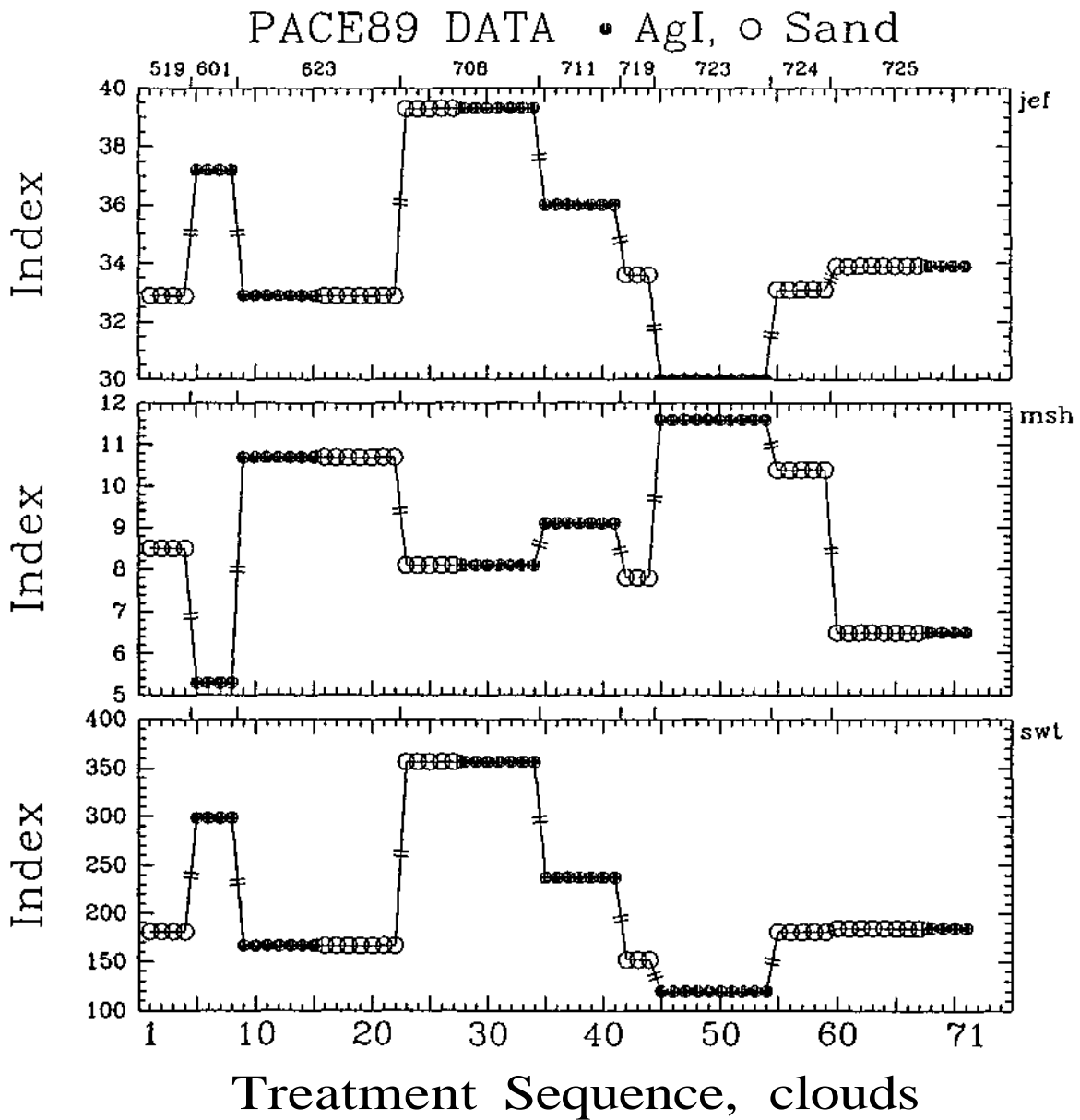


Figure B.12. Time history of the Jefferson (jef), modified Showalter (msh), and Sweat (swt) indices (measures of instability).

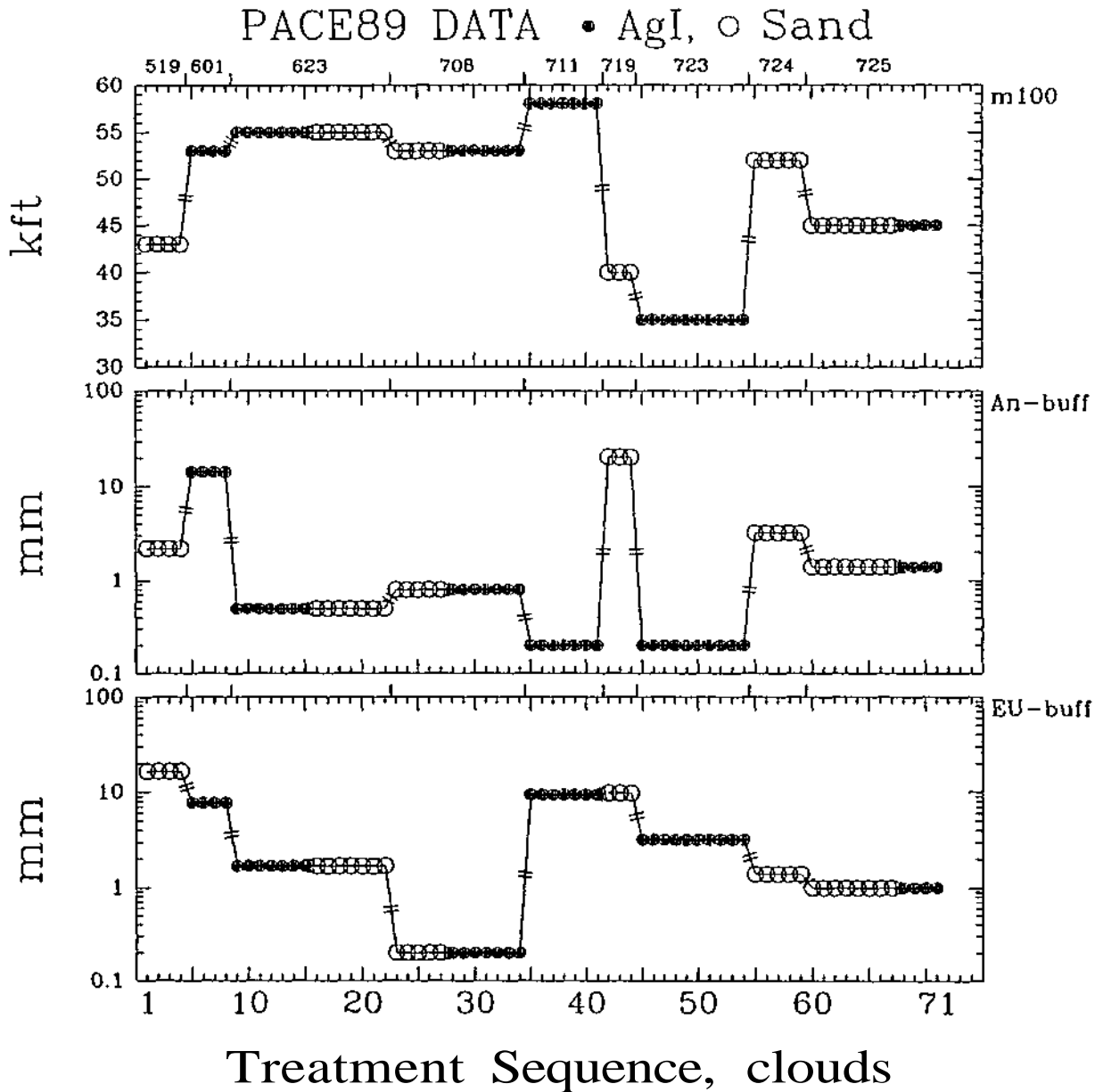


Figure B.13. Time history of the tallest maximum radar echo top within 100 nm of Champaign (CMI) observed between 1130 and 2030 CDT at the NWS site (MMO, STL, EVV) closest to the echo (m100), and of the 80-100 nm radius area (not including Indiana, centered on CMI) 24 hr (80-85% 7:00am obs) station averaged precipitation which fell on the day prior to the experimental unit (An-buff), and the day of the experimental unit (EU-buff).

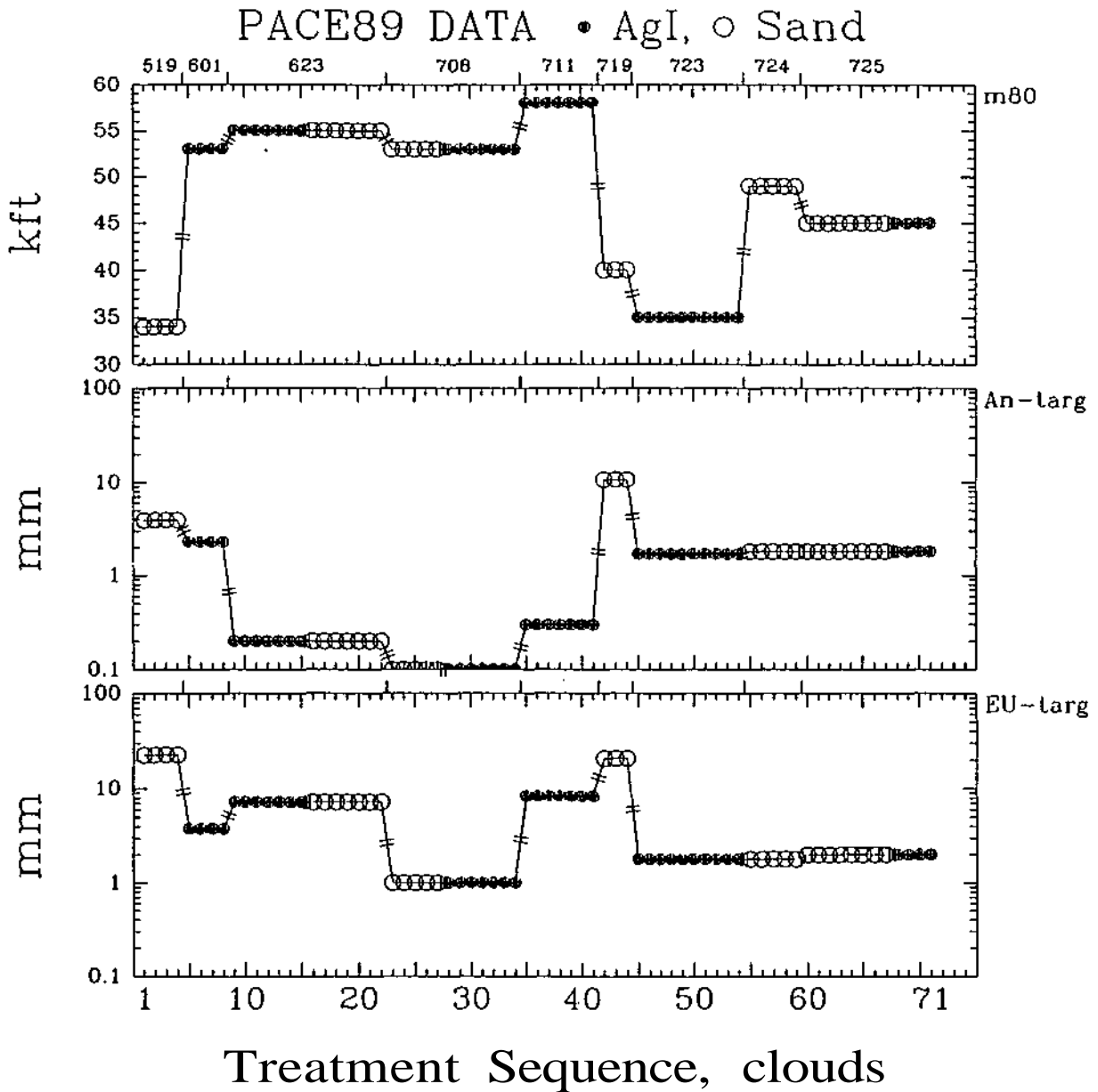


Figure B. 14. Time history of the tallest maximum radar echo top within 80 nm of Champaign (CMI) observed between 1130 and 1530 CDT at the NWS site (MMO, STL, EVV) closest to the echo (m80), and of the 80 nm radius area (not including Indiana, centered on CMI) 24 hr (80-85% 7:00am obs) station averaged precipitation which fell on the day prior to the experimental unit (An-targ), and the day of the experimental unit (EU-targ).

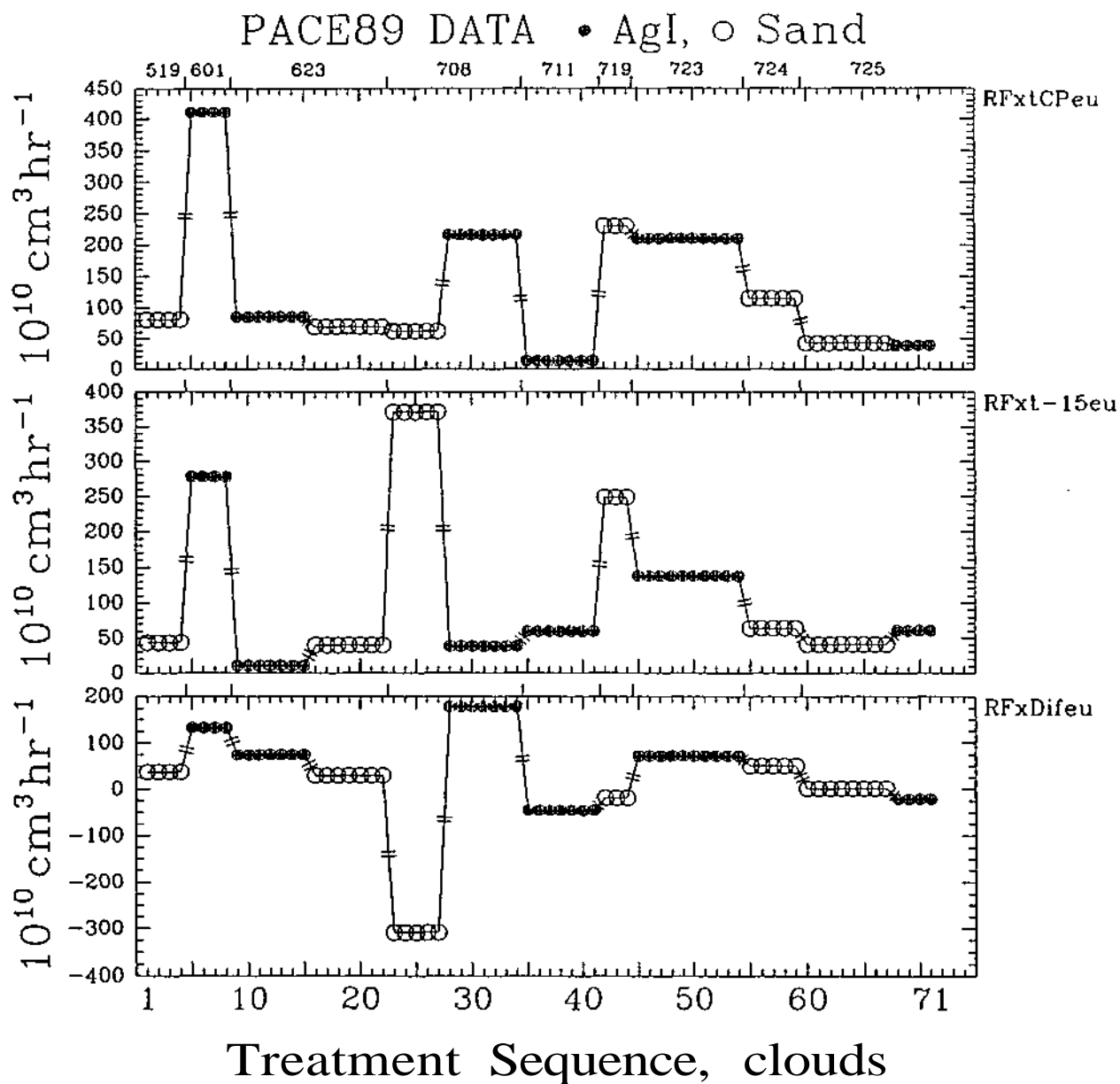


Figure B.15. Time history of the experimental unit rain flux at first treatment (RFxtCPeu), 15 minutes prior to the first treatment (RFxt-15eu), and the experimental unit rain flux change from 15 minutes prior to first treatment to the first treatment (RFxDifeu).

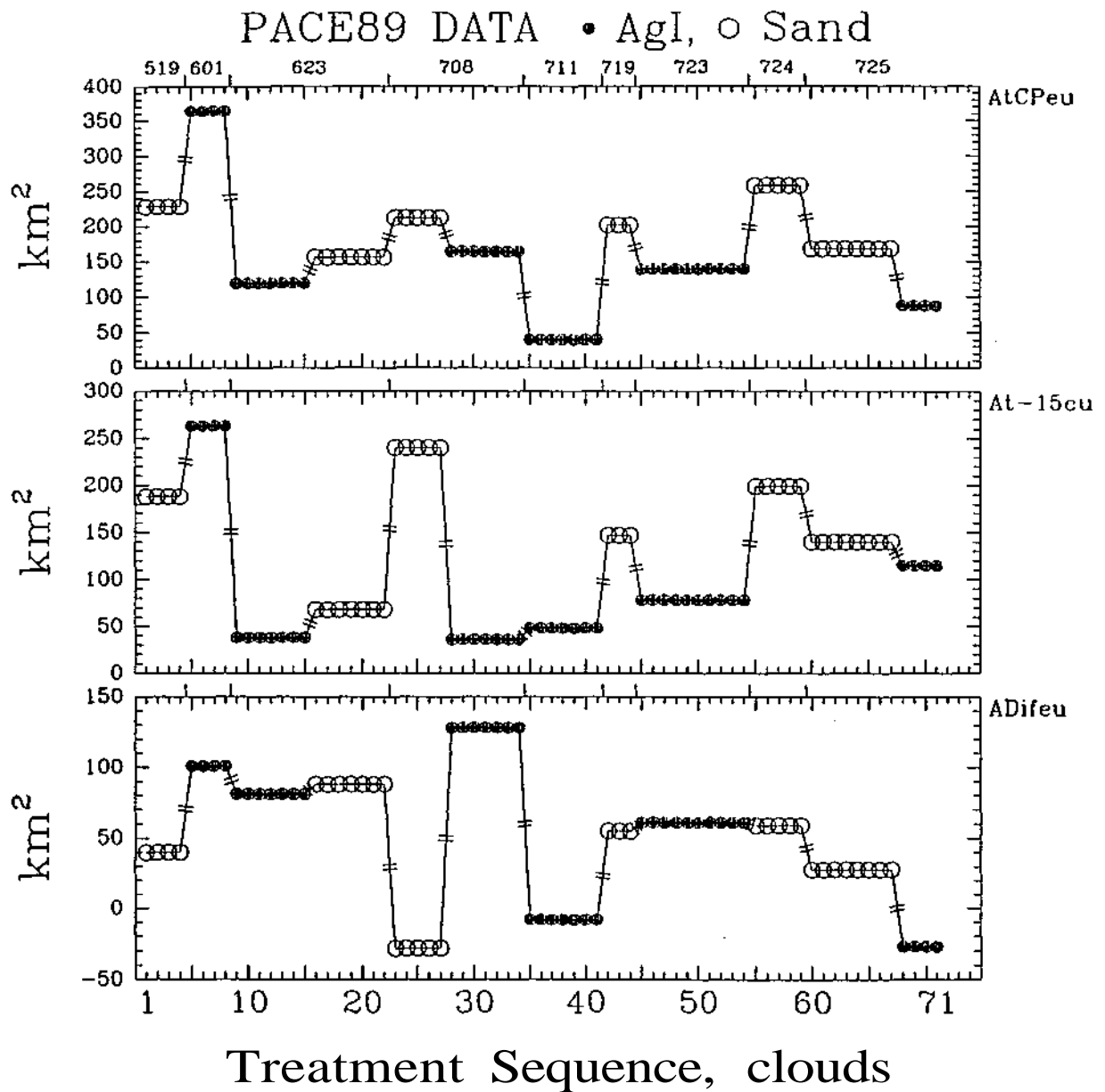


Figure B. 16. Time history of the experimental unit echo ureal coverage at first treatment (AtCpeu), 15 minutes prior to the first treatment (At-15eu), and the experimental unit echo areal coverage change from 15 minutes prior to first treatment to the first treatment (ADifeu).

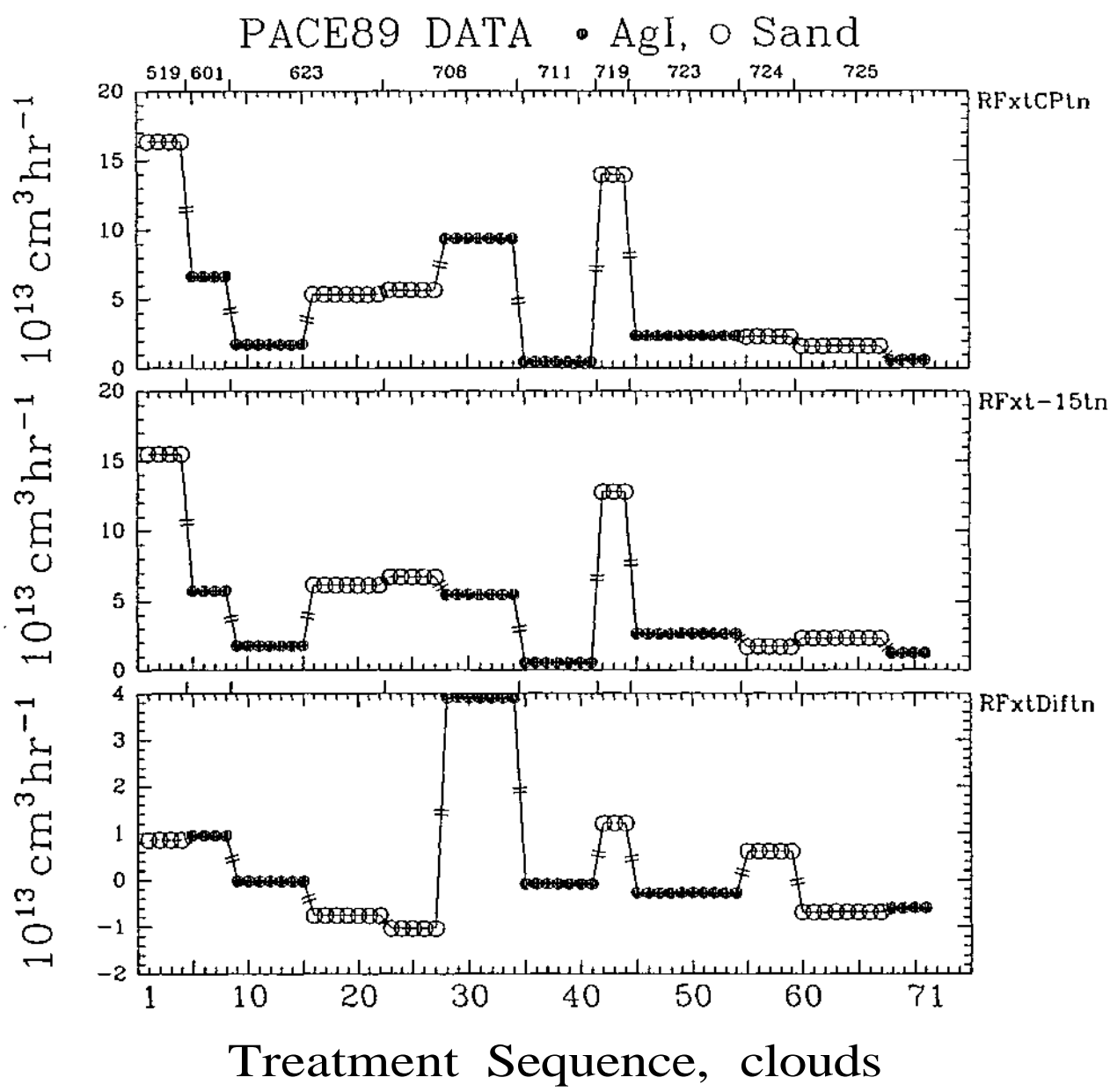


Figure B.17. Time history of the total network rain flux at first treatment (RFxtCPTn), 15 minutes prior to the first treatment (RFxt-15tn), and the total network rain flux change from 15 minutes prior to first treatment to the first treatment (RFxDiftn).

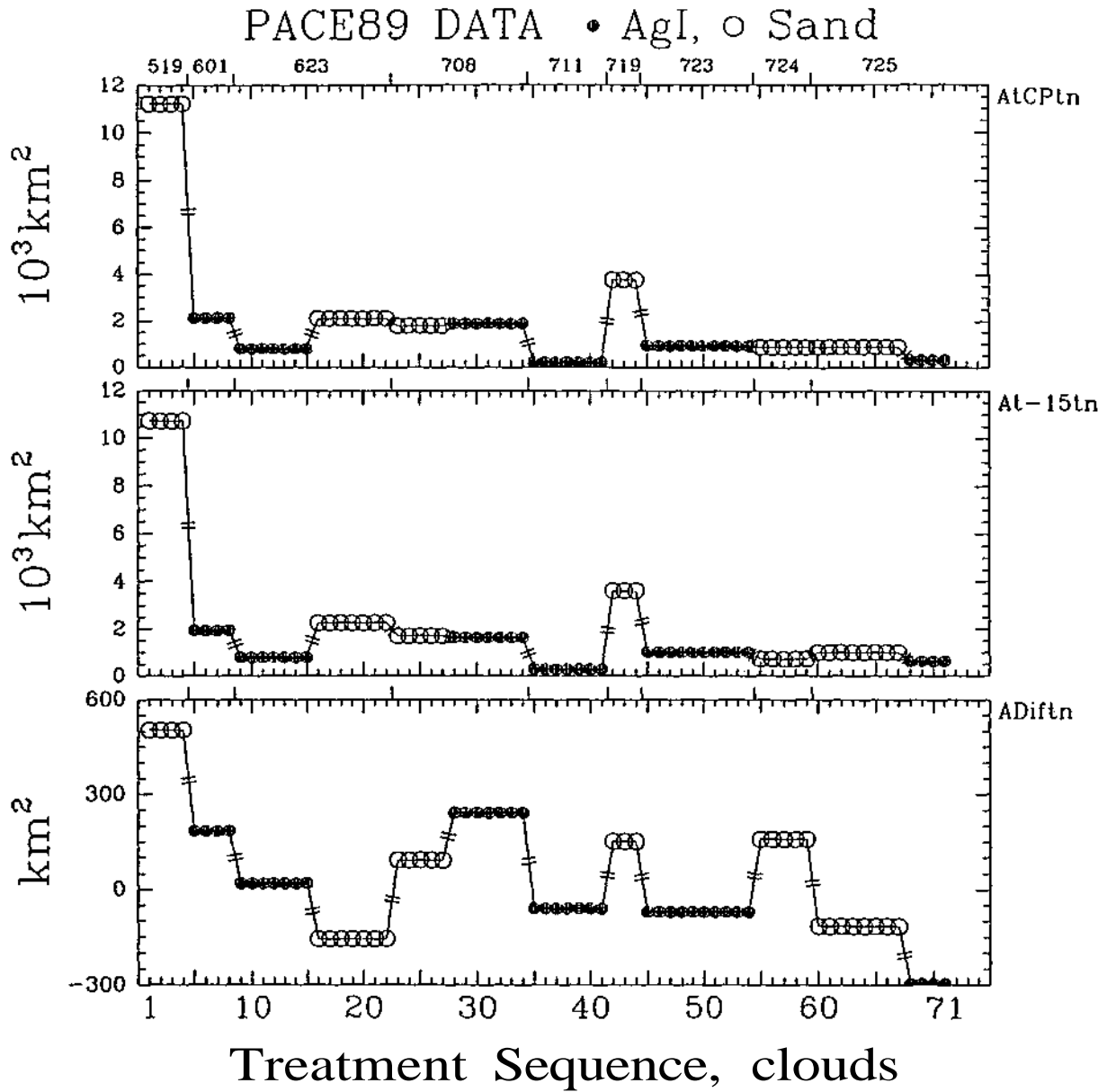


Figure B. IS. Time history of the total network echo areal coverage at first treatment (AtCPtn), 15 minutes prior to the first treatment (At-15tn), and the total network echo areal coverage change from 15 minutes prior to first treatment to the first treatment (ADiftn).

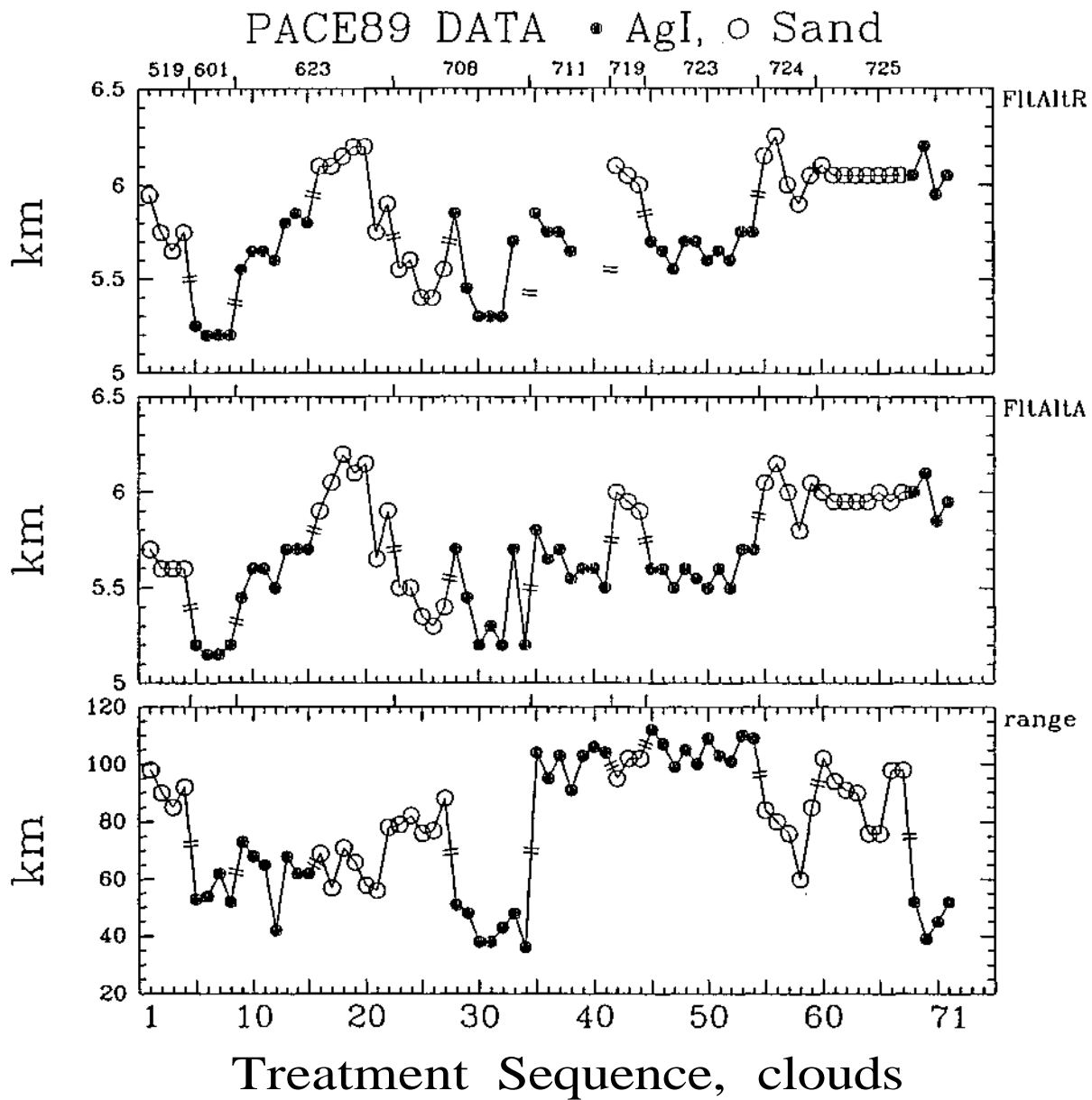


Figure B.19. Time history of the radar-data (RATS) derived (FltAltR), and aircraft-data derived (FltAltA) aircraft flight level at treatment, and the distance from the Champaign airport (radar site) to the echo/treatment (range).

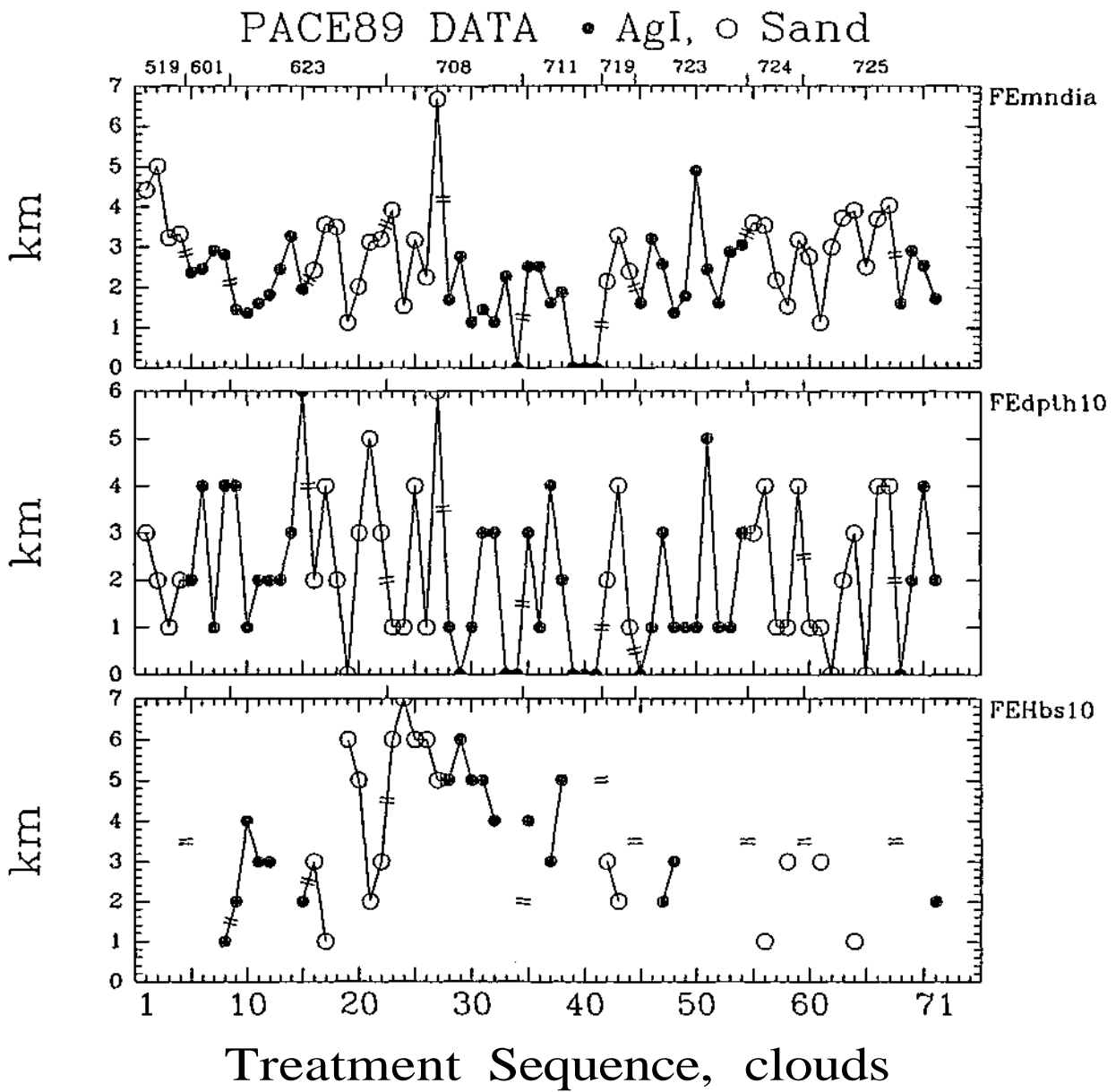


Figure B.20. Time history of the mean (averaged in height) echo diameter at first echo (FEmndia), the depth of the 10 dBZ contour at first echo (FEdpth10), and the base height of the 10 dBZ contour at first echo (FEHbs10).

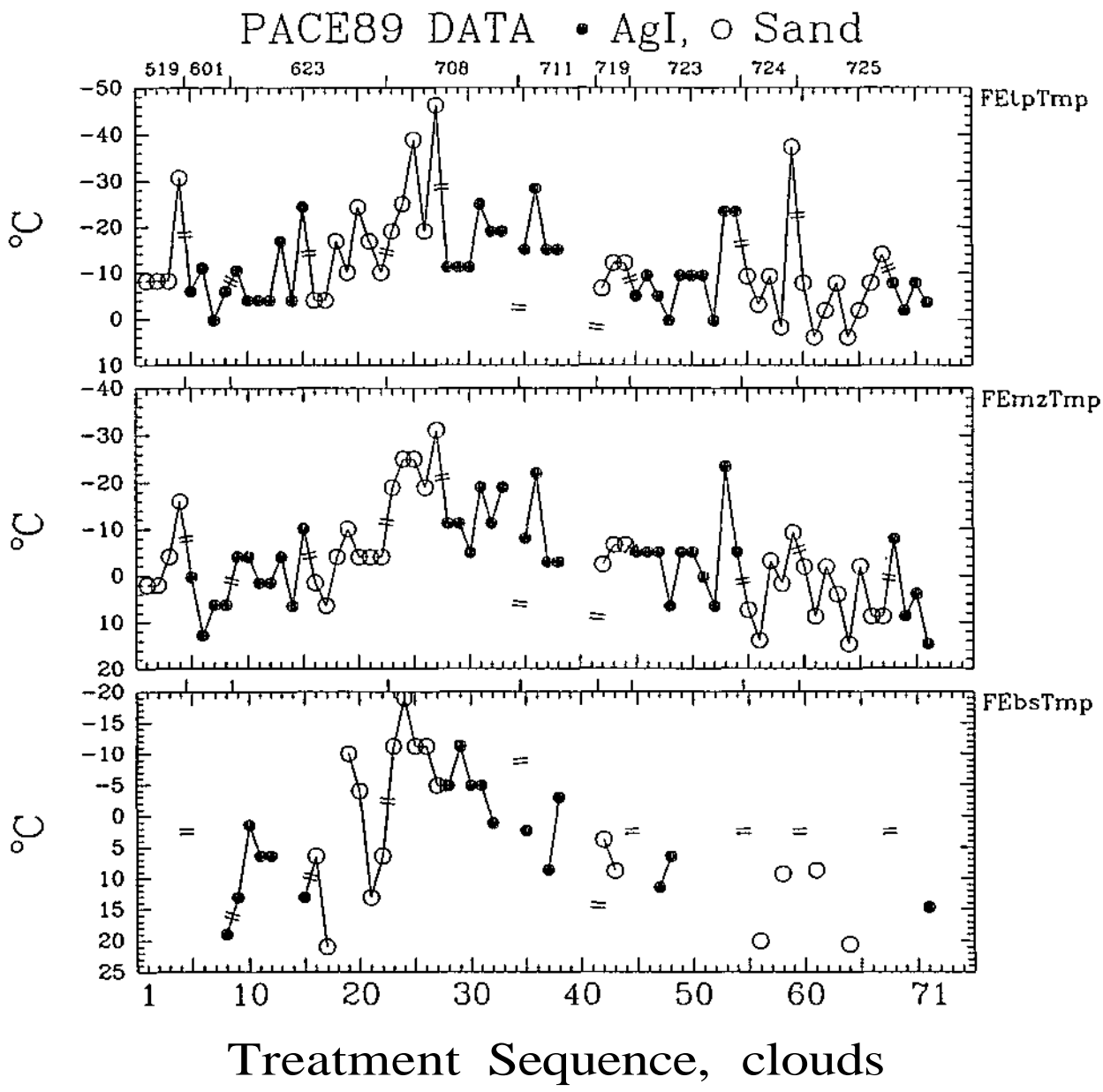


Figure B.21. Time history of the top of the echo temperature at first echo (FETpTmp), the temperature at the height of the maximum reflectivity at first echo (FEmzTmp), and the temperature at the base of the echo at first echo (FEbsTmp).

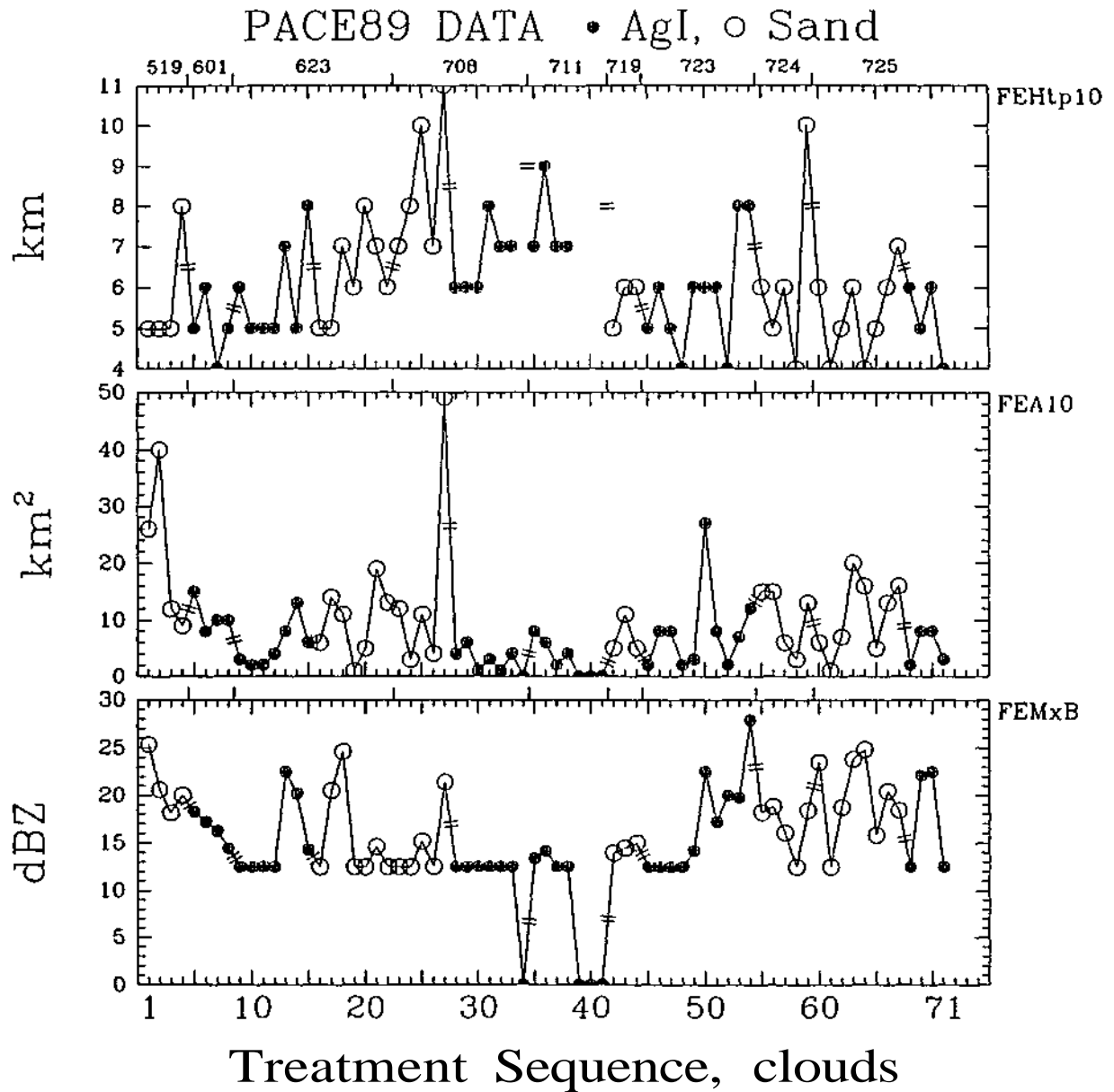


Figure B .22. Time history of the top height of the 10 dBZ contour at first echo (FEHtp10), the maximum area of the 10 dBZ contour at first echo (FEA10), and the maximum brightness at first echo (FEMxB).

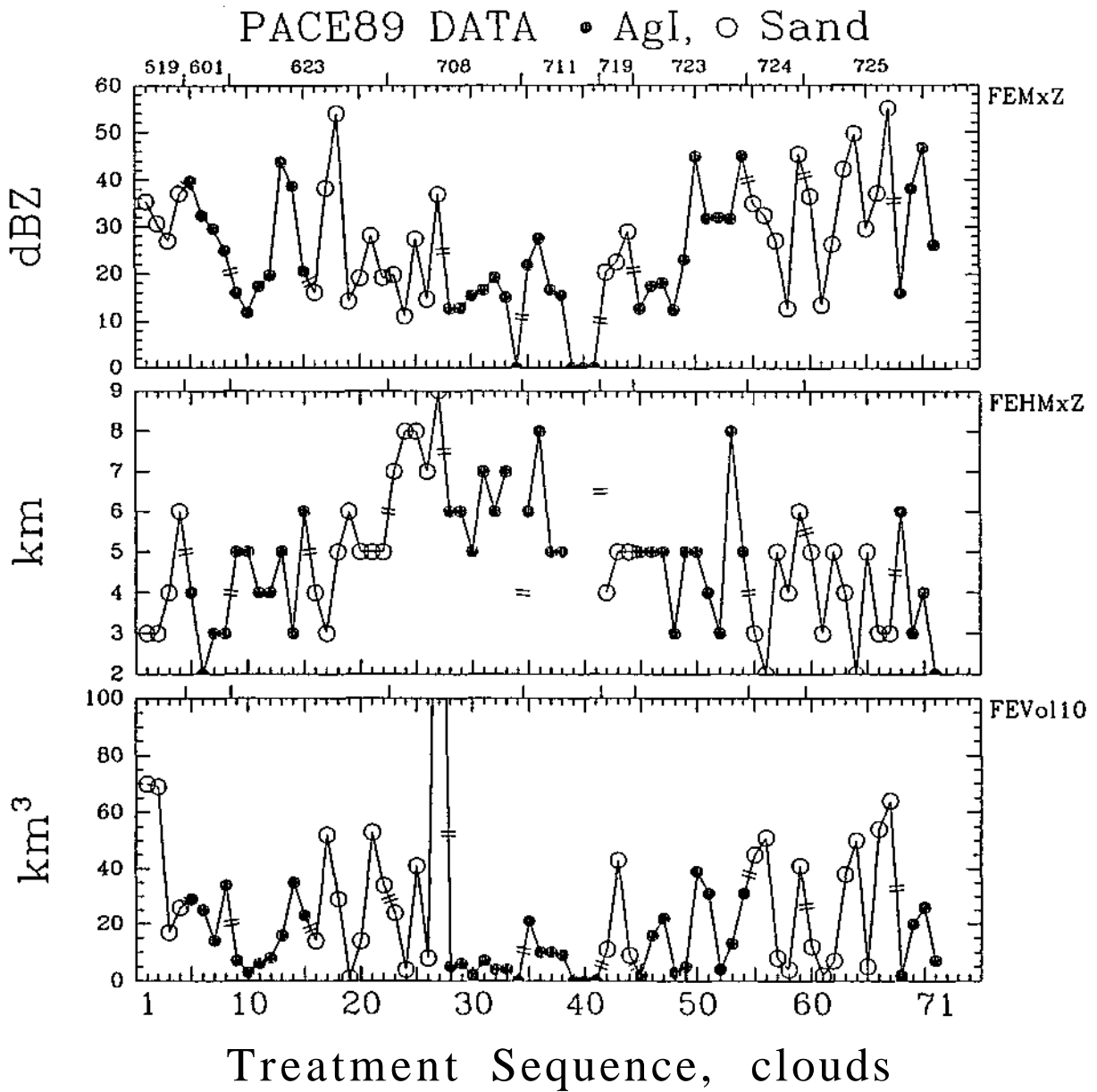


Figure B.23. Time history of the maximum reflectivity at first echo (FEMxZ), the height of the maximum reflectivity at first echo (FEHMxZ), and the volume of the 10 dBZ contour at first echo (FEVo110).

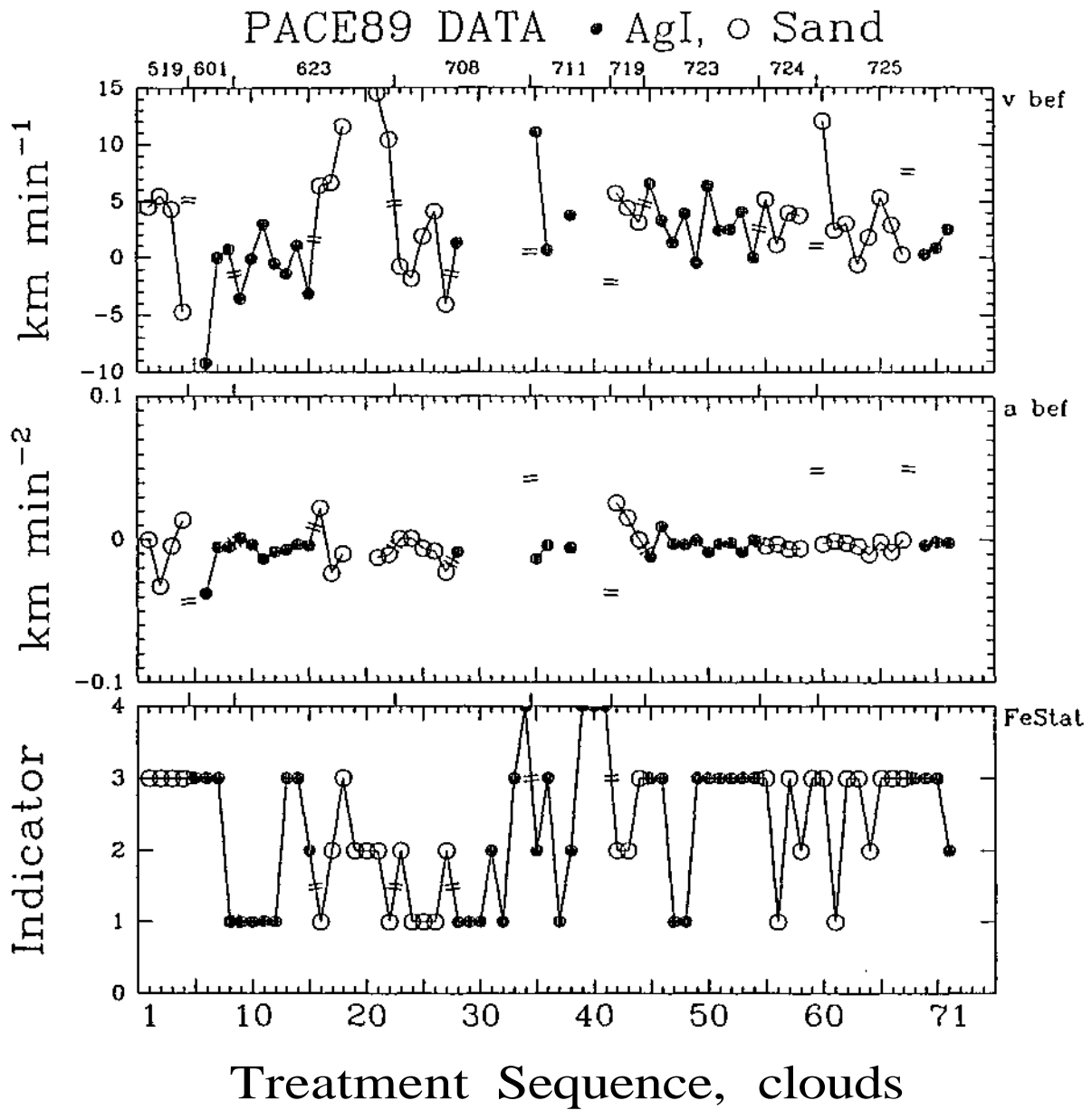


Figure B.24. Time history of the velocity ( $v_{bef}$ ) and acceleration ( $a_{bef}$ ) of the echo top 2 minutes before treatment, and the indicator of core merging at first echo (FeStat) (0 no echo at that time, 1 separate at all levels, 2 joined at some levels but can see base & top, 3 joined at lower levels but can see top, 4 no echo ever).

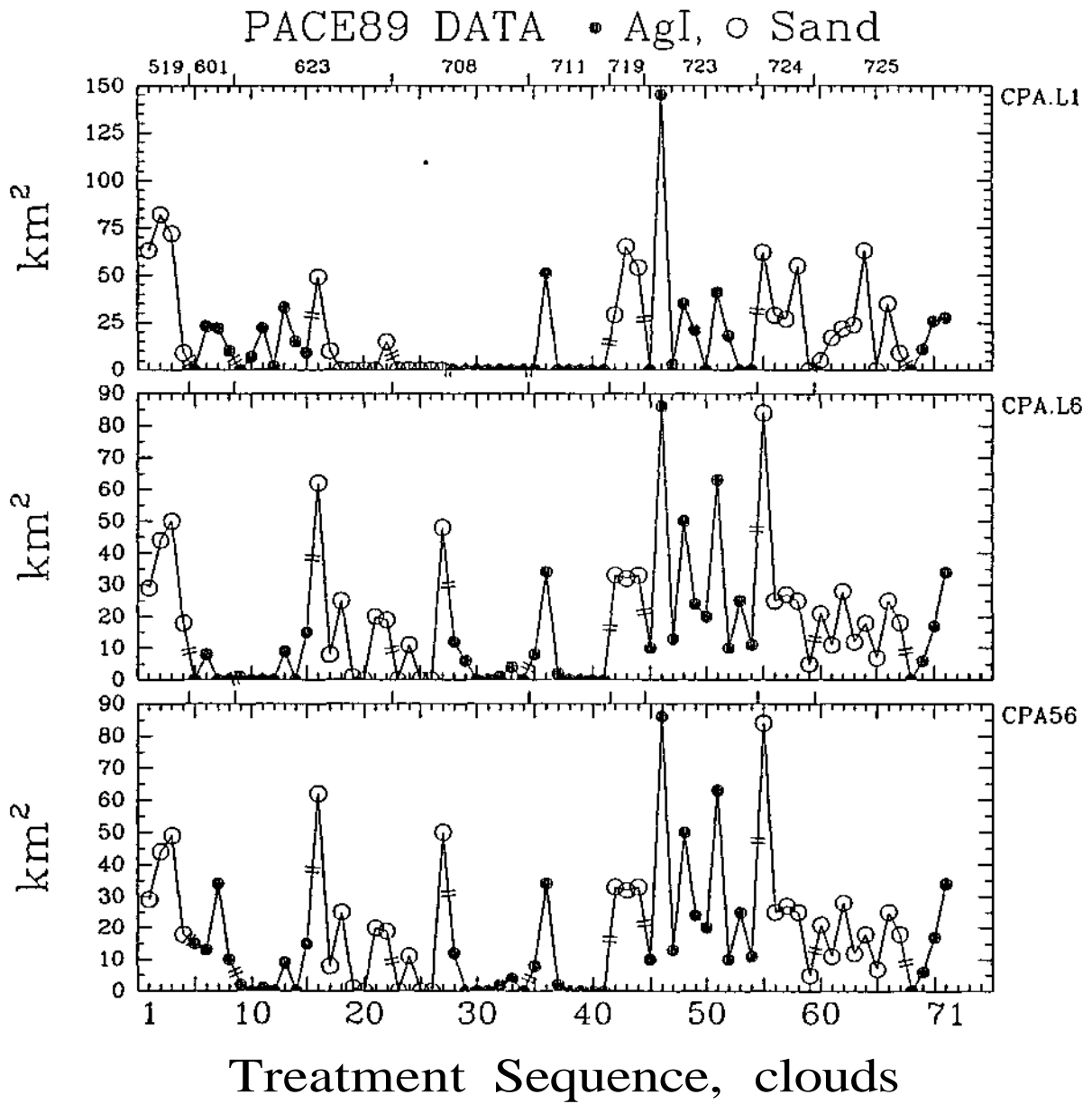


Figure B.25. Time history of the 1 kilometer (CPA.L1), 6 kilometer (CPA.L6), and flight level (CPA56) areas at treatment.

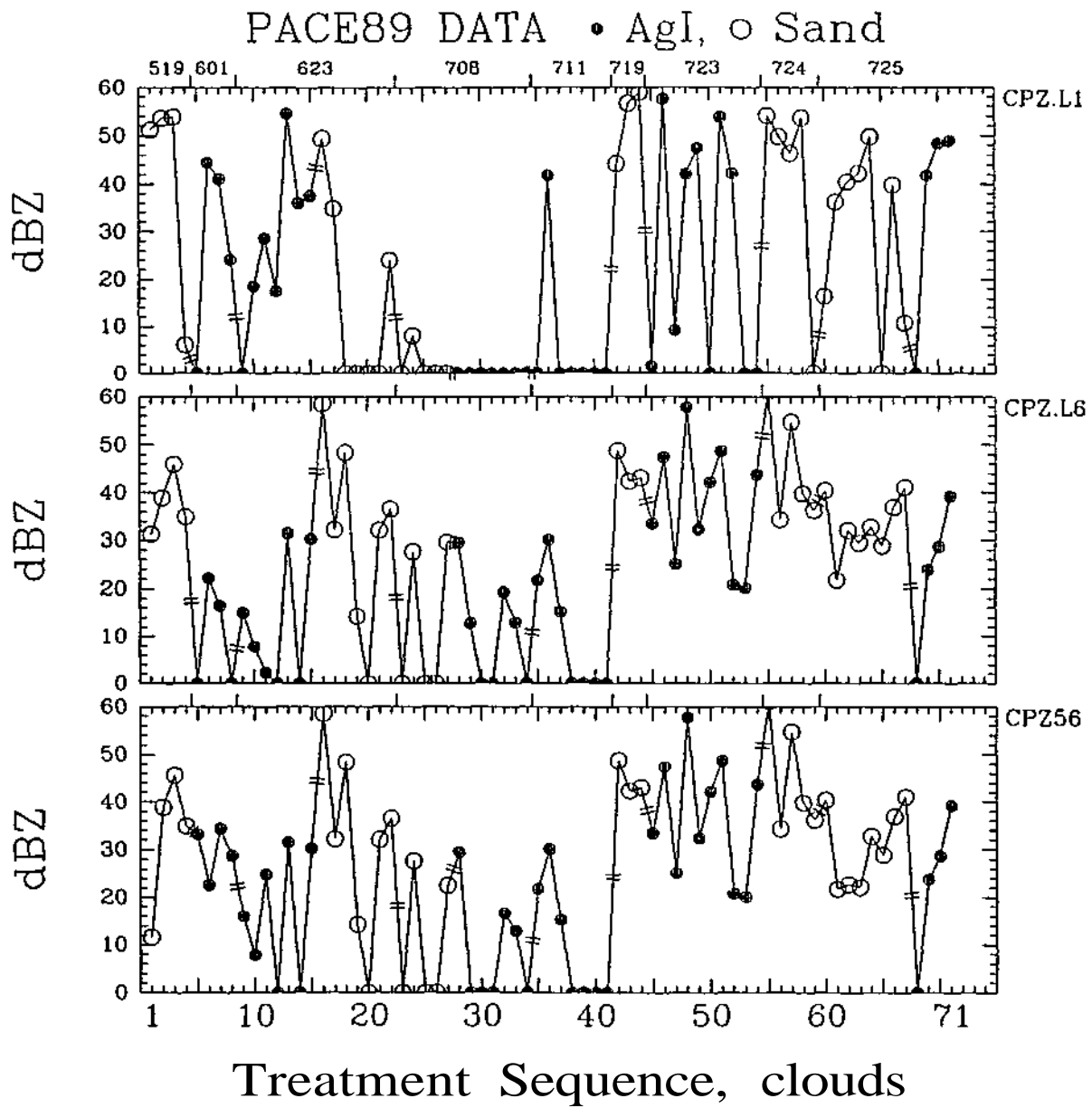


Figure B.26. Time history of the 1 kilometer (CPZ.L1), 6 kilometer (CPZ.L6), and flight level (CPZ56) maximum reflectivities at treatment.

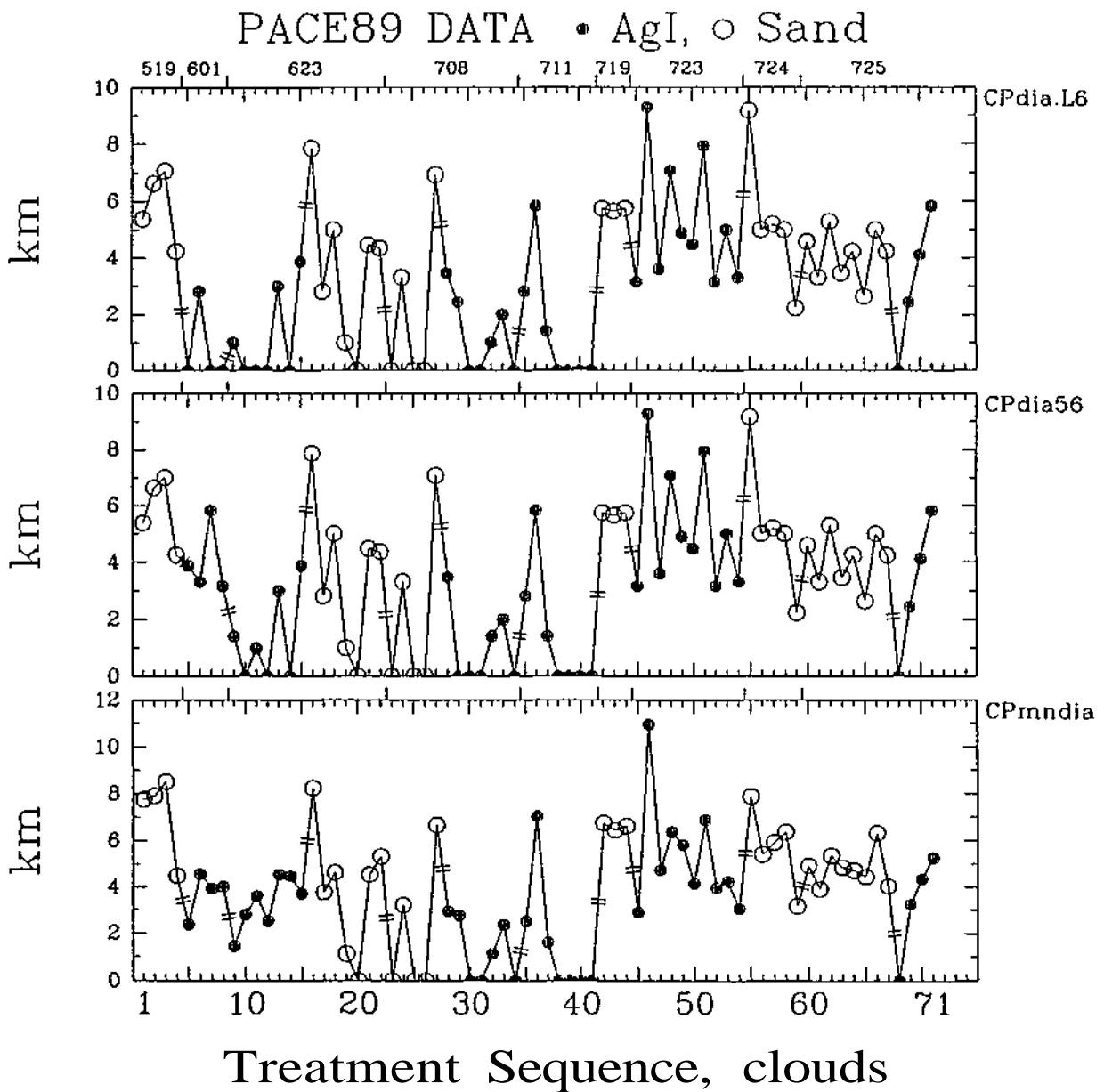


Figure B.27. Time history of the 6 kilometer (CPdia.L6) and flight level (CPdia56) echo diameters at treatment, and the mean (averaged in height) echo diameter at treatment (CPmndia).

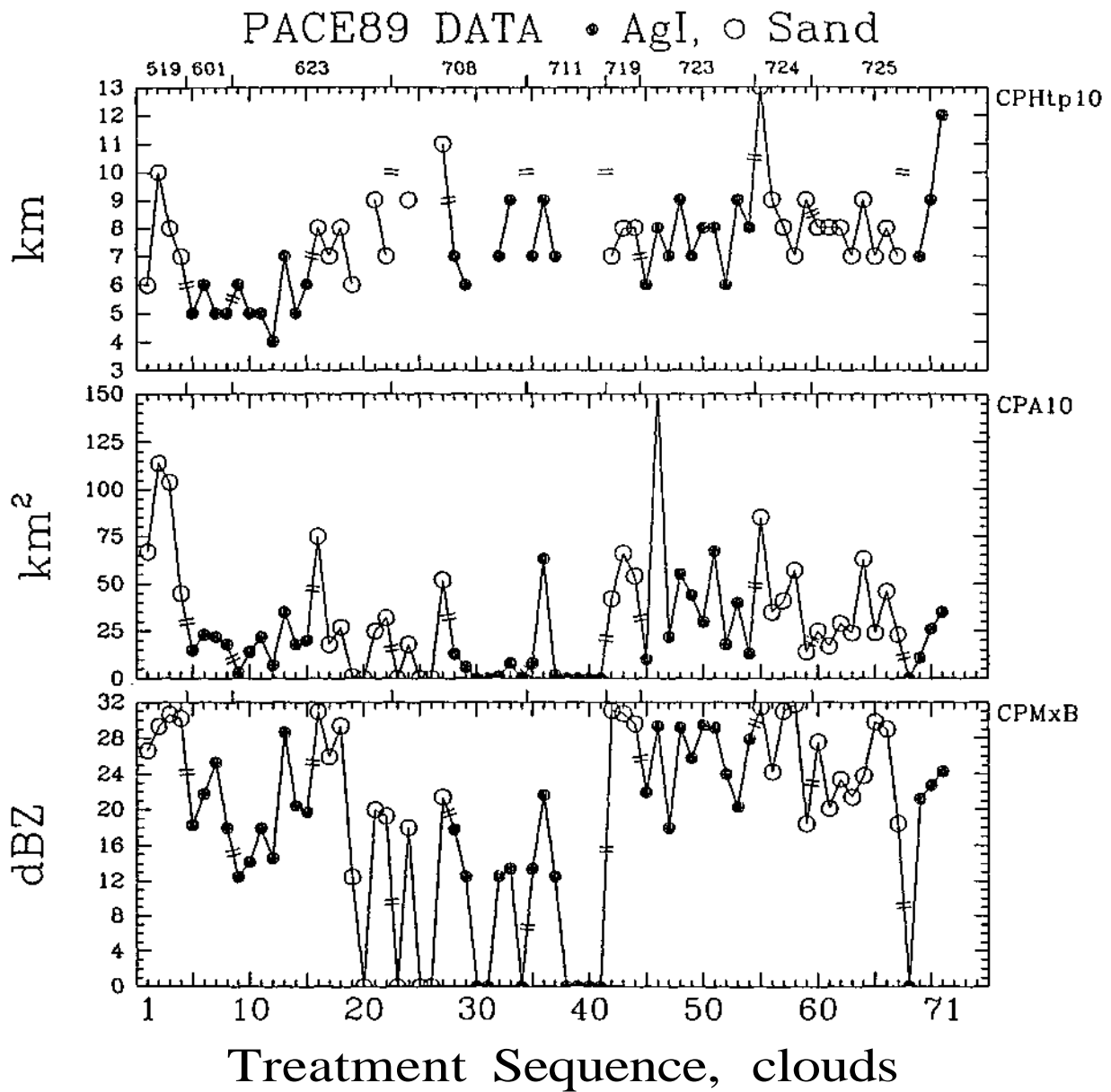


Figure B.28. Time history of the top height of the 10 dBZ contour at treatment (CPHtp10), the maximum area of the 10 dBZ contour at treatment (CPA10), and the maximum brightness at treatment (CPMxB).

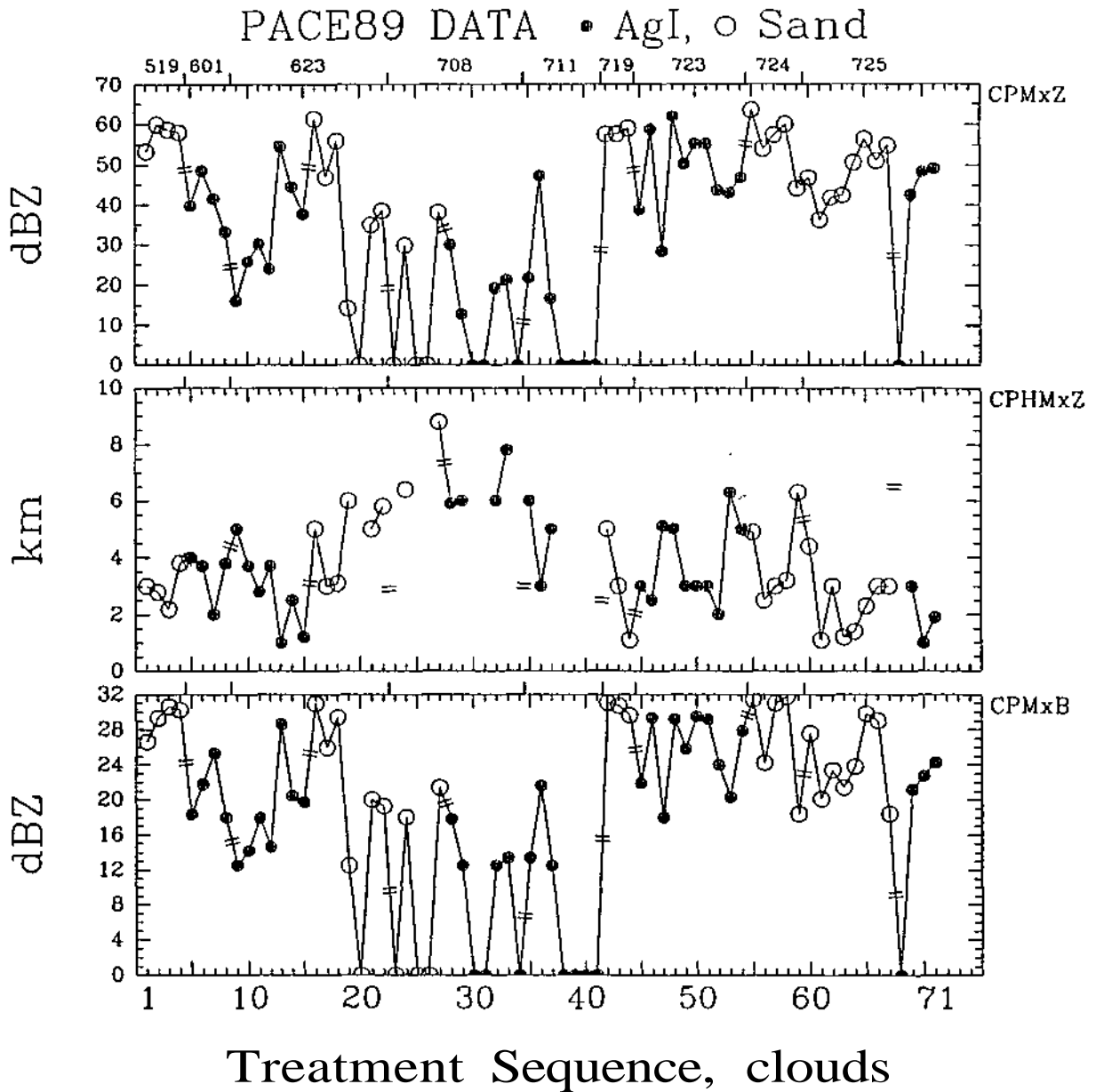


Figure B.29. Time history of the maximum reflectivity at treatment (CPMxZ), the height of the maximum reflectivity at treatment (CPHMxZ), and the maximum brightness at treatment (CPMxB).

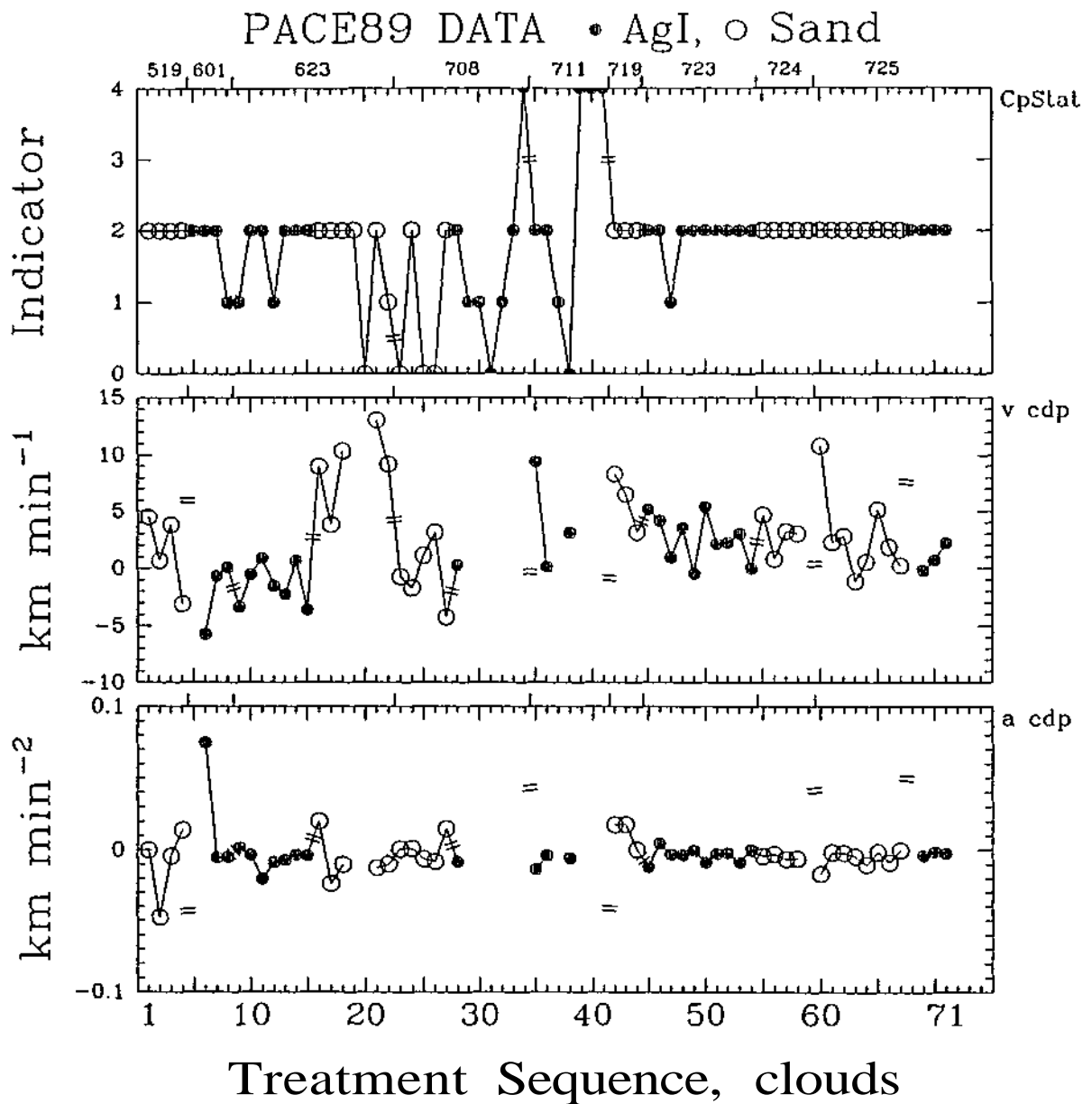


Figure B.30. Time history of the indicator of core merging at treatment ( $CpStat$ ) (0 no echo at that time, 1 isolated, 2 merged, 4 no echo ever), and the velocity ( $v_{cdp}$ ) and acceleration ( $a_{cdp}$ ) of the echo top at treatment.

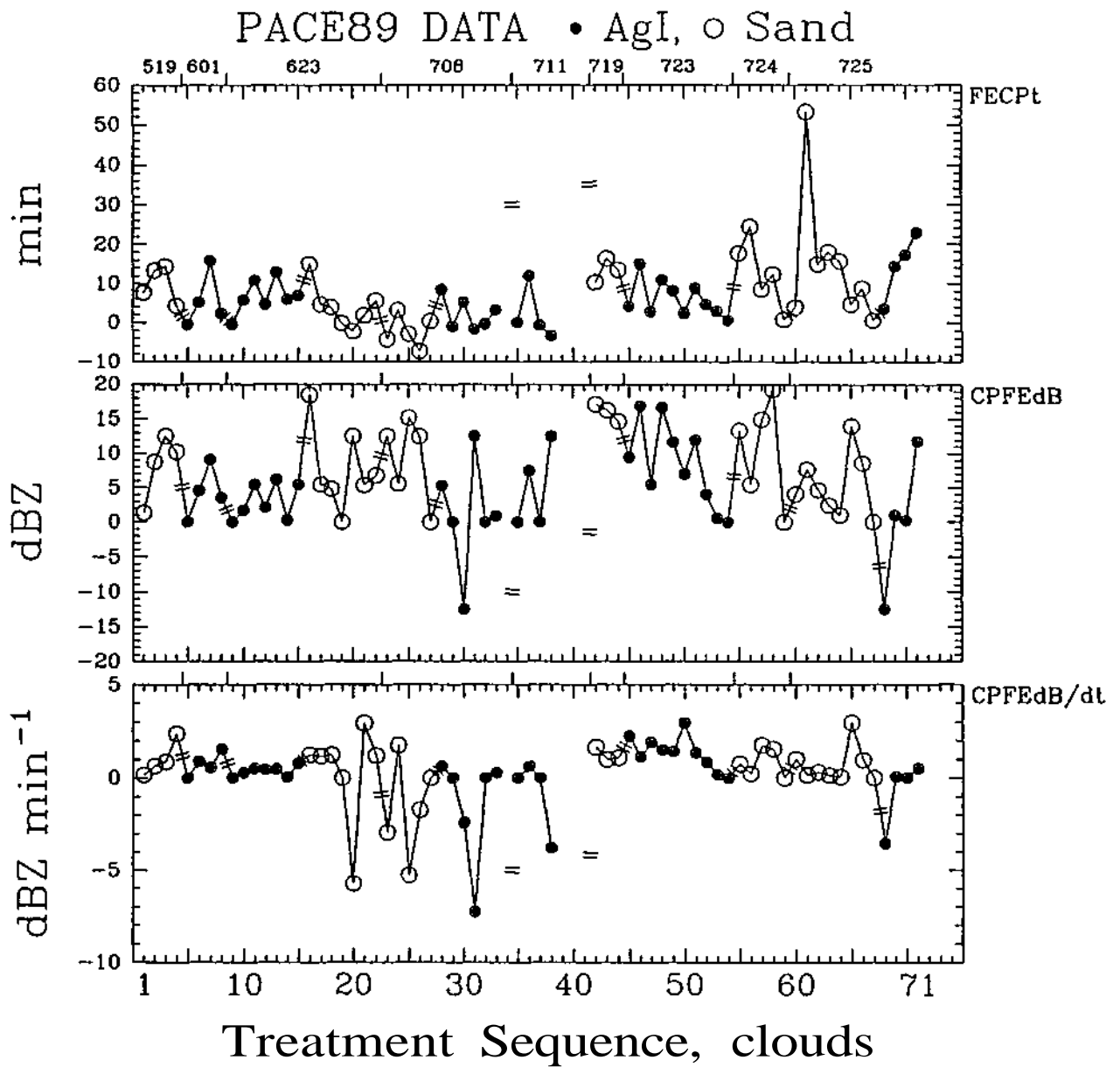


Figure B31. Time history of the time from first echo to treatment (FECPT), the change in maximum brightness from first echo to treatment (CPFEdB), and the rate of change of maximum brightness from first echo to treatment (CPFEdB/dt).

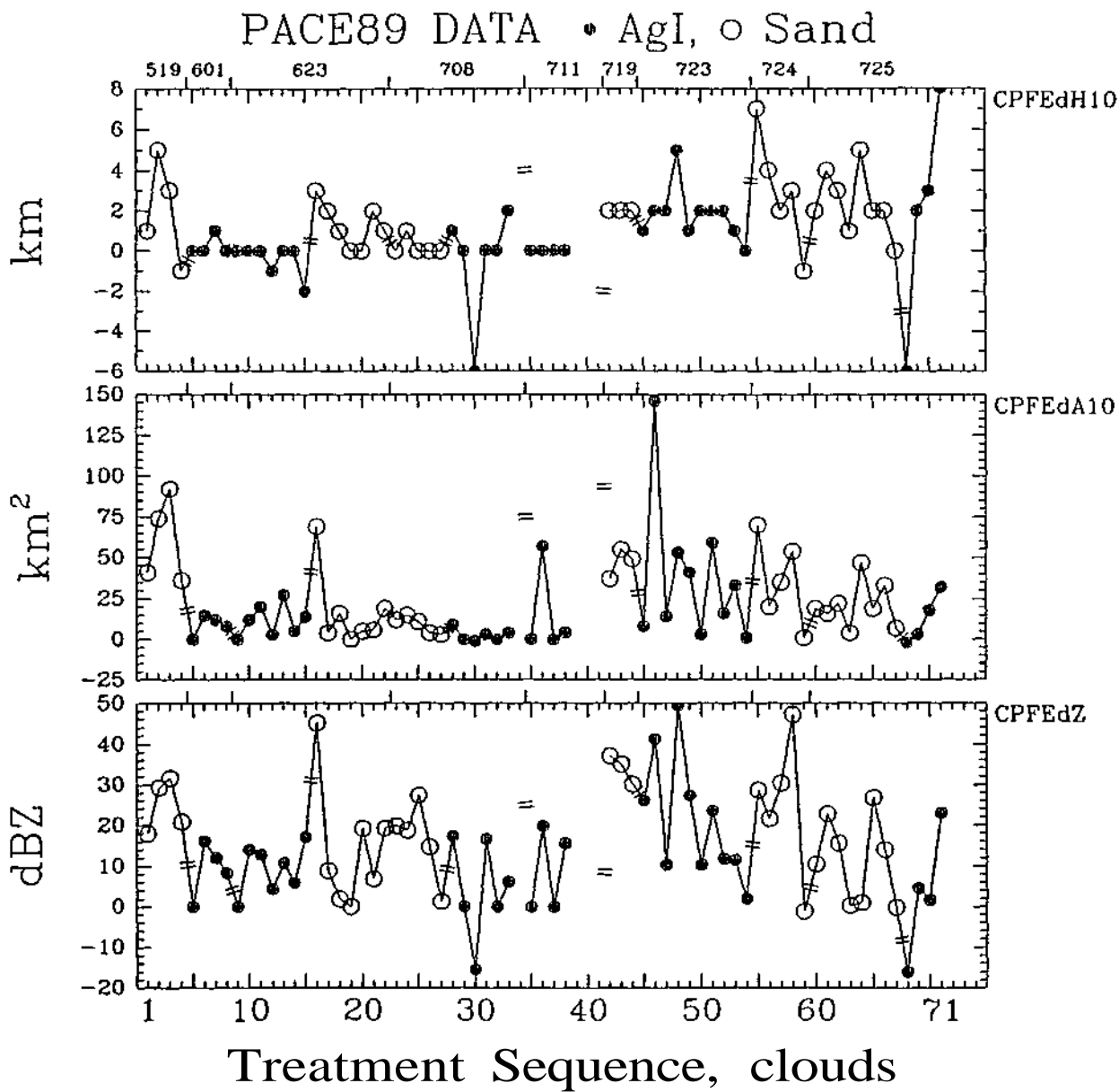


Figure B.32. Time history of the change in top height of the 10 dBZ contour from first echo to treatment (CPFE dH10), the change in area of the 10 dBZ contour from first echo to treatment (CPFE dA10), and the change in maximum reflectivity from first echo to treatment (CPFE dZ).

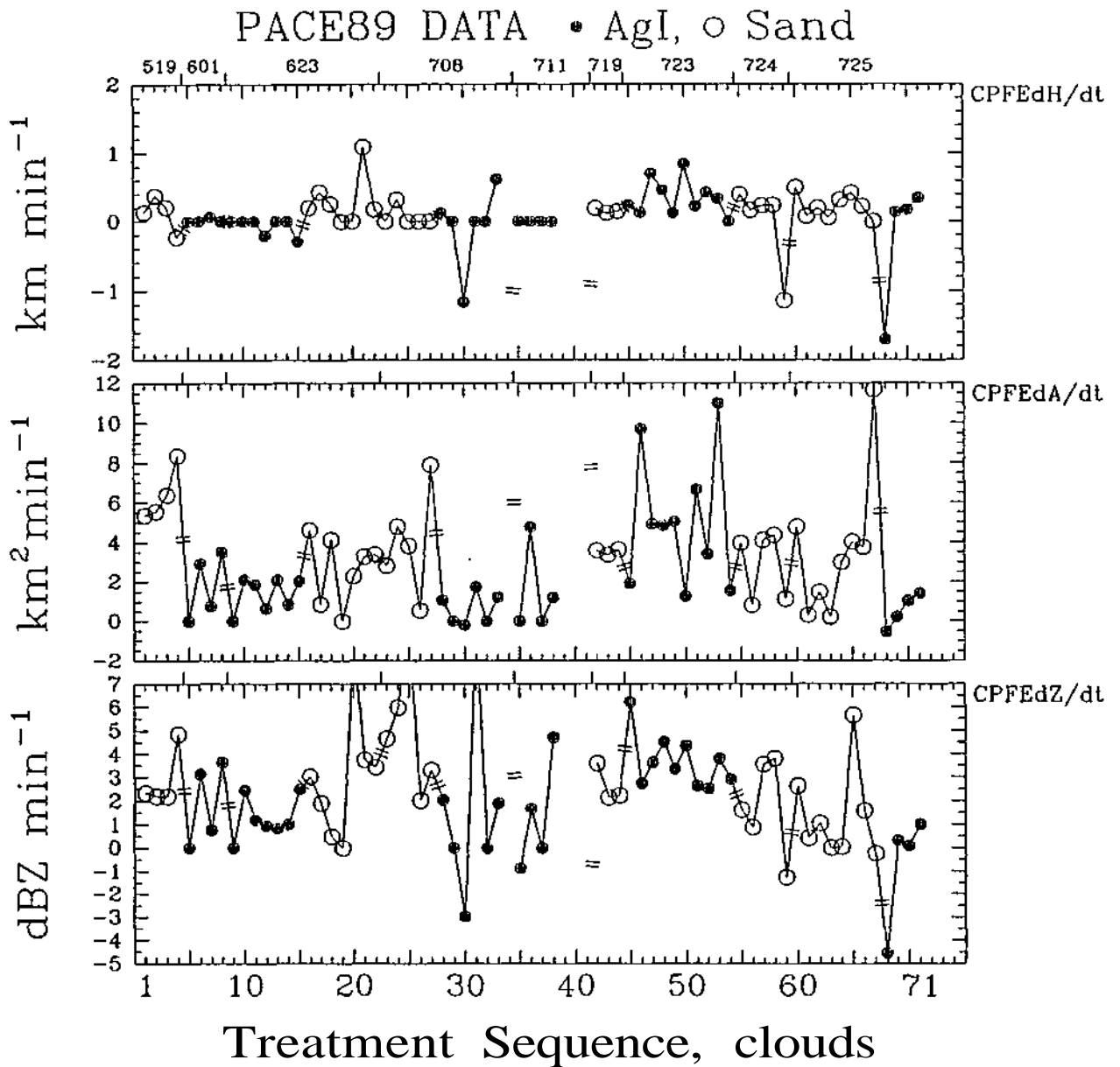


Figure B.33. Time history of the rate of change of the 10 dBZ echo top height from first echo to treatment (CPFE $dH/dt$ ), the rate of change of maximum area of the 10 dBZ contour from first echo to treatment (CPFE $dA/dt$ ), and the rate of change of maximum reflectivity from first echo to treatment (CPFE $dZ/dt$ ).

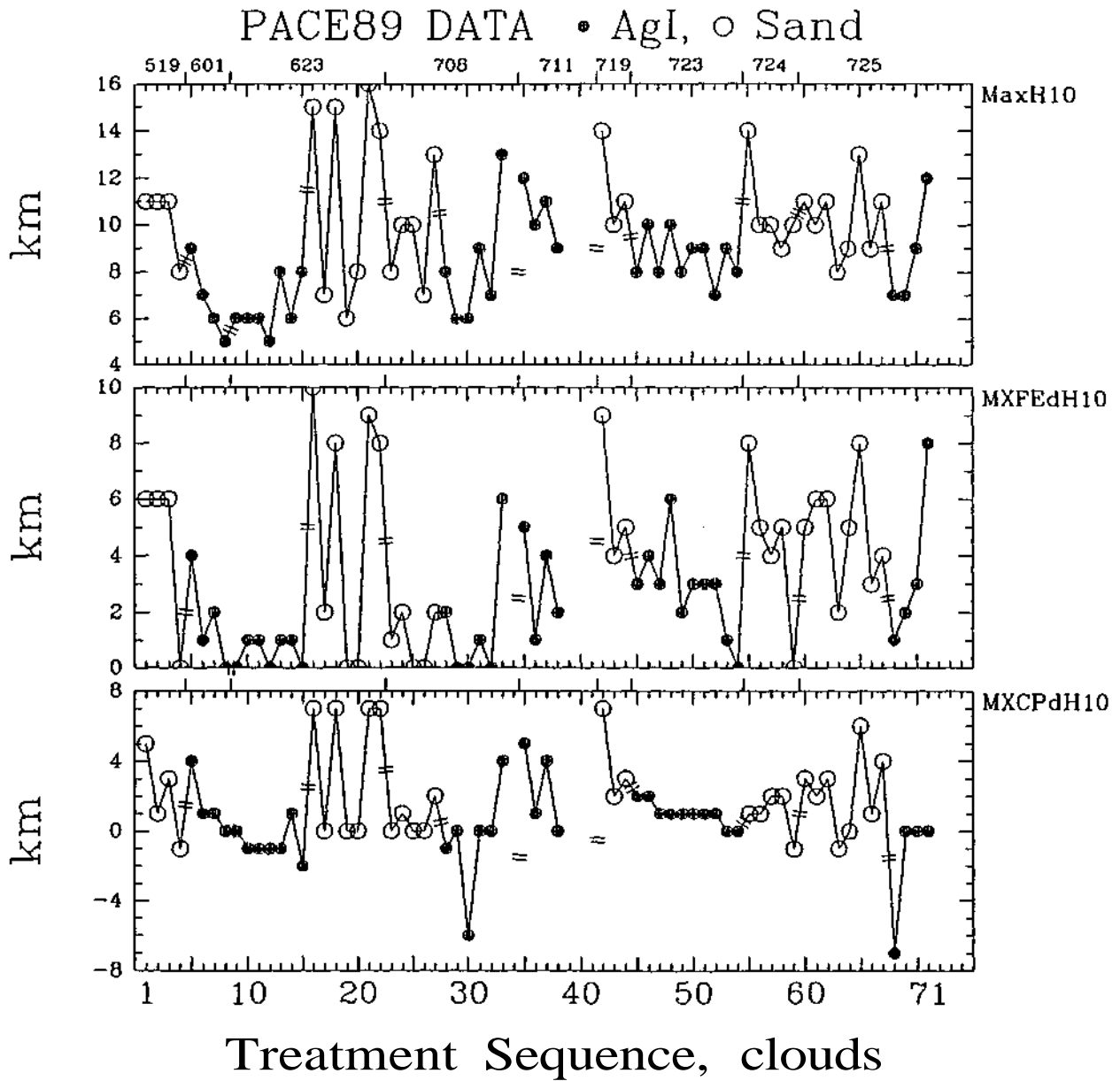


Figure B.34. Time history of the maximum top height of the 10 dBZ contour of the echo (MaxH10), the change in top height of the 10 dBZ contour from first echo to the maximum height of the echo core (MXFEdH10), and the change in top height of the 10 dBZ contour from treatment to the maximum height of the echo (MXCPdH10).

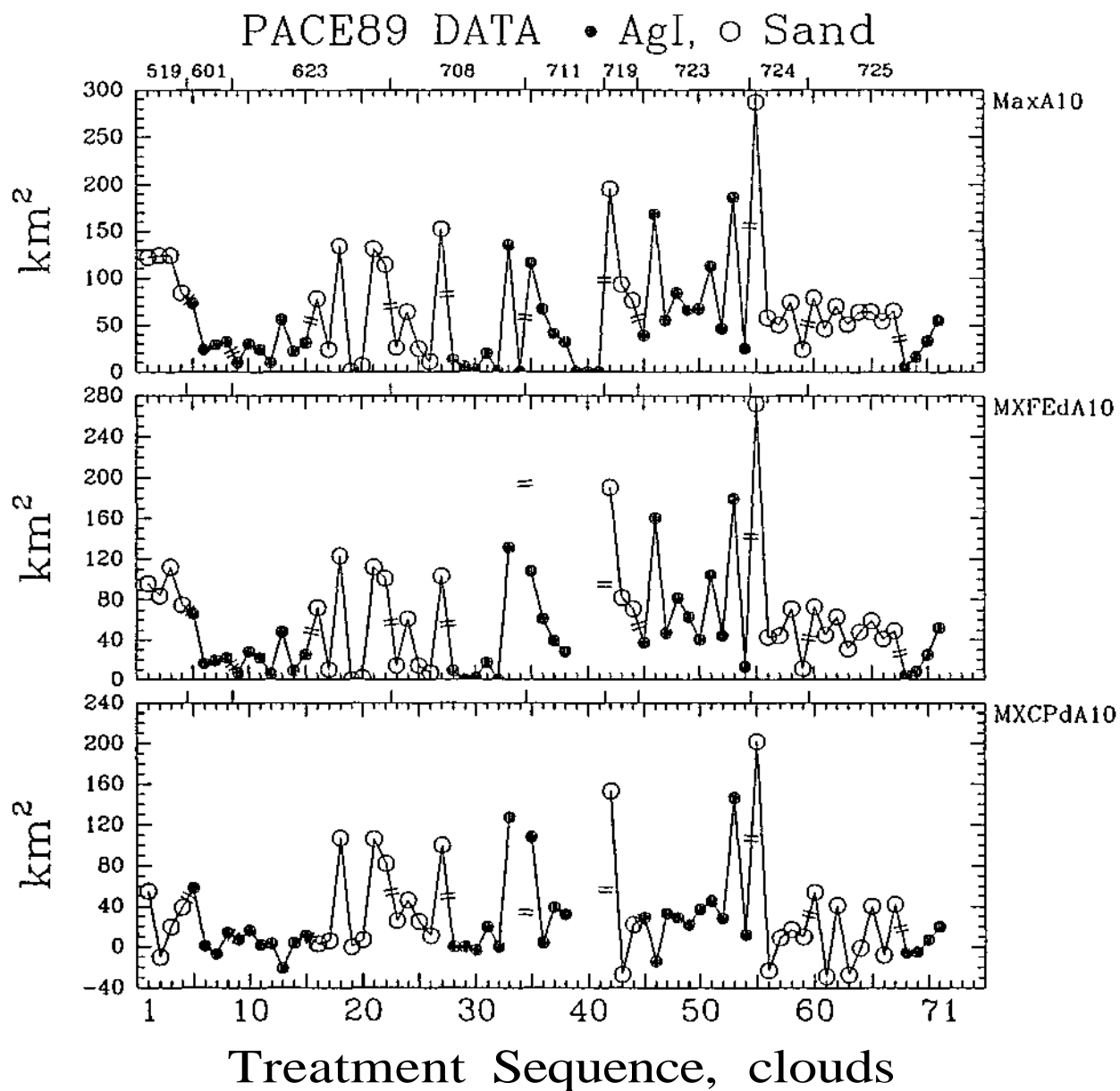


Figure B.35. Time history of the maximum area of the 10 dBZ contour of the echo (MaxA10), the change in area of the 10 dBZ contour from first echo to the maximum area of the echo core (MXFEdA10), and the change in area of the 10 dBZ contour from treatment to the maximum area of the echo (MXCPdA10).

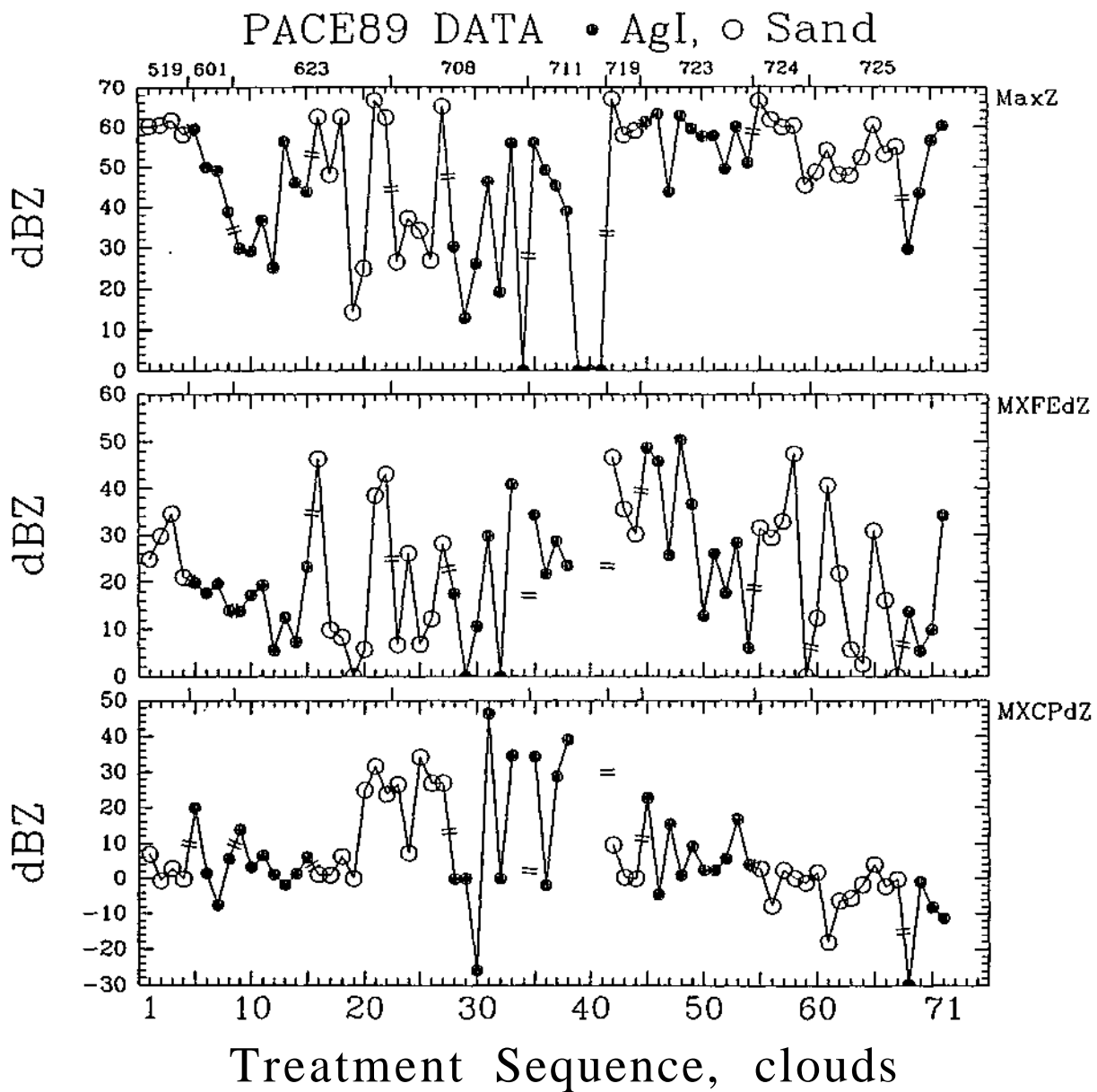


Figure B.36. Time history of the maximum reflectivity of the echo (MaxZ), the change in the maximum reflectivity from first echo to the maximum reflectivity of the echo core (MXFE dZ), and the change in maximum reflectivity from treatment to the maximum reflectivity of the echo (MXCP dZ).

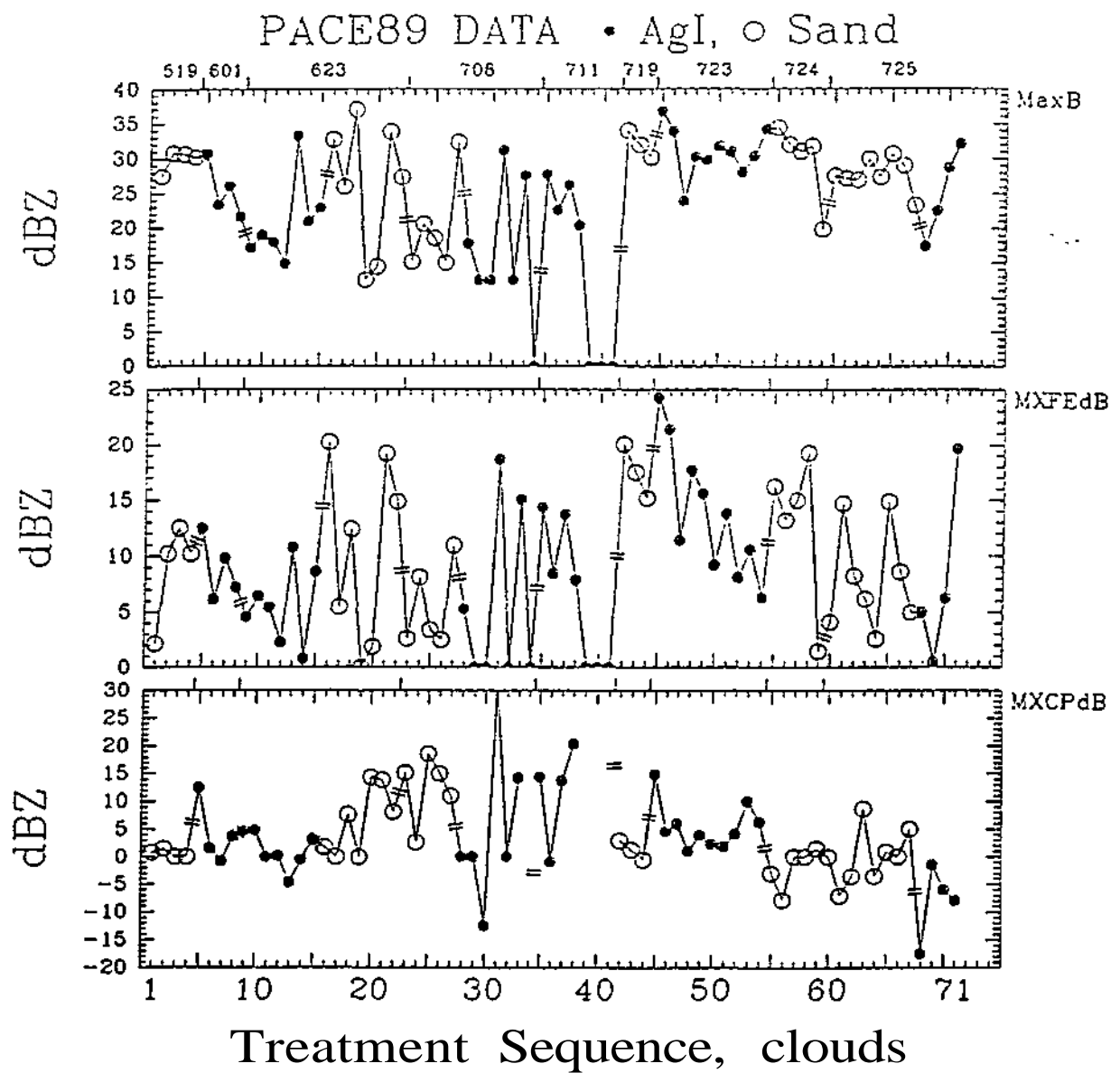


Figure D.37. Time history of the maximum brightness of the echo (MaxB), the change in the brightness from first echo to the maximum brightness of the echo core (MXFEdB), and the change in brightness from treatment to the maximum brightness of the echo (MXCPdB).

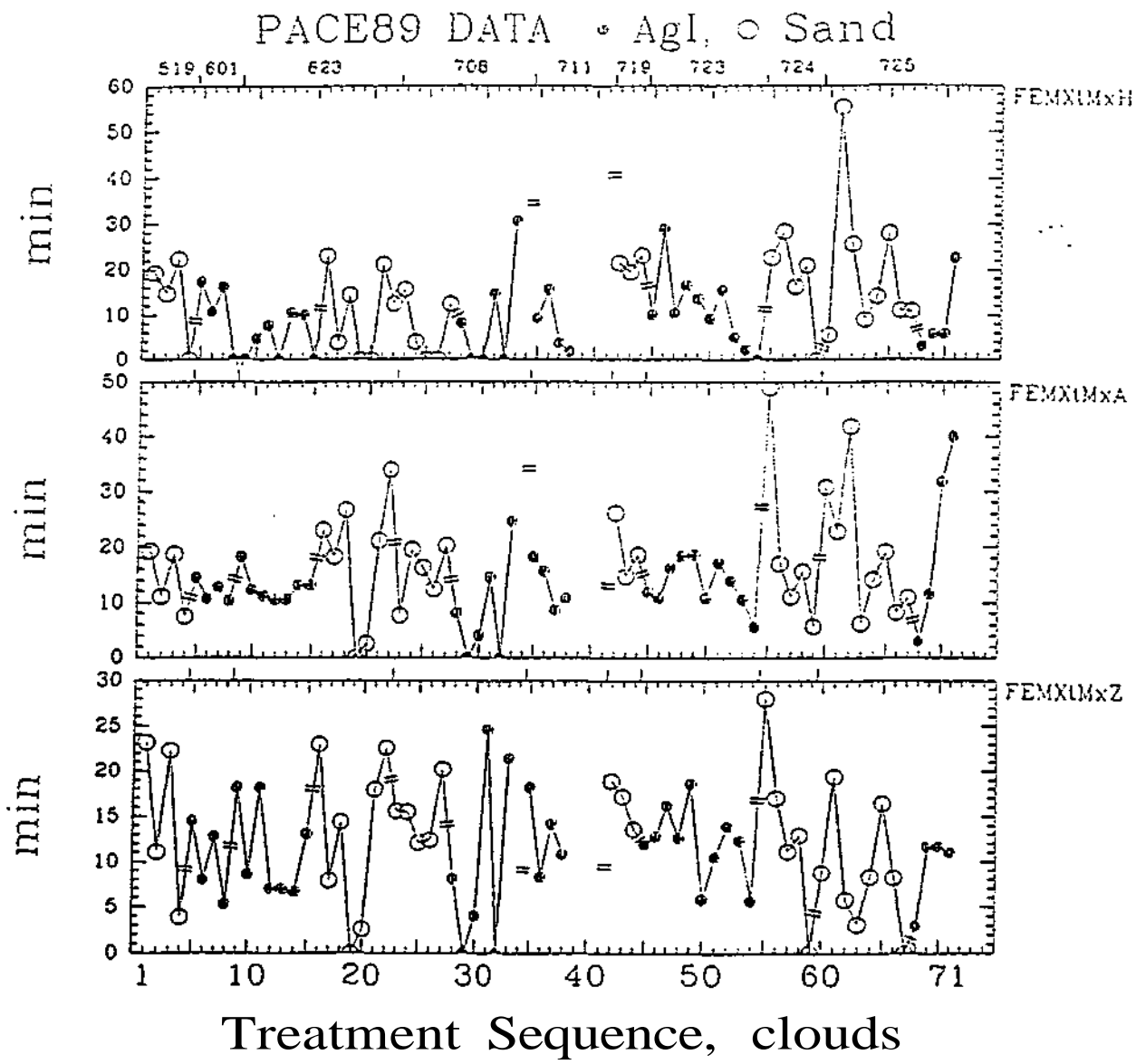


Figure B.38. Time history of the time from first echo to the time of maximum height (FEMXtMxH), area (FEMXtMxA), and reflectivity (FEMXtMxZ) of the echo core.

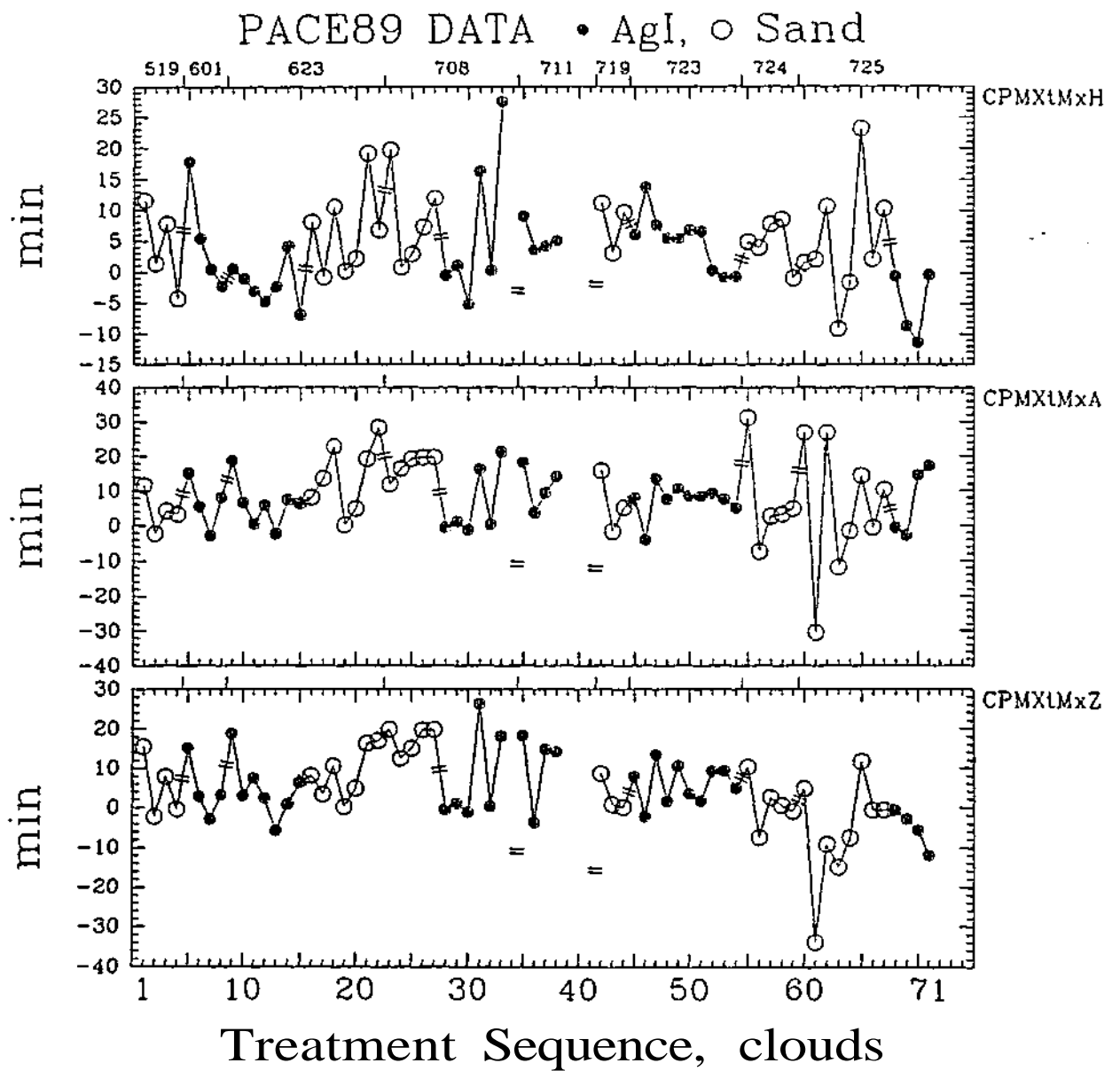


Figure B.39. Time history of the time from treatment to the time of maximum height (CPMXtMxH), area (CPMXtMxA), and reflectivity (CPMXtMxZ) of the echo core.

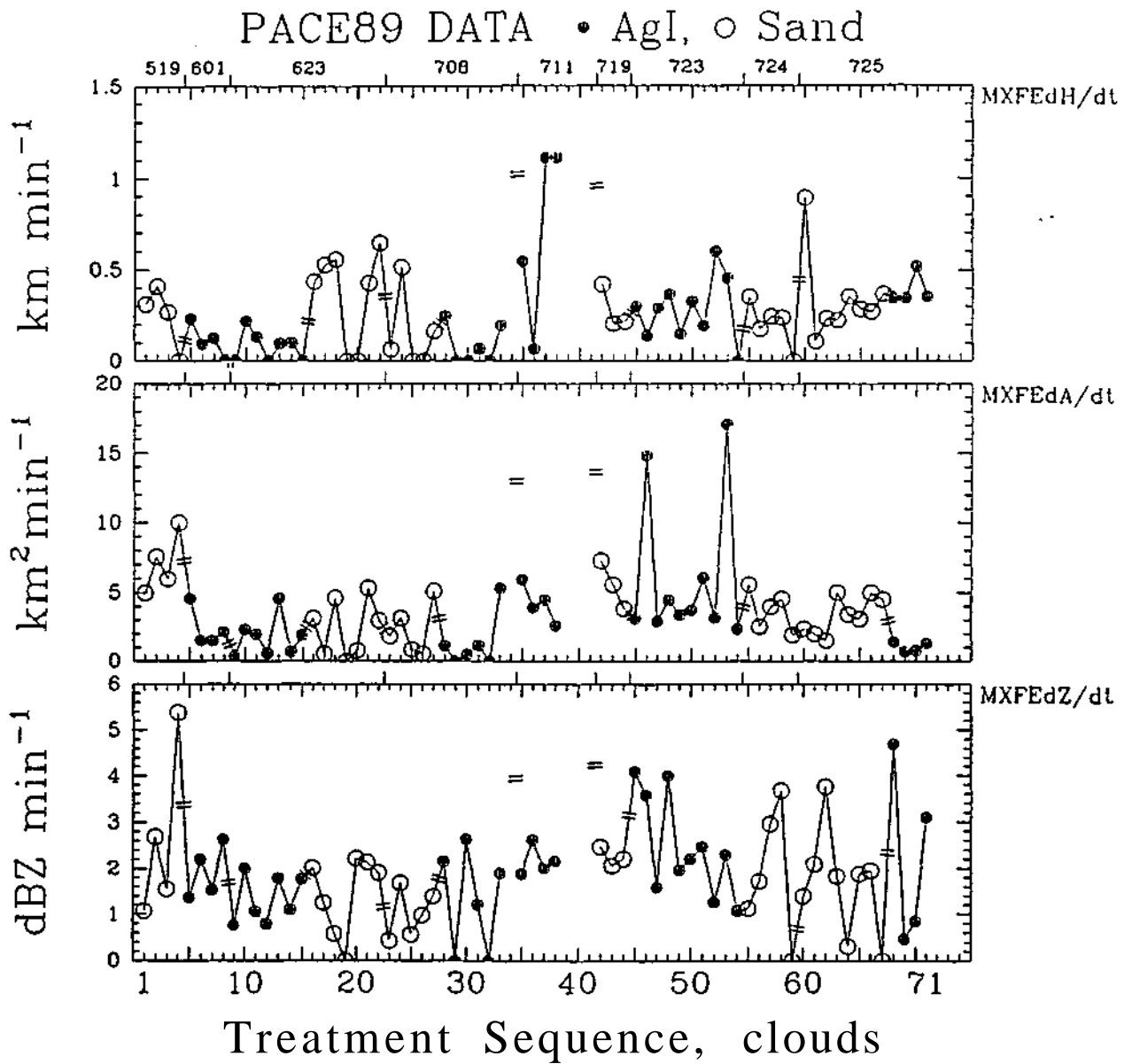


Figure B.40. Time history of the rate of changes of the 10 dBZ echo top height from first echo to the maximum height of the echo (MXFEH/dt), the maximum echo area from first echo to the maximum area of the echo (MXFEA/dt), and the maximum reflectivity from first echo to the maximum reflectivity of the echo (MXFEZ/dt).

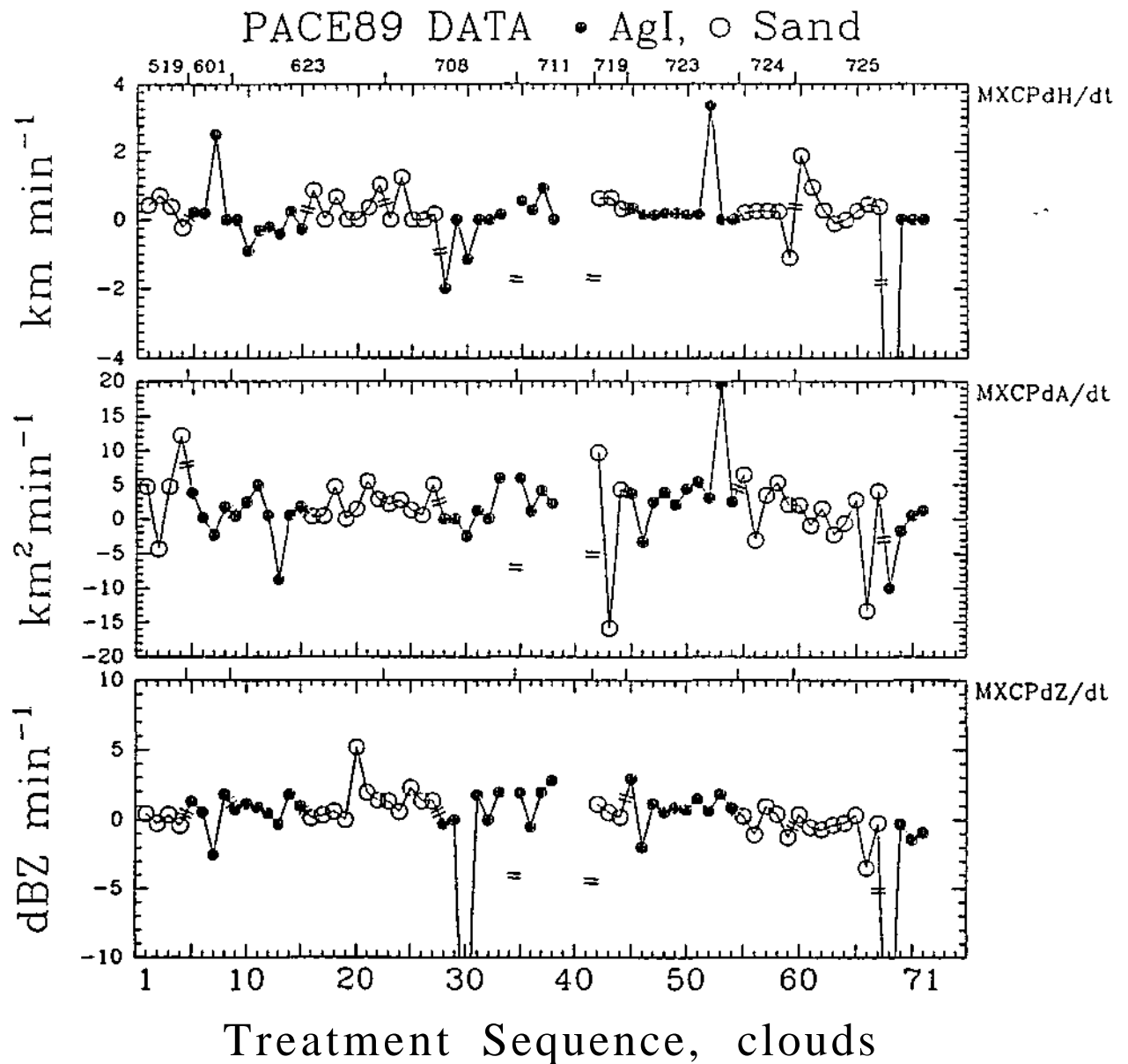


Figure B.41. Time history of the rate of changes of the 10 dBZ echo top height from treatment to the maximum height of the echo (MXCPdH/dt), the maximum echo area from treatment to the maximum area of the echo (MXCPdA/dt), and the maximum reflectivity from treatment to the maximum reflectivity of the echo (MXCPdZ/dt).

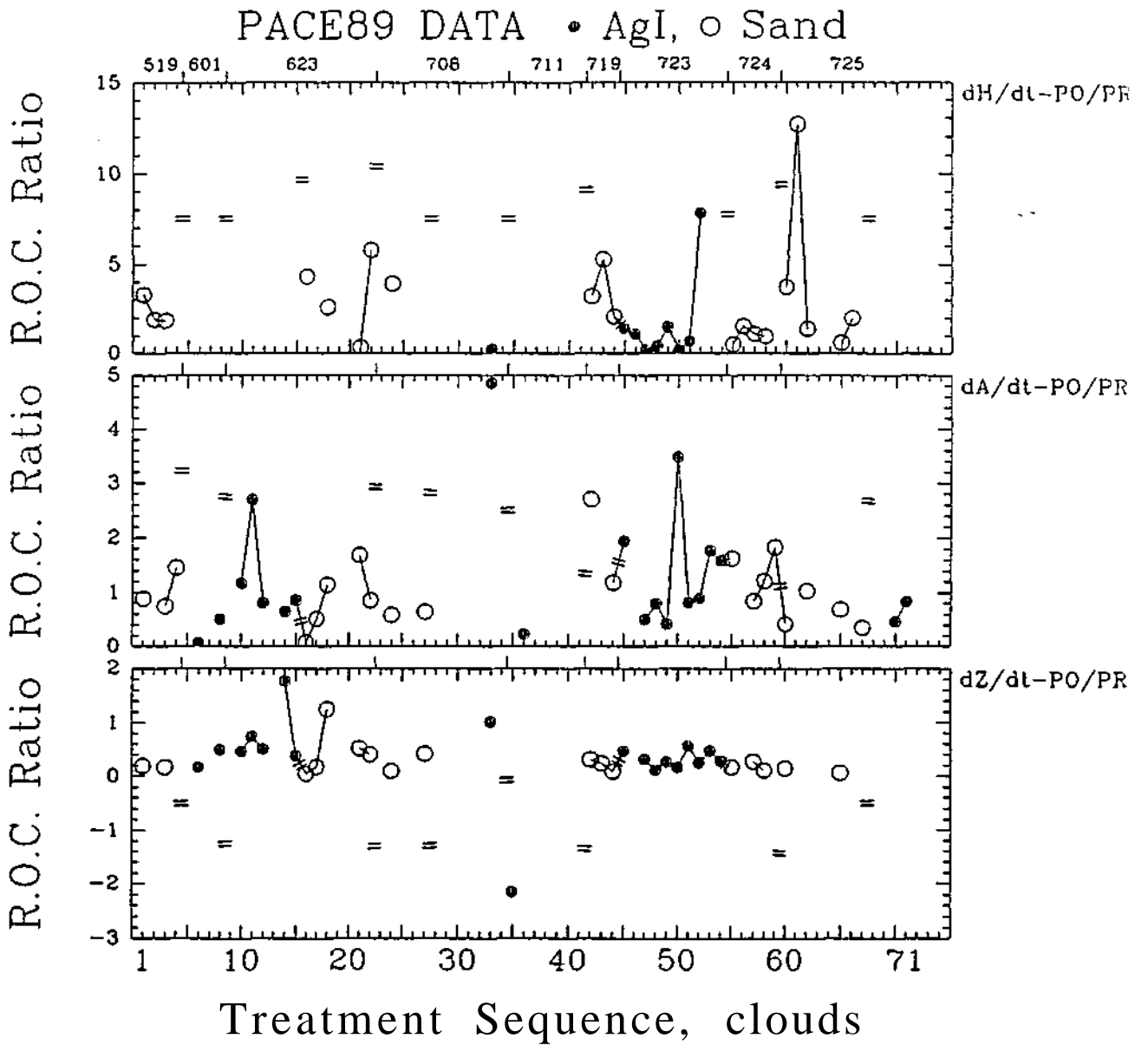


Figure B.42. Time history of the ratios of the rates of changes from treatment to the maximum and from first echo to treatment for the maximum echo top height ( $dH/dt$ -POIPR), area ( $dA/dt$ -POIPR), and reflectivity ( $dZ/dt$ -POIPR).

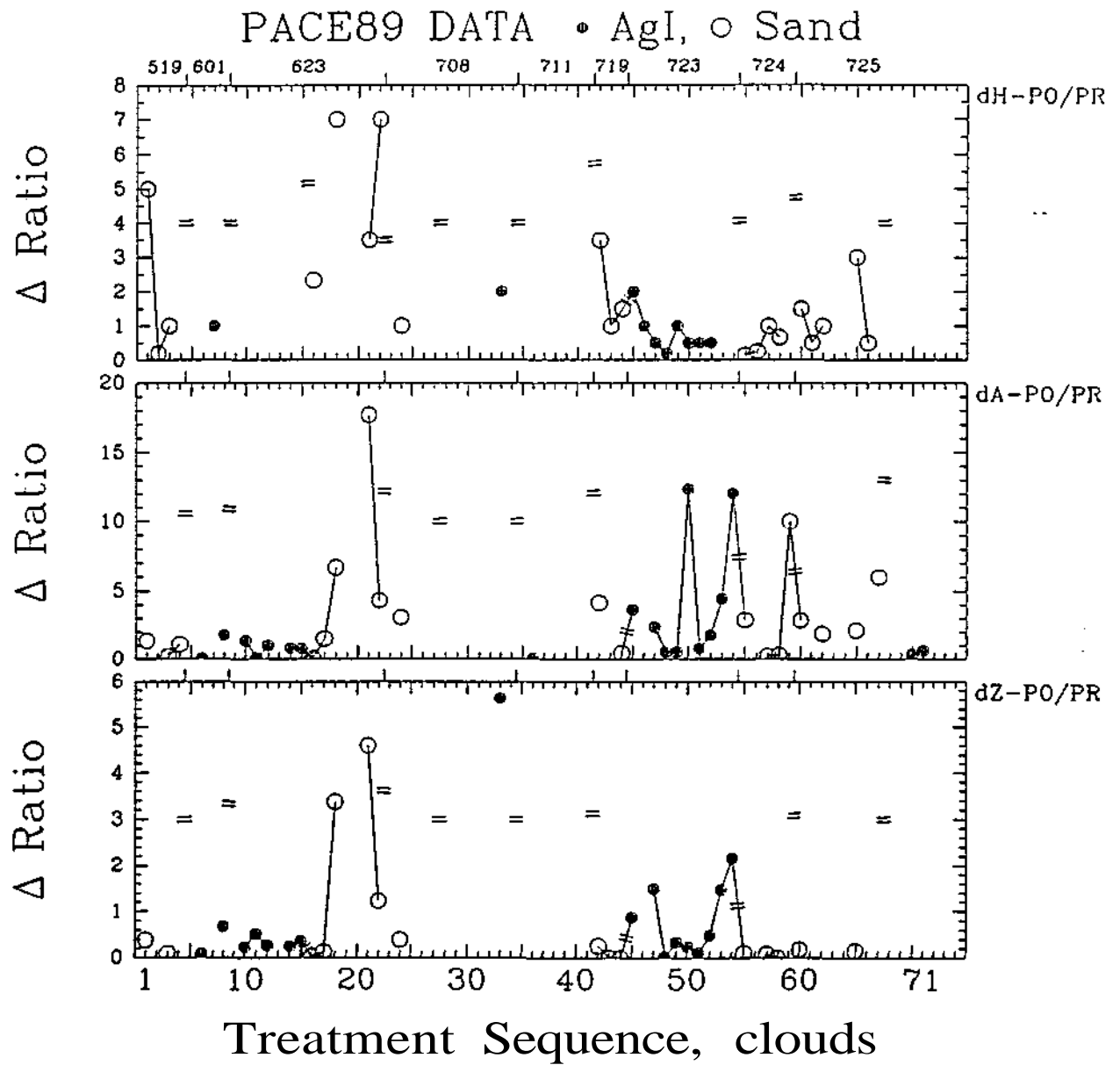


Figure B.43. Time history of the ratios of the changes from treatment to the maximum and from first echo to treatment for the maximum echo loop height (dH-POIPR), area (dA-POIPR), and reflectivity (dZ-POIPR).

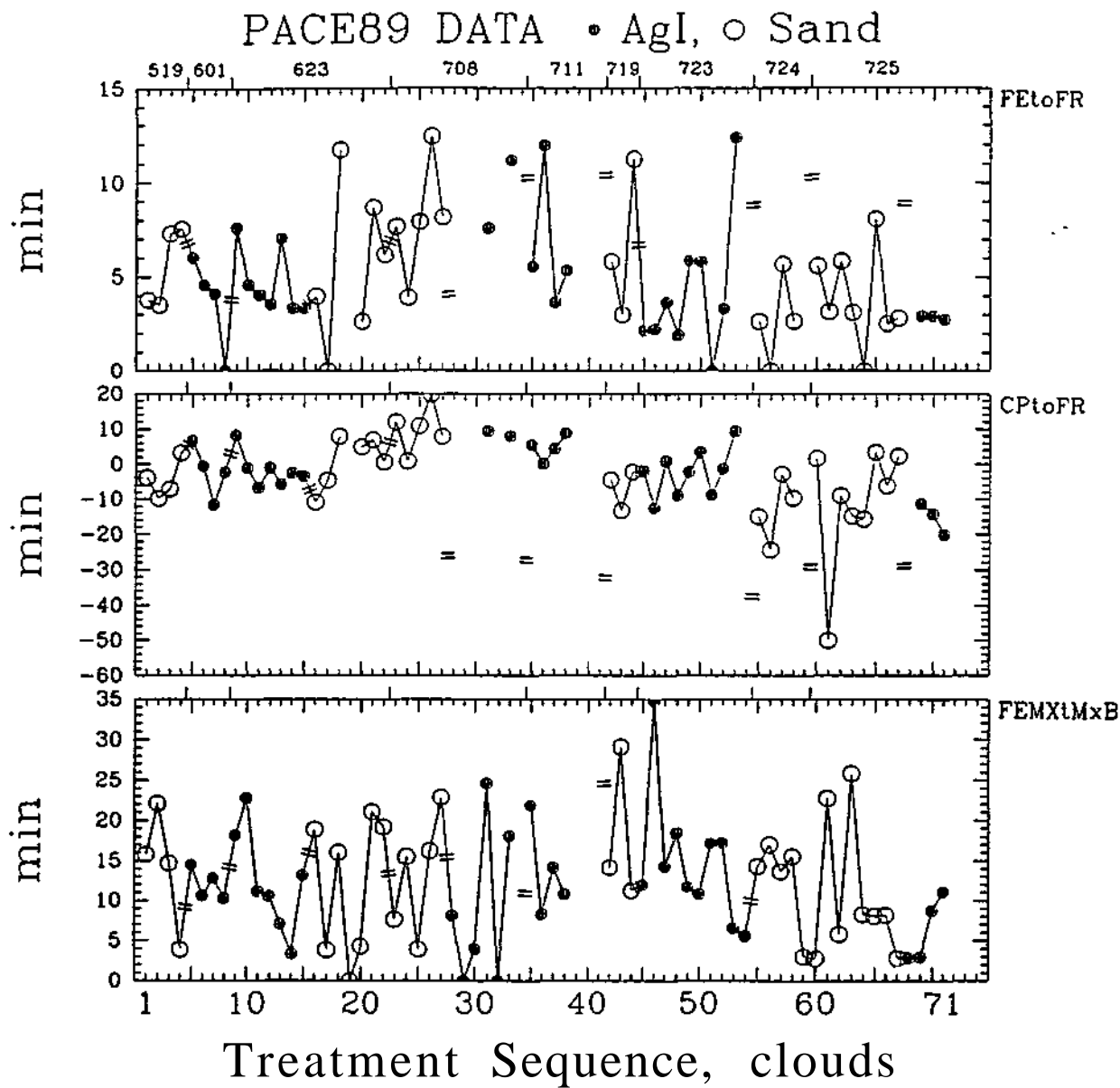


Figure B.44. Time history of the time from first echo to the time of first rain (FEtoFR), the time from treatment to the time of first rain (CPtoFR), and the time from first echo to the time of maximum brightness (FEMxMxB).

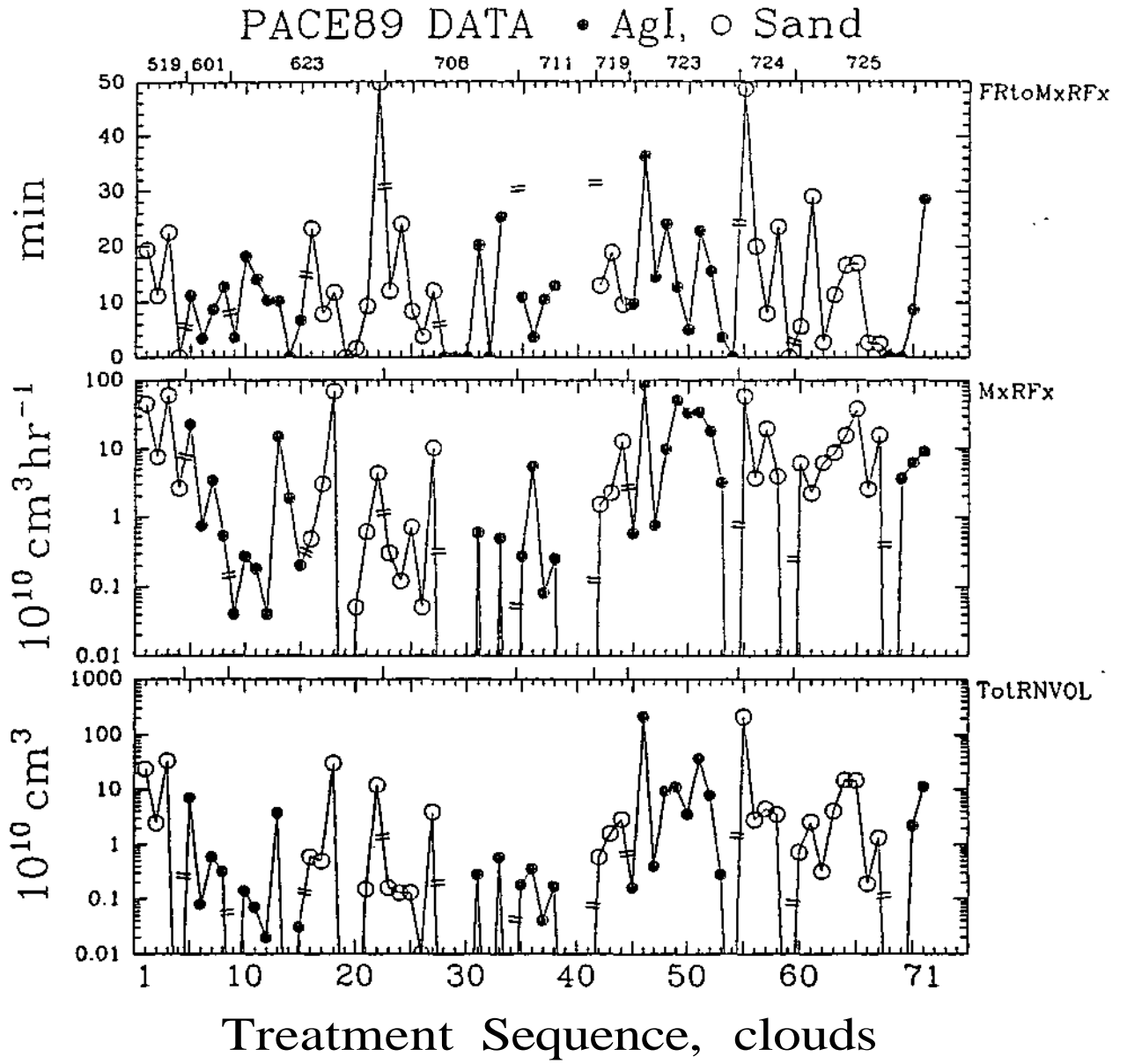


Figure B.45. Time history of the time from first rain to the time of maximum rain flux of the echo core (FRtoMxRFx), the maximum rain flux of the echo core (MxRFx), and the total accumulated rain volume of the echo core (TotRNVOL).

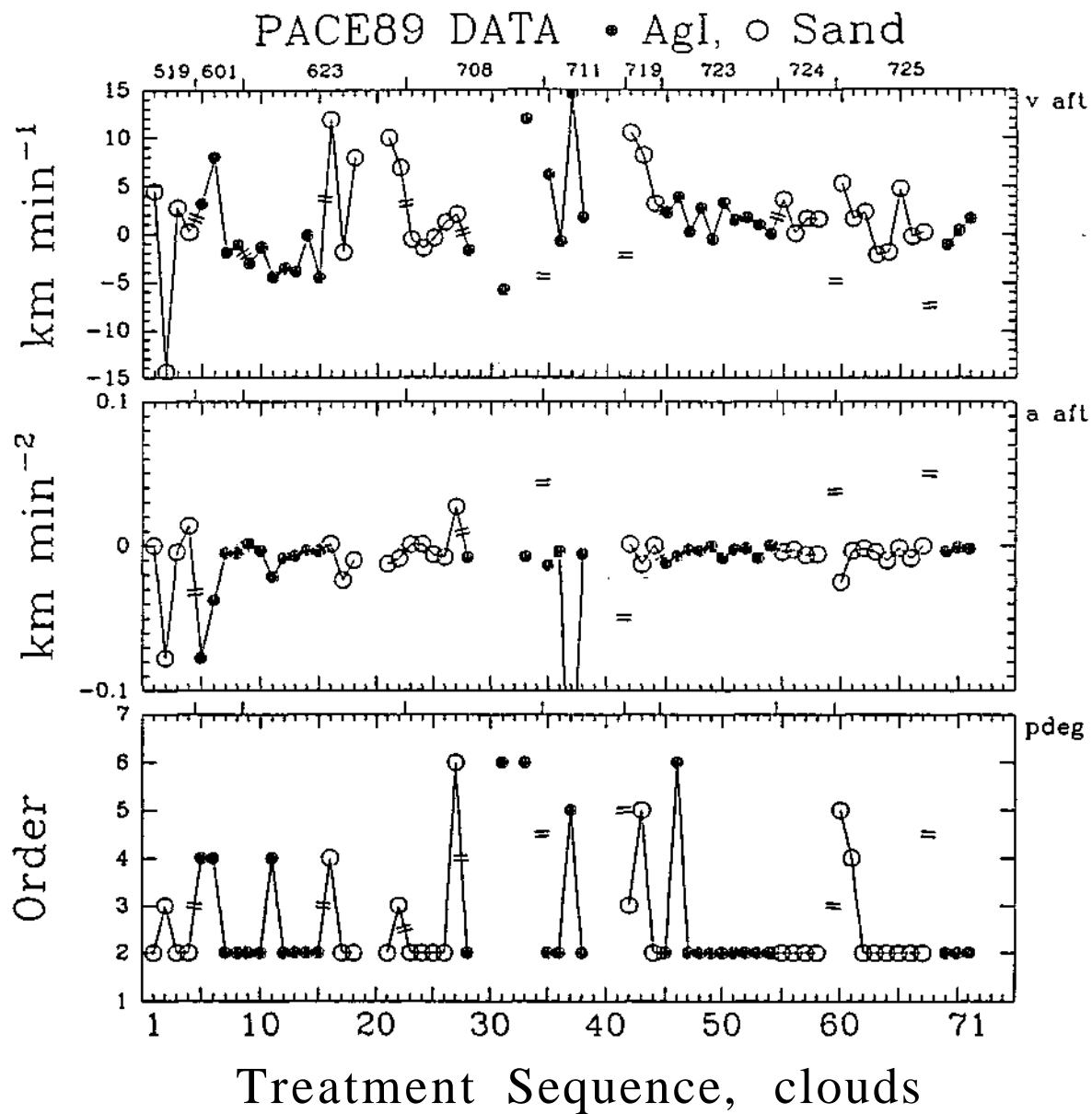


Figure B.46. Time history of the velocity ( $v_{aft}$ ) and acceleration ( $a_{aft}$ ) of the echo top 4 minutes after treatment, and the order of the polynomial used to determine velocities and accelerations of the echo top before, at, and after treatment ( $pdeg$ ).

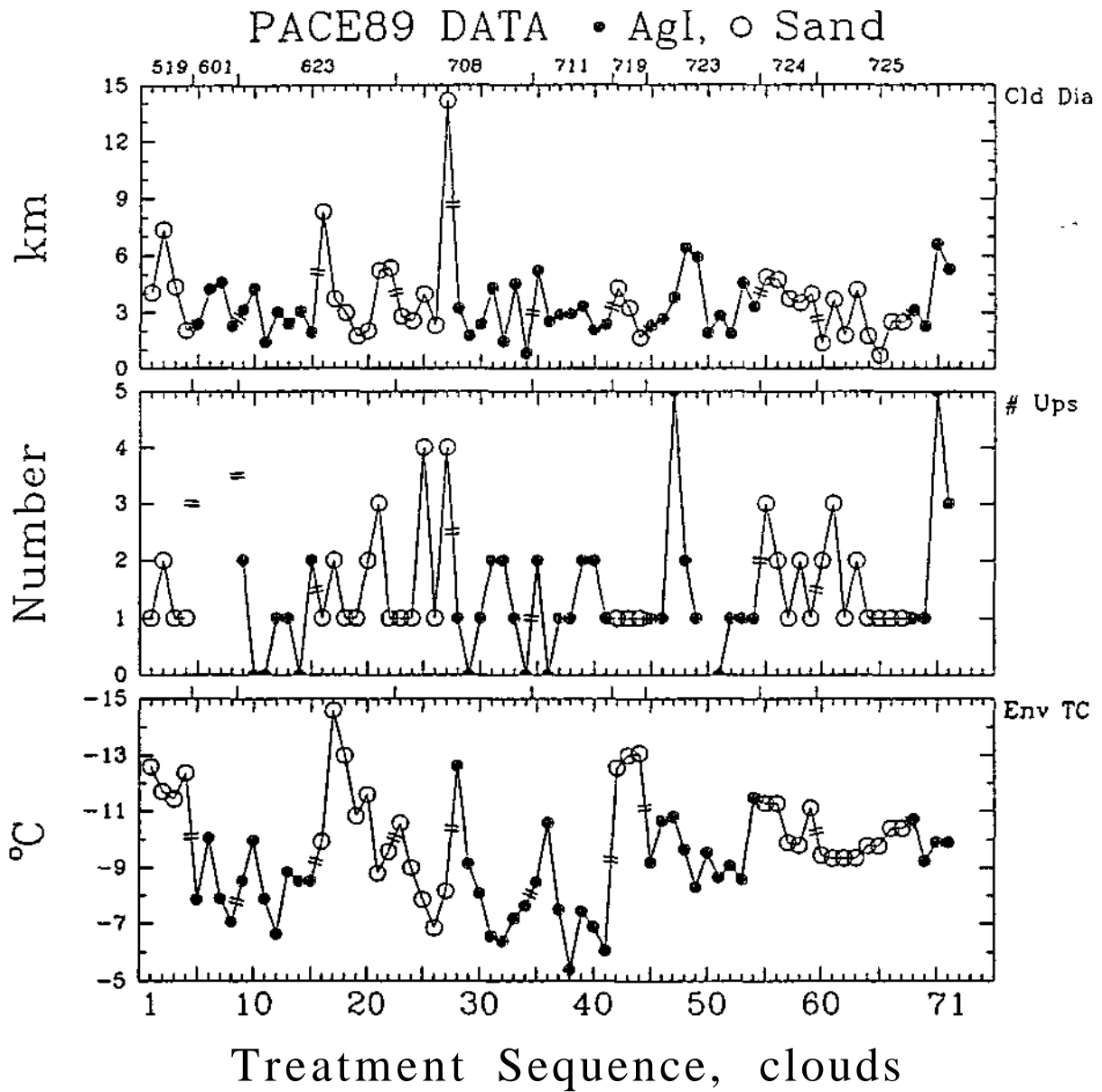


Figure B.47. Time history of the cloud diameter (Cld\_Dia), the number of updrafts in cloud (#\_Ups), and the temperature of the cloud's environment (Env\_TC).

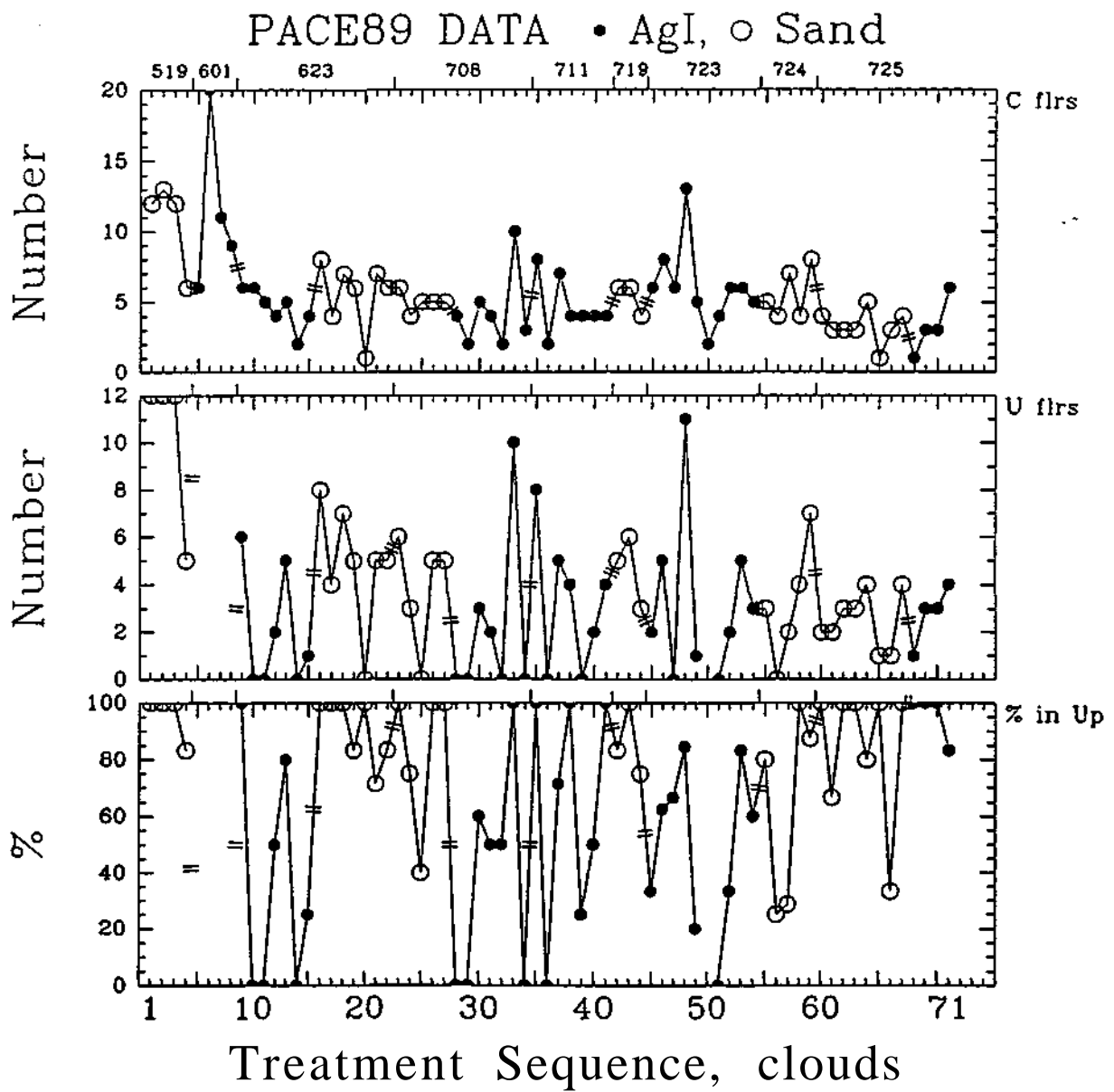


Figure B.48. Time history of the number of flares in the cloud ( $C\_flrs$ ), the number of flares in the main (broadest) updraft ( $U\_flrs$ ), and the percentage of flares released in any updraft ( $\%\_in\_Up$ ).

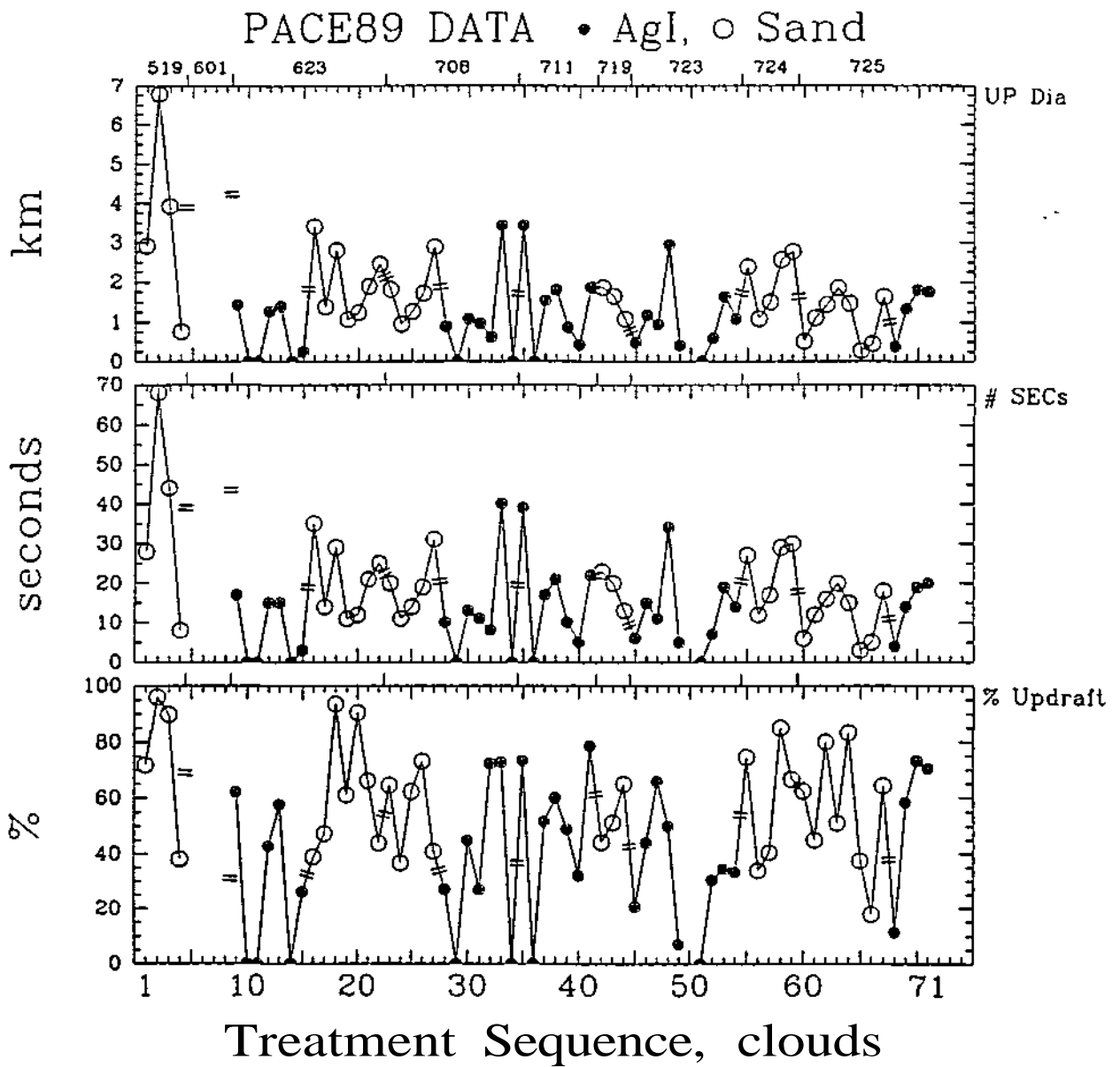


Figure B.49. Time history of the diameter of the main (broadest) updraft (UP\_Dia), the number of seconds of the broadest or main updraft (#\_SECs), and the percent of cloud which is updraft (%\_Updraft).

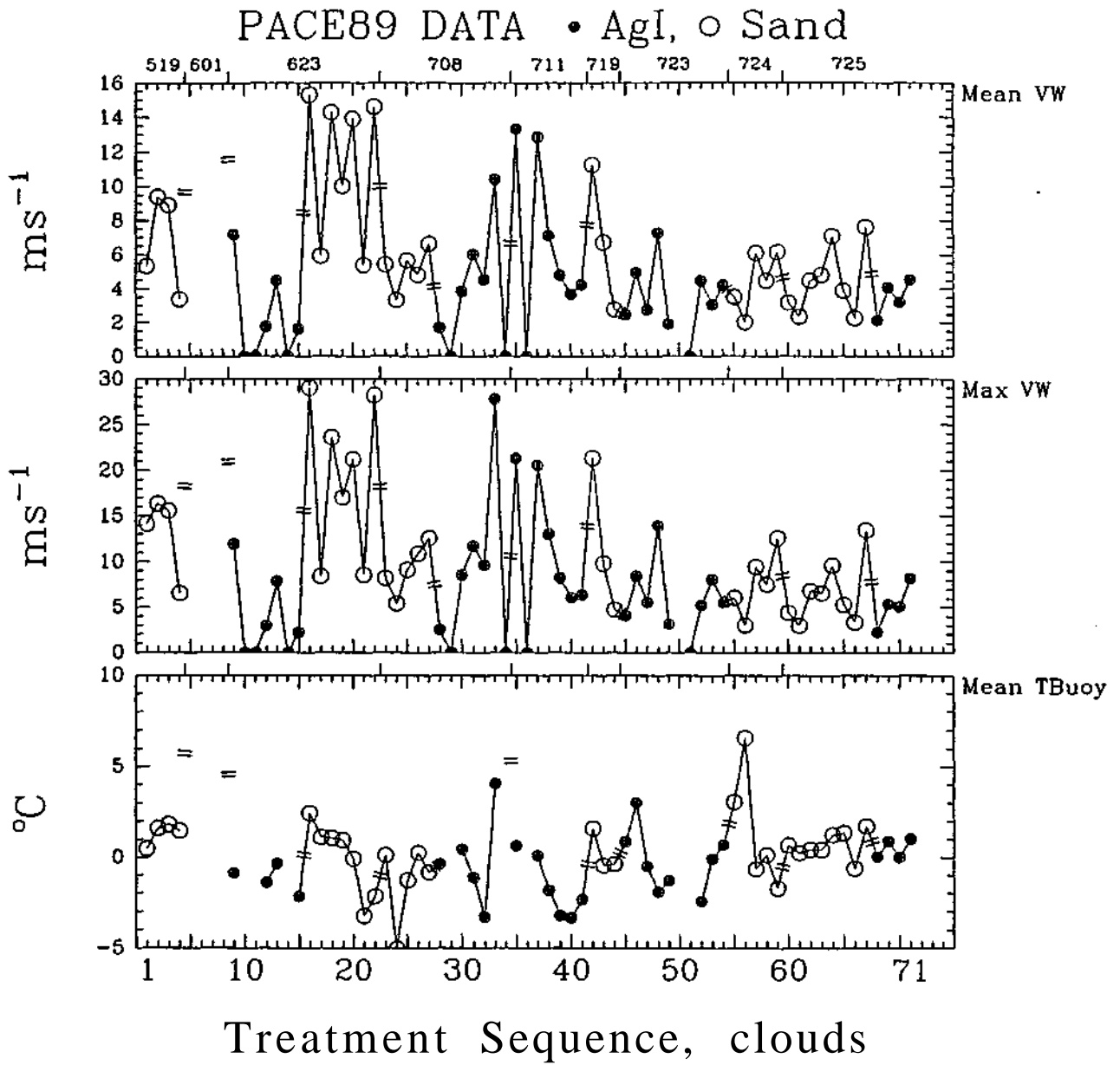


Figure B.50. Time history of the mean (Mean\_VW) and maximum (Max\_VW) vertical velocity of the main updraft, and the mean thermal buoyancy (Mean\_TBuoy).

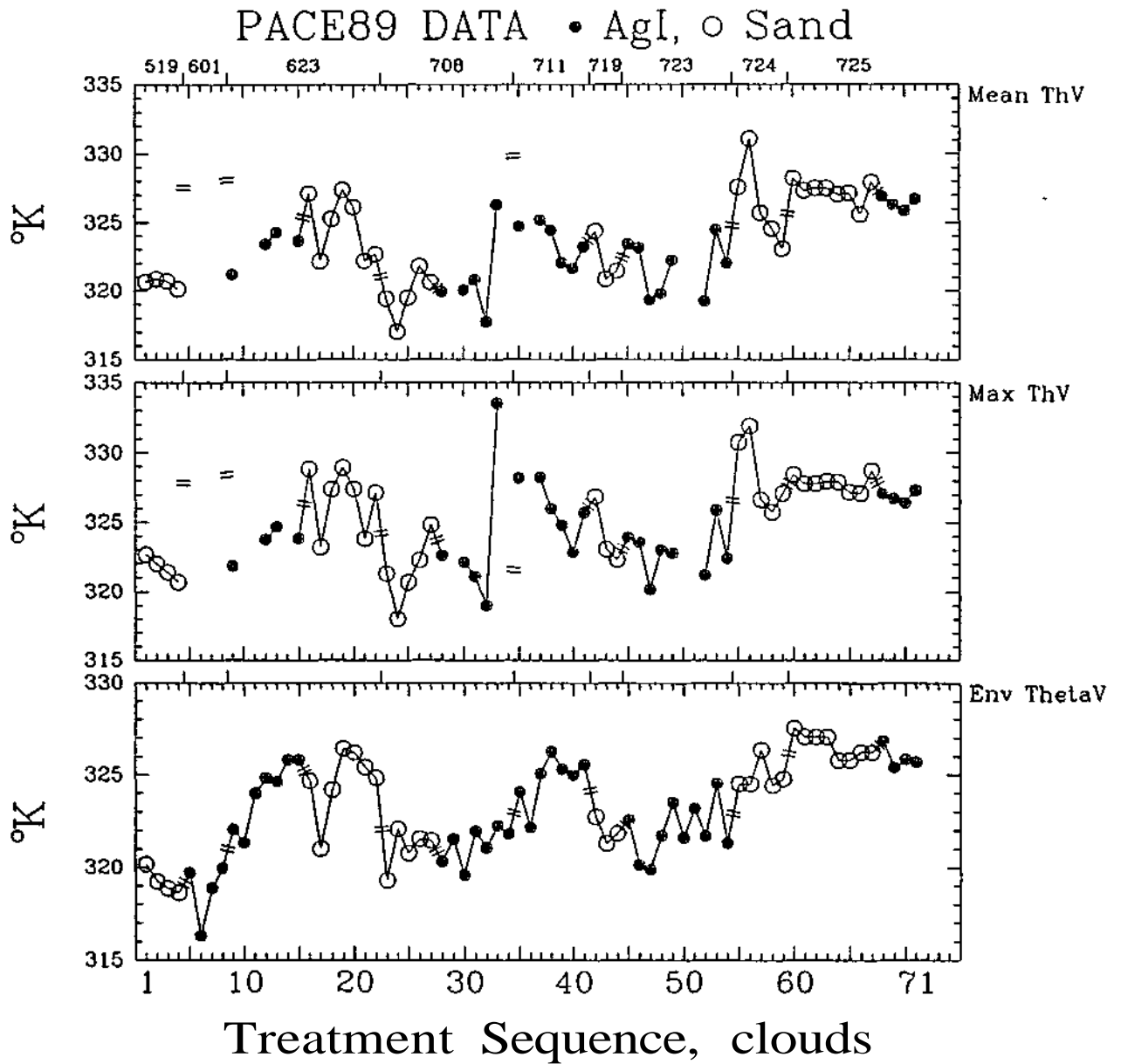


Figure B.51. Time history of the mean (*Mean\_ThV*) and maximum (*Max\_ThV*) virtual potential temperature of the main updraft, and the mean virtual potential temperature of the environment (*Env\_ThetaV*).

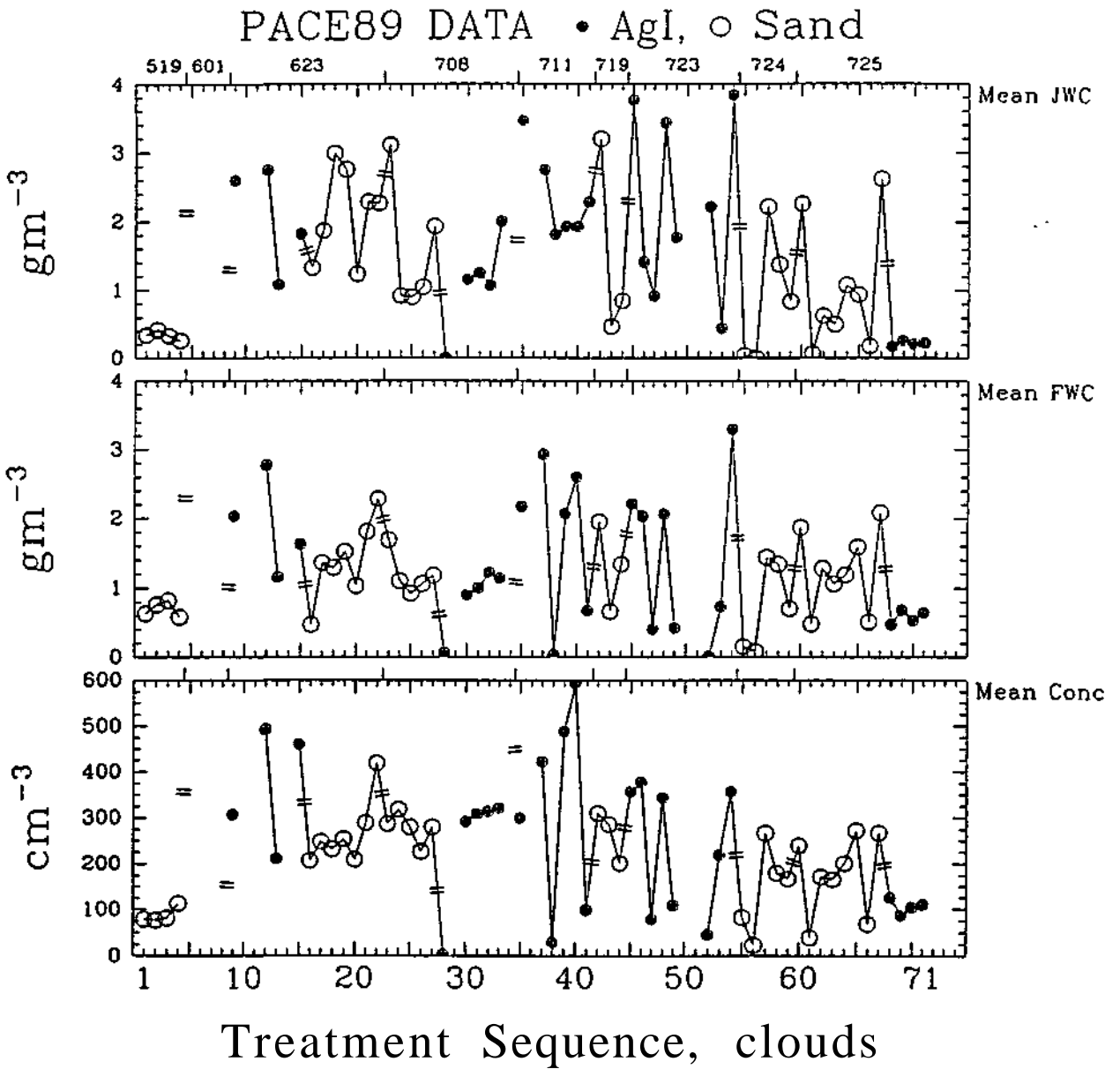


Figure B.52. Time history of the mean liquid water content in the main updraft from the JW (Mean\_JWC) and FSSP (Mean\_FWC) probes (i.e., cloud droplets), and the mean concentration of cloud droplets in the main updraft (Mean\_Conc).

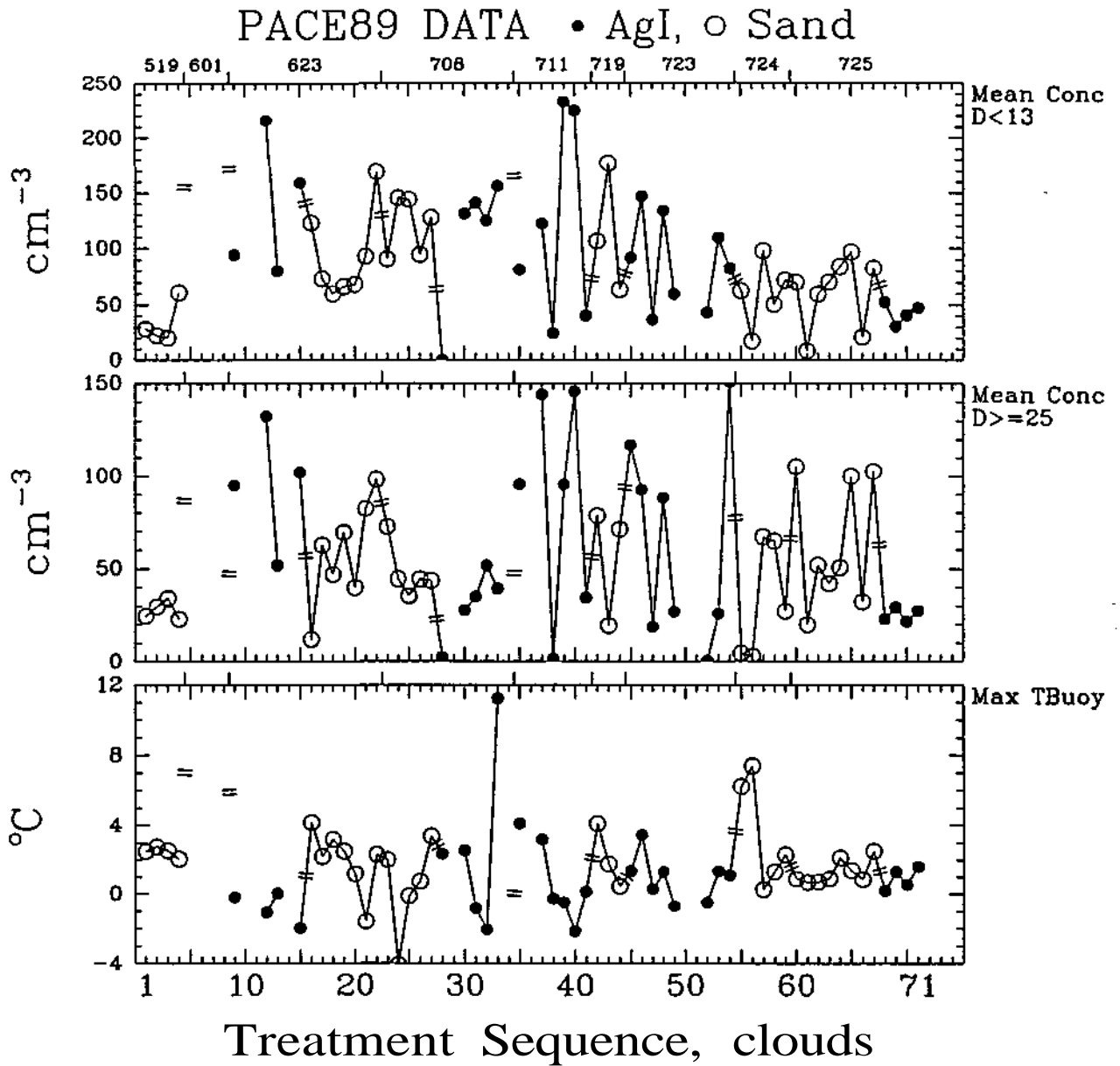


Figure B.53. Time history of the mean concentration in the main updraft of cloud droplets with  $d < 13 \mu\text{m}$  (Mean\_Conc\_D < 13) and cloud droplets with  $d \geq 25 \mu\text{m}$  (Mean\_Conc\_D  $\geq 25$ ), and the maximum thermal buoyancy of the main updraft (Max\_TBuoy).

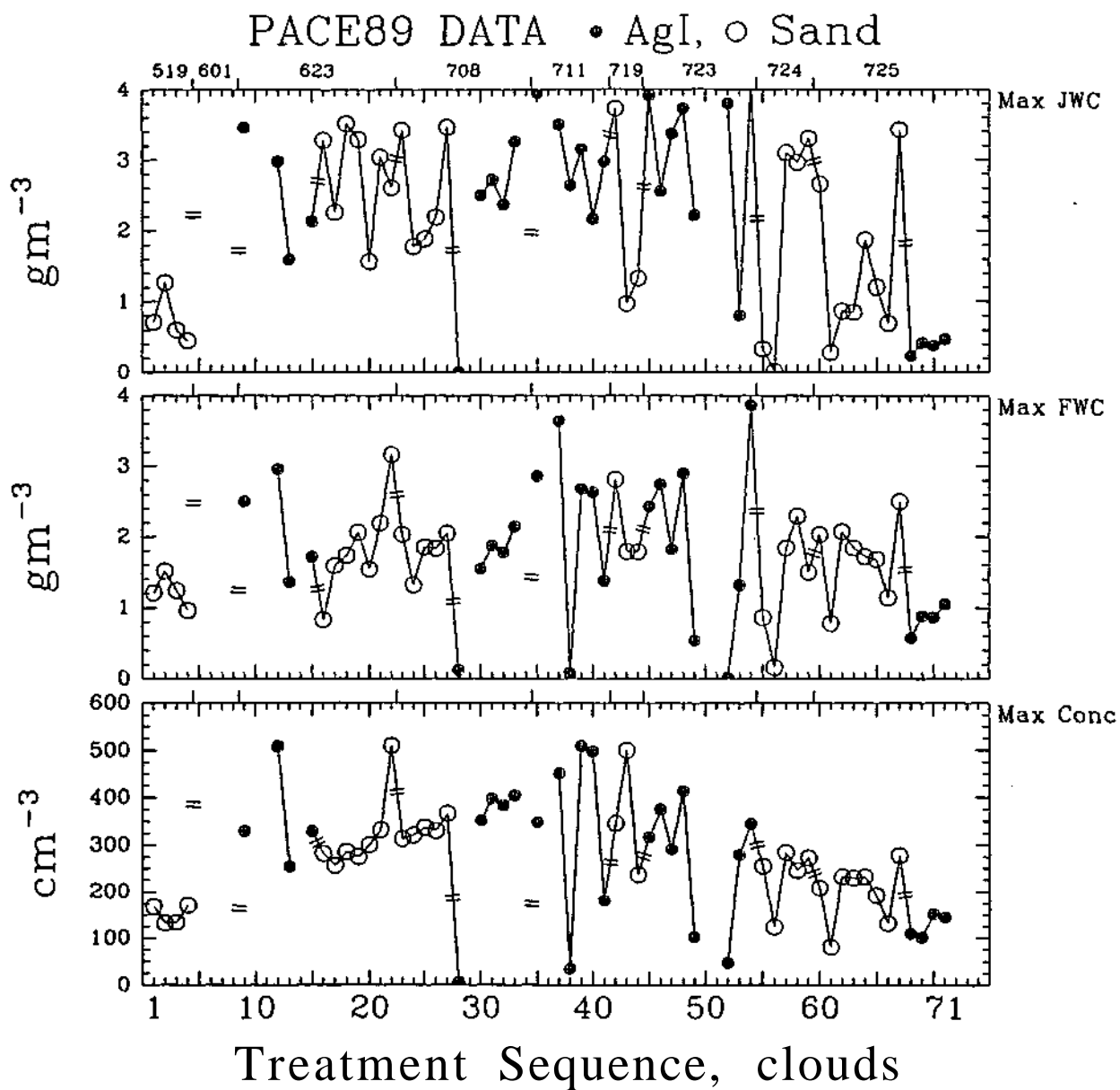


Figure B 54. Time history of the maximum liquid water content in the main updraft from the JW (Max\_JWC) and FSSP (Max\_FWC) probes (i.e., cloud droplets), and the maximum concentration of cloud droplets in the main updraft (Max\_Conc).

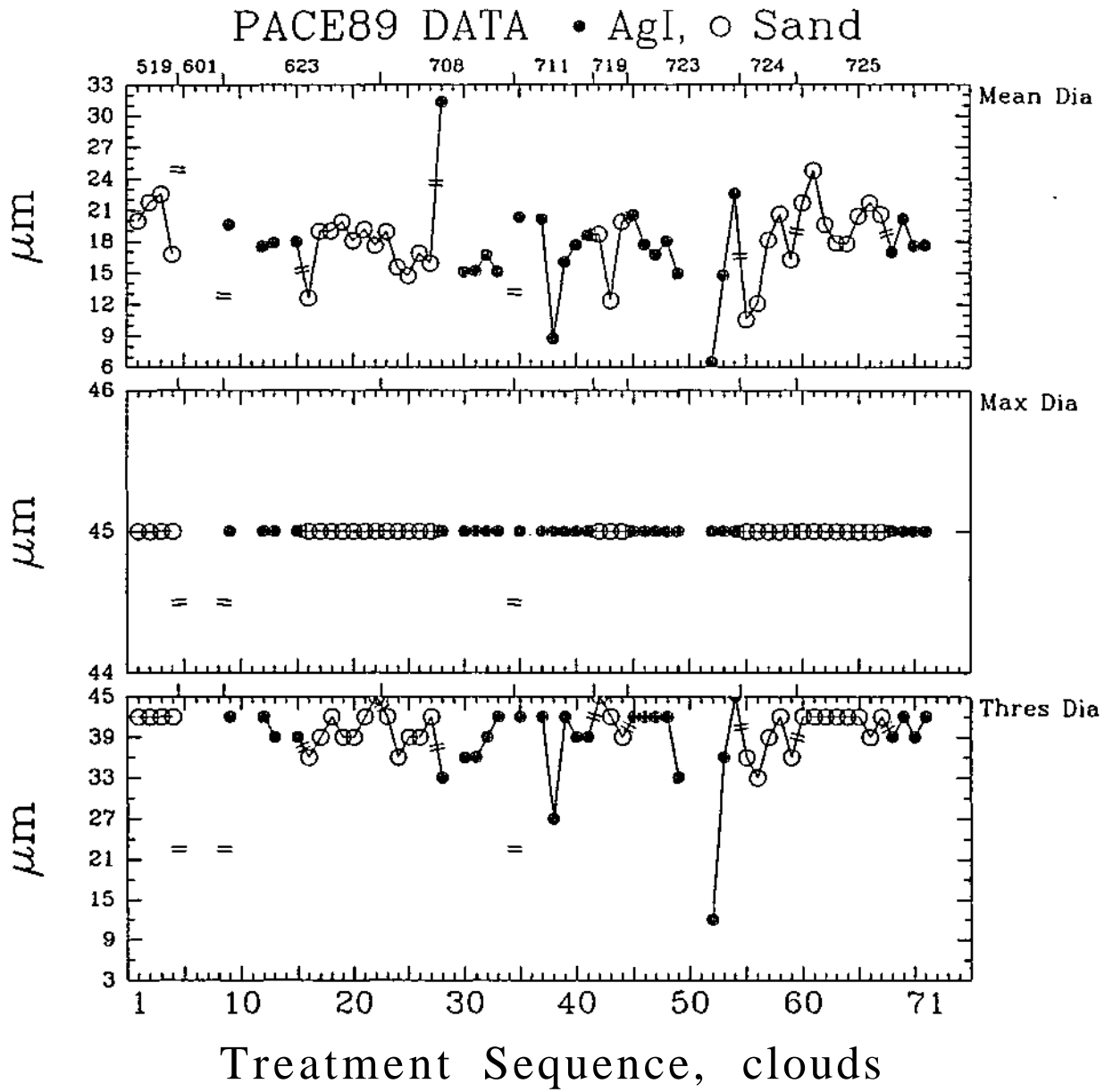


Figure B.55. Time history of the mean (Mean\_Dia) and maximum (Max\_Dia) diameter of cloud droplet particles (from FSSP data) found in the main updraft, and the threshold diameter of the main updraft (Thres\_Dia).

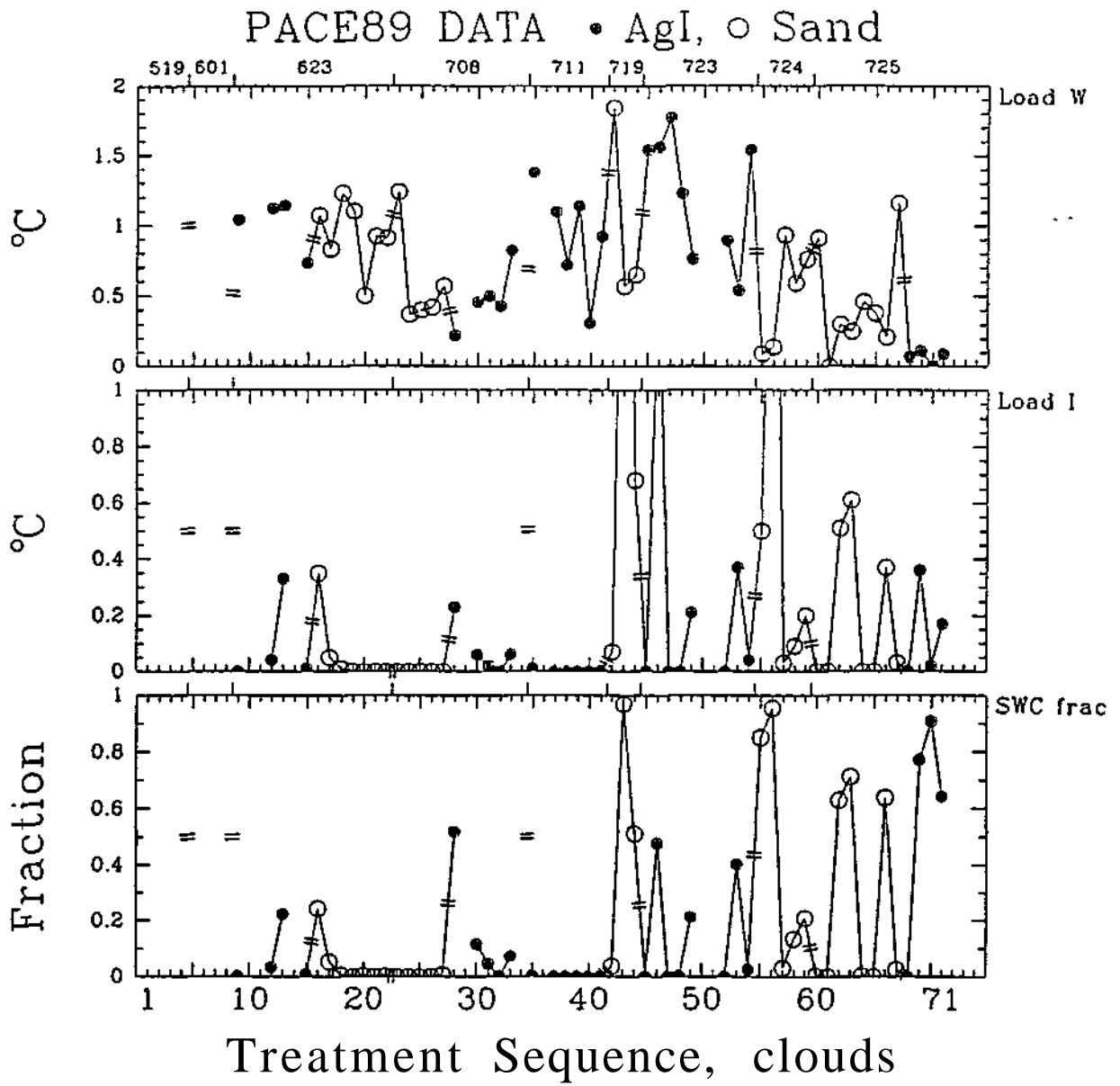


Figure B.56. Time history of the loading from water (liquid) (Load\_W) and from ice (solid) (Load\_I) in the main updraft, and the fraction of solid water content to the total condensate (SWC\_frac).

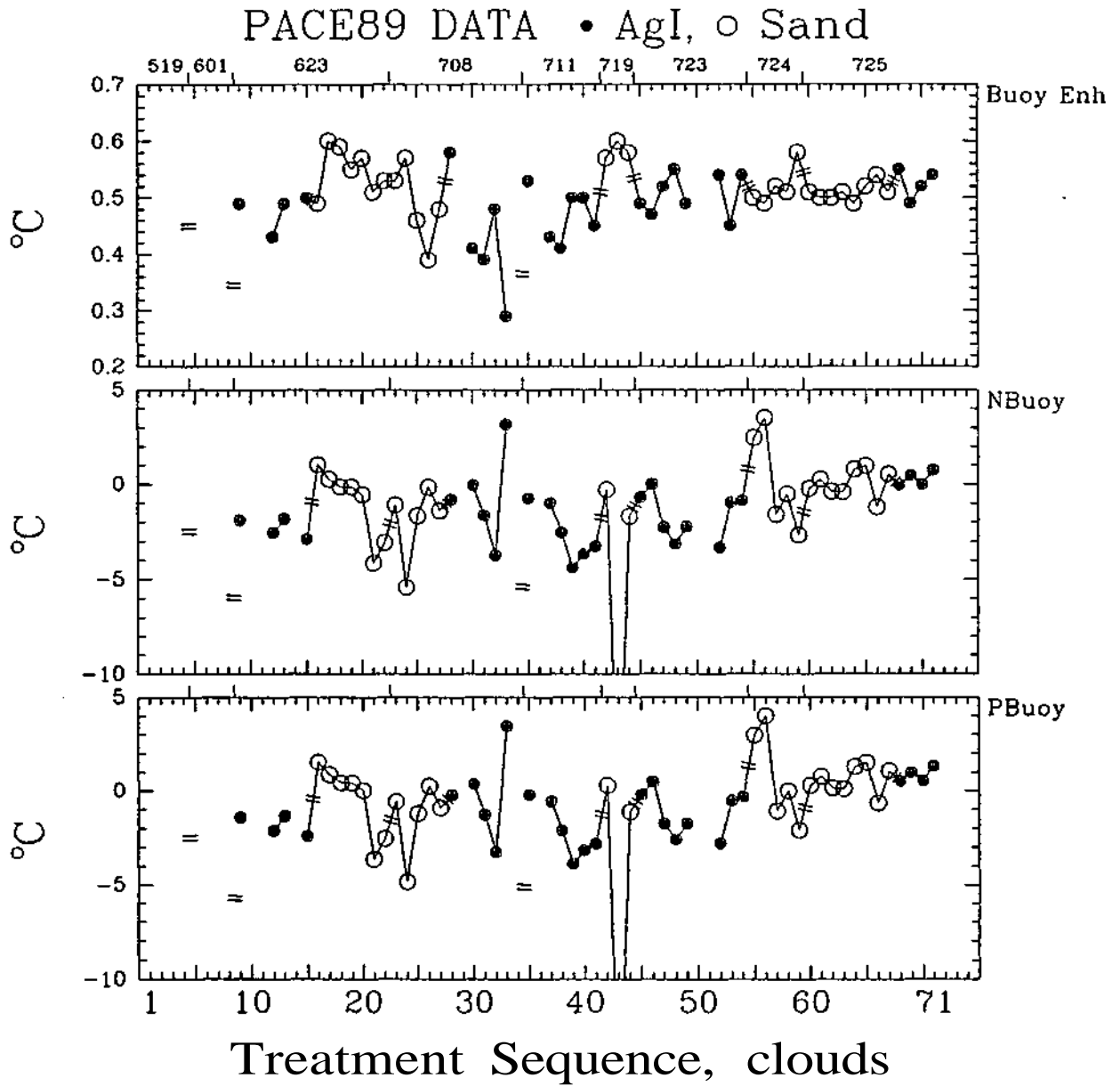


Figure B.57. Time history of the buoyancy enhancement (Buoy\_Enh), the net buoyancy (NBuoy), and the potential buoyancy (PBuoy) of the main up draft.

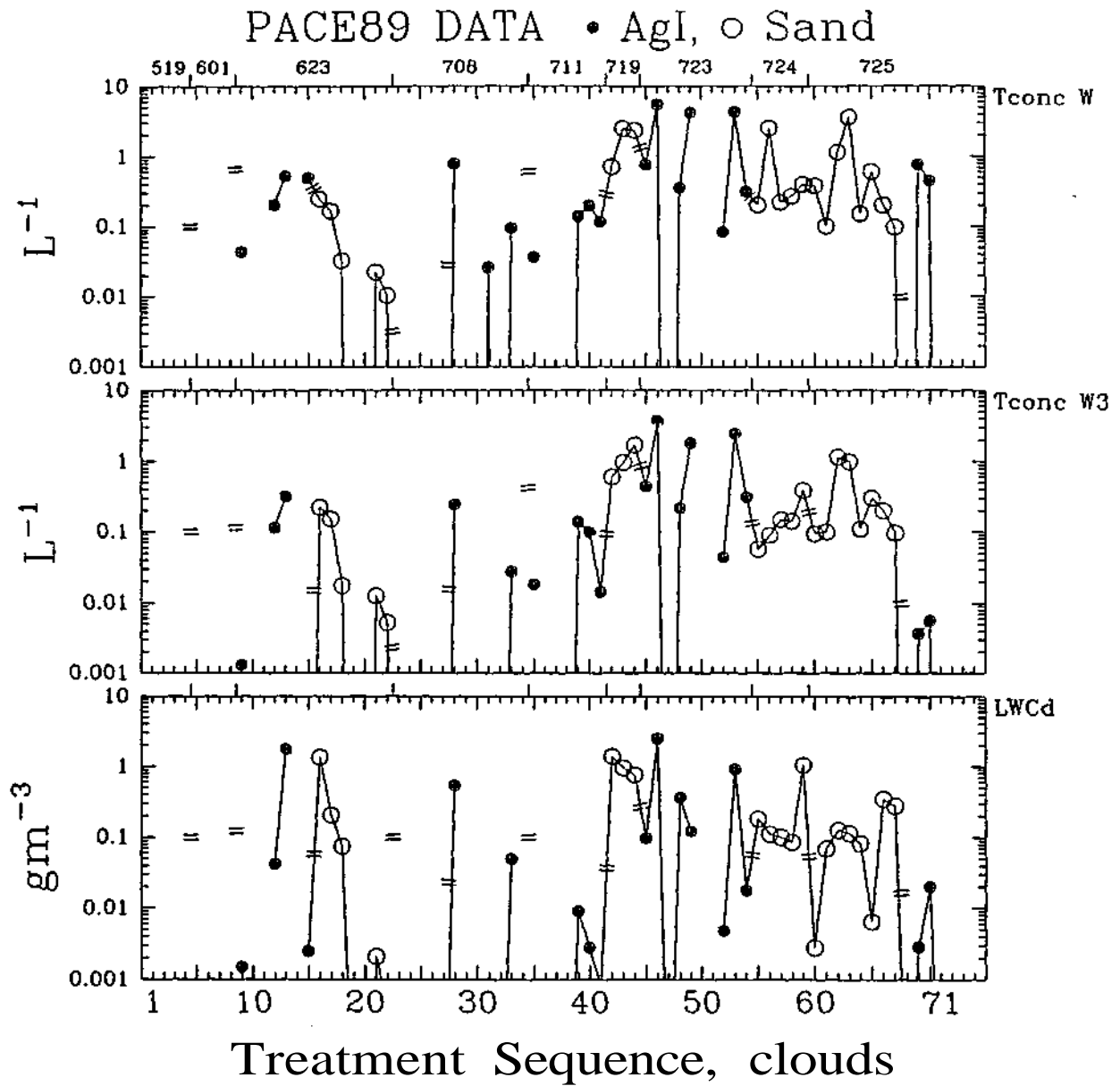


Figure B.58. Time history of the total concentration of water particles ( $Tconc\_W$ ), the total concentration of water particles with  $D > 300 \mu m$  ( $Tconc\_W3$ ), and the liquid water content by method I (i.e., discrete) ( $LWCd$ ) in the main updraft.

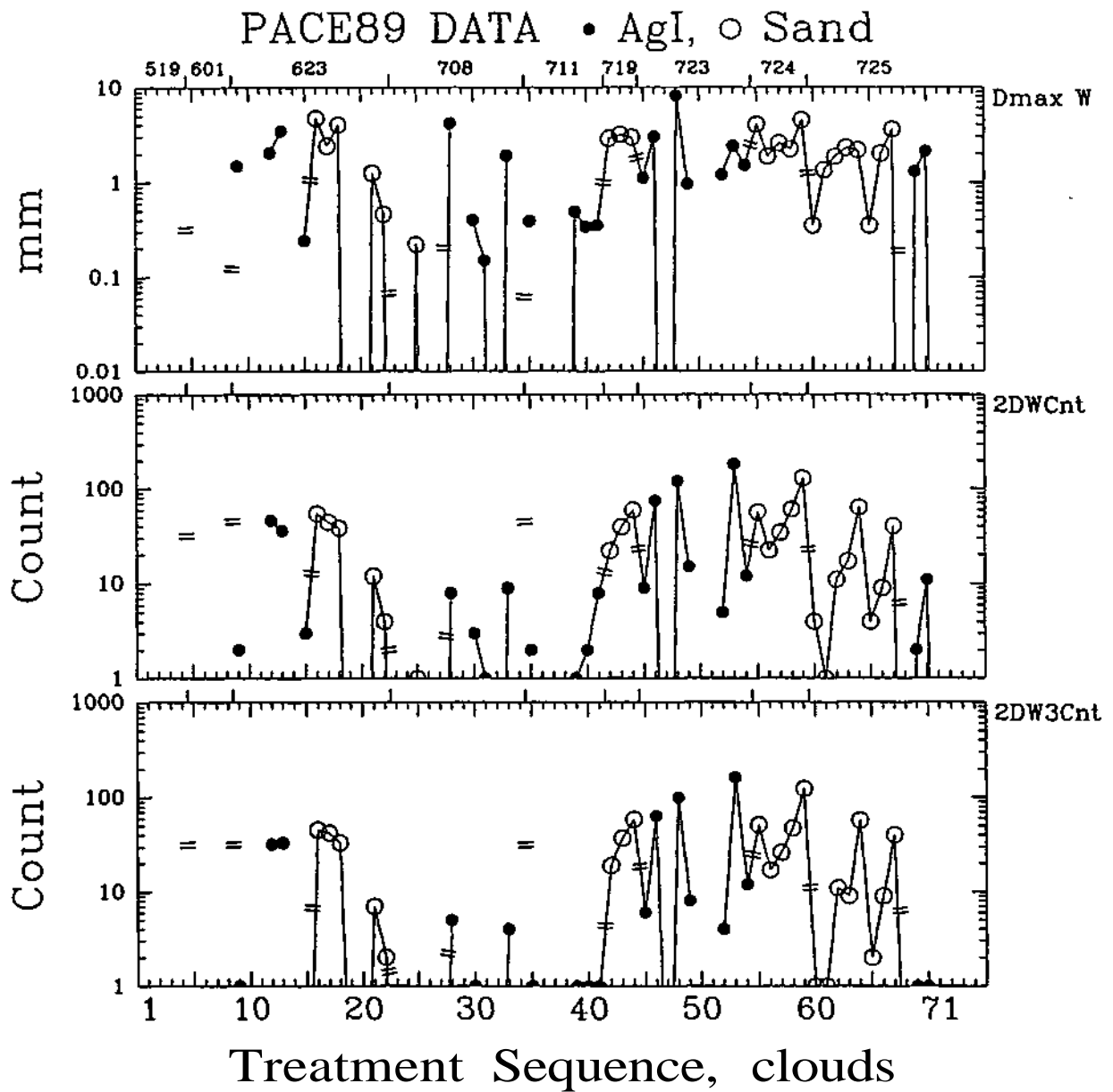


Figure B.59. Time history of the maximum diameter of supercooled liquid rain/drizzle drop particles in the main updraft ( $D_{max\_W}$ ), the 2D probes total particle count in  $T_{conc\_W}$  (2DWCnt), and the 2D probes total particle count in  $T_{conc\_W3}$  (2DW3Cnt).

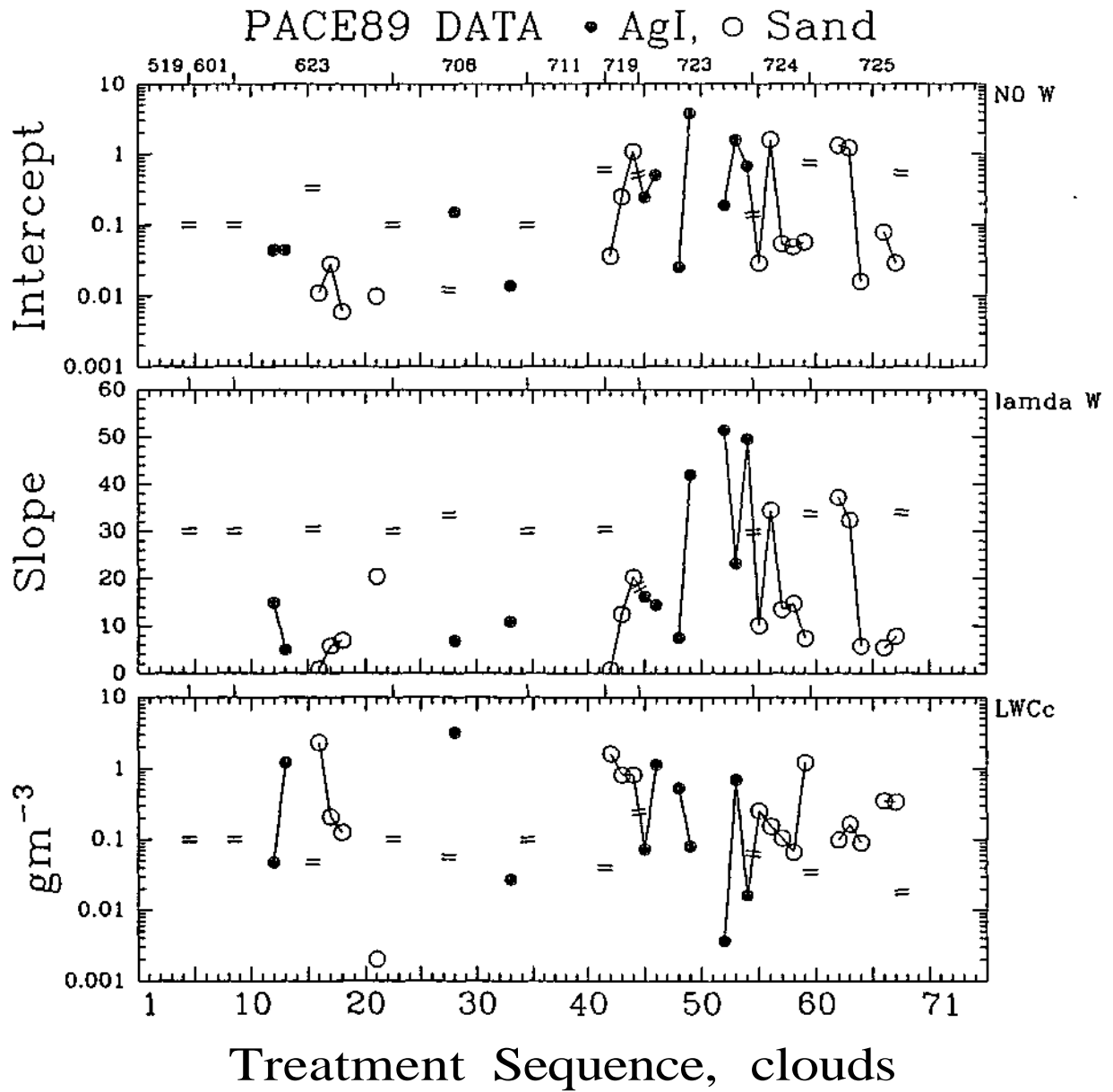


Figure B.60. Time history of the water size-distribution intercepts ( $NO\_W$ ) and slopes ( $lamda\_W$ ), and the liquid water content by method II (i.e., continuous; area under the line defined by  $NO\_W$  and  $lamda\_W$ ) ( $LWCc$ ) calculated for the main updraft.

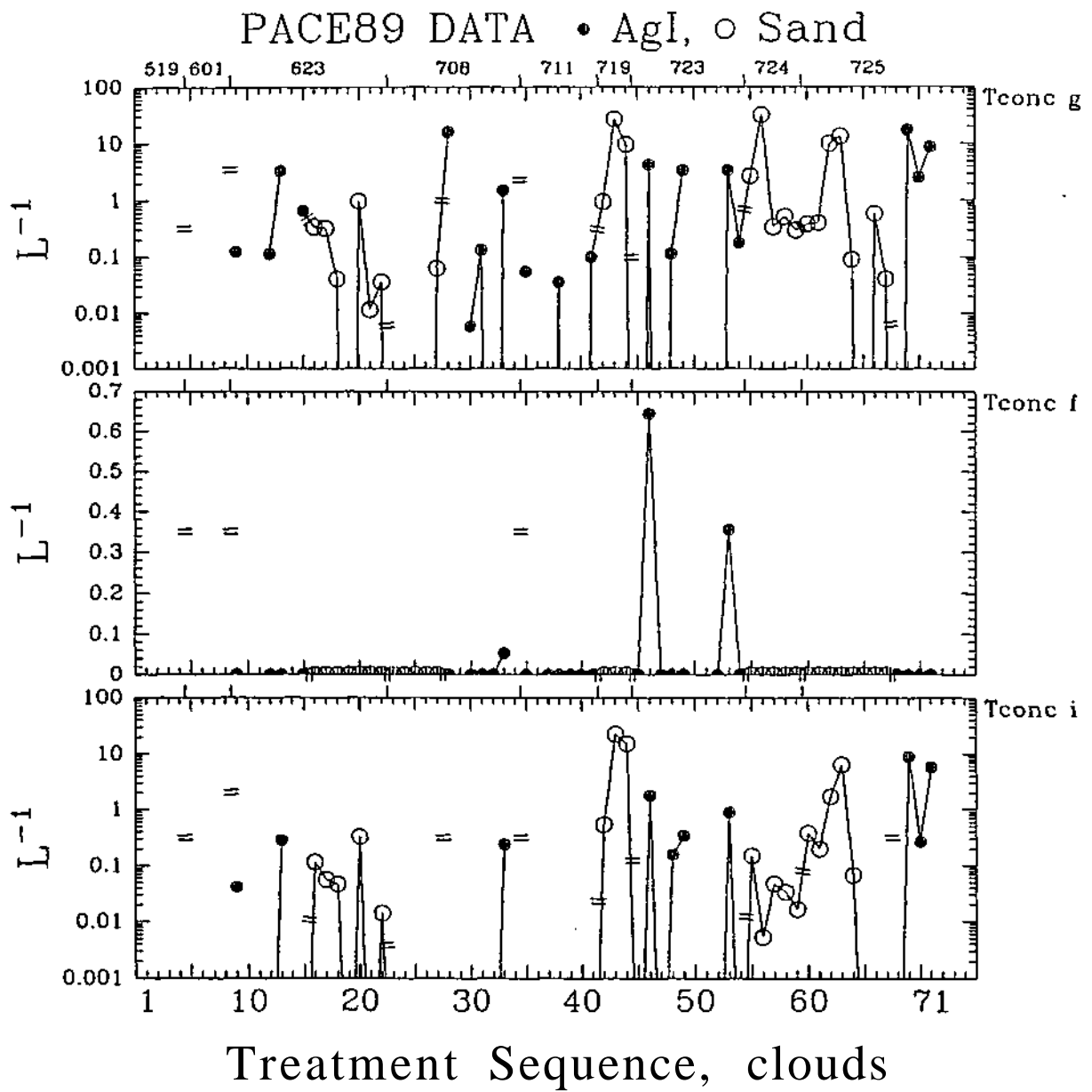


Figure B.61. Time history of the concentration of graupel ( $Tconc\_g$ ), ice fragment ( $Tconc\_f$ ), and ice crystal particles ( $Tconc\_i$ ) in the main updraft.

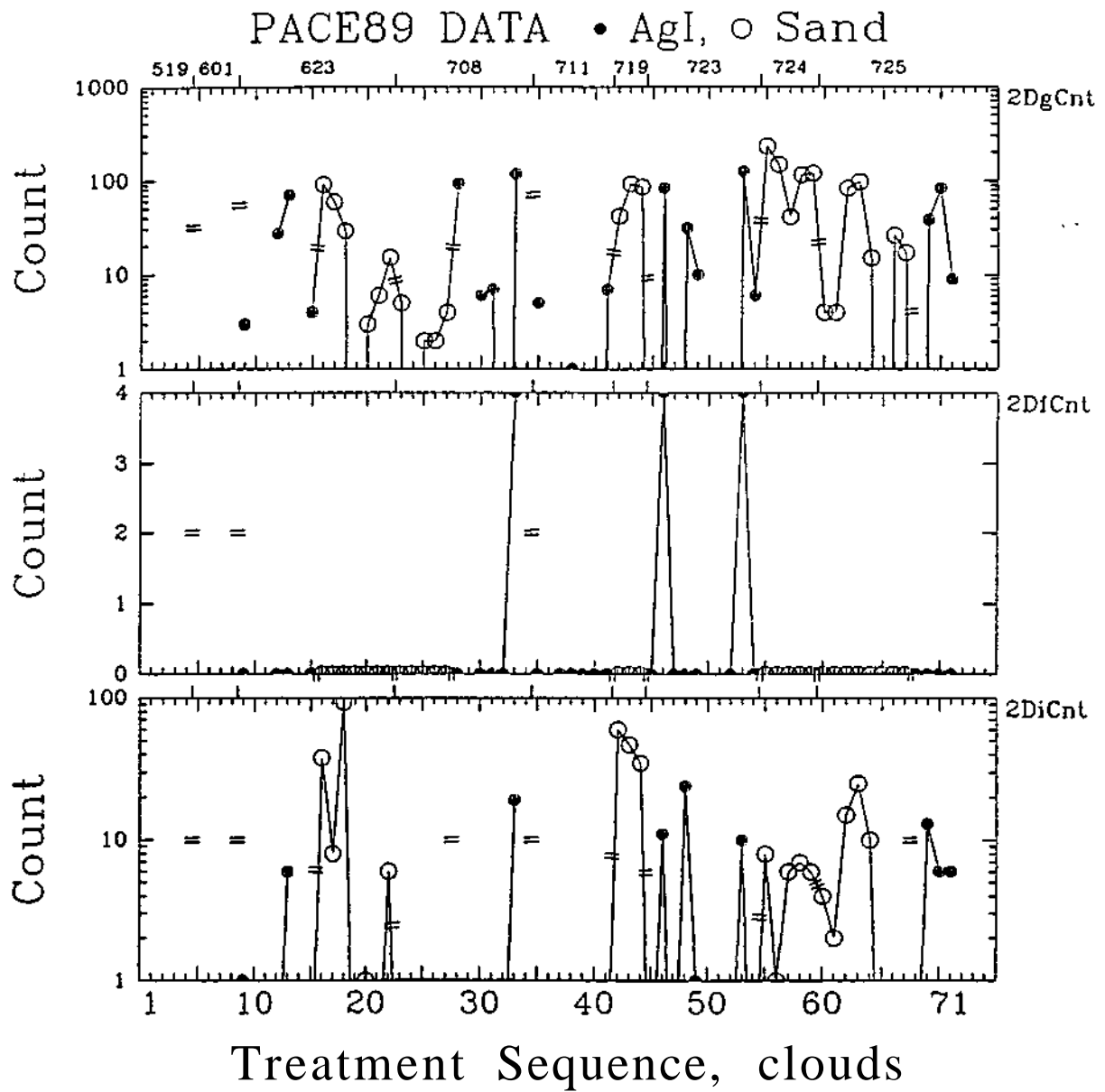


Figure B.62. Time history of the 2D probes total particle count (of graupel) in  $Tconc\_g$  (2DgCnt), (of ice fragments) in  $Tconc\_f$  (2DfCnt), and (of ice crystals) in  $Tconc\_i$  (2DiCnt).

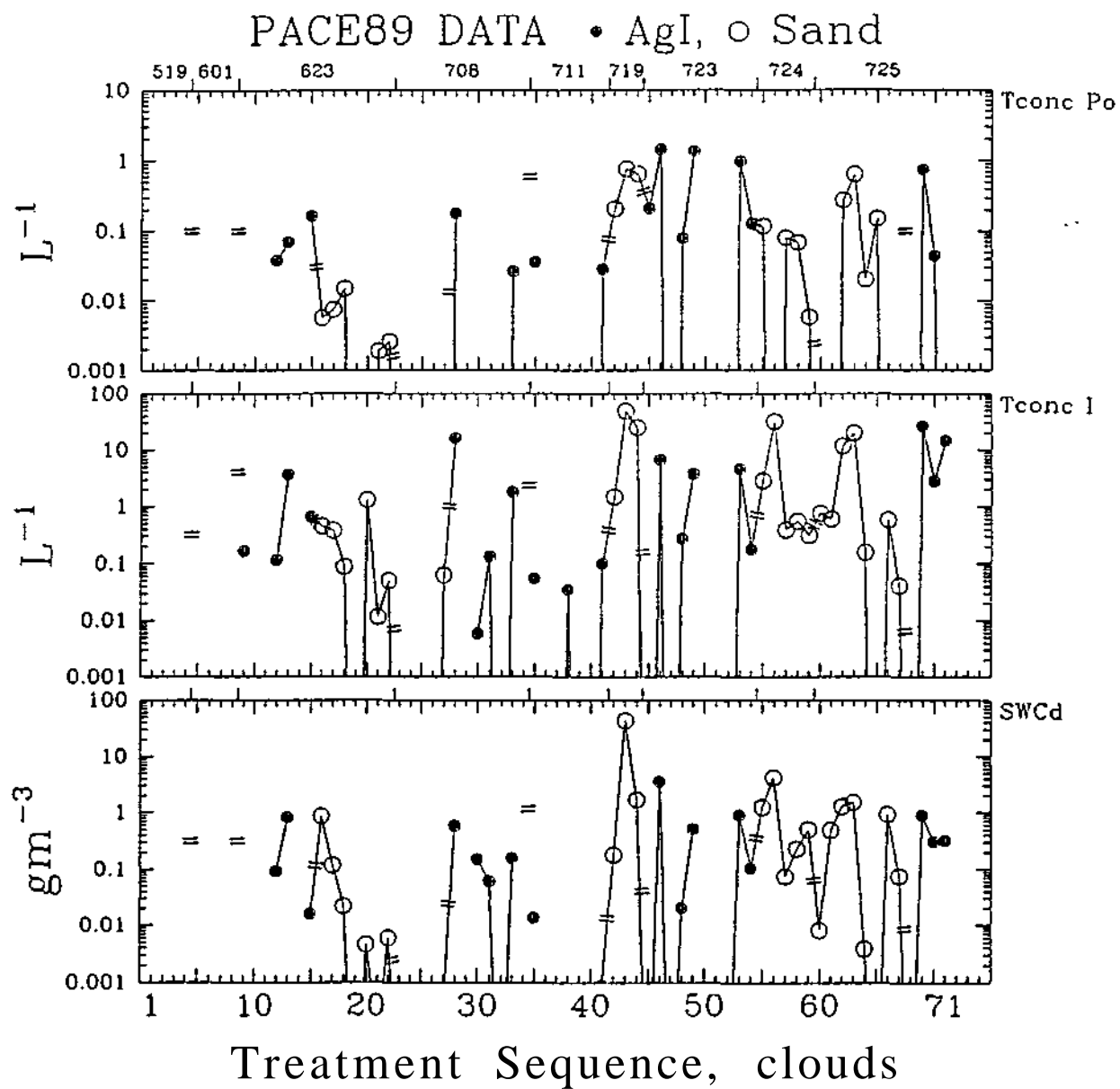


Figure B.63. Time history of the concentration of particles with depolarization signal  $> 0$  (Tconc\_Po), the total concentration of ice particles (Tconc\_I), and the solid water content by method I (i.e., discrete) (SWCd) in the main updraft.

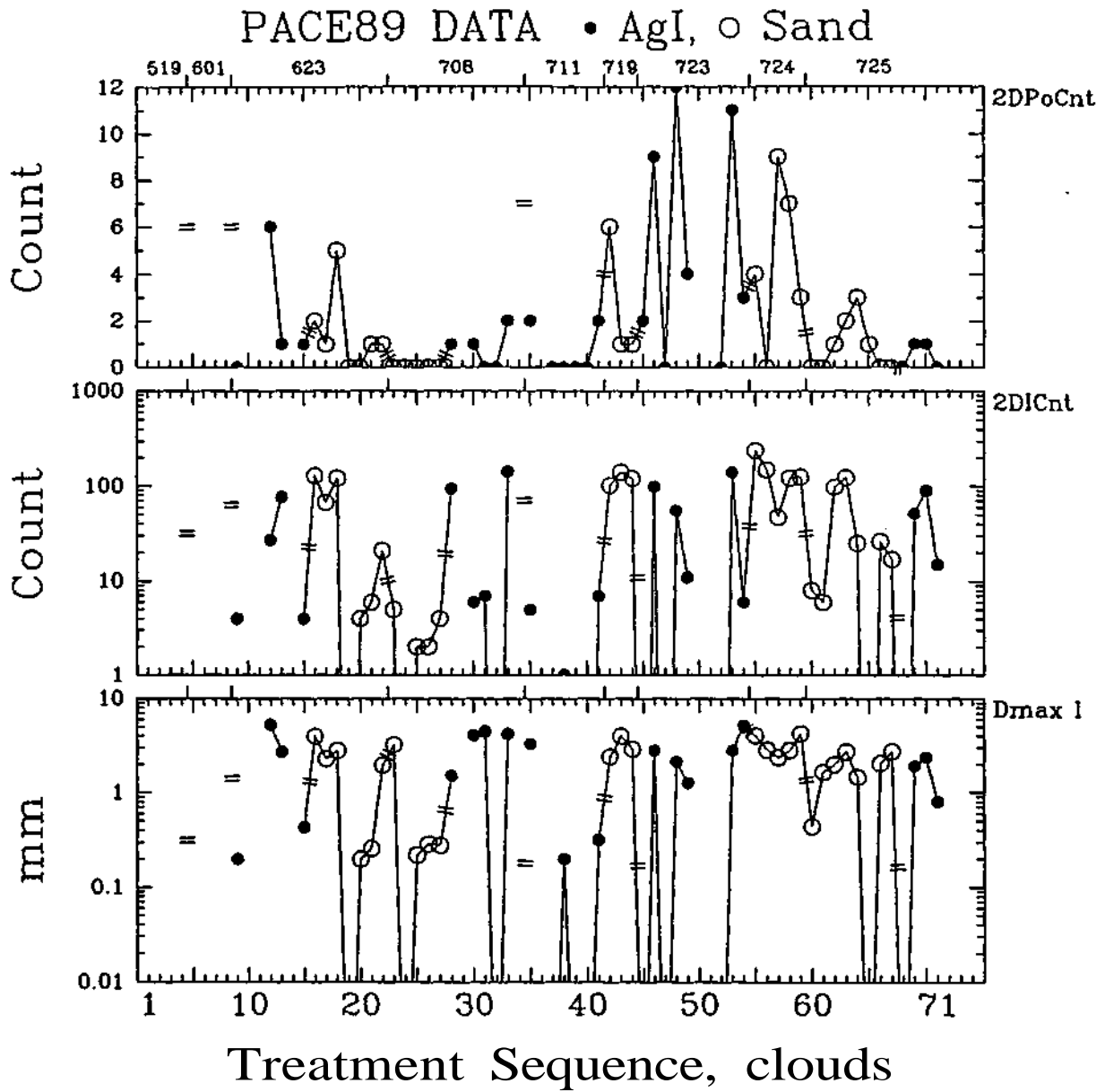


Figure B.64. Time history of the 2D probes total particle count (of particles with depolarization  $> 0$ ) in  $Tconc\_Po$  (2DPoCnt), and (of graupel, fragments and crystals) in  $Tconc\_I$  (2DICnt), and the maximum diameter of ice particles in the main updraft ( $Dmax\_I$ ).

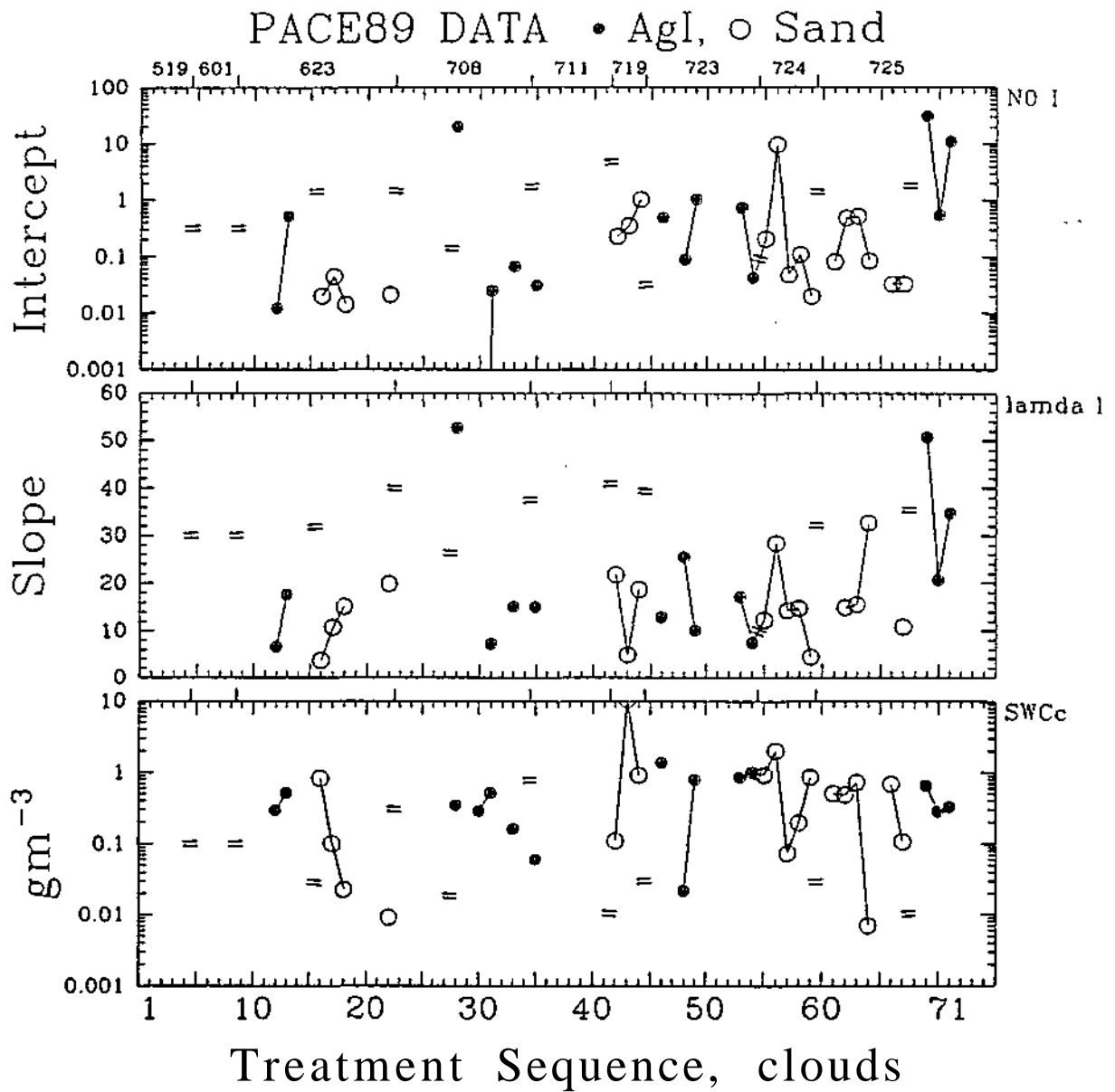


Figure B.65. Time history of the ice size-distribution intercepts ( $NO_I$ ) and slopes ( $lamda_I$ ), and the solid water content by method II (i.e., continuous; area under the line defined by  $NO_I$  and  $lamda_I$ ) ( $SWCc$ ) in the main updraft.

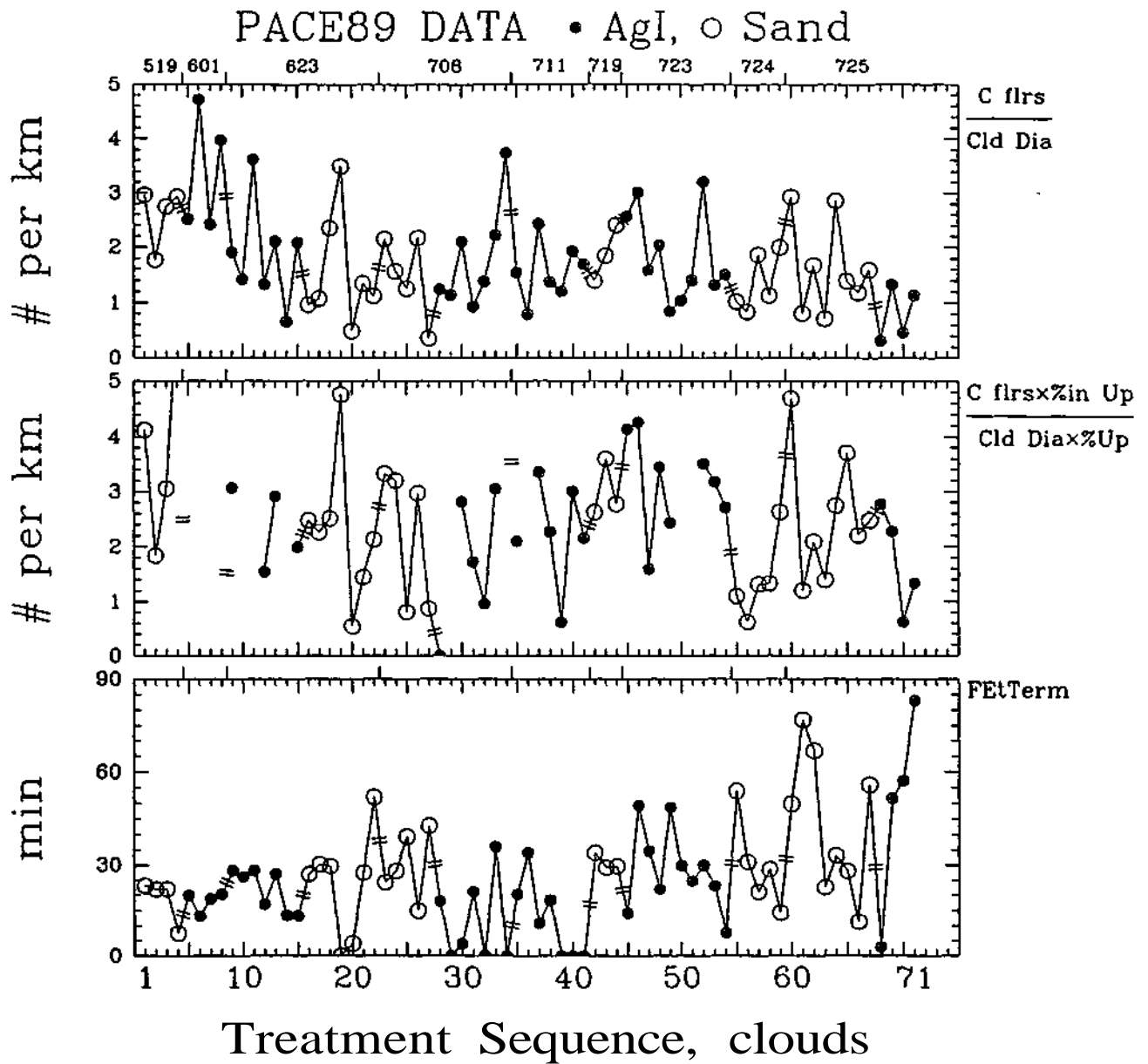


Figure B.66. Time history of the number of flares released in cloud per kilometer of cloud ( $C\_flrs/Cld\_Dia$ ), the number of flares released into updraft regions of the cloud per kilometer of updraft ( $C\_flrs \times \%In\_Up / Cld\_Dia \times \%Up$ ), and the time from first echo to termination of echo tracking ( $FEtTerm$ ).

**Part C**  
**Distributions of AgI- and Sand-Treated Cloud Populations**

Statistics and histograms of all 191 variables, and some derived from them, for the 71 "large" or " " type clouds are presented here. Tables C.1 and C.2 give the mean, standard deviation, and sample size for each predictor and response variable, respectively, for each population, and also present the p-values from rerandomization method 1 and rerandomization method 2 (see Part F of this Book) for Student's *t* test on the differences in the means, and for the Wilcoxon sum rank test on the differences in the distributions. Procedures used in method 2 most closely resemble the 1989 randomization scheme used in the field. In the figures, the top histograms are for the silver iodide (AgI)- treated clouds, while the sand-treated populations are shown in the bottom histograms.

Table C.1. Population statistics for all predictor variables for all of the sand- and AgI-treated clouds (N=71). Dark shading indicates significance levels of 0-5%; lighter shading indicates levels between 5% and 10%.

Variable	Mean		Standard Deviation		Sample Size		Rerandomized P-Values <sup>1</sup>		Rerandomized P-Values <sup>2</sup>	
	Sand	AgI	Sand	AgI	Sand	AgI	<i>t</i>	W*	<i>t</i>	W*
temp	20.31	20.77	1.27	2.08	32	39	0.637	0.654	0.577	0.635
dpt	18.76	19.10	2.11	2.47	32	39	0.785	0.990	0.808	1.000
ct	29.33	31.84	5.22	4.04	32	39	0.178	0.104	0.135	0.106
dbar	17.81	18.36	1.78	1.02	32	39	0.477	0.656	0.529	0.750
plcl	907.34	895.41	25.15	23.47	32	39	0.174	0.201	0.096	0.106
tlcl	17.23	17.60	1.89	1.15	32	39	0.613	0.969	0.644	0.981
hlcl	999.59	1130.41	238.12	217.83	32	39	0.092	0.064	0.067	0.058
pccl	854.41	832.44	57.93	50.45	32	39	0.229	0.094	0.135	0.087
tccl	16.28	16.44	2.11	1.60	32	39	0.818	0.828	0.827	0.846
hccl	1533.00	1770.54	608.16	524.72	32	39	0.184	0.053	0.125	0.048
pres0	613.12	604.33	24.58	16.58	32	39	0.465	0.613	0.471	0.606
hgt0	4266.66	4399.77	386.18	228.20	32	39	0.463	0.740	0.471	0.721
pres10	493.12	492.08	18.37	10.91	32	39	0.885	0.711	0.885	0.692
hgt10	5980.53	6022.56	368.85	194.65	32	39	0.770	0.711	0.798	0.692
dh38	788.09	757.77	116.20	126.80	32	39	0.574	0.895	0.577	0.875
pw	3.87	3.68	0.64	0.59	32	39	0.561	0.609	0.683	0.712
dir85	215.31	225.00	43.38	47.48	32	39	0.697	0.988	0.625	1.000
spd85	6.11	6.66	4.42	2.35	32	39	0.770	0.357	0.731	0.260
dir50	216.25	224.49	60.72	59.61	32	39	0.691	0.568	0.596	0.471
spd50	11.34	11.99	5.86	4.07	32	39	0.770	0.535	0.750	0.519

<sup>1</sup> Based on rerandomization method 1

<sup>2</sup> Based on rerandomization method 2

\* Wilcoxon sum rank test

Table C.1 (cont). Population statistics for all predictor variables for all of the sand- and AgI-treated clouds (N=71). Dark shading indicates significance levels of 0-5%; lighter shading indicates levels between 5% and 10%.

Variable	Mean		Standard Deviation		Sample Size		Rerandomized P-Values <sup>1</sup>		Rerandomized P-Values <sup>2</sup>	
	Sand	AgI	Sand	AgI	Sand	AgI	t	W*	t	W*
L	-0.56	1.89	4.66	4.02	32	39	0.102	0.047	0.029	0.019
cpe	9.17	-29.98	74.07	63.79	32	39	0.098	0.045	0.029	0.019
pb	4.12	5.65	2.18	1.86	32	39	0.113	0.082	0.087	0.019
li	-2.17	-3.32	1.13	1.46	32	39	0.154	0.438	0.231	0.442
ki	31.58	30.29	4.35	4.17	32	39	0.596	0.738	0.587	0.740
mki	36.62	35.28	4.66	4.23	32	39	0.535	0.779	0.548	0.712
jef	34.25	34.41	2.25	3.35	32	39	0.959	0.977	0.971	0.990
msh	8.65	9.19	1.66	2.13	32	39	0.648	0.545	0.673	0.615
swt	203.35	216.77	67.75	86.27	32	39	0.746	0.949	0.625	0.952
pbot	777.97	775.95	82.29	65.31	32	39	0.939	0.584	0.923	0.529
ptop	348.19	286.15	121.96	52.55	32	39	0.236	0.428	0.231	0.385
CAPE	482.16	773.00	217.41	340.36	32	39	0.113	0.330	0.173	0.231
vshr	12.80	9.79	12.76	5.52	32	39	0.662	0.875	0.558	0.788
Ri	62.07	88.75	31.02	45.76	32	39	0.371	0.604	0.452	0.654
m100	48.81	48.82	5.36	8.91	32	39	1.000	0.721	1.000	0.615
m80	47.22	48.82	6.96	8.91	32	39	0.795	0.580	0.788	0.500
An-targ	2.28	0.96	3.01	0.85	32	39	0.201	0.266	0.221	0.250
An-buff	3.29	1.93	5.73	4.25	32	39	0.580	0.102	0.615	0.183
EU-targ	7.28	4.02	8.13	2.94	32	39	0.281	0.668	0.279	0.606
EU-buff	3.87	3.74	5.54	3.39	32	39	0.961	0.516	0.962	0.462
RFxtCPeu	85.06	156.44	52.84	119.89	32	39	0.236	0.475	0.221	0.538
RFxt-15eu	115.56	89.47	126.63	79.03	32	39	0.764	0.822	0.779	0.856
RFxDifeu	-30.50	66.97	123.41	76.83	32	39	0.289	0.227	0.327	0.279
AtCPeu	197.00	139.97	36.87	87.16	32	39	0.189	0.037	0.202	0.067
At-15eu	155.75	80.67	58.23	67.27	32	39	0.131	0.109	0.221	0.173
ADifeu	41.25	59.31	37.17	52.52	32	39	0.686	0.490	0.808	0.635
RFxtCPtn	6174.43	3420.53	5210.71	3294.95	32	39	0.223	0.369	0.288	0.462
RFxt-15tn	6361.82	2776.66	4742.54	1896.31	32	39	0.057	0.090	0.144	0.202
RFxDiftn	-187.39	643.87	827.59	1592.78	32	39	0.621	0.318	0.462	0.212
AtCPtn	2860.22	1012.69	3323.85	667.14	32	39	0.090	0.176	0.135	0.346
At-15tn	2806.72	1006.56	3153.25	537.32	32	39	0.078	0.129	0.115	0.279
ADiftn	53.25	6.31	215.51	159.50	32	39	0.623	0.816	0.538	0.808
range	82.22	74.67	13.62	27.23	32	39	0.631	0.770	0.644	0.740

<sup>1</sup> Based on rerandomization method 1

<sup>2</sup> Based on rerandomization method 2

\* Wilcoxon sum rank test

Table C.1 (cont). Population statistics for all predictor variables for all of the sand- and AgI-treated clouds (N=71). Dark shading indicates significance levels of 0-5%; lighter shading indicates levels between 5% and 10%.

Variable	Mean		Standard Deviation		Sample Size		Rerandomized P-Values <sup>1</sup>		Rerandomized P-Values <sup>2</sup>	
	Sand	AgI	Sand	AgI	Sand	AgI	t	W*	t	W*
FeStat	2.25	2.36	0.80	1.04	32	39	0.664	0.590	0.587	0.462
FEmndia	3.09	1.99	1.13	1.00	32	39	0.016	0.012	0.019	0.019
FEHtp10	6.28	5.38	1.73	2.21	32	39	0.088	0.182	0.019	0.077
FEdpth10	2.34	1.90	1.56	1.57	32	39	0.299	0.250	0.173	0.163
FEA10	12.25	5.64	10.36	5.19	32	39	0.025	0.027	0.029	0.038
FEVol10	35.97	12.79	44.75	11.48	32	39	0.010	0.016	0.019	0.019
FEMxZ	29.46	22.14	11.93	12.79	32	39	0.076	0.086	0.048	0.067
FEHMxZ	4.75	4.31	1.74	2.05	32	39	0.361	0.607	0.231	0.519
FEMxB	17.29	13.89	4.28	6.18	32	39	0.109	0.084	0.067	0.067
FEtpTmp	-12.83	-10.71	12.15	7.79	32	35	0.475	0.744	0.529	0.721
FEmzTmp	-3.73	-3.43	11.20	9.17	32	35	0.912	0.611	0.894	0.538
CpStat	1.72	1.90	0.68	0.91	32	39	0.363	0.873	0.240	0.856
CPmndia	4.79	3.18	2.46	2.39	32	39	0.086	0.033	0.048	0.019
CPA.L1	24.88	13.38	26.61	25.62	32	39	0.107	0.078	0.058	0.077
CPZ.L1	27.50	18.87	23.24	21.62	32	39	0.172	0.186	0.183	0.173
CPA.L6	23.09	12.03	19.12	18.91	32	39	0.117	0.049	0.058	0.029
CPZ.L6	32.91	18.72	15.96	16.74	32	39	0.051	0.045	0.019	0.019
CPdia.L6	4.24	2.41	2.30	2.53	32	39	0.076	0.049	0.038	0.029
CPA56	23.12	13.59	19.16	18.91	32	39	0.160	0.084	0.087	0.077
CPZ56	31.55	20.98	16.64	16.53	32	39	0.113	0.098	0.048	0.038
CPdia56	4.24	2.74	2.30	2.49	32	39	0.135	0.080	0.106	0.077
FltAltR	5.94	5.64	0.24	0.25	32	35	0.004	0.008	0.010	0.019
FltAltA	5.85	5.56	0.25	0.23	32	39	0.004	0.006	0.010	0.010
CPHtp10	7.09	5.51	3.05	3.22	32	39	0.090	0.037	0.010	0.010
CPA10	38.22	21.10	29.55	28.08	32	39	0.104	0.055	0.067	0.038
CPMxZ	43.21	30.43	19.75	19.89	32	39	0.115	0.064	0.067	0.019
CPHMxZ	3.23	3.00	2.12	2.18	32	39	0.572	0.656	0.587	0.663
CPMxB	22.39	16.37	9.97	9.84	32	39	0.145	0.066	0.096	0.038
FECpt	8.79	5.99	11.08	6.20	32	35	0.150	0.287	0.154	0.279
CPFEdH10	1.81	0.57	1.84	2.40	32	35	0.035	0.059	0.010	0.029
CPFEdA10	27.97	17.63	24.70	28.02	32	35	0.229	0.049	0.125	0.029
CPFEdZ	18.82	11.07	13.48	13.17	32	35	0.078	0.070	0.019	0.029
CPFEdB	8.60	4.24	6.00	6.56	32	35	0.039	0.037	0.010	0.019

<sup>1</sup> Based on rerandomization method 1

<sup>2</sup> Based on rerandomization method 2

\* Wilcoxon sum rank test

Table C.1 (cont). Population statistics for all predictor variables for all of the sand- and AgI-treated clouds (N=71). Dark shading indicates significance levels of 0-5%; lighter shading indicates levels between 5% and 10%.

Variable	Mean		Standard Deviation		Sample Size		Rerandomized P-Values <sup>1</sup>		Rerandomized P-Values <sup>2</sup>	
	Sand	AgI	Sand	AgI	Sand	AgI	t	W*	t	W*
CPFE <sub>d</sub> H/dt	0.16	0.04	0.33	0.44	32	35	0.402	0.260	0.356	0.192
CPFE <sub>d</sub> A/dt	3.70	2.26	2.54	2.69	32	35	0.234	0.154	0.163	0.087
CPFE <sub>d</sub> Z/dt	2.69	1.89	2.43	2.54	32	35	0.342	0.496	0.260	0.404
FE <sub>t</sub> Term	30.64	22.21	17.22	18.03	32	39	0.119	0.076	0.087	0.038
pdeg	2.59	2.68	1.12	1.35	29	31	0.764	0.846	0.721	0.817
v_bef	3.89	1.37	4.44	3.69	29	27	0.197	0.158	0.173	0.163
v_cdp	3.47	0.94	4.25	3.10	29	27	0.193	0.186	0.163	0.154
a_bef	-0.00	-0.01	0.01	0.01	29	27	0.449	0.570	0.433	0.558
a_cdp	-0.00	-0.00	0.01	0.02	29	27	0.734	0.820	0.779	0.827
FEH <sub>bs</sub> 10	3.71	3.47	2.02	1.42	17	17	0.680	0.727	0.740	0.702
FE <sub>bs</sub> Temp	2.75	4.45	12.56	8.41	17	17	0.617	0.699	0.615	0.683
FE <sub>t</sub> toFR	5.25	4.80	3.32	3.07	30	29	0.486	0.545	0.327	0.423
Cld_Dia	3801.13	3213.23	2508.69	1390.15	32	39	0.402	0.645	0.337	0.663
#_Ups	1.59	1.32	0.91	1.20	32	34	0.395	0.141	0.365	0.250
%_Updraft	59.91	37.53	20.25	26.60	32	34	0.008	0.012	0.038	0.058
C#_flrs	5.53	5.51	2.81	3.51	32	39	0.971	0.748	0.971	0.788
%_in_Up	84.24	52.60	22.77	38.09	32	34	0.012	0.023	0.038	0.058
#_SECs	20.50	12.18	12.72	10.68	32	34	0.035	0.027	0.106	0.096
Env_ThetaV	323.69	322.80	2.77	2.47	32	39	0.422	0.422	0.385	0.394
Env_TC	-10.58	-8.65	1.72	1.58	32	39	0.008	0.008	0.019	0.019
UP_Dia	1900.03	1050.76	1243.50	928.72	32	34	0.027	0.023	0.077	0.096
Mean_VW	6.59	3.90	3.78	3.41	32	34	0.090	0.031	0.163	0.115
Max_VW	11.31	6.93	7.07	6.58	32	34	0.125	0.043	0.250	0.135
Mean_ThV	324.08	322.89	3.42	2.54	32	27	0.309	0.328	0.365	0.365
Max_ThV	325.55	324.39	3.33	3.03	32	27	0.383	0.332	0.433	0.385
U#_flrs	4.50	2.71	3.19	2.91	32	34	0.066	0.043	0.115	0.096
Mean_TBuoy	0.39	-0.55	1.99	1.79	32	27	0.109	0.035	0.106	0.058
Max_TBuoy	1.87	0.96	2.05	2.62	32	27	0.199	0.027	0.221	0.058
Load_W	0.67	0.82	0.42	0.51	28	27	0.492	0.484	0.567	0.510
Load_I	0.85	0.12	3.27	0.29	28	27	0.297	0.711	0.404	0.731
Buoy_Enh	0.53	0.48	0.05	0.06	28	27	0.031	0.039	0.058	0.058
NBuoy	-1.26	-1.50	3.80	1.70	28	27	0.820	0.133	0.827	0.115
PBuoy	-0.74	-1.01	3.78	1.68	28	27	0.781	0.133	0.769	0.115
SWC_frac	0.22	0.17	0.33	0.27	28	27	0.633	0.805	0.567	0.798

<sup>1</sup> Based on rerandomization method 1

<sup>2</sup> Based on rerandomization method 2

\* Wilcoxon sum rank test

Table C.1 (cont). Population statistics for all predictor variables for all of the sand- and AgI-treated clouds (N=71). Dark shading indicates significance levels of 0-5%; lighter shading indicates levels between 5% and 10%.

Variable	Mean		Standard Deviation		Sample Size		Rerandomized P-Values <sup>1</sup>		Rerandomized P-Values <sup>2</sup>	
	Sand	AgI	Sand	AgI	Sand	AgI	t	W*	t	W*
Mean_JWC	1.29	1.72	0.99	1.14	32	27	0.289	0.336	0.240	0.279
Max_JWC	1.96	2.42	1.18	1.27	32	27	0.309	0.336	0.260	0.269
Mean_FWC	1.13	1.33	0.55	0.96	32	27	0.406	0.797	0.346	0.808
Max_FWC	1.68	1.79	0.61	1.07	32	27	0.652	0.723	0.596	0.731
Mean_Dia	18.15	17.45	3.23	4.32	32	27	0.562	0.355	0.606	0.404
Max_Dia	45.00	45.00	0.00	0.00	32	27	0.562	1.000	0.606	1.000
Thres_Dia	40.41	38.33	2.75	6.52	32	27	0.078	0.293	0.125	0.375
Mean_Conc	204.06	257.11	94.14	162.03	32	27	0.191	0.121	0.115	0.096
Max_Conc	261.27	283.85	96.80	151.12	32	27	0.473	0.223	0.337	0.135
Mean_Conc_D<13	78.90	100.00	42.83	62.98	32	27	0.133	0.289	0.096	0.308
Mean_Conc_D>=25	50.11	62.00	28.60	48.18	32	27	0.387	0.848	0.346	0.894
Dmax_W	1.83	1.38	1.53	1.78	28	27	0.438	0.398	0.433	0.433
Tconc_W	0.57	0.72	0.96	1.46	28	27	0.828	0.992	0.692	1.000
2DWCnt	25.82	20.44	30.05	42.21	28	27	0.719	0.398	0.769	0.308
Tconc_W3	0.27	0.37	0.42	0.87	28	27	0.820	0.695	0.673	0.606
2DW3Cnt	22.75	16.15	28.27	36.90	28	27	0.547	0.312	0.337	0.183
LWCd	0.26	0.24	0.42	0.59	28	27	0.898	0.477	0.865	0.404
Dmax_I	1.94	1.70	1.40	1.79	28	27	0.734	0.500	0.769	0.510
Tconc_g	3.55	2.29	8.03	4.58	28	27	0.523	0.734	0.481	0.760
2DgCnt	47.79	26.93	57.36	39.72	28	27	0.406	0.273	0.385	0.298
Tconc_f	0.00	0.04	0.00	0.14	28	27	0.203	0.133	0.288	0.202
2DfCnt	0.00	0.44	0.00	1.28	28	27	0.125	0.133	0.202	0.202
Tconc_i	1.71	0.69	5.08	2.02	28	27	0.648	0.320	0.817	0.442
2DiCnt	13.29	3.59	22.31	6.47	28	27	0.109	0.078	0.250	0.125
Tconc_I	5.25	3.02	11.85	6.23	28	27	0.539	0.680	0.615	0.673
2DICnt	61.07	30.96	65.33	44.89	28	27	0.188	0.180	0.231	0.183
Tconc_Po	0.11	0.21	0.22	0.41	28	27	0.578	0.680	0.471	0.663
2DPoCnt	1.71	2.19	2.42	3.40	28	27	0.734	0.844	0.692	0.740
SWCd	2.02	0.32	8.12	0.71	28	27	0.352	0.578	0.558	0.615
NO_W	0.35	0.65	0.56	1.11	17	11	0.500	0.500	0.442	0.471
lamda_W	13.91	21.99	11.38	17.35	17	11	0.359	0.391	0.327	0.356
LWCC	0.51	0.63	0.65	0.96	17	11	0.688	0.500	0.644	0.692
NO_I	0.72	4.33	2.24	9.14	18	15	0.336	0.445	0.192	0.481
lamda_I	15.18	20.93	8.00	15.08	16	14	0.227	0.281	0.087	0.125
SWCC	1.05	0.50	2.39	0.37	18	15	0.516	0.961	0.587	0.971

<sup>1</sup> Based on rerandomization method 1

<sup>2</sup> Based on rerandomization method 2

\* Wilcoxon sum rank test

Table C.2. Population statistics for all response variables for all of the sand- and AgI-treated clouds (N=71). Dark shading indicates significance levels of 0-5%; lighter shading indicates levels between 5% and 10%.

Variable	Mean		Standard Deviation		Sample Size		Rerandomized P-Values <sup>1</sup>		Rerandomized P-Values <sup>2</sup>	
	Sand	AgI	Sand	AgI	Sand	AgI	t	W*	t	W*
MaxH10	10.62	7.28	2.54	3.13	32	39	0.002	0.002	0.010	0.010
MaxA10	80.34	44.44	58.89	45.73	32	39	0.031	0.039	0.019	0.038
MaxZ	52.12	41.02	13.77	19.03	32	39	0.096	0.064	0.058	0.048
MaxB	27.26	22.30	6.50	10.01	32	39	0.164	0.193	0.115	0.135
MxRFx	12.51	7.85	19.28	17.03	32	39	0.453	0.150	0.375	0.106
TotRNVOL	11.67	7.90	37.46	34.04	32	39	0.627	0.105	0.327	0.077
FRtoMxRFx	13.95	10.41	12.21	9.23	32	35	0.072	0.178	0.019	0.048
FEMXtMxH	14.83	8.83	11.71	8.13	32	35	0.037	0.037	0.038	0.048
FEMXtMxA	17.80	13.19	10.66	7.74	32	35	0.006	0.002	0.010	0.010
FEMXtMxZ	12.92	11.04	7.55	5.71	32	35	0.145	0.119	0.125	0.096
FEMXtMxB	12.77	11.94	7.73	7.31	32	35	0.533	0.396	0.471	0.298
MXFEdH10	4.34	2.11	3.08	2.00	32	35	0.006	0.018	0.019	0.029
MXFEdA10	68.09	43.46	55.92	44.98	32	35	0.086	0.088	0.029	0.058
MXFEdZ	22.66	21.04	15.18	13.09	32	35	0.688	0.664	0.587	0.529
MXFEdH/dt	0.28	0.25	0.21	0.27	32	35	0.719	0.375	0.692	0.423
MXFEdA/dt	3.73	3.21	2.28	3.61	32	35	0.678	0.242	0.587	0.173
MXFEdZ/dt	1.73	1.92	1.17	1.09	32	35	0.539	0.494	0.481	0.423
CPMXtMxH	6.04	2.82	6.96	7.68	32	35	0.115	0.084	0.173	0.125
CPMXtMxA	9.01	7.20	13.02	6.93	32	35	0.512	0.553	0.404	0.462
CPMXtMxZ	4.13	5.05	11.33	8.39	32	35	0.729	0.994	0.731	0.990
MXCPdH10	2.31	0.31	2.63	2.31	32	35	0.047	0.068	0.106	0.125
MXCPdA10	34.31	22.80	52.80	37.05	32	35	0.188	0.469	0.173	0.462
MXCPdZ	6.22	6.57	12.69	16.32	32	35	0.930	0.799	0.942	0.769
MXCPdB	3.28	3.62	6.64	9.07	32	35	0.879	0.877	0.875	0.856
MXCPdH/dt	0.35	-0.21	0.52	2.17	32	35	0.383	0.088	0.413	0.173
MXCPdA/dt	1.57	1.63	5.43	4.67	32	35	0.965	0.549	0.971	0.471
MXCPdZ/dt	0.41	-1.38	1.37	9.25	32	35	0.410	0.420	0.375	0.356
v_aft	2.31	0.95	5.05	4.51	29	31	0.465	0.307	0.596	0.442
a_aft	-0.01	-0.02	0.02	0.04	29	31	0.240	0.422	0.144	0.337
CPtoFR	-4.10	-1.86	12.98	7.80	30	29	0.426	0.551	0.356	0.442
dH/dt-PO/PR	2.95	5.30	2.77	12.26	20	10	0.609	0.211	0.721	0.240
dA/dt-PO/PR	1.02	1.27	0.61	1.20	20	20	0.533	0.922	0.548	0.942
dZ/dt-PO/PR	0.27	0.35	0.28	0.73	17	18	0.707	0.094	0.779	0.144
dH-PO/PR	2.08	0.92	2.13	0.63	20	10	0.383	0.398	0.317	0.337
dA-PO/PR	5.01	3.85	7.87	7.46	20	20	0.418	0.305	0.317	0.231
dZ-PO/PR	1.91	-26.39	5.21	115.74	17	18	0.465	0.332	0.519	0.471

<sup>1</sup> Based on rerandomization method 1

<sup>2</sup> Based on rerandomization method 2

\* Wilcoxon sum rank test

# PACE89 DATA

## Total Sample

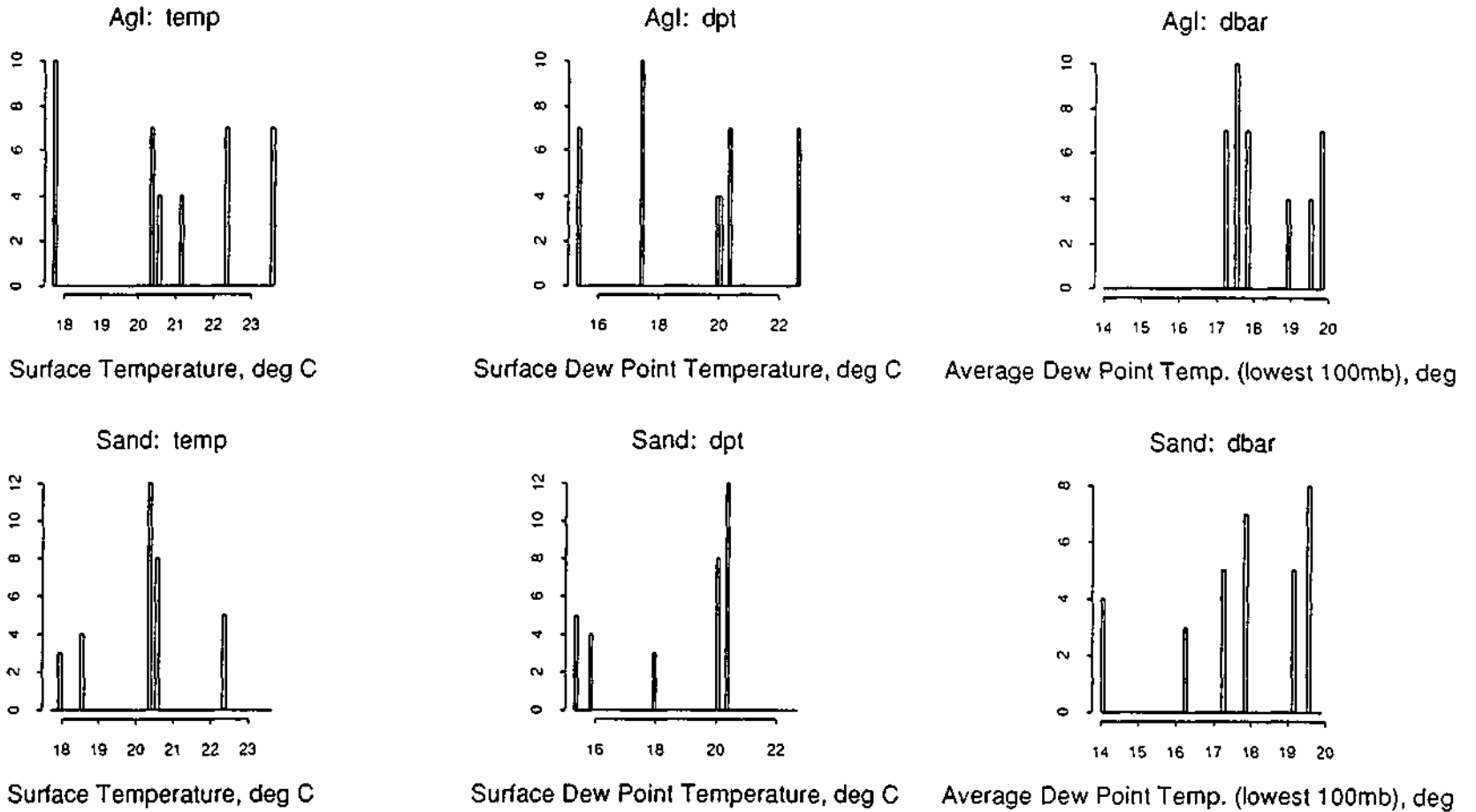


Figure C.1. Histograms of the surface temperature (temp), the surface dew point temperature (dpt), and the average dew point temperature in lowest 100 mb layer (dbar) (these and the following synoptic variables are all from 0700 CDT Peoria sounding).

# PACE89 DATA

## Total Sample

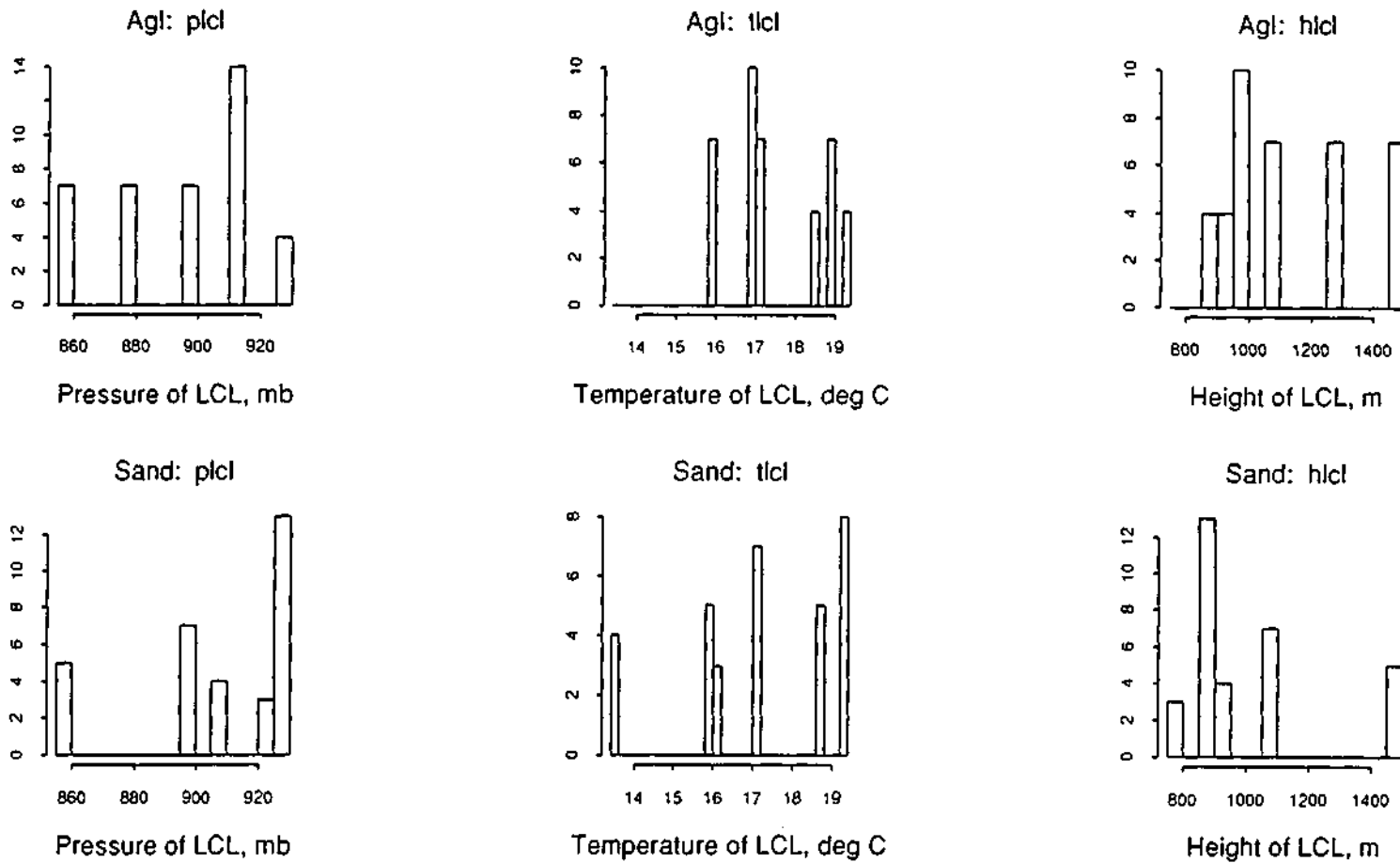


Figure C.2. Histograms of the pressure (plcl), temperature (tlcl), and height (hlcl) of the lifting condensation level (LCL) using averaged data in lowest 100 mb.

# PACE89 DATA

## Total Sample

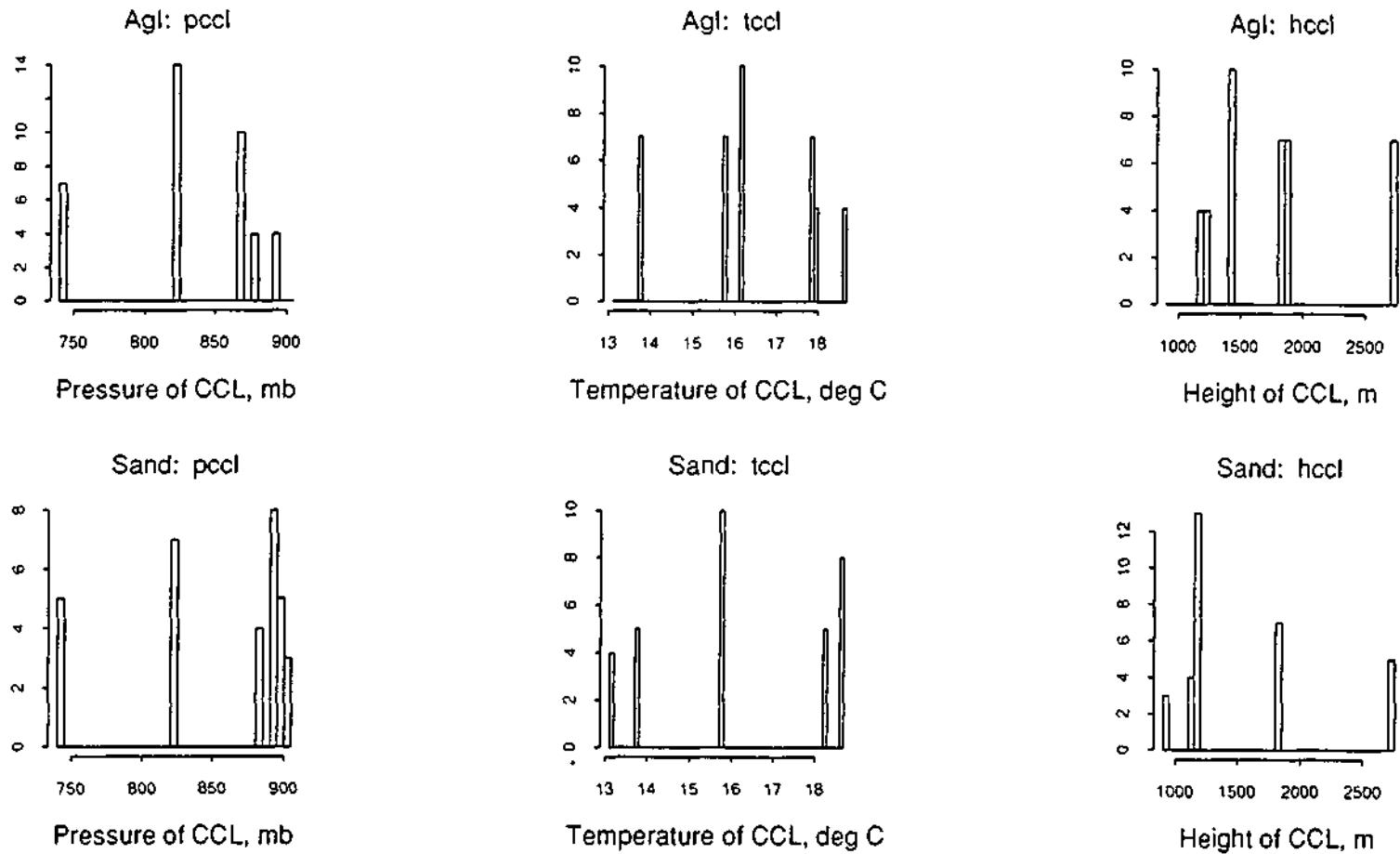


Figure C.3. Histograms of the pressure (pccl), temperature (tccl), and height (hccl) of the convective condensation level (CCL) using averaged data in lowest 100 mb.

# PACE89 DATA

## Total Sample

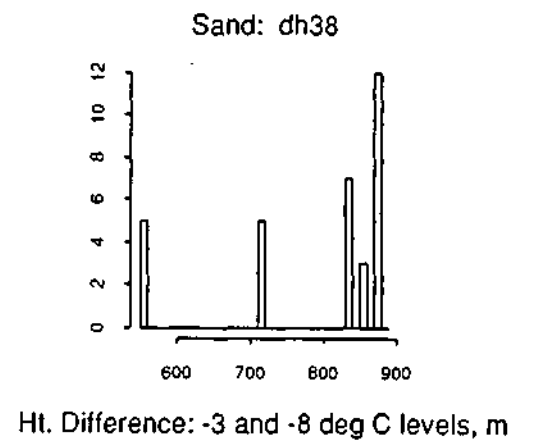
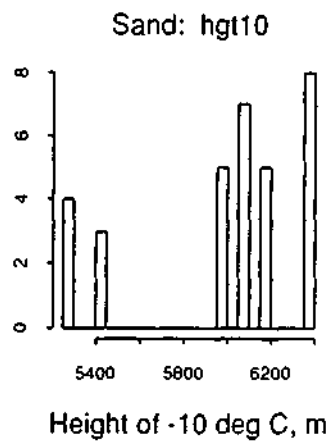
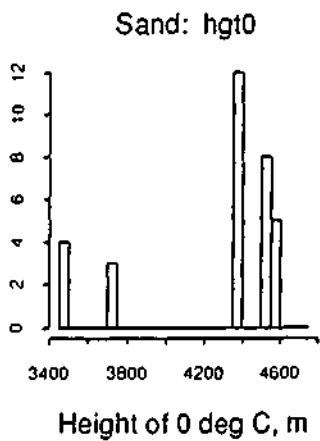
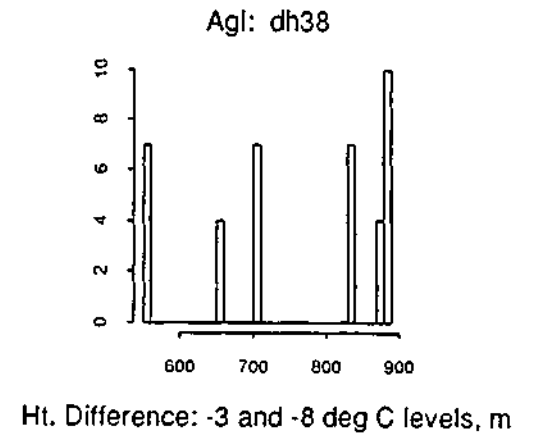
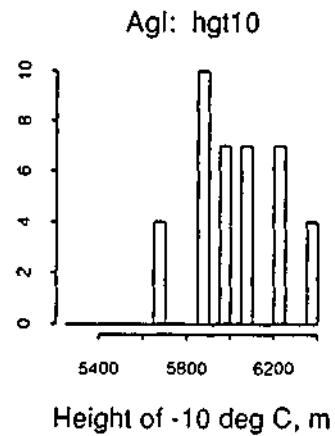
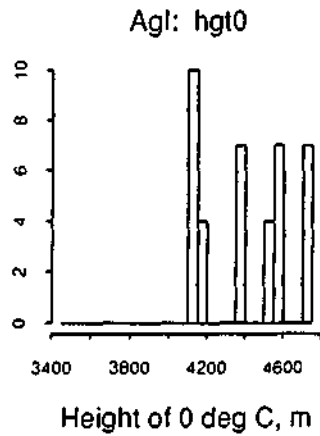


Figure C.4. Histograms of the heights of the 0°C (hgt0) and -10°C (hgt10) levels, and the height difference between the heights of the -3°C and -8°C levels (dh38).

# PACE89 DATA

## Total Sample

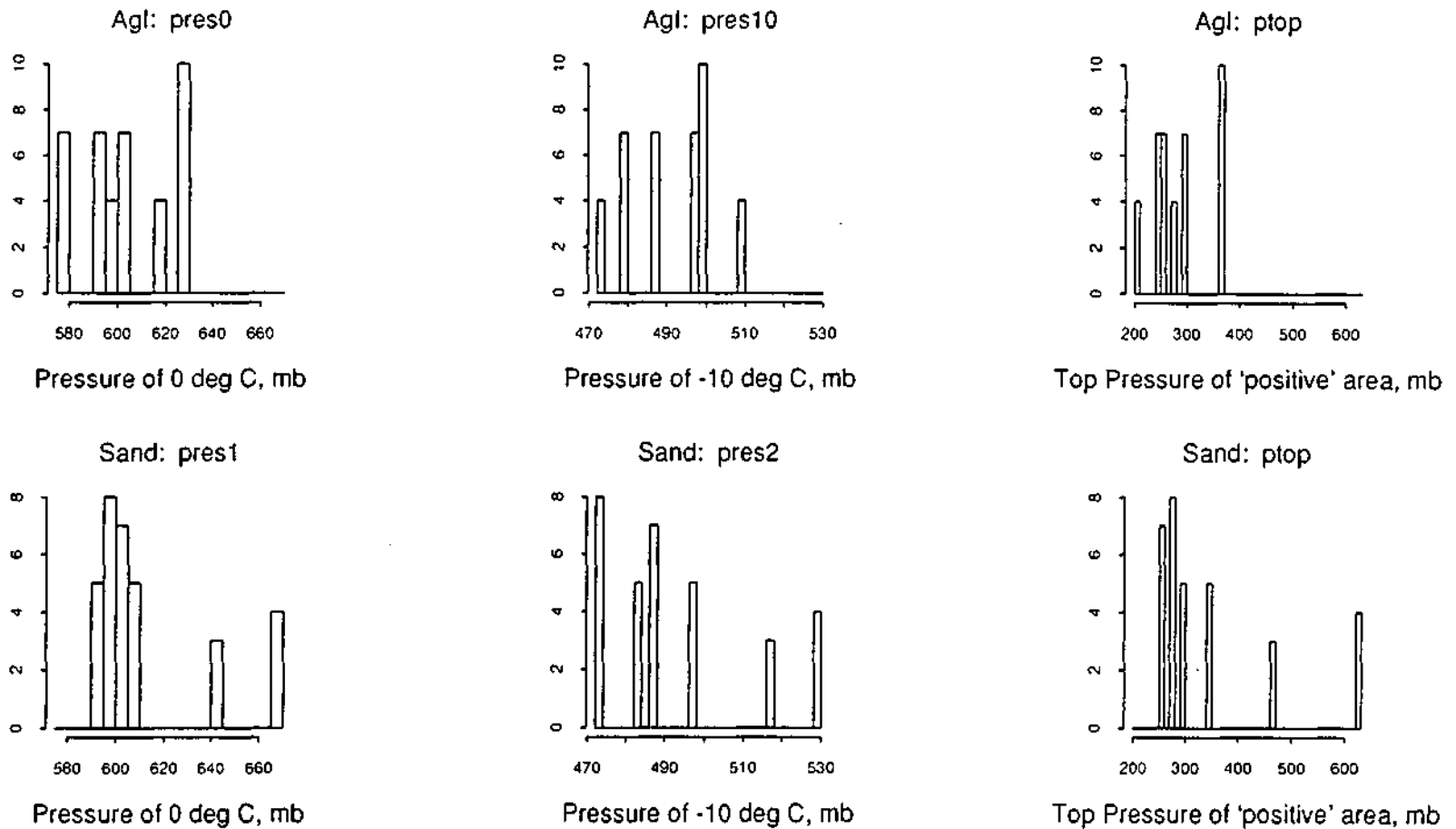


Figure C.5. Histograms of the pressures of the 0°C (pres0) and -10°C (pres10) levels, and the pressure of the top of the "positive area" on the sounding (ptop).

# PACE89 DATA

Total Sample

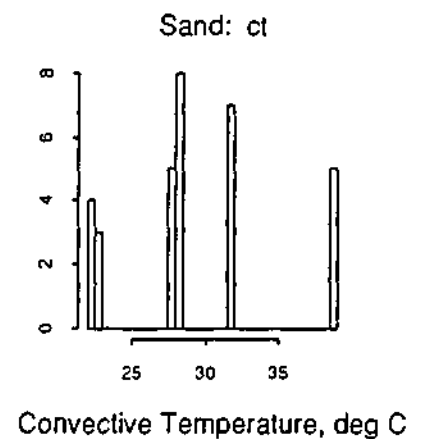
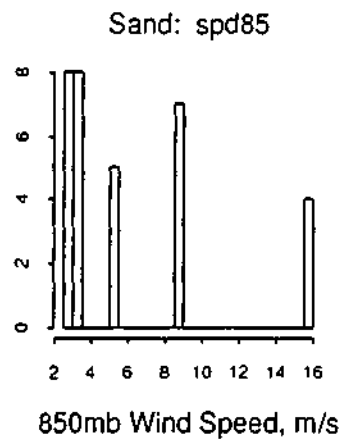
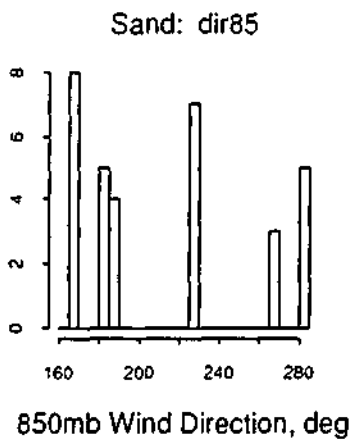
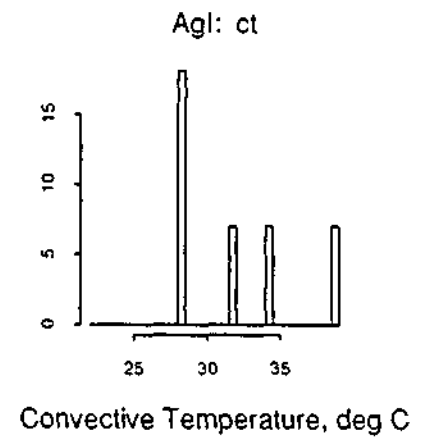
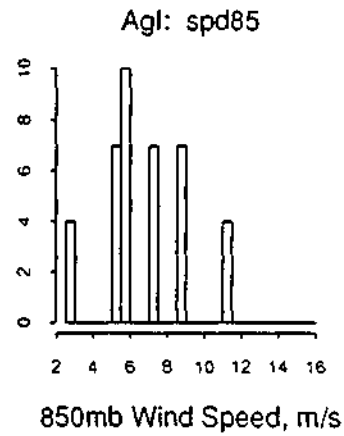
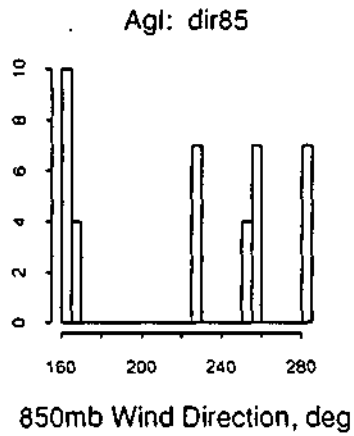


Figure C.6. Histograms of the 850 mb wind direction (*dir85*) and speed (*spd85*), and the convective temperature using average mixing ratio in lowest 100 mb (*ct*).

# PACE89 DATA

Total Sample

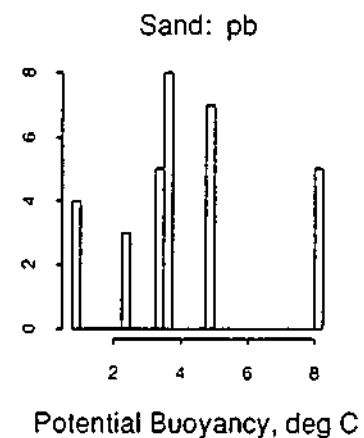
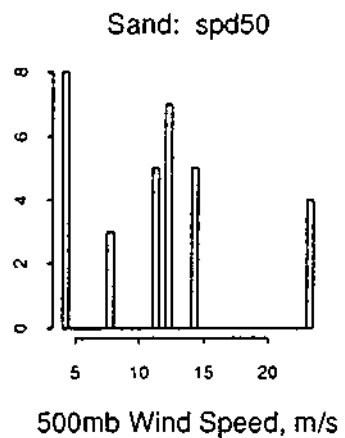
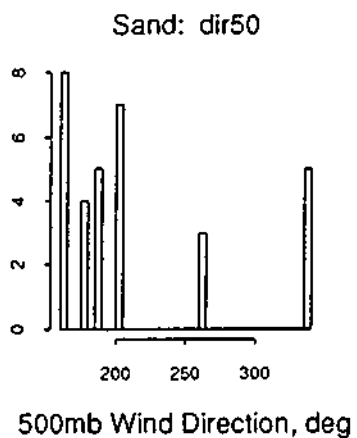
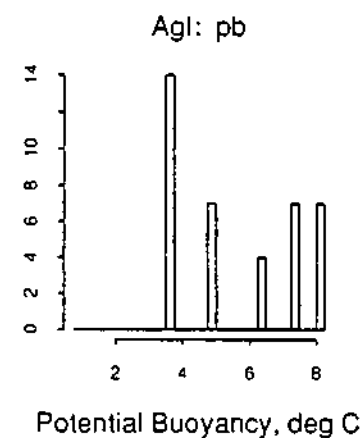
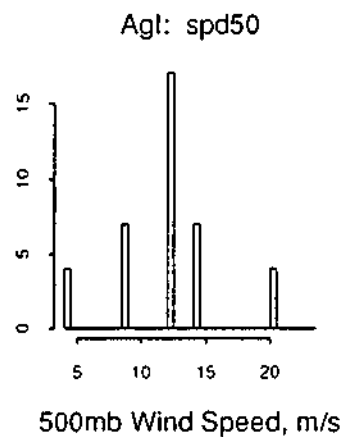
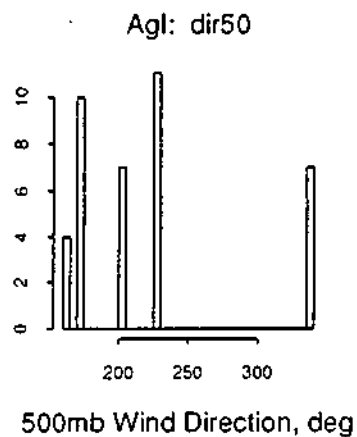


Figure C.7. Histograms of the 500 mb wind direction (dir50) and speed (spd50), and the synoptic (parcel) potential buoyancy (pb).

# PACE89 DATA

Total Sample

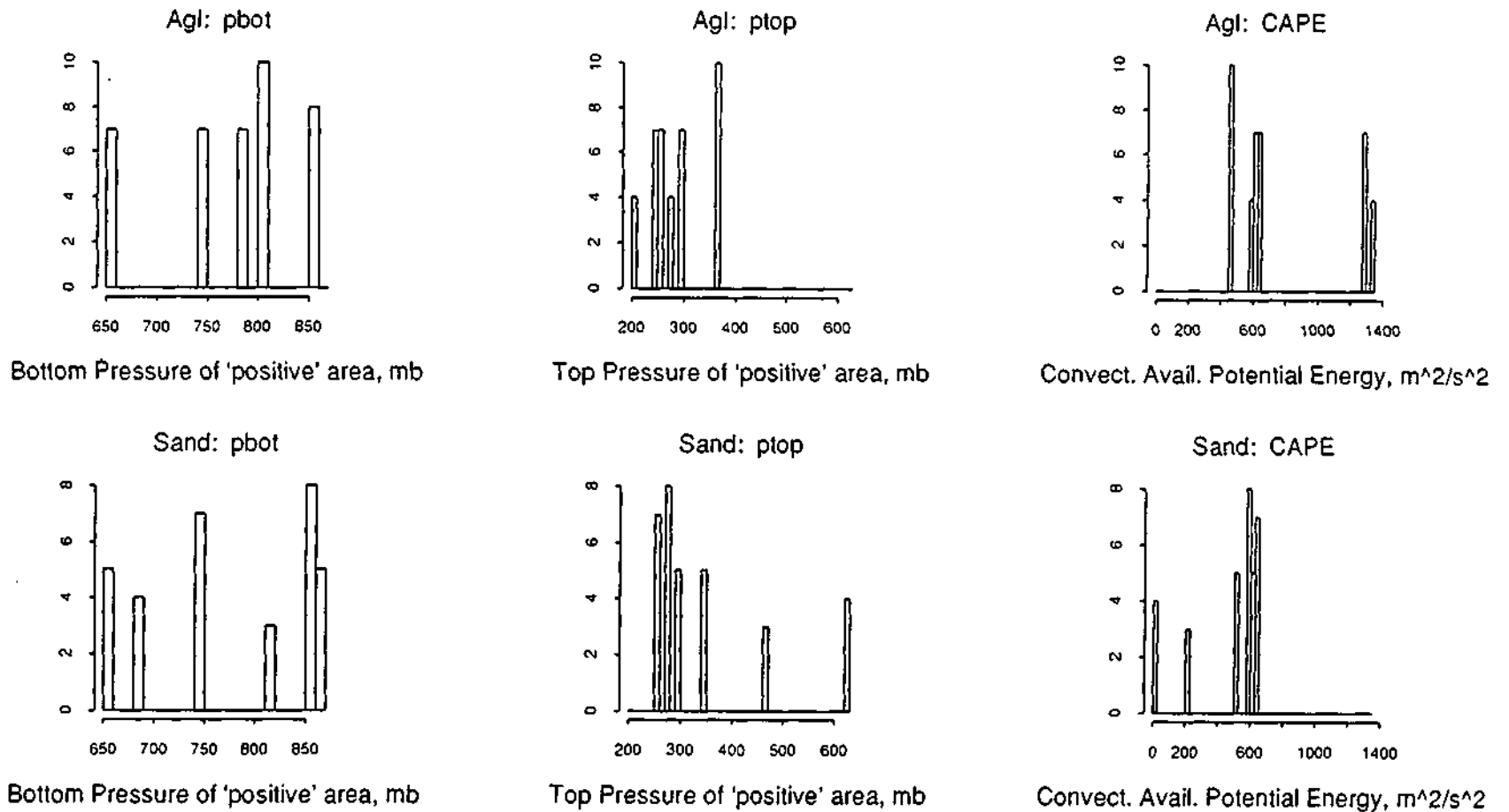


Figure C.8. Histograms of the pressure at the bottom (pbot) and the top (ptop) of the "positive area" of the rawinsonde, and the convective available potential energy (CAPE).

# PACE89 DATA

Total Sample

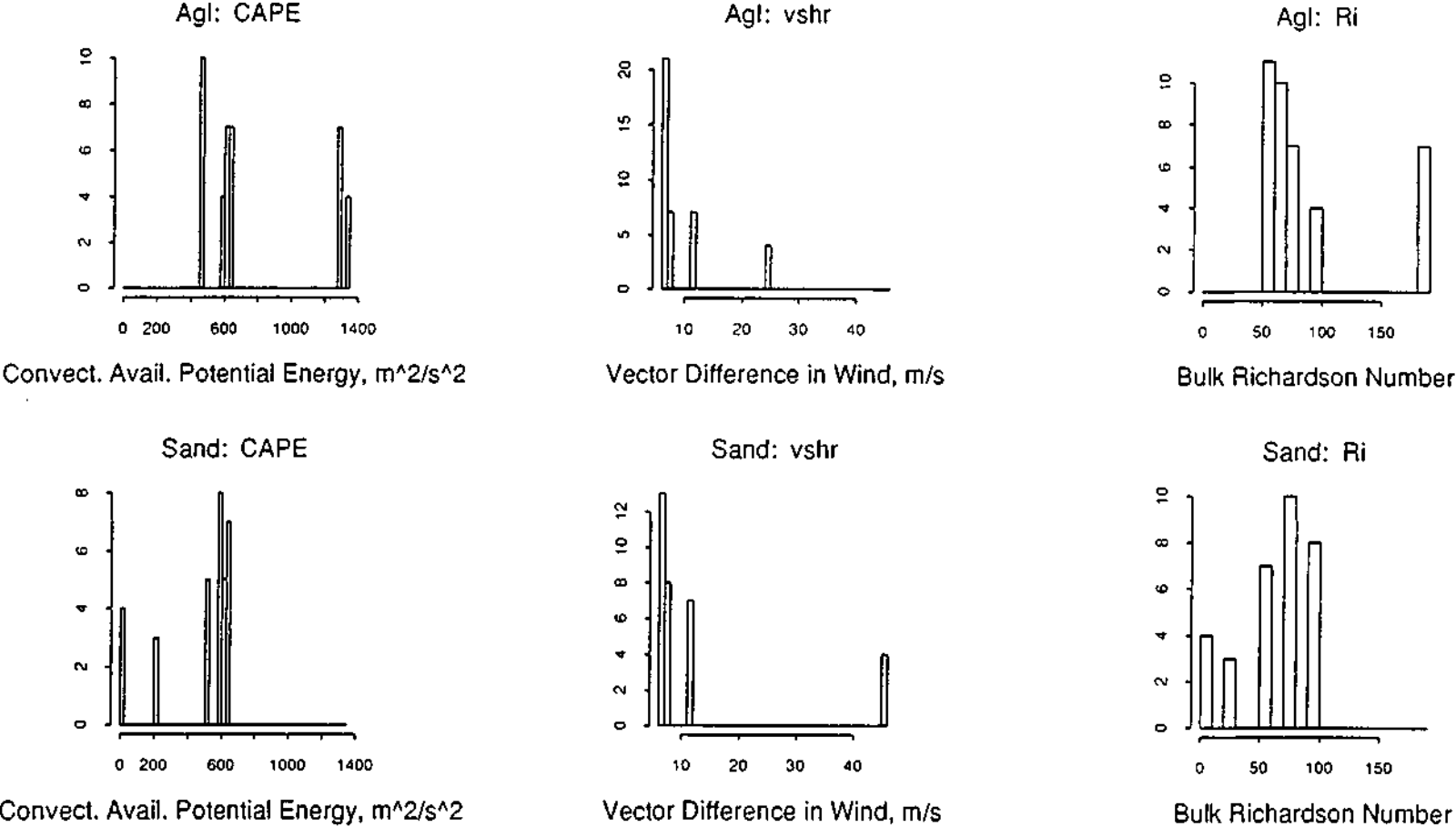


Figure C.9. Histograms of the convective available potential energy (CAPE), the vector difference between the wind at 4 km and the average wind in lowest 500 m (vshr), and the Bulk Richardson number (Ri), calculated using CAPE and vshr.

# PACE89 DATA

## Total Sample

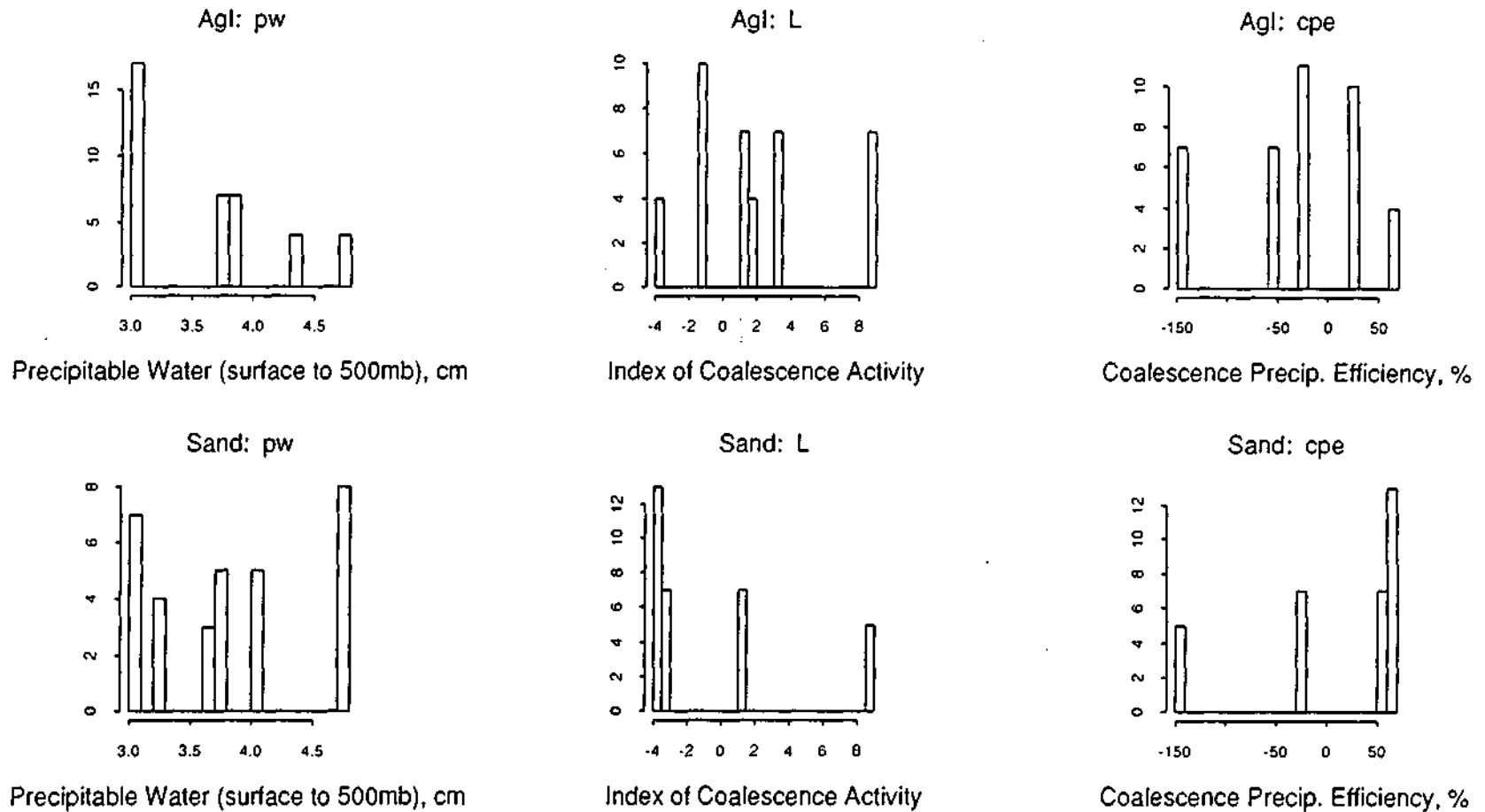


Figure C.10. Histograms of the precipitable water between the surface and 500 mb (pw), the index of coalescence activity (L) (i.e., a raindrop size discriminant function based on tccl and pb), and the coalescence precipitation efficiency (cpe) (i.e., relative size of L).

# PACE89 DATA

## Total Sample

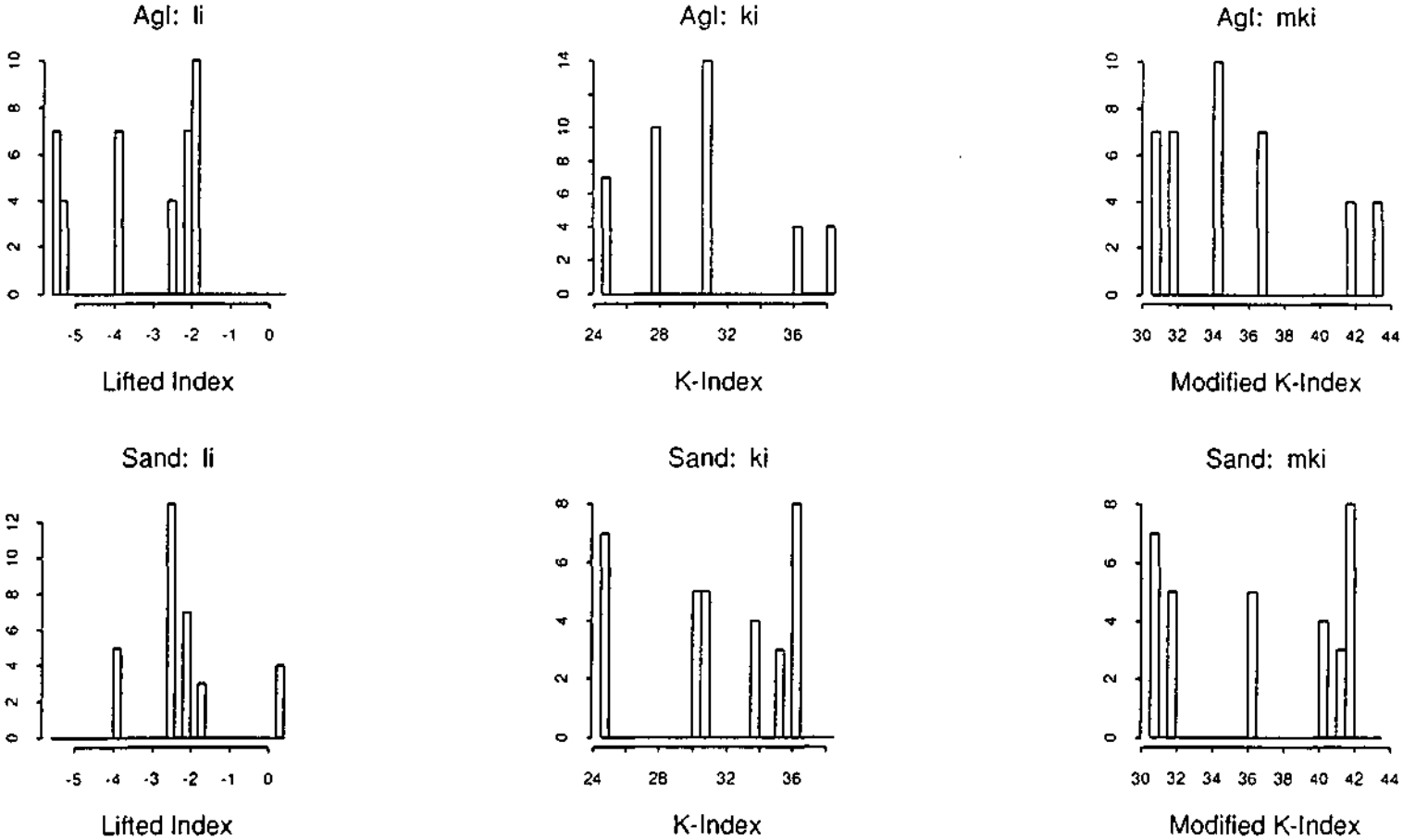


Figure C.11. Histograms of the lifted index (li) (measure of latent instability), the K-index (ki) (heat differential and moisture depth in the lower levels of the atmosphere), and the Modified K-index (mki).

# PACE89 DATA

## Total Sample

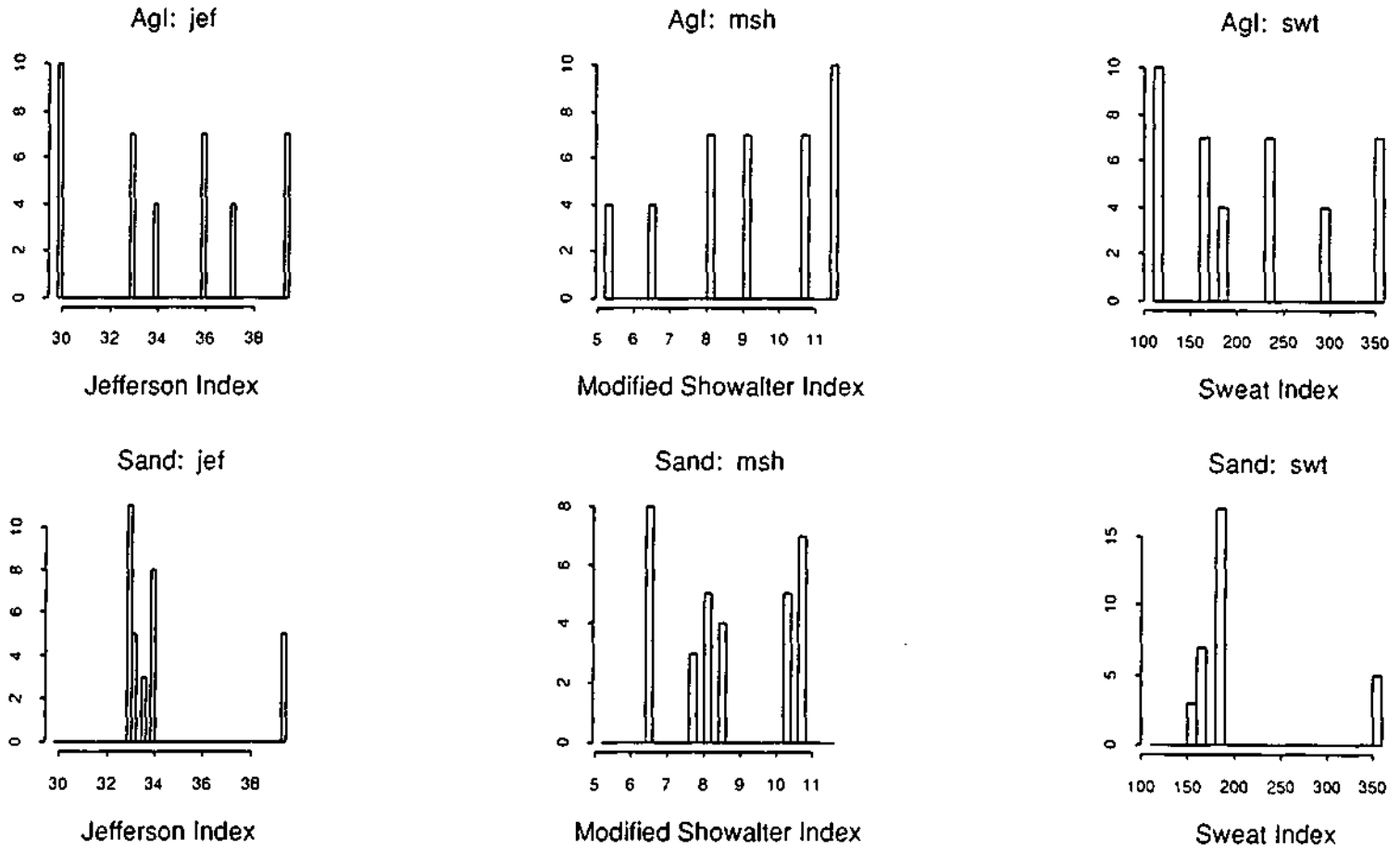


Figure C.12. Histograms of the Jefferson (jef), modified Showalter (msh), and Sweat (swt) indices (measures of instability).

# PACE89 DATA

## Total Sample

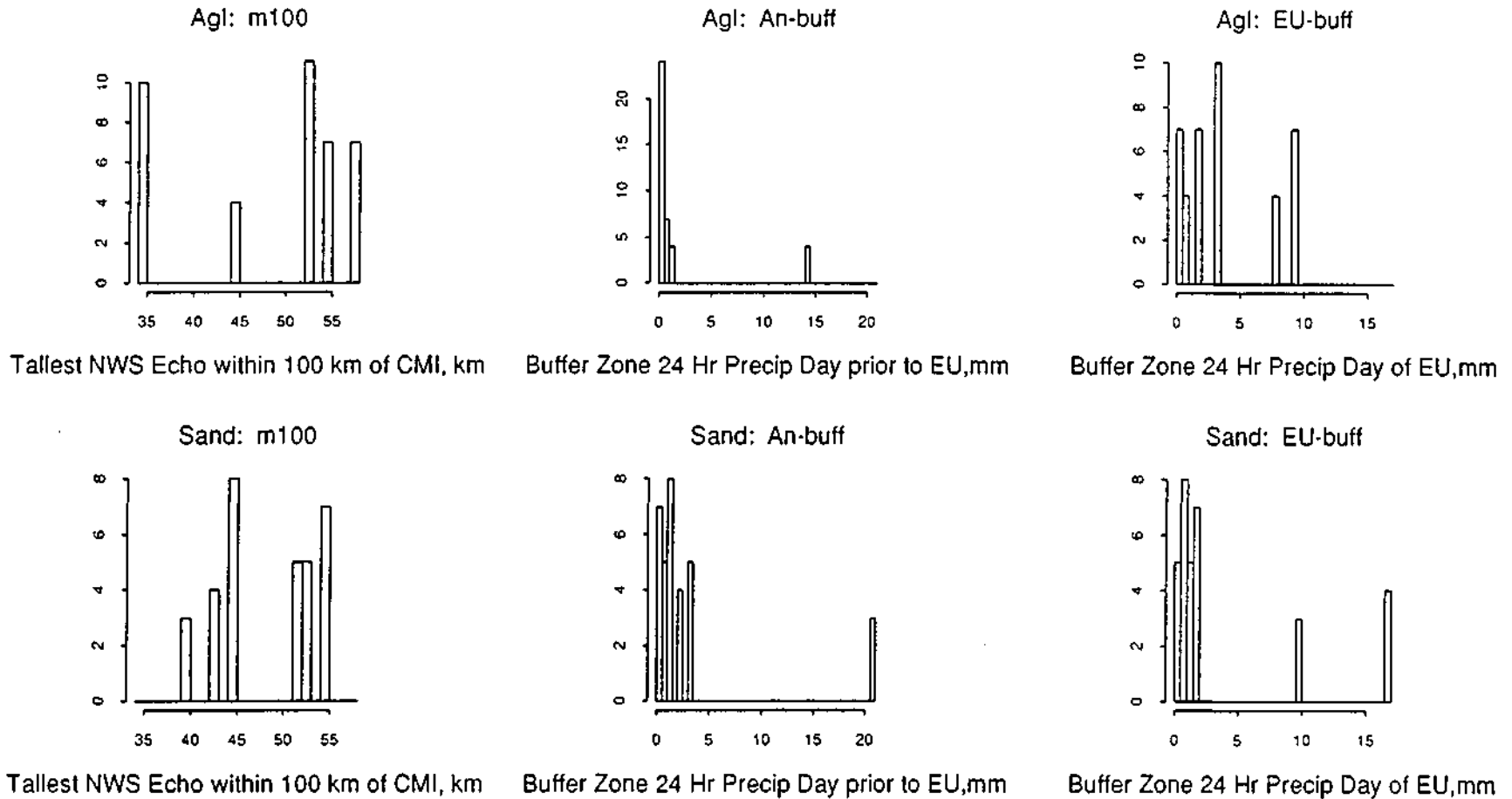


Figure C.13. Histograms of the tallest maximum radar echo top within 100 nm of Champaign (CMI) observed between 1130 and 2030 CDT at the NWS site (MMO, STL, EW) closest to the echo (m100), and of the 80-100 nm radius area (not including Indiana, centered on CMI) 24 hr (80-85% 7:00am obs) station averaged precipitation which fell on the day prior to the experimental unit (An-buff), and the day of the experimental unit (EU-buff).

# PACE89 DATA

## Total Sample

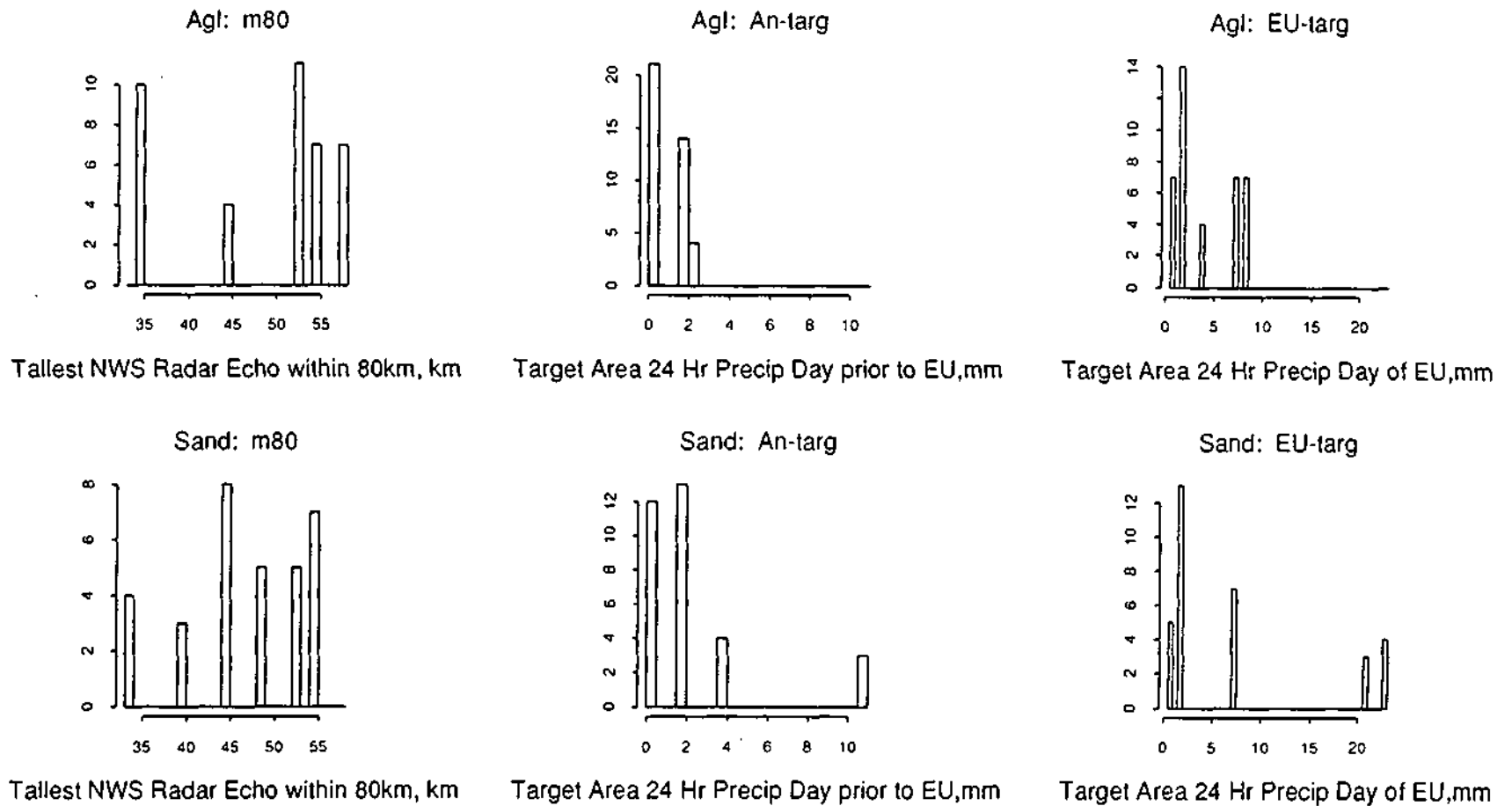


Figure C.14. Histograms of the tallest maximum radar echo top within 80 nm of Champaign (CMI) observed between 1130 and 1830 CDT at the NWS site (MMO, STL, EVV) closest to the echo (m80), and of the 80 nm radius area (not including Indiana, centered on CMI) 24 hr (80-85% 7:00am obs) station averaged precipitation which fell on the day prior to the experimental unit (An-targ), and the day of the experimental unit (EU-targ).

# PACE89 DATA

## Total Sample

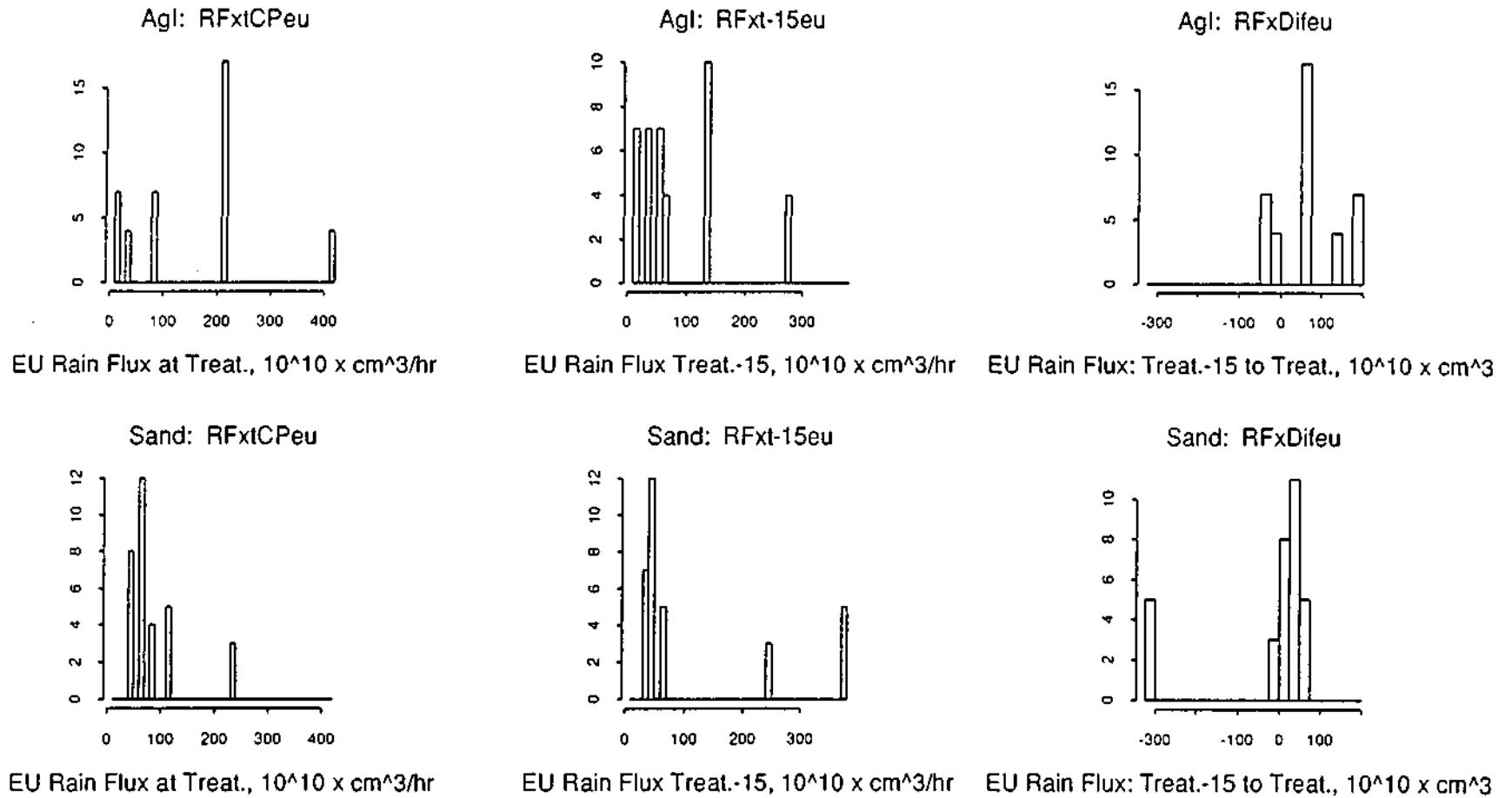


Figure C.15. Histograms of the experimental unit rain flux at first treatment (RFxtCpeu), 15 minutes prior to the first treatment (RFxt-15eu), and the experimental unit rain flux change from 15 minutes prior to first treatment to the first treatment (RFxDifeu).

# PACE89 DATA

## Total Sample

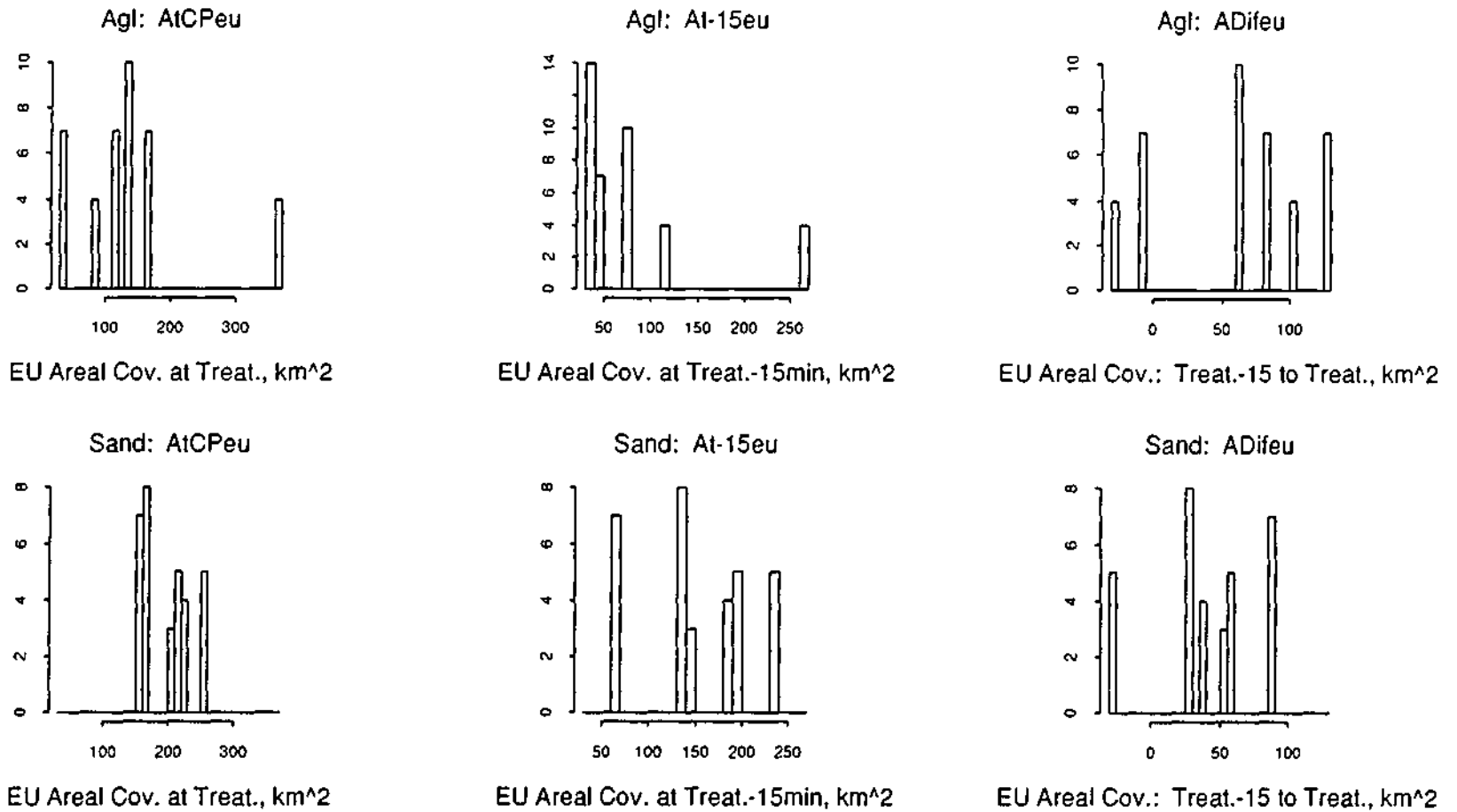


Figure C.16. Histograms of the experimental unit echo areal coverage at first treatment (AtCpeu), 15 minutes prior to the first treatment (At-15eu), and the experimental unit echo areal coverage change from 15 minutes prior to first treatment to the first treatment (ADifeu).

# PACE89 DATA

## Total Sample

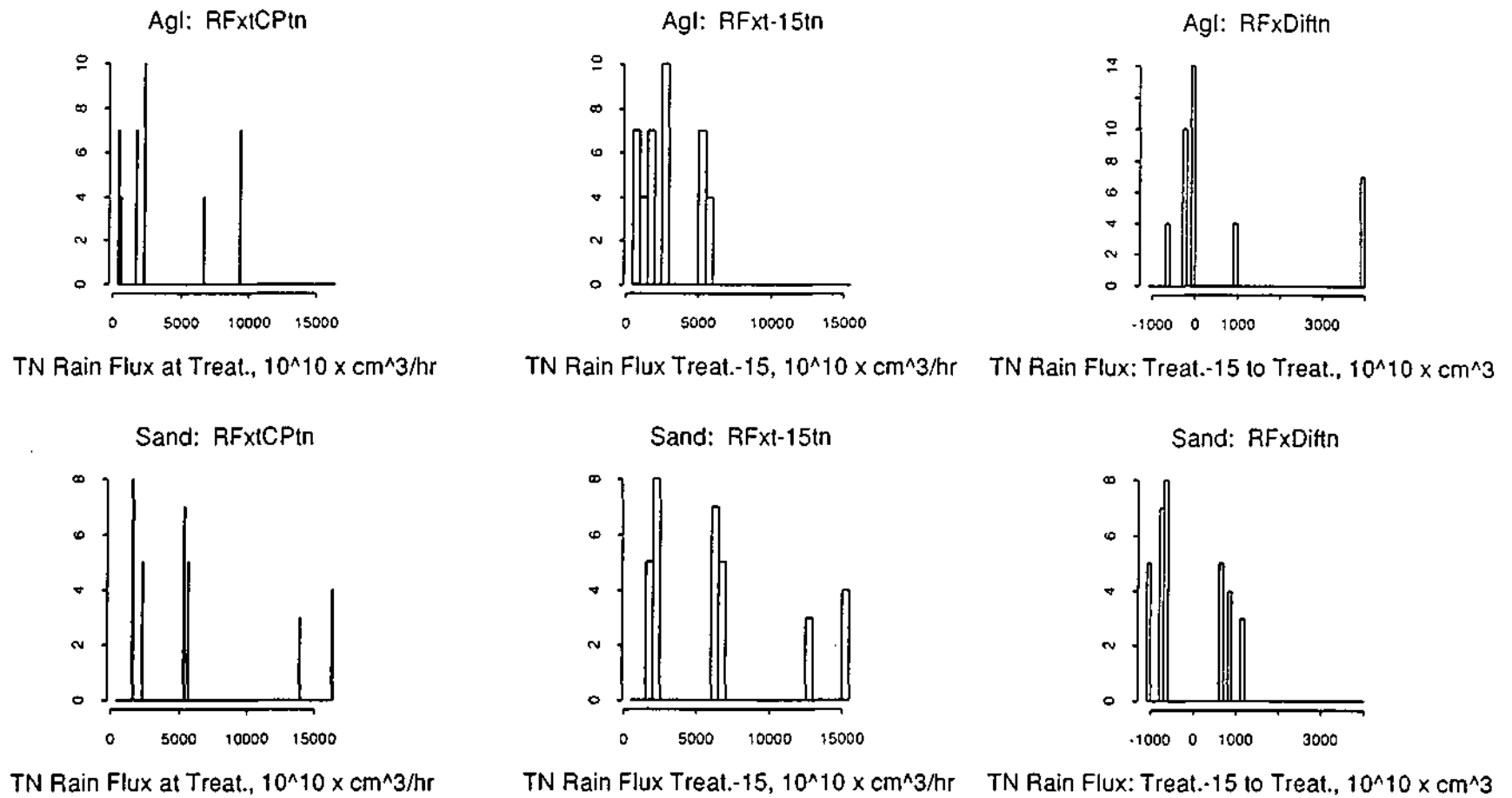


Figure C.17. Histograms of the total network rain flux at first treatment (RFxtCPtn), 15 minutes prior to the first treatment (RFxt-15tn), and the total network rain flux change from 15 minutes prior to first treatment to the first treatment (RFXDiftn).

# PACE89 DATA

## Total Sample

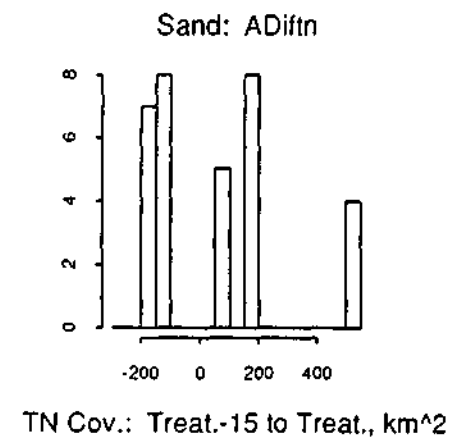
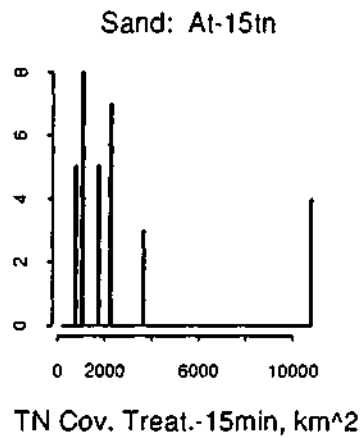
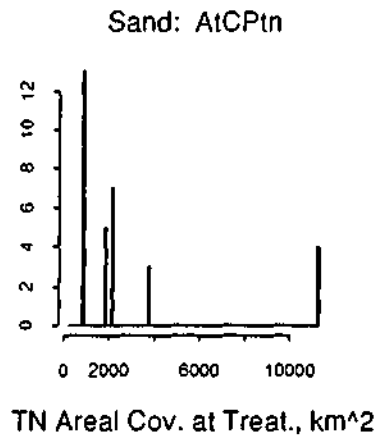
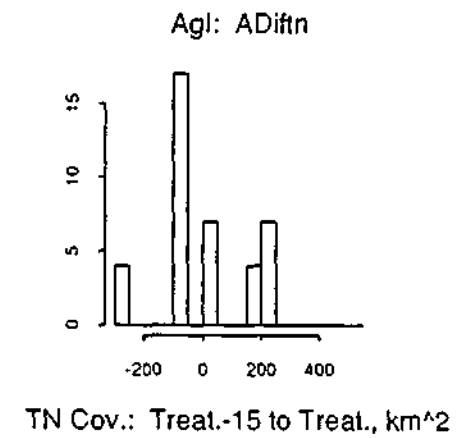
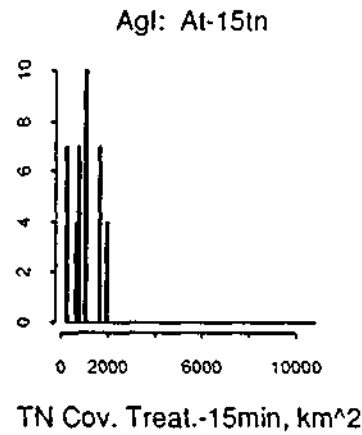
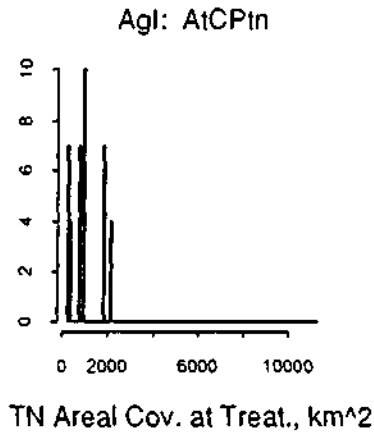


Figure C.18. Histograms of the total network echo areal coverage at first treatment (AtCPtn), 15 minutes prior to the first treatment (At-15tn), and the total network echo areal coverage change from 15 minutes prior to first treatment to the first treatment (ADiftn).

# PACE89 DATA

Total Sample

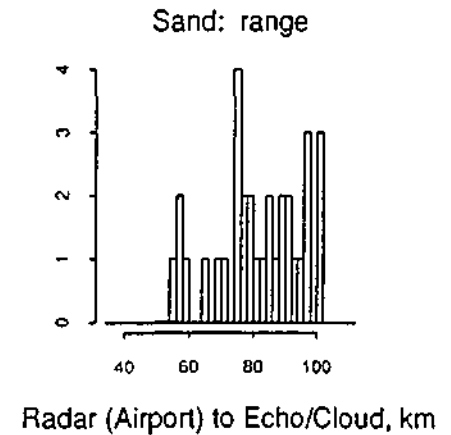
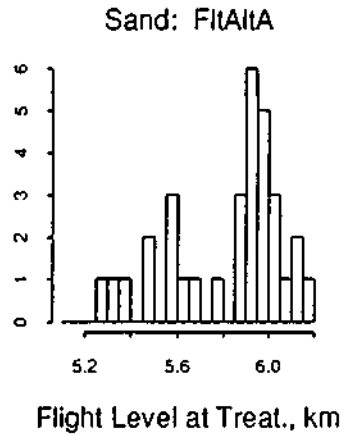
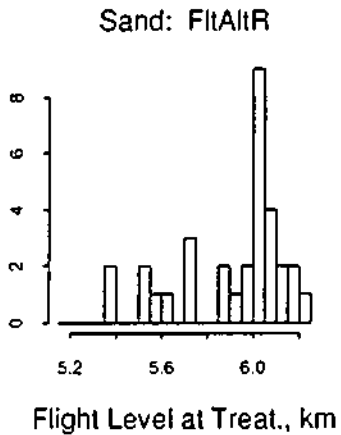
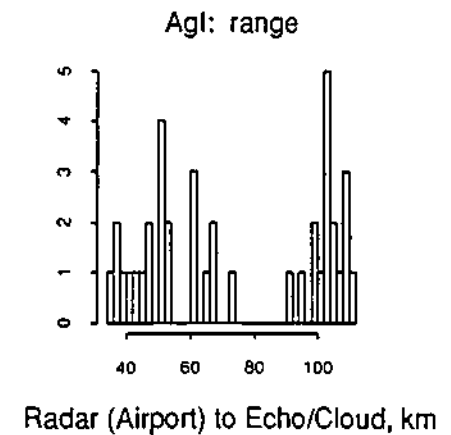
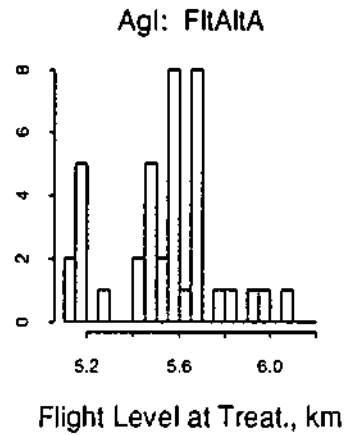
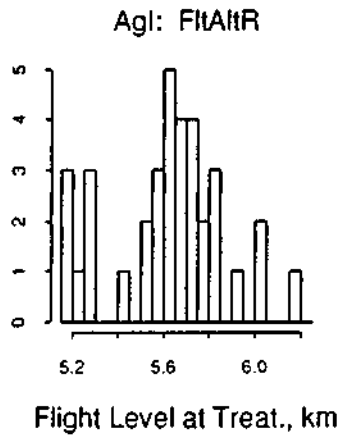


Figure C.19. Histograms of the radar-data (RATS) derived (FltAltR), and aircraft-data derived (FltAltA) aircraft flight level at treatment, and the distance from the Champaign airport (radar site) to the echo/treatment (range).

# PACE89 DATA

## Total Sample

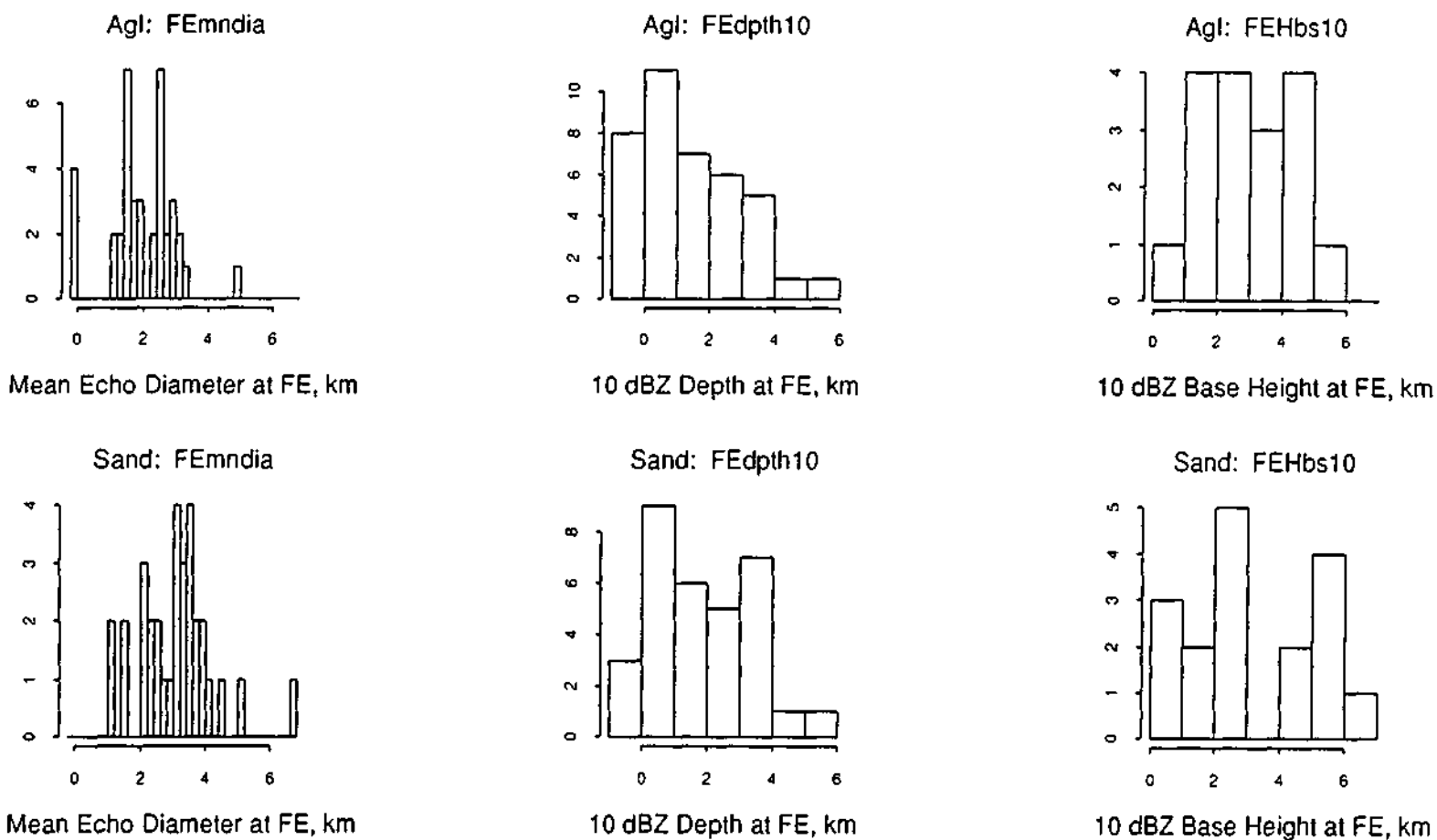


Figure C.20. Histograms of the mean (averaged in height) echo diameter at first echo (FEmndia), the depth of the 10 dBZ contour at first echo (FEdpth10), and the base height of the 10 dBZ contour at first echo (FEHbs10).

# PACE89 DATA

Total Sample

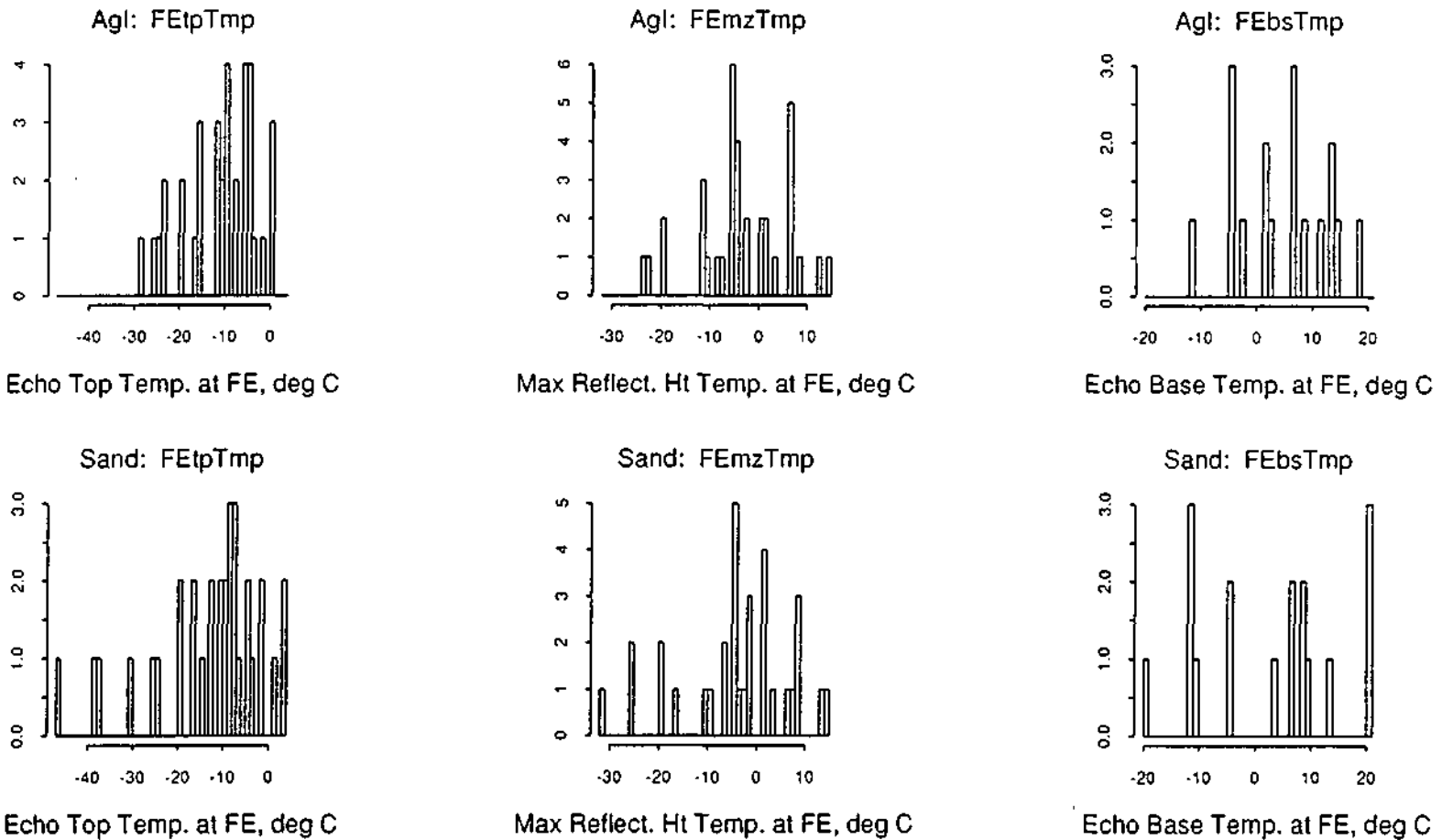


Figure C.21. Histograms of the top of the echo temperature at first echo (FEtpTmp), the temperature at the height of the maximum reflectivity at first echo (FEmzTmp), and the temperature at the base of the echo at first echo (FEbsTmp).

# PACE89 DATA

Total Sample

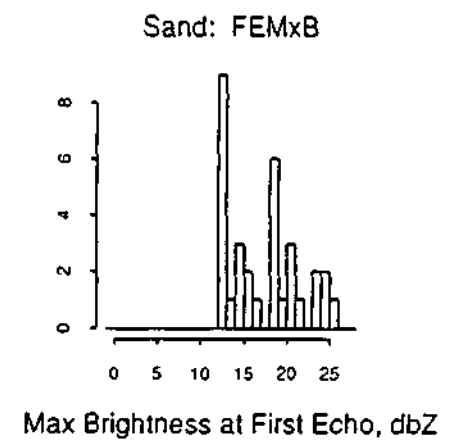
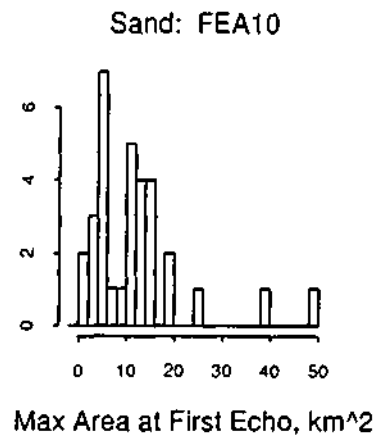
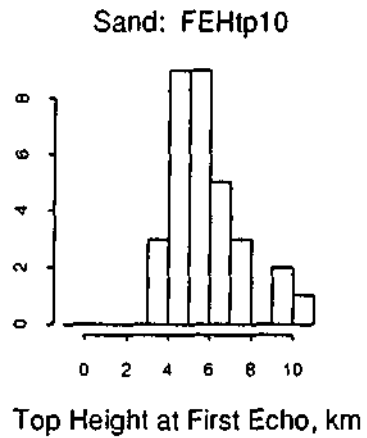
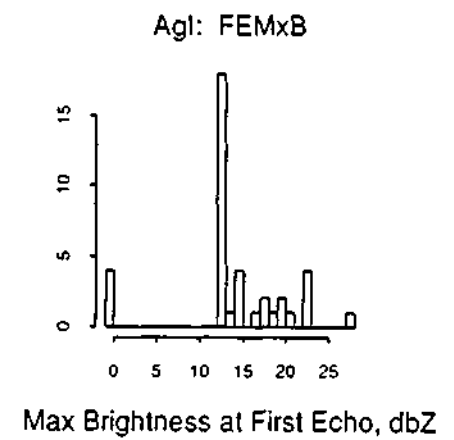
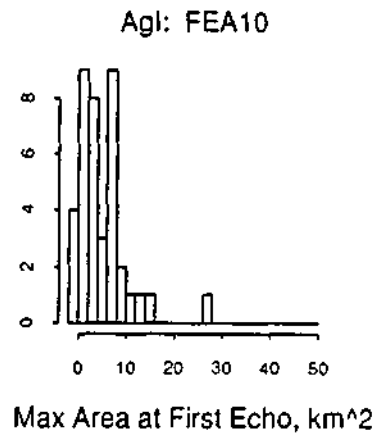
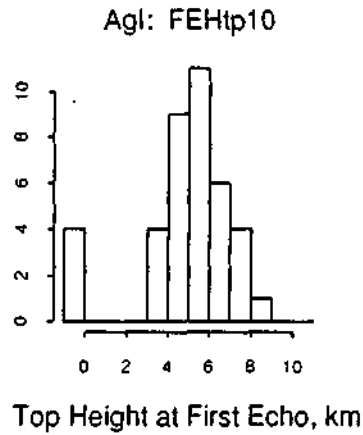


Figure C.22. Histograms of the top height of the 10 dBZ contour at first echo (FEHtp10), the maximum area of the 10 dBZ contour at first echo (FEA10), and the maximum brightness at first echo (FEMxB).

# PACE89 DATA

Total Sample

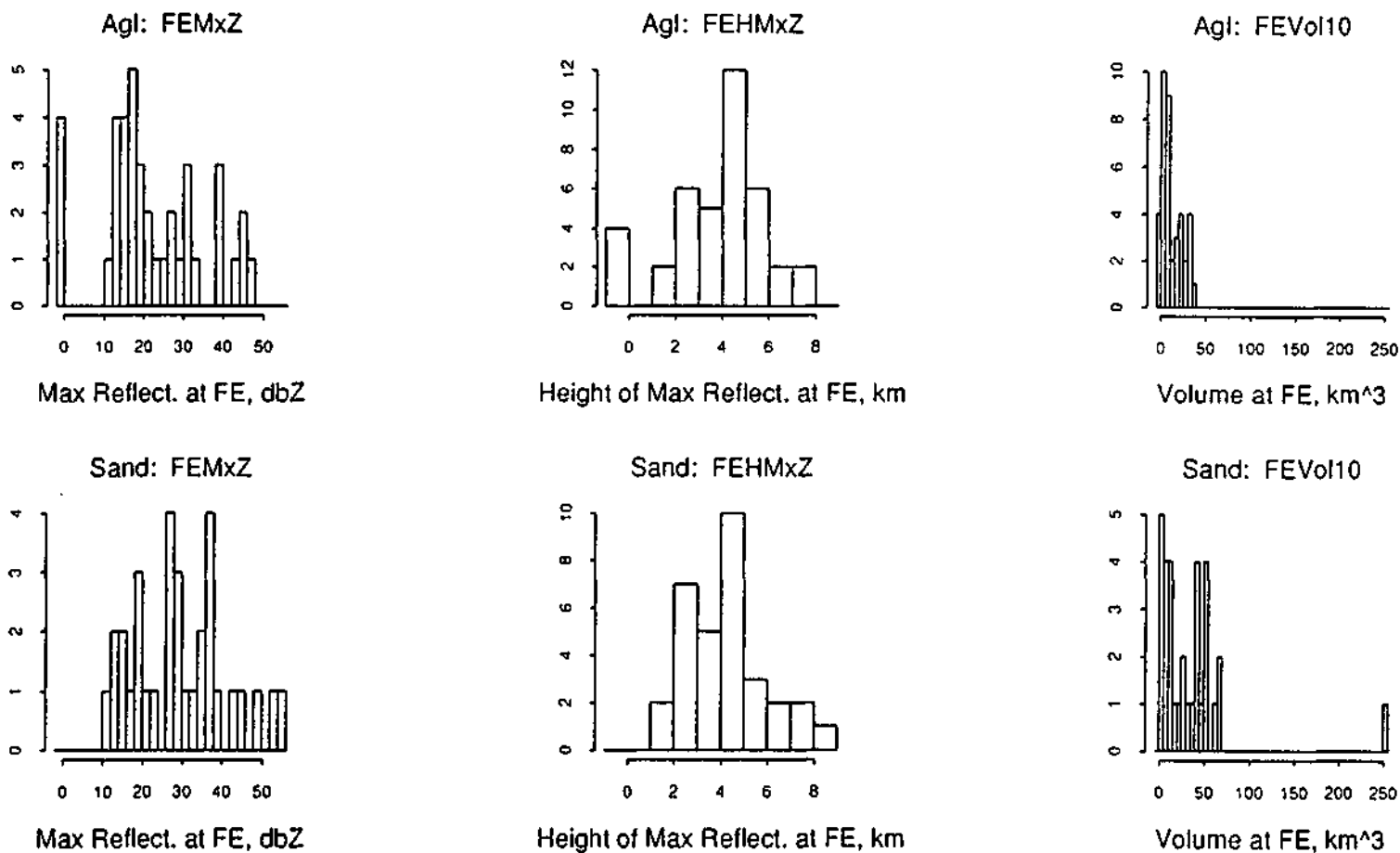


Figure C..23. Histograms of the maximum reflectivity at first echo (FEMxZ), the height of the maximum reflectivity at first echo (FEHMxZ), and the volume of the 10 dBZ contour at first echo (FEVol10).

# PACE89 DATA

## Total Sample

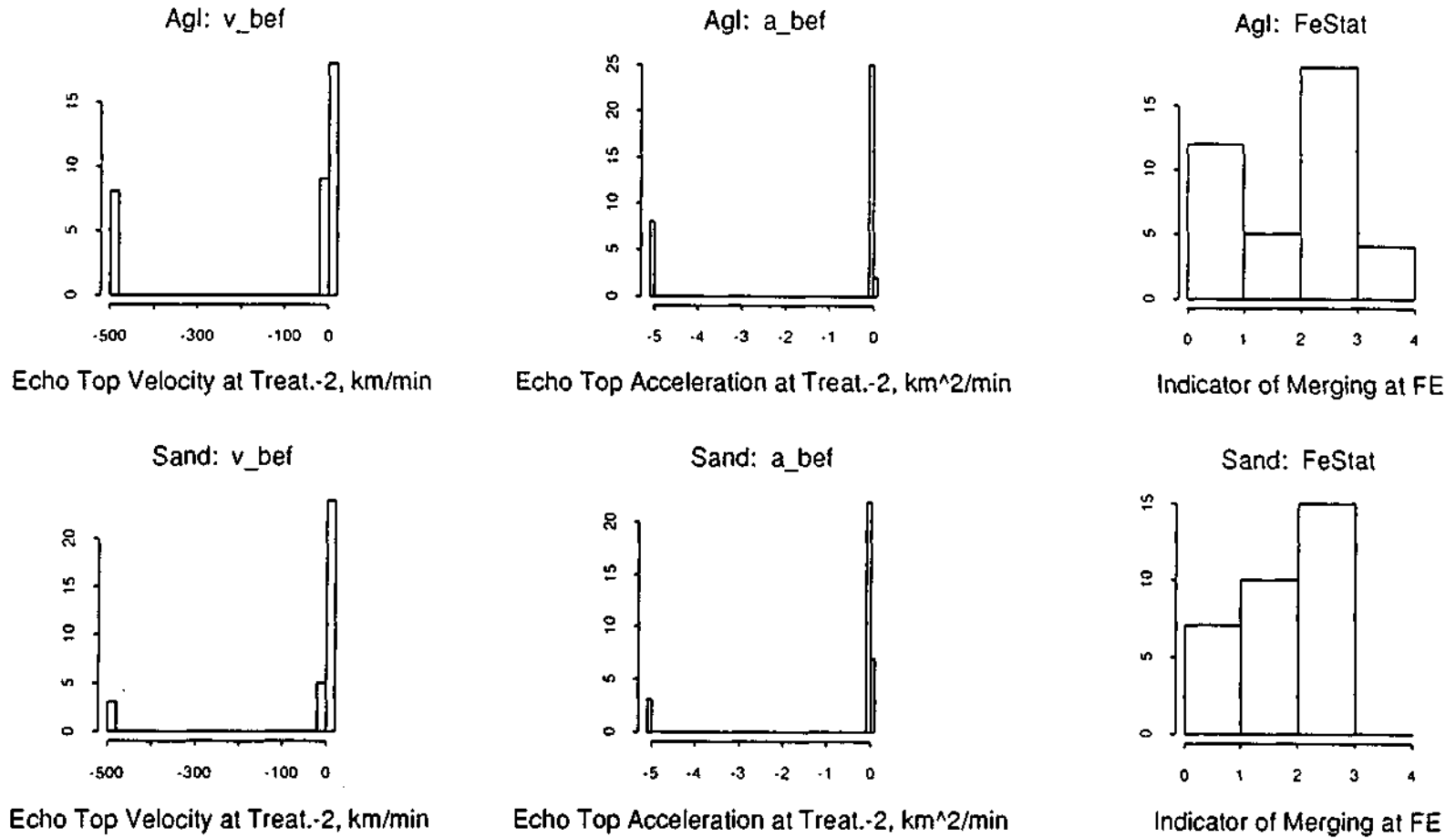


Figure C.24. Histograms of the velocity ( $v_{bef}$ ) and acceleration ( $a_{bef}$ ) of the echo top 2 minutes before treatment, and the indicator of core merging at first echo ( $FeStat$ ) (0 no echo at that time, 1 separate at all levels, 2 joined at some levels but can see base & top, 3 joined at lower levels but can see top, 4 no echo ever).

# PACE89 DATA

## Total Sample

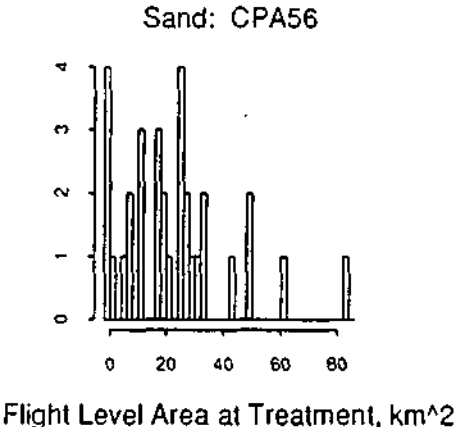
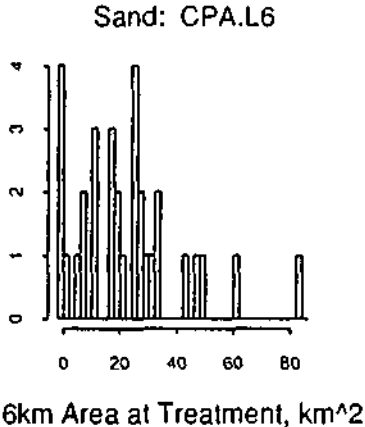
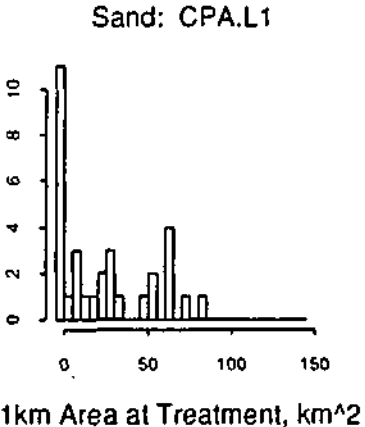
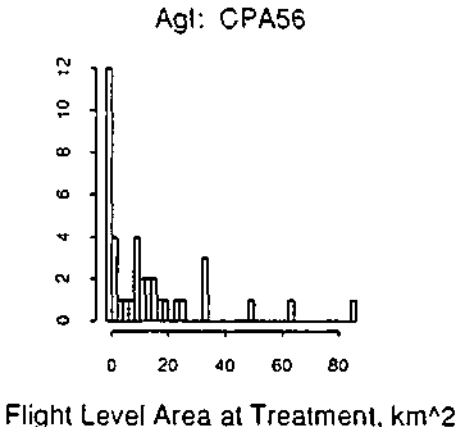
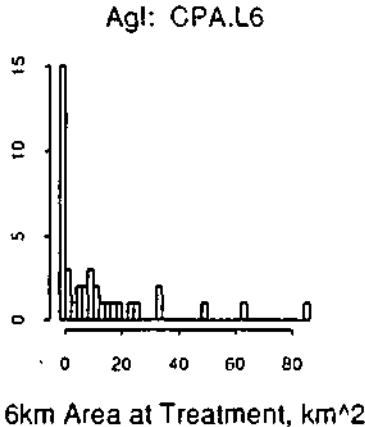
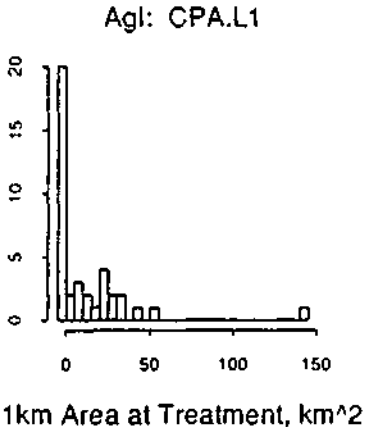


Figure C.25. Histograms of the 1 kilometer (CPA.L1), 6 kilometer (CPA.L6), and flight level (CPA56) areas at treatment.

# PACE89 DATA

## Total Sample

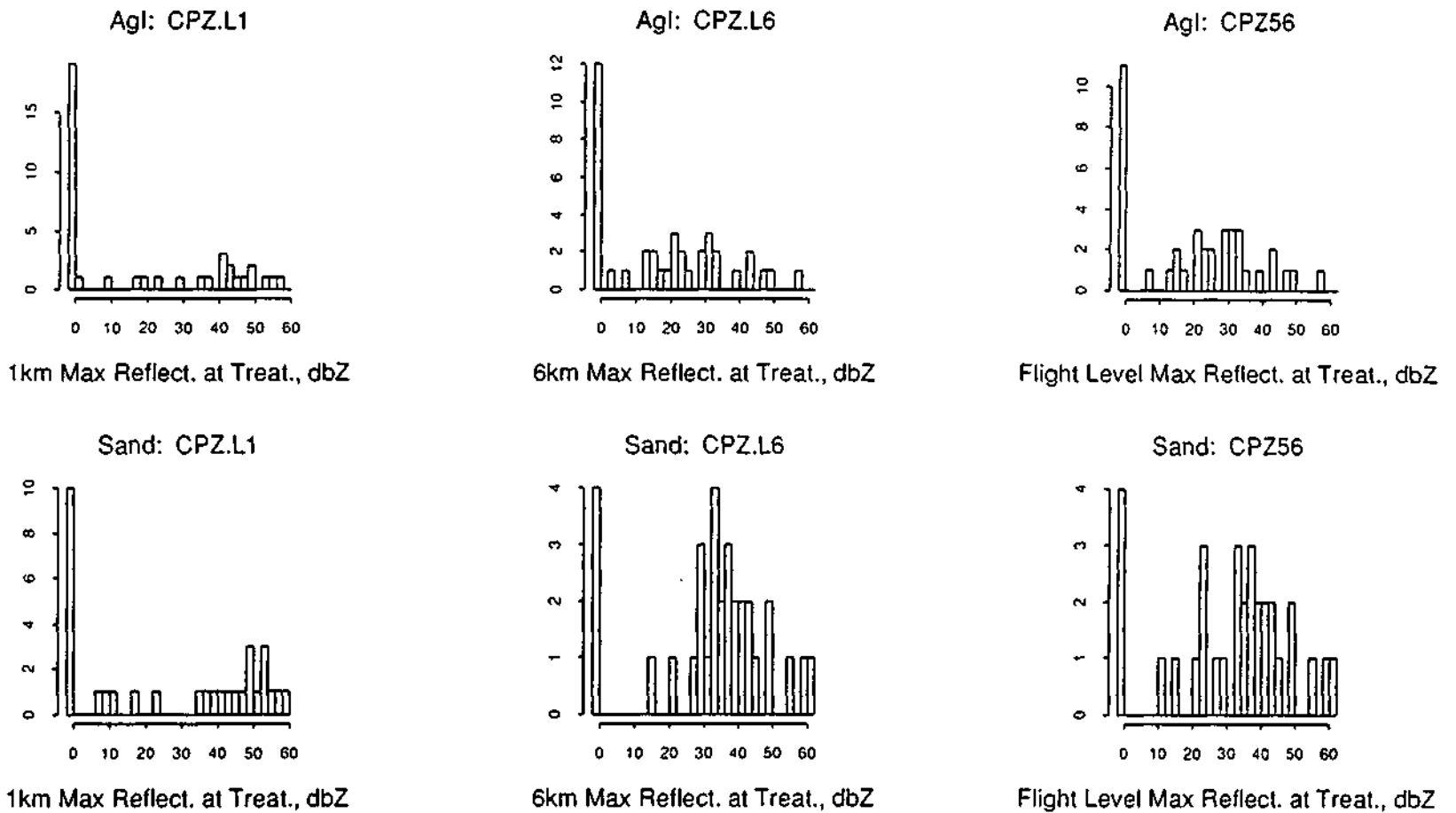


Figure C.26. Histograms of the 1 kilometer (CPZ.L1), 6 kilometer (CPZ.L6), and flight level (CPZ56) maximum reflectivities at treatment.

# PACE89 DATA

## Total Sample

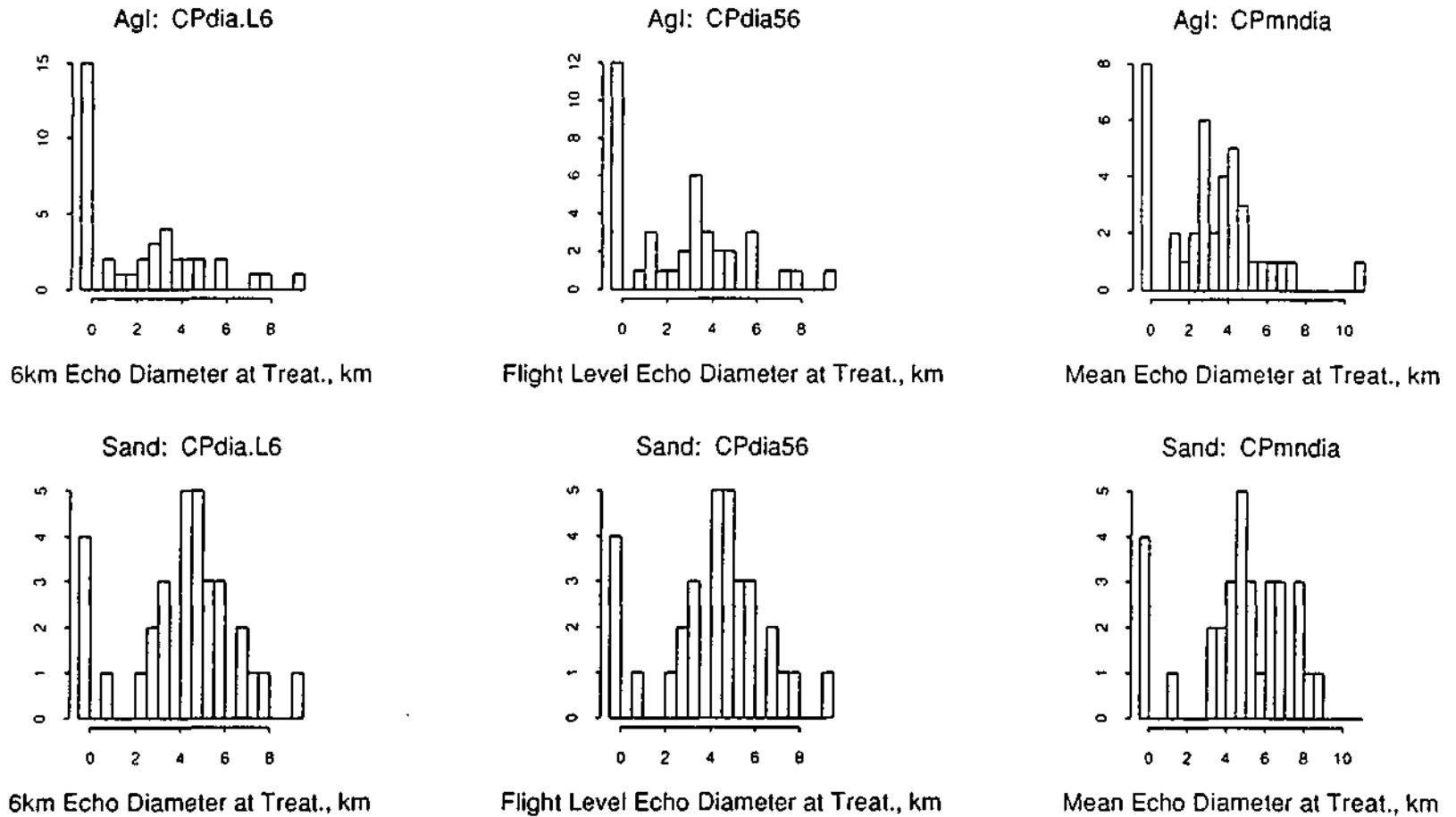


Figure C.27. Histograms of the 6 kilometer (CPdia.L6) and flight level (CPdia56) echo diameters at treatment, and the mean (averaged in height) echo diameter at treatment (CPmndia).

# PACE89 DATA

## Total Sample

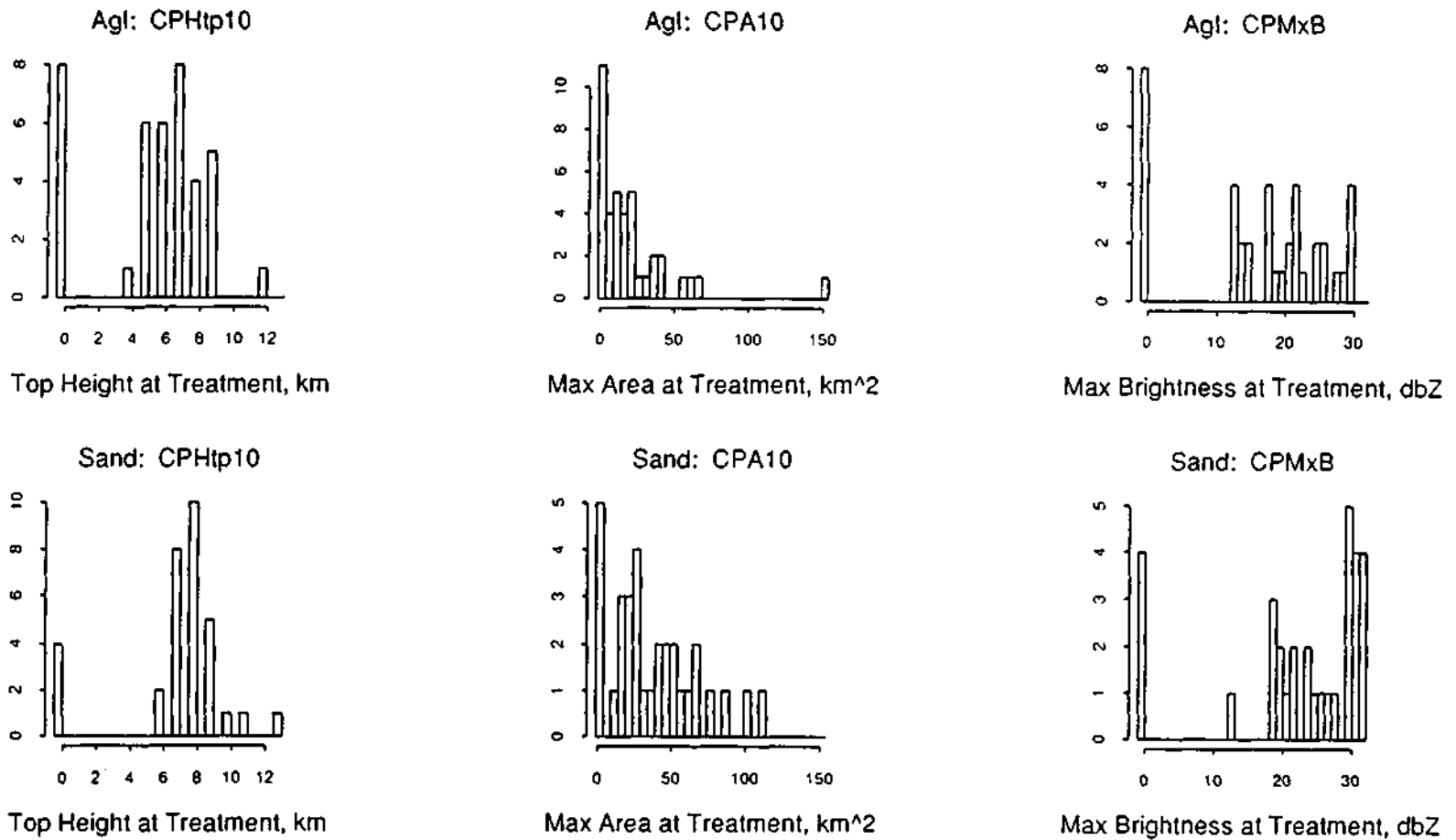


Figure C.28. Histograms of the top height of the 10 dBZ contour at treatment (CPHtp10), the maximum area of the 10 dBZ contour at treatment (CPA10), and the maximum brightness at treatment (CPMxB).

# PACE89 DATA

## Total Sample

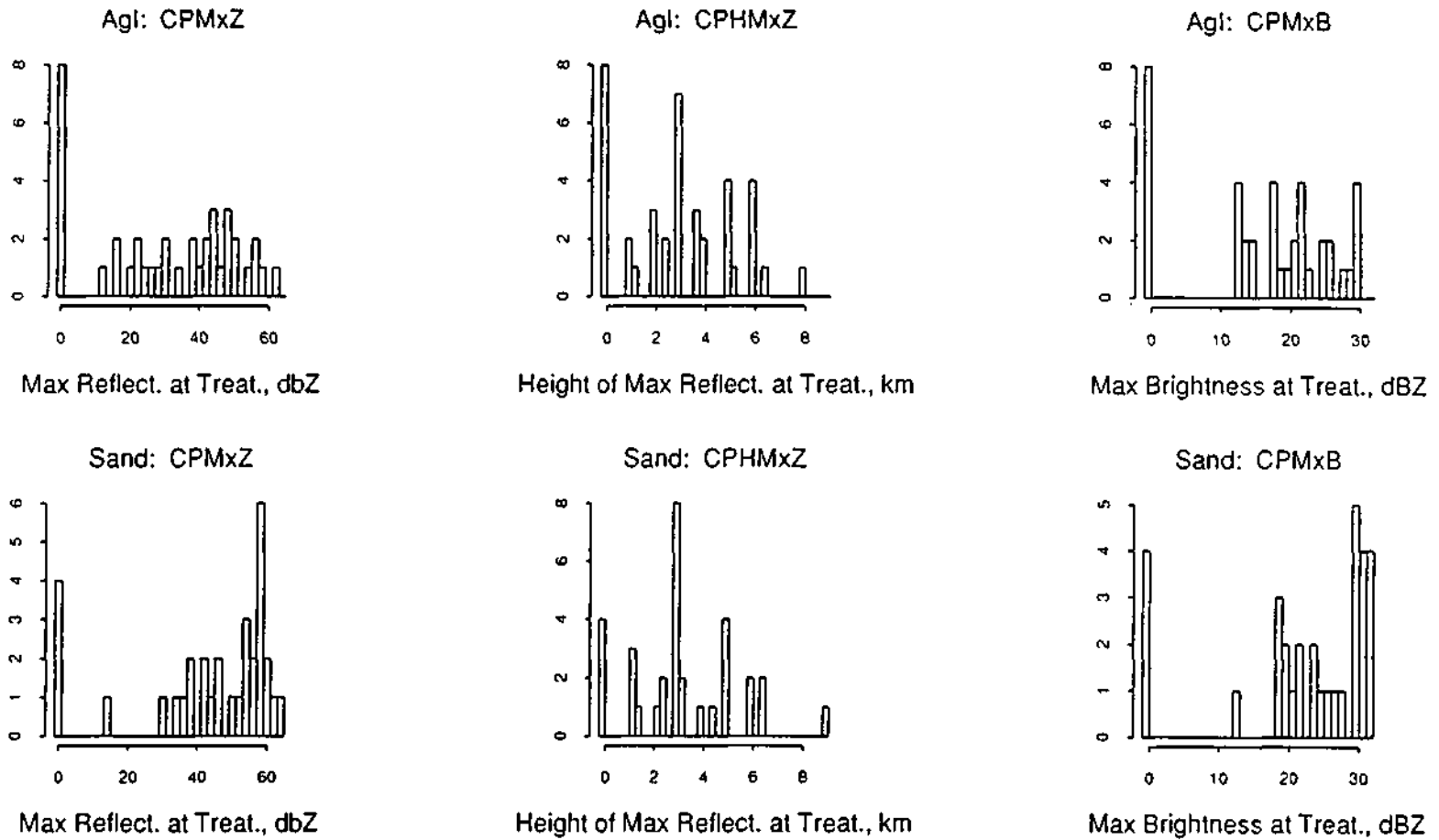


Figure C.29. Histograms of the maximum reflectivity at treatment (CPMxZ), the height of the maximum reflectivity at treatment (CPHMxZ), and the maximum brightness at treatment (CPMxB).

# PACE89 DATA

## Total Sample

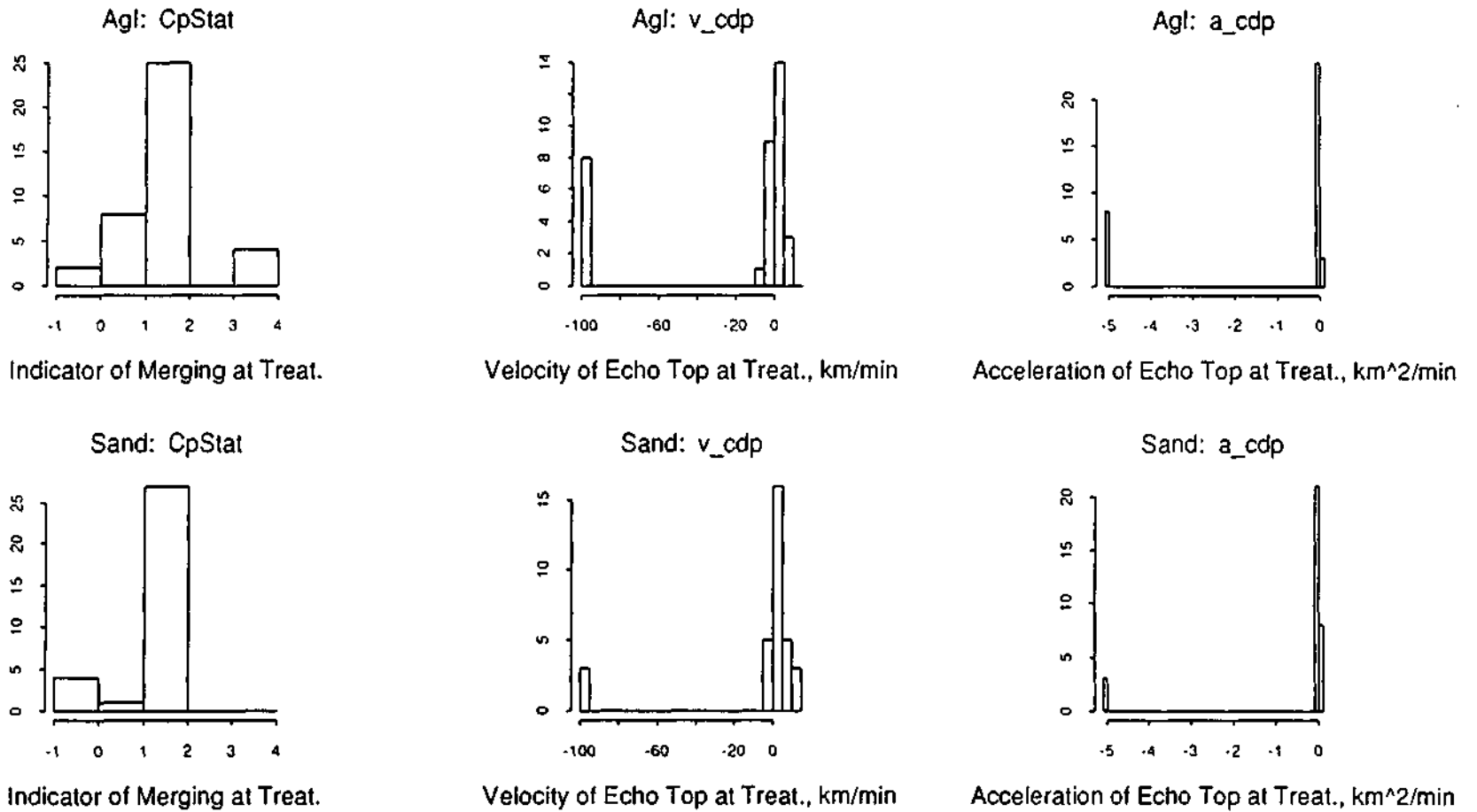


Figure C.30. Histograms of the indicator of core merging at treatment (CpStat) (0 = no echo at that time, 1 = isolated, 2 = merged, 4 = no echo ever), and the velocity (v\_cdp) and acceleration (a\_cdp) of the echo top at treatment.

# PACE89 DATA

Total Sample

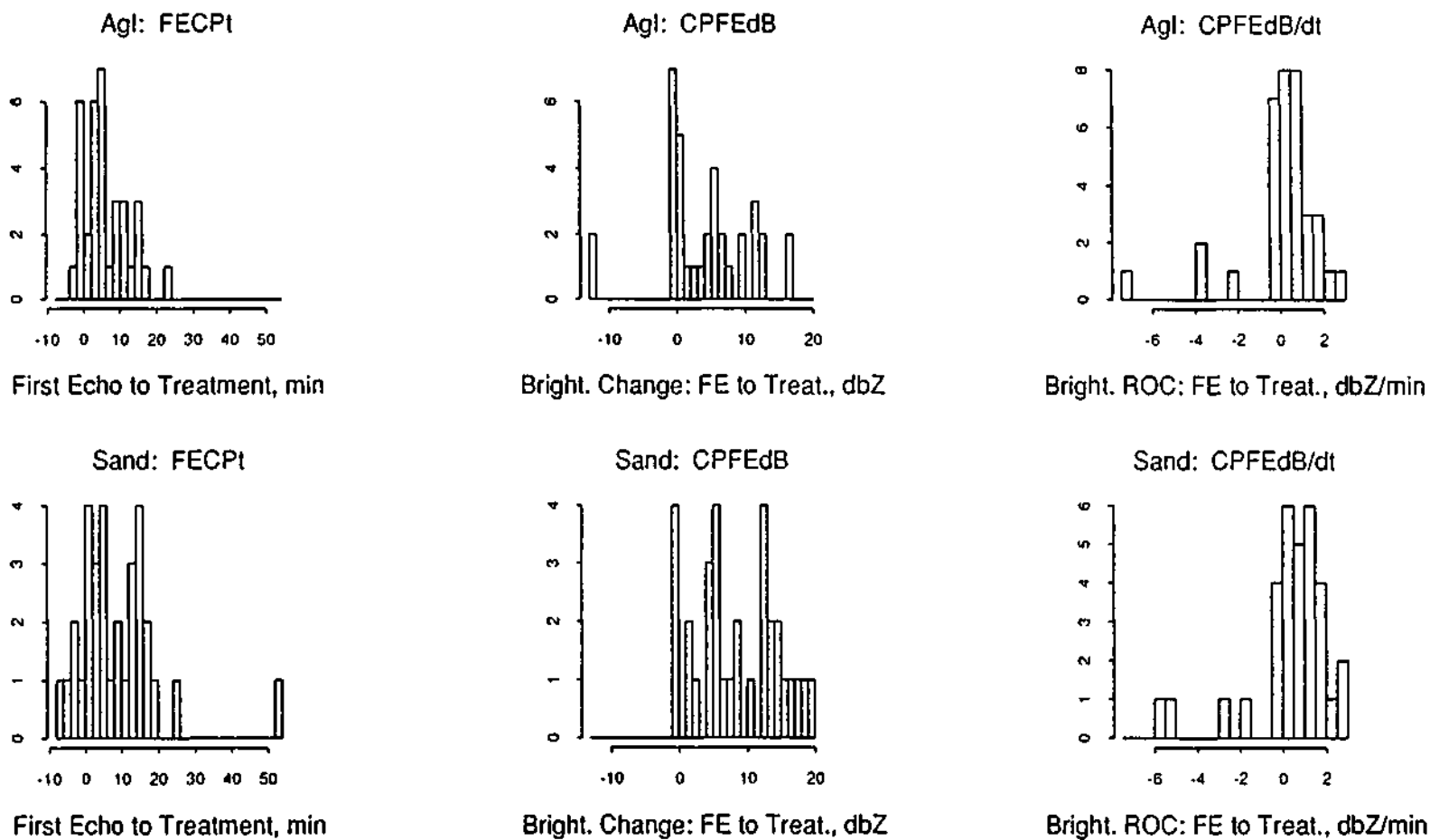


Figure C.31. Histograms of the time from first echo to treatment (FECPt), the change in maximum brightness from first echo to treatment (CPFEdB), and the rate of change of maximum brightness from first echo to treatment (CPFEdB/dt).

# PACE89 DATA

## Total Sample

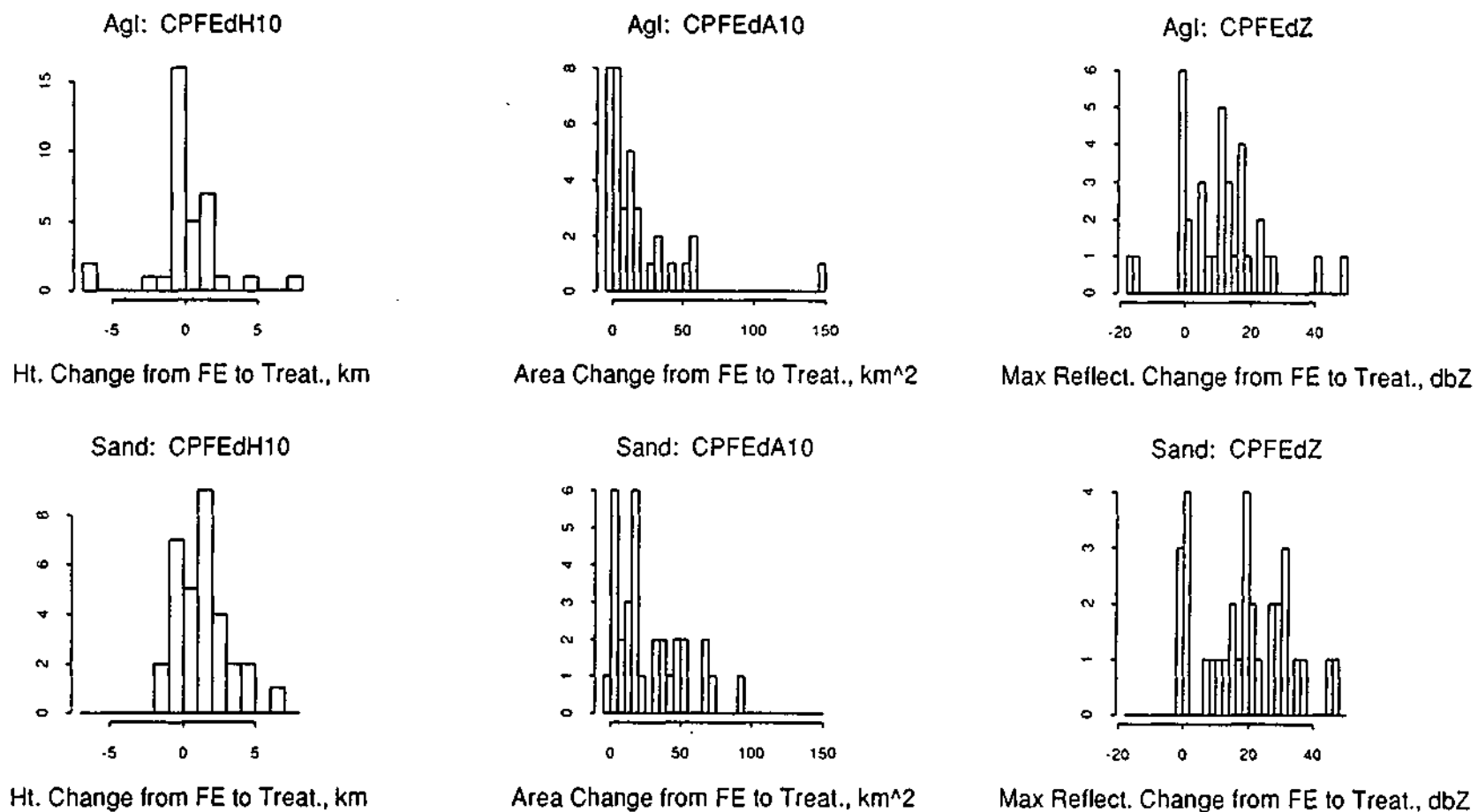


Figure C.32. Histograms of the change in top height of the 10 dBZ contour from first echo to treatment (CPFEdH10), the change in area of the 10 dBZ contour from first echo to treatment (CPFEdA10), and the change in maximum reflectivity from first echo to treatment (CPFEdZ).

# PACE89 DATA

## Total Sample

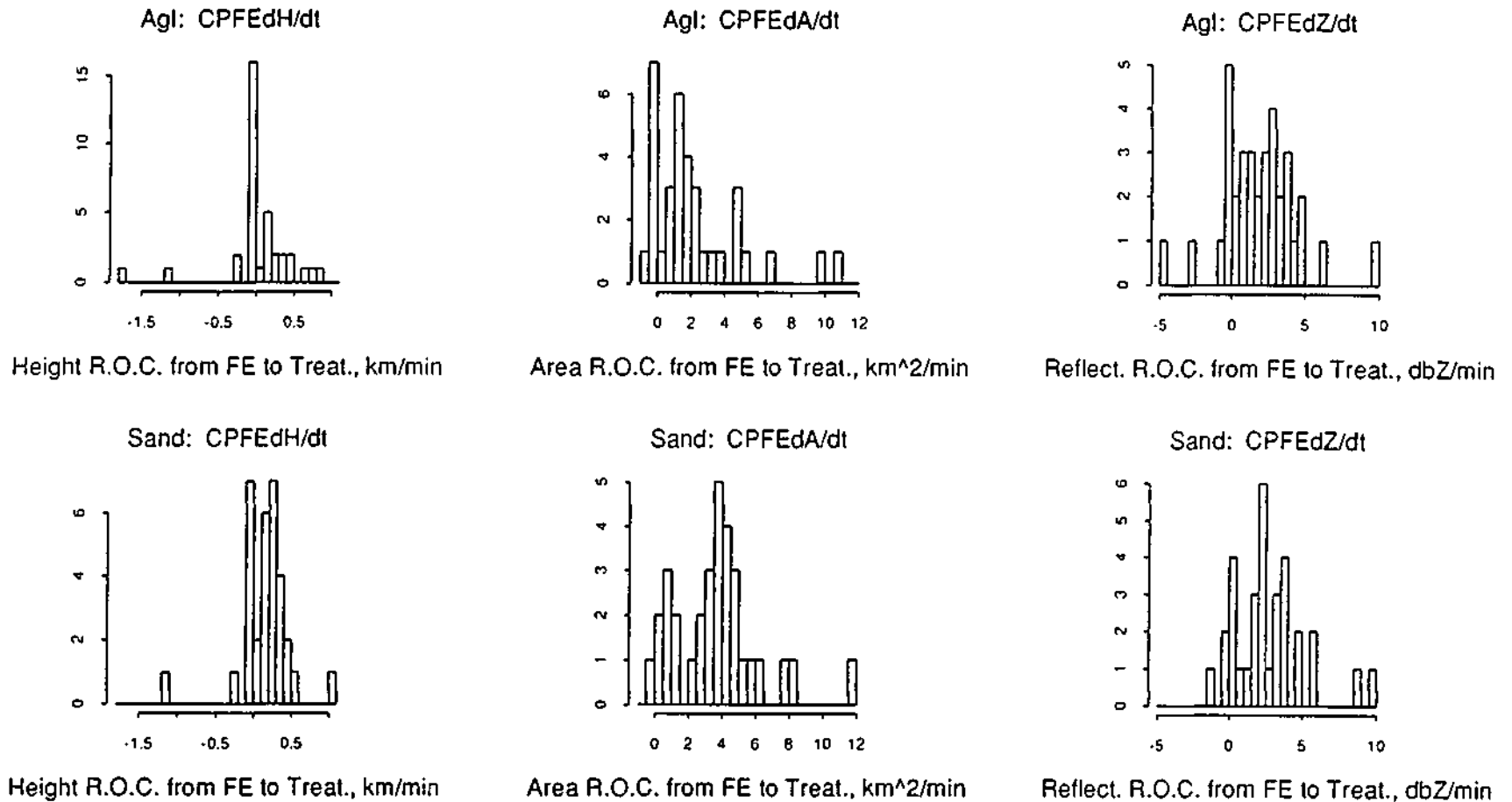


Figure C.33. Histograms of the rate of change of the 10 dBZ echo top height from first echo to treatment (CPFEdH/dt), the rate of change of maximum area of the 10 dBZ contour from first echo to treatment (CPFEdA/dt), and the rate of change of maximum reflectivity from first echo to treatment (CPFEdZ/dt).

# PACE89 DATA

Total Sample

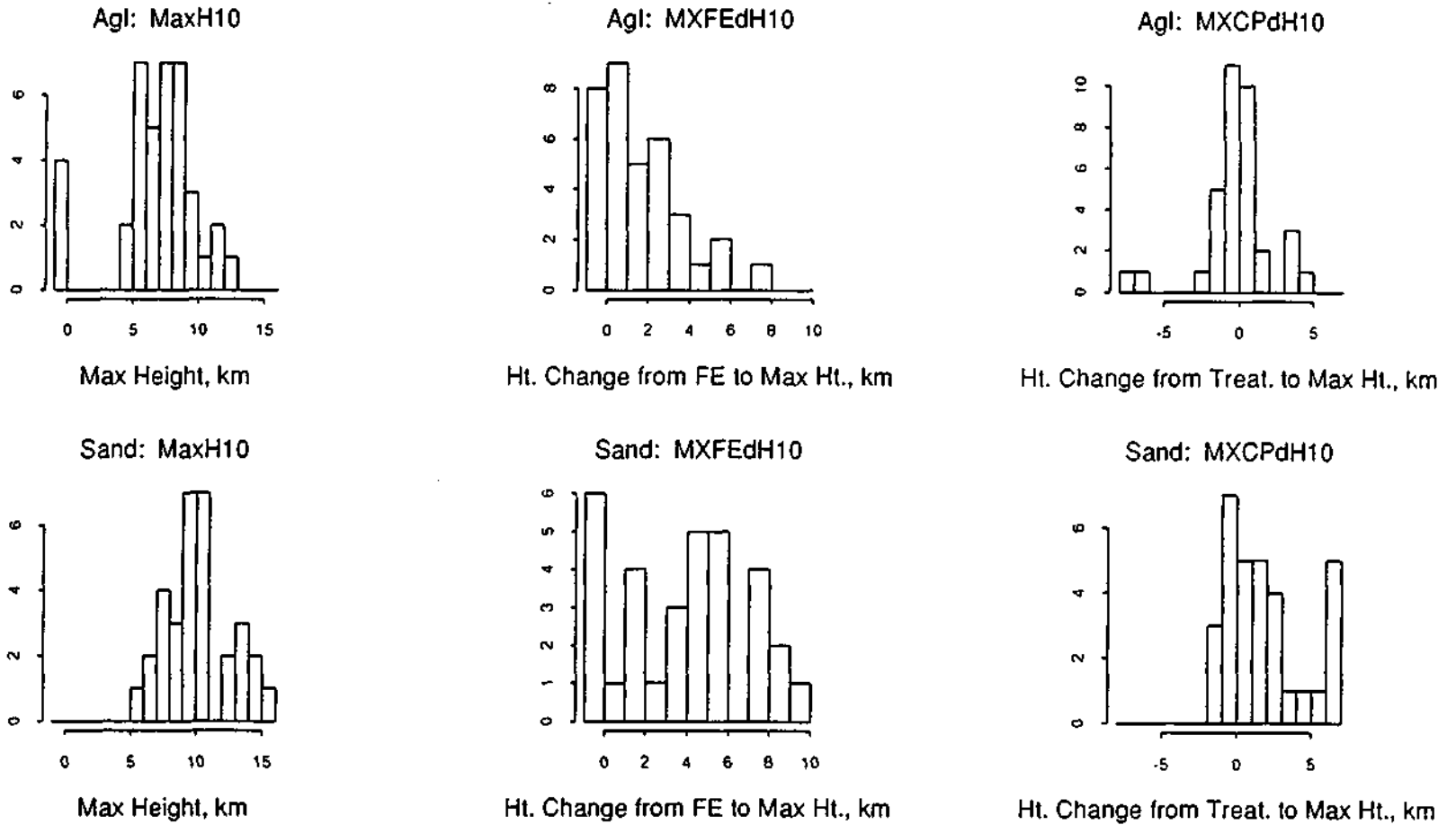


Figure C.34. Histograms of the maximum top height of the 10 dBZ contour of the echo (MaxH10), the change in top height of the 10 dBZ contour from first echo to the maximum height of the echo core (MXFEdH10), and the change in top height of the 10 dBZ contour from treatment to the maximum height of the echo (MXCPdH10).

# PACE89 DATA

## Total Sample

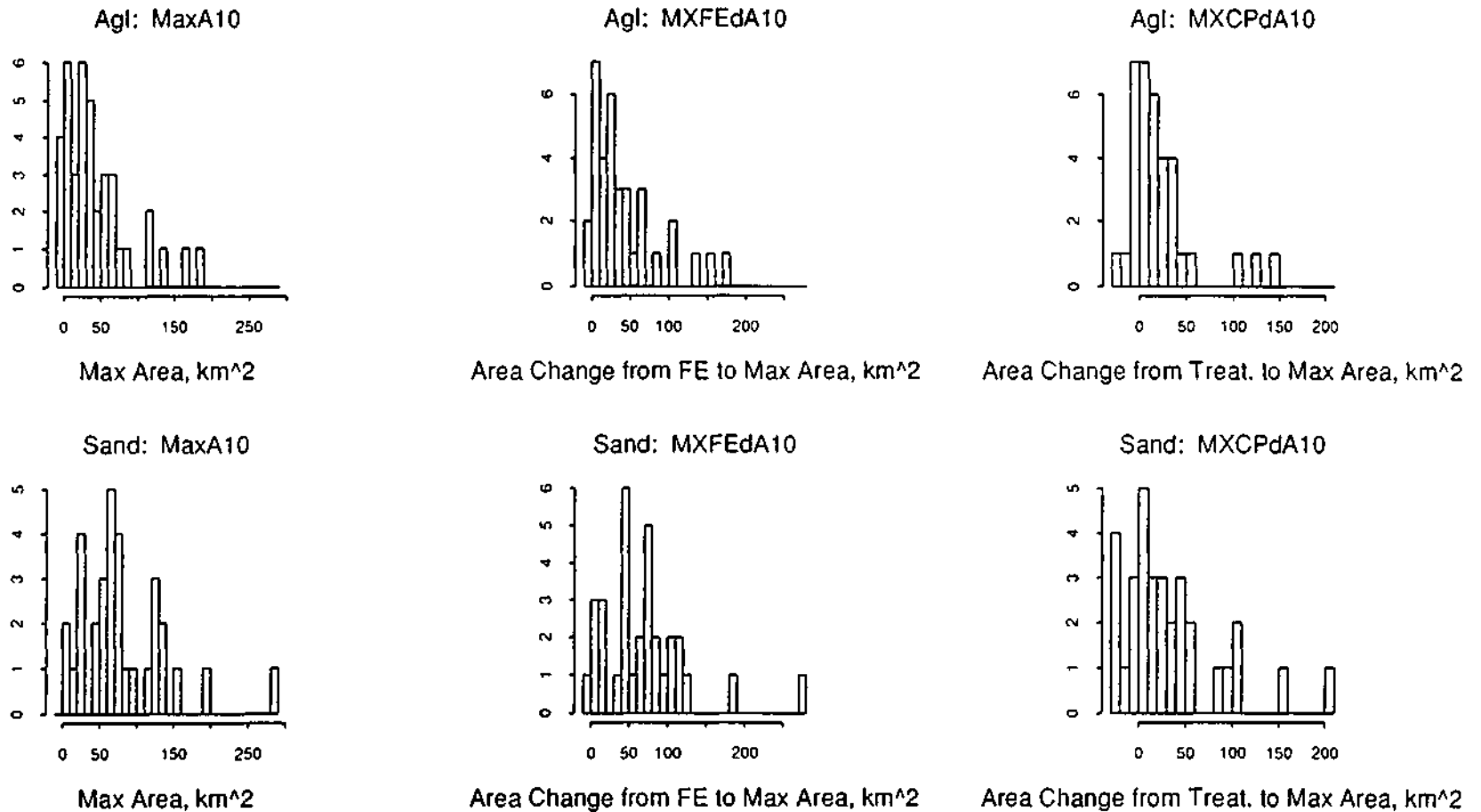


Figure C.35. Histograms of the maximum area of the 10 dBZ contour of the echo (MaxA10), the change in area of the 10 dBZ contour from first echo to the maximum area of the echo core (MXFEA10), and the change in area of the 10 dBZ contour from treatment to the maximum area of the echo (MXCPdA10).

# PACE89 DATA

Total Sample

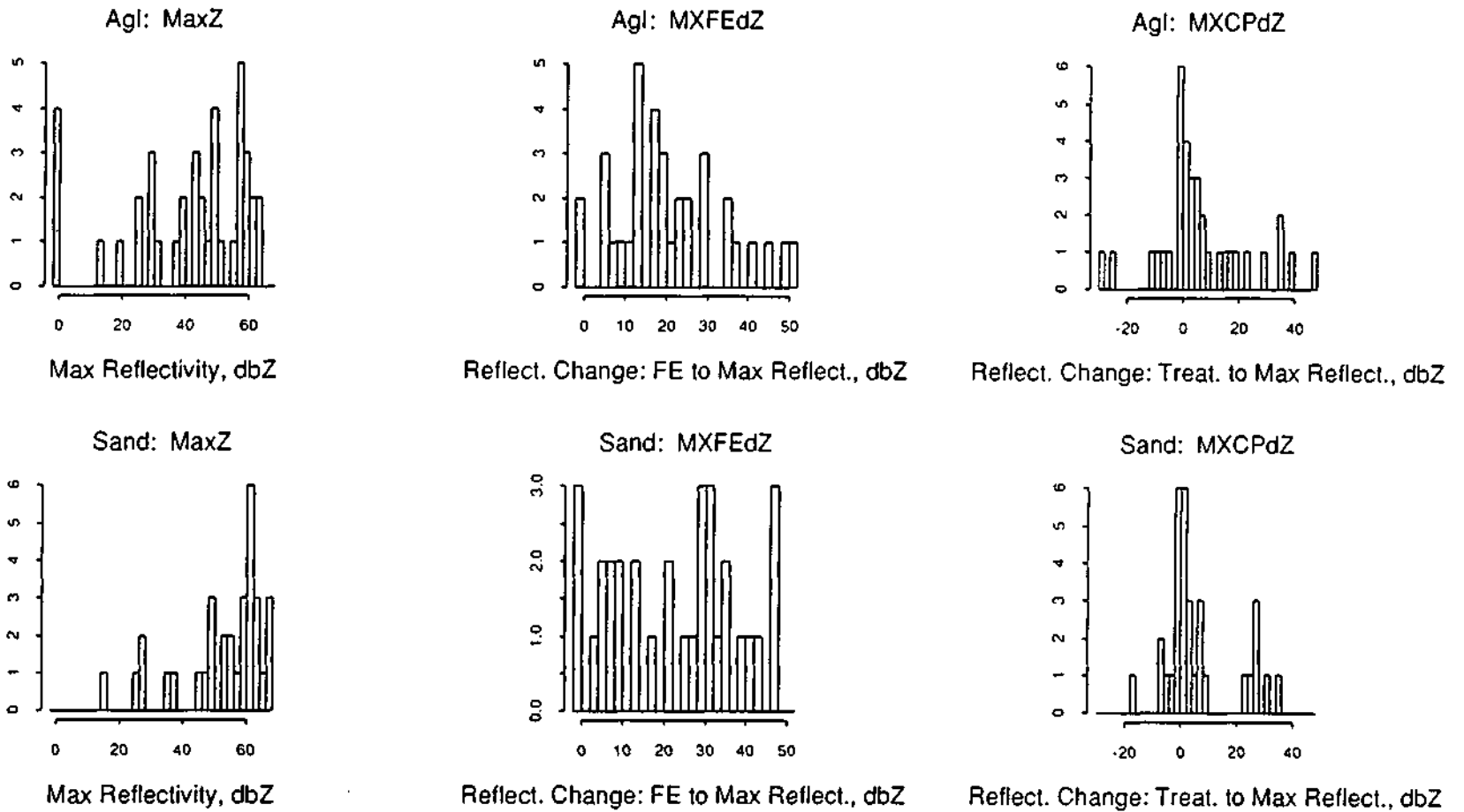


Figure C.36. Histograms of the maximum reflectivity of the echo (MaxZ), the change in the maximum reflectivity from first echo to the maximum reflectivity of the echo core (MXFE dZ), and the change in maximum reflectivity from treatment to the maximum reflectivity of the echo (MXCPdZ).

# PACE89 DATA

Total Sample

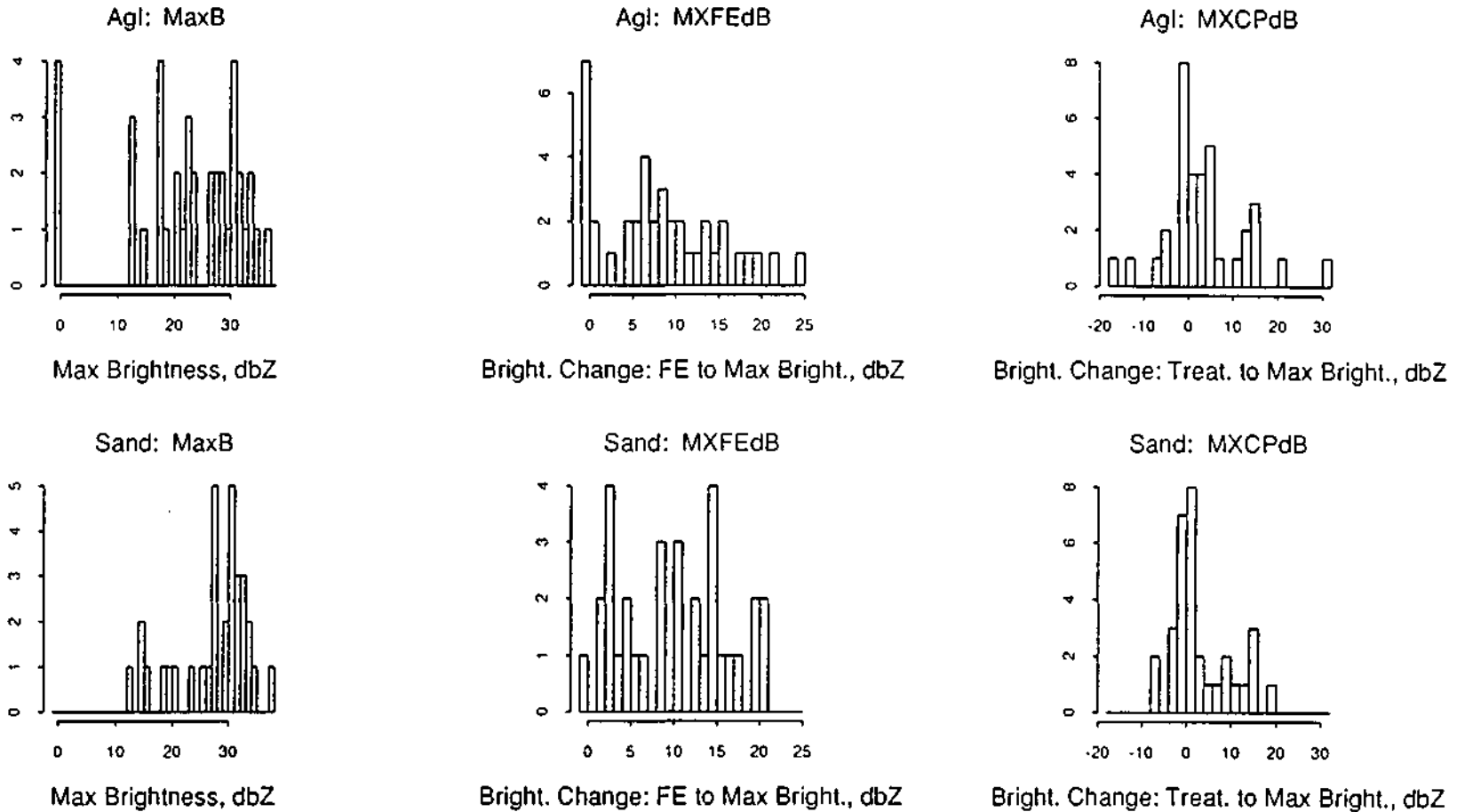
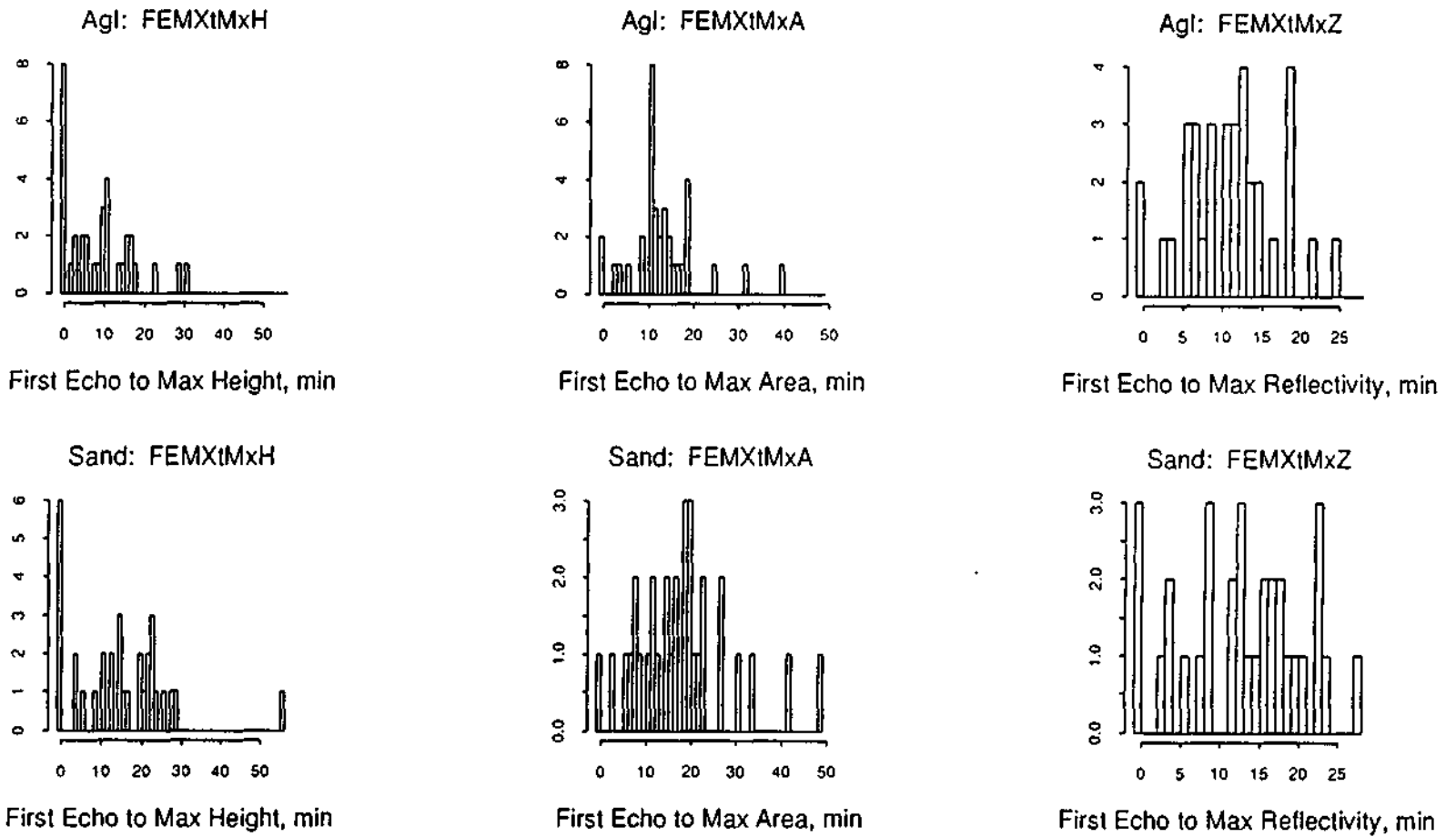


Figure C.37. Histograms of the maximum brightness of the echo (MaxB), the change in the brightness from first echo to the maximum brightness of the echo core (MXFEdB), and the change in brightness from treatment to the maximum brightness of the echo (MXCPdB).

# PACE89 DATA

Total Sample



120

Figure C.38. Histograms of the time from first echo to the time of maximum height (FEMXtMxH), area (FEMXtMxA), and reflectivity (FEMXtMxZ) of the echo core.

# PACE89 DATA

Total Sample

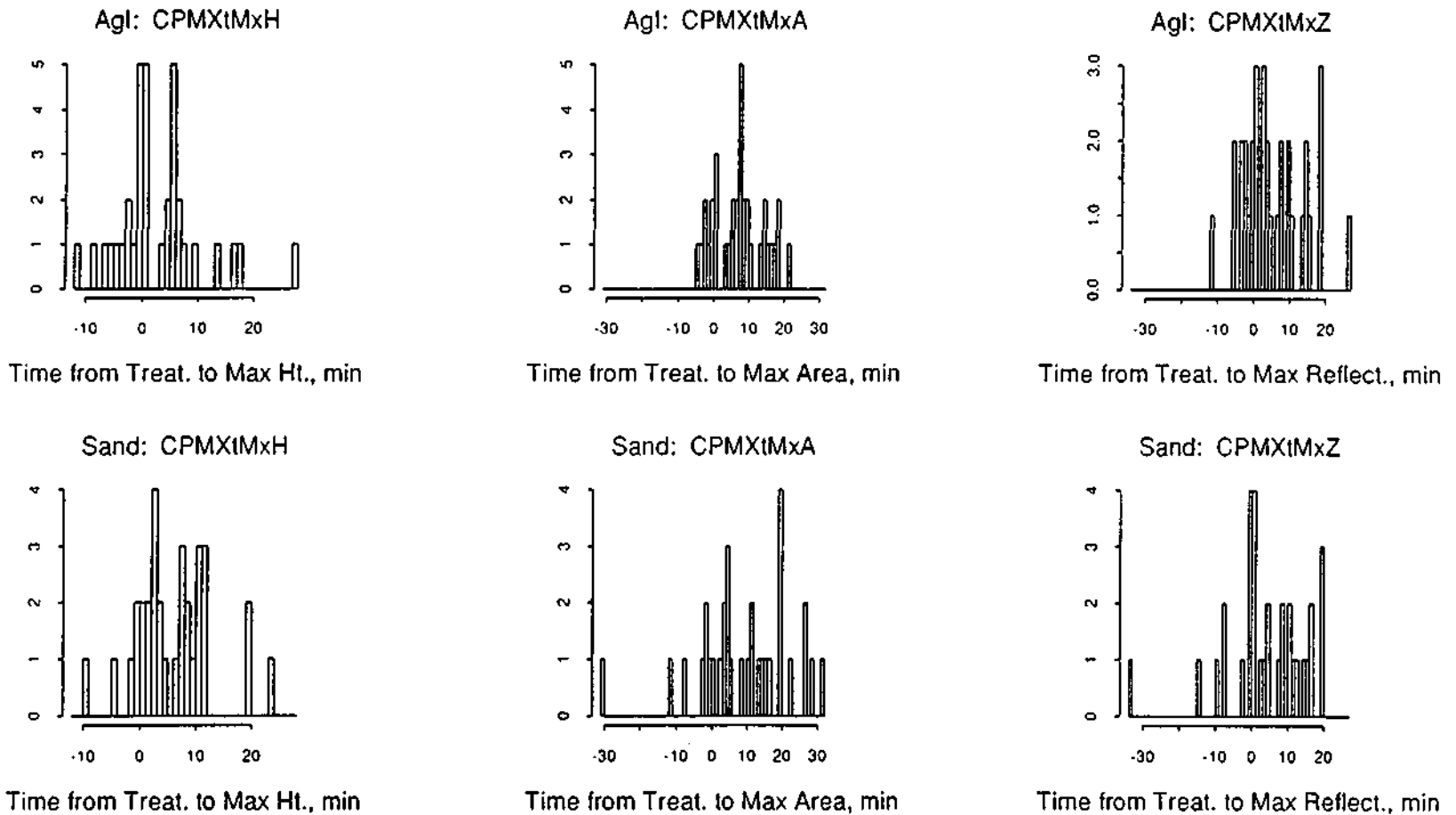


Figure C.39. Histograms of the time from treatment to the time of maximum height (CPMXtMxH), area (CPMXtMxA), and reflectivity (CPMXtMxZ) of the echo core.

# PACE89 DATA

## Total Sample

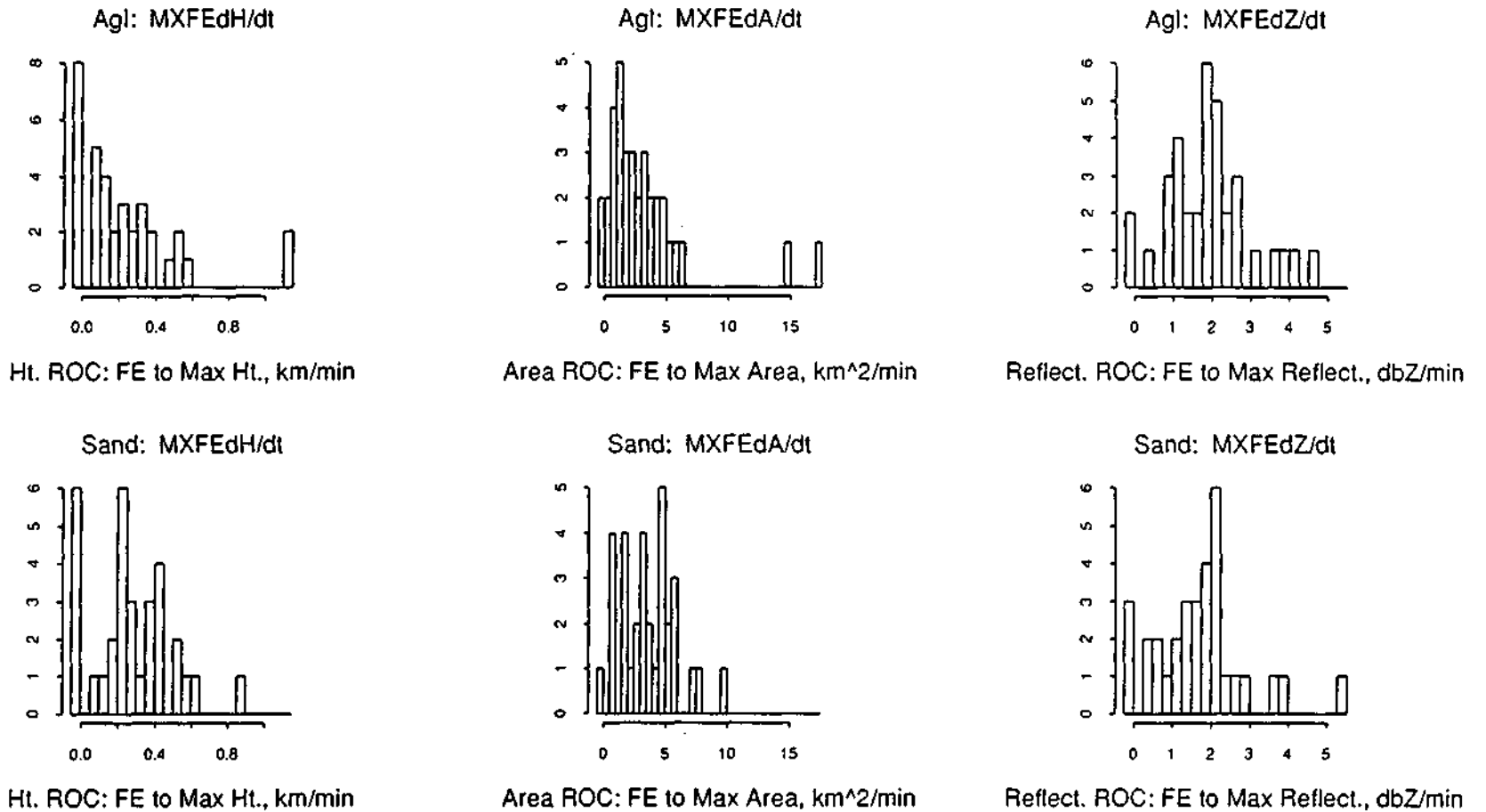


Figure C.40. Histograms of the rate of changes of the 10 dBZ echo top height from first echo to the maximum height of the echo (MXFE<sub>d</sub>H/dt), the maximum echo area from first echo to the maximum area of the echo (MXFE<sub>d</sub>A/dt), and the maximum reflectivity from first echo to the maximum reflectivity of the echo (MXFE<sub>d</sub>Z/dt).

# PACE89 DATA

## Total Sample

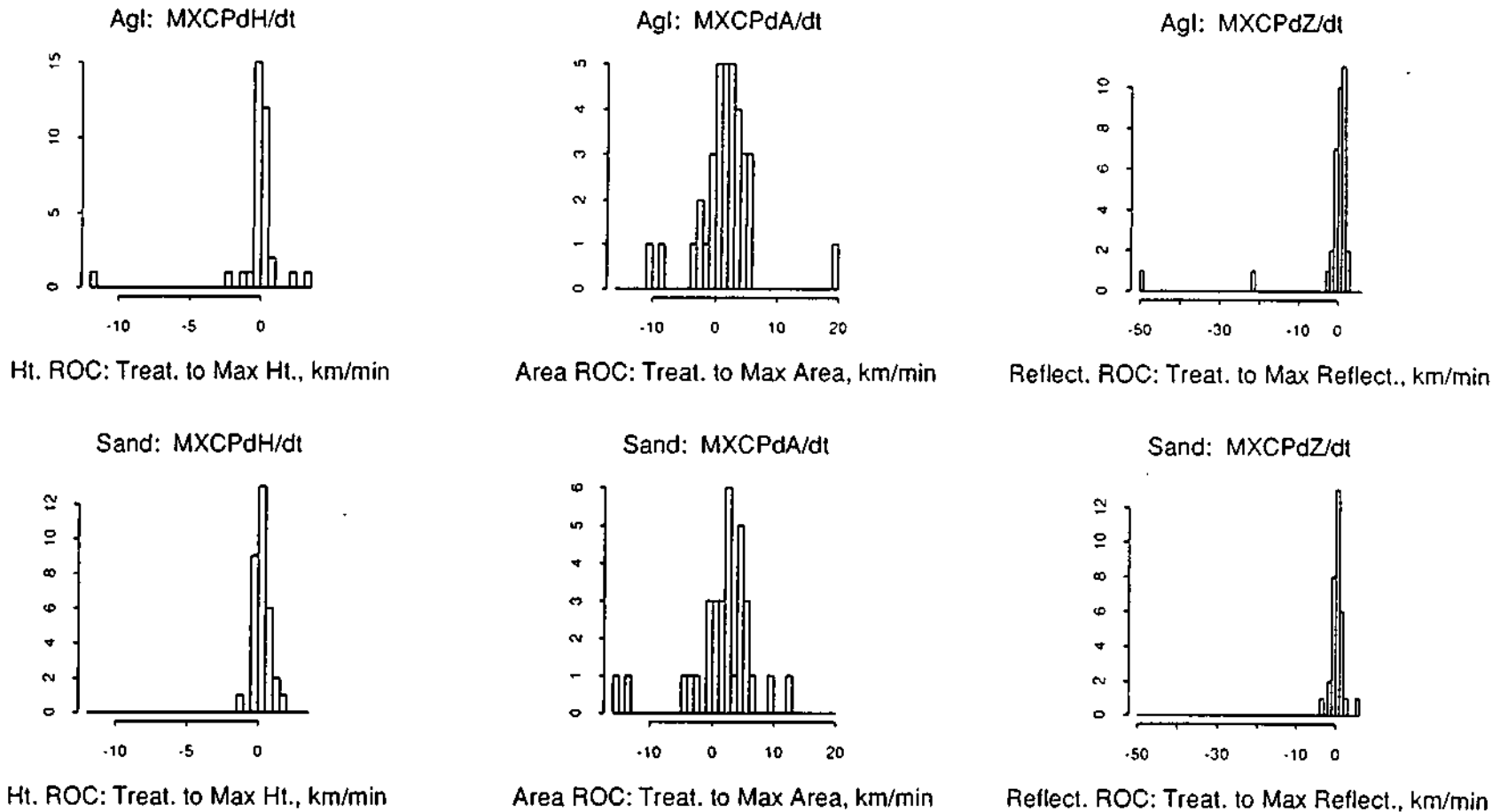


Figure C.41. Histograms of the rate of changes of the 10 dBZ echo top height from treatment to the maximum height of the echo (MXCPdH/dt), the maximum echo area from treatment to the maximum area of the echo (MXCPdA/dt), and the maximum reflectivity from treatment to the maximum reflectivity of the echo (MXCPdZ/dt).

# PACE89 DATA

## Total Sample

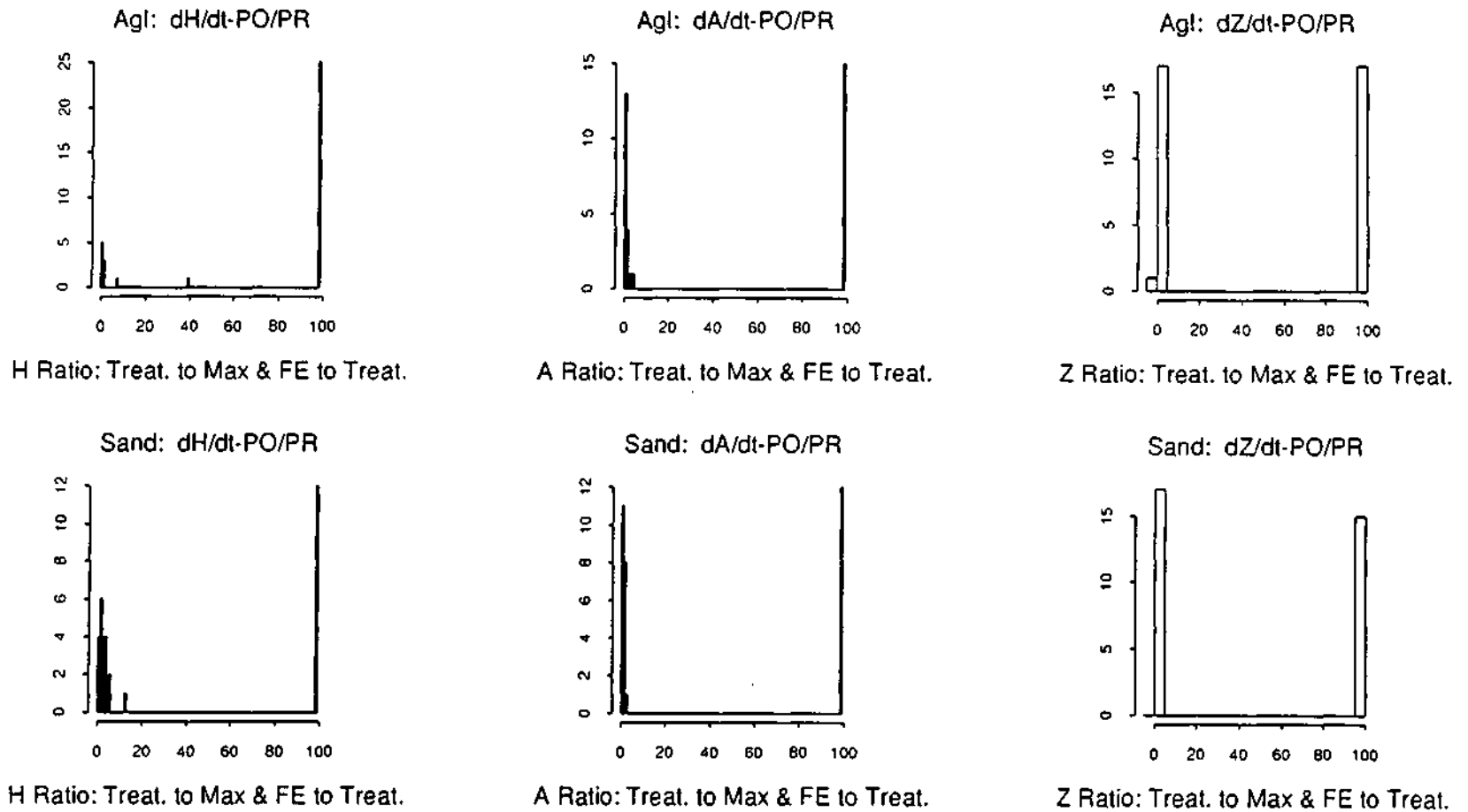


Figure C.42. . Histograms of the ratios of the rates of changes from treatment to the maximum and from first echo to treatment for the maximum echo top height ( $dH/dt-PO/PR$ ), area ( $dA/dt-PO/PR$ ), and reflectivity ( $dZ/dt-PO/PR$ ).

# PACE89 DATA

## Total Sample

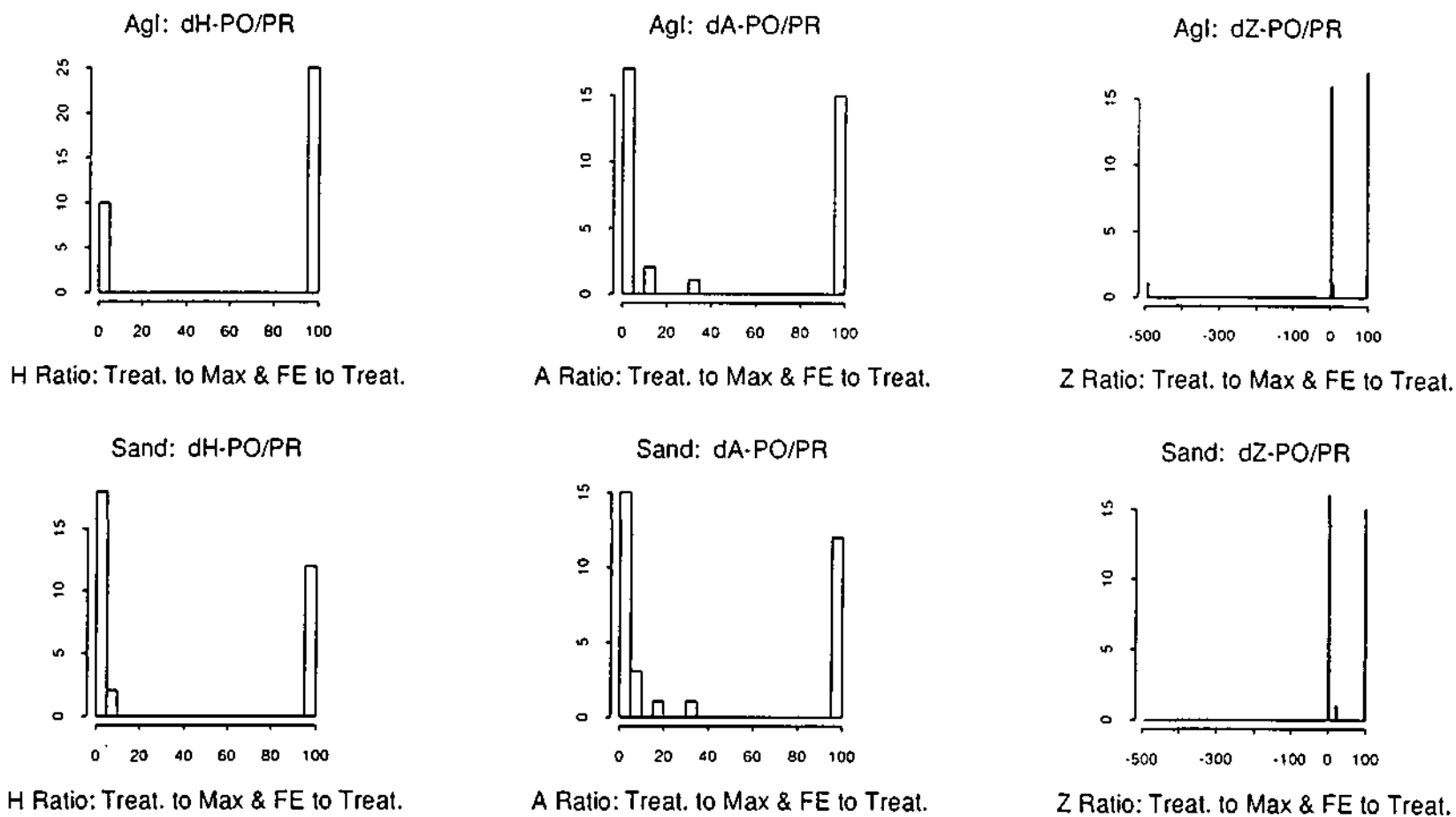


Figure C.43. Histograms of the ratios of the changes from treatment to the maximum and from first echo to treatment for the maximum echo top height (dH-PO/PR), area (dA-PO/PR), and reflectivity (dZ-PO/PR).

# PACE89 DATA

Total Sample

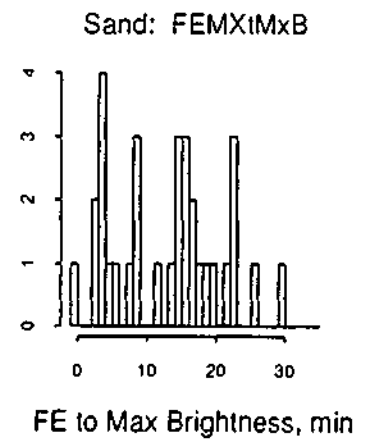
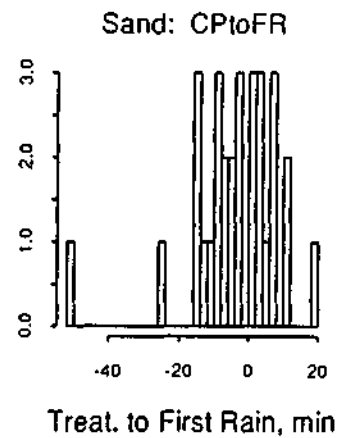
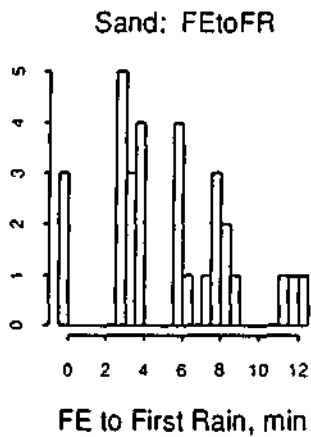
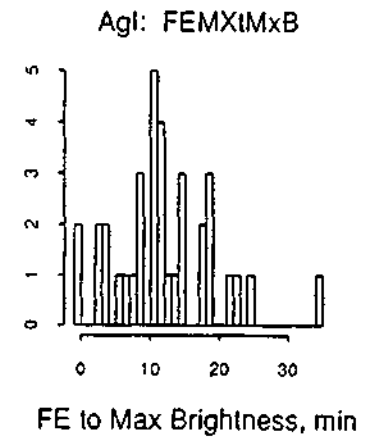
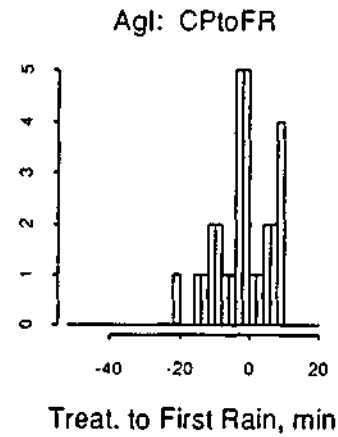
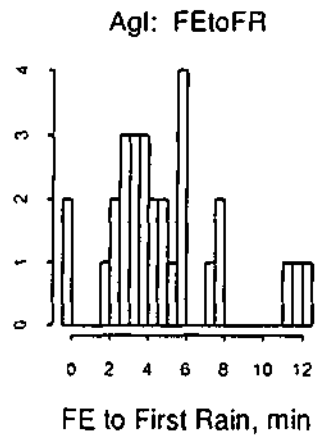


Figure C.44. Histograms of the time from first echo to the time of first rain (FEtoFR), the time from treatment to the time of first rain (CPtoFR), and the time from first echo to the time of maximum brightness (FEMXtMxB).

# PACE89 DATA

Total Sample

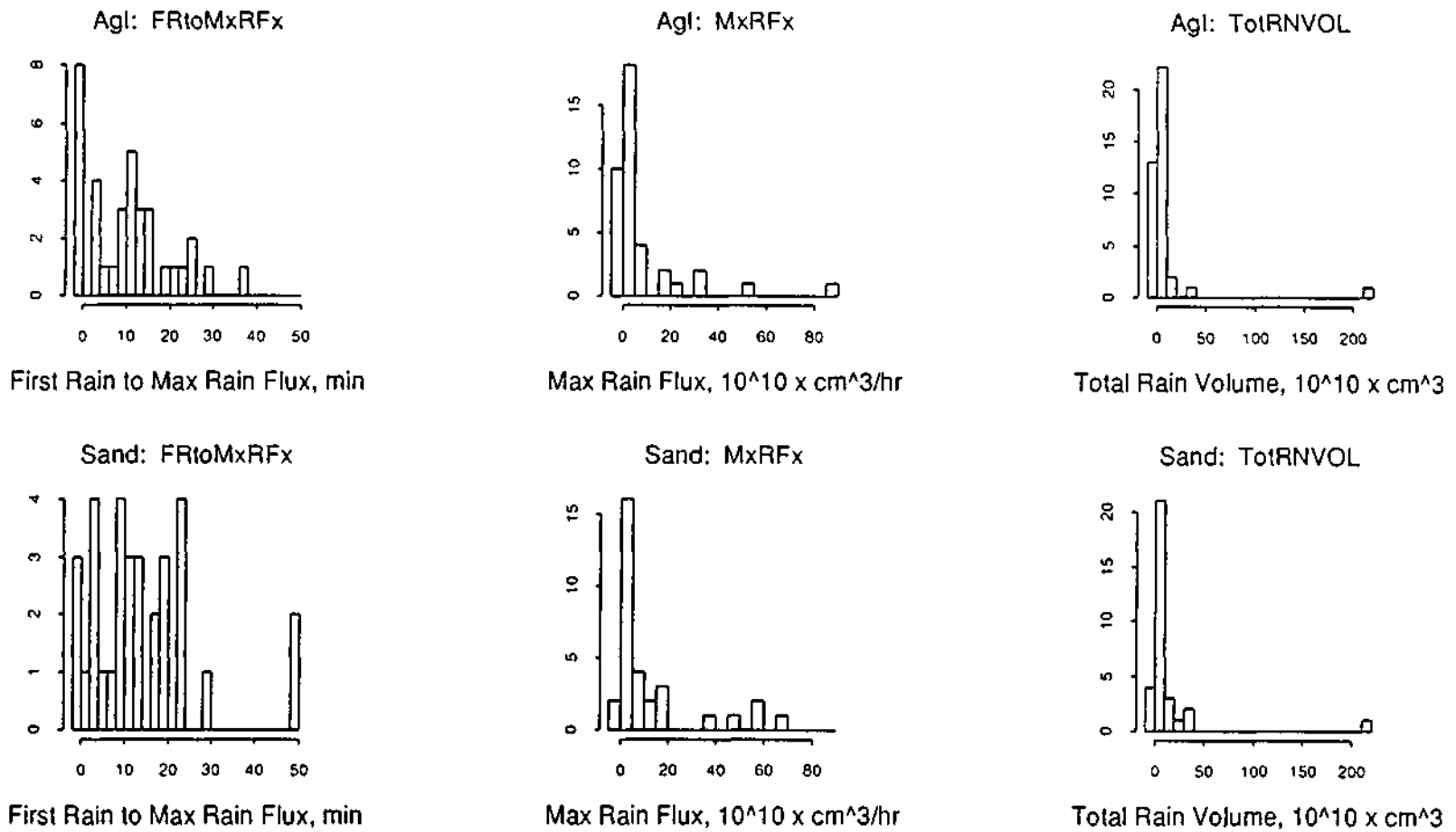


Figure C.45. Histograms of the time from first rain to the time of maximum rain flux of the echo core (FRtoMxRFx), the maximum rain flux of the echo core (MxRFx), and the total accumulated rain volume of the echo core (TotRNVOL).

# PACE89 DATA

Total Sample

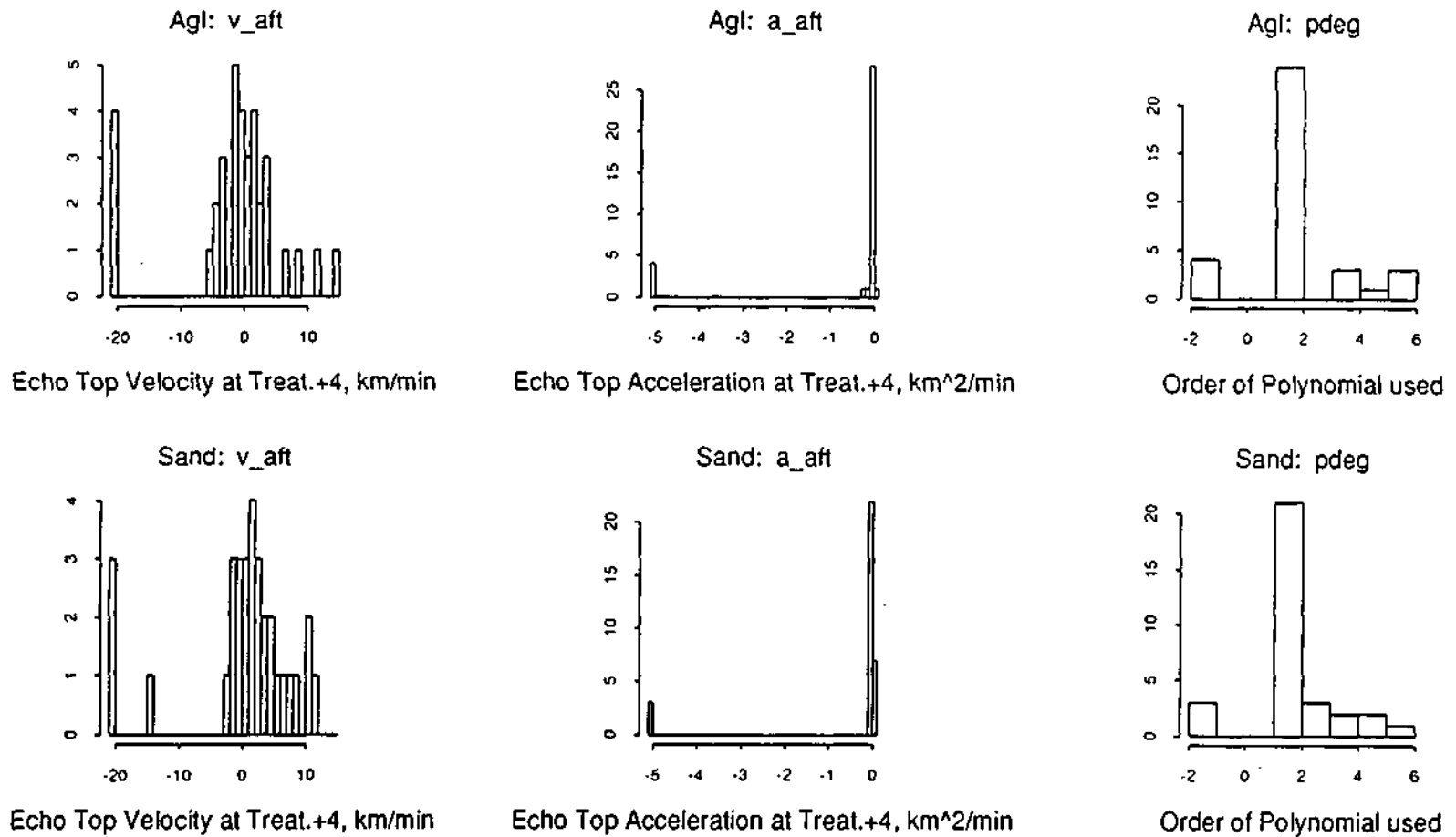


Figure C.46. Histograms of the velocity ( $v_{aft}$ ) and acceleration ( $a_{aft}$ ) of the echo top 4 minutes after treatment, and the order of the polynomial used to determine velocities and accelerations of the echo top before, at, and after treatment ( $pdeg$ ).

# PACE89 DATA

Total Sample

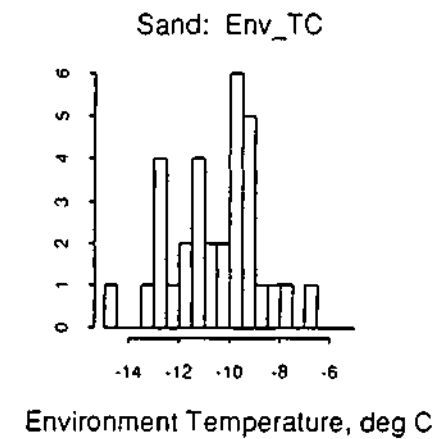
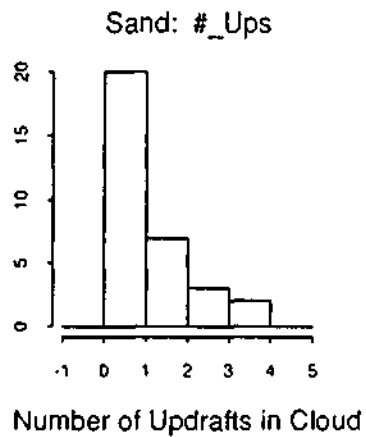
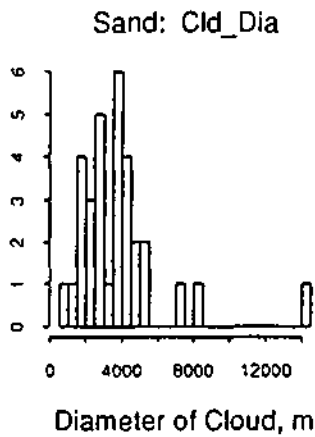
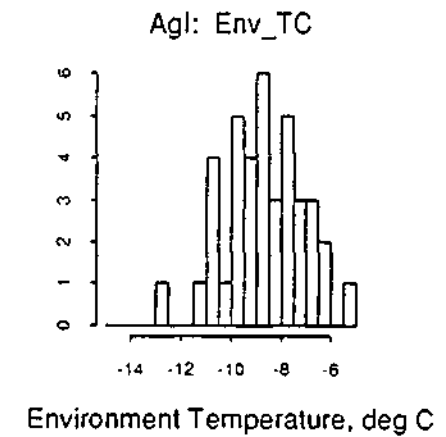
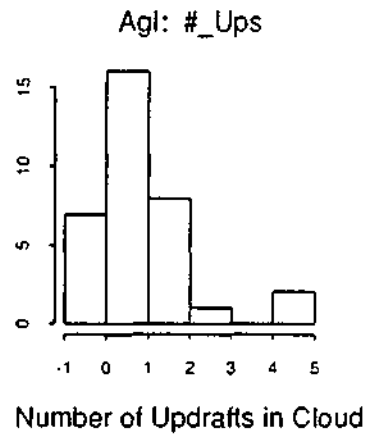
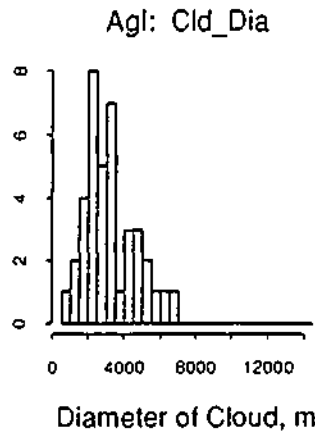


Figure C.47. Histograms of the cloud diameter (Cld\_Dia), the number of updrafts in cloud (#\_Ups), and the temperature of the cloud's environment (Env\_TC).

# PACE89 DATA

Total Sample

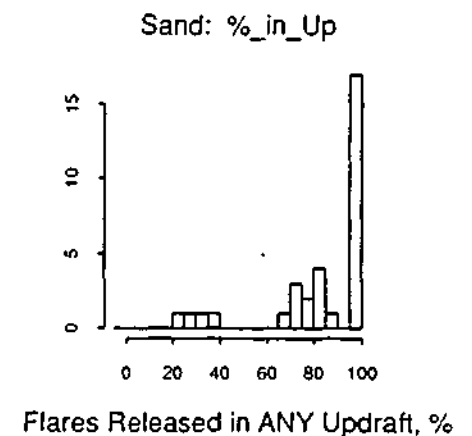
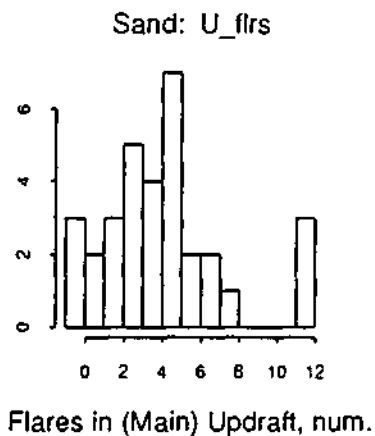
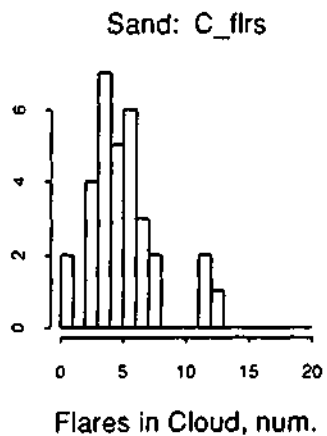
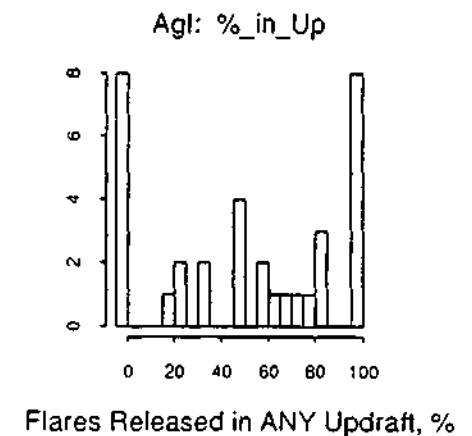
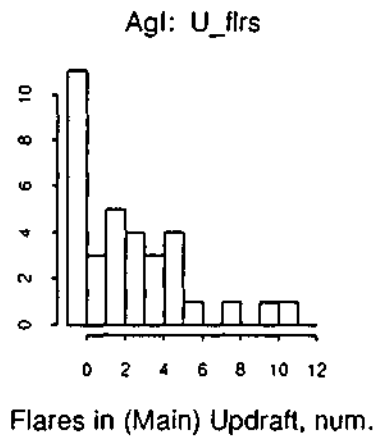
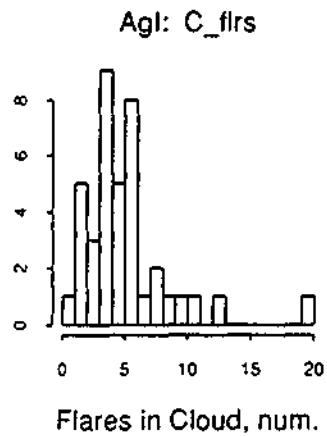


Figure C.48. Histograms of the number of flares in the cloud (*C\_flr*), the number of flares in the main (broadest) updraft (*U\_flr*), and the percentage of flares released in any updraft (*%\_in\_Up*).

# PACE89 DATA

Total Sample

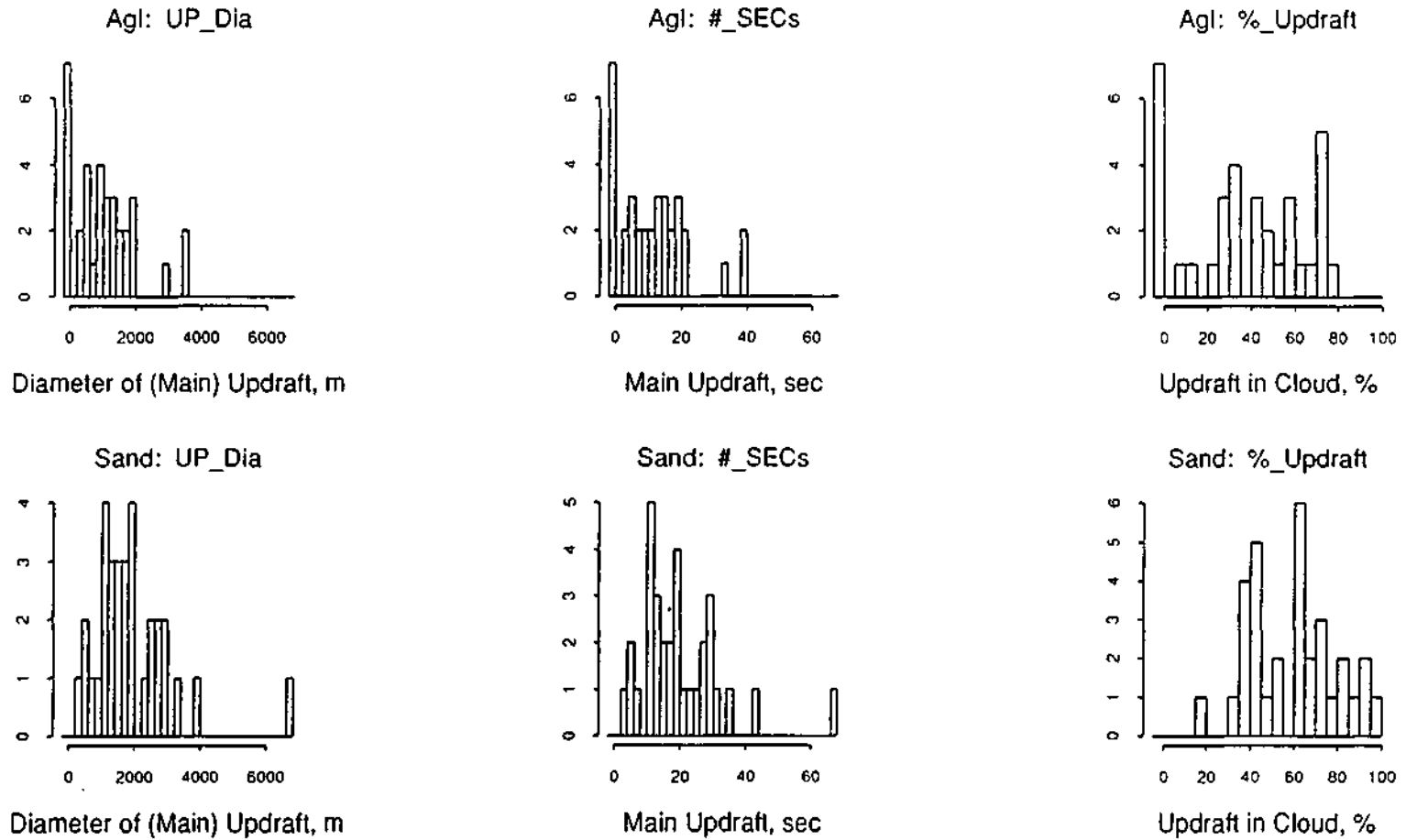


Figure C.49. Histograms of the diameter of the main (broadest) updraft (UP\_Dia), the number of seconds of the broadest or main updraft (#\_SECs), and the percent of cloud which is updraft (%\_Updraft).

# PACE89 DATA

Total Sample

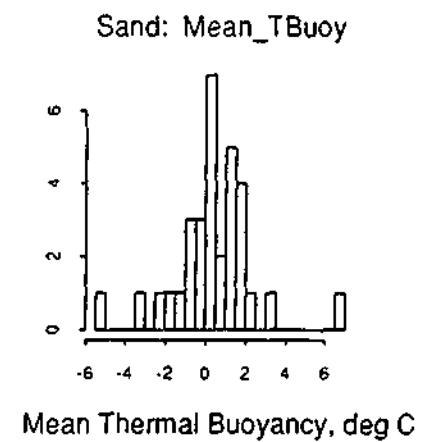
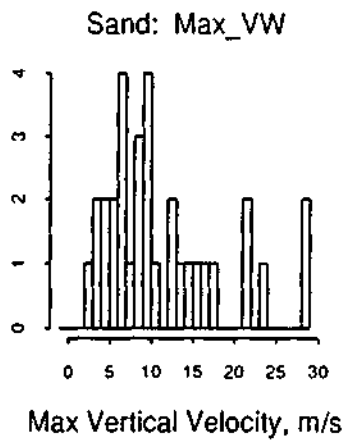
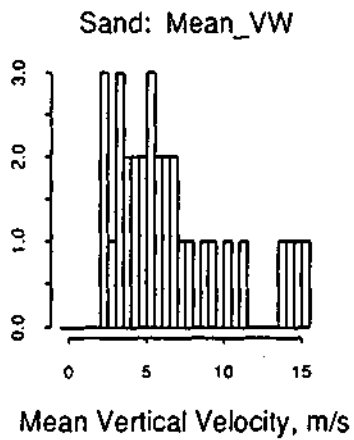
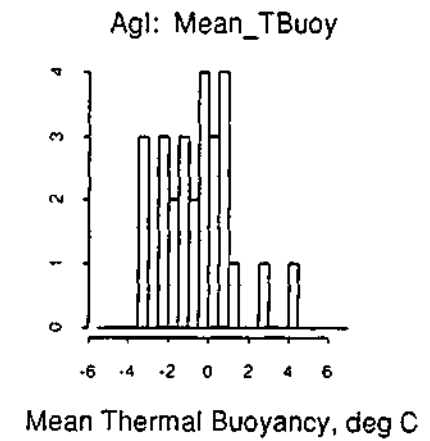
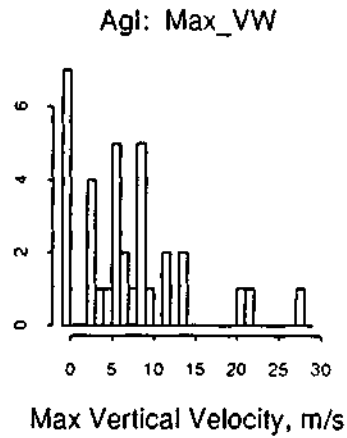
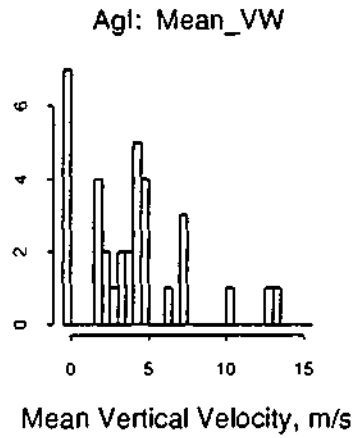


Figure C.50. Histograms of the mean (Mean\_VW) and maximum (Max\_VW) vertical velocity of the main updraft, and the mean thermal buoyancy (Mean\_TBuoy).

# PACE89 DATA

## Total Sample

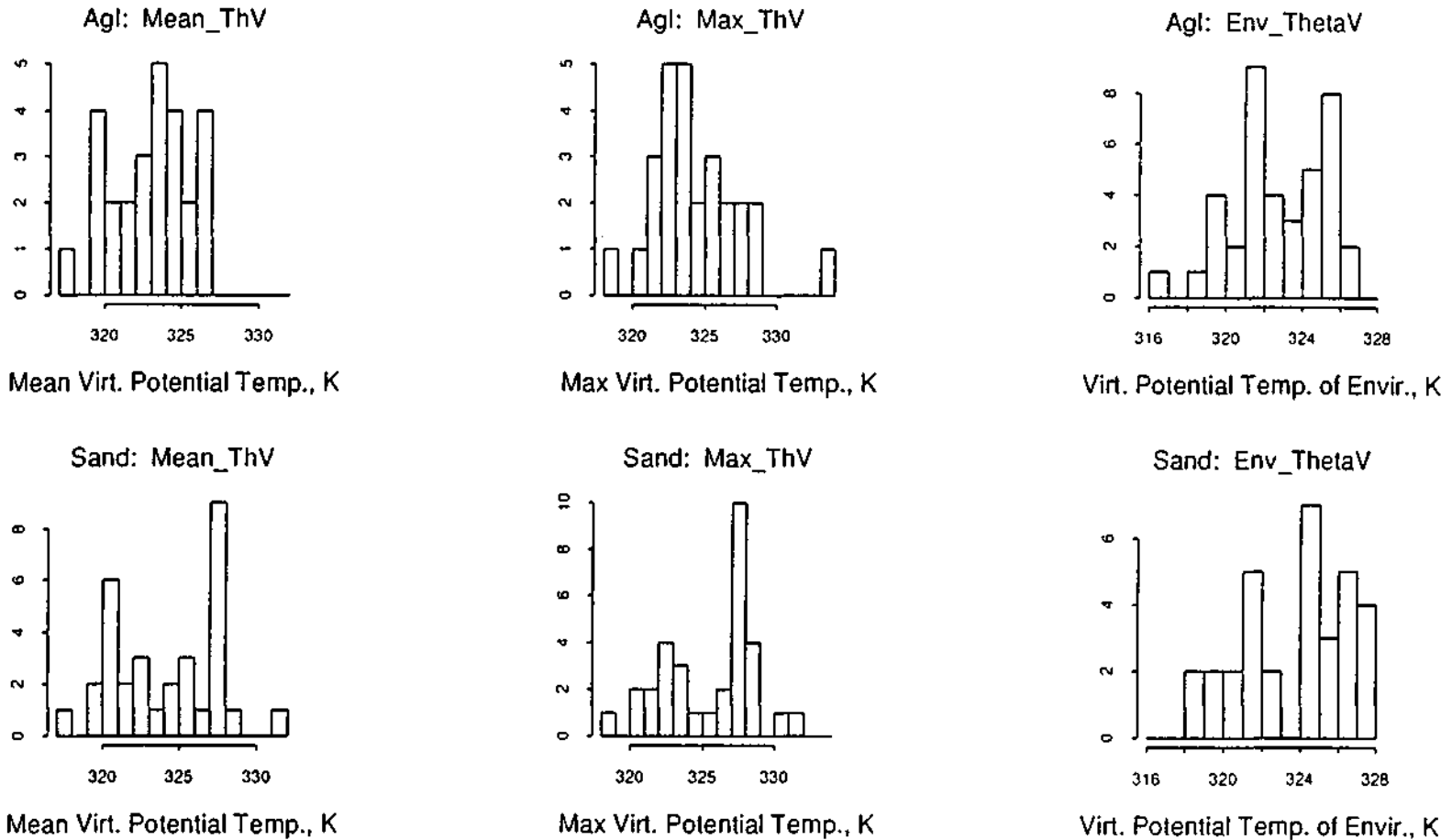


Figure C.51. Histograms of the mean (Mean\_ThV) and maximum (Max\_ThV) virtual potential temperature of the main updraft, and the mean virtual potential temperature of the environment (Env\_ThetaV).

# PACE89 DATA

## Total Sample

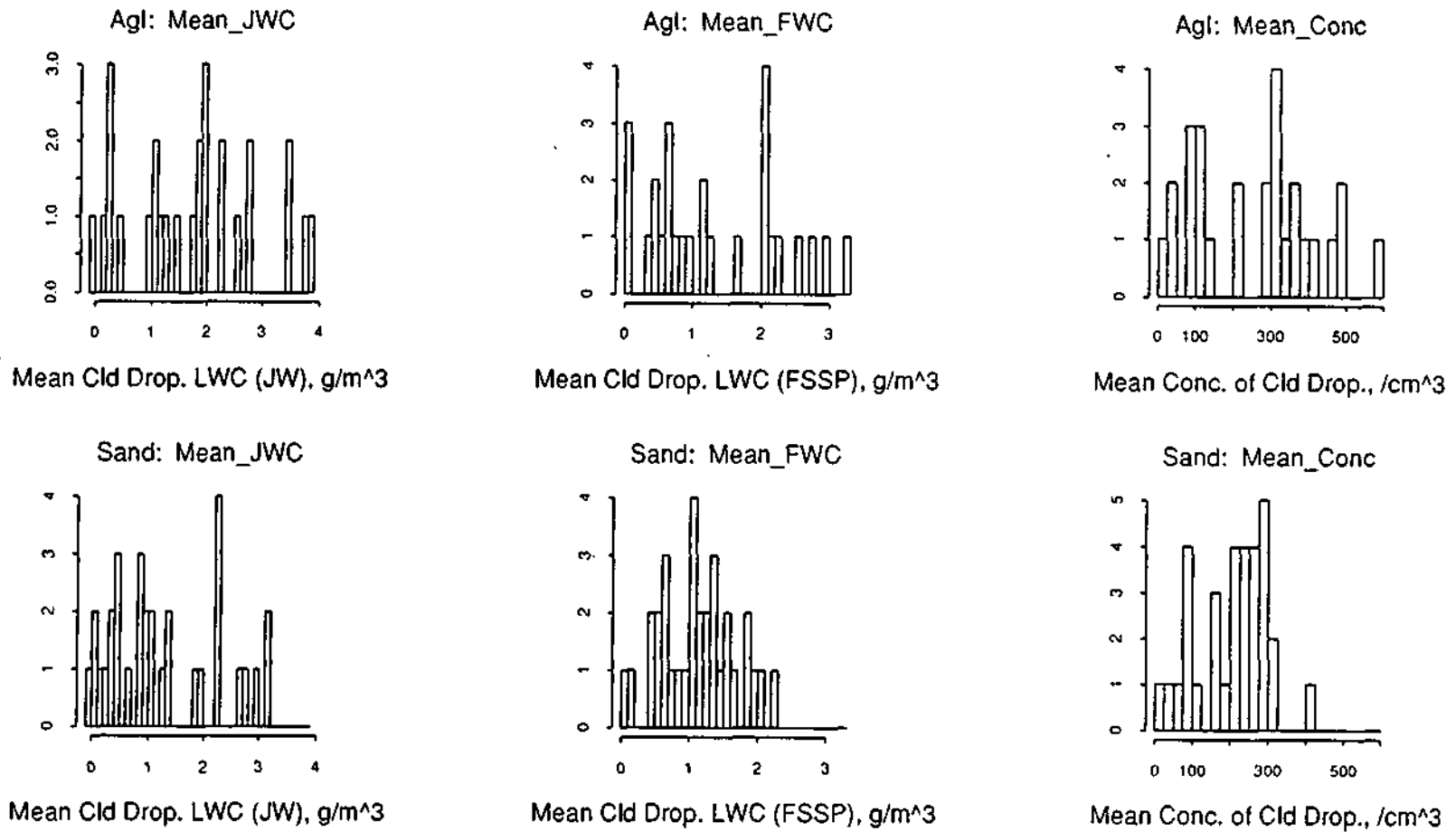


Figure C.52. Histograms of the mean liquid water content in the main updraft from the JW (Mean\_JWC) and FSSP (Mean\_FWC) probes (i.e., cloud droplets), and the mean concentration of cloud droplets in the main updraft (Mean\_Conc).

# PACE89 DATA

## Total Sample

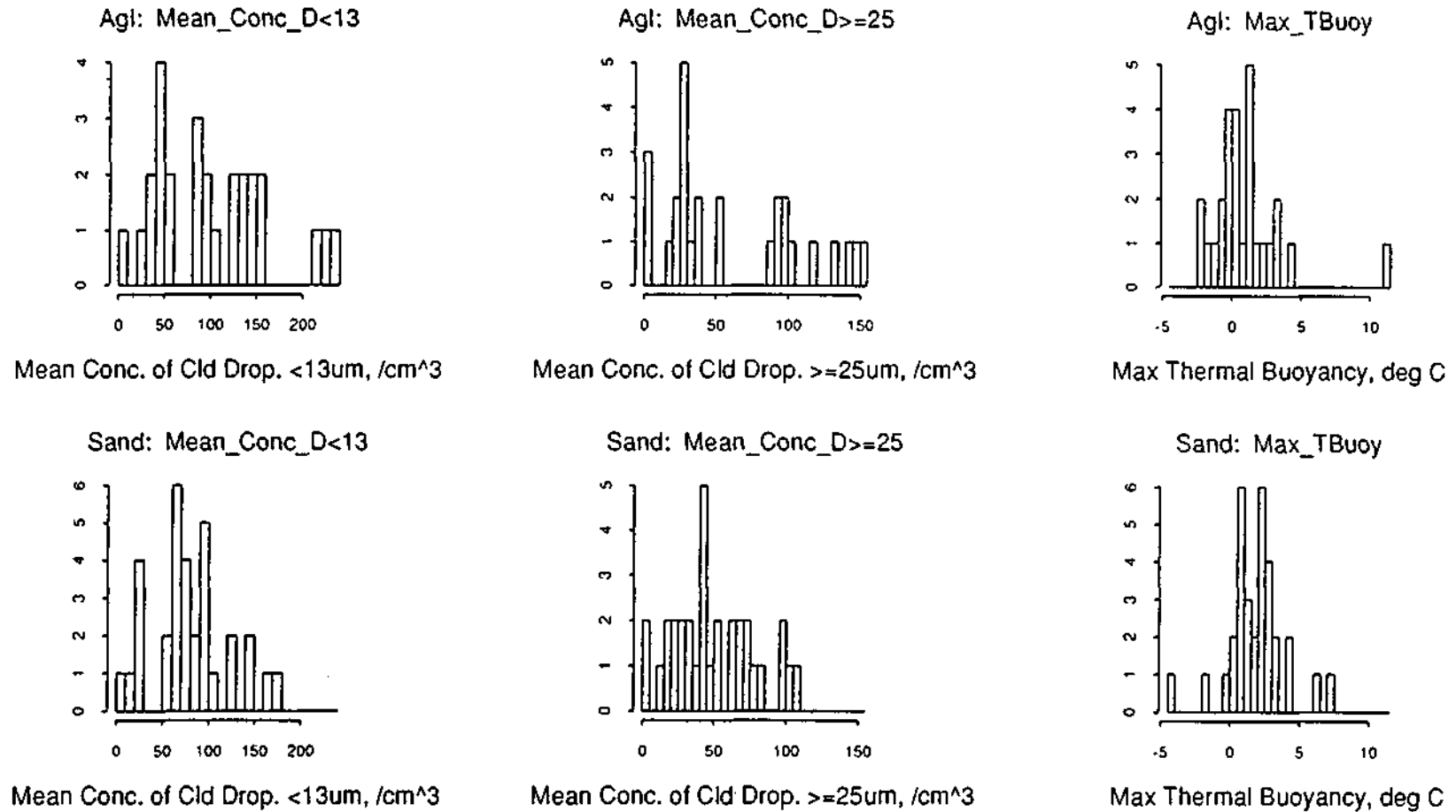


Figure C.53. Histograms of the mean concentration in the main updraft of cloud droplets with  $d < 13 \mu\text{m}$  (*Mean\_Conc\_D<13*) and cloud droplets with  $d \geq 25 \mu\text{m}$  (*Mean\_Conc\_D>=25*), and the maximum thermal buoyancy of the main updraft (*Max\_TBuoy*).

# PACE89 DATA

## Total Sample

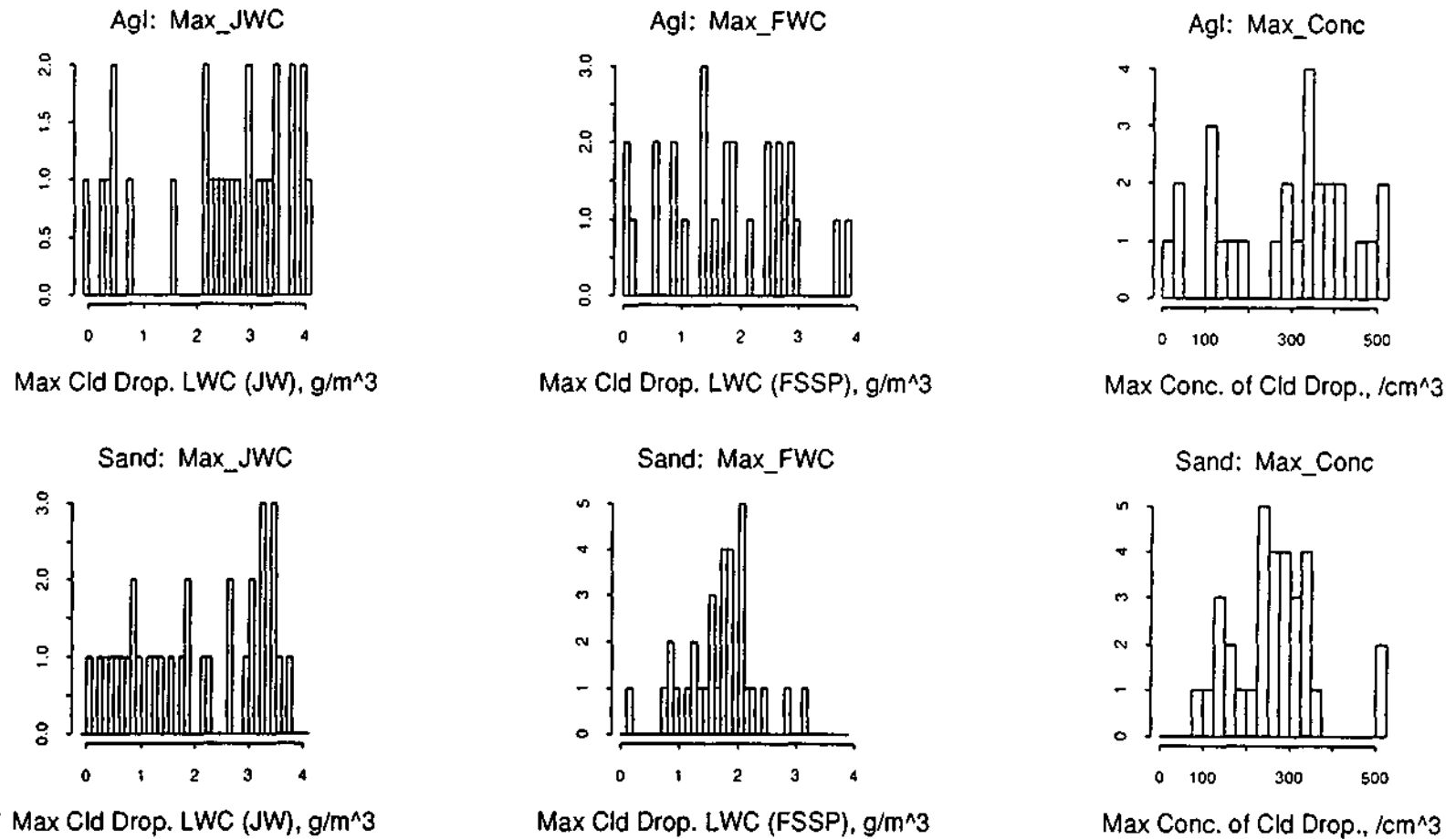
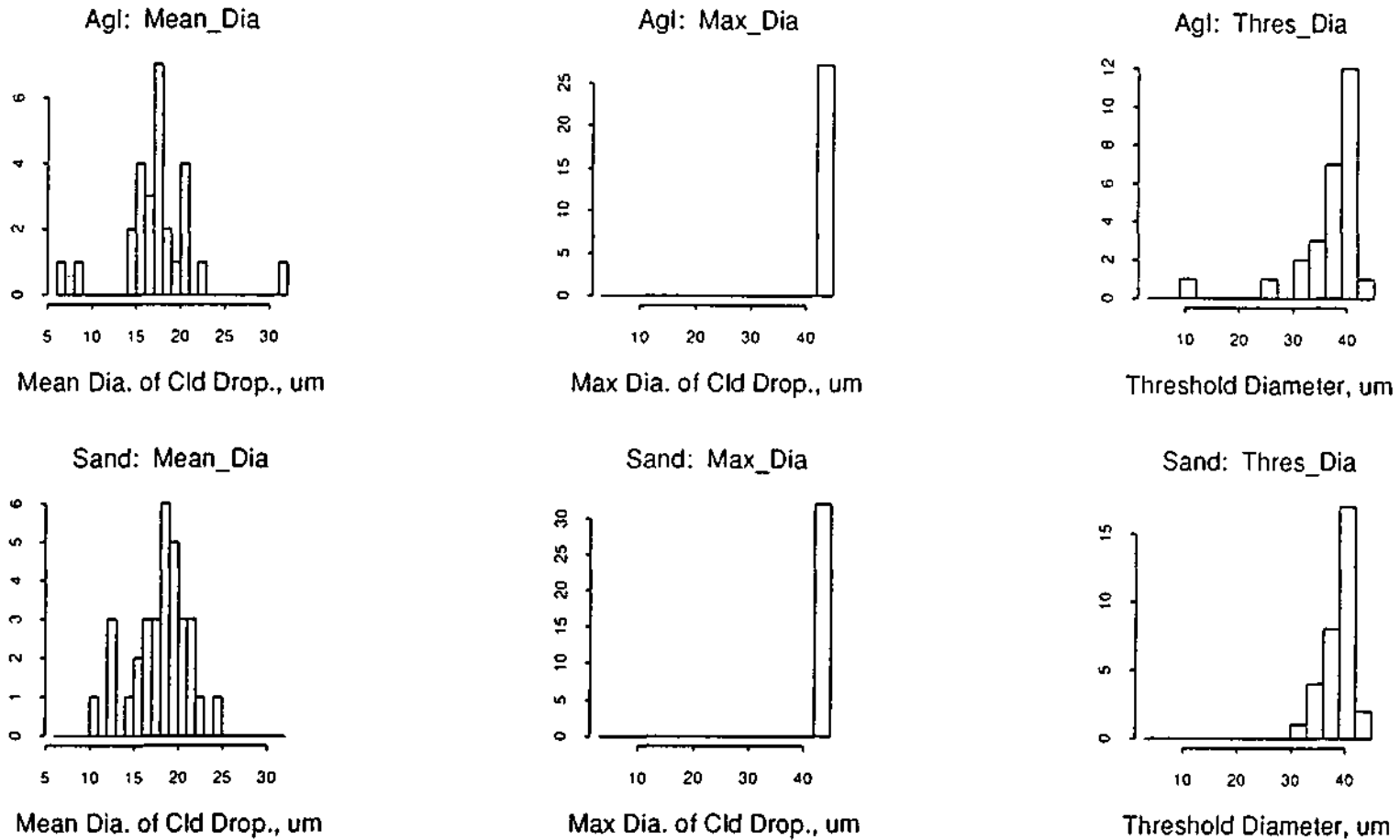


Figure C.54. Histograms of the maximum liquid water content in the main updraft from the JW (*Max\_JWC*) and FSSP (*Max\_FWC*) probes (i.e., cloud droplets), and the maximum concentration of cloud droplets in the main updraft (*Max\_Conc*).

# PACE89 DATA

Total Sample



137

Figure C.55. Histograms of the mean (Mean\_Dia) and maximum (Max\_Dia) diameter of cloud droplet particles (from FSSP data) found in the main updraft, and the threshold diameter of the main updraft (Thres\_Dia).

# PACE89 DATA

## Total Sample

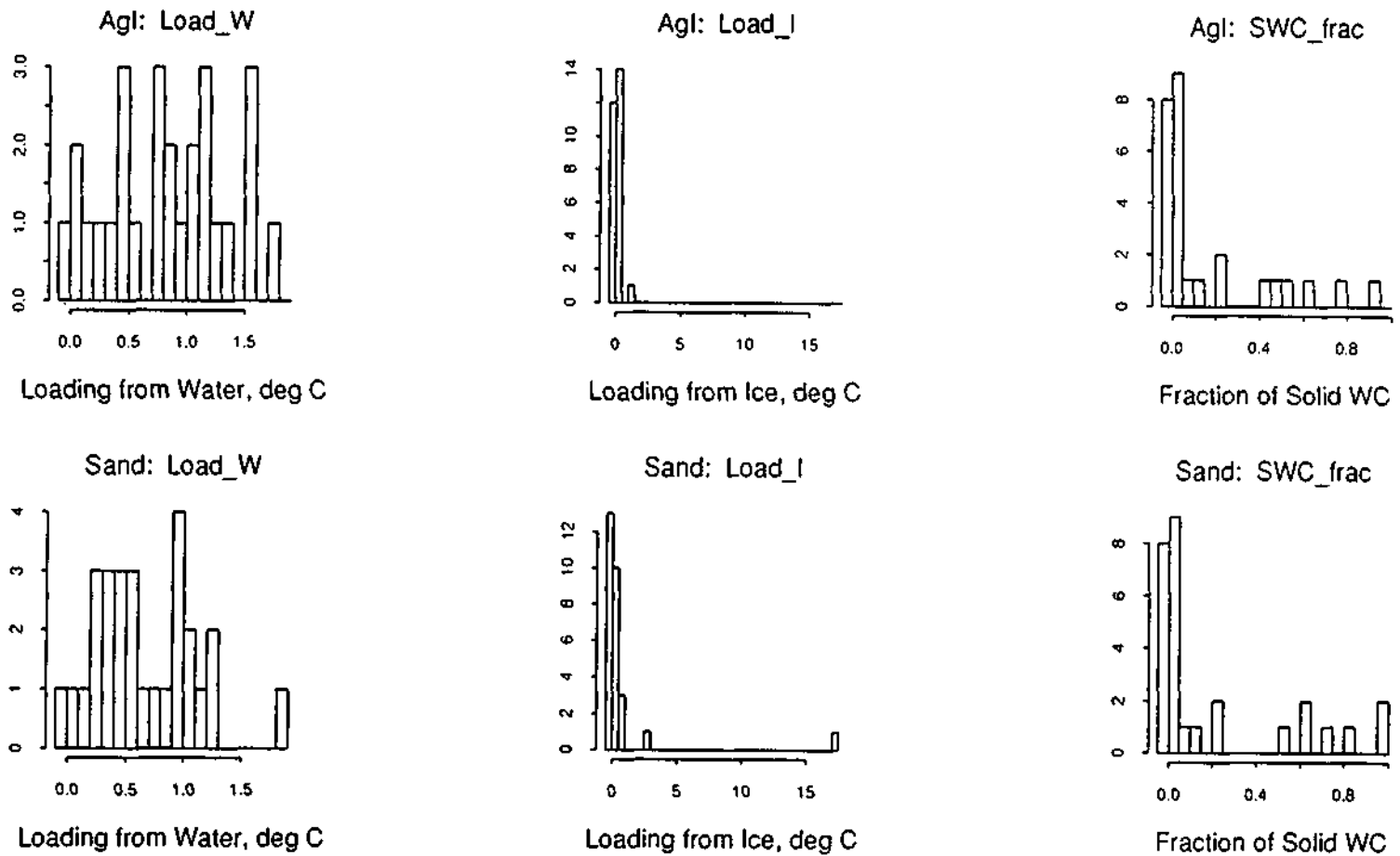


Figure C.56. Histograms of the loading from water (liquid) (Load\_W) and from ice (solid) (Load\_I) in the main updraft, and the fraction of solid water content to the total condensate (SWC\_frac).

# PACE89 DATA

Total Sample

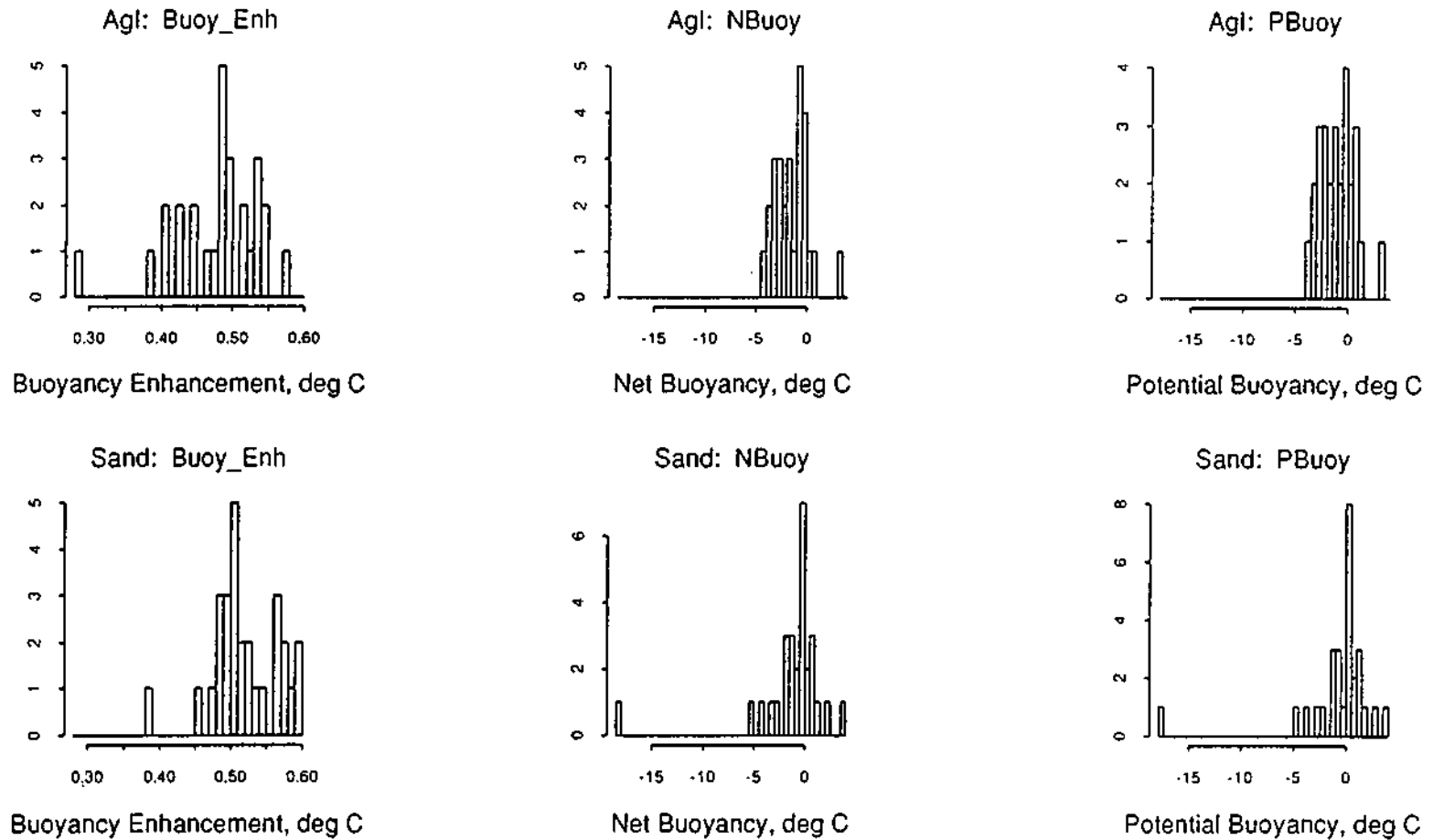


Figure C.57. Histograms of the buoyancy enhancement (Buoy\_Enh), the net buoyancy (NBUoy), and the potential buoyancy (PBuoy) of the main updraft.

# PACE89 DATA

## Total Sample

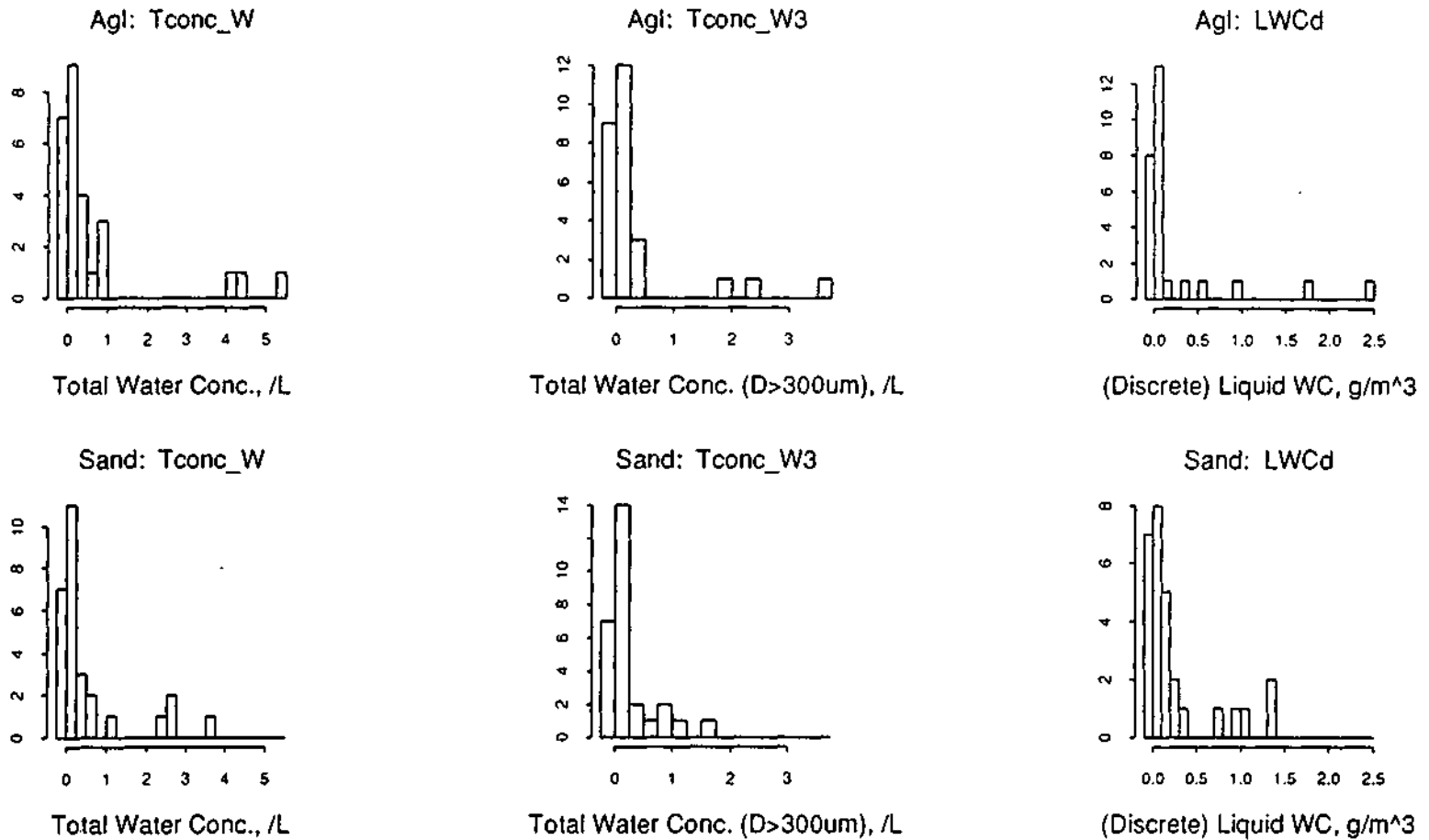


Figure C.58. Histograms of the total concentration of water particles (Tconc\_W), the total concentration of water particles with  $D > 300 \mu\text{m}$  (Tconc\_W3), and the liquid water content by method/ (i.e., discrete) (LWCd) in the main updraft.

# PACE89 DATA

Total Sample

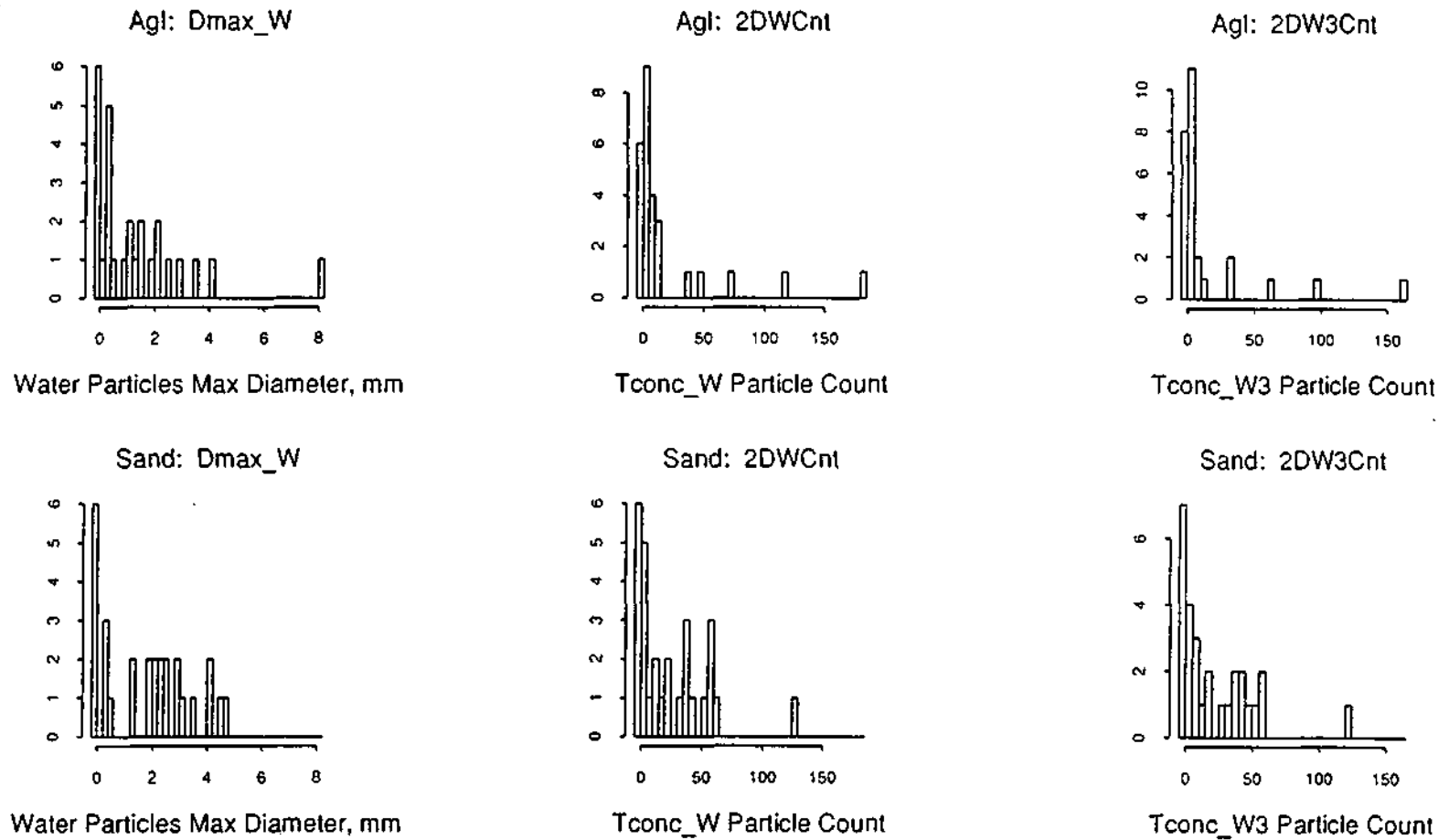


Figure C.59. Histograms of the maximum diameter of supercooled liquid rain/drizzle drop particles in the main updraft ( $D_{max\_W}$ ), the 2D probes total particle count in  $T_{conc\_W}$  (2DWCnt), and the 2D probes total particle count in  $T_{conc\_W3}$  (2DW3Cnt).

# PACE89 DATA

Total Sample

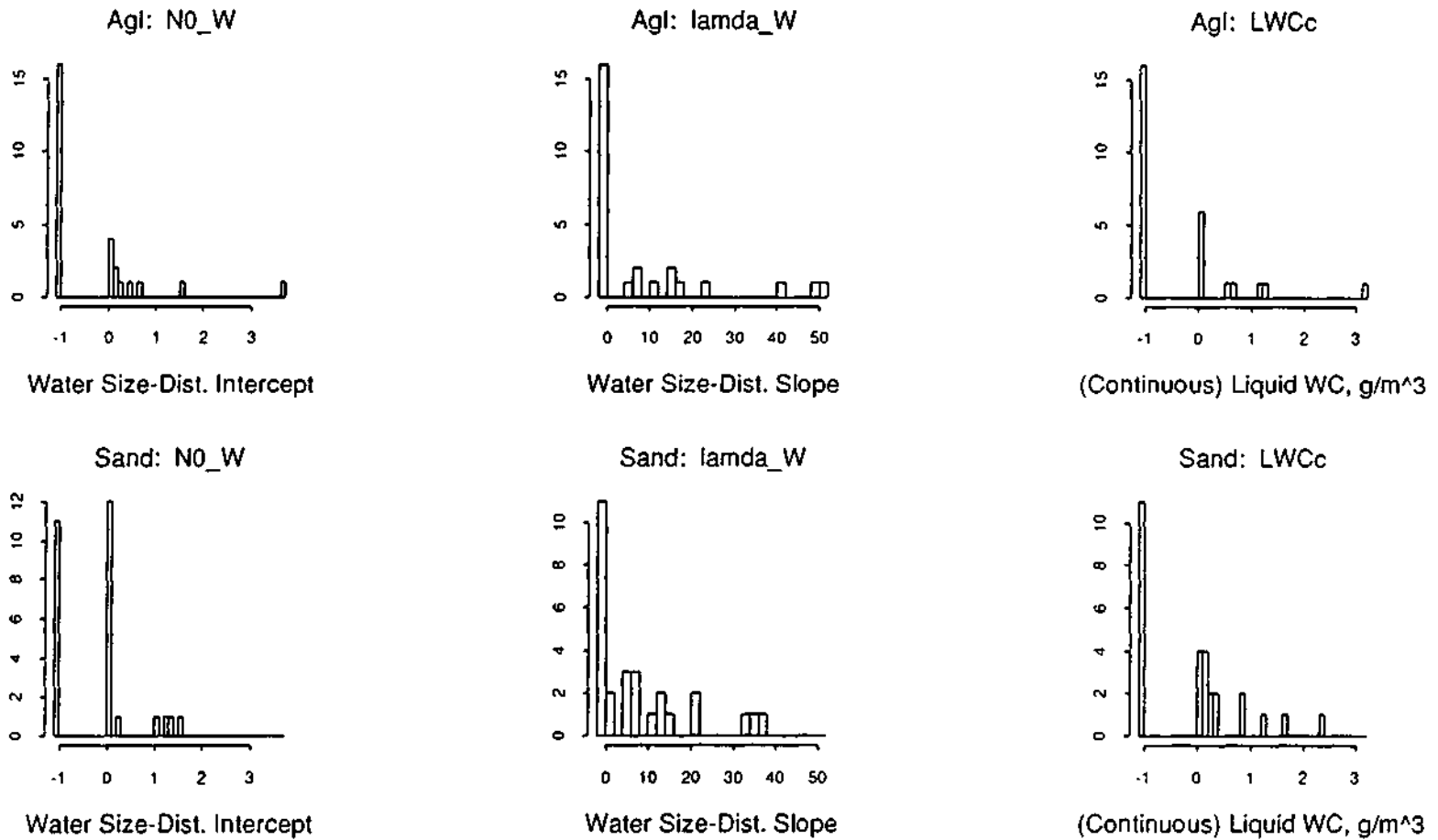


Figure C.60. Histograms of the water size-distribution intercepts ( $NO\_W$ ) and slopes ( $lamda\_W$ ), and the liquid water content by method II (i.e., continuous; area under the line defined by  $NO\_W$  and  $lamda\_W$ ) ( $LWCc$ ) calculated for the main updraft.

# PACE89 DATA

## Total Sample

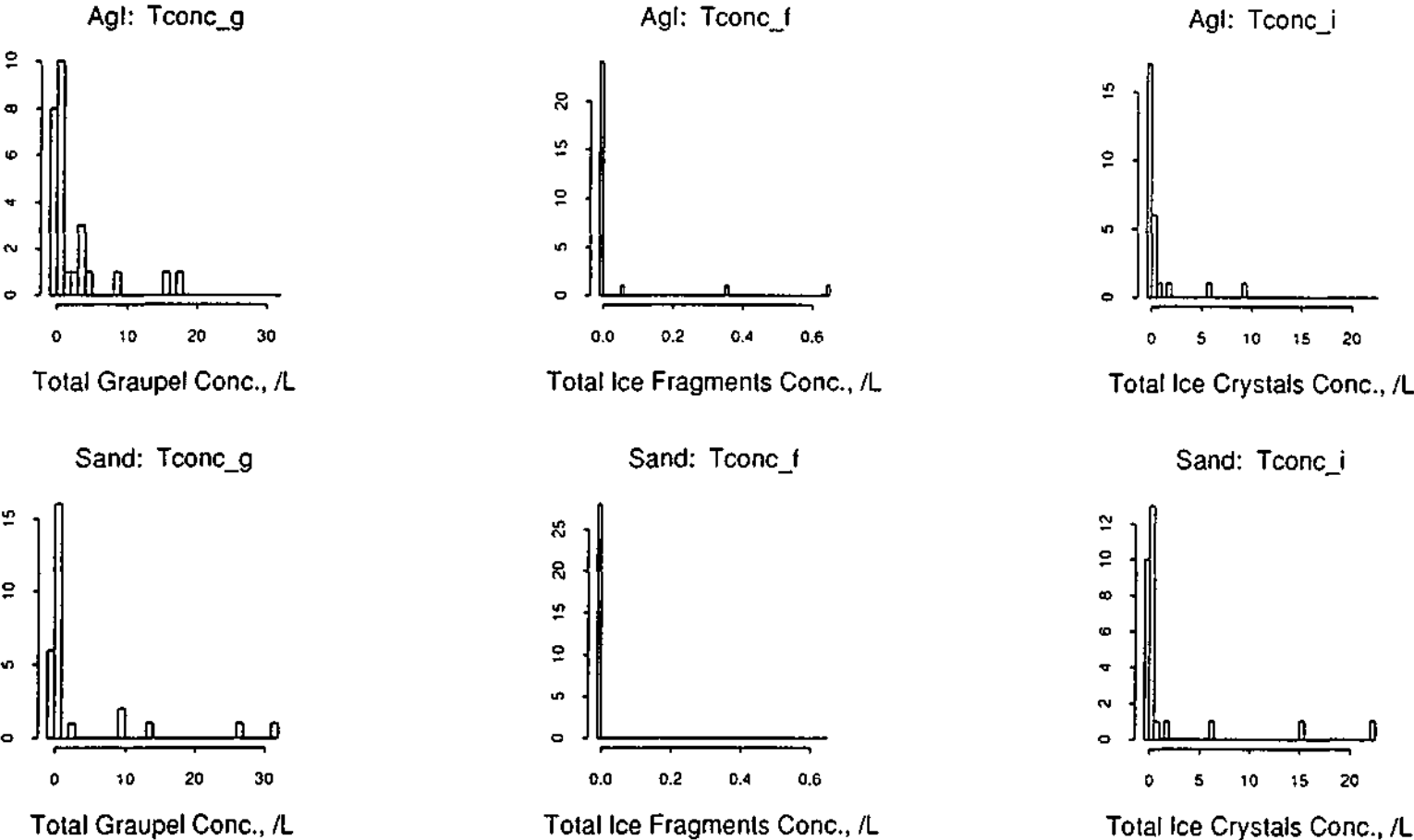
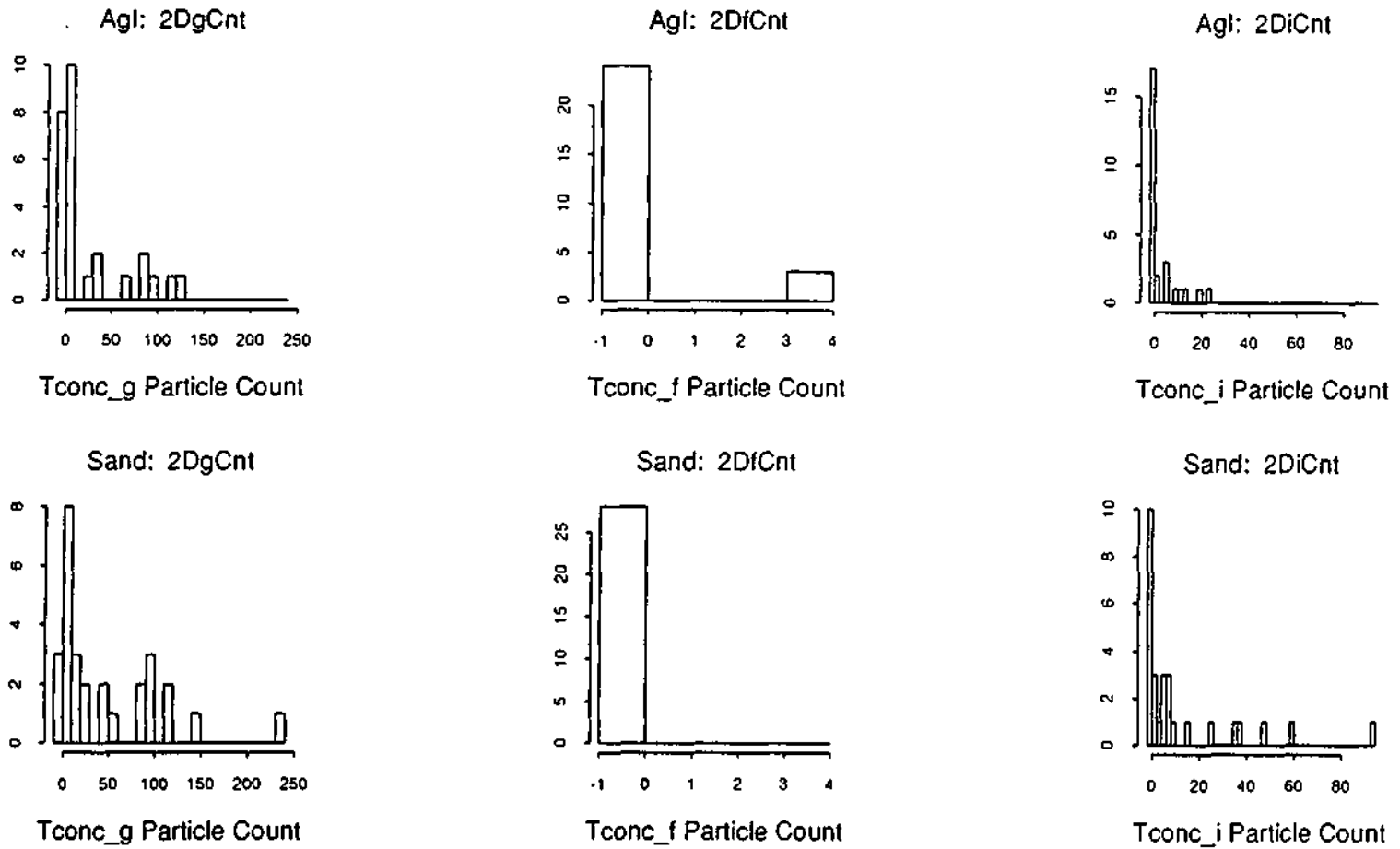


Figure C.61. Histograms of the concentration of graupel ( $Tconc_g$ ), ice fragment ( $Tconc_f$ ), and ice crystal particles ( $Tconc_i$ ) in the main updraft .

# PACE89 DATA

Total Sample



144

Figure C.62. Histograms of the 2D probes total particle count (of graupel) in *Tconc\_g* (2DgCnt), (of ice fragments) in *Tconc\_f* (2DfCnt), and (of ice crystals) in *Tconc\_i* (2DiCnt).

# PACE89 DATA

## Total Sample

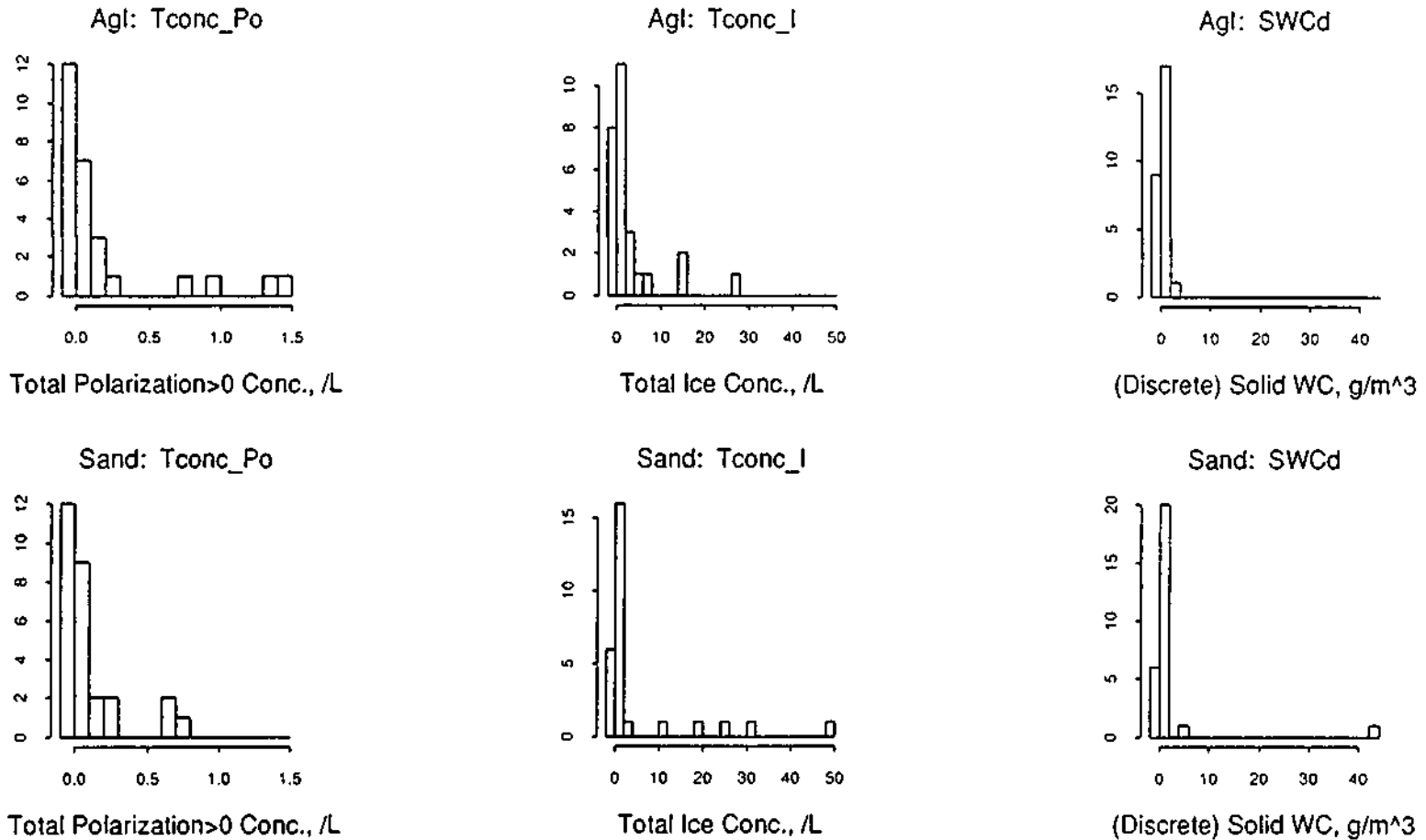


Figure C.63. Histograms of the concentration of particles with depolarization signal  $> 0$  ( $Tconc\_Po$ ), the total concentration of ice particles ( $Tconc\_I$ ), and the solid water content by method I (i.e., discrete) ( $SWCd$ ) in the main updraft.

# PACE89 DATA

## Total Sample

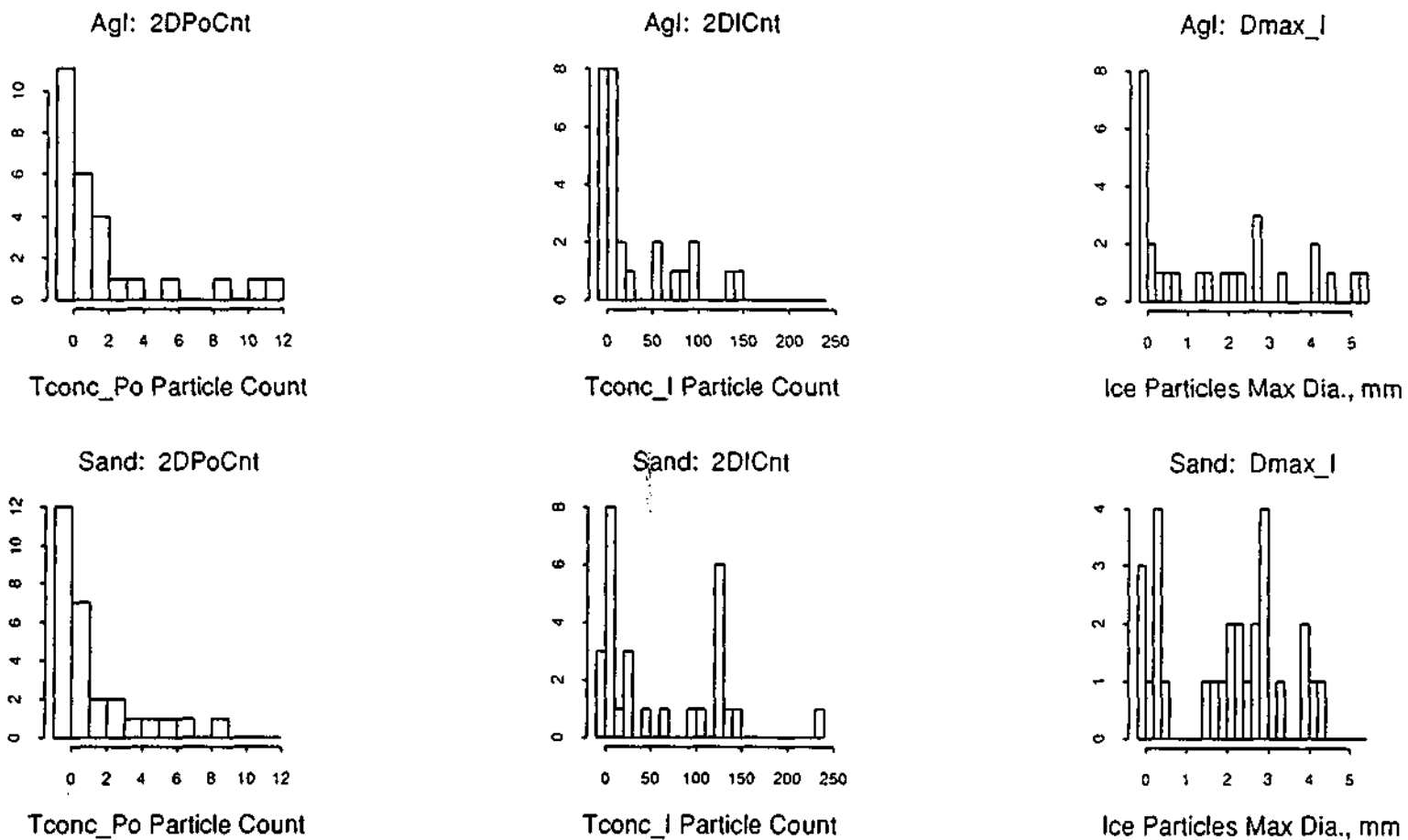


Figure C.64. Histograms of the 2D probes total particle count (of particles with depolarization  $> 0$ ) in *Tconc\_Po* (2DPoCnt), and (of graupel, fragments and crystals) in *Tconc\_I* (2DICnt), and the maximum diameter of ice particles in the main updraft (*Dmax\_I*).

# PACE89 DATA

Total Sample

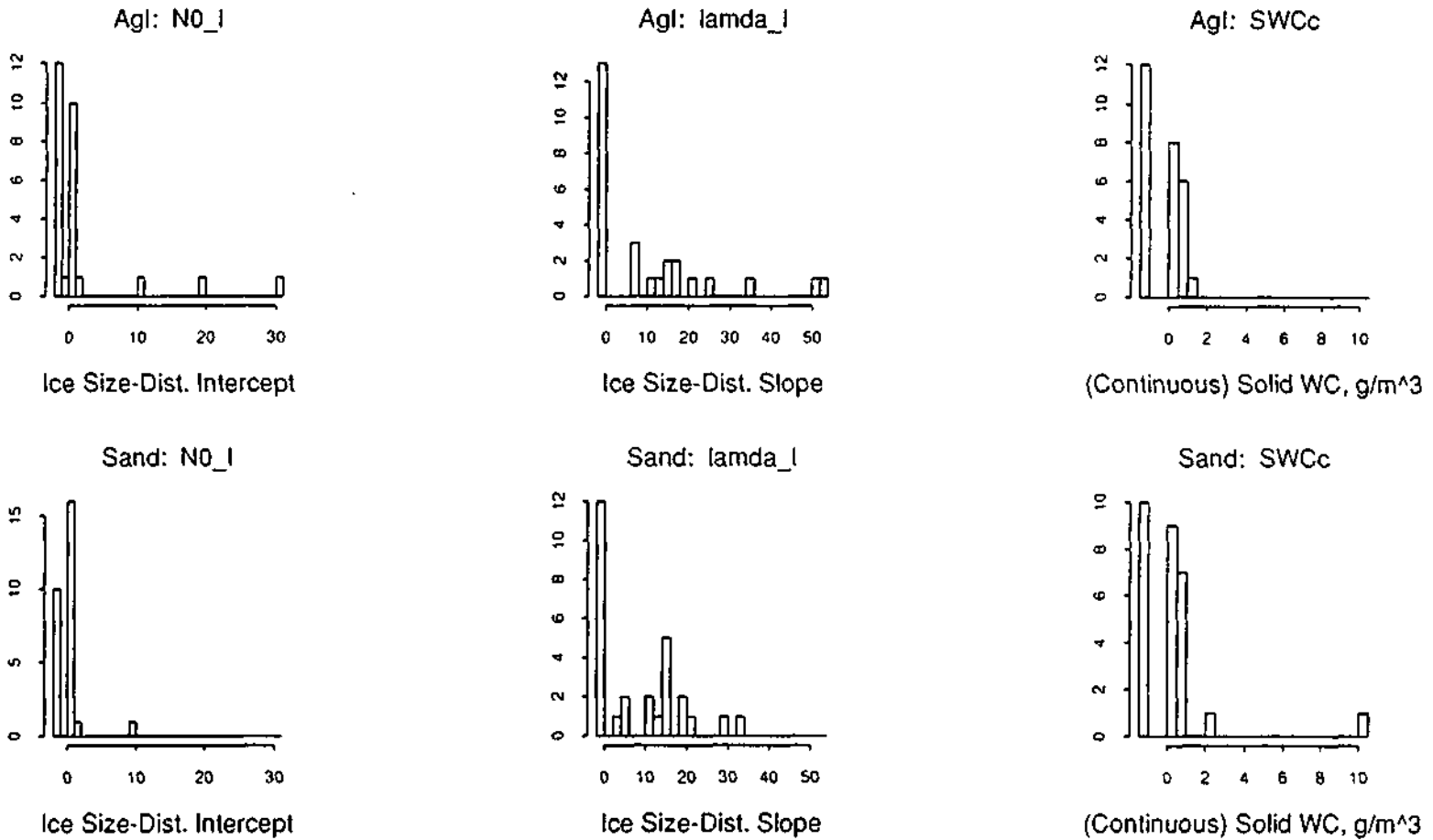


Figure C.65. Histograms of the ice size-distribution intercepts ( $NO_I$ ) and slopes ( $lamda_I$ ), and the solid water content by method II (i.e., continuous; area under the line defined by  $NO_I$  and  $lamda_I$ ) ( $SWCc$ ) in the main updraft.

# PACE89 DATA

Total Sample

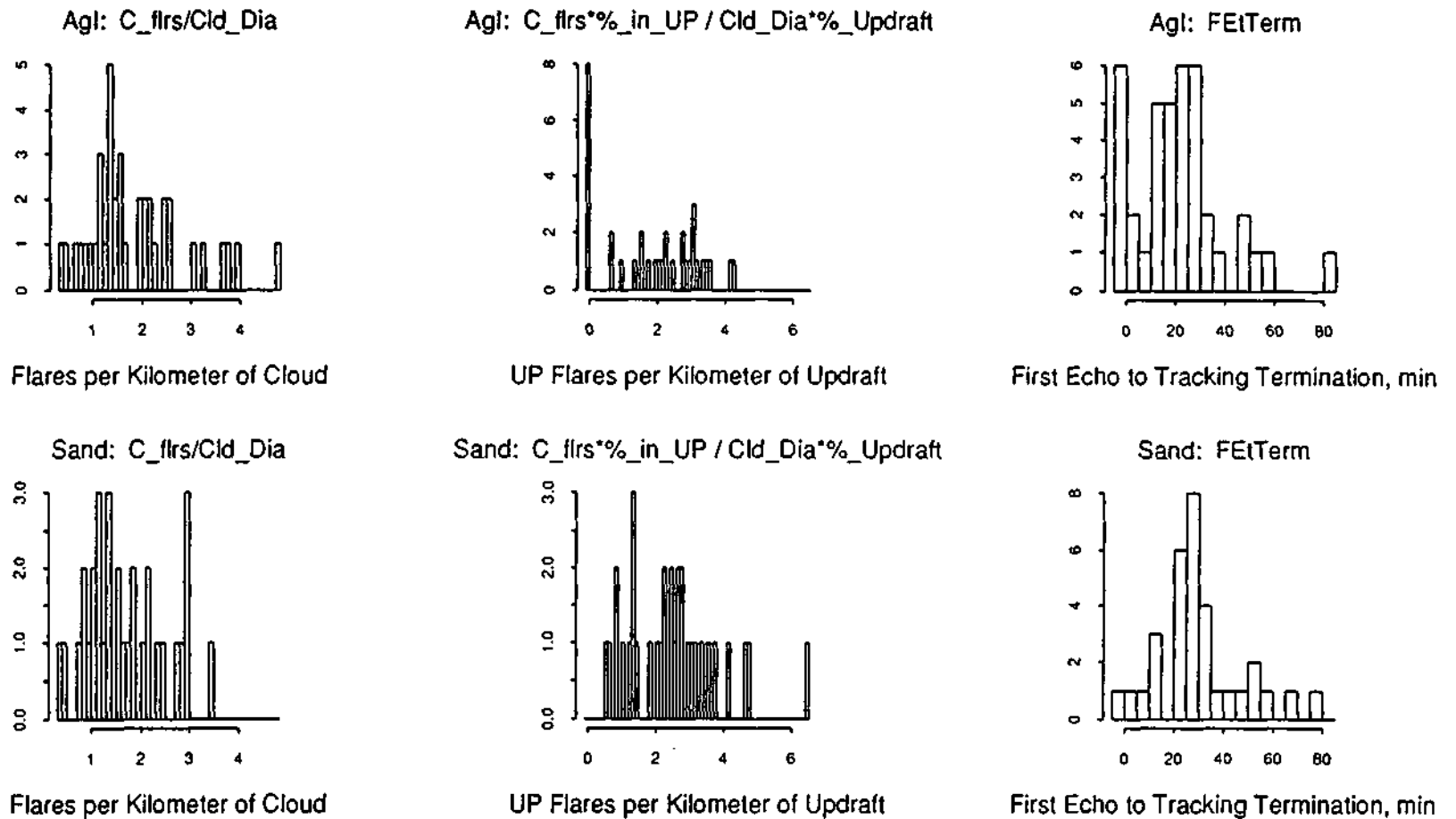


Figure C.66. Histograms of the number of flares released in cloud per kilometer of cloud ( $C\_flrs + Cld\_Dia$ ), the number of flares released into updraft regions of the cloud per kilometer of updraft ( $C\_flrs \times \%\_in\_UP + Cld\_Dia \times \%\_Updraft$ ), and the time from first echo to termination of echo tracking ( $FEtTerm$ ).

**Part D**  
**Subpopulation Composite Diagrams and Comparisons**

This Part presents composite diagrams and corresponding tables of population statistics according to different levels of the Seedability Index (SI) and synoptic types. P-Values are from rerandomization method 2 (see Part F of this Book);  $t$  is Student's  $t$  test for differences in the means, and  $W$  stands for the Wilcoxon sum rank test for differences in the distributions.

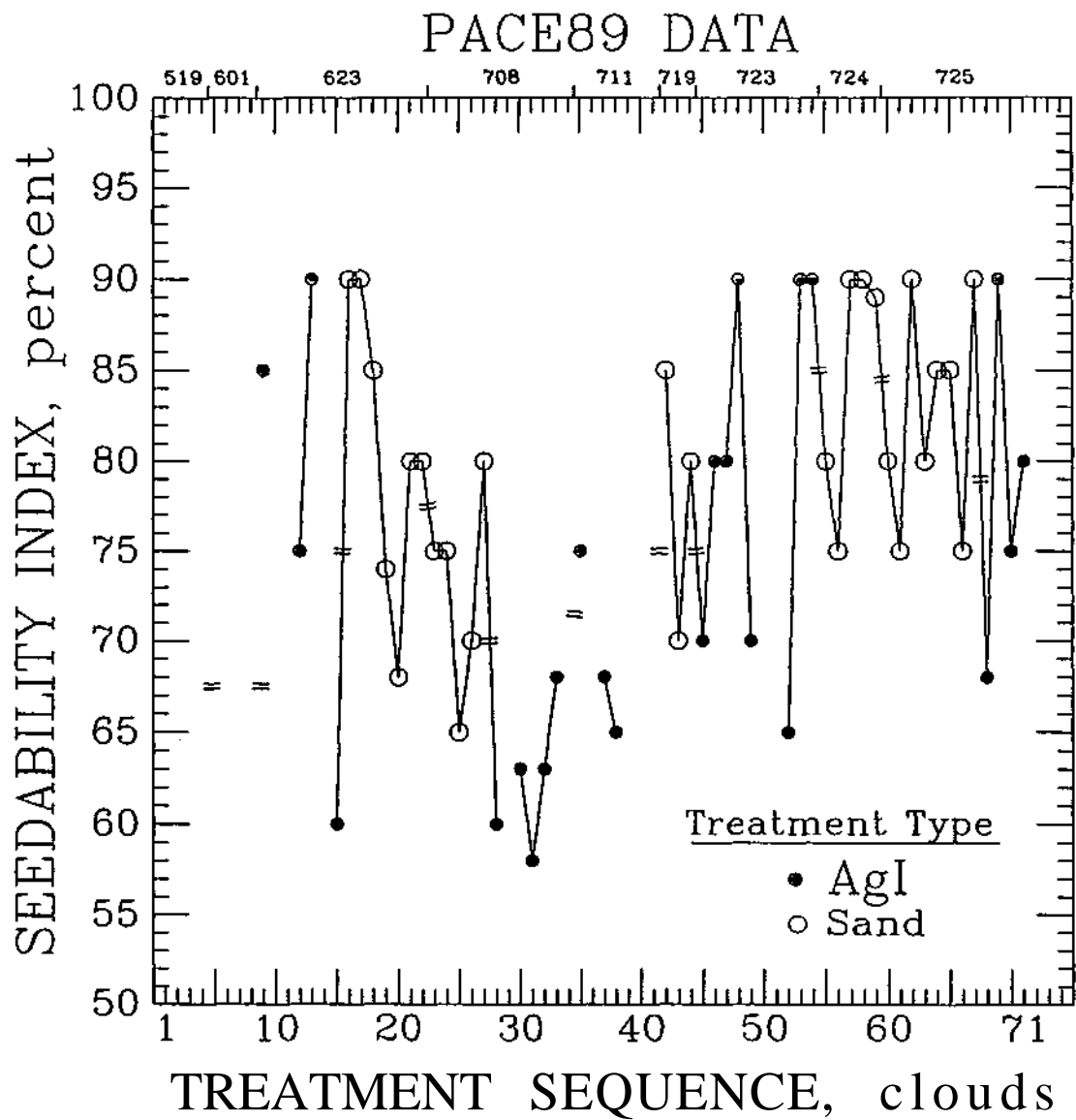


Figure D.1. Temporal variation of the Seedability Index (SI). Values of the index are not joined by a solid line if an intervening value was missing.



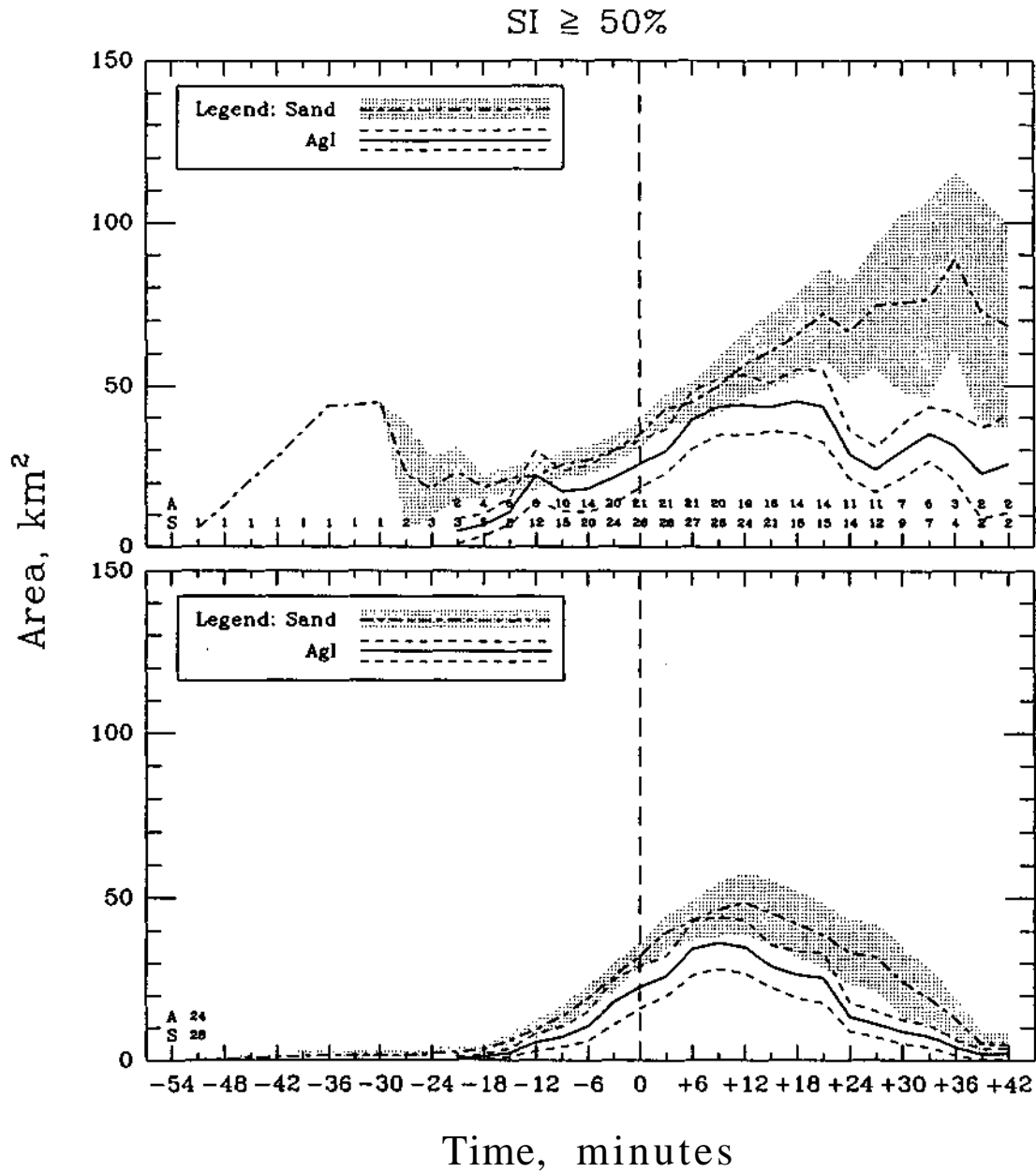


Figure D.3. Variation with time of means of the 10 dBZ defined echo areas for sand- and AgI-treated echoes in existence at each interpolated volume scan (top) and all treated echoes (bottom) for the subpopulation of clouds with SI  $\geq$  50%.

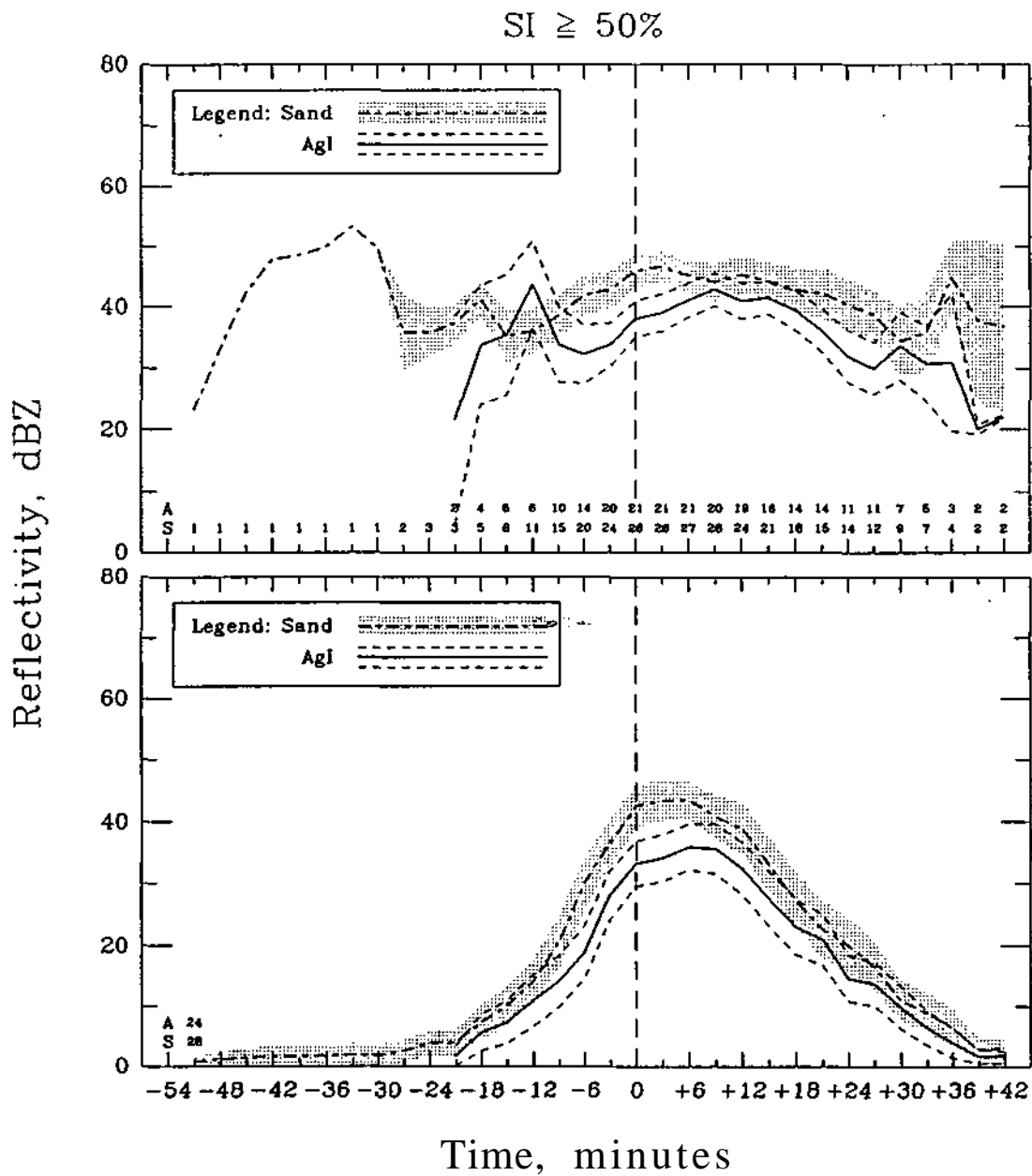


Figure D.4. Variation with time of means of maximum reflectivities for sand- and AgI-treated echoes in existence at each interpolated volume scan (top) and all treated echoes (bottom) for the subpopulation of clouds with SI  $\geq$  50%.

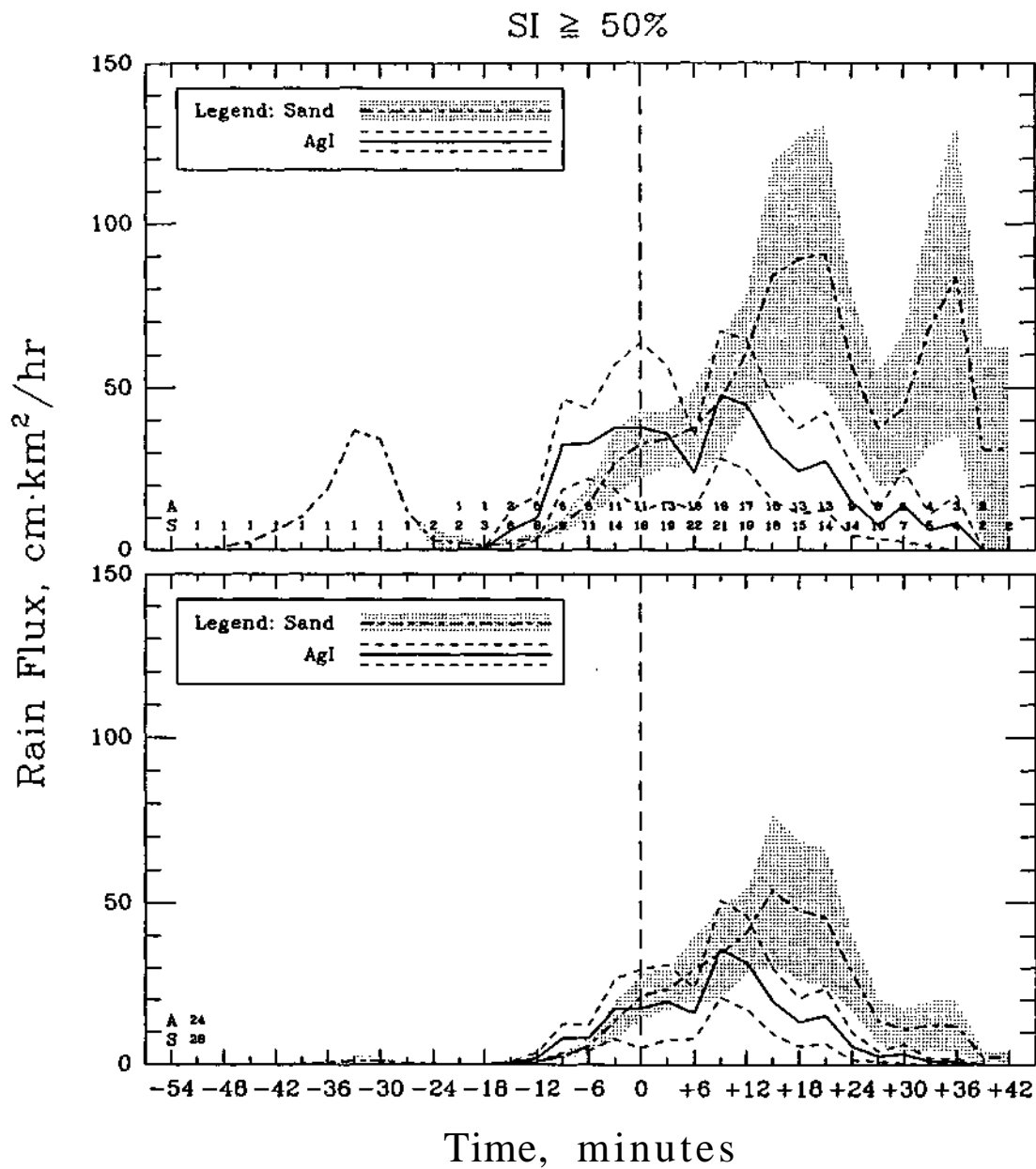


Figure D.5. Variation with time of means of rain fluxes for sand- and AgI-treated echoes in existence at each interpolated volume scan (top) and all treated echoes (bottom) for the subpopulation of clouds with  $SI \geq 50\%$ .

Table D.1. Population statistics of predictor variables for clouds with SI 50% (N = 52).

Variable	Mean		Standard Deviation		Sample Size		P-Values	
	Sand	AgI	Sand	AgI	Sand	AgI	t	W
CPmndia	4.4	3.2	2.4	2.5	28	24	0.08	0.03
CPHip10	7.0	6.2	3.2	3.2	28	24	0.11	0.05
CPMxZ	41.2	31.4	20.3	19.5	28	24	0.08	0.05
CPMxB	21.4	17.1	10.3	9.5	28	24	0.18	0.03
CPA10	31.9	21.9	23.6	32.2	28	24	0.13	0.05
FECPt	8.6	5.9	11.8	6.7	28	24	0.24	0.49
NBuoy	-1.3	-1.2	3.8	1.6	28	24	0.97	0.20
Buoy_Enh	0.5	0.5	0.0	0.1	28	24	0.06	0.06
Mean_VW	6.6	5.0	3.9	3.3	28	24	0.53	0.26
SWC_frac	0.2	0.2	0.3	0.3	28	24	0.75	0.94
pb	4.6	5.3	1.9	2.0	28	24	0.29	0.19
tccl	16.7	16.3	1.9	1.7	28	24	0.44	0.70
Ri	70.9	86.2	21.4	39.0	28	24	0.44	0.70

Table D.2. Population statistics of response variables for clouds with SI 50% (N = 52).

Variable	Mean		Standard Deviation		Sample Size		P-Values	
	Sand	AgI	Sand	AgI	Sand	AgI	t	W
MaxH10	10.7	8.5	2.7	2.0	28	24	0.06	0.06
MaxA10	75.6	52.0	61.3	51.2	28	24	0.03	0.11
MaxZ	51.0	46.4	14.4	13.6	28	24	0.10	0.06
MaxB	26.9	25.5	6.9	7.2	28	24	0.34	0.31
MXCPdH10	2.4	0.1	2.7	2.6	28	24	0.12	0.12
MXCPdA10	35.5	26.0	55.7	42.4	28	24	0.38	0.71
MXCPdZ	6.8	8.2	13.4	19.1	28	24	0.83	0.83
MXCPdB	3.7	4.3	7.0	10.7	28	24	0.84	0.81
CPMXtMxA	9.7	8.0	13.7	7.7	28	24	0.54	0.43
FEMXtMxA	18.3	13.9	11.2	8.9	28	24	0.03	0.03
TotRNVOL	11.2	10.8	39.7	42.9	28	24	0.86	0.10
MxRFx	10.2	8.5	17.2	19.6	28	24	0.69	0.13
FETTerm	32.3	26.6	17.6	19.8	28	24	0.16	0.09

$p \leq 5\%$

$5 < p \leq 10\%$

$p > 10\%$

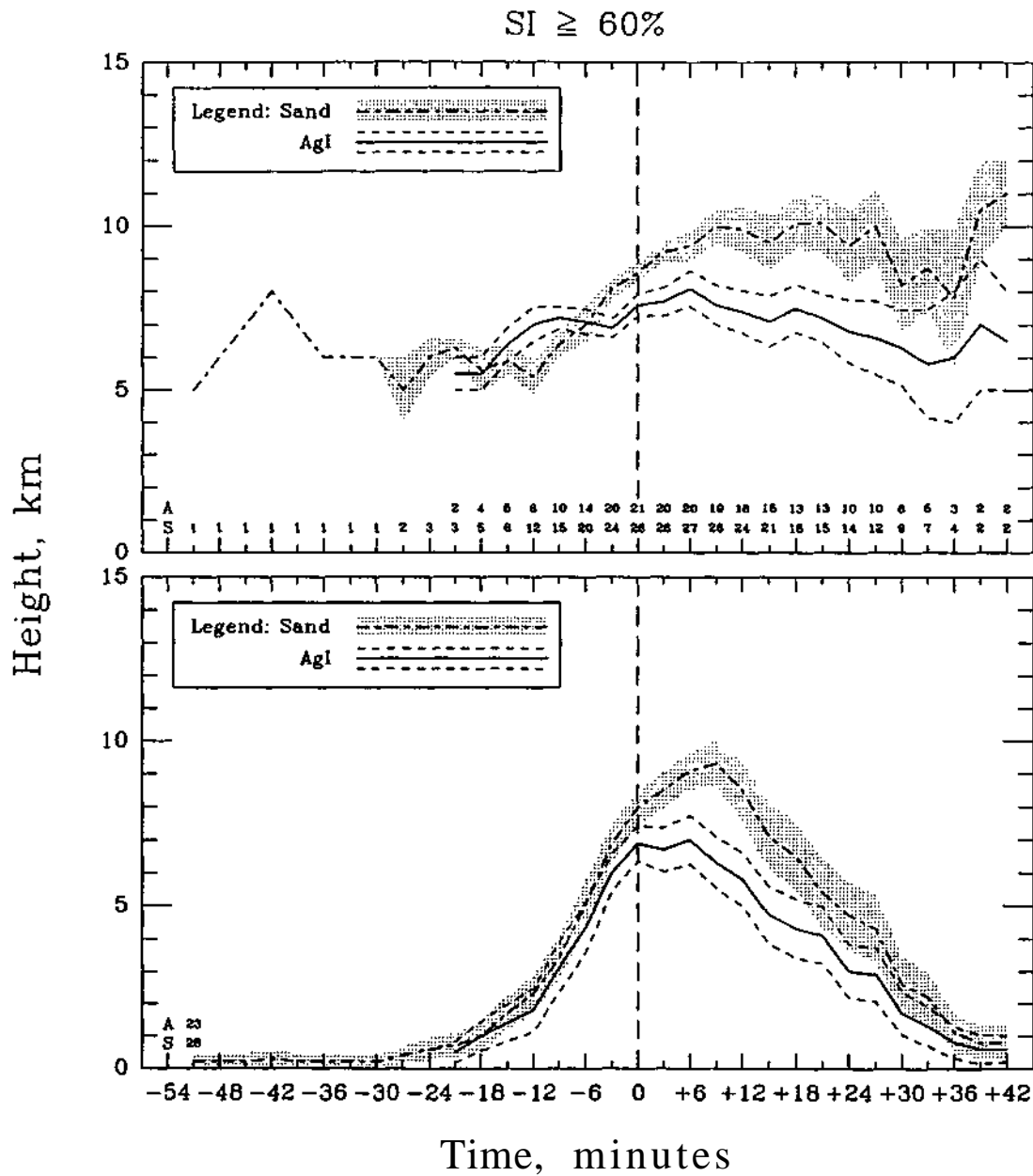


Figure D.6. Variation with time of means of the 10 dBZ echo top heights for sand- and AgI-treated echoes in existence at each interpolated volume scan (top) and all treated echoes (bottom) for the subpopulation of clouds with SI  $\geq$  60%.

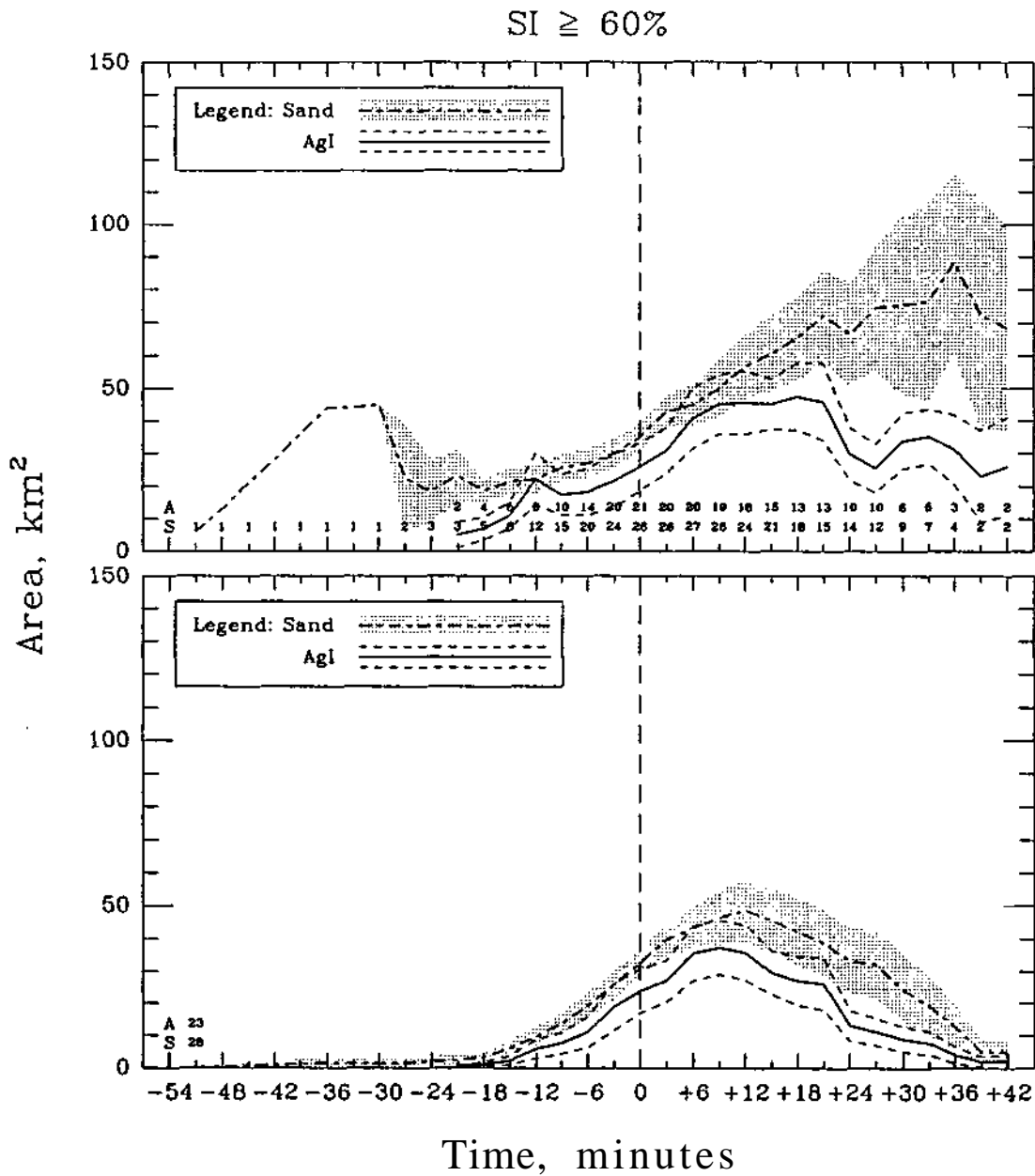


Figure D.7. Variation with time of means of the 10 dBZ defined echo areas for sand- and AgI-treated echoes in existence at each interpolated volume scan (top) and all treated echoes (bottom) for the subpopulation of clouds with  $SI \geq 60\%$ .

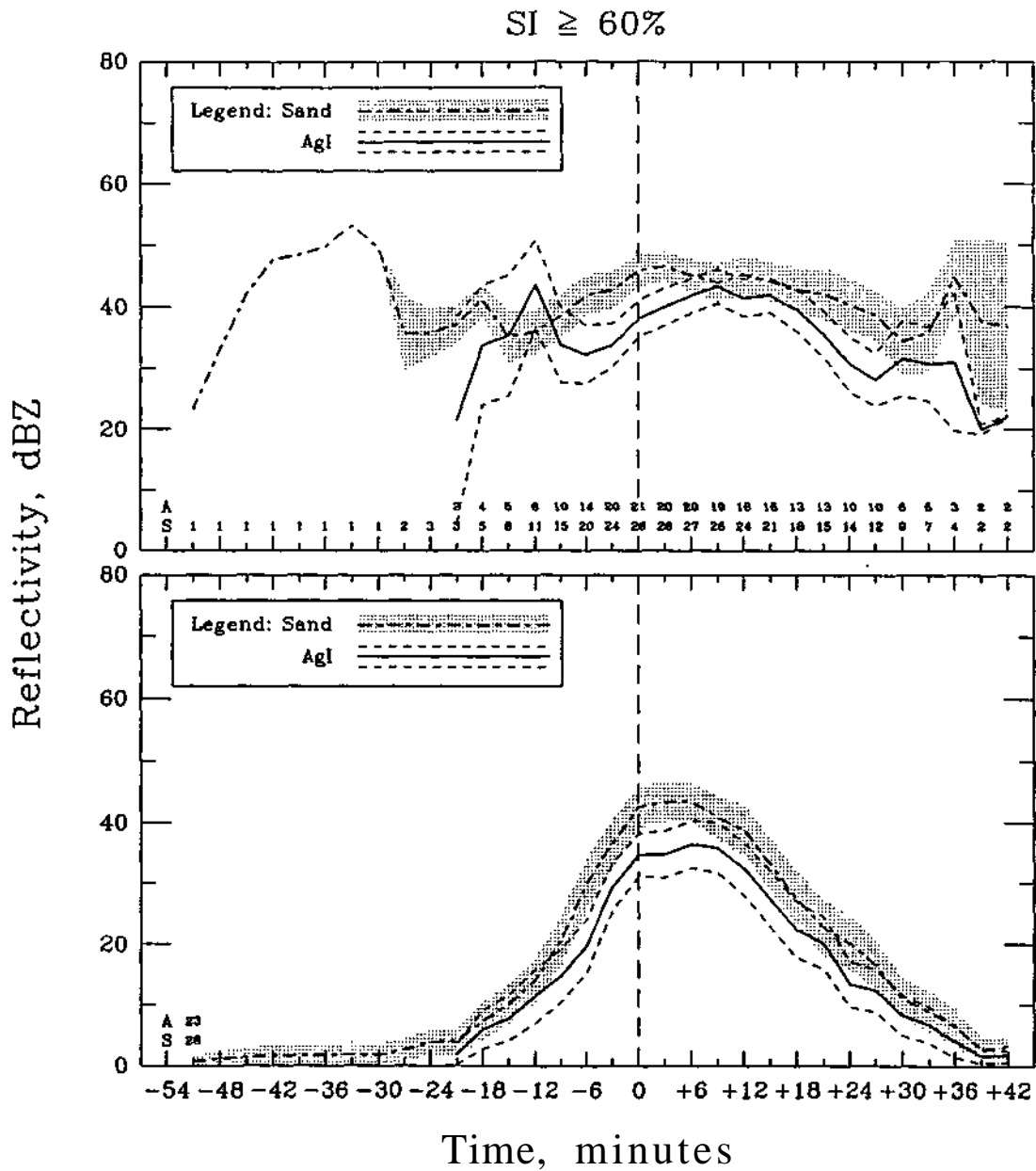


Figure D.8. Variation with time of means of maximum reflectivities for sand- and AgI-treated echoes in existence at each interpolated volume scan (top) and all treated echoes (bottom) for the subpopulation of clouds with SI  $\geq$  60%.

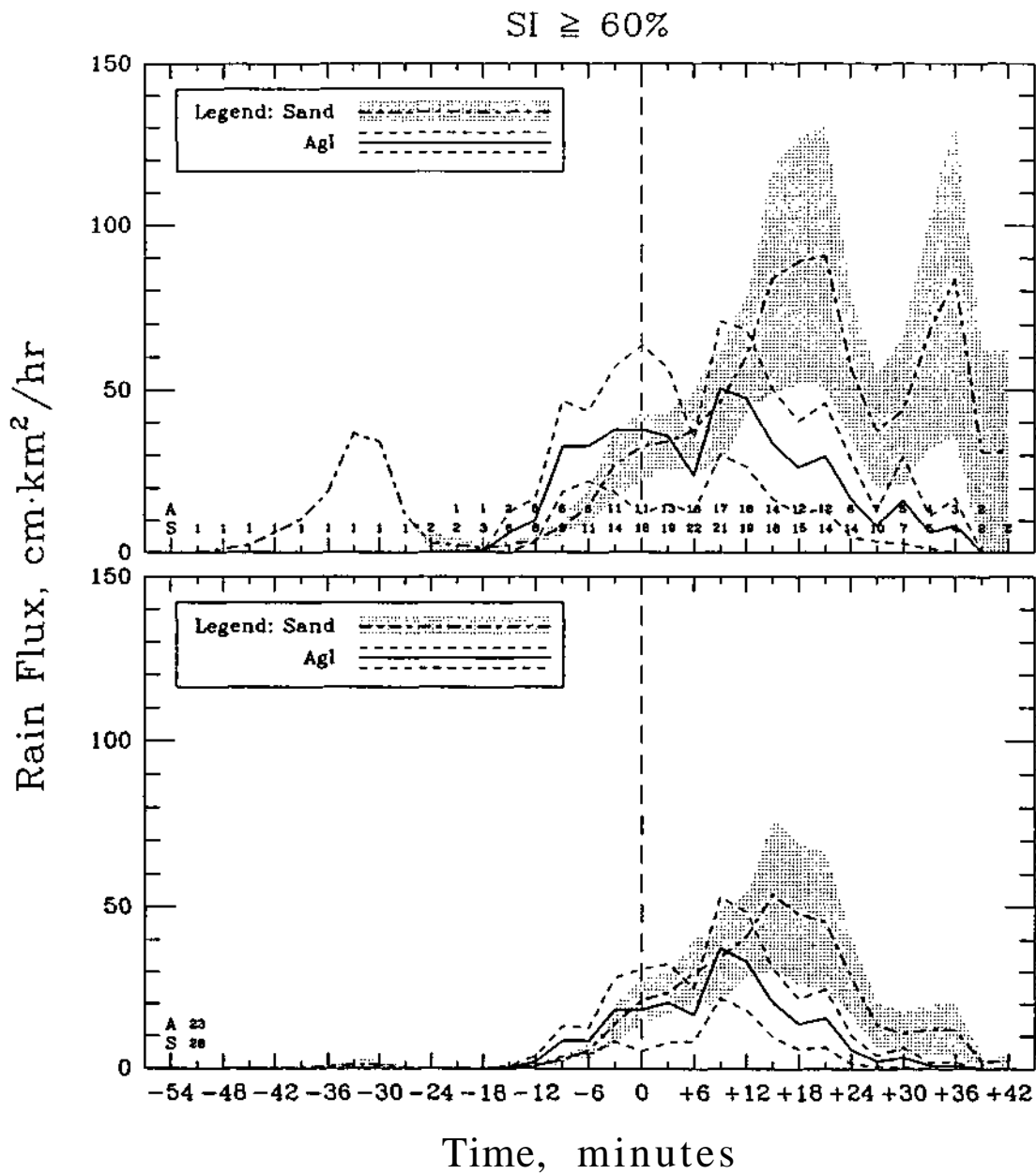


Figure D.9. Variation with time of means of rain fluxes for sand- and AgI-treated echoes in existence at each interpolated volume scan (top) and all treated echoes (bottom) for the subpopulation of clouds with  $SI \geq 60\%$ .

Table D.3. Population statistics of predictor variables for clouds with SI 60% (N = 51).

Variable	Mean		Standard Deviation		Sample Size		P-Values	
	Sand	AgI	Sand	AgI	Sand	AgI	t	W
CPmndia	4.4	3.4	2.4	2.4	28	23	0.15	0.05
CPHtp10	7.0	6.4	3.2	3.0	28	23	0.38	0.08
CPMxZ	41.2	32.7	20.3	18.7	28	23	0.20	0.13
CPMxB	21.4	17.8	10.3	9.0	28	23	0.25	0.08
CPA10	31.9	22.8	23.6	32.6	28	23	0.15	0.05
FECPI	8.6	6.3	11.8	6.6	28	23	0.37	0.63
NBuoy	-1.3	-1.2	3.8	1.6	28	23	0.97	0.22
Buoy_Enh	0.5	0.5	0.0	0.1	28	23	0.06	0.09
Mean_VW	6.6	4.9	3.9	3.4	28	23	0.53	0.26
SWC_frac	0.2	0.2	0.3	0.3	28	23	0.83	0.88
pb	4.6	5.1	1.9	1.9	28	23	0.46	0.28
tccl	16.7	16.4	1.9	1.6	28	23	0.55	0.88
Ri	70.9	86.6	21.4	39.8	28	23	0.41	0.76

Table D.4. Population statistics of response variables for clouds with SI 60% (N = 51).

Variable	Mean		Standard Deviation		Sample Size		P-Values	
	Sand	AgI	Sand	AgI	Sand	AgI	t	W
MaxH10	10.7	8.5	2.7	2.0	28	23	0.06	0.06
MaxA10	75.6	53.3	61.3	51.9	28	23	0.03	0.11
MaxZ	51.0	46.4	14.4	13.9	28	23	0.13	0.06
MaxB	26.9	25.3	6.9	7.3	28	23	0.18	0.29
MXCPdH10	2.4	0.1	2.7	2.7	28	23	0.12	0.12
MXCPdA10	35.5	26.3	55.7	43.3	28	23	0.41	0.71
MXCPdZ	6.8	6.5	13.4	17.7	28	23	0.98	1.00
MXCPdB	3.7	3.1	7.0	9.2	28	23	0.87	1.00
CPMXtMxA	9.7	7.6	13.7	7.6	28	23	0.51	0.43
FEMXtMxA	18.3	13.9	11.2	9.1	28	23	0.03	0.03
TotRNVOL	11.2	11.2	39.7	43.8	28	23	0.97	0.10
MxRFx	10.2	8.8	17.2	20.0	28	23	0.77	0.13
FEtTerm	32.3	26.8	17.6	20.2	28	23	0.23	0.09

$p \leq 5\%$

$5 < p \leq 10\%$

$p > 10\%$



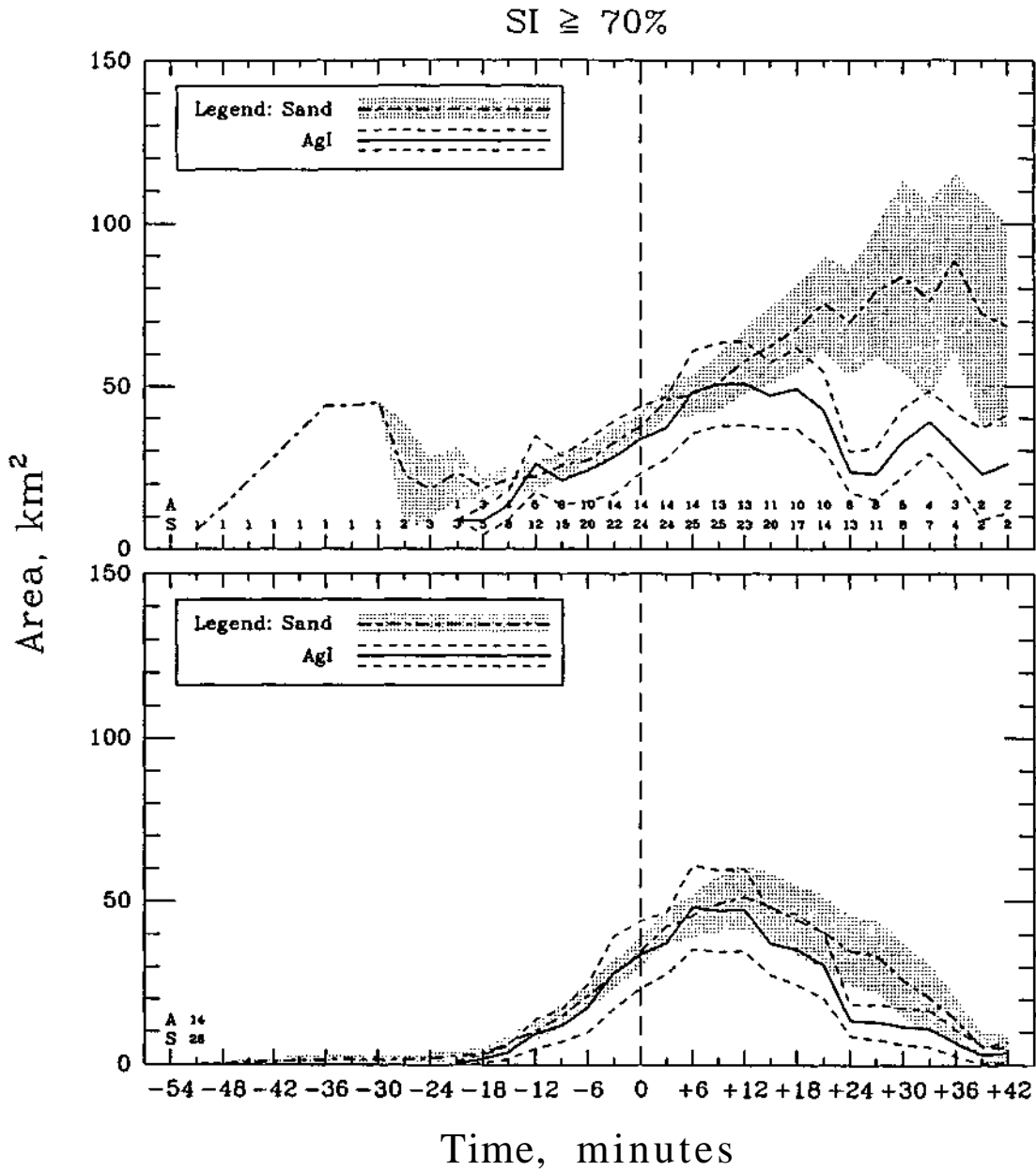


Figure D.11. Variation with time of means of the 10 dBZ defined echo areas for sand- and AgI-treated echoes in existence at each interpolated volume scan (top) and all treated echoes (bottom) for the subpopulation of clouds with SI  $\geq$  70%.

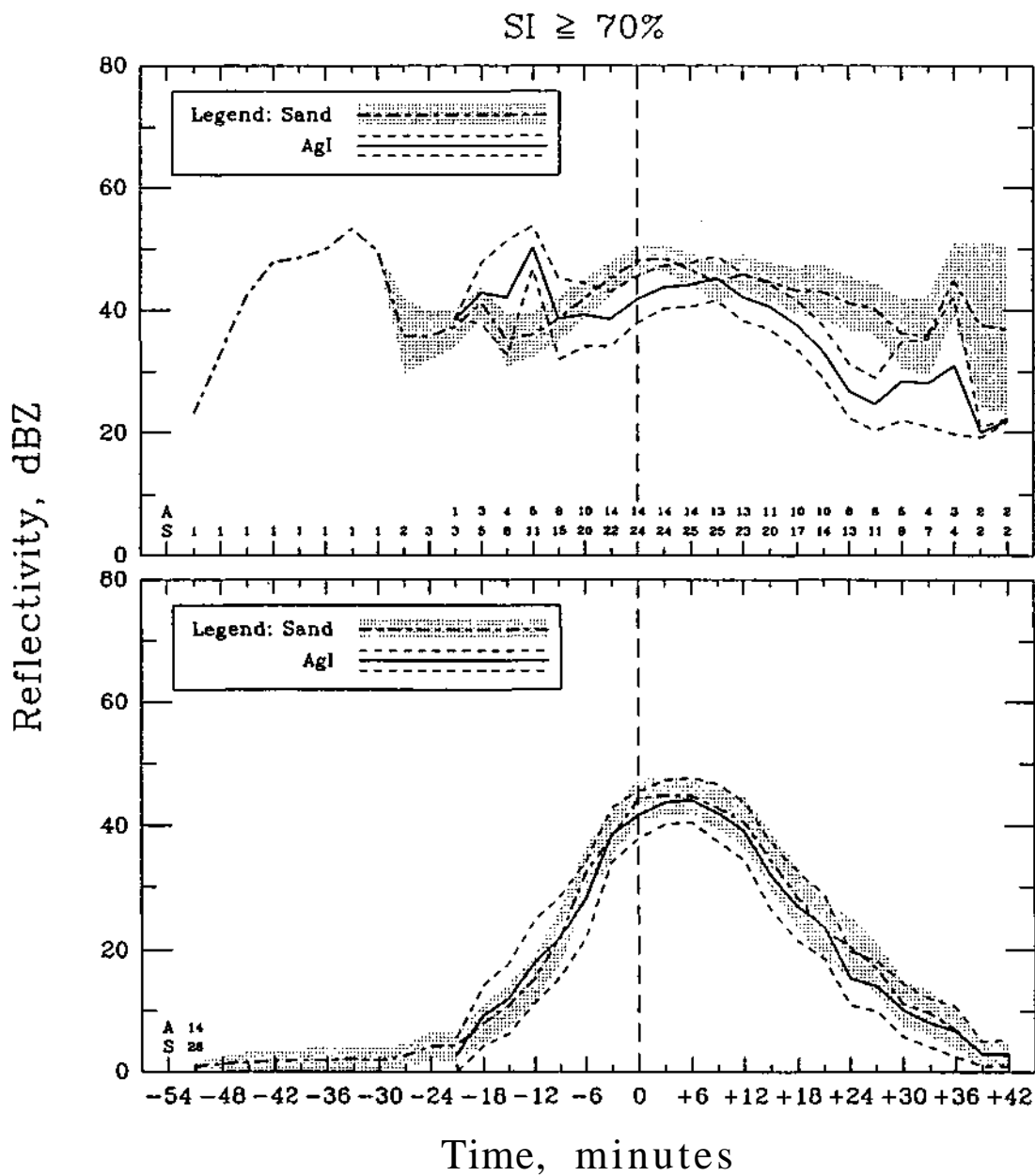


Figure D.12. Variation with time of means of maximum reflectivities for sand- and AgI-treated echoes in existence at each interpolated volume scan (top) and all treated echoes (bottom) for the subpopulation of clouds with SI  $\geq$  70%.

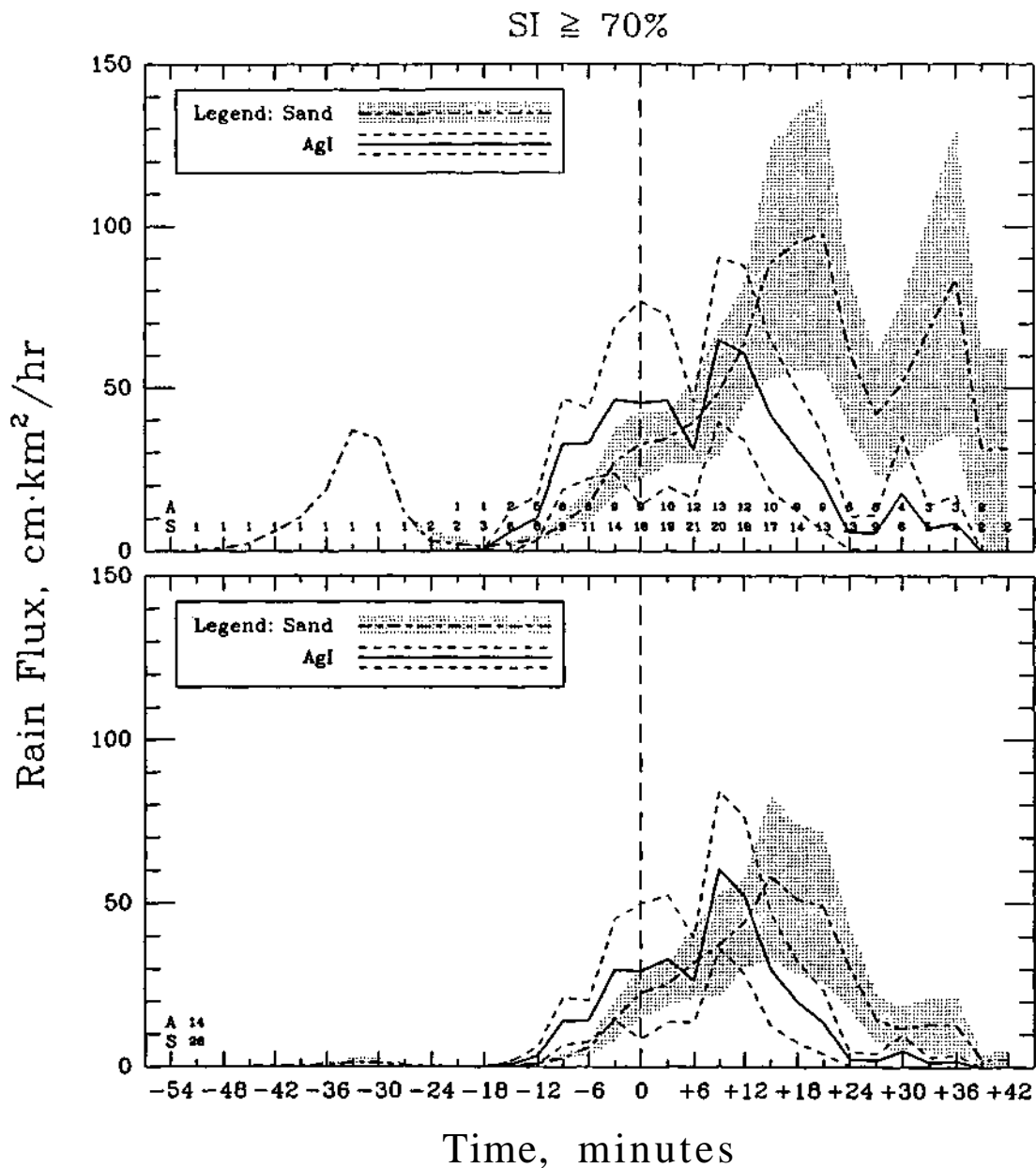


Figure D.13. Variation with time of means of rain fluxes for sand- and Agl-treated echoes in existence at each interpolated volume scan (top) and all treated echoes (bottom) for the subpopulation of clouds with  $SI \geq 70\%$ .

Table D.5. Population statistics of predictor variables for clouds with SI 70% (N = 40).

Variable	Mean		Standard Deviation		Sample Size		P-Values	
	Sand	Agl	Sand	Agl	Sand	Agl	t	W
CPmndia	4.8	4.4	2.1	2.3	26	14	0.65	0.16
CPHlp10	7.5	7.6	2.6	1.9	26	14	0.98	0.42
CPMxZ	44.3	41.7	17.3	14.2	26	14	0.78	0.45
CPMxB	23.1	22.1	8.7	5.8	26	14	0.81	0.32
CPA10	34.3	33.1	22.6	38.3	26	14	0.88	0.27
FECPt	9.5	8.3	11.8	7.3	26	14	0.69	0.88
NBuoy	-1.3	-1.2	3.9	1.2	26	14	0.95	0.24
Buoy_Enh	0.5	0.5	0.0	0.0	26	14	0.23	0.23
Mean_VW	6.3	4.7	3.8	3.0	26	14	0.53	0.32
SWC_frac	0.2	0.3	0.3	0.3	26	14	0.86	0.75
pb	4.4	4.2	1.8	1.1	26	14	0.82	0.74
tccl	16.9	16.8	1.8	1.2	26	14	0.94	0.88
Ri	71.3	78.9	21.9	32.9	26	14	0.64	0.91

Table D.6. Population statistics of response variables for clouds with SI 70% (N = 40).

Variable	Mean		Standard Deviation		Sample Size		P-Values	
	Sand	Agl	Sand	Agl	Sand	Agl	t	W
MaxH10	10.8	8.6	2.7	2.0	26	14	0.09	0.09
MaxA10	80.2	65.6	61.2	55.6	26	14	0.25	0.28
MaxZ	52.6	52.1	13.5	12.2	26	14	0.98	0.88
MaxB	27.7	28.2	6.4	6.5	26	14	0.85	0.72
MXCPdH10	2.5	0.7	2.7	1.5	26	14	0.25	0.20
MXCPdA10	37.0	26.9	57.5	46.0	26	14	0.49	0.75
MXCPdZ	5.0	6.6	12.2	12.8	26	14	0.81	0.86
MXCPdB	2.7	3.3	6.2	7.0	26	14	0.88	0.79
CPMxtMxA	9.5	8.3	14.1	7.7	26	14	0.83	0.44
FEMXtMxA	19.0	16.6	11.1	9.2	26	14	0.44	0.34
TotRNVOL	12.1	17.9	41.2	55.8	26	14	0.39	0.24
MxRFx	10.9	13.1	17.6	24.6	26	14	0.72	0.56
FEtTerm	33.2	34.5	17.3	20.8	26	14	0.55	0.47

$p \leq 5\%$

$5 < p \leq 10\%$

$p > 10\%$

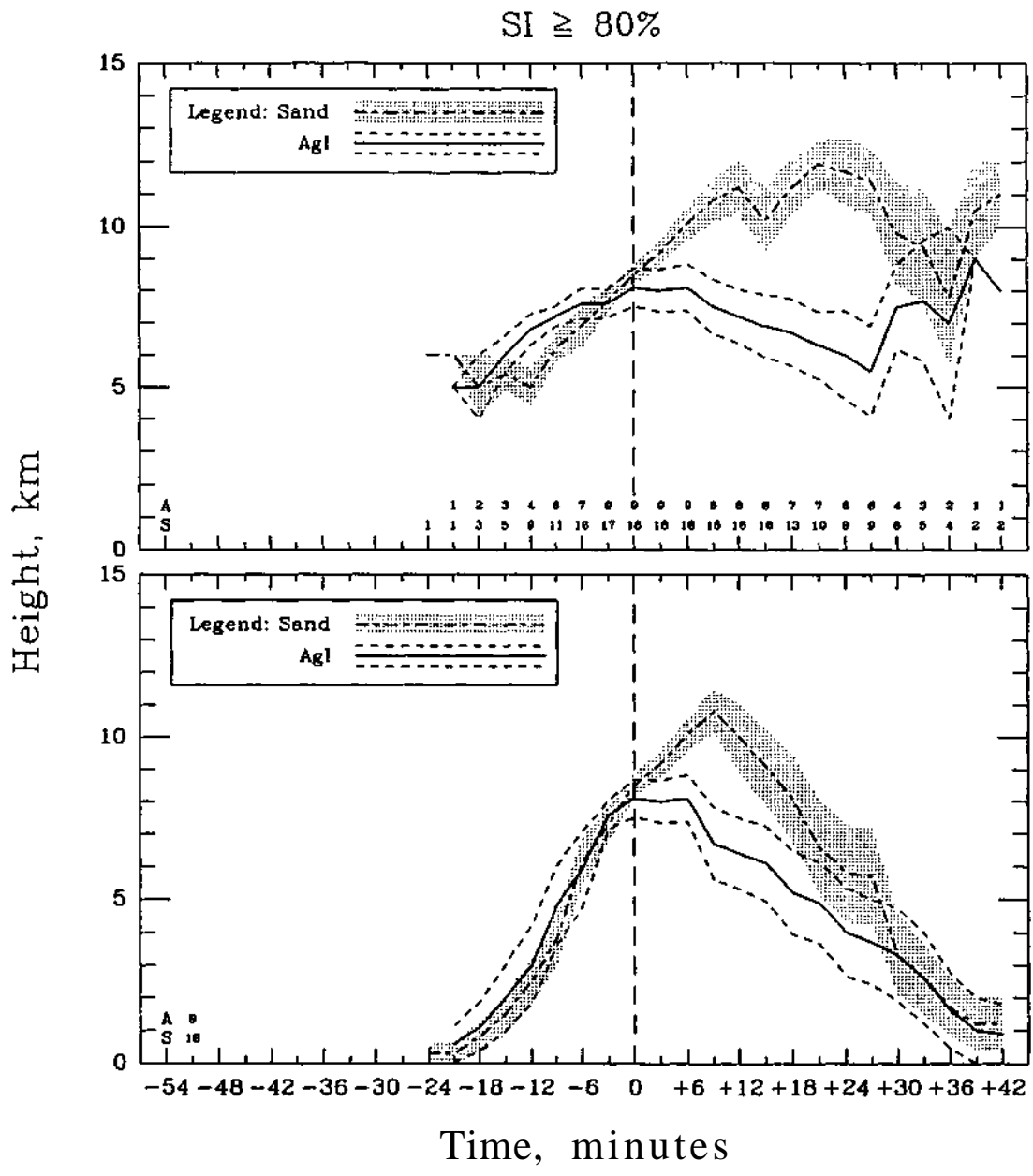


Figure D.14. Variation with time of means of the 10 dBZ echo top heights for sand- and AgI-treated echoes in existence at each interpolated volume scan (top) and all treated echoes (bottom) for the subpopulation of clouds with  $SI \geq 80\%$ .

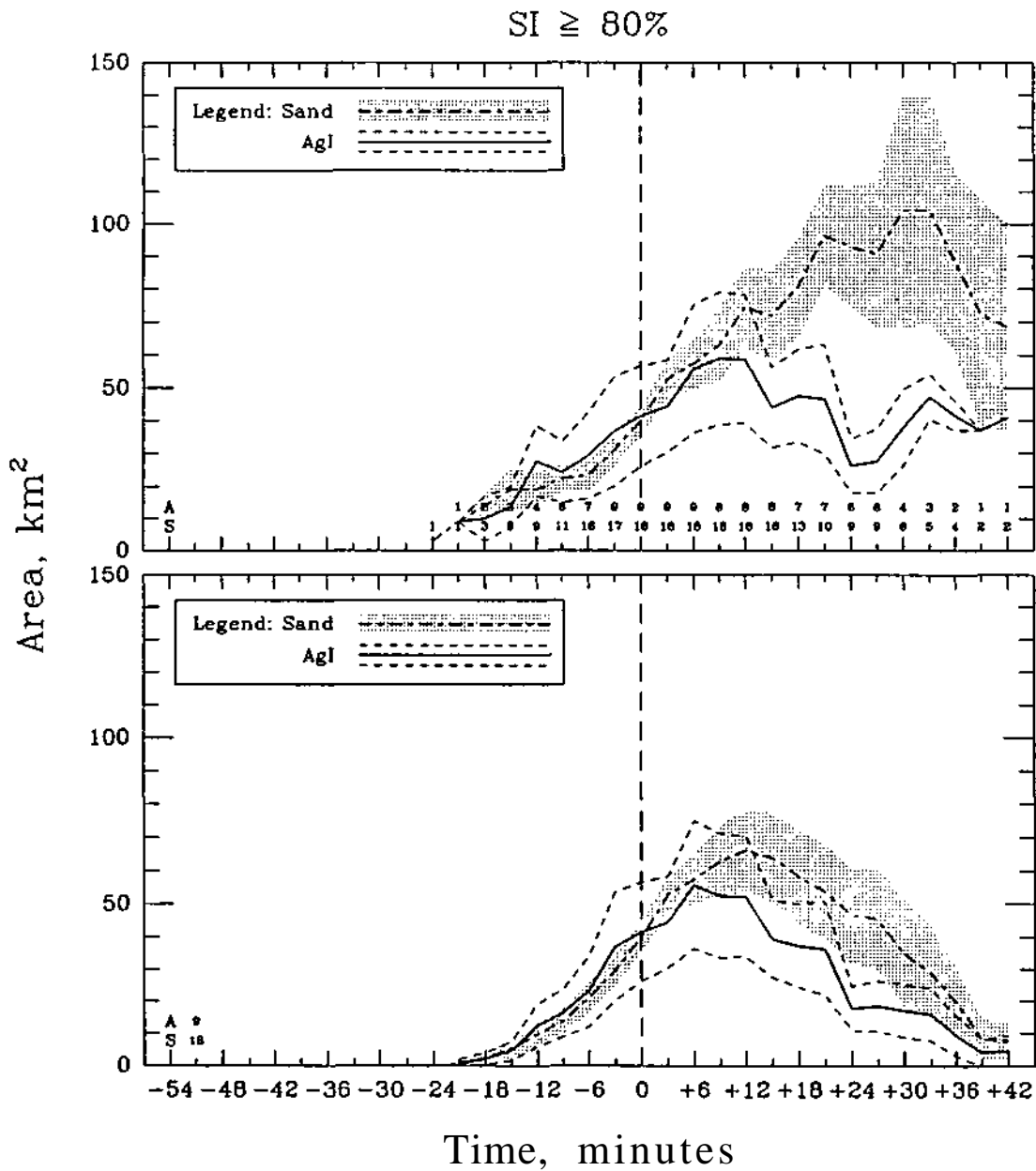


Figure D.15. Variation with time of means of the 10 dBZ defined echo areas for sand- and Agl-treated echoes in existence at each interpolated volume scan (top) and all treated echoes (bottom) for the subpopulation of clouds with SI  $\geq$  80%.

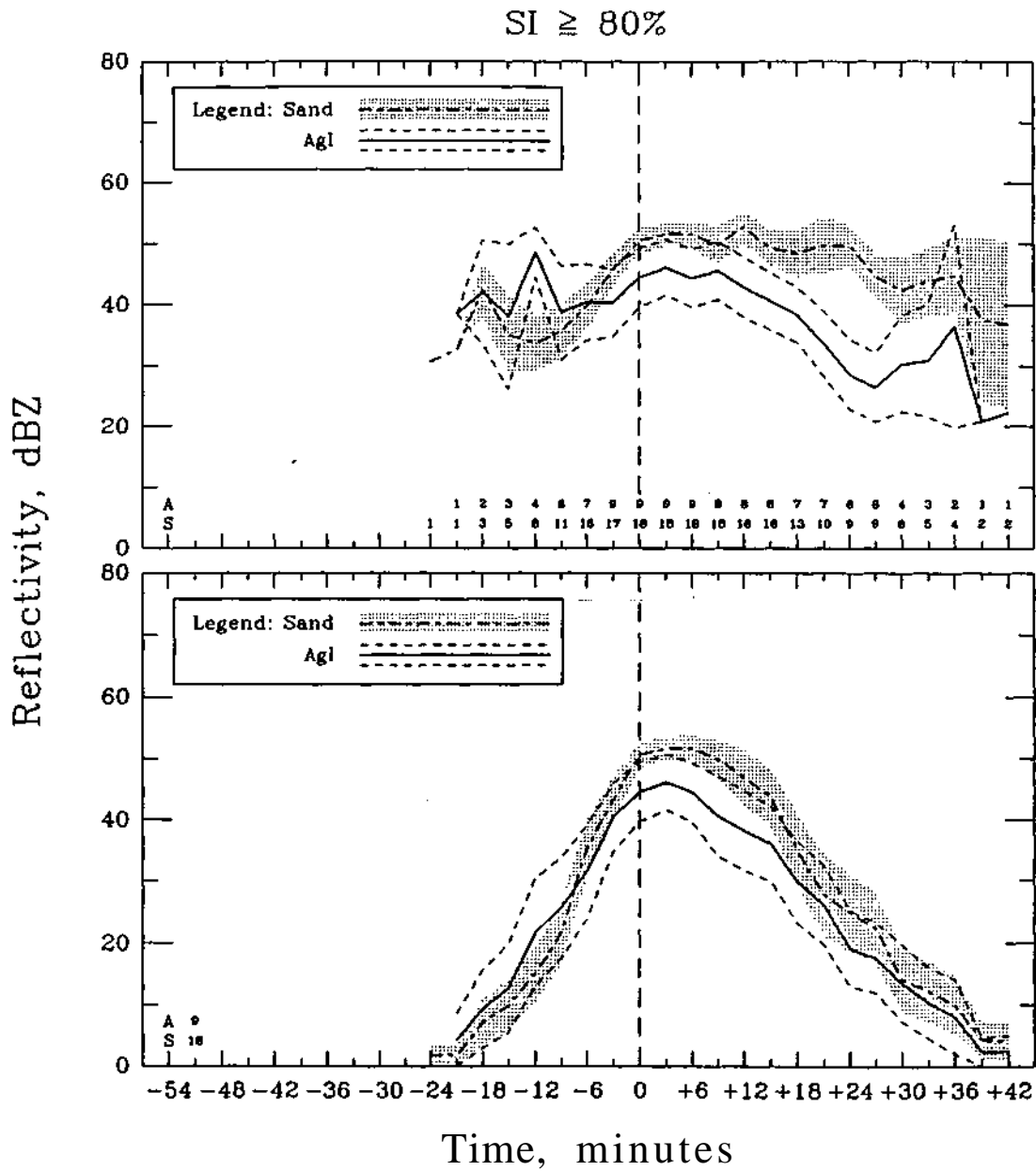


Figure D.16. Variation with time of means of maximum reflectivities for sand- and AgI-treated echoes in existence at each interpolated volume scan (top) and all treated echoes (bottom) for the subpopulation of clouds with SI  $\geq$  80%.

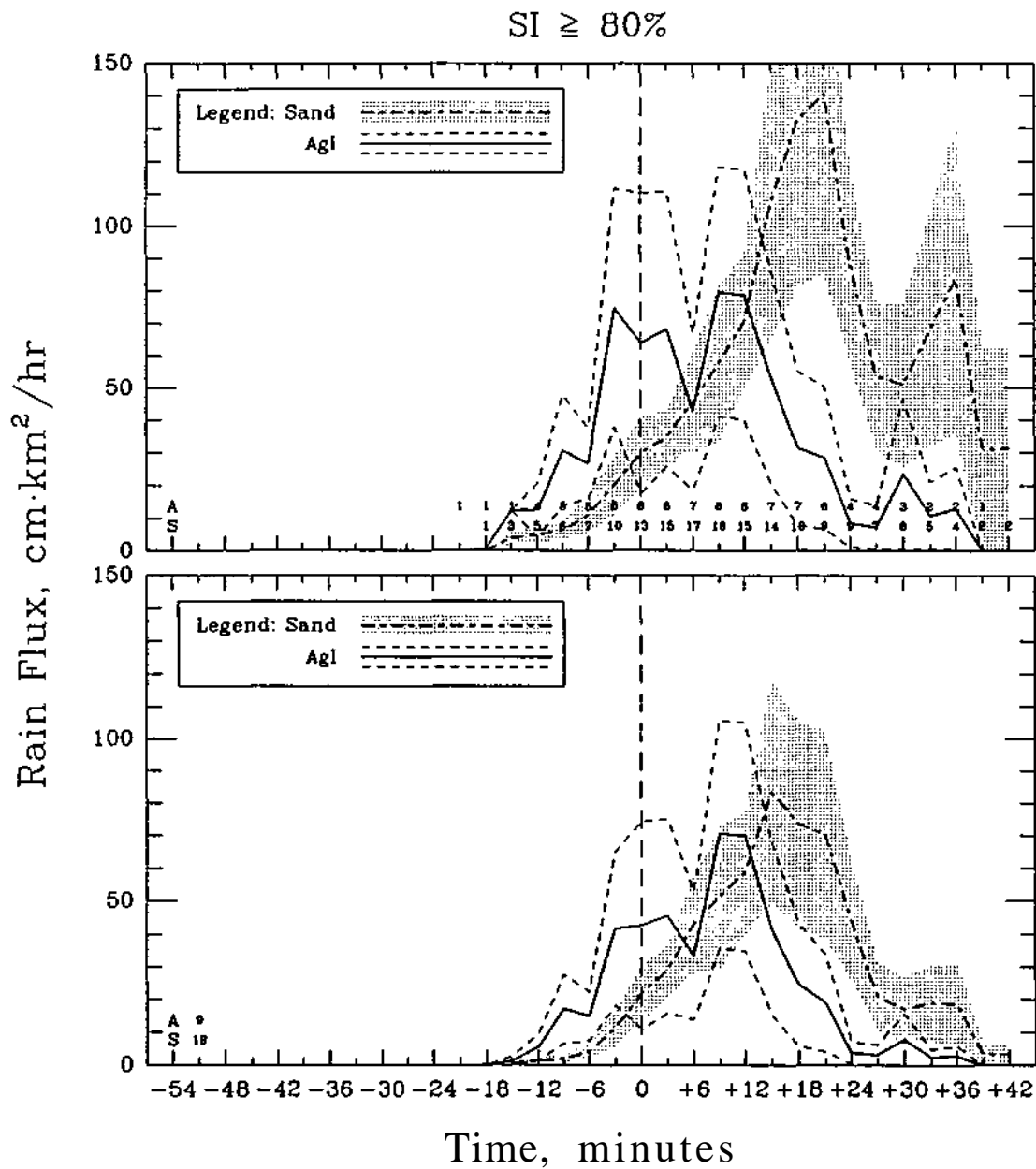


Figure D.17. Variation with time of means of rain fluxes for sand- and AgI-treated echoes in existence at each interpolated volume scan (top) and all treated echoes (bottom) for the subpopulation of clouds with  $SI \geq 80\%$ .

Table D.7. Population statistics of predictor variables for clouds with SI 80% (N = 27).

Variable	Mean		Standard Deviation		Sample Size		P-Values	
	Sand	Agl	Sand	Agl	Sand	Agl	t	W
CPmndia	5.5	4.9	14	2.7	18	9	0.33	0.15
CPHtpIO	8.2	8.1	1.6	1.8	18	9	0.95	0.88
CPMxZ	50.6	44.6	9.0	14.6	18	9	0.15	0.33
CPMxB	25.8	23.5	5.0	5.9	18	9	0.21	0.25
CPA10	39.4	40.9	20.5	45.5	18	9	0.87	0.19
FECPt	8.5	9.1	6.2	8.0	18	9	0.73	0.90
NBuoy	-0.6	-1.1	1.6	1.3	18	9	0.33	0.33
Buoy_Enh	0.5	0.5	0.0	0.0	18	9	0.25	0.28
Mean_VW	7.1	4.7	4.0	1.6	18	9	0.33	0.21
SWC_frac	0.2	0.3	0.3	0.3	18	9	0.46	0.77
pb	4.1	3.9	1.3	0.6	18	9	0.79	0.76
tccl	17.2	16.7	1.6	1.2	18	9	0.53	0.92
Ri	71.0	70.9	22.6	14.8	18	9	1.00	0.83

Table D.8. Population statistics of response variables for clouds with SI 80% (N = 27).

Variable	Mean		Standard Deviation		Sample Size		P-Values	
	Sand	Agl	Sand	Agl	Sand	Agl	t	W
MaxH10	11.7	8.7	2.6	1.8	18	9	0.06	0.06
MaxA10	96.2	72.8	65.1	63.6	18	9	0.17	0.25
MaxZ	57.6	52.3	7.4	11.3	18	9	0.20	0.29
MaxB	29.8	28.6	4.3	6.0	18	9	0.59	0.88
MXCPdH10	3.3	0.3	2.9	0.9	18	9	0.14	0.14
MXCPdA10	53.7	23.0	60.1	49.7	18	9	0.12	0.06
MXCPdZ	5.4	3.6	10.8	9.7	18	9	0.76	0.73
MXCPdB	2.8	2.0	5.1	5.8	18	9	0.80	0.95
CPMXtMxA	13.3	6.6	11.7	8.6	18	9	0.12	0.12
FEMXtMxA	21.8	15.8	11.6	10.0	18	9	0.20	0.20
TotRNVOL	17.0	26.2	49.1	69.5	18	9	0.42	0.11
MxRFx	15.2	14.1	19.8	27.2	18	9	0.82	0.45
FEtTerm	35.9	36.3	14.2	22.2	18	9	0.95	0.42

$p \leq 5\%$

$5 < p \leq 10\%$

$p > 10\%$

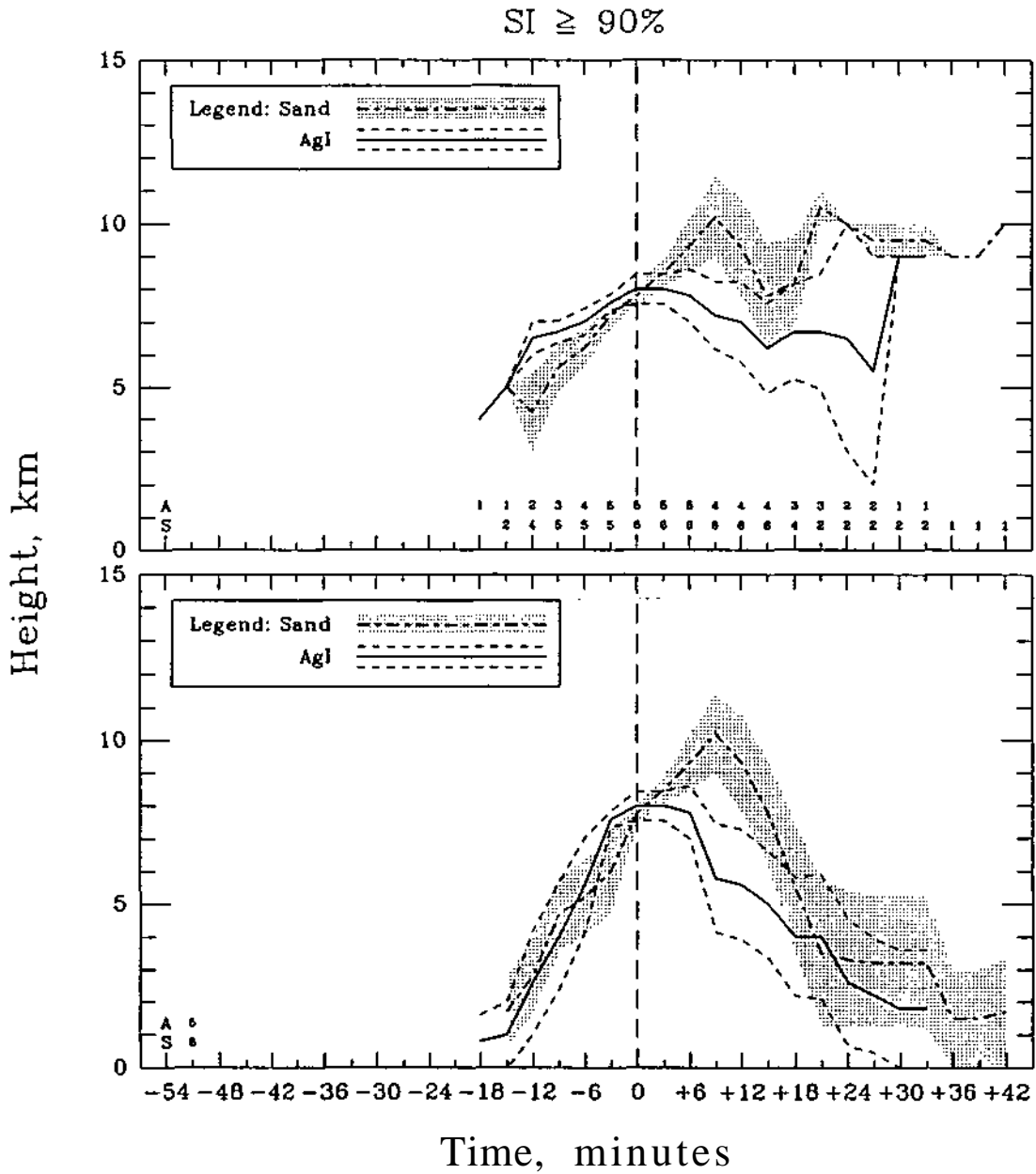


Figure D.18. Variation with time of means of the 10 dBZ echo top heights for sand- and AgI-treated echoes in existence at each interpolated volume scan (top) and all treated echoes (bottom) for the subpopulation of clouds with  $SI \geq 90\%$ .

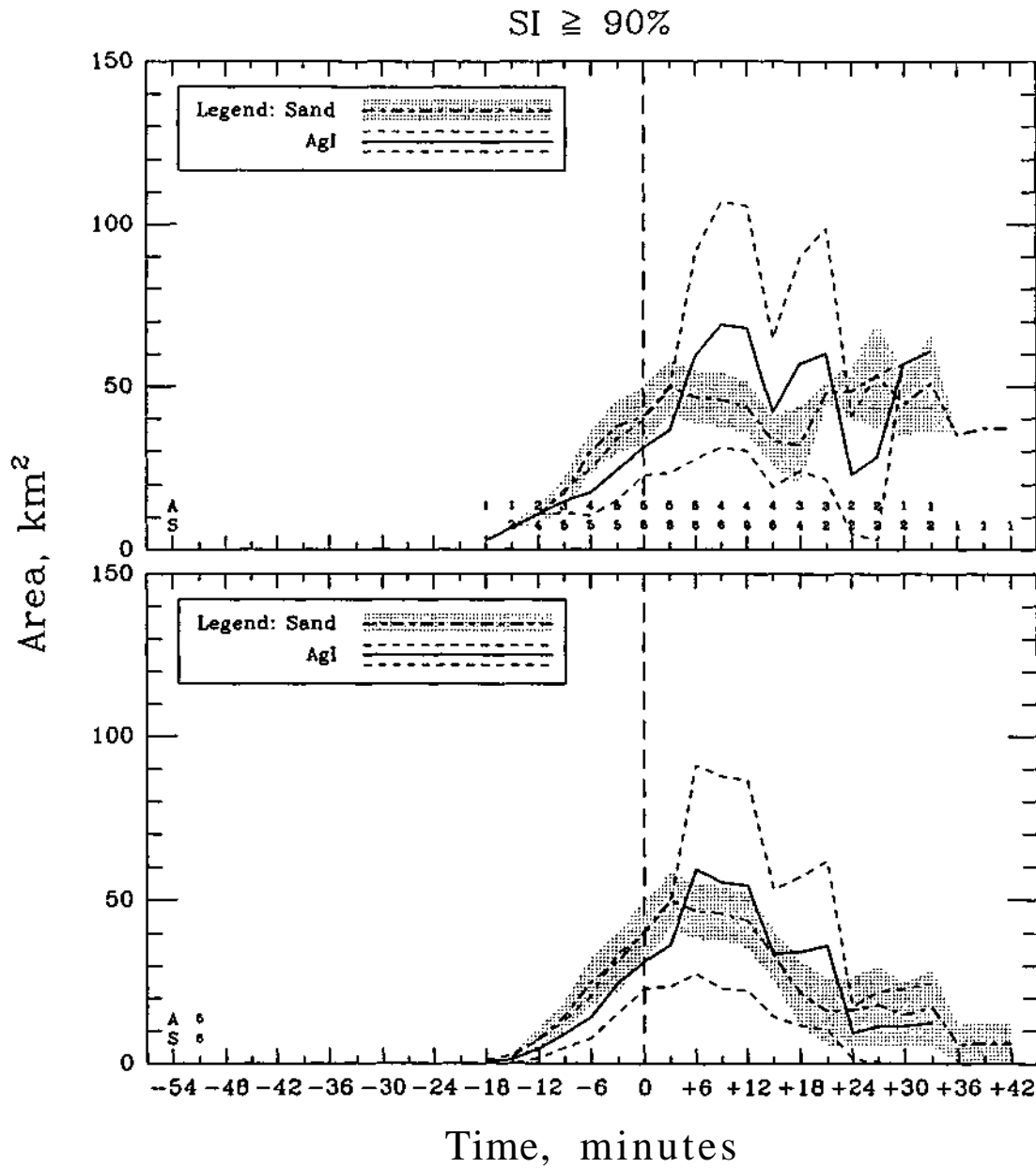


Figure D.19. Variation with time of means of the 10 dBZ defined echo areas for sand- and AgI-treated echoes in existence at each interpolated volume scan (top) and all treated echoes (bottom) for the subpopulation of clouds with SI  $\geq$  90%.

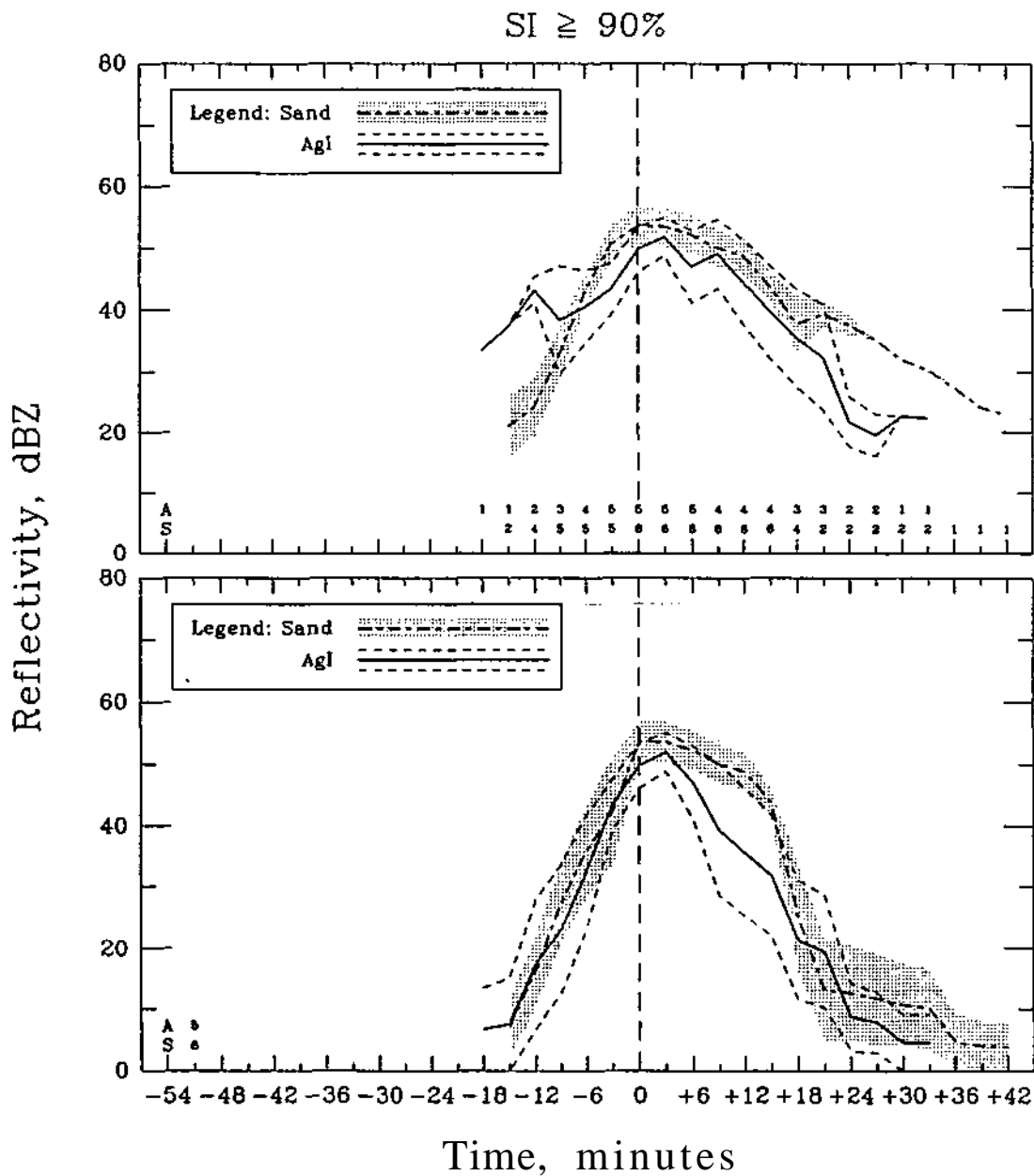


Figure D.20. Variation with time of means of maximum reflectivities for sand- and AgI-treated echoes in existence at each interpolated volume scan (top) and all treated echoes (bottom) for the subpopulation of clouds with SI  $\geq$  90%.

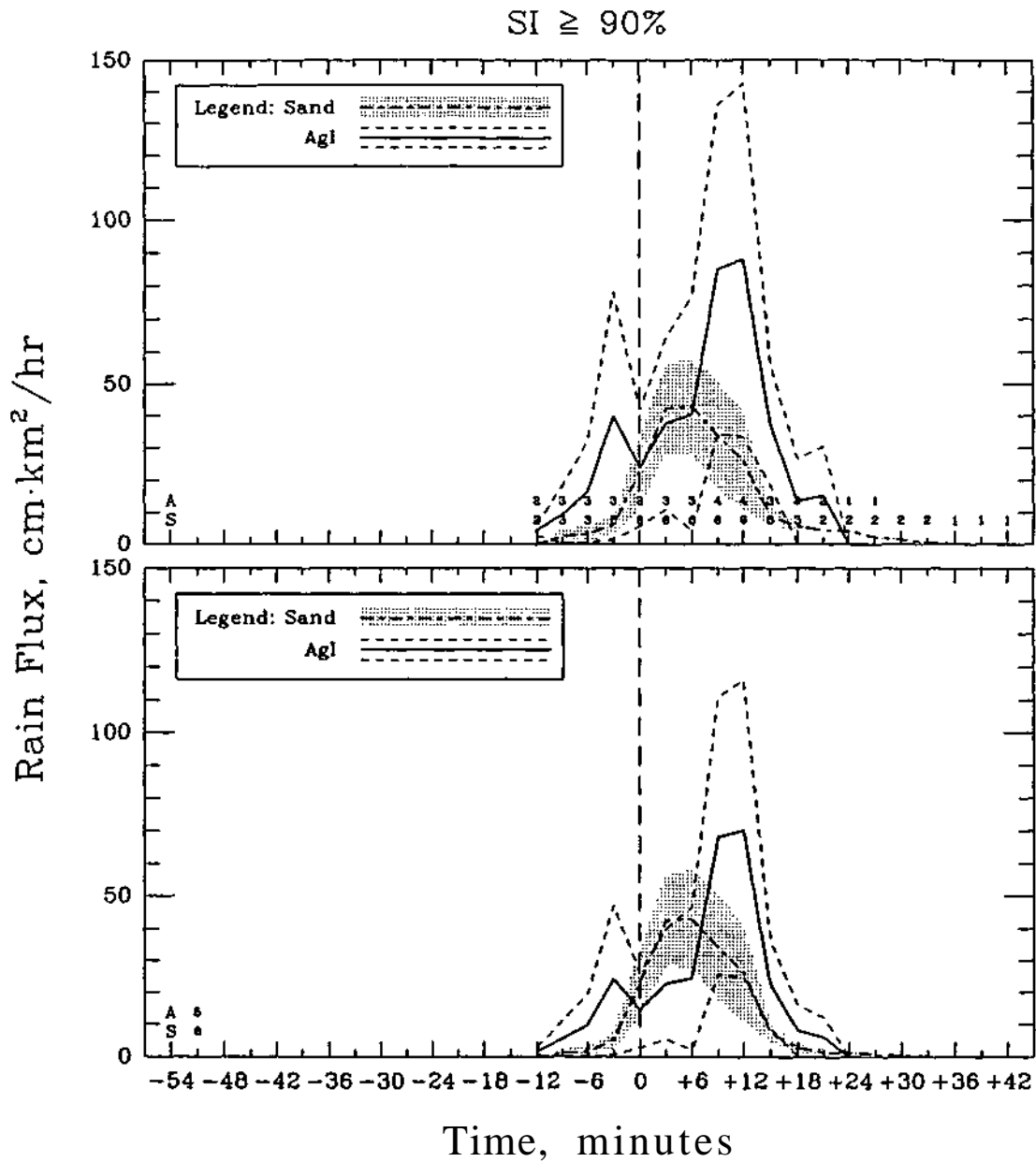


Figure D.21. Variation with time of means of rain fluxes for sand- and Agl-treated echoes in existence at each interpolated volume scan (top) and all treated echoes (bottom) for the subpopulation of clouds with SI  $\geq$  90%.

Table D.9. Population statistics of predictor variables for clouds with SI 90% (N = 11).

Variable	Mean		Standard Deviation		Sample Size		P-Values	
	Sand	Agl	Sand	Agl	Sand	Agl	t	W
CPmndia	5.6	4.3	1.6	1.3	6	5	0.14	0.18
CPHlp10	7.5	8.0	0.5	1.0	6	5	0.67	0.82
CPMxZ	53.7	49.8	7.7	8.2	6	5	0.22	0.49
CPMxB	26.9	25.4	5.3	4.3	6	5	0.78	0.80
CPA10	40.5	30.8	21.9	18.7	6	5	0.14	0.18
FECPt	9.3	8.4	5.8	6.2	6	5	0.77	0.67
NBuoy	-0.1	-1.3	0.9	1.3	6	5	0.23	0.23
Buoy_Enh	0.5	0.5	0.0	0.0	6	5	0.14	0.14
Mean_VW	7.3	4.6	4.1	1.6	6	5	0.25	0.18
SWC_frac	0.2	0.3	0.2	0.3	6	5	0.24	0.92
pb	4.0	3.9	0.8	0.6	6	5	1.00	0.82
tecl	17.6	16.6	14	1.2	6	5	0.44	0.73
Ri	75.1	70.6	18.2	14.8	6	5	0.59	0.73

Table D. 10. Population statistics of response variables for clouds with SI 90% (N = 11).

Variable	Mean		Standard Deviation		Sample Size		P-Values	
	Sand	Agl	Sand	Agl	Sand	Agl	t	W
MaxH10	10.5	8.4	2.7	1.1	6	5	0.23	0.18
MaxA10	60.2	73.4	20.2	68.4	6	5	0.59	1.00
MaxZ	55.6	54.7	6.3	7.6	6	5	0.56	1.00
MaxB	28.7	30.1	3.7	4.6	6	5	0.43	0.33
MXCPdH10	3.0	0.0	2.4	0.7	6	5	0.14	0.14
MXCPdA10	19.7	32.2	17.5	66.3	6	5	0.77	1.00
MXCPdZ	-0.2	3.8	3.1	7.6	6	5	0.47	0.94
MXLPdB	0.5	2.3	2.8	5.9	6	5	0.82	0.88
CPMXtMxA	10.8	2.9	8.9	5.2	6	5	0.41	0.49
FEMXtMxA	20.1	11.3	11.6	4.6	6	5	0.27	0.23
TotRNVOL	1.8	2.7	1.7	4.0	6	5	0.58	0.53
MxRFx	8.2	6.3	7.7	6.1	6	5	0.86	0.86
FEITcrm	38.3	26.2	18.5	16.0	6	5	0.58	0.38

$p \leq 5\%$

$5 < p \leq 10\%$

$p > 10\%$

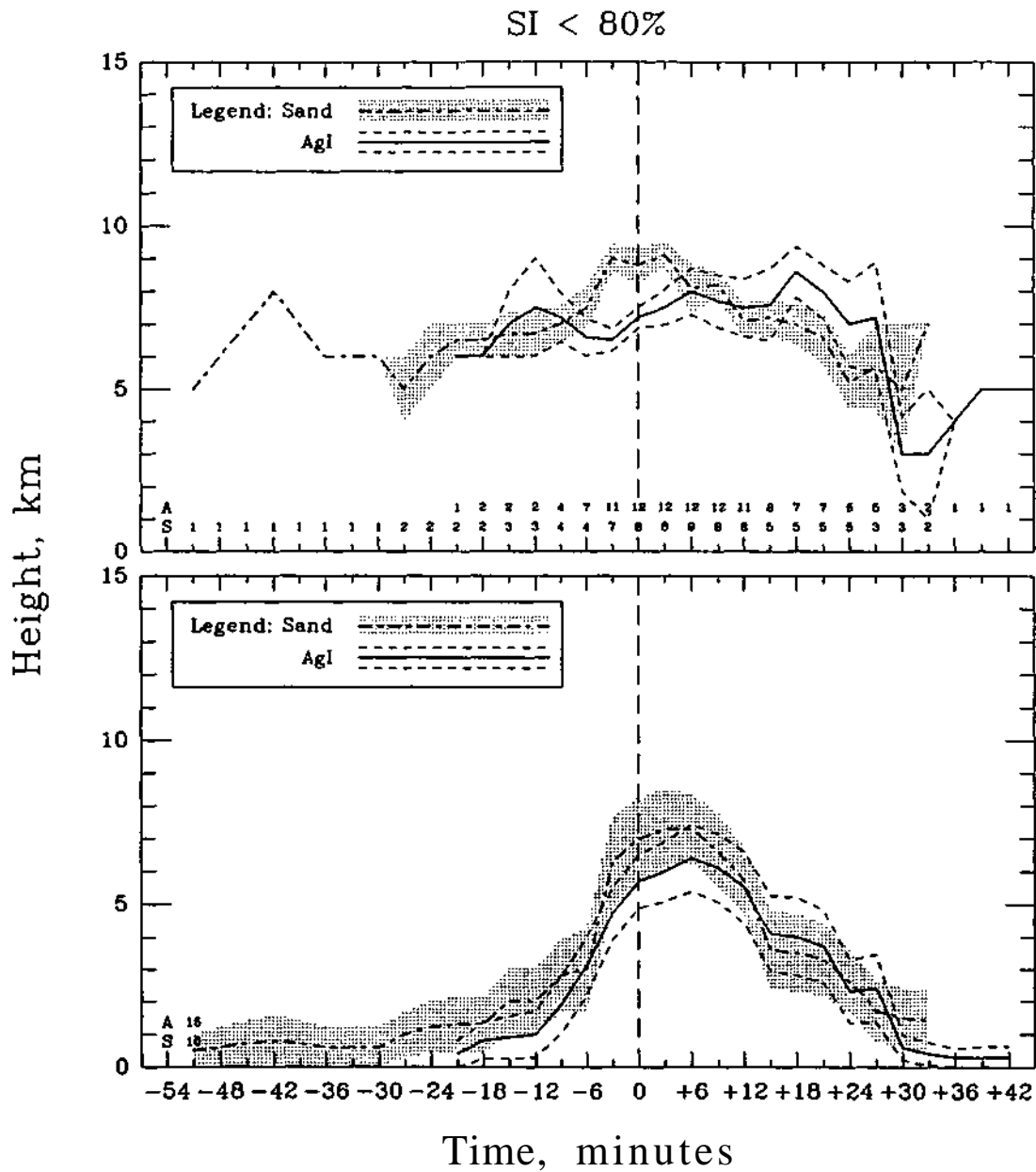


Figure D.22. Variation with time of means of the 10 dBZ echo top heights for sand- and AgI-treated echoes in existence at each interpolated volume scan (top) and all treated echoes (bottom) for the subpopulation of clouds with SI < 80%.

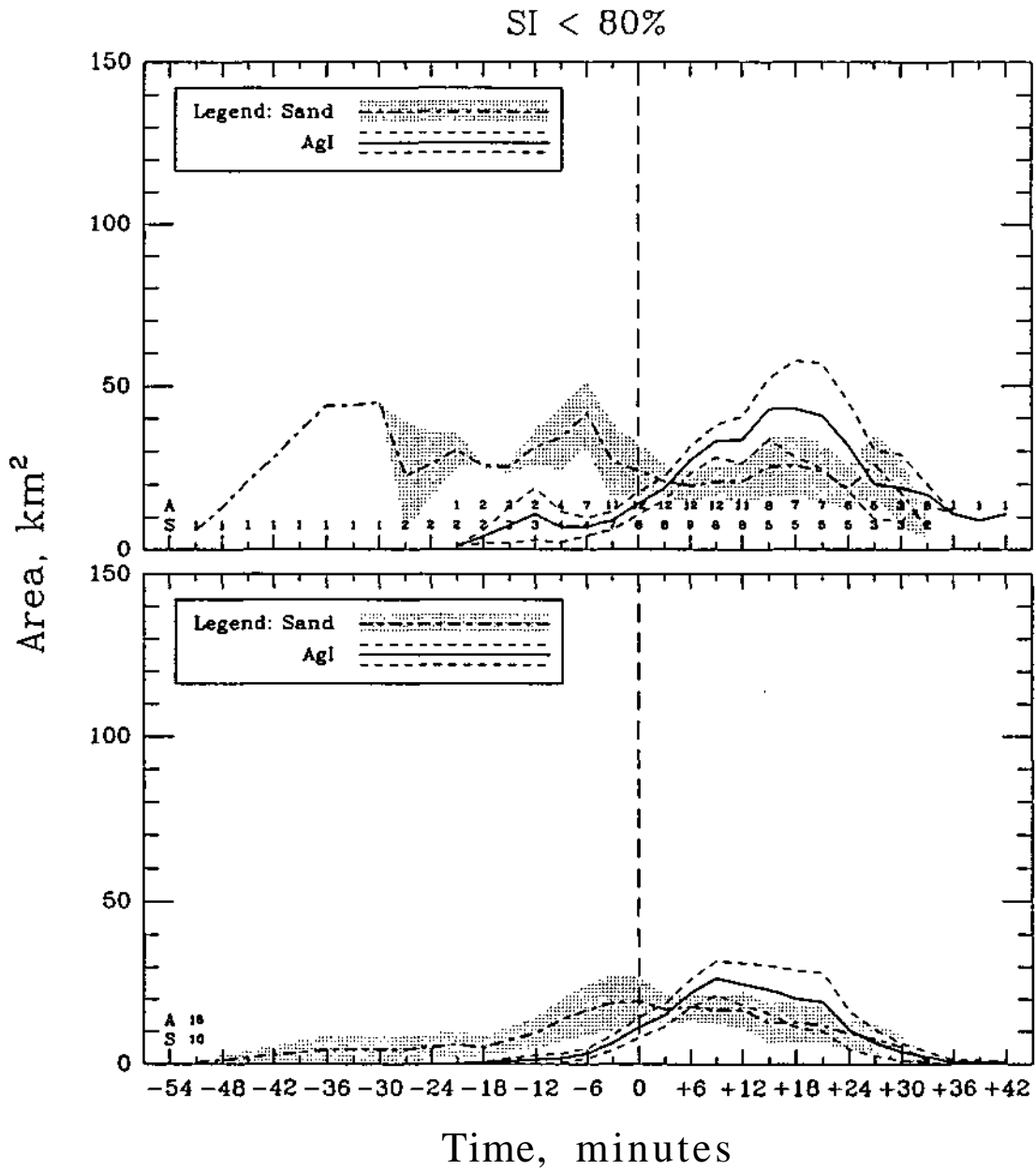


Figure D.23. Variation with time of means of the 10 dBZ defined echo areas for sand- and AgI-treated echoes in existence at each interpolated volume scan (top) and all treated echoes (bottom) for the subpopulation of clouds with SI < 80%.

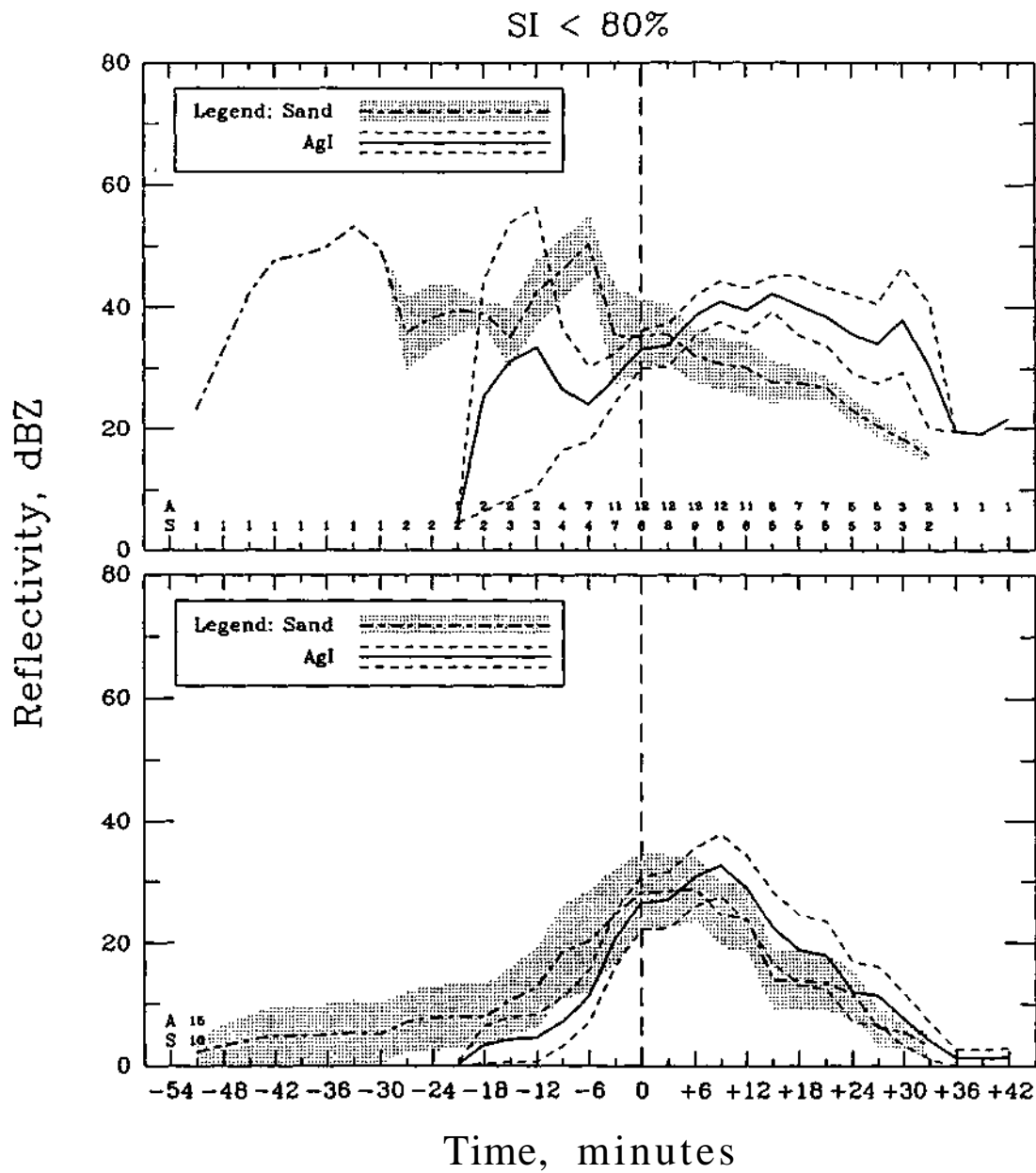


Figure D.24. Variation with time of means of maximum reflectivities for sand- and Agl-treated echoes in existence at each interpolated volume scan (top) and all treated echoes (bottom) for the subpopulation of clouds with SI < 80%.

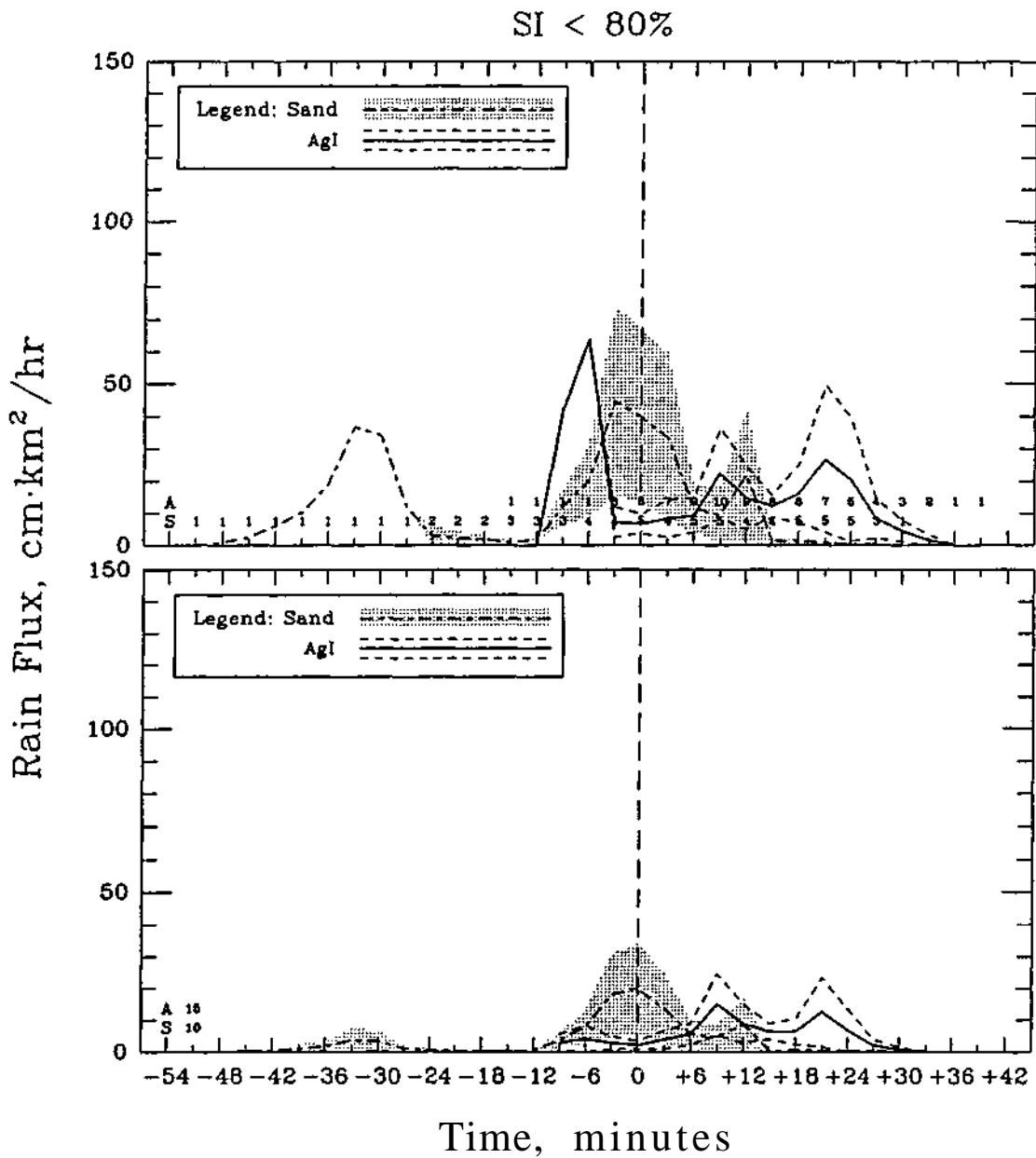


Figure D.25. Variation with time of means of rain fluxes for sand- and AgI-treated echoes in existence at each interpolated volume scan (top) and all treated echoes (bottom) for the subpopulation of clouds with SI < 80%.

Table D.11. Population statistics of predictor variables for clouds with SI < 80% (N = 25).

Variable	Mean		Standard Deviation		Sample Size		P-Values	
	Sand	Agl	Sand	Agl	Sand	Agl	t	W
CPmndia	2.6	2.3	2.7	1.8	10	15	0.64	0.81
CPHlp10	4.8	5.0	4.2	3.3	10	15	0.89	0.50
CPMxZ	24.3	23.4	24.4	17.9	10	15	0.93	0.98
CPMxB	13.5	13.2	12.7	9.3	10	15	1.00	0.85
CPA10	18.3	10.5	23.5	12.4	10	15	0.28	0.78
FECpt	8.9	4.0	18.5	5.1	10	15	0.37	0.81
NBuoy	-2.5	-1.3	6.0	1.7	10	15	0.67	0.74
Buoy_Enh	0.5	0.5	0.1	0.1	10	15	0.14	0.14
Mean_VW	5.6	5.2	3.8	4.0	10	15	0.74	0.59
SWC_frac	0.3	0.1	0.4	0.3	10	15	0.33	0.82
pb	5.6	6.1	2.4	2.1	10	15	0.54	0.56
tccl	15.8	16.0	2.1	1.9	10	15	0.96	0.75
Ri	70.8	95.3	20.3	46.2	10	15	0.67	0.67

Table D. 12. Population statistics of response variables for clouds with SI < 80% (N = 25).

Variable	Mean		Standard Deviation		Sample Size		P-Values	
	Sand	Agl	Sand	Agl	Sand	Agl	t	W
MaxH10	8.8	8.5	1.5	2.2	10	15	0.70	0.55
MaxA10	38.5	39.5	29.4	39.4	10	15	0.92	0.83
MaxZ	39.1	42.9	16.5	13.9	10	15	0.38	0.43
MaxB	21.6	23.6	7.7	7.4	10	15	0.38	0.56
MXCPdH10	0.7	0.0	0.8	3.3	10	15	0.55	0.58
MXCPdA10	2.8	27.8	25.1	39.2	10	15	0.05	0.26
MXCPdZ	9.3	10.9	17.6	22.9	10	15	0.85	0.75
MXCPdB	5.2	5.6	9.7	12.7	10	15	0.91	1.00
CPMxtMxA	3.2	8.8	15.2	7.2	10	15	0.36	0.56
FEMxtMxA	12.1	12.8	7.4	8.2	10	15	0.77	0.94
TotRNVOL	0.8	1.5	1.1	3.4	10	15	0.91	0.87
MxRFx	1.2	5.1	1.3	13.3	10	15	0.86	0.56
FEITerm	25.9	20.1	21.9	16.2	10	15	0.47	0.63

$p \leq 5\%$

$5 < p \leq 10\%$

$p > 10\%$

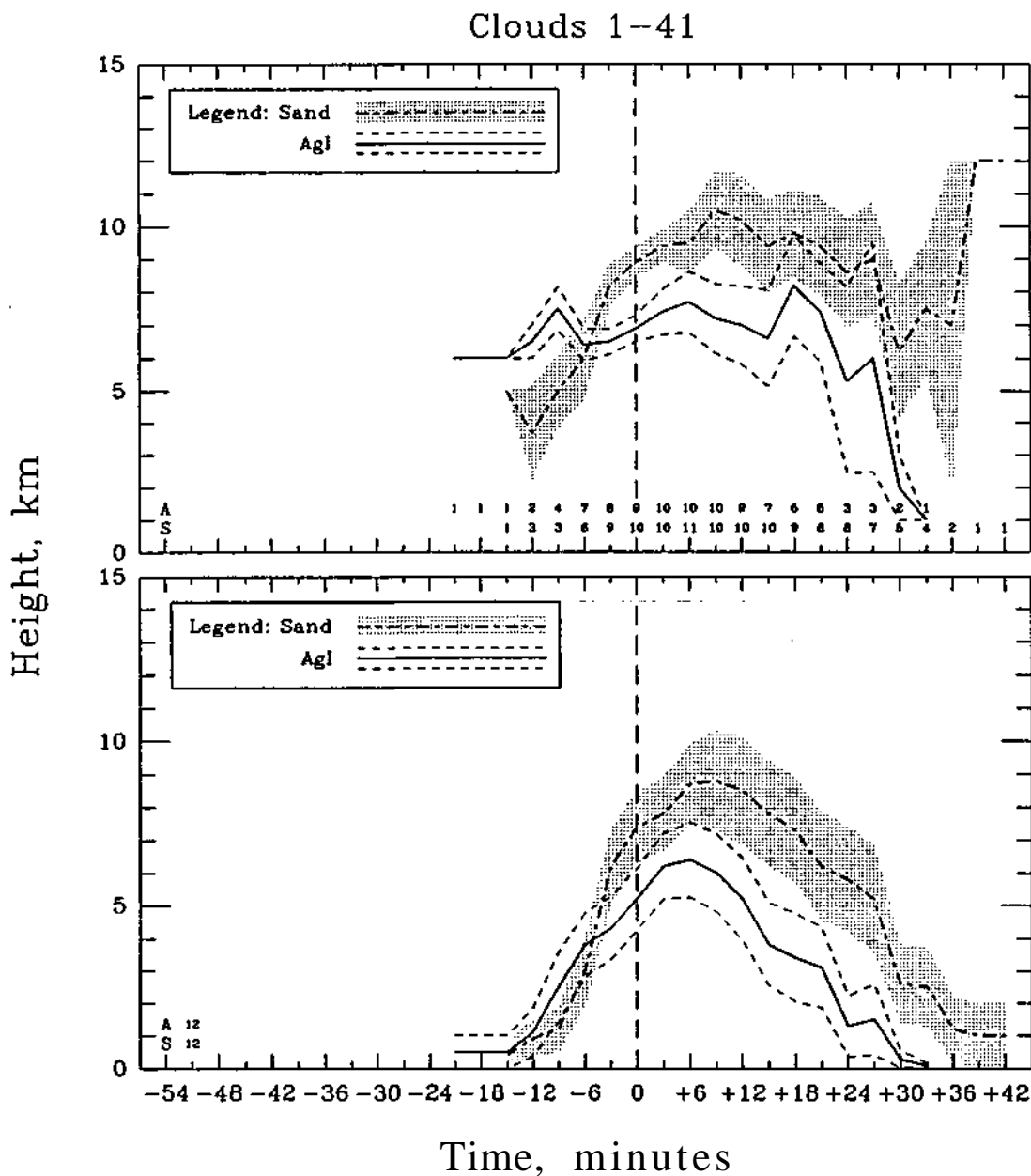


Figure D.26. Variation with time of means of the 10 dBZ echo top heights for sand- and AgI-treated echoes in existence at each interpolated volume scan (top) and all treated echoes (bottom) for the subpopulation of clouds in treatment sequence 1-41 with SI.

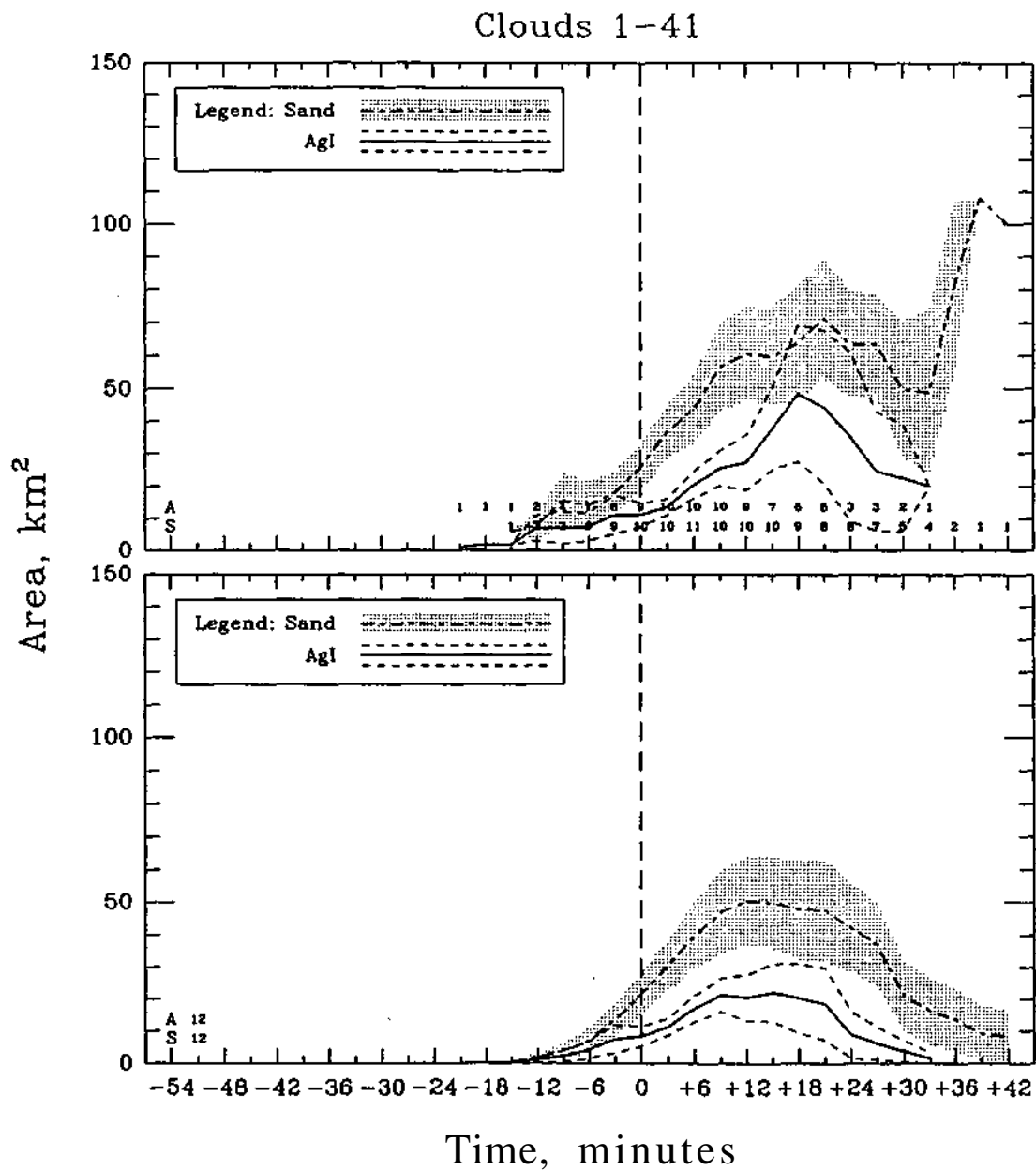


Figure D.27. Variation with time of means of the 10 dBZ defined echo areas for sand- and AgI-treated echoes in existence at each interpolated volume scan (top) and all treated echoes (bottom) for the subpopulation of clouds in treatment sequence 1-41 with SI.

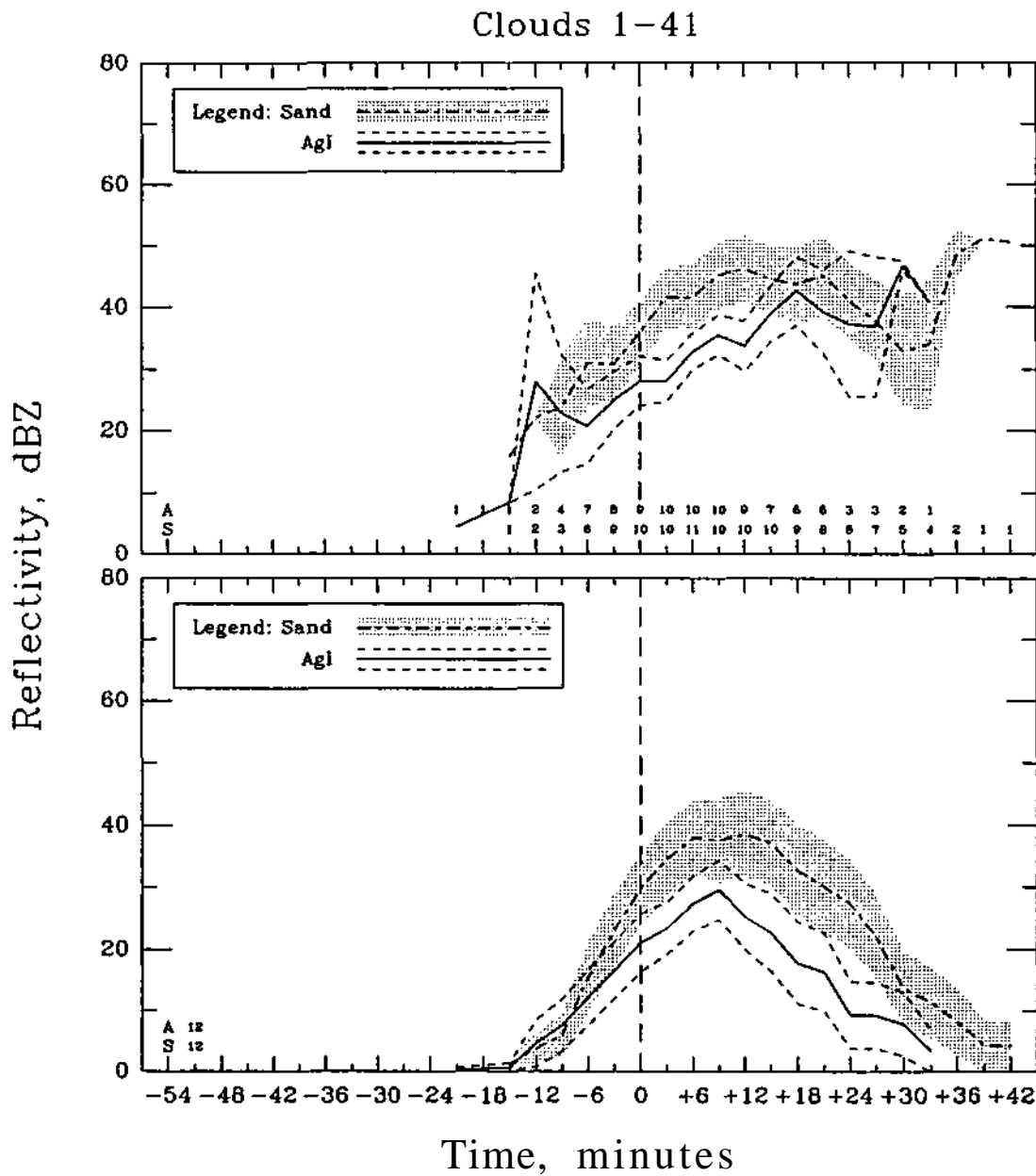


Figure D.28. Variation with time of means of maximum reflectivities for sand- and AgI-treated echoes in existence at each interpolated volume scan (top) and all treated echoes (bottom) for the subpopulation of clouds in treatment sequence 1-41 with SI.

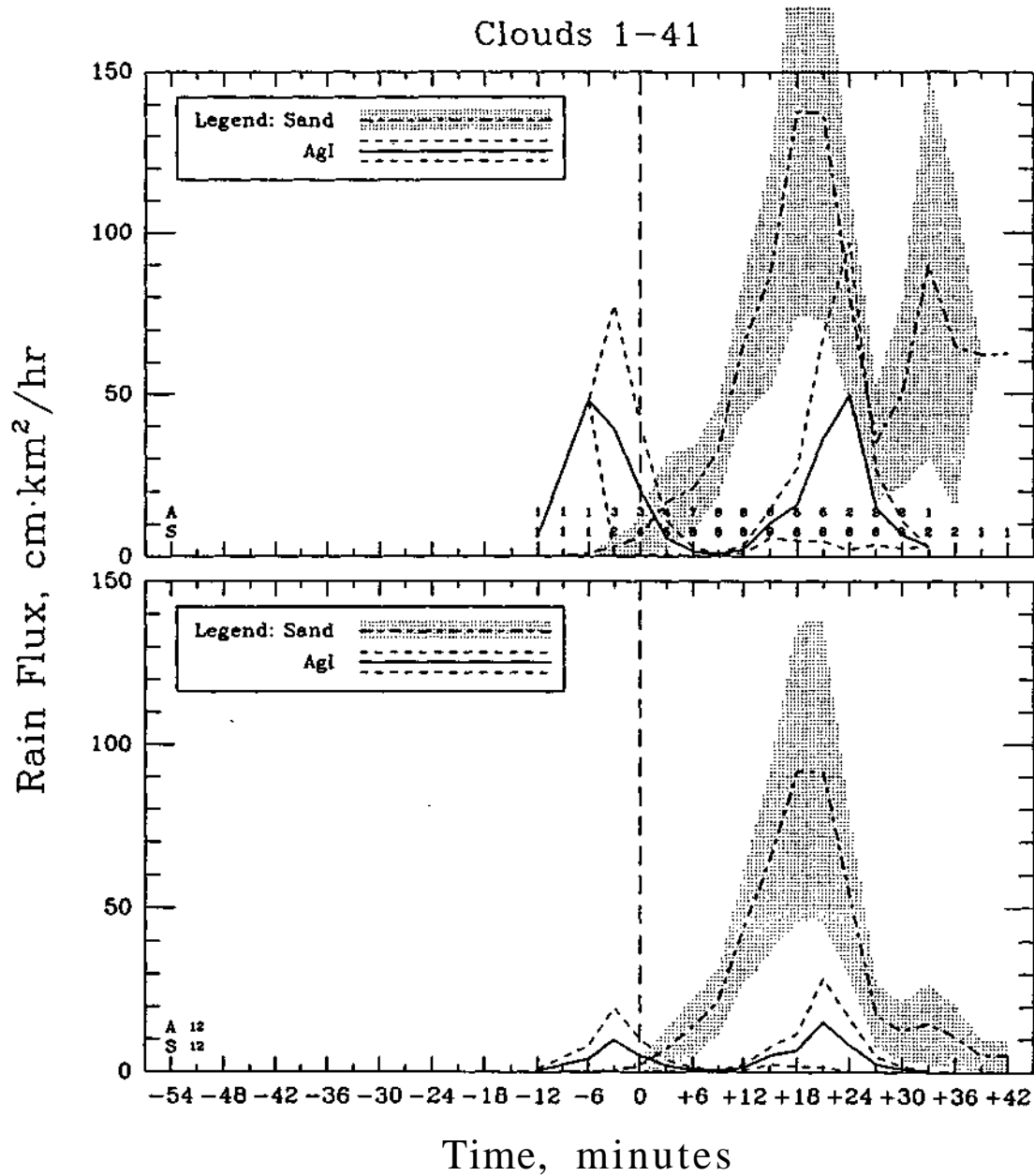


Figure D.29. Variation with time of means of rain fluxes for sand- and AgI-treated echoes in existence at each interpolated volume scan (top) and all treated echoes (bottom) for the subpopulation of clouds in treatment sequence 1-41 with SI.

Table D. 13. Population statistics of predictor variables for treatment sequence 1-41 (N = 24).

Variable	Mean		Standard Deviation		Sample Size		P-Values	
	Sand	Agl	Sand	Agl	Sand	Agl	t	W
CPmndia	3.1	1.9	2.9	1.5	12	12	0.14	0.30
CPHlp10	5.4	5.0	4.2	3.2	12	12	0.77	0.38
CPMxZ	26.6	20.1	23.0	16.1	12	12	0.63	0.63
CPMxB	14.8	12.1	12.0	8.6	12	12	0.63	0.39
CPA10	20.7	8.1	23.8	10.4	12	12	0.14	0.30
FECPt	1.5	2.9	5.7	4.8	12	12	0.86	0.86
NBuoy	-1.4	-1.4	1.9	1.8	12	12	1.00	0.52
Buoy_Enh	0.5	0.5	0.1	0.1	12	12	0.14	0.14
Mean_VW	8.8	6.2	4.5	4.1	12	12	0.75	0.52
SWC_frac	0.0	0.1	0.1	0.2	12	12	0.76	0.86
pb	6.3	6.9	1.6	1.5	12	12	0.63	0.63
tccl	15.0	15.5	1.0	1.7	12	12	0.85	0.85
Ri	63.5	95.4	11.5	53.1	12	12	0.53	0.53

Table D.14. Population statistics of response variables for treatment sequence 1-41 (N = 24).

Variable	Mean		Standard Deviation		Sample Size		P-Values	
	Sand	Agl	Sand	Agl	Sand	Agl	t	W
MaxH10	10.8	8.5	3.6	2.5	12	12	0.38	0.38
Max A10	63.9	39.0	55.9	43.7	12	12	0.38	0.53
MaxZ	44.2	39.4	19.0	13.1	12	12	0.52	0.38
MaxB	23.8	22.0	8.8	7.2	12	12	0.62	0.62
MXCPdH10	2.6	0.2	3.3	3.0	12	12	0.38	0.38
MXCPdA10	43.2	26.9	43.3	45.4	12	12	0.68	0.63
MXCPdZ	17.5	14.7	13.1	21.7	12	12	0.86	1.00
MXCPdB	9.0	7.1	6.6	12.0	12	12	0.86	0.86
CPMXUMxA	15.3	8.9	8.0	8.7	12	12	0.38	0.38
FEMXtMxA	16.8	11.8	9.8	6.6	12	12	0.14	0.14
TotRNVOL	4.0	0.4	9.0	1.0	12	12	0.14	0.38
MxRFx	7.4	14	19.5	4.3	12	12	0.14	0.14
FEtTerm	26.6	17.8	14.9	10.1	12	12	0.14	0.14

$p \leq 5\%$

$5 < p \leq 10\%$

$p > 10\%$

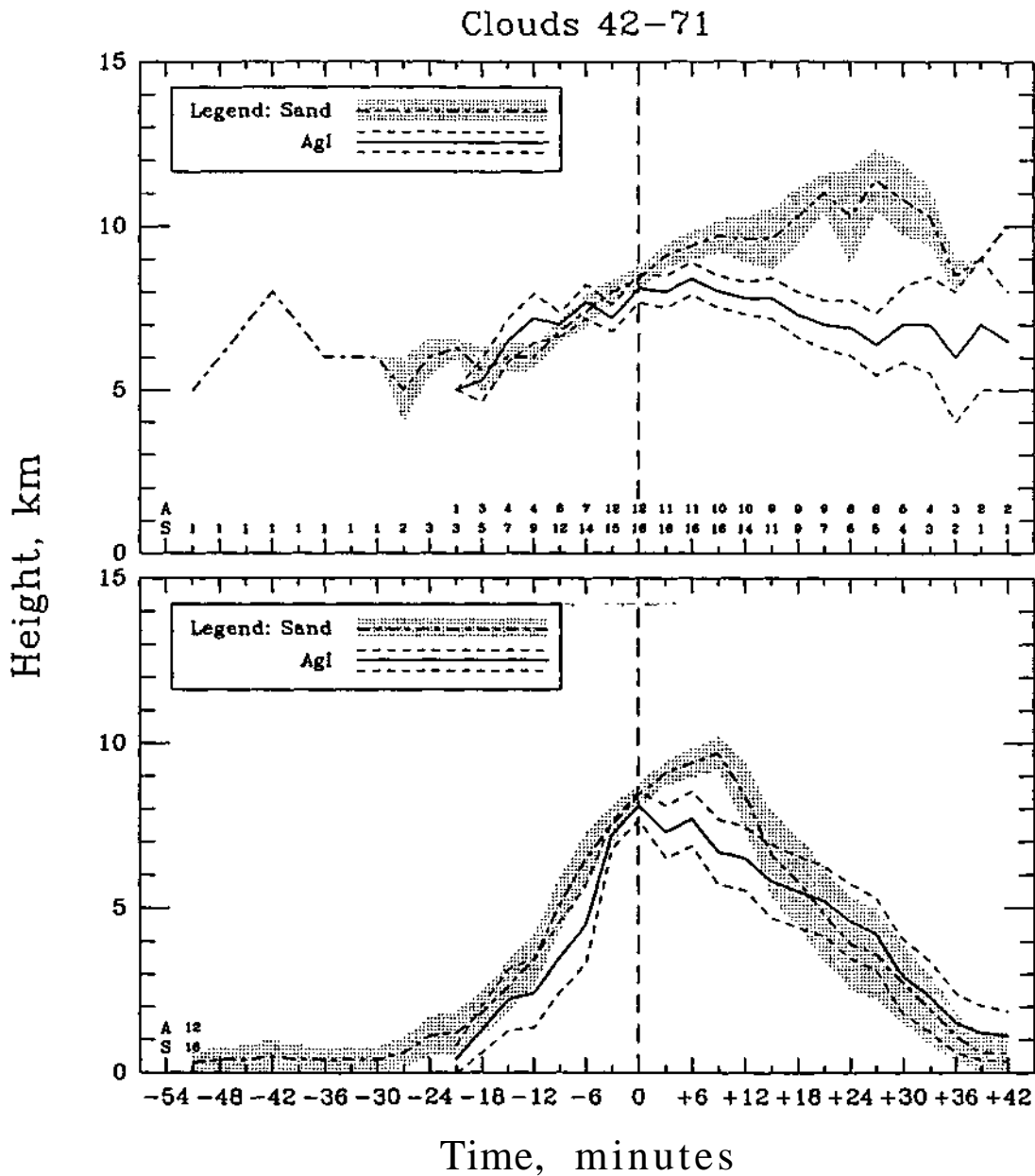


Figure D.30. Variation with time of means of the 10 dBZ echo top heights for sand- and AgI-treated echoes in existence at each interpolated volume scan (top) and all treated echoes (bottom) for the subpopulation of clouds in treatment sequence 42-71 with

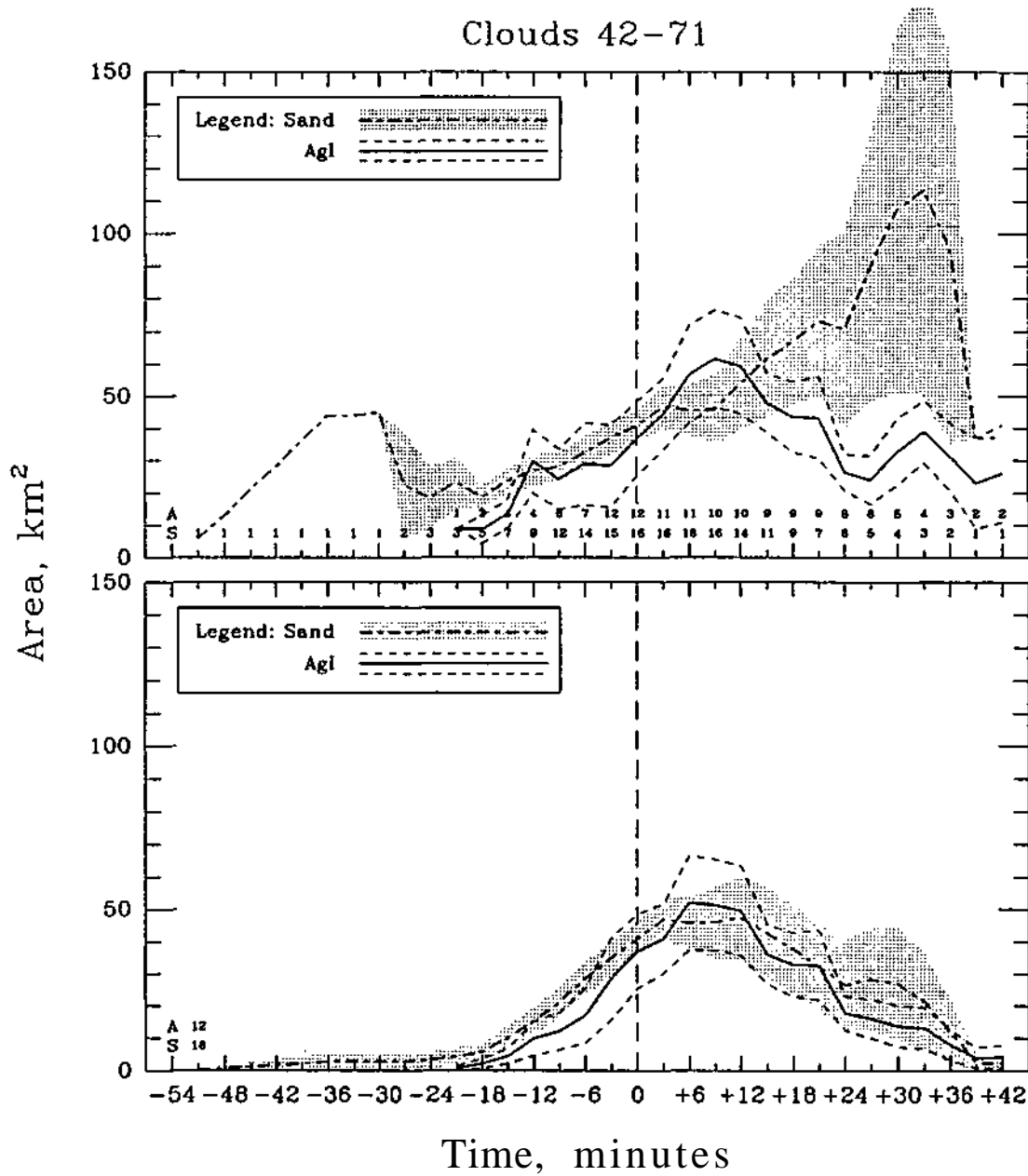


Figure D.31. Variation with time of means of the 10 dBZ defined echo areas for sand- and Agl-treated echoes in existence at each interpolated volume scan (top) and all treated echoes (bottom) for the subpopulation of clouds in treatment sequence 42-71 with SI.

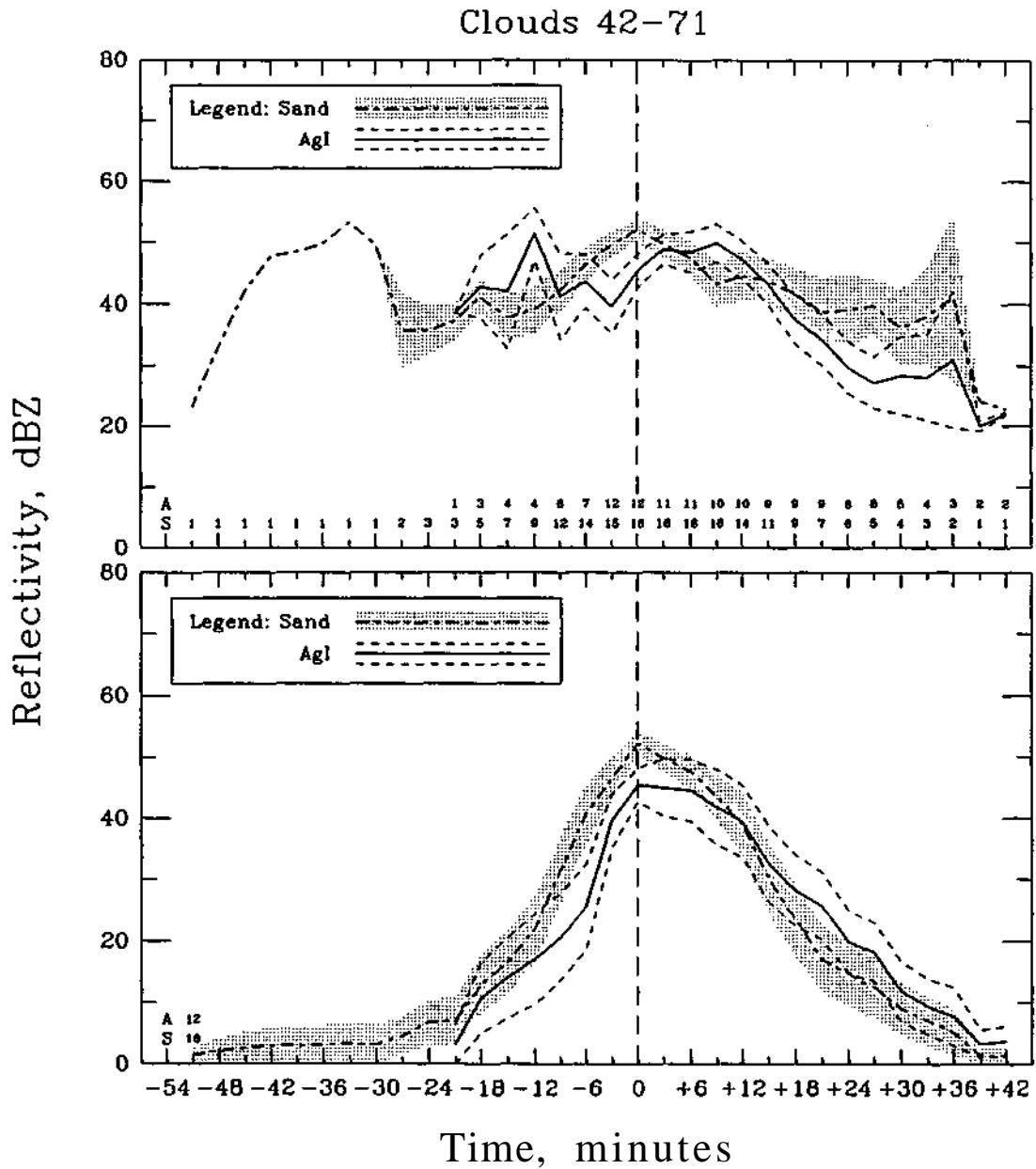


Figure D.32. Variation with time of means of maximum reflectivities for sand- and AgI-treated echoes in existence at each interpolated volume scan (top) and all treated echoes (bottom) for the subpopulation of clouds in treatment sequence 42-71 with SI.

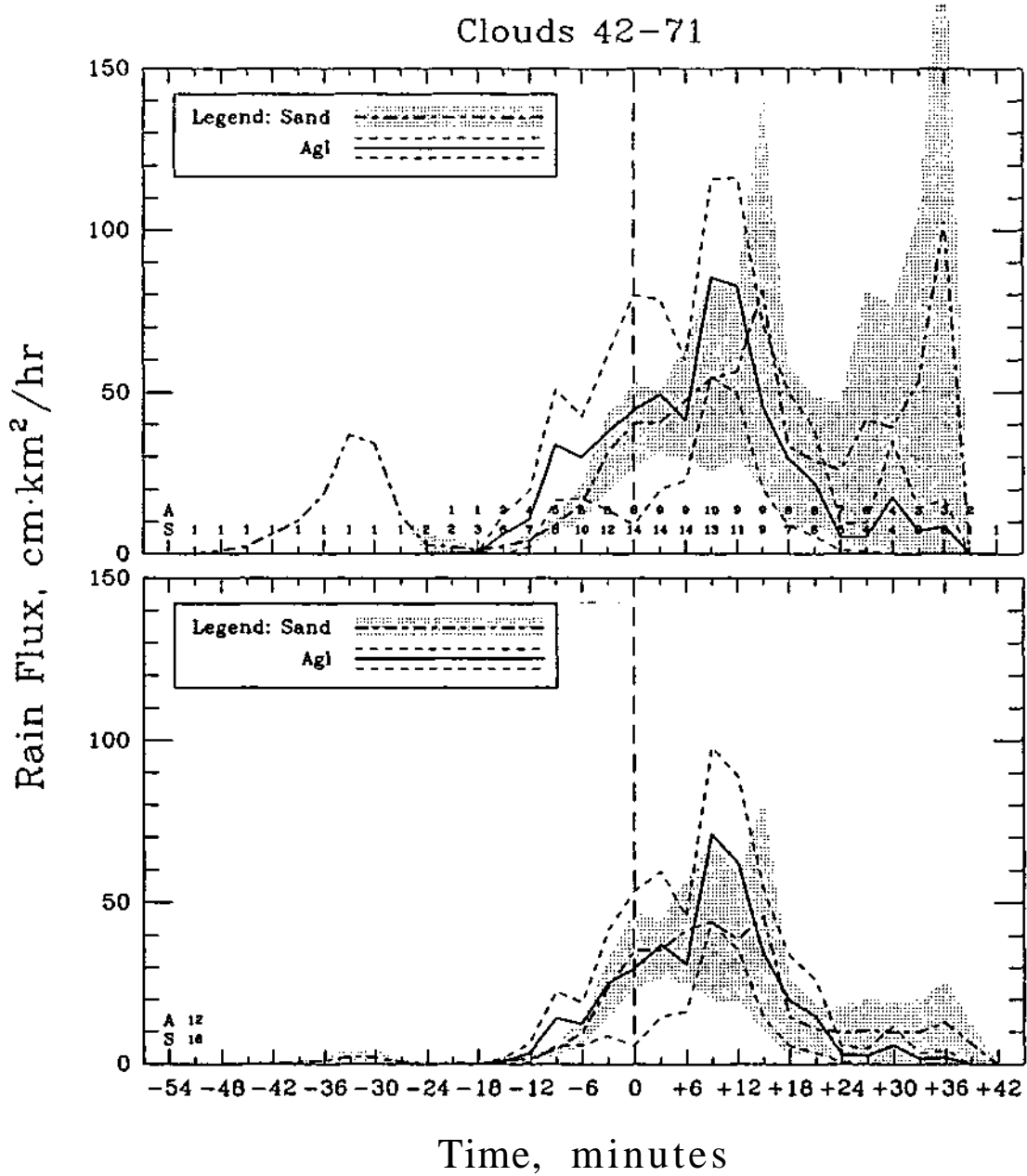


Figure D.33. Variation with time of means of rain fluxes for sand- and Agl-treated echoes in existence at each interpolated volume scan (top) and all treated echoes (bottom) for the subpopulation of clouds in treatment sequence 42-71 with SI.

Table D.15. Population statistics of predictor variables for treatment sequence 42-71 (N = 28).

Variable	Mean		Standard Deviation		Sample Size		P-Values	
	Sand	Agl	Sand	Agl	Sand	Agl	t	W
CPmndia	5.4	4.6	1.3	2.6	16	12	0.23	0.23
CPHtp10	8.2	7.3	1.5	2.8	16	12	0.38	0.77
CPMxZ	52.1	42.7	7.7	16.0	16	12	0.23	0.23
CPMxB	26.4	22.1	4.9	7.8	16	12	0.23	0.23
CPA10	40.3	35.7	20.2	40.6	16	12	0.38	0.23
FECPt	14.0	9.0	12.4	7.1	16	12	0.23	0.46
NBuoy	-1.2	-1.0	4.8	14	16	12	1.00	0.53
Buoy_Enh	0.5	0.5	0.0	0.0	16	12	0.69	0.85
Mean_VW	4.9	3.7	2.5	1.5	16	12	0.23	0.23
SWC_frac	0.4	0.3	0.4	0.3	16	12	0.62	0.62
pb	3.3	3.6	0.5	0.0	16	12	0.46	0.46
tccl	18.0	17.0	1.1	1.2	16	12	0.54	0.77
Ri	76.5	76.9	25.5	13.2	16	12	0.77	0.77

Table D. 16. Population statistics of response variables for treatment sequence 42-71 (N = 28).

Variable	Mean		Standard Deviation		Sample Size		P-Values	
	Sand	Agl	Sand	Agl	Sand	Agl	t	W
MaxH10	10.6	8.6	1.7	1.5	16	12	0.23	0.23
MaxA10	84.4	64.9	65.3	56.7	16	12	0.23	0.38
MaxZ	56.1	53.4	6.6	10.3	16	12	0.23	0.85
MaxB	29.2	29.0	3.8	5.4	16	12	1.00	0.85
MXCPdH10	2.2	0.1	2.2	2.4	16	12	0.46	0.46
MXCPdA10	29.7	25.1	64.2	41.2	16	12	0.85	0.77
MXCPdZ	-1.3	1.7	6.1	14.2	16	12	0.77	0.77
MXCPdB	-0.3	1.5	4.1	8.7	16	12	0.77	0.77
CPMXtMxA	5.5	7.1	15.7	6.7	16	12	0.62	0.38
FEMXtMxA	19.5	16.0	12.3	10.5	16	12	0.62	0.46
TotRNVOL	16.6	21.2	52.1	60.0	16	12	0.62	0.38
MxRFx	12.3	15.5	15.5	26.0	16	12	0.69	0.62
FEtTerm	36.6	35.3	18.7	23.4	16	12	0.77	0.77

$p \leq 5\%$

$5 < p \leq 10\%$

$p > 10\%$

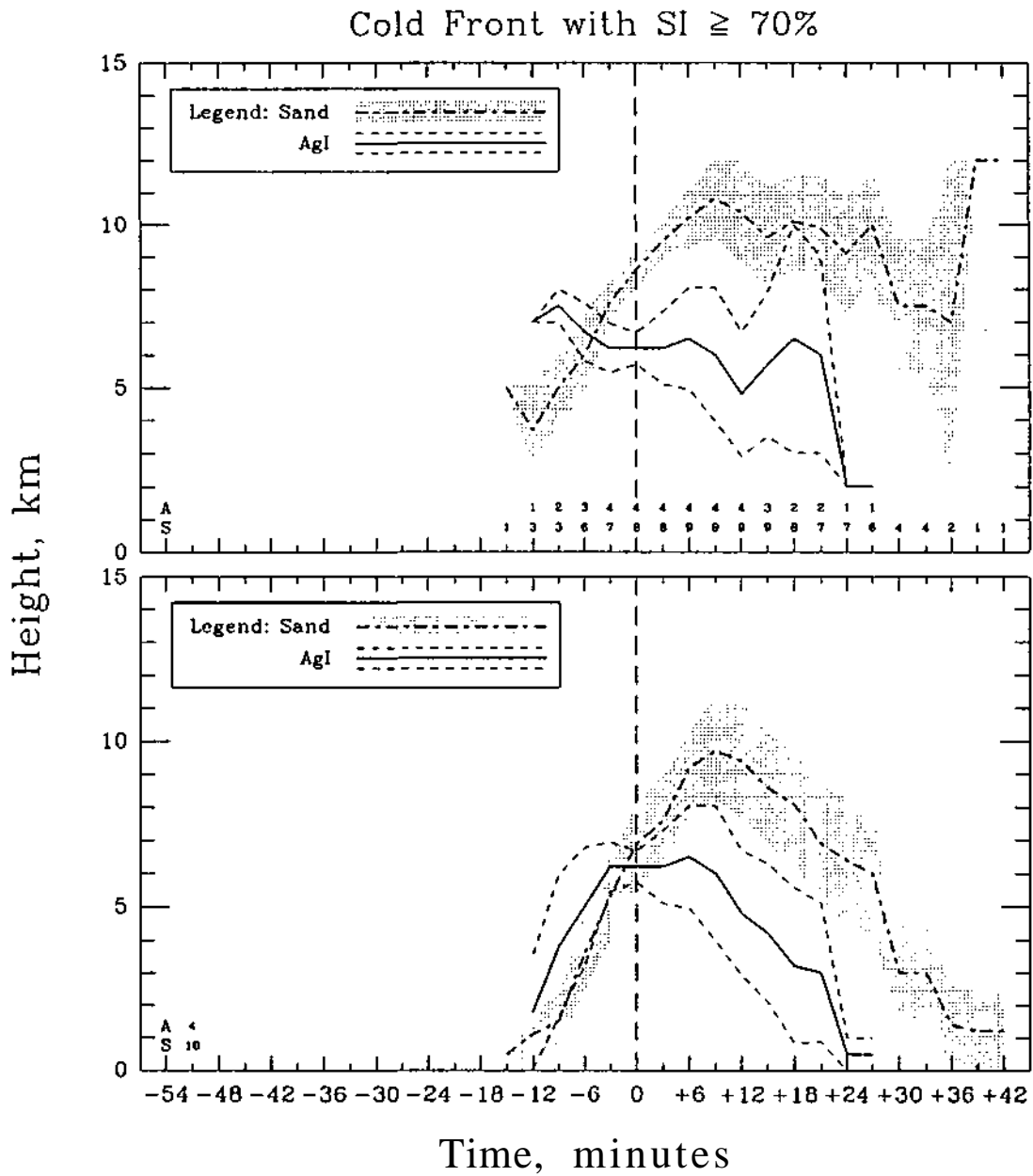


Figure D.34. Variation with time of means of the 10 dBZ echo top heights for sand- and AgI-treated echoes in existence at each interpolated volume scan (top) and all treated echoes (bottom) for the subpopulation of clouds associated with cold fronts and had SI  $\geq 70\%$ .

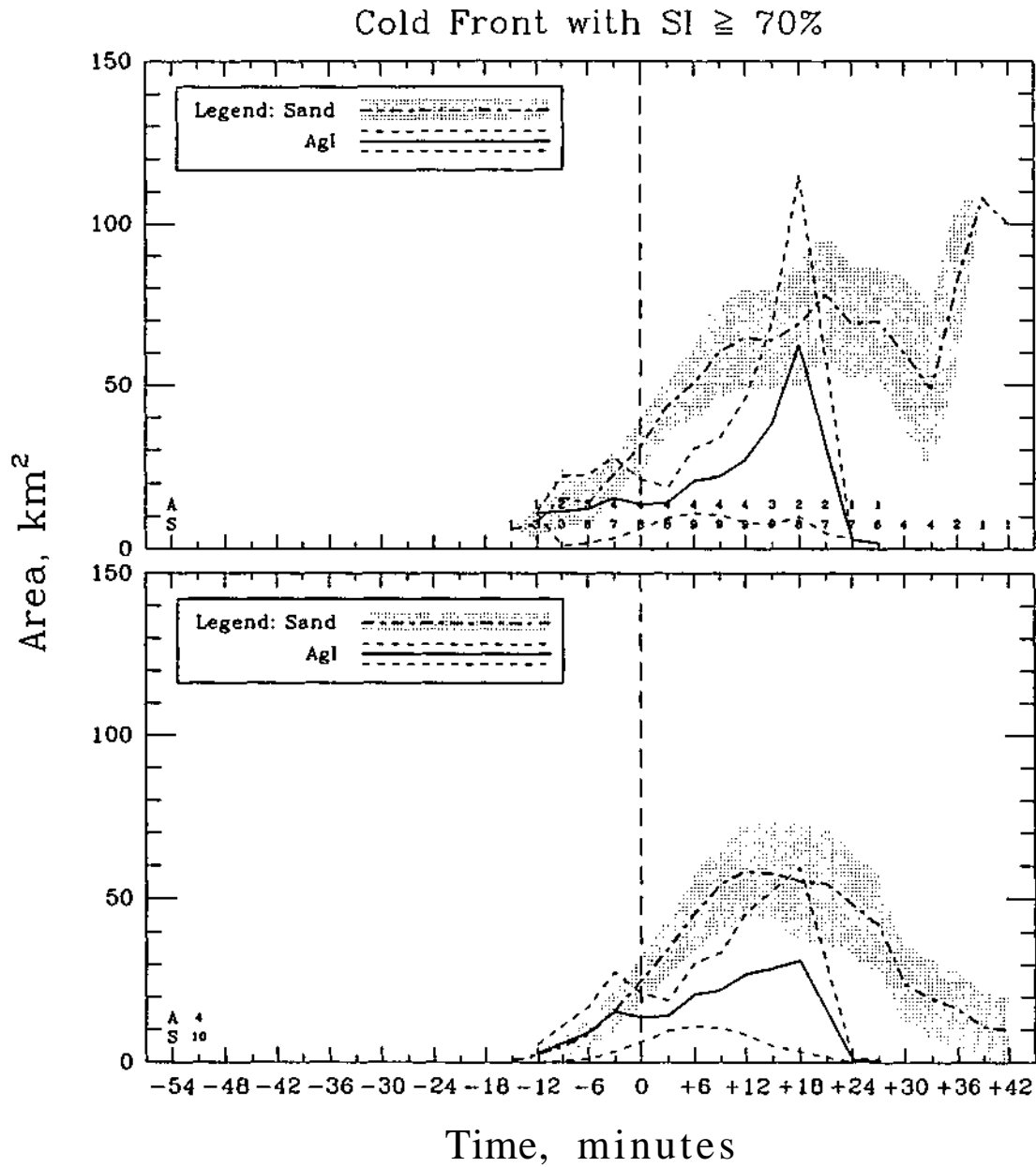


Figure D.35. Variation with time of means of the 10 dBZ defined echo areas for sand- and AgI-treated echoes in existence at each interpolated volume scan (top) and all treated echoes (bottom) for the subpopulation of clouds associated with cold fronts and had SI  $\geq 70\%$ .

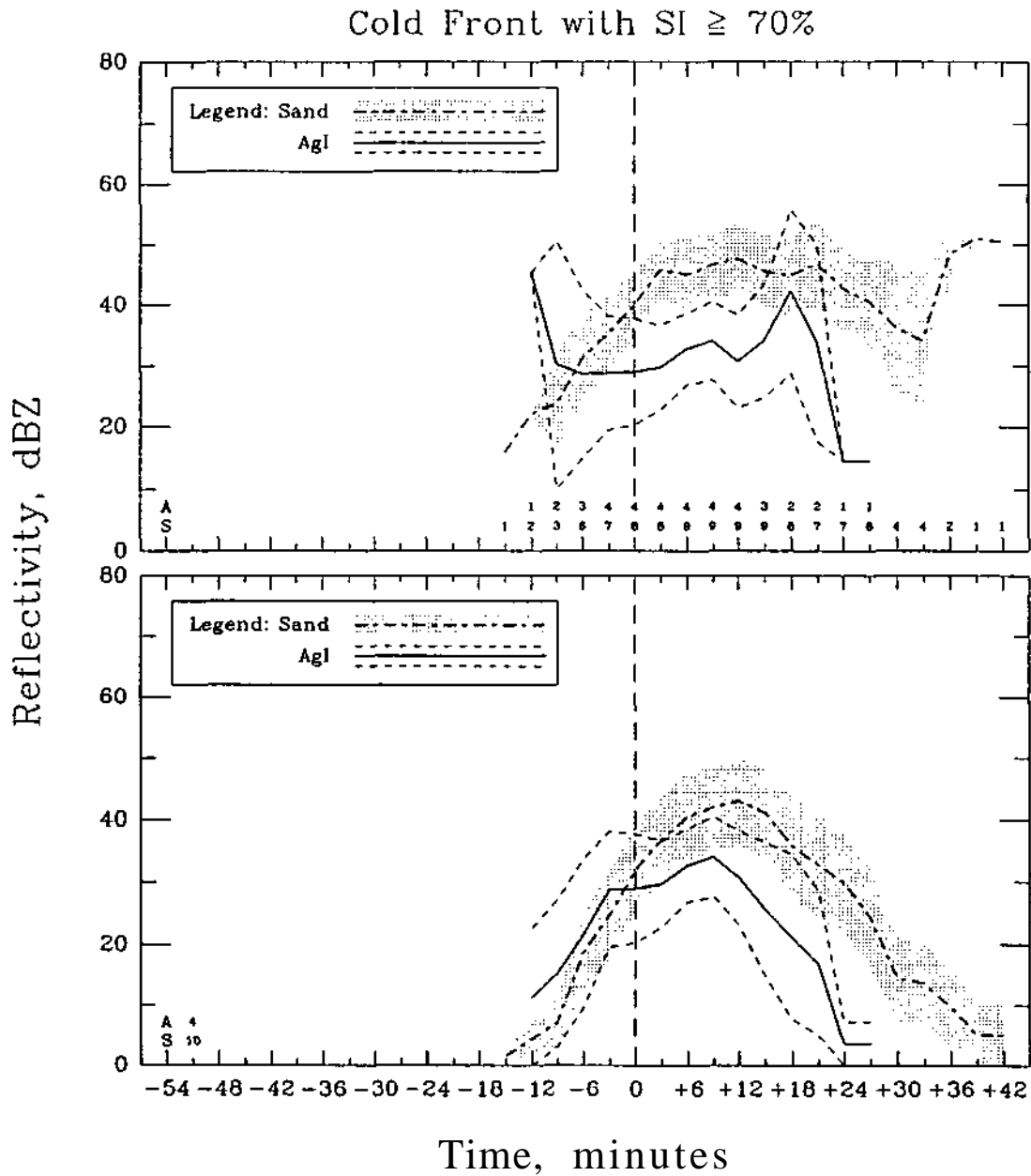


Figure D.36. Variation with time of means of maximum reflectivities for sand- and Agl-treated echoes in existence at each interpolated volume scan (top) and all treated echoes (bottom) for the subpopulation of clouds associated with cold fronts and had SI 70%.

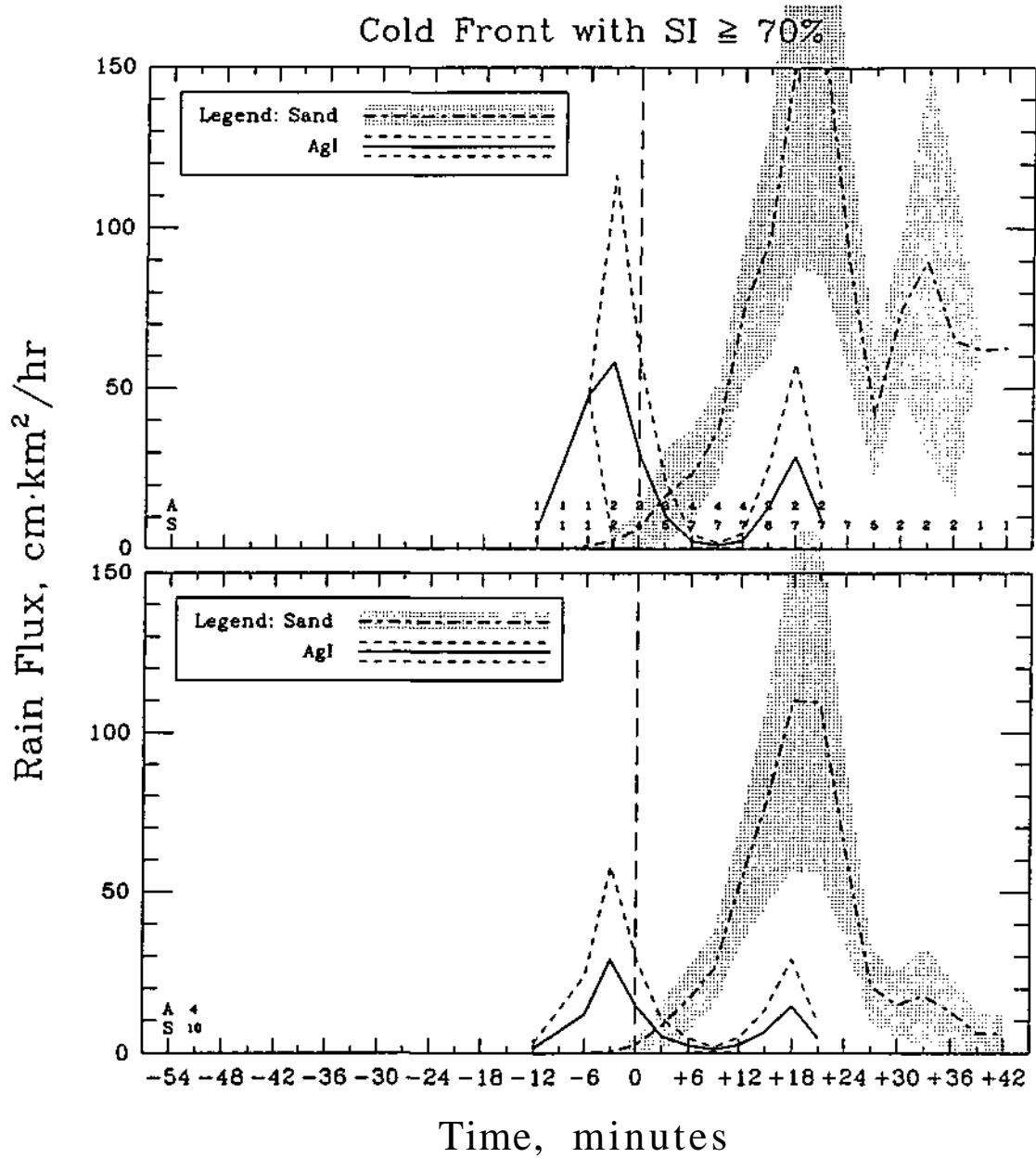


Figure D.37. Variation with time of means of rain fluxes for sand- and AgI-treated echoes in existence at each interpolated volume scan (top) and all treated echoes (bottom) for the subpopulation of clouds associated with cold fronts and had  $SI \geq 70\%$ .

Table D.17. Population statistics of predictor variables for cold front clouds with SI 70(N = 14).

Variable	Mean		Standard Deviation		Sample Size		P-Value	
	Sand	Agl	Sand	Agl	Sand	Agl	t	W
CPmndia	3.7	2.8	2.7	1.3	10	4	0.77	0.77
CPHip10	6.5	6.0	3.7	1.4	10	4	1.00	0.38
CPMxZ	32.0	29.1	21.4	17.3	10	4	0.77	0.77
CPMxB	17.8	17.3	10.8	7.6	10	4	1.00	0.77
CPA10	24.8	13.2	24.0	14.7	10	4	0.38	0.77
FECpt	2.3	4.3	6.0	6.2	10	4	1.00	1.00
NBuoy	-1.4	-1.8	2.1	0.7	10	4	1.00	0.75
Buoy_Enh	0.5	0.5	0.1	0.0	10	4	0.75	0.75
Mean_VW	8.6	6.7	4.6	4.9	10	4	1.00	1.00
SWC_frac	0.0	0.1	0.1	0.1	10	4	0.63	0.63
pb	6.3	5.6	1.7	1.2	10	4	1.00	1.00
tccl	15.0	16.3	1.0	1.1	10	4	0.38	0.54
Ri	63.1	86.1	11.5	63.9	10	4	0.53	1.00

Table D.18. Population statistics of response variables for cold front clouds with SI 70 (N = 14).

Variable	Mean		Standard Deviation		Sample Size		P-Values	
	Sand	Agl	Sand	Agl	Sand	Agl	t	W
MaxH10	11.1	7.8	3.9	3.1	10	4	0.75	0.52
MaxA10	73.5	48.0	56.5	50.3	10	4	0.75	0.52
MaxZ	47.1	41.8	19.5	16.7	10	4	1.00	0.75
MaxB	25.3	23.2	8.9	8.8	10	4	1.00	1.00
MXCPdH10	3.1	0.8	3.4	2.9	10	4	0.85	0.75
MXCPdA10	48.7	24.2	45.5	57.2	10	4	0.67	0.67
MXCPdZ	15.1	11.9	12.9	16.4	10	4	0.86	0.86
MXCPdB	7.5	3.6	6.1	8.1	10	4	0.63	0.86
CPMXtMxA	16.0	10.1	8.0	10.2	10	4	0.38	0.38
FEMXIMxA	18.3	14.3	9.6	4.4	10	4	0.75	0.75
ToiRNVOL	4.8	1.0	9.8	1.8	10	4	0.67	0.75
MxRFx	8.8	3.9	21.2	7.5	10	4	0.77	0.38
FEtTerm	27.6	23.1	14.0	5.4	10	4	0.14	0.38

$p \leq 5\%$

$5 < p \leq 10\%$

$p > 10\%$

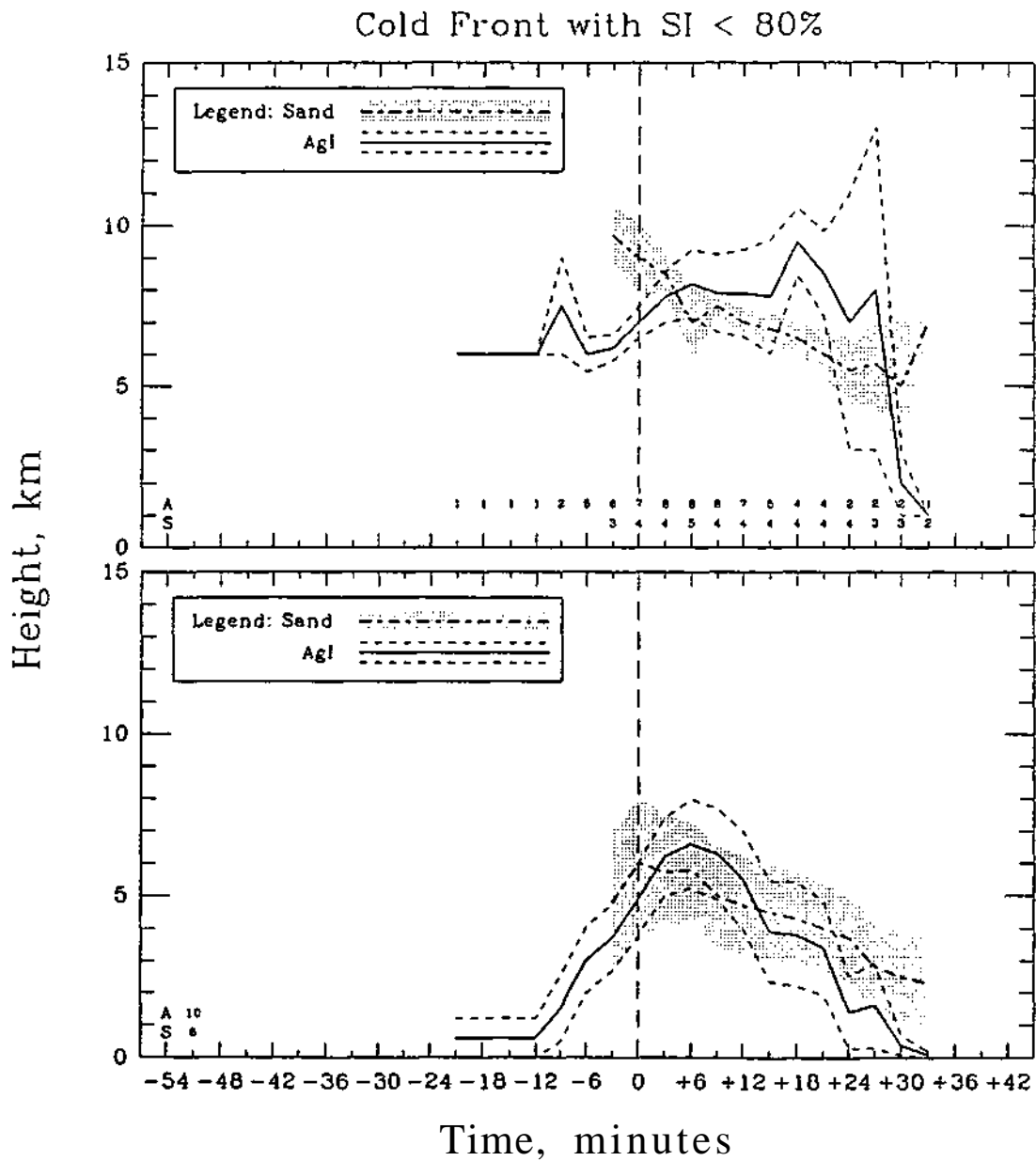


Figure D.38. Variation with time of means of the 10 dBZ echo top heights for sand- and Agl-treated echoes in existence at each interpolated volume scan (top) and all treated echoes (bottom) for the subpopulation of clouds associated with cold fronts and had SI < 80%.



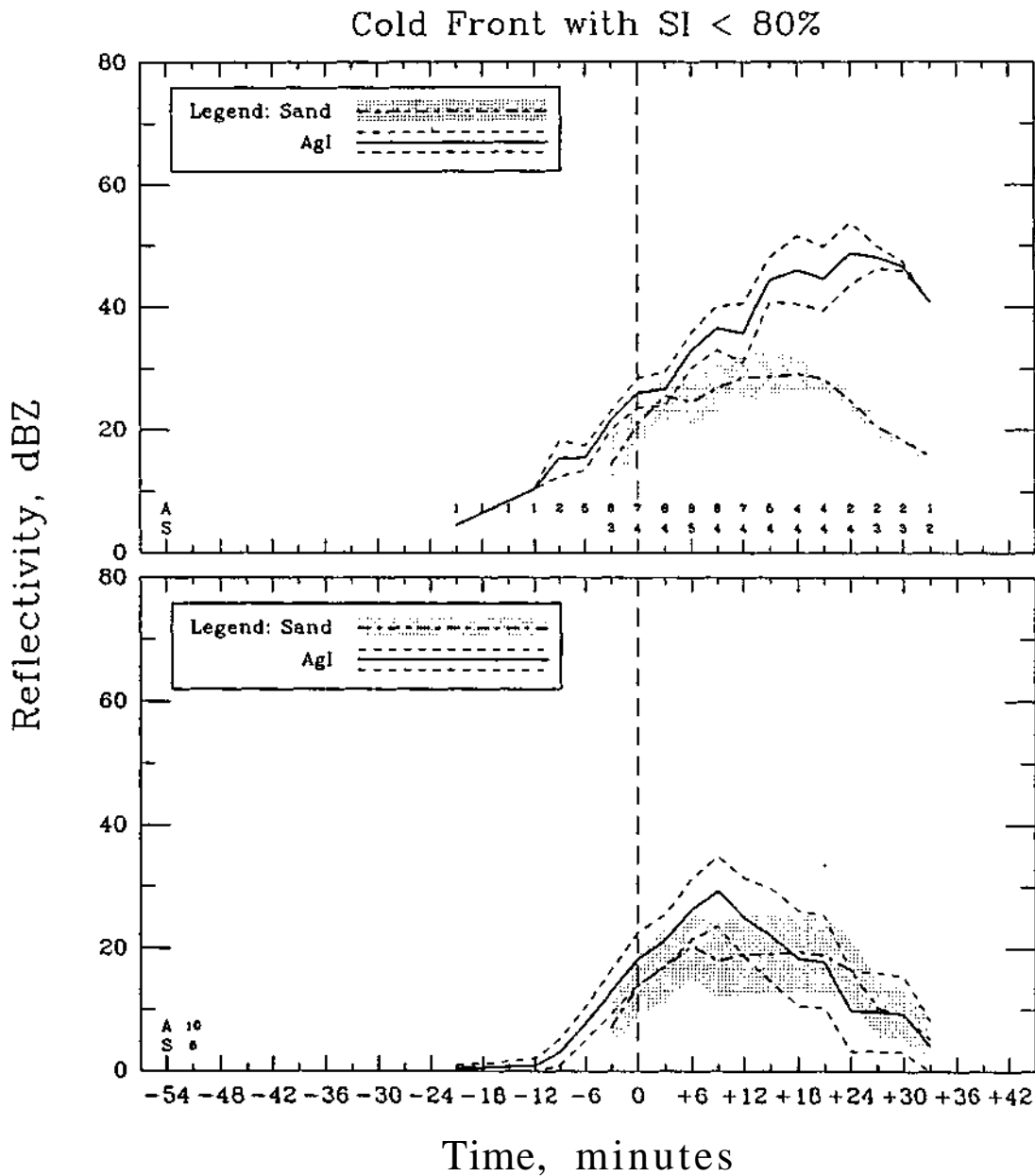


Figure D.40. Variation with time of means of maximum reflectivities for sand- and AgI-treated echoes in existence at each interpolated volume scan (top) and all treated echoes (bottom) for the subpopulation of clouds associated with cold fronts and had SI < 80%.

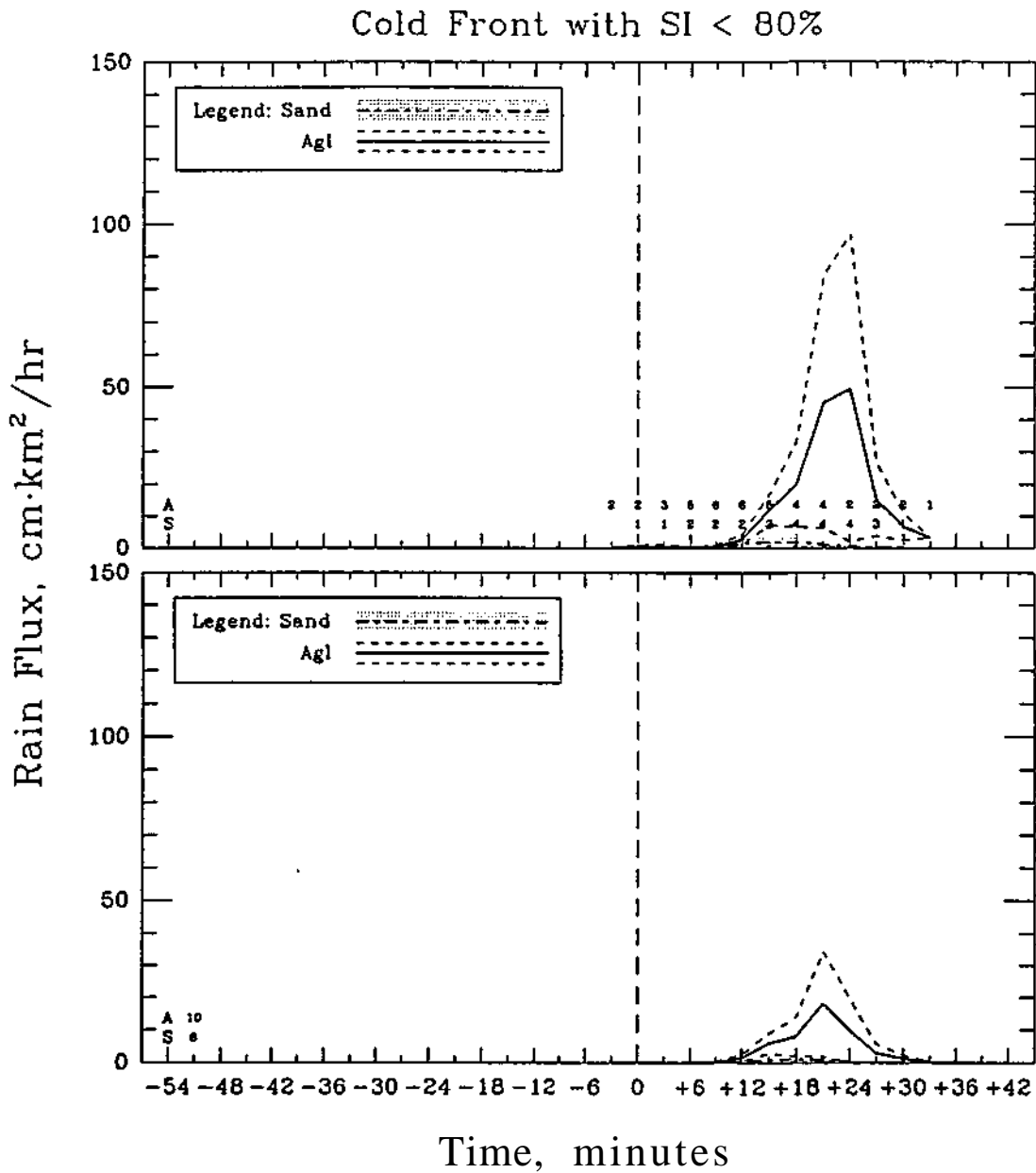


Figure D.41. Variation with time of means of rain fluxes for sand- and AgI-treated echoes in existence at each interpolated volume scan (top) and all treated echoes (bottom) for the subpopulation of clouds associated with cold fronts and had SI < 80%.

Table D.19. Population statistics of predictor variables for cold front clouds with SI < 80 (N = 16).

Variable	Mean		Standard Deviation		Sample Size		P-Values	
	Sand	Agl	Sand	Agl	Sand	Agl	t	W
CPmndia	0.7	1.7	1.3	1.3	6	10	0.14	0.14
CPHIp10	2.5	4.7	4.0	3.5	6	10	0.14	0.14
CPMxZ	7.3	17.0	12.4	13.1	6	10	0.38	0.38
CPMxB	5.1	10.4	8.1	7.5	6	10	0.14	0.38
CPA10	3.2	5.9	7.3	6.7	6	10	0.75	0.14
FECPt	-2.3	2.3	3.5	4.0	6	10	0.53	0.53
NBuoy	-1.5	-1.3	2.0	1.9	6	10	1.00	0.77
Buoy_Enh	0.5	0.4	0.1	0.1	6	10	0.14	0.14
Mean_VW	7.2	6.3	4.0	4.5	6	10	1.00	0.77"
SWC_frac	0.0	0.1	0.0	0.2	6	10	0.76	0.53
pb	7.1	7.3	1.7	1.3	6	10	0.54	1.00
tccl	14.5	15.4	1.0	1.9	6	10	0.85	0.85
Ri	69.1	103.7	11.5	54.7	6	10	0.90	0.44

Table D.20. Population statistics of response variables for cold front clouds with SI < 80 (N = 16).

Variable	Mean		Standard Deviation		Sample Size		P-Values	
	Sand	Agl	Sand	Agl	Sand	Agl	t	W
MaxH10	8.2	8.8	1.6	2.6	6	10	0.90	0.90
MaxA10	22.3	40.2	22.7	47.0	6	10	0.30	0.76
MaxZ	27.3	38.7	8.0	13.0	6	10	0.14	0.14
MaxB	16.0	21.4	3.0	6.8	6	10	0.14	0.14
MXCPdH10	0.2	0.3	0.4	3.3	6	10	0.90	1.00
MXCPdA10	19.2	33.7	16.6	46.6	6	10	0.30	1.00
MXCPdZ	20.0	16.4	13.2	23.3	6	10	0.86	1.00
MXCPdB	10.9	8.5	7.7	12.6	6	10	0.86	0.86
CPMXtMxA	12.0	9.0	8.0	8.2	6	10	1.00	1.00
FEMXIMxA	9.8	11.3	7.7	7.0	6	10	0.77	0.77
TotRNVOL	0.1	0.1	0.1	0.2	6	10	0.14	0.53
MxRFx	0.2	0.2	0.3	0.2	6	10	1.00	1.00
FEITerm	18.4	15.9	15.0	9.9	6	10	0.77	1.00

$p \leq 5\%$

$5 < p \leq 10\%$

$p > 10\%$

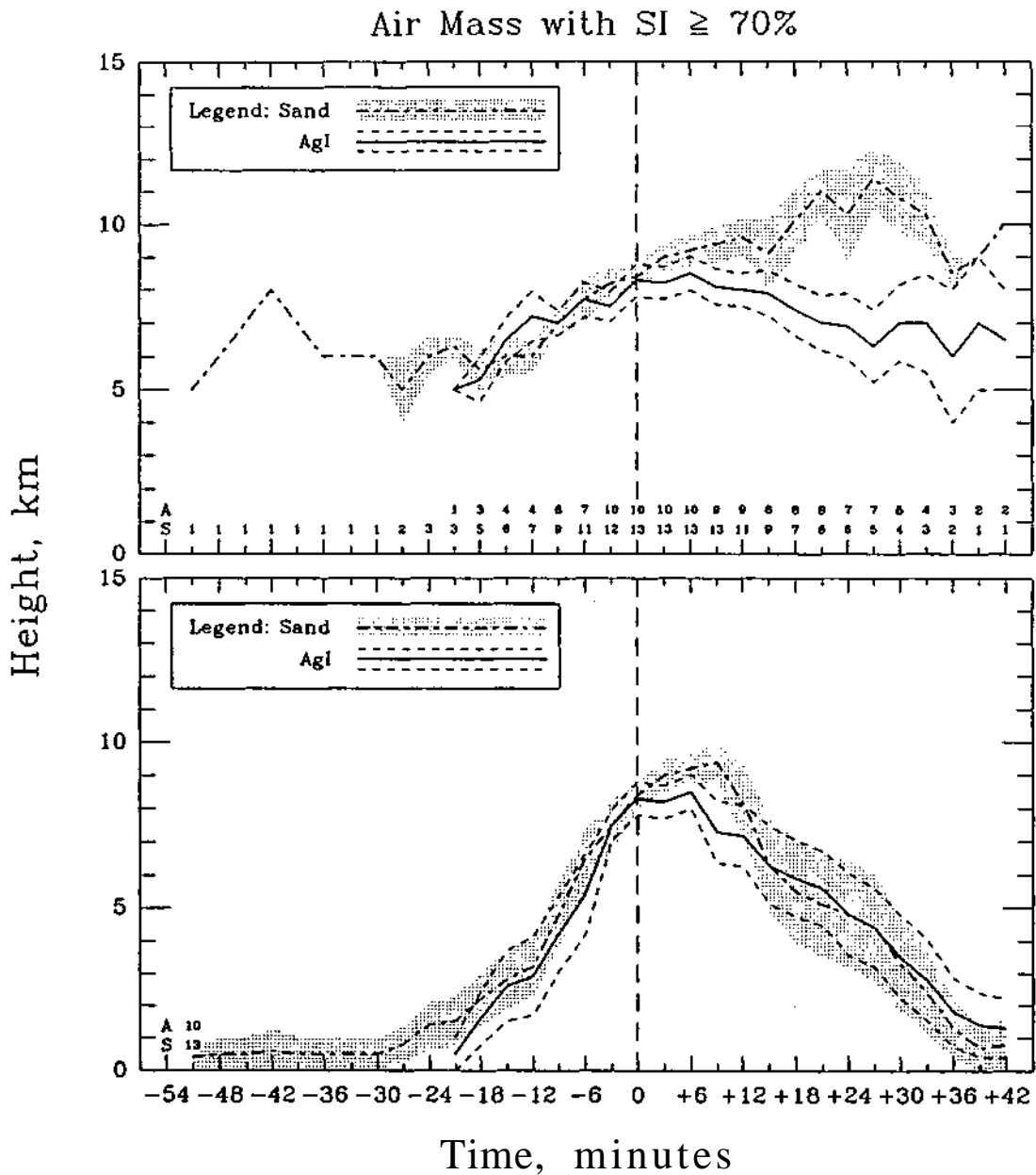


Figure D.42. Variation with time of means of the 10 dBZ echo top heights for sand- and AgI-treated echoes in existence at each interpolated volume scan (top) and all treated echoes (bottom) for the subpopulation of clouds associated with air mass convection and had  $SI \geq 70\%$ .

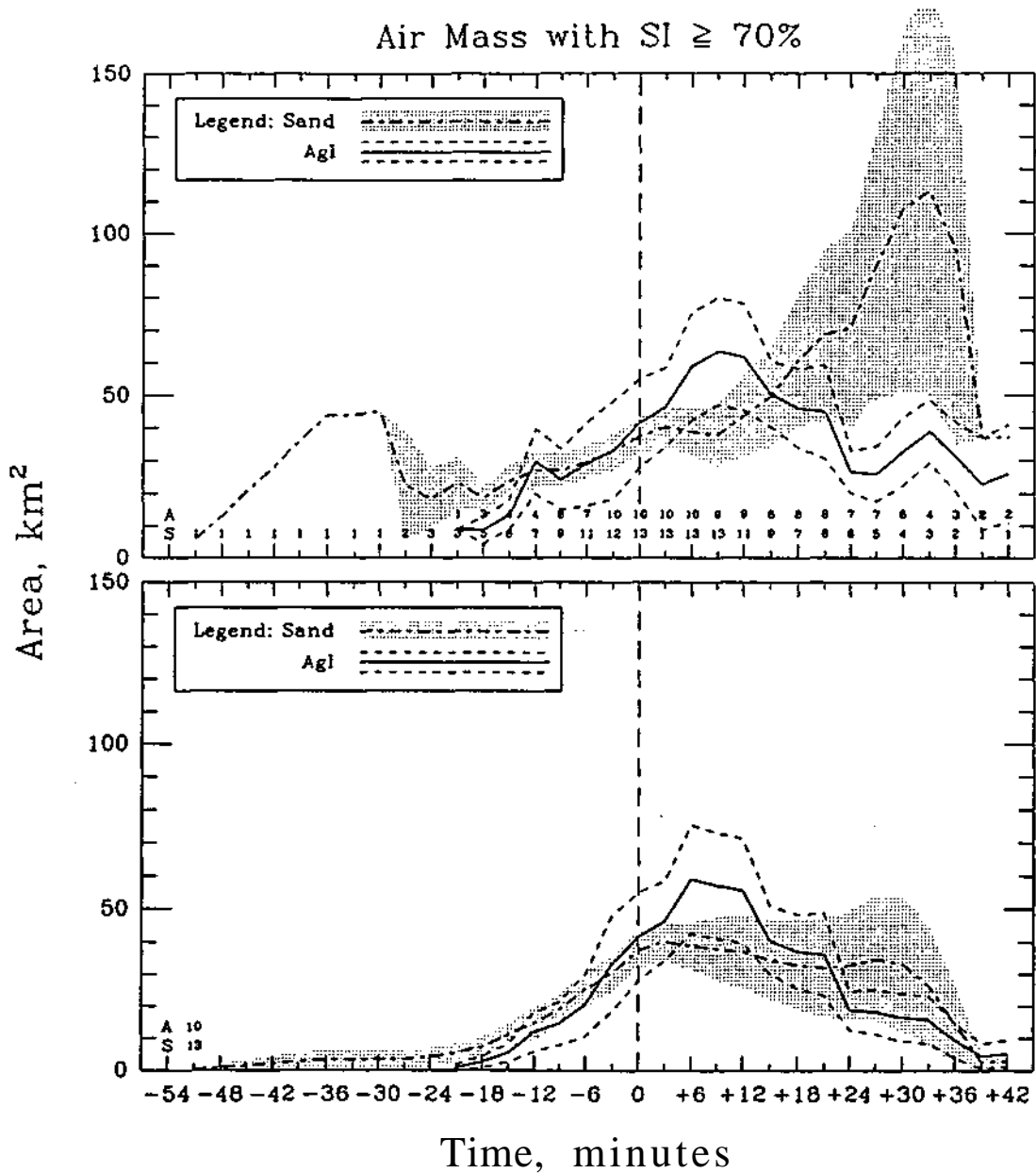


Figure D.43. Variation with time of means of the 10 dBZ defined echo areas for sand- and AgI-treated echoes in existence at each interpolated volume scan (top) and all treated echoes (bottom) for the subpopulation of clouds associated with air mass convection and had SI  $\geq 70\%$ .

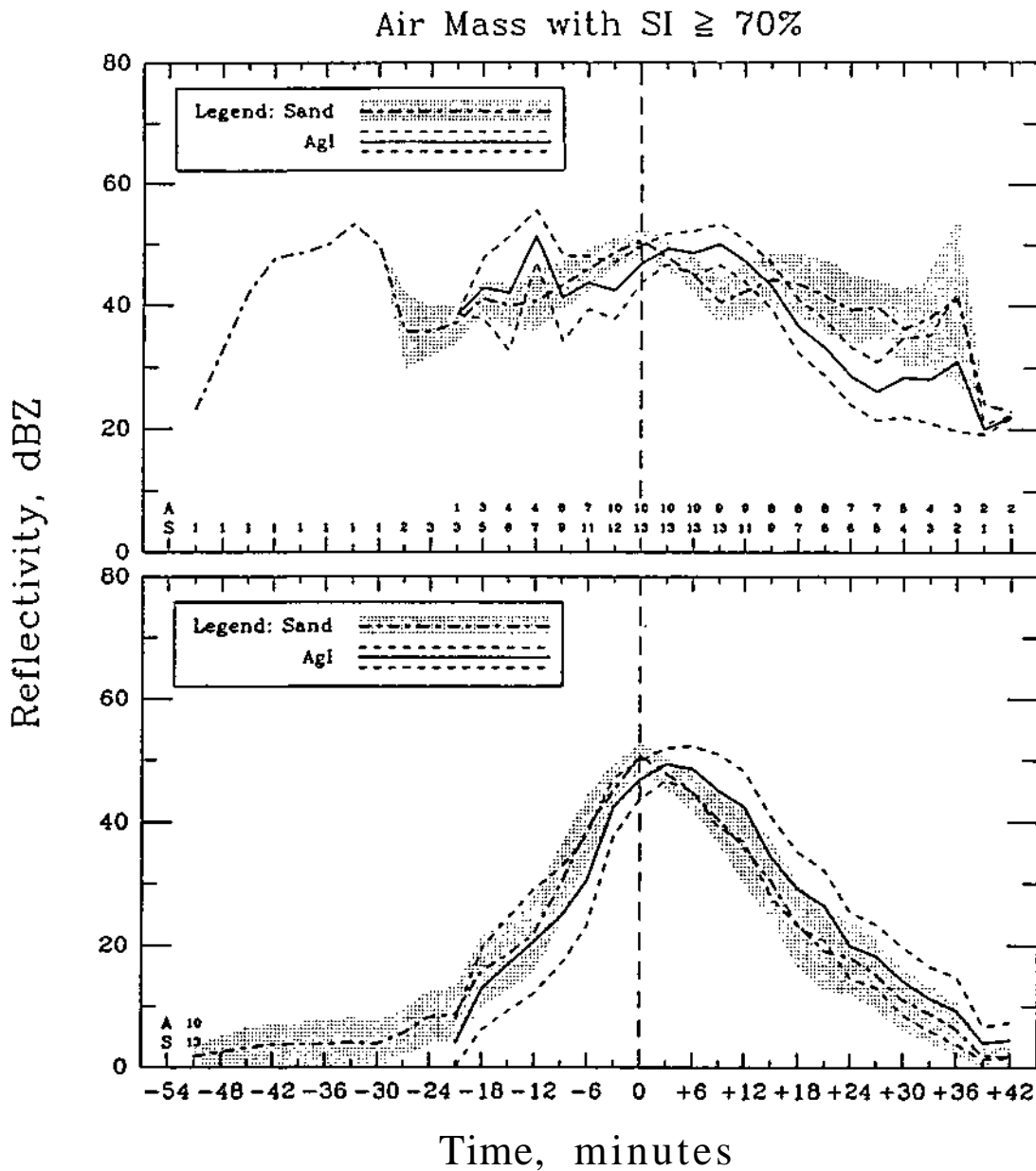


Figure D.44. Variation with time of means of maximum reflectivities for sand- and AgI-treated echoes in existence at each interpolated volume scan (top) and all treated echoes (bottom) for the subpopulation of clouds associated with air mass convection and had SI  $\geq$  70%.

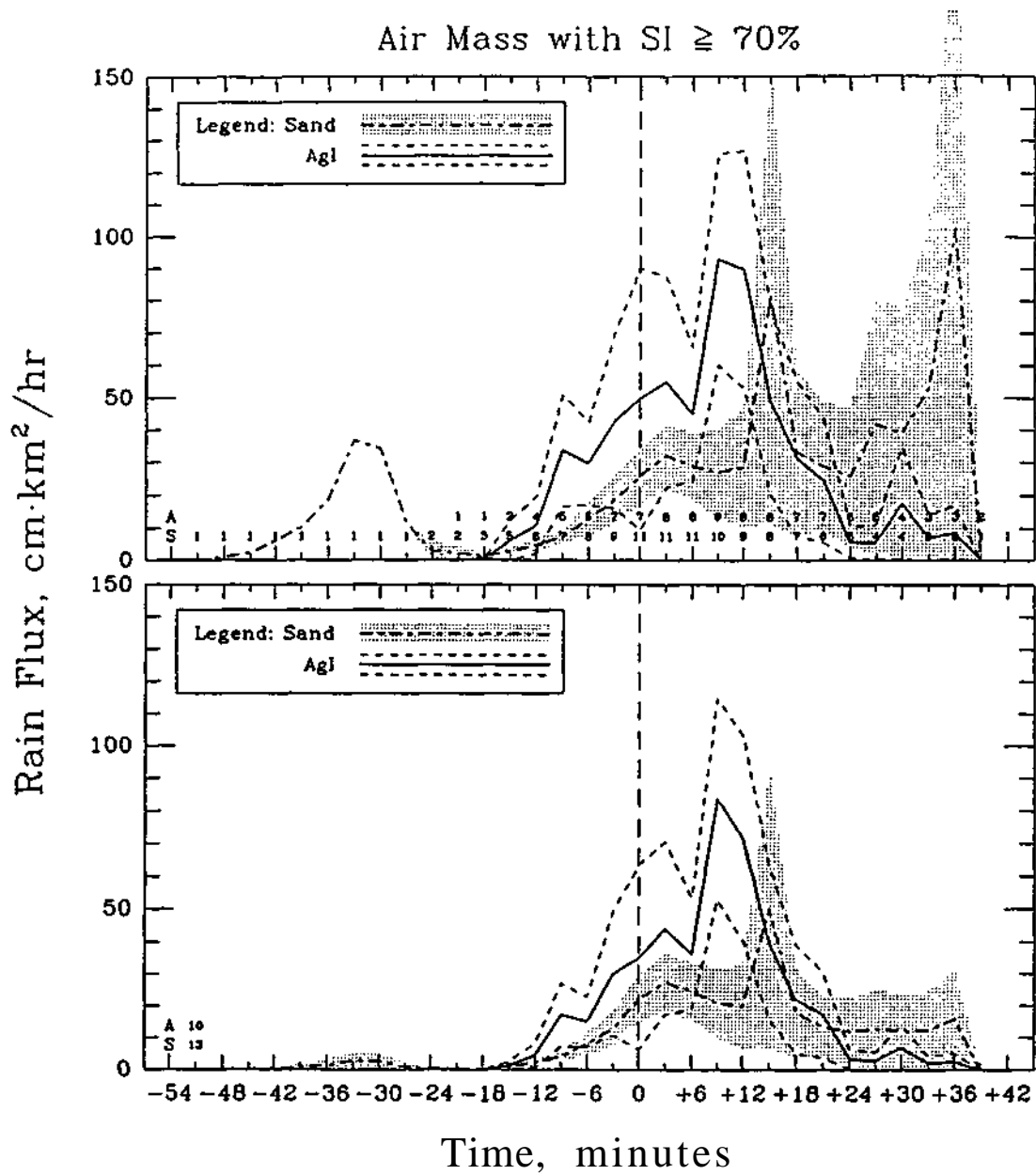


Figure D.45. Variation with time of means of rain fluxes for sand- and AgI-treated echoes in existence at each interpolated volume scan (top) and all treated echoes (bottom) for the subpopulation of clouds associated with air mass convection and had  $SI \geq 70\%$ .

Table D.21. Population statistics of precursor variables for air mass clouds with SI 70 (N = 23).

Variable	Mean		Standard Deviation		Sample Size		P-Values	
	Sand	Agl	Sand	Agl	Sand	Agl	t	W
CPmndia	5.2	5.1	1.2	2.4	13	10	0.62	0.38
CPHplO	8.3	8.2	1.6	1.7	13	10	1.00	1.00
CPMxZ	50.7	46.8	8.0	9.5	13	10	0.77	0.77
CPMxB	25.4	24.1	5.0	3.9	13	10	0.38	0.77
CPAIO	37.2	41.0	20.7	42.5	13	10	0.62	0.38
FECpt	14.1	9.9	13.8	7.4	13	10	0.38	0.77
NBuoy	0.1	-0.9	1.6	1.3	13	10	0.38	0.38
Buoy_Enh	0.5	0.5	0.0	0.0	13	10	0.77	0.77
Mcan_VW	4.4	3.8	1.8	1.5	13	10	0.38	0.38
SWC_frac	0.3	0.3	0.4	0.3	13	10	1.00	1.00
pb	3.5	3.6	0.1	0.0	13	10	0.77	0.77
tccl	18.5	16.9	0.2	1.2	13	10	0.38	0.62
Ri	87.6	76.0	9.4	12.9	13	10	0.62	0.62

Table D.22. Population statistics of response variables for air mass clouds with SI 70 (N = 23).

Variable	Mean		Standard Deviation		Sample Size		P-Values	
	Sand	Agl	Sand	Agl	Sand	Agl	t	W
MaxH10	10.4	8.9	1.7	1.4	13	10	0.38	0.38
MaxA10	75.8	72.7	65.0	58.6	13	10	0.62	0.77
MaxZ	54.9	56.2	6.4	7.5	13	10	1.00	1.00
MaxB	28.6	30.3	3.9	4.4	13	10	0.62	0.62
MXCPdH10	1.8	0.7	2.0	0.8	13	10	0.62	0.62
MXCPdA10	25.2	27.9	60.0	44.2	13	10	1.00	0.77
MXCPdZ	-2.3	4.4	5.9	11.3	13	10	0.38	0.62
MXCPdB	-0.7	3.1	4.5	7.0	13	10	0.77	0.77
CPMXIMxA	5.3	7.6	17.2	6.9	13	10	1.00	0.38
FEMXIMxA	19.4	17.5	13.5	10.6	13	10	0.77	1.00
TolRNVOL	20.0	24.6	57.6	65.7	13	10	1.00	0.38
MxRFx	13.9	16.9	16.8	28.3	13	10	1.00	0.38
FEtTerm	37.9	39.1	20.6	23.1	13	10	1.00	1.00

$p \leq 5\%$

$5 < p \leq 10\%$

$p > 10\%$

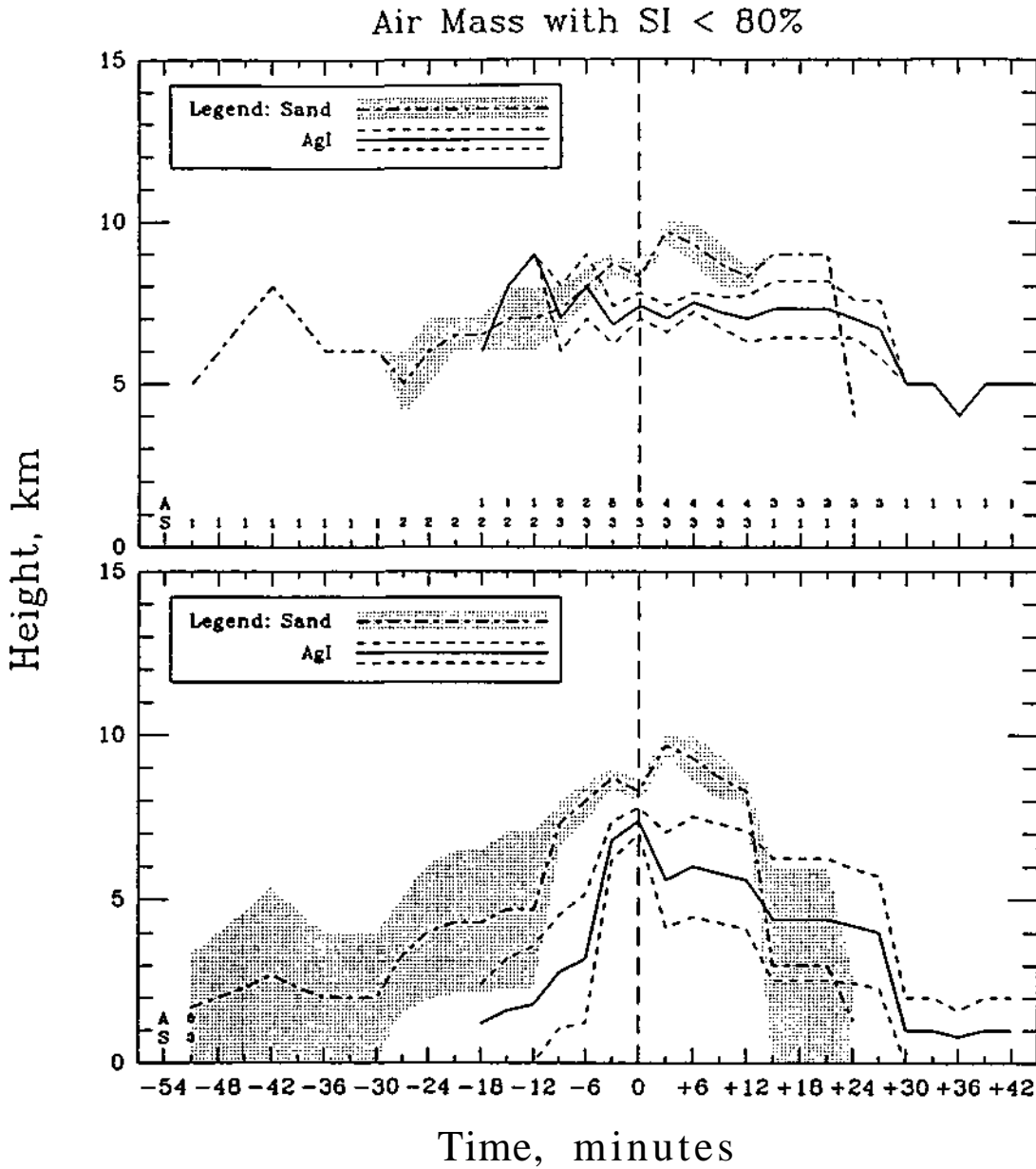


Figure D.46. Variation with time of means of the 10 dBZ echo top heights for sand- and AgI-treated echoes in existence at each interpolated volume scan (top) and all treated echoes (bottom) for the subpopulation of clouds associated with air mass convection and had SI < 80%.



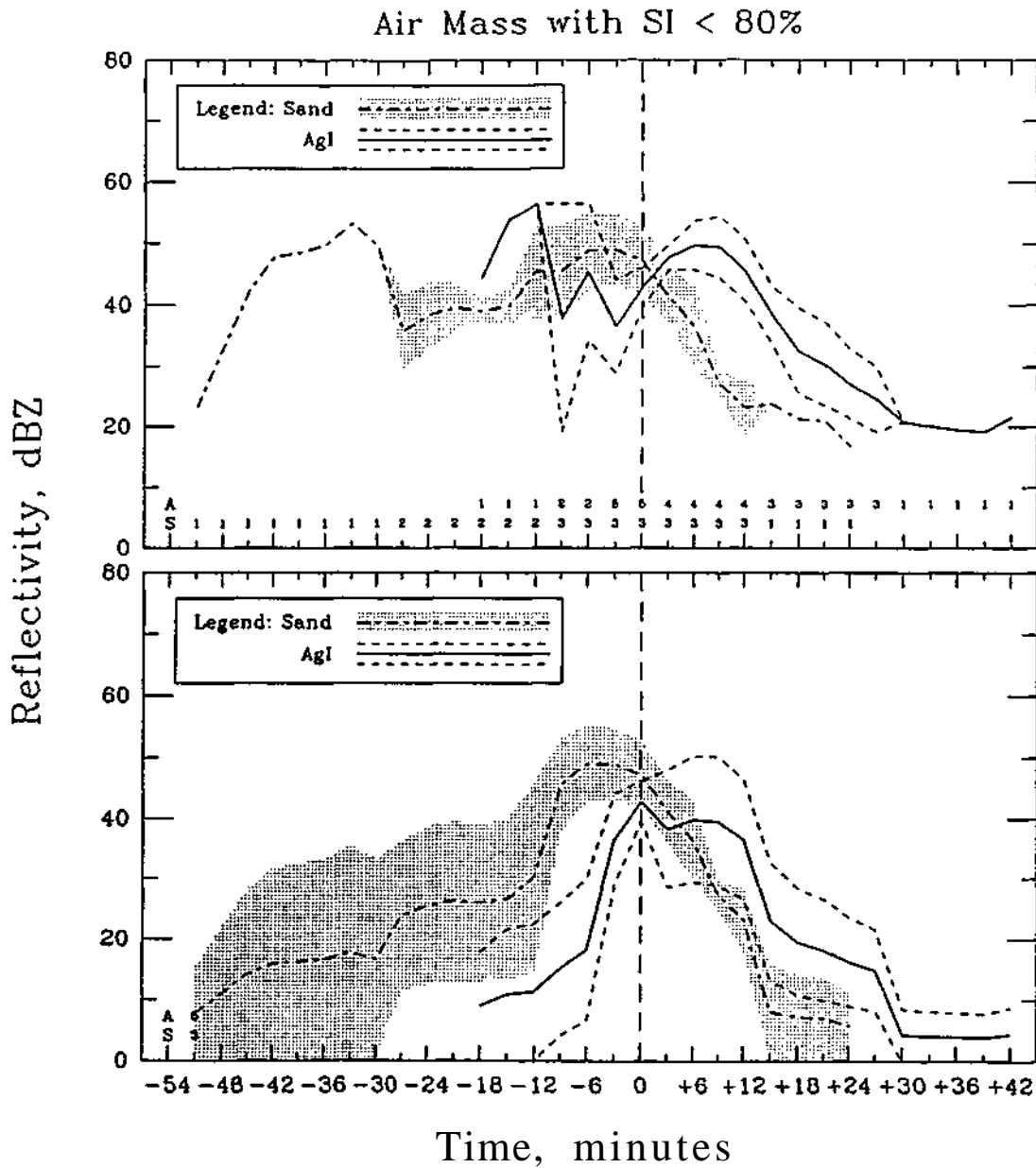


Figure D.48. Variation with time of means of maximum reflectivities for sand- and AgI-treated echoes in existence at each interpolated volume scan (top) and all treated echoes (bottom) for the subpopulation of clouds associated with air mass convection and had SI < 80%.

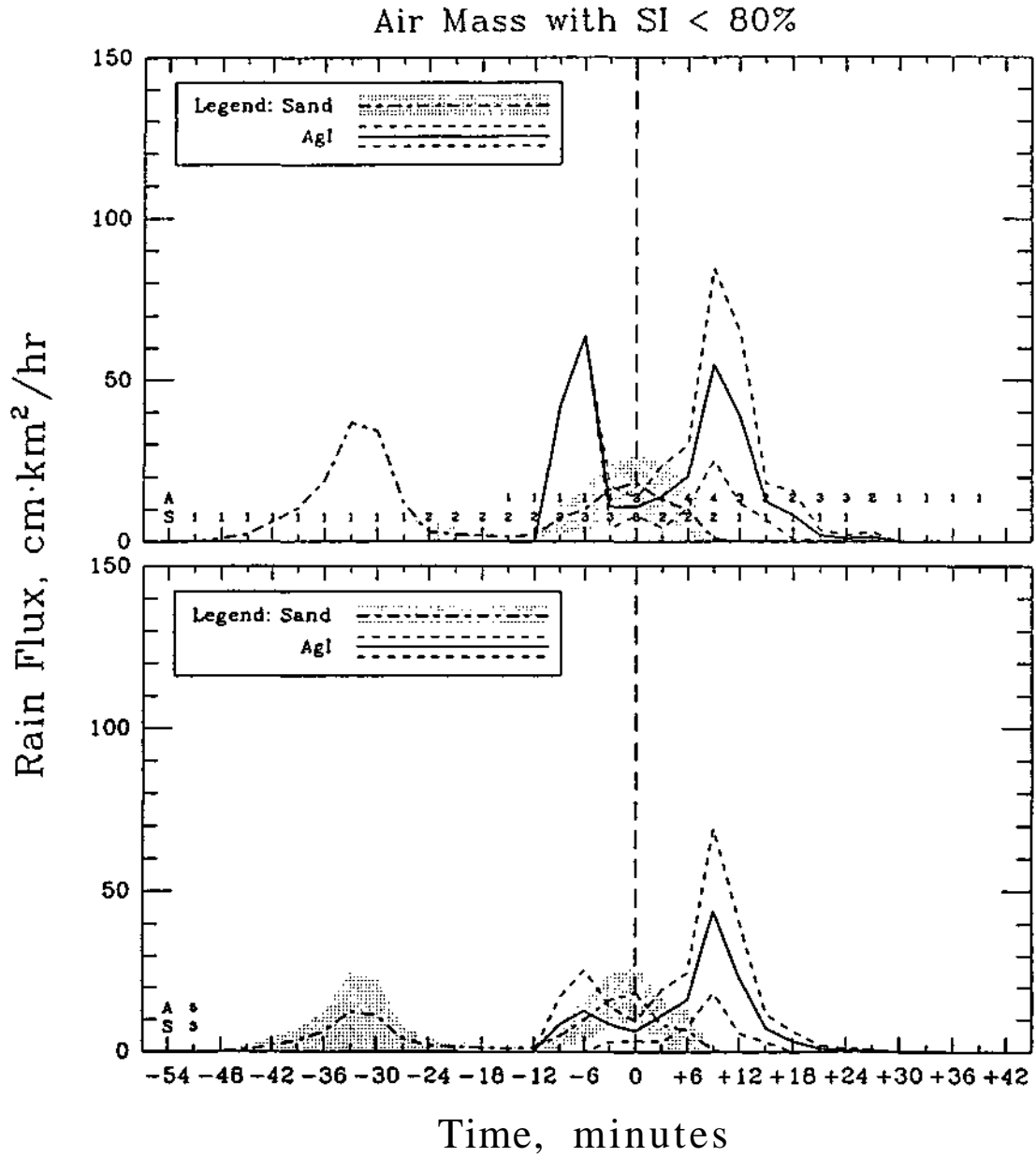


Figure D.49. Variation with time of means of rain fluxes for sand- and Agl-treated echoes in existence at each interpolated volume scan (top) and all treated echoes (bottom) for the subpopulation of clouds associated with air mass convection and had SI < 80%.

Table D.23. Population statistics of predictor variables for air mass elmds will) SI < 80(N = 8).

Variable	Mean		Standard Deviation		Sample Size		P-Values	
	Sand	Agl	Sand	Agl	Sand	Agl	t	W
CPmndia	5.2	3.4	1.2	2.2	3	5	0.38	0.38
CPHlp10	8.3	5.6	0.6	3.4	3	5	0.38	0.3S
CPMxZ	47.1	36.2	9.5	20.7	3	5	0.38	0.38
CPMxB	24.5	18.9	4.5	10.7	3	5	0.77	0.77
CPA10	32.7	19.6	14.6	16.7	3	5	0.38	0.38
FECPt	28.8	7.6	22.5	5.7	3	5	0.38	0.38
NBuoy	0.8	-1.3	2.4	1.5	3	5	0.77	0.77
Buoy_Enh	0.5	0.5	0.0	0.0	3	5	0.77	1.00
Mean_VW	2.2	2.8	0.2	1.0	3	5	0.38	0.38
SWC_frac	0.5	0.2	0.5	0.4	3	5	0.77	0.77
pb	3.5	3.6	0.1	0.0	3	5	0.77	0.77
tccl	18.6	17.2	0.2	1.4	3	5	0.77	1.00
<b>Ri</b>	88.6	78.7	10.7	14.7	3	5	1.00	1.00

Table D.24. Population statistics of response variables for air mass clouds with SI < 80 (N = 8).

Variable	Mean		Standard Deviation		Sample Size		P-Values	
	Sand	Agl	Sand	Agl	Sand	Agl	t	W
MaxH10	9.7	7.8	0.6	0.8	3	5	0.38	0.38
MaxA10	52.7	38.0	6.1	21.8	3	5	0.77	0.38
MaxZ	56.3	51.3	4.7	12.9	3	5	0.77	0.62
MaxB	29.4	28.2	2.4	6.9	3	5	0.77	1.00
MXCPdH10	1.3	-0.6	0.6	3.6	3	5	0.77	1.00
MXCPdA10	-20.0	16.0	10.8	15.1	3	5	0.38	0.38
MXCPdZ	-9.2	-0.0	8.0	19.8	3	5	0.77	0.77
MXCPdB	-5.0	-0.1	4.3	12.2	3	5	0.77	0.77
CPMxtMxA	-12.8	8.3	15.6	5.6	3	5	0.38	0.38
FEMXtMxA	16.0	15.8	7.4	10.6	3	5	1.00	0.77
TotRNVOL	19	4.3	14	5.0	3	5	0.77	1.00
MxRFx	2.8	15.0	0.8	20.9	3	5	0.38	1.00
FEtTcrm	39.7	30.6	33.6	22.8	3	5	0.62	0.38

**p ≤ 5%**

**5 < p ≤ 10%**

**p > 10%**

## Part E Review of the Experiment's Randomization Outcome

### 1. Background

Randomization of treatment types used during the 1989 PACE Field Experiment was to be conducted on experimental units (EUs). Balancing of the treatment data was to be undertaken by randomizing the EUs in pairs. This was to avoid major discrepancy in the number of silver iodide (AgI) and sand samples obtained (Changnon, et al. 1989).

Separate randomization tables were computed for experiments on "large" clouds (tops reaching higher than 30,000 ft) conducted within the confines of the designated experiment (target) area, and for all other experiments. All other experiments included 1) "small" cloud experiments (tops not reaching 30,000 ft or higher) within the target area, 2) (any) clouds outside the target area, 3) experiments with the T-28 aircraft in use, and 4) experiments conducted when the radar (or other equipment) was down. The "large" cloud experiments in the target area are referred to as " " experiments, while all other experiments are grouped together and referred to as "8" experiments.

Tables E.1 and E.2 are the randomization schemes for these " " and " " experiments, respectively, created before operations began. These indicate precisely what type of flares were to be used throughout the summer's EUs, and where in the flare banks on the aircraft the flares were to be put. It is apparent from these tables and the description in the operations manual (see above), that an attempt was made to follow the rule of "No more than two EUs in a row of the same treatment type" (hereafter referred to as "the rule").

However, the tables are not flawless, since up to four EUs were allowed in one flight. That is, the rule should have been valid if one or two or three or four EUs were treated in one flight. In checking the table, it appears that this flaw is revealed, for example, if " " Flight 5 (Table E.1) had three EUs in the flight: the first EU of this flight would have had treatment P (placebo/sand), the second EU treatment A (silver iodide/AgI), and the third EU treatment A. According to the table, the first EU of the next flight (6) would have also gotten treatment type A, thus creating three EUs in a row with the same treatment type (A in this example); therefore, the preset rule would have not been followed. Note, however, that if all flights have only one EU, the rule is followed, and if all flights have only two EUs, the rule is also followed. And, of course, if all flights have four EUs, the rule is also followed.

As it turned out, no flight during the summer of 1989 had more than two EUs during the flight. Thus, according to Tables E.1 and E.2, the rule of no more than two in a row of the same treatment type should have nearly resulted if the correct envelopes had been used/given and treatment types had been subsequently recorded correctly. Envelopes containing which flare bank numbers to use in the flight were developed before operations began. This may have contributed to the confusion of the treatment type the EUs should have gotten as the summer progressed and to the (wrong) outcome of treatment types the EUs received, as will now be described.

## 2. Transcript of the summer

Tables E.3 and E.4, and E.5 and E.6 are exact copies of Tables E. 1 and E.2 respectively, but show how the randomization officer (RO) kept track of the treatments through the summer (Tables E.3 and E.4) and show how the "Rerandomization Officer" (ReRO) believes the EUs and treatments should have been recorded (Tables E.5 and E.6).

The first flight was carried out on May 19. It was a scheduled " " experiment and was carried out as such. The plane was loaded with flares according to " " Flare Loading (FL) #1. Silver iodide (AgI) flares were used in one EU. Thus, Tables E.4 and E.6 indicate " " FL #1 and " " Flight #1 were used on 5/19a (where " " indicates the first flight on 5/19).

The second flight on 5/19 (5/19b), was a scheduled " ", and was carried out successfully, " " FL #1 was used. Placebo flares were used in one EU. Thus, Tables E.3 and E.5 indicate that " " FL #1 and " " Flight #1 were used on 5/19b.

The next flight occurred on 5/25. It was a scheduled " ", and therefore " " FL #2 was used. However, " " clouds did not materialize, so type " " was carried out. Placebo flares were used in one EU. Tables E.5 and E.6 (ReRO) reflect that " " FL #2 was used on 5/25, and " " Flight #2 was carried out on 5/25. However, Table E.3 (RO " ") records that a " " (backup) experiment was carried out as " " Flight #2. Assumably, it was recorded this way because " " FL #2 was used for this flight.

There was much confusion relating to 5/30. As recorded by the RO:

This was an unscheduled flight that was formulated in the early forenoon and people called out to the airport to perform it. The recorded message for the previous evening indicated no early flight would occur. Neither the Randomization Officer (Huff) nor the Randomization Technician (Walters) could be located, so the Baron pilot selected the Type " " loaded rack for the flight. Walters had both Type " " and Type "8" flare racks loaded and identified in the storage closet.

Since this was a T-28 flight, the Type "8" rack should have been used. The pilot took the proper set of envelopes for the Type " " flight (" " FL #3 in Tables) from the Huff-Walters file, but took a scheduled Type " " set of envelopes ("8" FL #3 in Tables) instead of the Type "8" backup set from the files.

The experiment was changed to a " " type in the air, and the " " envelopes used. Fortunately this did not cause a major problem -- just a little adjustment of the randomization tables. However, treatment was accomplished with placebo flares, whereas with use of the " " backup set of envelopes the treatment would have been with AgI flares.

Because of the above occurrence, experiment 3 of the Type " " randomizations (" " FL #3) and experiment 3 of the " " type group (" " FL #3) have been eliminated from the randomization tables for future use.

So the flight on 5/30 was a " " flight where placebo flares treated one EU. The tables indicate (with horizontal lines through the numbers) " " and " " #3 FLs and " " and " " #3 Flights were eliminated. However, the RO's notes indicate " " Flight #3, which should have been blank or eliminated, was carried out as " " (backup) on 5/30.

The flight on 6/1 was a scheduled " " and carried out as such, " " FL #4 was used, and Agl flares treated one EU. Table E.5 (ReRO's recording notes) indicates that " " FL #4 was used on 6/1. However, " " Flight #2 had not been carried out yet at this point; thus the ReRO believes this was " " Flight #2 on 6/1, and should have used placebos, not Agl. In contrast, Table E.3 (RO's notes) has recorded a " " event in Flight #2 of this " " table, so thus records 6/1 as " " Flight #4.

On June 3, an " " flight was planned. Therefore flare banks were loaded using " " FL #5 and the aircraft went up. An in-flight switch was made to " ", and one (" ") EU was treated with placebo flares. Another EU was treated, but was type " ". This resulted in Agl flares being used. Table E.3 shows that the RO recorded both EUs in the " " table. The ReRO's recording of the treatments is shown in Tables E.5 and E.6. The first EU was a " ", and according to the next flight in the " " table (" " Flight #5), it should have been an Agl unit. However, placebos were used. The second EU was an " ", and Table E.5 shows that the next EU (" " Flight #4) was to use Agl flares, which were used in this second EU of 6/3.

The next date with flights was 6/12. A type " " experiment was planned, so " " FL #2 was used on the aircraft. Two EUs were treated; the first received Agl flares, and the second received placebos. Table E.4 shows these recorded under " " flight #2. However, this wasn't the 2nd flight with " " units but was " " Flight #6. Table E.6 reflects that the first unit should have gotten placebo flares, while the second unit in the flight should have received Agl flares.

June 18 had one EU in a flight that was scheduled " " and carried out as such. Thus, " " FL #4 was used, and placebo flares were released. Both tables reflect this.

June 23 had two flights. The first flight was scheduled " " and carried out as such. Thus, " " FL #6 was used, and Agl flares were released. Note, according to the next " " flight in Table E.5 (Flight #5), this unit should have been treated with placebos. The second flight on this day was also scheduled " " and carried out as such; " " FL #7 was used. Two EUs were treated during this flight. The first one got Agl flares, the second received placebos. The tables agree, though written under different flight numbers, that the treatment types on this flight were "correct."

An " " experiment was planned on 6/27. Therefore, " " FL #8 was used. During the flight, however, the mission was changed to a " ". Two EUs were treated; the first received placebos,

and the second received Agl flares. According to Table E.6, the next " " flight was #8, so the first EU on this flight should have received Agl flares, and the second EU should have gotten placebos.

An " " FL (#9) was used on 7/2, anticipating "big" clouds. However, the shift to a " " experiment was made. Placebo flares were fired into one EU. Table E.6 shows that this flight was " " flight #9, and should have received Agl flares.

On July 8, an " " experiment was scheduled and carried out; " " FL #11 was used (skipping FL #10 by mistake, perhaps?). Two EUs were treated. The first received placebos, the second got Agl flares. Table E.5 (" " Flight #7) indicates that the first EU should have gotten Agl, while the second should have gotten placebos.

July 11 was an " " experiment; " " FL #10 was used (since it was missed last time?). Agl flares treated one EU. According to Table E.5, this was " " Flight #8, which should have received placebos.

There were two flights on 7/19. The first flight was scheduled " ", and used " " FL #13 (skipping FL #12). One EU was treated with placebo flares. Both tables show this was "correct" treatment. The second flight on 7/19 was scheduled and carried out a " ". " " FL #5 was used, and Agl flares were released into one EU. Table E.6 shows this was " " Flight #10, and should have received placebo flares.

On July 23, a " " experiment was planned. " " FL #8 was used (skipping FL #6 and #7). The experiment was changed to an " " in flight, and one EU was treated with Agl flares. Table E.5 indicates this was " " Flight #10, so should and did get Agl flares.

An " " experiment was planned and carried out on 7/24. " " FL #16 was used (again skipping two FLs). One EU was treated with placebos. Table E.5 indicates this was " " Flight #11, so was "correct" in getting placebo flares.

The last date with experiments was 7/25. An " " experiment was planned, so " " FL #17 was used. (Note that " " FL #s 12, 14, and 15 were never used, but 16 and 17 were.) Two EUs were treated; the first received placebos, the second received Agl flares. Table E.5 shows that this was " " Flight #12, so the first EU should have gotten Agl flares, and the second EU should have gotten placebos, when, in fact, the opposite occurred.

### **3. Summary**

Tables E.7 and E.8 show the results of the " " and " " experiment treatments declared and treated using the " " type and " " type treatment tables, respectively. In the Tables, the last column indicates what the "correct" treatment should have been. Note that the flaw mentioned earlier is revealed: Because " " Flight #7 had two EUs and " " Flights #8 and #9 each had one EU, three EUs in a row would have occurred with the same treatment type of sand. Thus, even if

Tables E. 1 and E.2 would have been followed perfectly, the rule of no more than 2 in row of the same treatment type would not have been followed exactly.

The ReRO believes that the recording practice of the RO resulted from insisting that the Flare Loading (FL) numbers corresponded with the Flight numbers. Thus, had the forecasts been perfect, the " " FLs would have occurred with " " experiments and confusion in recording (that is, recording " " events in the " " Table) would not have happened. The fact that the envelopes were pre-prepared probably also added to the "wrong" randomization results. The ReRO suggests that separate " " and " " FLs were not necessary, since the intent of different FLs per flight was to keep airplane crew unaware of which type of treatment was in which flare bank. Thus, one sequence of Flare Loadings would be used for the entire summer; FL #1 would be used on Flight #1, FL #2 on Flight #2, etc., regardless of type " " or " ". However, the envelopes to use on any particular flight would be unknown until the previous flight was Finished. That is, when Flare Loading #7, for example, was used, one would not know ahead of time which banks to use, without knowing if the treatment type for the next EU was to receive placebos or Agl.

#### **4. References**

Changnon, S.A., Jr., R.R. Czys, F.A. Huff, E.A. Mueller, J.B. Nespor, R.W. Scott, and N.E. Westcott, 1989: Operations Manual: The Precipitation Augmentation for Crops Experiment - 1989, Phase II: Exploratory Modification Phase, Illinois State Water Survey Miscellaneous Publication 143, Champaign, Illinois, 48 pp.

Table E.1. Pre-determined 1989 " " experiment treatment types.

FL <sup>1</sup>	Flare Bank <sup>2</sup>									Flight	Experimental Unit
	1	2	3	4	5	6	7	8,9			
1	P	A	P	A	A	P	P	A		1	P A A P
2	A	P	P	A	A	P	A	P		2	P A P A
3	P	A	P	A	P	A	A	P		3	A P A P
4	A	P	A	P	P	A	A	P		4	A P A P
5	A	P	P	A	P	A	P	A		5	P A A P
6	A	P	A	P	P	A	P	A		6	A P P A
7	P	A	P	A	P	A	P	A		7	A P A P
8	A	P	P	A	A	P	A	P		8	P A P A
9	A	P	P	A	A	P	P	A		9	P A P A
10	A	P	A	P	P	A	A	P		10	A P P A
11	P	A	P	A	P	P	A	A		11	P A P A
12	A	P	A	P	A	P	P	A		12	A P P A
13	A	P	P	A	A	P	A	P		13	P A A P
14	P	A	P	P	P	A	A	A		14	A P A P
15	P	A	P	P	P	A	P	A		15	A P P A
16	A	P	P	A	A	P	A	P		16	P A P A
17	A	P	A	P	P	P	A	A		17	P A A P
18	A	P	P	A	A	P	A	P		18	A P A P
19	P	A	P	A	A	P	A	P		19	A P P A
20	A	P	P	A	A	P	P	A		20	P A A P

<sup>1</sup>FL Flight Loading

<sup>2</sup>Banks 8 and 9 were loaded with the same treatment type.

P Placebo (sand), A Sliver Iodide (Agl)

Table E.2. Pre-determined 1989 " " experiment treatment types.

FL <sup>1</sup>	Flare Bank <sup>2</sup>									Flight	Experimental Unit
	1	2	3	4	5	6	7	8,9			
1	P	A	P	P	A	P	A	A		1	A P A P
2	A	P	P	A	P	P	A	A		2	P A A P
3	A	P	A	P	A	P	P	A		3	A P P A
4	P	A	P	A	P	P	A	A		4	P A P A
5	P	A	A	P	P	A	P	A		5	A P P A
6	A	P	P	A	A	P	A	P		6	P A P A
7	A	P	P	A	A	P	A	P		7	P A P A
8	P	A	P	A	P	A	P	A		8	A P A P
9	A	P	A	P	P	A	P	A		9	A P P A
10	A	P	P	A	P	A	P	A		10	P A A P
11	A	P	A	P	P	A	A	P		11	A P A P
12	P	A	P	A	P	A	A	P		12	A P A P
13	A	P	P	A	A	P	A	P		13	P A P A
14	P	A	P	A	A	P	P	A		14	P A A P
15	P	A	P	P	P	A	P	A		15	A P P A
16	A	P	P	A	A	P	A	P		16	P A P A
17	A	P	A	P	P	A	P	A		17	P A P A
18	P	A	P	P	P	A	P	A		18	A P A P
19	A	P	P	A	A	P	P	A		19	A P P A
20	A	P	P	A	P	P	A	A		20	P A A P

<sup>1</sup>FL Flight Loading Number

<sup>2</sup>Banks 8 and 9 were loaded with the same treatment type.

P Placebo (sand), A Silver Iodide (AgI)

Table E.3. 1989 " " experiment treatment types recorded by the Randomization Officer (RO).

FL*	Flare Bank**									Flight	Experimental Unit	Date Used
	1	2	3	4	5	6	7	8,9				
1	P	A	P	A	A	P	P	A		1	P <sup>1</sup> A A P	5/19b
2	A	P	P	A	A	P	A	P		2	P <sup>1</sup> A P A	5/25 "β" backup
3	<del>P</del>	<del>A</del>	<del>P</del>	<del>A</del>	<del>A</del>	<del>P</del>	<del>A</del>	<del>P</del>		3	<del>A</del> -P <sup>1</sup> <del>A</del> -P	5/30 "β" backup
4	A	P	A	P	P	A	A	P		4	A <sup>1</sup> P A P	6/1
5	A	P	P	A	P	A	P	A		5	P <sup>1</sup> A <sup>2</sup> A P	6/13 "β" backup, "α"
6	A	P	A	P	P	A	P	A		6	A <sup>1</sup> P P A	6/23a
7	P	A	P	A	P	A	P	A		7	A <sup>1</sup> P <sup>2</sup> A P	6/23b
8	A	P	P	A	A	P	A	P		8	P <sup>1</sup> A <sup>2</sup> P A	6/27 "β" backup
9	A	P	P	A	A	P	P	A		9	P <sup>1</sup> A P A	7/2 "β" backup
10	A	P	A	P	P	A	A	P		10	A <sup>1</sup> P P A	7/11
11	P	A	P	A	P	P	A	A		11	P <sup>1</sup> A <sup>2</sup> P A	7/8
12	A	P	A	P	A	P	P	A		12	A P P A	
13	A	P	P	A	A	P	A	P		13	P <sup>1</sup> A A P	7/19a
14	P	A	P	P	A	P	A	A		14	A P A P	
15	P	A	P	P	A	P	A	A		15	A P P A	
16	A	P	P	A	A	P	A	P		16	P <sup>1</sup> A P A	7/24
17	A	P	A	P	P	A	P	A		17	P <sup>1</sup> A <sup>2</sup> A P	7/25
18	A	P	P	A	A	P	A	P		18	A P A P	
19	P	A	P	A	A	P	A	P		19	A P P A	
20	A	P	P	A	A	P	P	A		20	P A A P	

\* FL Flight Loading

\*\*Banks 8 and 9 were loaded with the same treatment type.

P Placebo (sand), A Sliver Iodide (Agl)

<sup>1</sup> The first EU of the flight received this treatment type.

<sup>2</sup> The second EU of the flight received this treatment type.

Table E.4. 1989 " " experiment treatment types recorded by the Randomization Officer.

FL*	Flare Bank**									Flight	Experimental Unit	Date Used
	1	2	3	4	5	6	7	8,9				
1	P	A	P	P	A	P	A	A		1	A <sup>1</sup> P A P	5/19a
2	A	P	P	A	P	P	A	A	2	P <sup>1</sup> A <sup>2</sup> A P	6/12	
3	<del>A</del>	<del>P</del>	<del>A</del>	<del>P</del>	<del>A</del>	<del>P</del>	<del>P</del>	<del>A</del>	3	<del>A P P A</del>	5/30	
4	P	A	P	A	P	P	A	A	4	P <sup>1</sup> A P A	6/18	
5	P	A	A	P	P	A	P	A	5	A <sup>1</sup> P P A	7/19b	
6	A	P	P	A	A	P	A	P	6	P A P A		
7	A	P	P	A	A	P	A	P	7	P A P A		
8	P	A	P	A	P	A	P	A	8	A <sup>1</sup> P A P	7/23 "α" backup	
9	A	P	A	P	P	A	P	A	9	A P P A		
10	A	P	P	A	P	A	P	A	10	P A A P		
11	A	P	A	P	P	A	A	P	11	A P A P		
12	P	A	P	A	P	A	A	P	12	A P A P		
13	A	P	P	A	A	P	A	P	13	P A P A		
14	P	A	P	A	A	P	P	A	14	P A A P		
15	P	A	P	P	A	P	A	A	15	A P P A		
16	A	P	P	A	A	P	A	P	16	P A P A		
17	A	P	A	P	P	A	P	A	17	P A P A		
18	P	A	P	P	A	P	A	A	18	A P A P		
19	A	P	P	A	A	P	P	A	19	A P P A		
20	A	P	P	A	P	P	A	A	20	P A A P		

\*FL Flight Loading

\*\*Banks 8 and 9 were loaded with the same treatment type.

P Placebo (sand), A Silver Iodide (AgI)

<sup>1</sup> The first EU of the flight received this treatment type.

<sup>2</sup> The second EU of the flight received this treatment type.

Table E.5. 1989 " " experiment treatment types recorded by the ReRandomization Officer (ReRO).

FL*	Flare Bank**									Date Used	Flight	Experimental Unit	Date Used
	1	2	3	4	5	6	7	8,9					
1	P	A	P	A	A	P	P	A		5/19b	1	P <sup>1</sup> A A P	5/19b
2	A	P	P	A	A	P	A	P		5/25	2	P A <sup>1</sup> P A	6/1
3	<del>P</del>	<del>A</del>	<del>P</del>	<del>A</del>	<del>A</del>	<del>P</del>	<del>A</del>	<del>P</del>		5/30	3	<del>A</del> <del>P</del> <del>A</del> <del>P</del>	
4	A	P	A	P	P	A	A	P		6/1	4	A <sup>1</sup> P A P	6/3
5	A	P	P	A	P	A	P	A		6/3	5	P A <sup>1</sup> A P	6/23a
6	A	P	A	P	P	A	P	A		6/23a	6	A <sup>1</sup> P <sup>2</sup> P A	6/23b
7	P	A	P	A	P	A	P	A		6/23b	7	A <sup>2</sup> P <sup>1</sup> A P	7/8
8	A	P	P	A	A	P	A	P		6/27	8	P A <sup>1</sup> P A	7/11
9	A	P	P	A	A	P	A	P		7/2	9	P <sup>1</sup> A P A	7/19
10	A	P	A	P	P	A	A	P		7/11	10	A <sup>1</sup> P P A	7/23
11	P	A	P	A	P	P	A	A		7/8	11	P <sup>1</sup> A P A	7/24
12	A	P	A	P	A	P	P	A			12	A <sup>2</sup> P <sup>1</sup> P A	7/25
13	A	P	P	A	A	P	A	P		7/19a	13	P A A P	
14	P	A	P	P	A	P	A	A			14	A P A P	
15	P	A	P	P	A	P	A	A			15	A P P A	
16	A	P	P	A	A	P	A	P		7/24	16	P A P A	
17	A	P	A	P	P	A	P	A		7/25	17	P A A P	
18	A	P	P	A	A	P	A	P			18	A P A P	
19	P	A	P	A	A	P	A	P			19	A P P A	
20	A	P	P	A	A	P	A	P			20	P A A P	

\* FL Flight Loading

\*\*Banks 8 and 9 were loaded with the same treatment type.

P Placebo (sand), A Silver Iodide (AgI)

<sup>1</sup> The first EU of the flight received this treatment type.

<sup>2</sup> The second EU of the flight received this treatment type.

Table E.6. 1989 " " experiment treatment types recorded by the ReRandomization Officer.

FL*	Flare Bank**									Date Used	Flight	Experimental Unit	Date Used
	1	2	3	4	5	6	7	8,9					
1	P	A	P	P	A	P	A	A		5/19a	1	A <sup>1</sup> P A P	5/19a
2	A	P	P	A	P	P	A	A		6/12	2	P <sup>1</sup> A A P	5/25
3	<del>A</del>	<del>P</del>	<del>A</del>	<del>P</del>	<del>P</del>	<del>P</del>	<del>A</del>	<del>A</del>			3	<del>A P P A</del>	
4	P	A	P	A	P	P	A	A		6/18	4	P <sup>1</sup> A P A	5/30
5	P	A	A	P	P	A	P	A		7/19b	5	A P <sup>1</sup> P A	6/3
6	A	P	P	A	A	P	A	P			6	P <sup>2</sup> A <sup>1</sup> P A	6/12
7	A	P	P	A	A	P	A	P			7	P <sup>1</sup> A P A	6/18
8	P	A	P	A	P	A	P	A		7/23	8	A <sup>2</sup> P <sup>1</sup> A P	6/27
9	A	P	A	P	P	A	P	A			9	A P <sup>1</sup> P A	7/2
10	A	P	P	A	P	A	P	A			10	P A <sup>1</sup> A P	7/19b
11	A	P	A	P	P	A	A	P			11	A P A P	
12	P	A	P	A	P	A	A	P			12	A P A P	
13	A	P	P	A	A	P	A	P			13	P A P A	
14	P	A	P	A	A	P	P	A			14	P A A P	
15	P	A	P	P	A	P	A	A			15	A P P A	
16	A	P	P	A	A	P	A	P			16	P A P A	
17	A	P	A	P	P	A	P	A			17	P A P A	
18	P	A	P	P	A	P	A	A			18	A P A P	
19	A	P	P	A	A	P	P	A			19	A P P A	
20	A	P	P	A	P	P	A	A			20	P A A P	

\* FL Flight Loading

\*\*Banks 8 and 9 were loaded with the same treatment type.

P Placebo (sand), A Silver Iodide (AgI)

<sup>1</sup> The first EU of the flight received this treatment type.

<sup>2</sup> The second EU of the flight received this treatment type.

Table. E.7. Summary of experimental units (EUs) treated as type " ". Shading indicates discrepancy.

Date	EU Number	Seeding Material	
		Used	Intended
May 19 (b)	2	Sand	Sand
June 1	5	AgI	Sand
June 3	7	AgI	AgI
June 23 (a)	11	AgI	Sand
June 23 (b)	12	AgI	AgI
June 23 (b)	13	Sand	Sand
July 8	17	Sand	AgI
July 8	18	AgI	Sand
July 11	19	AgI	Sand
July 19 (a)	20	Sand	Sand
July 23	22	AgI	AgI
July 24	23	Sand	Sand
July 25	24	Sand	AgI
July 25	25	AgI	Sand

Table. E.8. Summary of experimental units (EUs) treated as type " ". Shading indicates discrepancy.

Date	EU Number	Seeding Material	
		Used	Intended
May 19 (a)	1	AgI	AgI
May 25	3	Sand	Sand
May 30	4	Sand	Sand
June 3	6	Sand	AgI
June 12	8	AgI	Sand
June 12	9	Sand	AgI
June 18 (b)	10	Sand	Sand
June 27	14	Sand	AgI
June 27	15	AgI	Sand
July 2	16	Sand	AgI
July 19 (b)	21	AgI	Sand

## Part F Rerandomization Procedures

### 1. Background

The development of analytical tools for discerning seeding effects (objective #3 of the 1989 PACE exploratory cloud seeding experiment; see Czys, et al 1992) includes the formation of permutation tests, where judging the strength of evidence offered by an apparent result against the background of the distribution of such results is obtained by replacing the actual randomizations by randomizations that might have happened -- i.e., re-randomizing (Gabriel 1979).

Seeding flights were initiated in 1989 when conditions seemed suitable for precipitation augmentation. Once a flight started, the first storm with "large" cloud or " " conditions that was chosen for experimentation was defined as an experimental unit of type " ". This was randomly allocated to be seeded with either sand and Agl. The randomization of the experiment was supposed to have followed the rule of no more than two experimental units (EUs) in a row of the same treatment type ("the rule"); however, records show that the rule was not followed, as is pointed out in Part E of this Book. It is clear, however, that if a second storm of type " " was subsequently located on the same flight, it was defined as another experimental unit and received the alternative treatment to that of the first unit, i.e., if the first was Agl seeded, then the second was sand seeded, and vice versa.

### 2. Methods for rerandomization

#### a. *Rerandomization method 1*

Rerandomization 1 (hereafter referred to as rerand1) is the rerandomization where "the rule" is **not** followed. Each experimental unit (EU) was randomly selected to have treatment type sand or Agl, except for the 2nd EU of a flight. Table F.1 shows the 12 type " " EUs on which this and the following (rerand2) rerandomizations were made. A total of 10 EUs were to be randomly assigned "new" treatment types, since 2 EUs were the second ones of the flight and were assigned treatments based on the first EU of the flight. Therefore, rerand1 had  $2^{10} = 1024$  (unique) permutations of the two treatment types, one of these 1024 sequences identical to the sequence of treatments actually given (Table F. 1). Table F.2 shows some example sequences of the 1024 rerand1 permutations. Sand treatments are denoted as "0", while Agl treatments are shown as "1". All clouds within an EU received the same treatment type; thus, Table F.2 lists sequences of 71 treatment types. The EUs are separated with spaces.

Student's  $t$  statistic was to be used to test for differences in the means of the Agl- and sand-treated samples, and the Wilcoxon sum rank test was to be used to determine the level of significance for differences in the distributions of the two samples. For each of the 1024 treatment permutations, the 71 clouds were divided into 2 populations, according to each cloud's treatment type. A  $t$  statistic and a Z statistic were then calculated (for each variable) based on this permutation's sand- and Agl-treated populations.  $t$  and Z statistics were also computed (for

each variable) from the actual treatment sequence, as shown in Table F.1. The 1024 permutation statistics were then compared to the actual treatment statistics. The resulting  $t$  or  $Z$  p-value is the fraction of the 1024 statistics that were greater than or equal to the statistic calculated from the actual treatment sequence.

*b. Rerandomization method 2*

Rerandomization 2 (hereafter referred to as rerand2) is the rerandomization analysis where "the rule" is followed. Each experimental unit (EU) was randomly selected to have treatment type sand or Agl, except that there could be no more than two EUs in a row of the same treatment type, and again the 2nd EU of a flight was to be of opposite treatment type from the first EU of the flight. Rerand2 had a total of 208 unique permutations of the two treatment types, again one of these 208 being the sequence actually carried out (Table F.1). Table F.3 shows some example sequences of the 208 rerand2 permutations. Again, "0" sand, "1" Agl, and the EUs are separated with spaces.

As was done in rerand1, for each of the 208 treatment permutations, the 71 clouds were divided into 2 populations, according to each cloud's treatment type. A  $t$  statistic and a  $Z$  statistic were then calculated (for each variable) based on this permutation's sand- and Agl-treated populations. The 208 permutation statistics were then compared to the actual treatment statistics, where the resulting  $t$  or  $Z$  p-value was the fraction of the 208 statistics that were greater than or equal to the statistic calculated from the actual treatment sequence.

### **3. References**

- Czys, R.R., S.A. Changnon, M.S. Petersen, R.W. Scott, and N.E. Westcott, 1992: Initial results from the 1989 cloud seeding experiment in Illinois. *J. Wea. Mod.*, 24, 13-18.
- Gabriel, K.R., 1979: Some statistical issues in weather experimentation. *Communications in Statistics, Part A: Theory and Methods*, 8, 975-1015.

Table F.1. Summary of " " or large clouds in the analysis.

Date	Experimental Unit Number	Number of Clouds	Treatment Material
May 19 (b)	2	4	Sand
June 1	5	4	Agl
June 23 (a)	11	7	Agl
June 23 (b)	13	7	Sand
July 8	17	5	Sand
July 8	18	7	Agl
July 11	19	7	Agl
July 19 (a)	20	3	Sand
July 23	22	10	Agl
July 24	23	5	Sand
July 25	24	8	Sand
July 25	25	4	Agl

Table F.2. Sample permutations of treatment type sequences from the rerandomization method 1 (rerand1). A "0" indicates the sand treatments, a "1" indicates the Agl treatment types. The experimental units (EUs) are separated by spaces.

0000	1111	0000000	0000000	11111	0000000	0000000	000	0000000000	00000	111111111	0000
1111	0000	0000000	1111111	00000	1111111	1111111	000	0000000000	11111	00000000	1111
1111	1111	1111111	0000000	00000	1111111	1111111	111	0000000000	00000	111111111	0000
0000	1111	1111111	0000000	11111	0000000	1111111	111	0000000000	00000	00000000	1111
0000	1111	0000000	1111111	00000	1111111	0000000	111	0000000000	11111	00000000	1111
0000	0000	0000000	0000000	00000	1111111	1111111	111	0000000000	00000	111111111	0000

Table F.3. Sample permutations of treatment type sequences from the rcrandomization method 2 (rerand2). A "0" indicates the sand treatments, a "1" indicates the Agl treatment types. The experimental units (EUs) are separated by spaces.

0000	1111	1111111	0000000	11111	0000000	1111111	000	1111111111	00000	111111111	0000
1111	0000	0000000	1111111	00000	1111111	0000000	111	0000000000	00000	111111111	0000
1111	1111	0000000	1111111	00000	1111111	1111111	000	0000000000	11111	111111111	0000
0000	1111	0000000	0000000	11111	0000000	1111111	111	0000000000	00000	111111111	0000
0000	1111	0000000	1111111	11111	0000000	1111111	000	0000000000	11111	00000000	1111
0000	0000	1111111	0000000	11111	0000000	1111111	000	1111111111	00000	00000000	1111

**Part G**  
**Radar Cloud Description:**  
**Experimental Unit and Echo Core Histories**

Figures for each of the 12 experimental units are presented in this Part in groups of three:

1. The cloud fields at the time of first treatment and 30 minutes following the last treatment are depicted by CAPPIs of radar reflectivity interpolated to the 1 km AGL level. Reflectivity contours are in 10 dBZ increments from 15 to 65 dBZ. The circle (28 km radius) in each figure delineates the experimental unit.
2. The time-history of the radar-estimated rain volume and the echo area coverage ( 30 dBZ) are shown from 15 minutes prior to treatment to 90 minutes following the last treatment. Values are noted at the beginning time of the first cloud treatment pass (BT), and at the ending time of treatment for the last cloud treatment pass (ET). The lines labeled EU refer to values for the experimental unit, and the lines labeled TN-EU refer to values for the 240 km x 240 km area usually centered on the radar site near Champaign (CMI), minus the value within the experimental unit.
3. The maximum reflectivity time-height histories of the treated and tracked echo cores are shown for cores with sufficient data for contouring (more than 4 data points). Reflectivity is contoured in 5 dBZ increments from 10 to 70 dBZ. A cross indicates the midtime and approximate location of the aircraft pass at treatment. The cloud identifier and date are given at the top of each graph. EU02EC01a refers to the treated cloud 01 in the large cloud experimental unit 02.

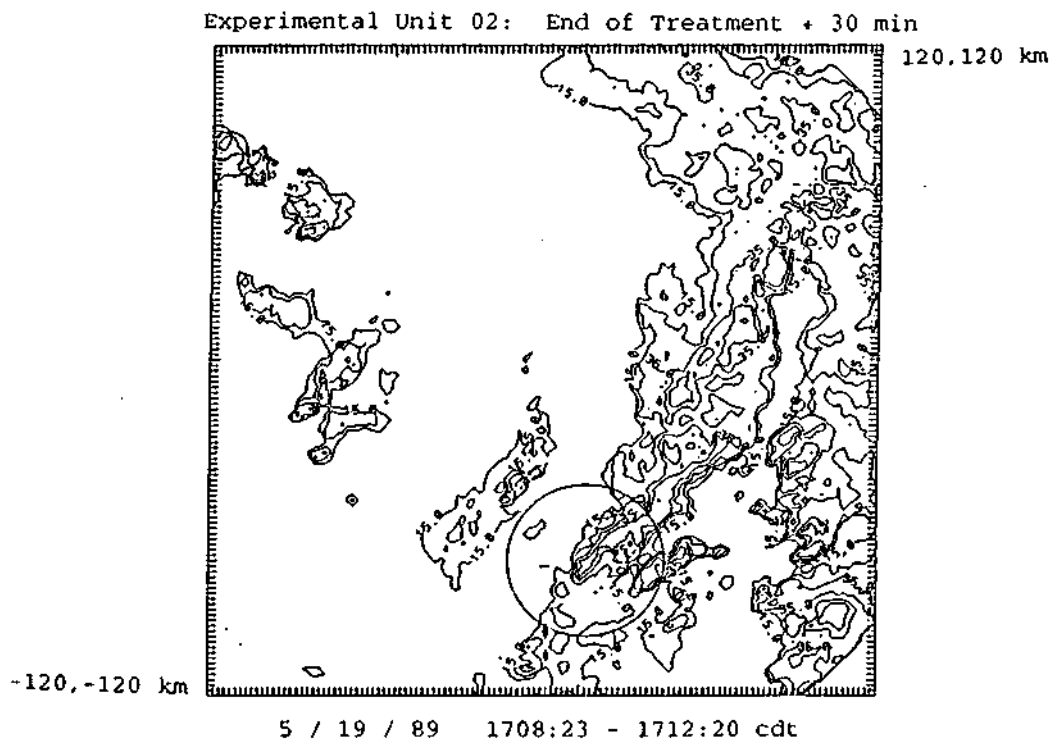
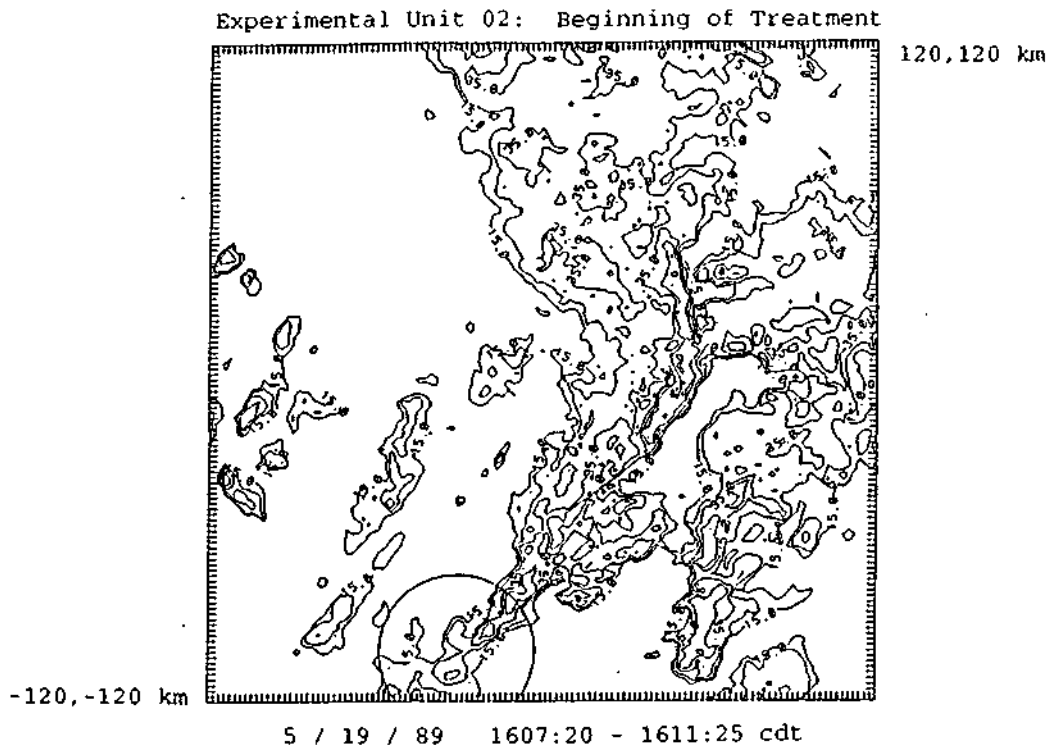


Figure G.1. CAPPIs of radar reflectivity at the 1 km AGL level for Experimental Unit 02, on May 19, 1989.

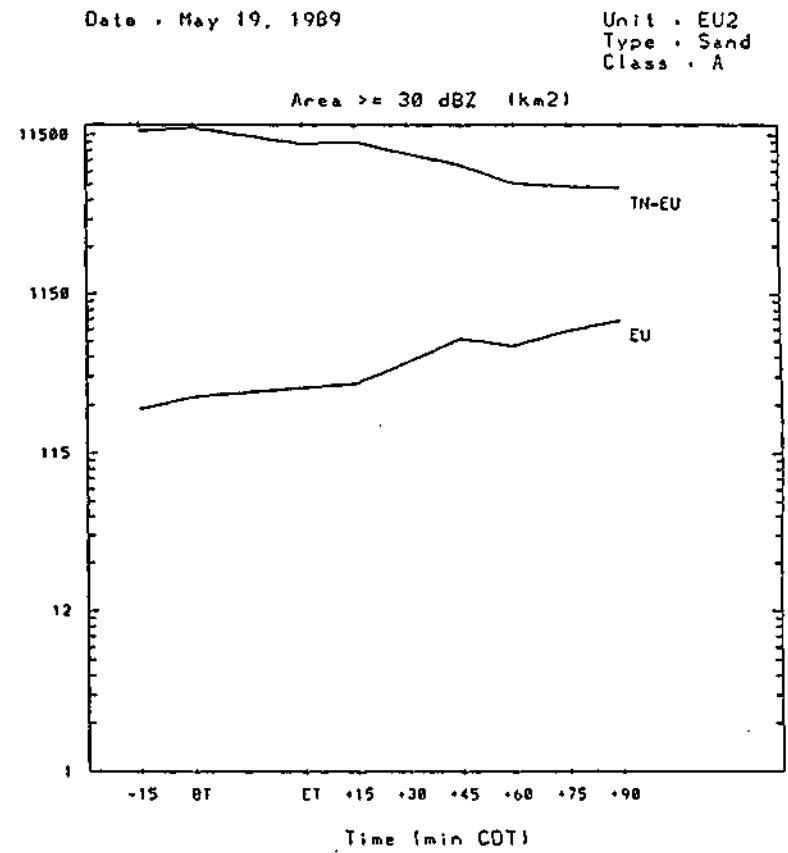
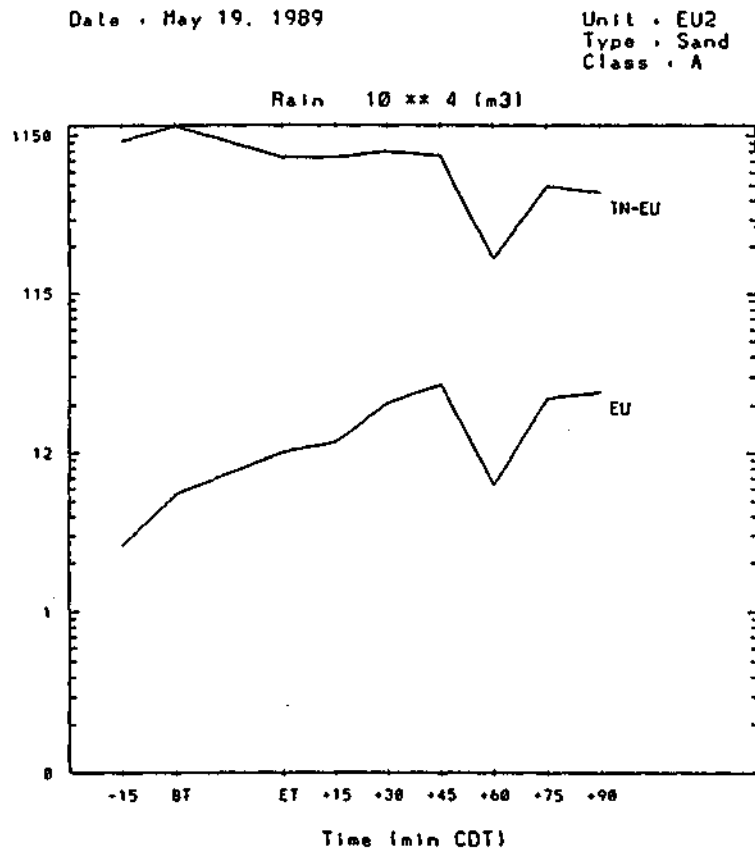
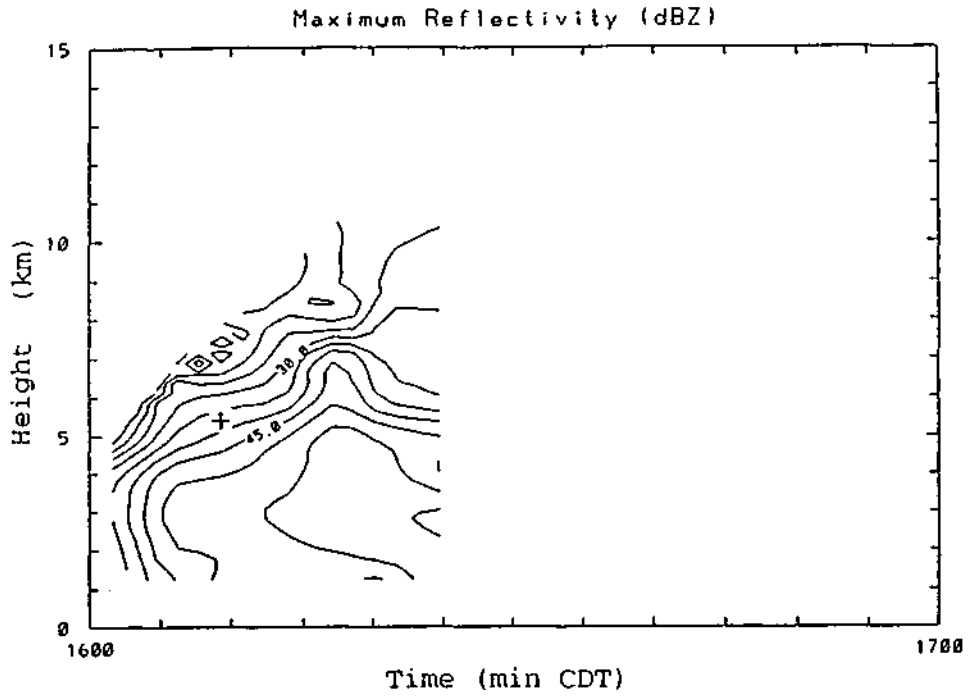


Figure G.2. Time history of radar-estimated rain volume ( $10^4$  m<sup>3</sup>) and echo area for reflectivities  $\geq 30$  dBZ (km<sup>2</sup>) in and around Experimental Unit 02, on May 19, 1989.

EU02EC01a 051989



EU02EP03a 051989

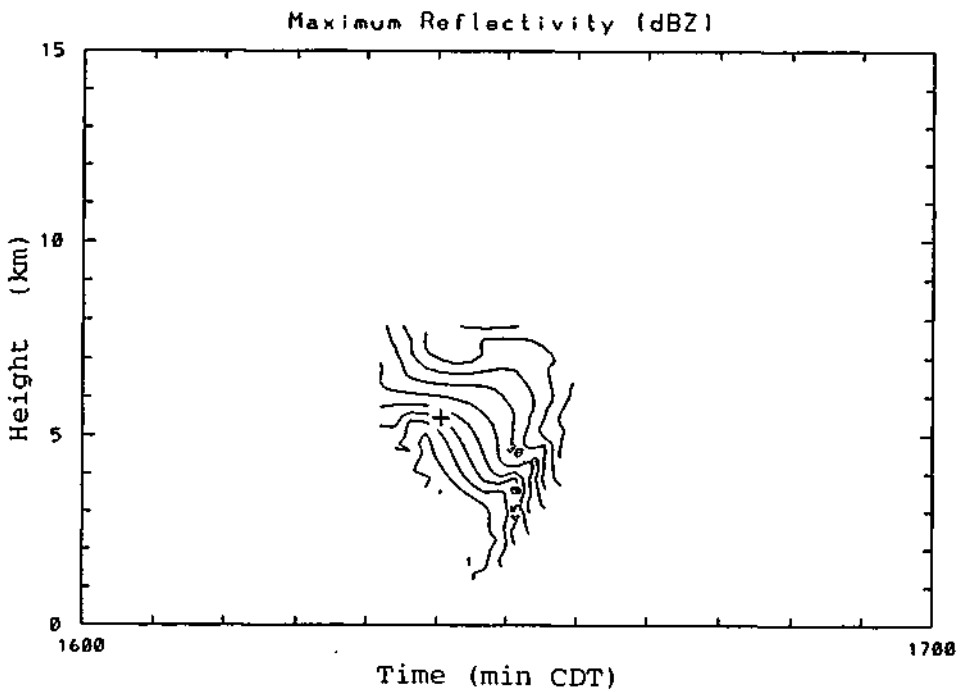
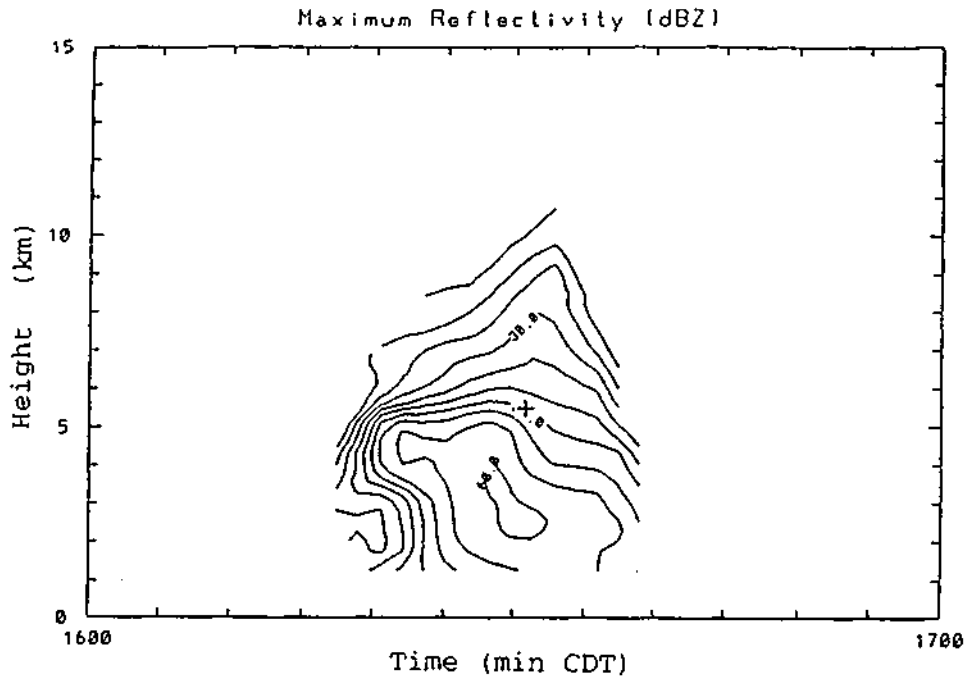


Figure G.3. Time-height histories of the reflectivity cores for clouds EU02EC01a and EU02EP03a in Experimental Unit 02, on May 19, 1989. EU02EP03a was tracked only through a portion of its history.

EU02EC04a 051989



EU02EC05a 051989

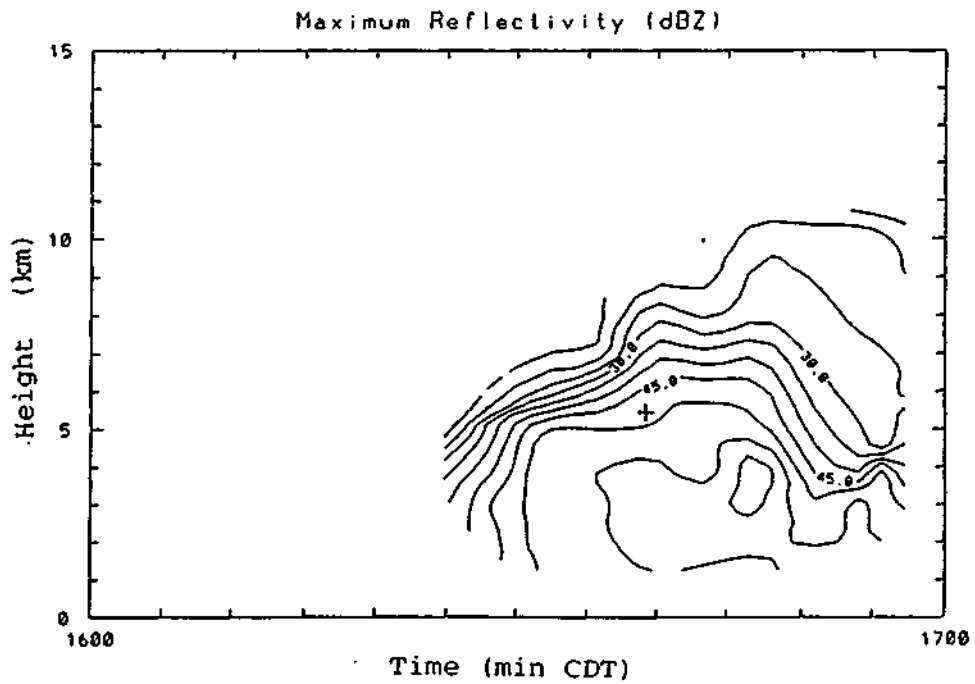


Figure G.4. Time-height histories of the reflectivity cores for clouds EU02EC04a and EU02EC05a in Experimental Unit 02, on May 19, 1989.

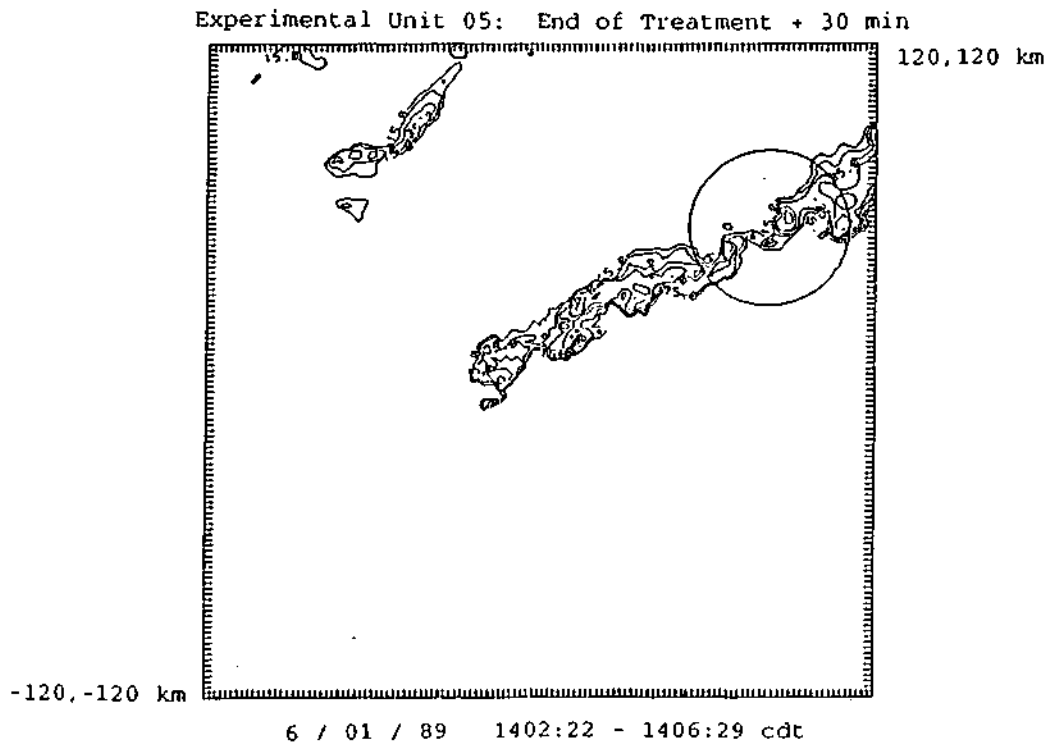
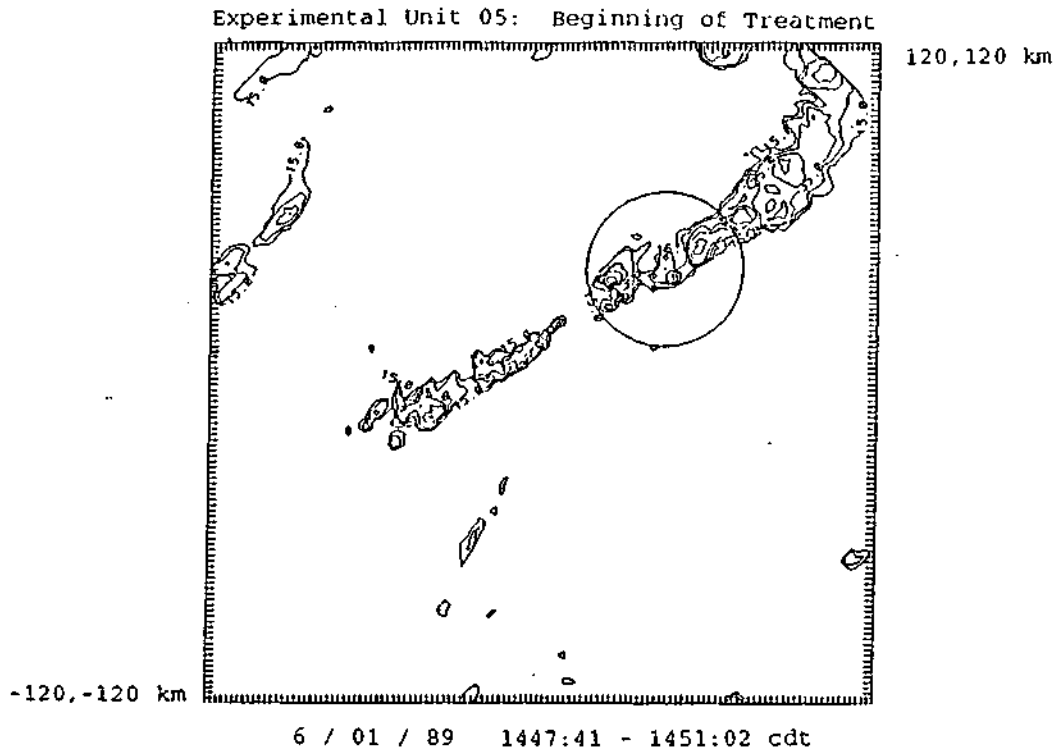


Figure G.5. CAPPIs of radar reflectivity at the 1 km AGL level for Experimental Unit 05, on June 1, 1989.

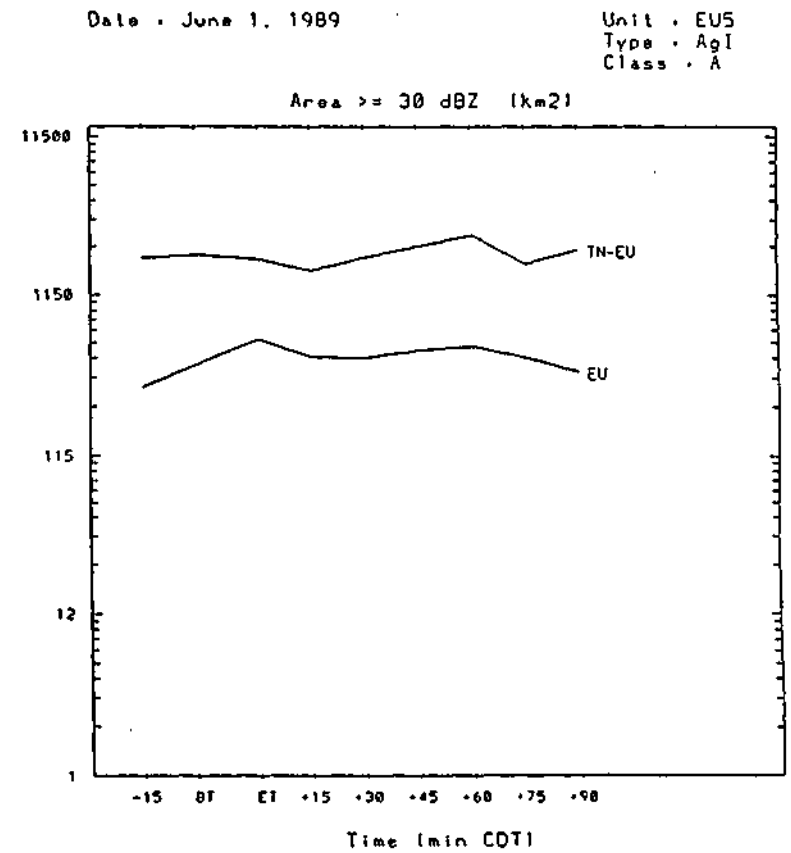
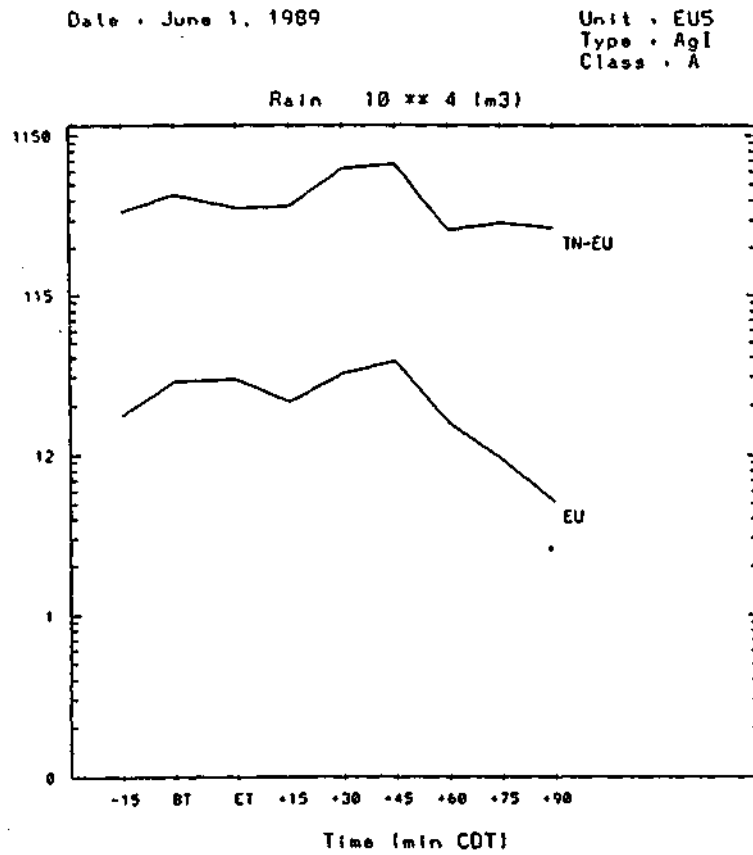
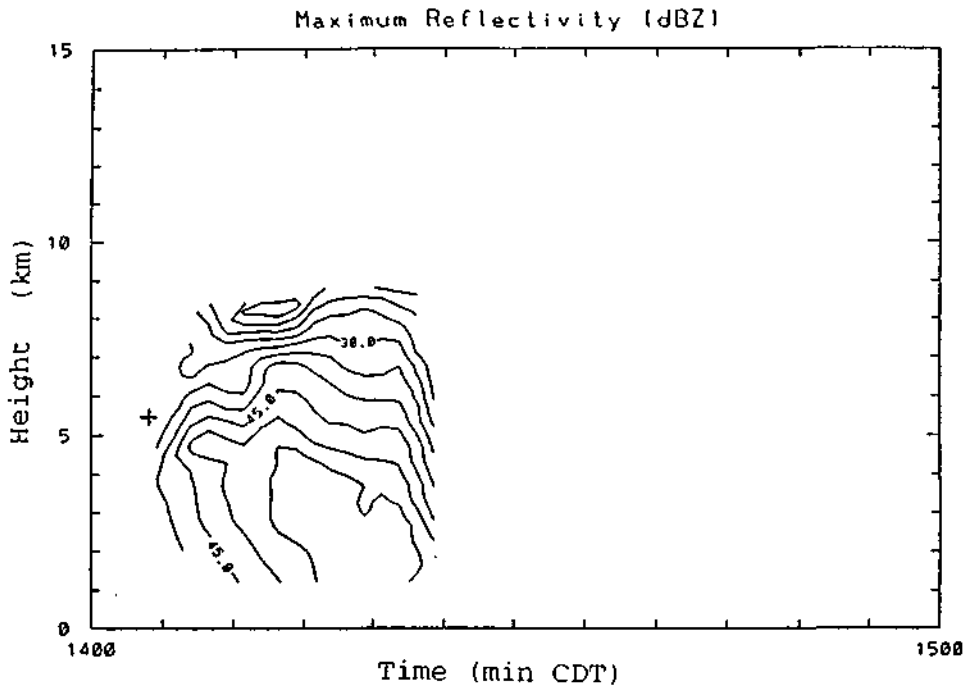


Figure G.6. Time history of radar-estimated rain volume ( $10^4 \text{ m}^3$ ) and echo area for reflectivities  $\geq 30 \text{ dBZ}$  ( $\text{km}^2$ ) in and around Experimental Unit 05, on June 1, 1989.

EU05EC01a 060189



EU05EC02a 060189

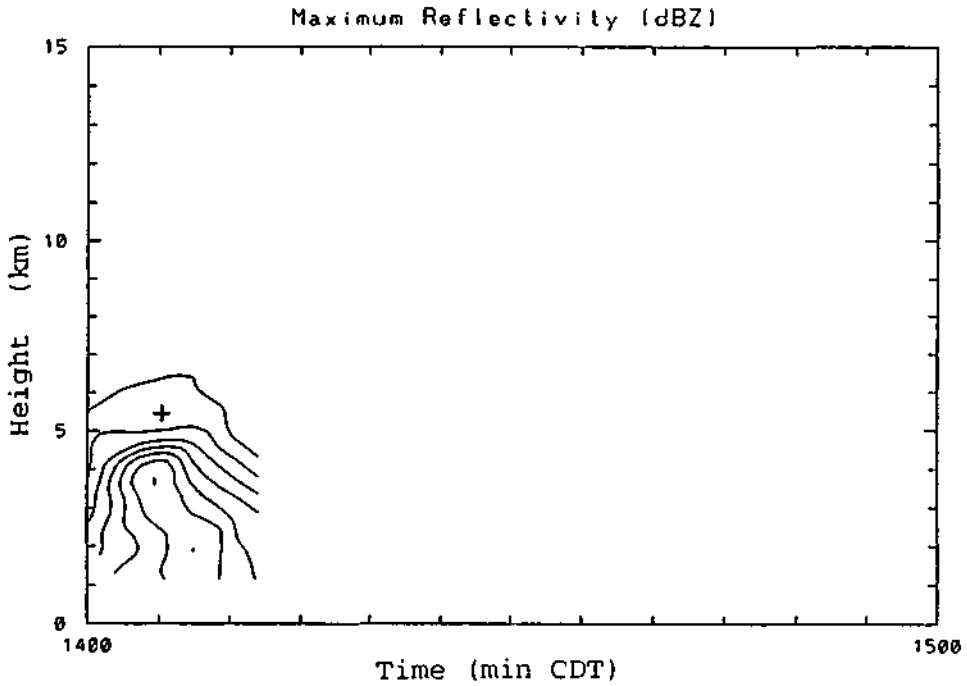
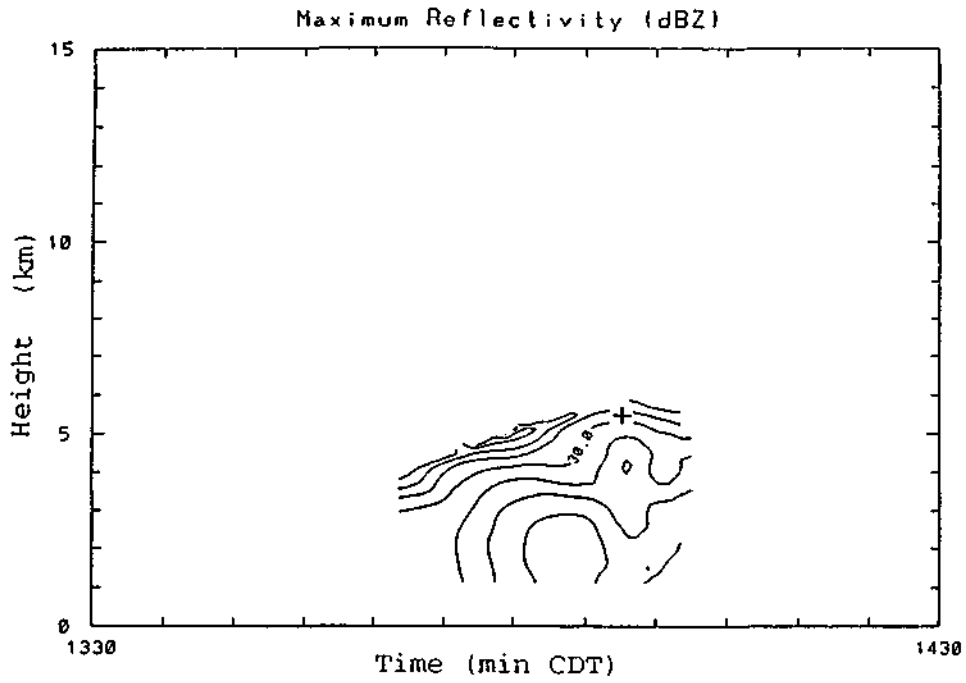


Figure G.7. Time-height histories of the reflectivity cores for clouds EU05EC01a and EU05EC02a in Experimental Unit 05, on June 1, 1989.

EU05EC03a 060189



EU05EC04a 060189

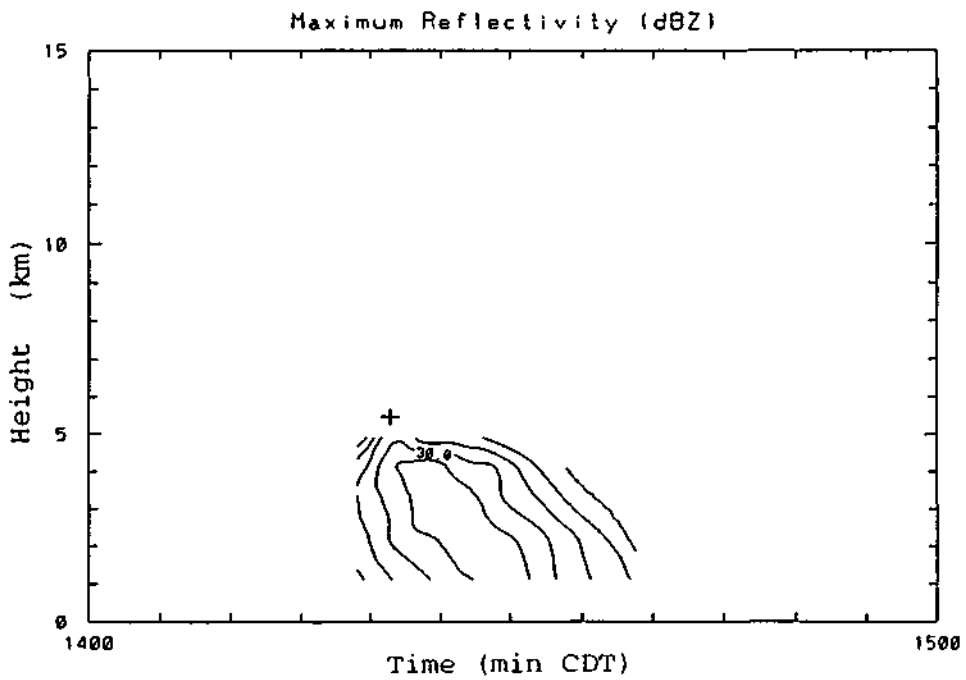
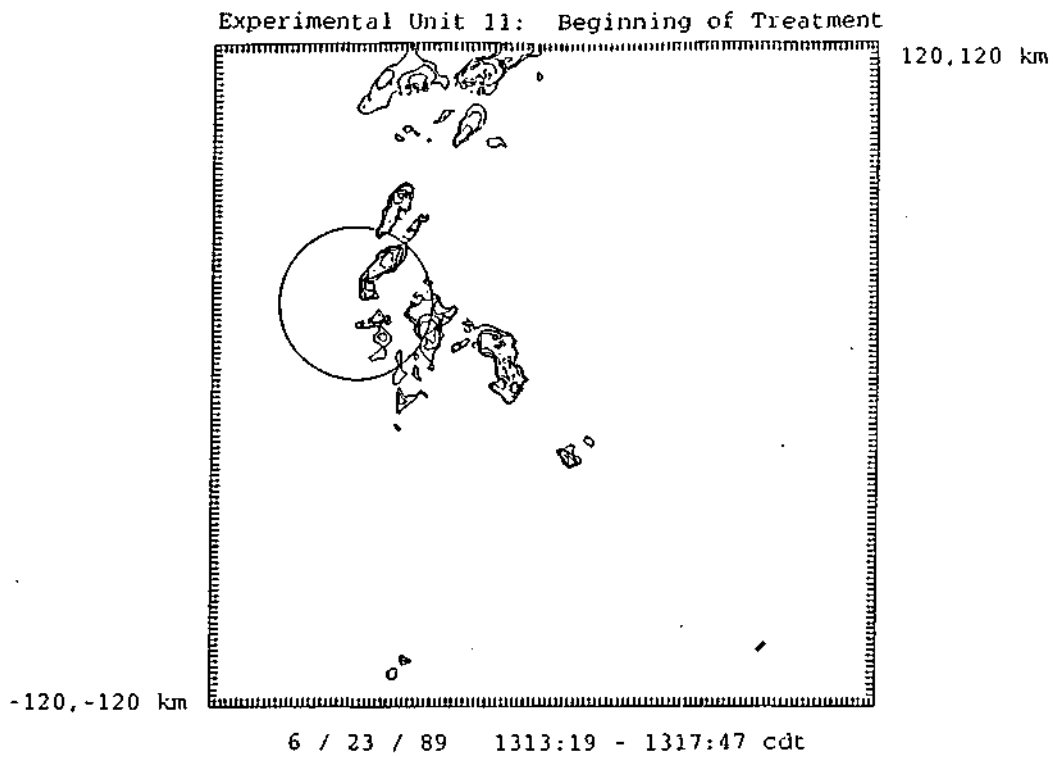


Figure G.8. Time-height histories of the reflectivity cores for clouds EU05EC03a and EU05EC04a in Experimental Unit 05, on June 1, 1989.



*Figure G.9. CAPPIS of radar reflectivity at the 1 km AGL level for Experimental Unit 11, on June 23, 1989. The radar was down from 13:55 - 15:10 CDT.*

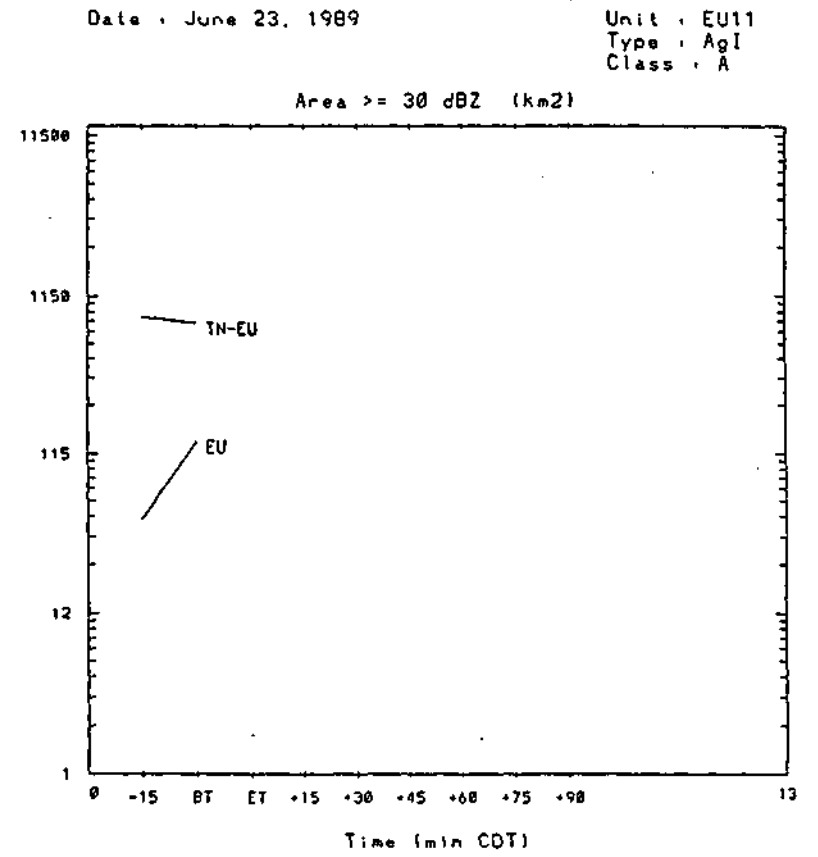
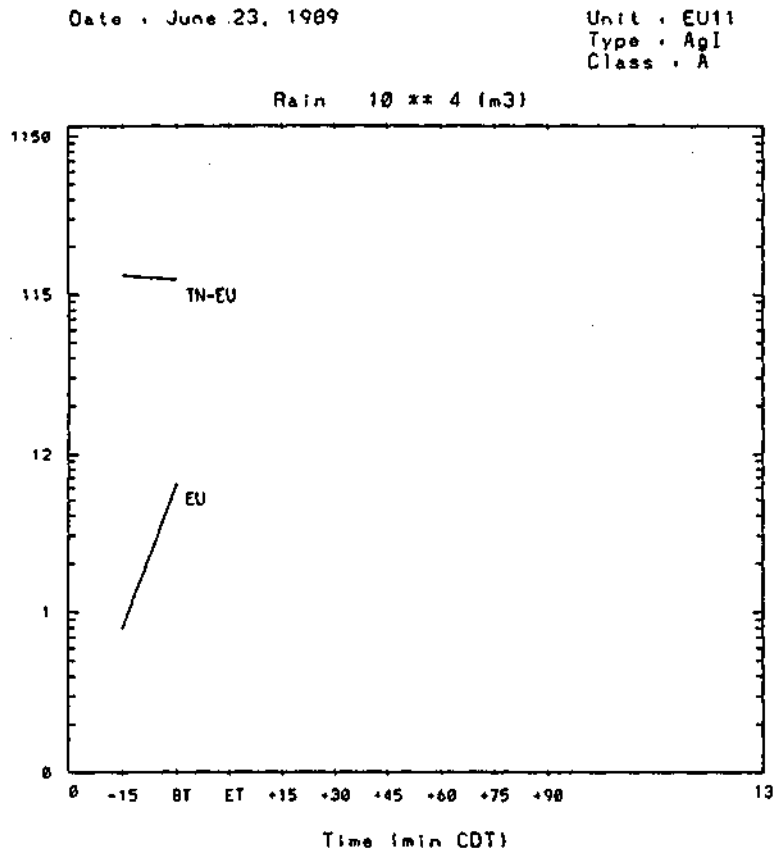
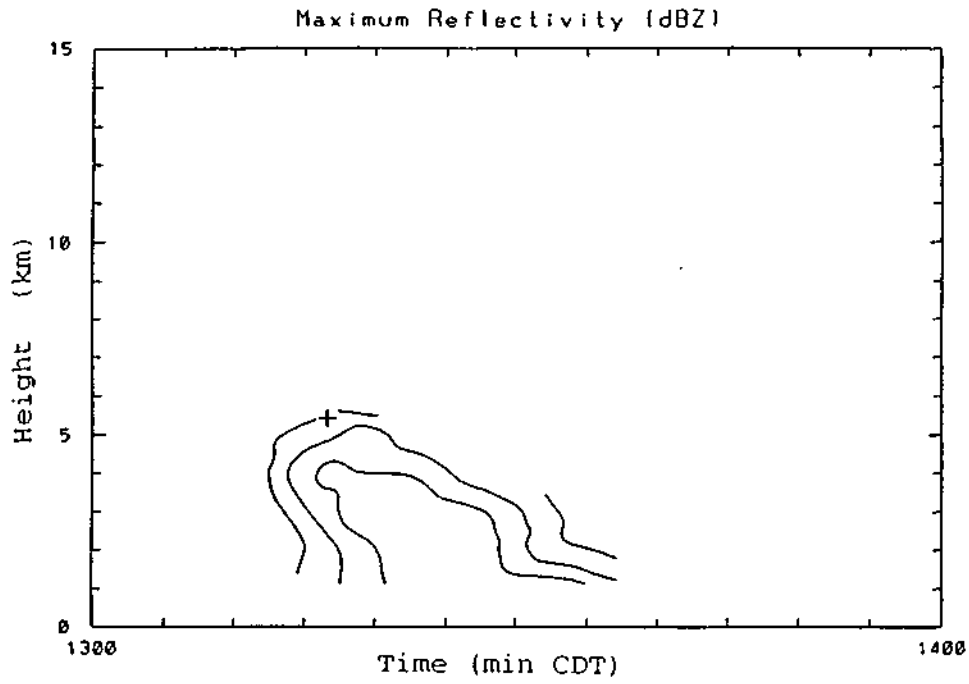


Figure G.10. Time history of radar-estimated rain volume ( $10^4 \text{ m}^3$ ) and echo area for reflectivities  $\geq 30 \text{ dBZ}$  ( $\text{km}^2$ ) in and around Experimental Unit 11, on June 23, 1989.

EU11EC02a 062389



EU11EC01a 062389

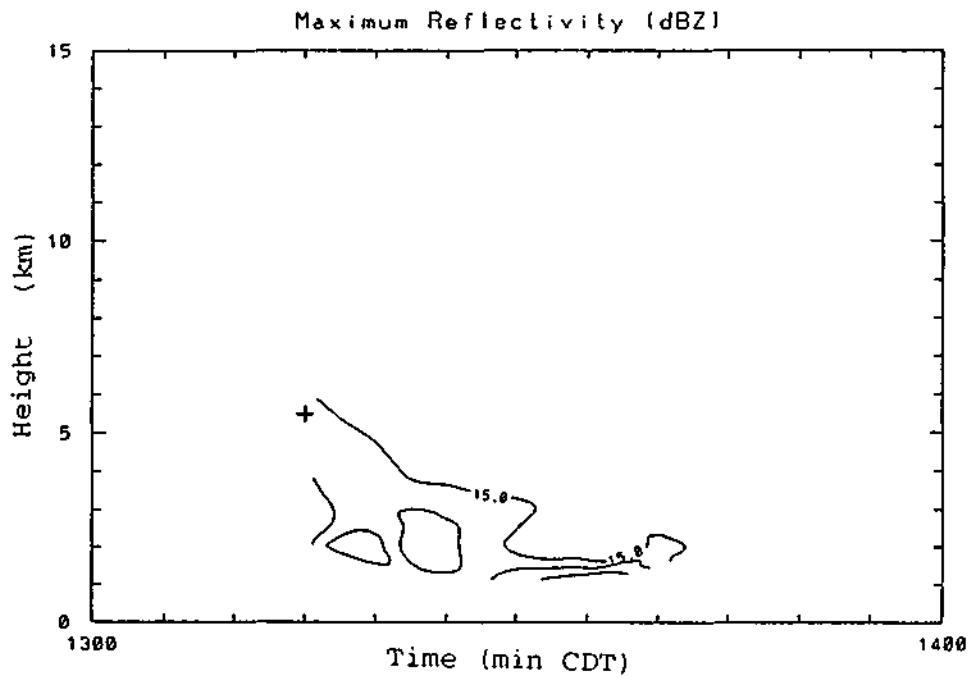
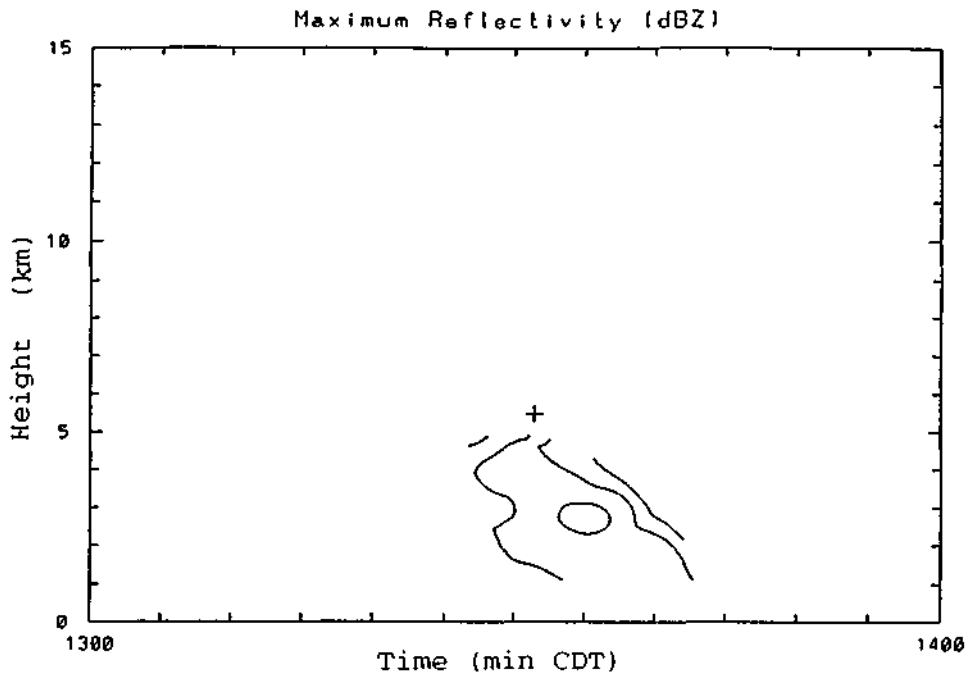


Figure G.11. Time-height histories of the reflectivity cores for clouds EU11EC01a and EU11EC02a in Experimental Unit 11, on June 23, 1989.

EU11EC05a 062389



EU11EC04a 062389

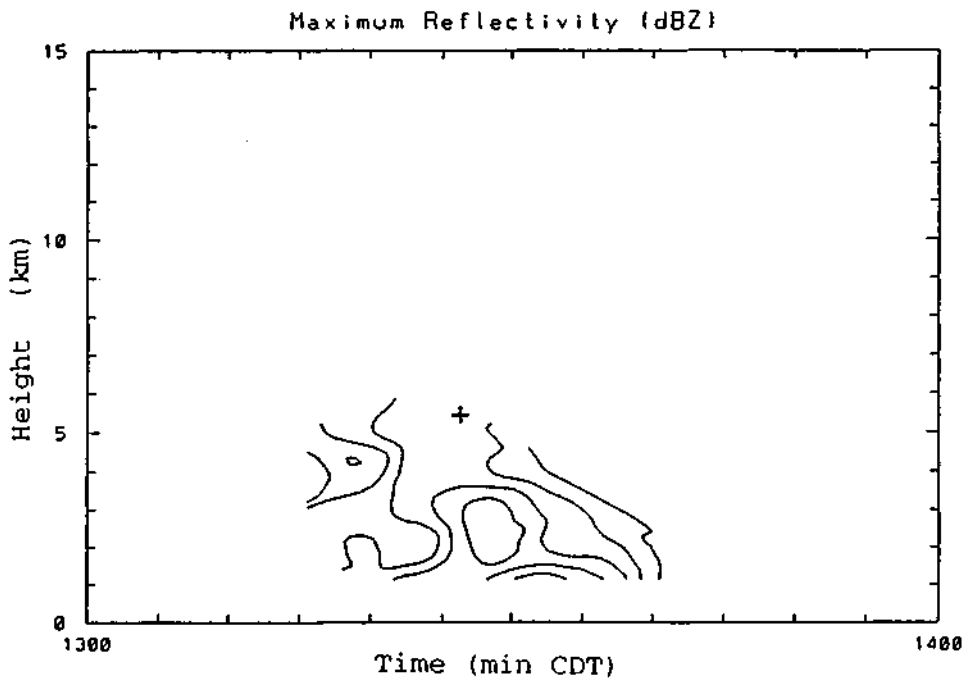
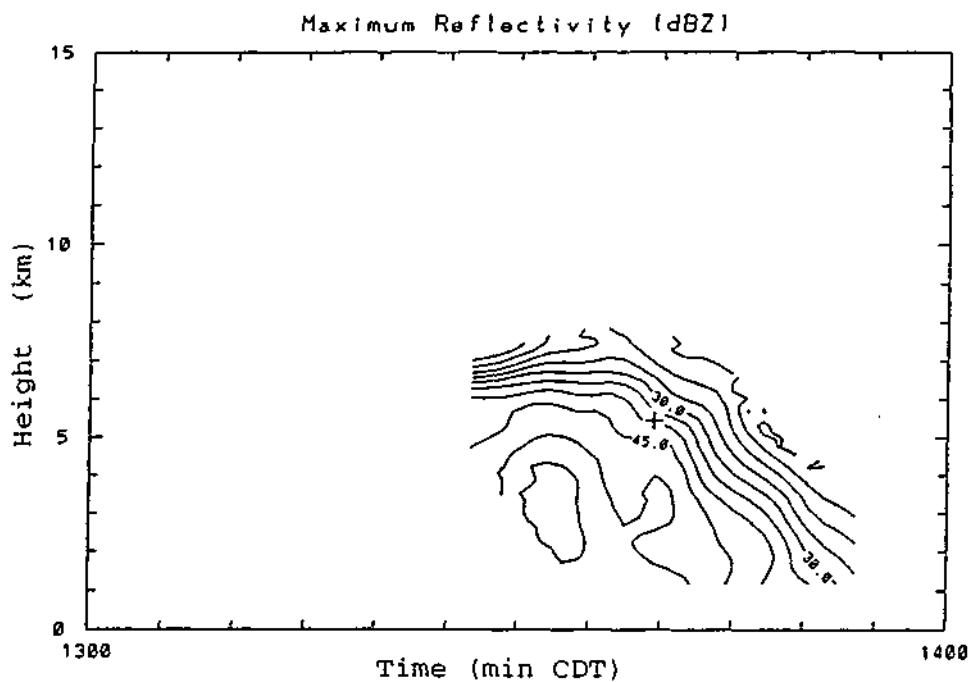


Figure G.12. Time-height histories of the reflectivity cores for clouds EU11EC04a and EU11EC05a in Experimental Unit II, on June 23, 1989.

EU11EC06a 062389



EU11EC07a 062389

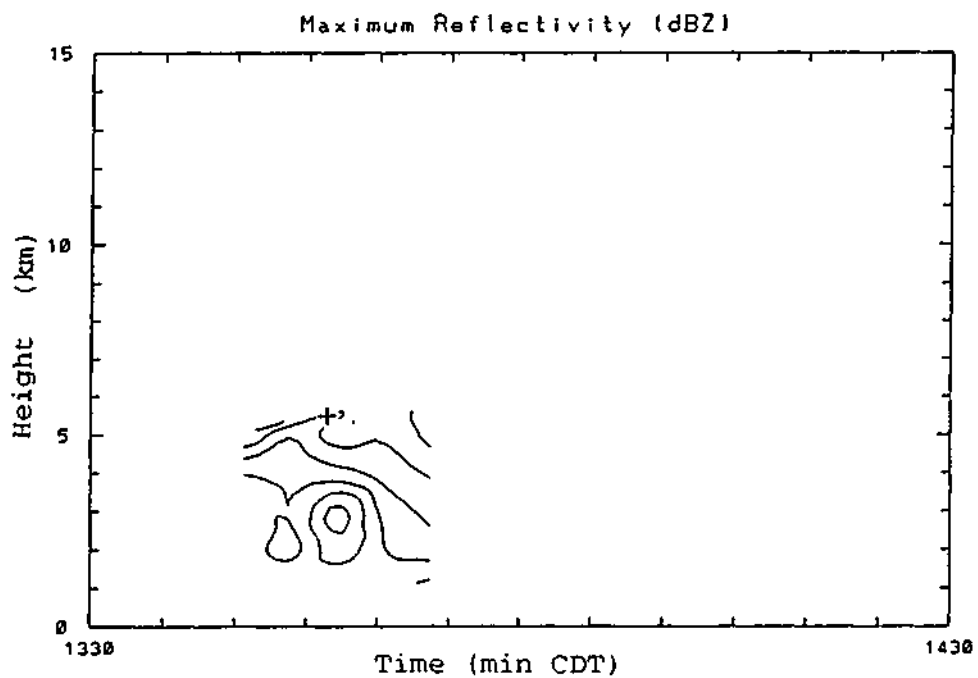


Figure G.13. Time-height histories of the reflectivity cores for clouds EU11EC06a and EU11EC07a in Experimental Unit 11, on June 23, 1989.

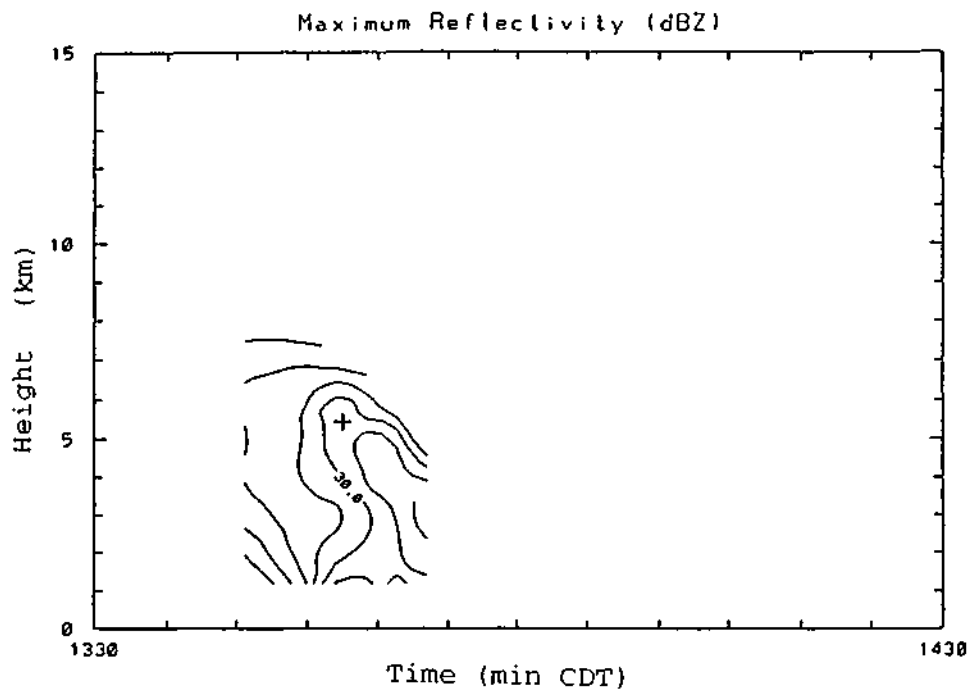


Figure G.14. Time-height histories of the reflectivity cores for clouds EU11EC08a in Experimental Unit 11, on June 23, 1989.

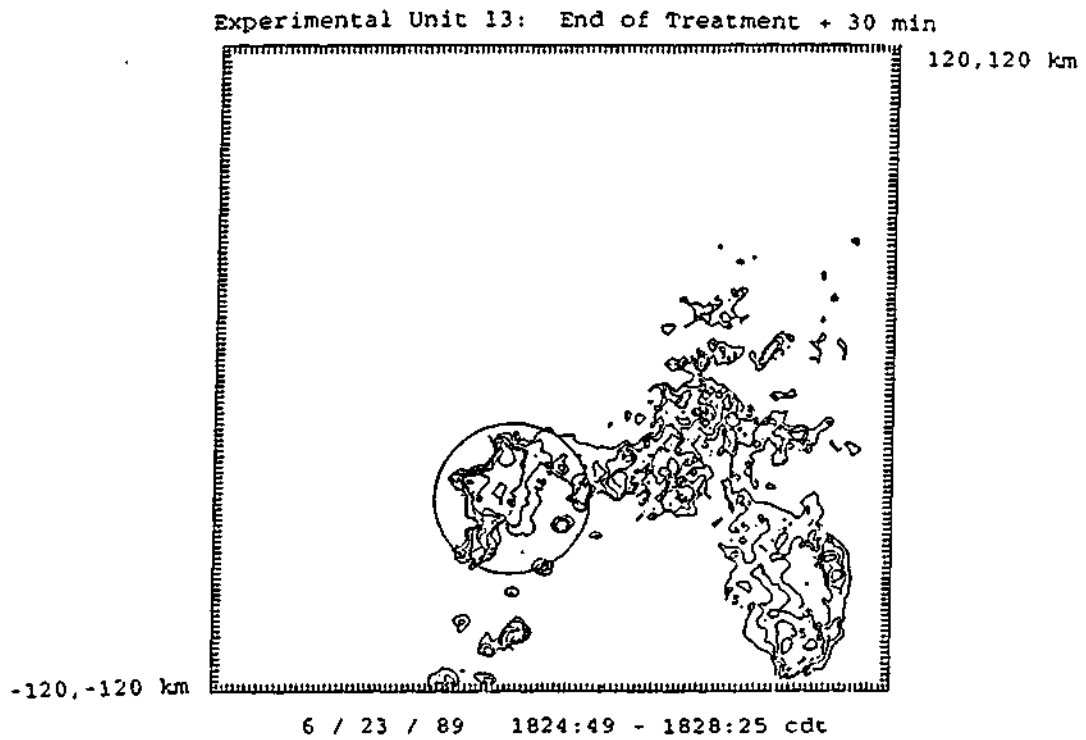
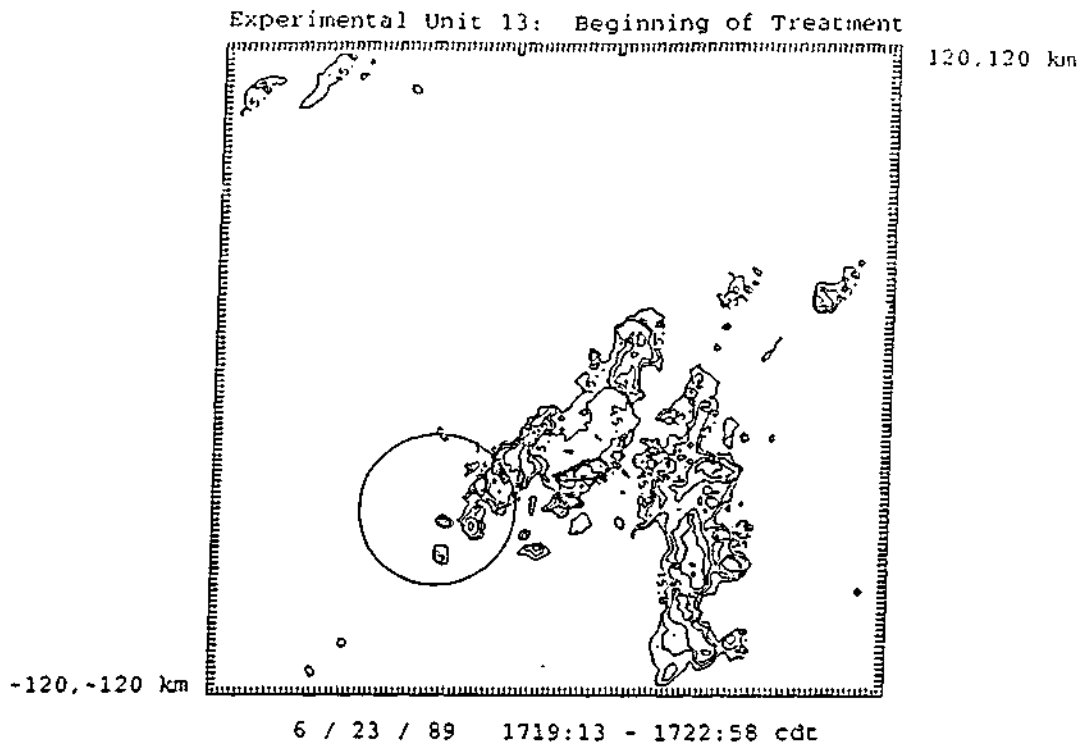


Figure C.15. CAPPi of radar reflectivity at the 1 km AGL level for Experimental Unit 13 on June 23, 1989.

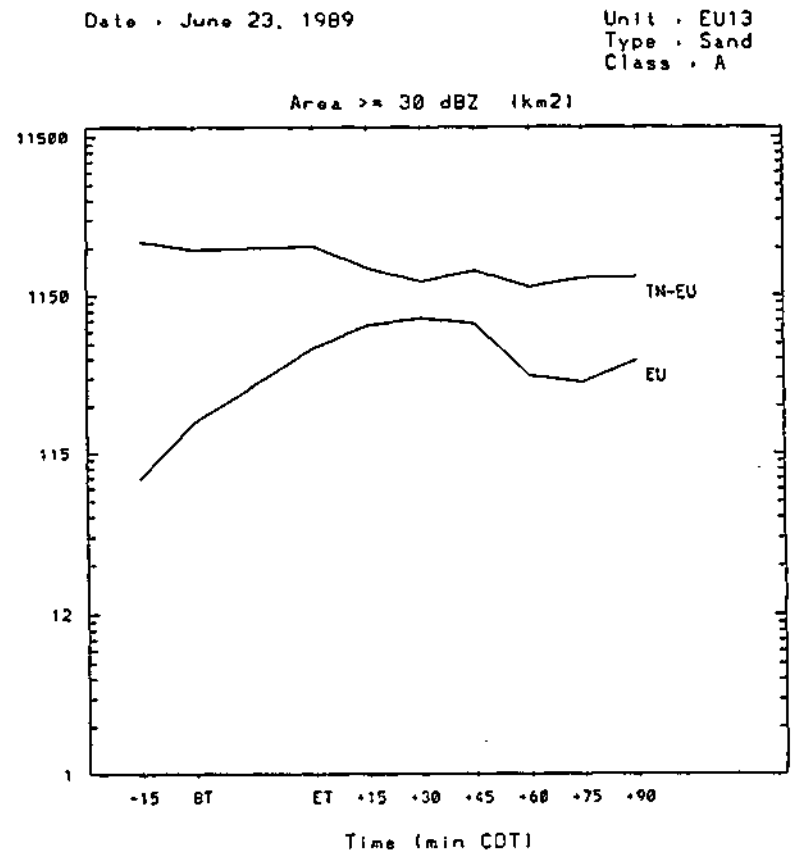
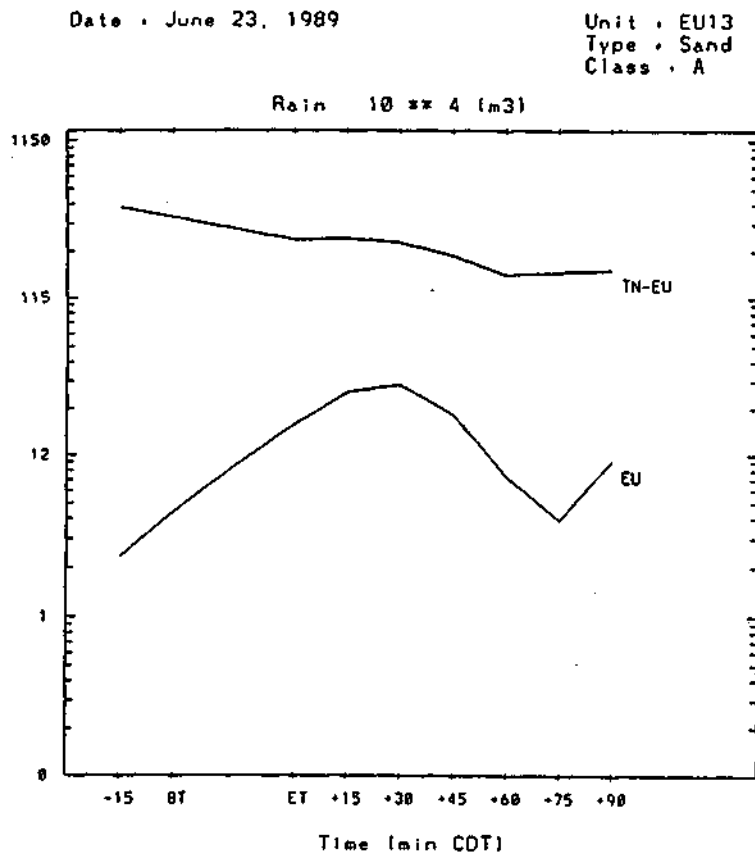
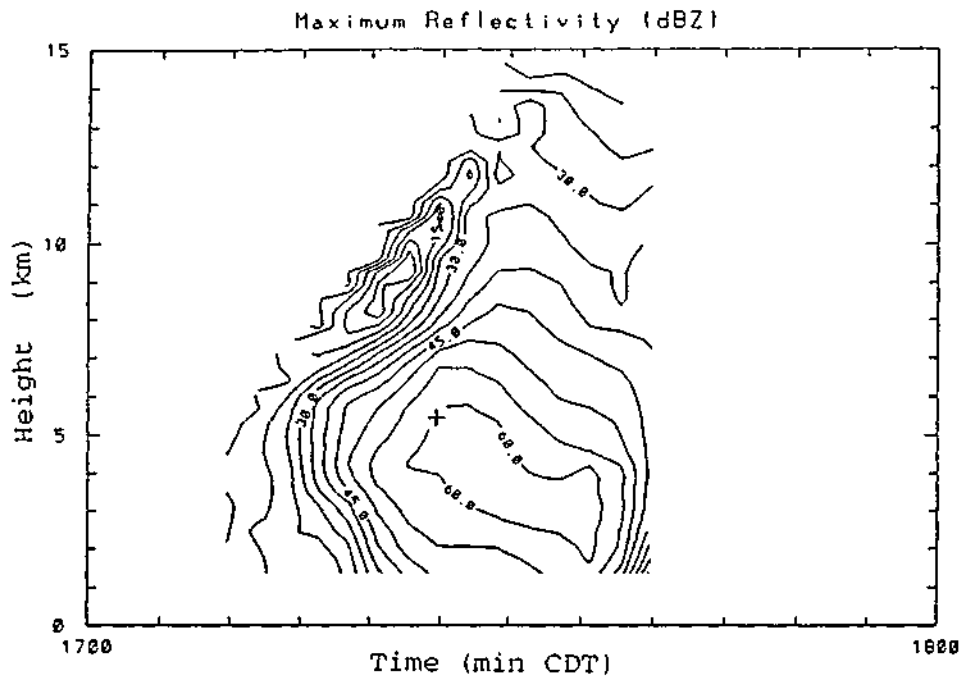


Figure G.16. Time history of radar-estimated rain volume ( $10^4 \text{ m}^3$ ) and echo area for reflectivities  $\geq 30 \text{ dBZ}$  ( $\text{km}^2$ ) in and around Experimental Unit 13, on June 23, 1989.

EU13EC08a 062389



EU13EC09a 062389

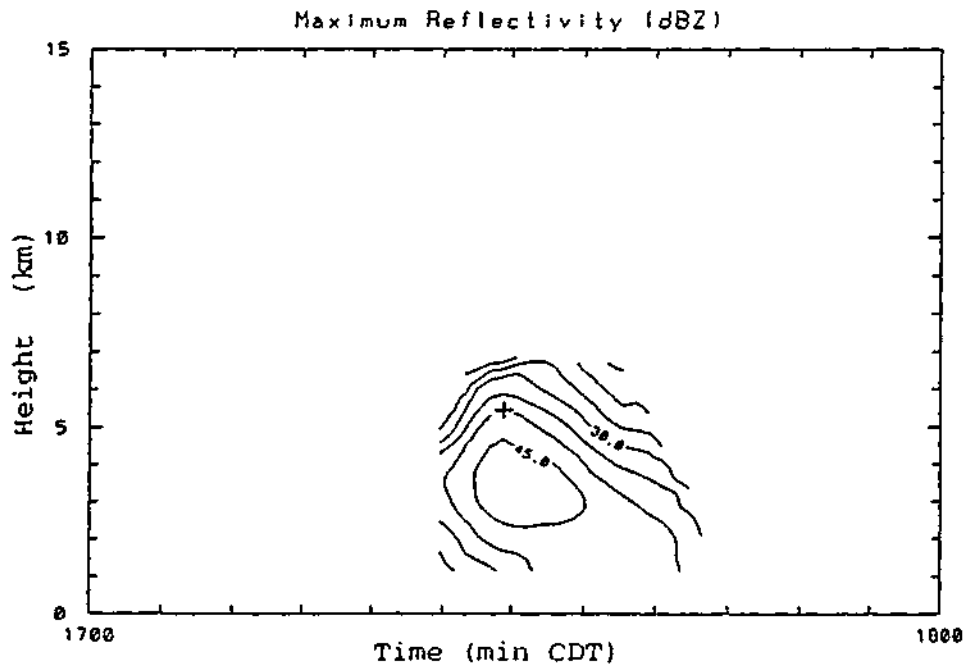


Figure G.17. Time-height histories of the reflectivity cores for clouds EU13EC08a and EU13EC09a in Experimental Unit 13, on June 23, 1989.

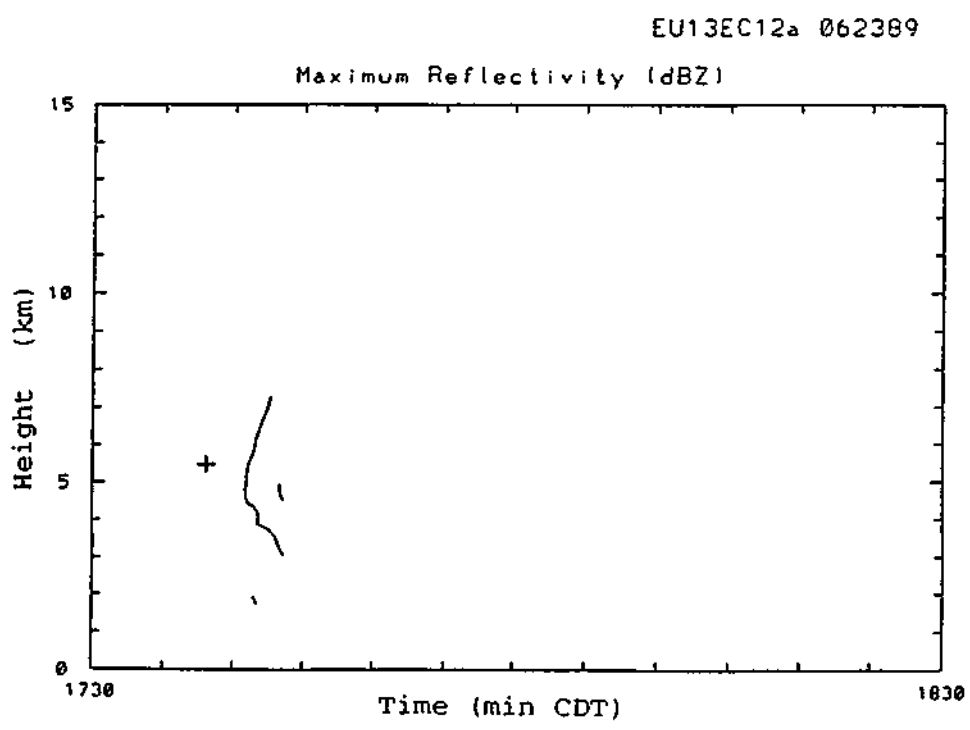
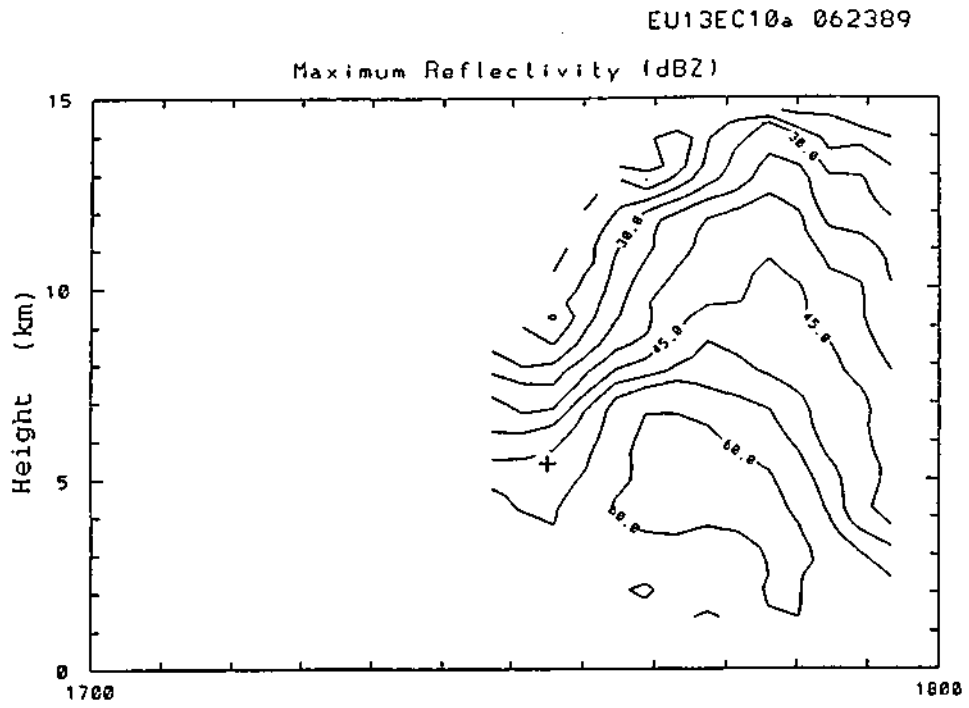
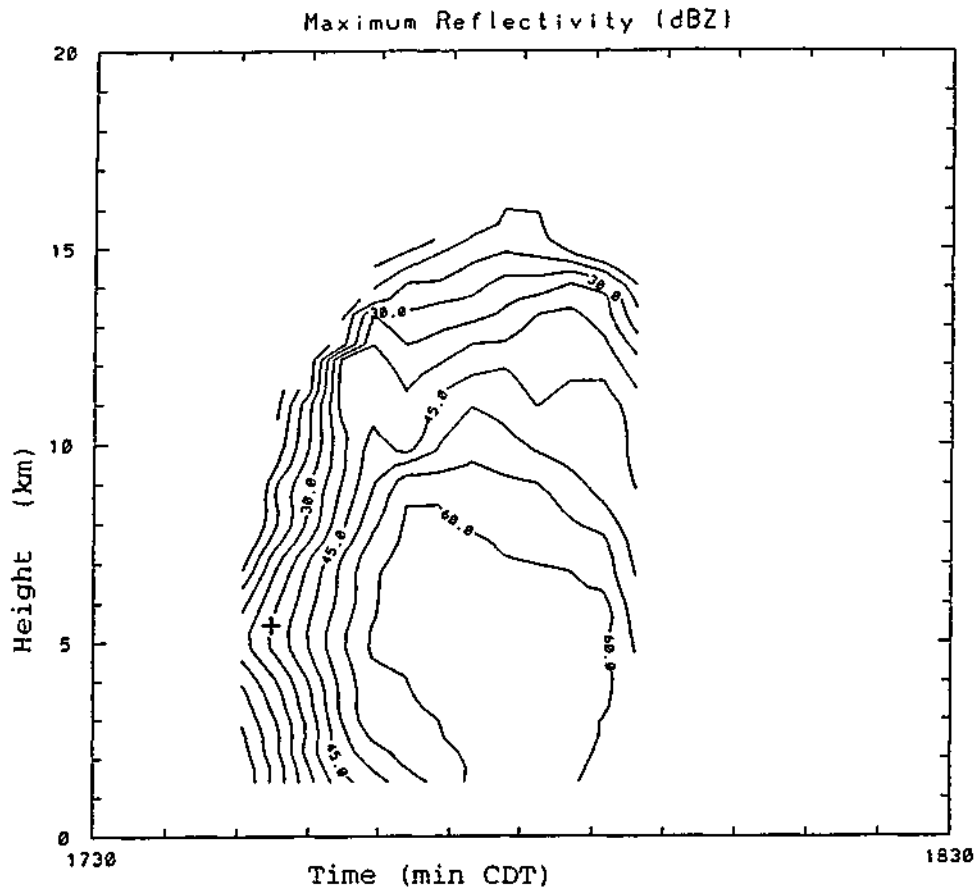


Figure G.18. Time-height histories of the reflectivity cores for clouds EU13EC10a and EU13EC12a in Experimental Unit 13, on June 23, 1989.

EU13EC13a 062389



EU13EC14a

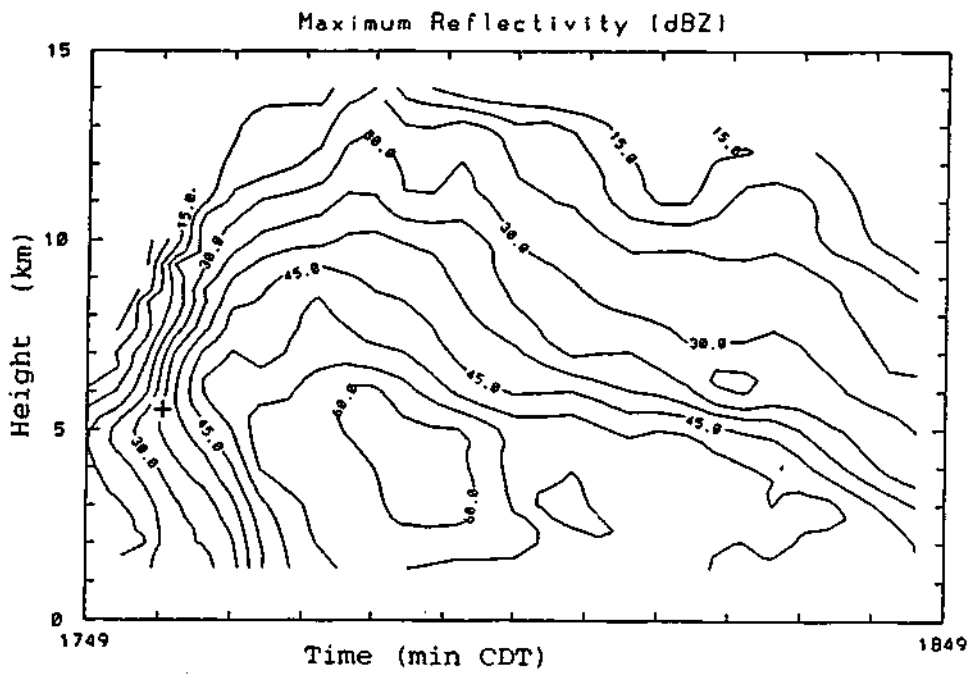


Figure G.19. Time-height histories of the reflectivity cores for clouds EU13EC13a and EU13EC14a in Experimental Unit 13, on June 23, 1989.

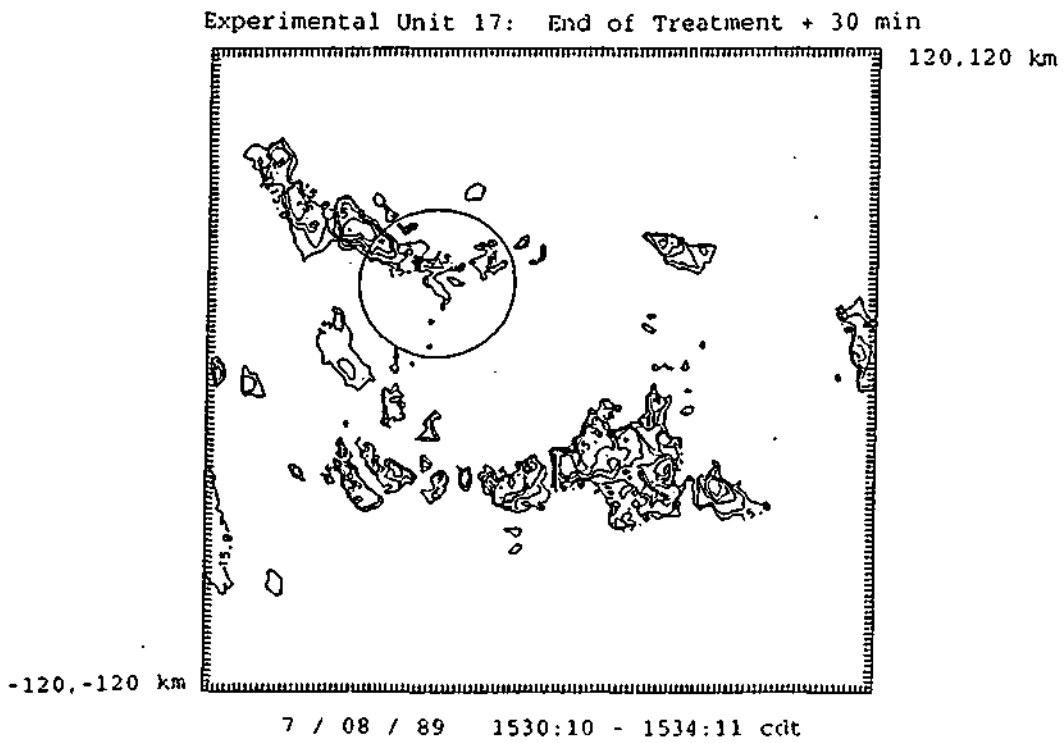
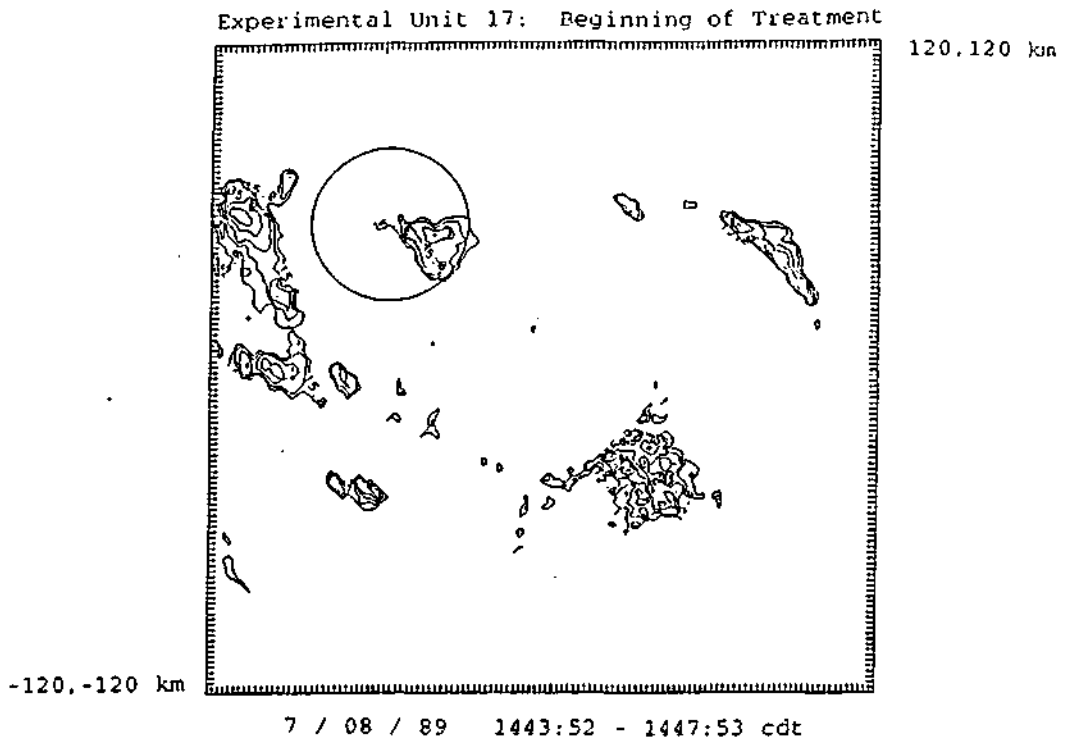


Figure G.20. CAPPi's of radar reflectivity at the 1 km AGL level for Experimental Unit 17 on July 08, 1989.

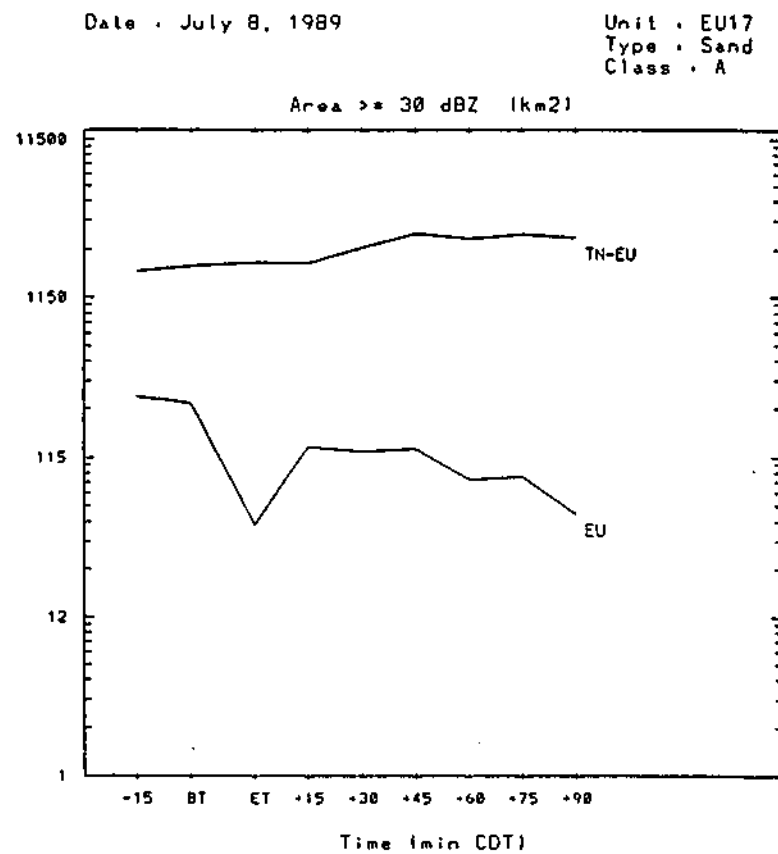
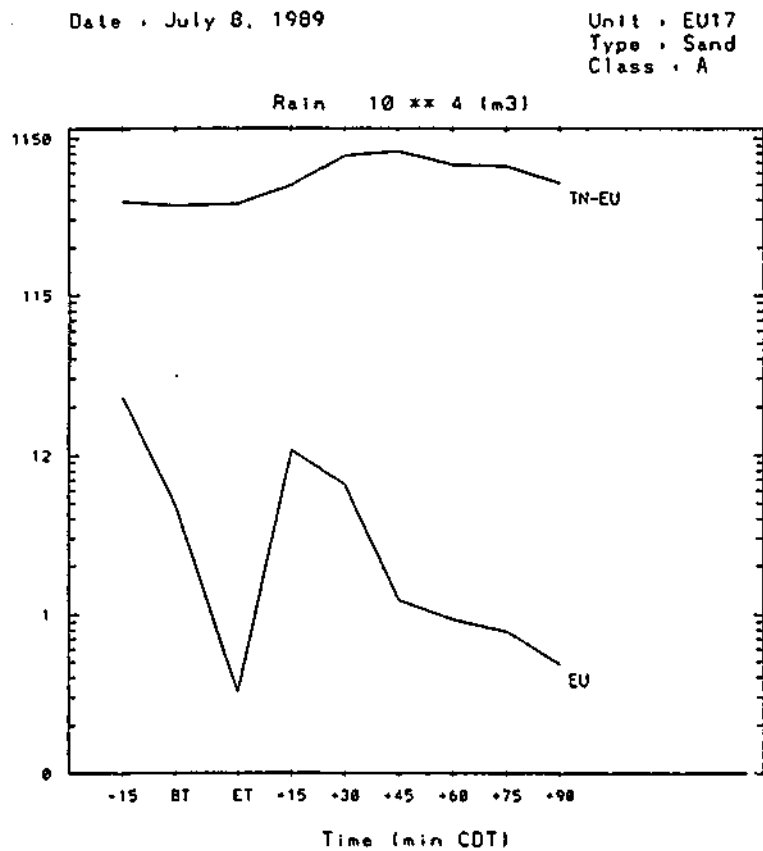
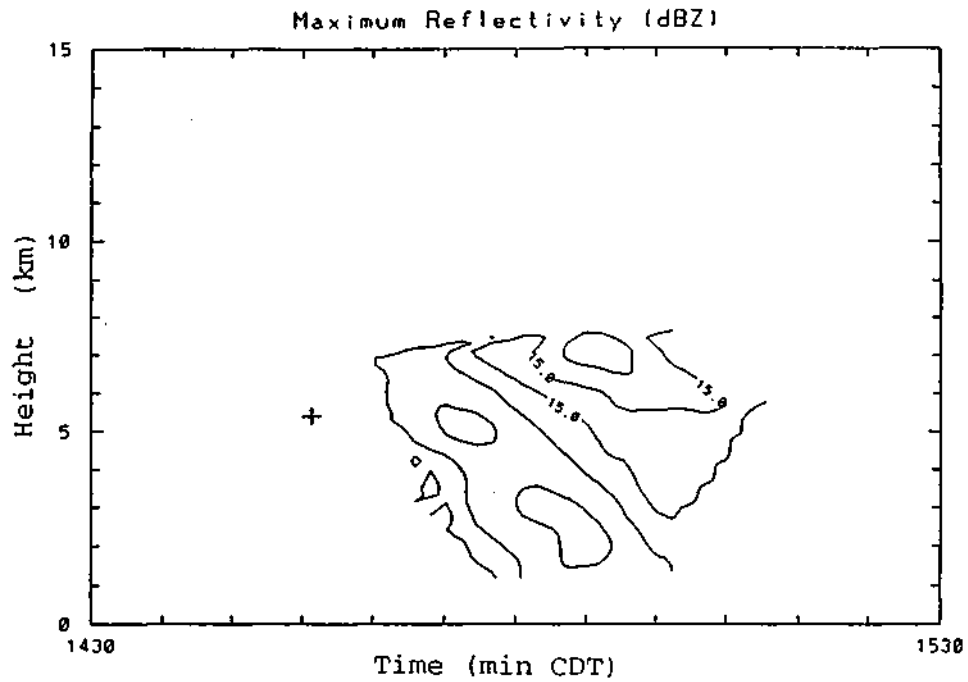


Figure G.21. Time history of radar-estimated rain volume ( $10^4 \text{ m}^3$ ) and echo area for reflectivities  $\geq 30 \text{ dBZ}$  ( $\text{km}^2$ ) in and around Experimental Unit 17, on July 08, 1989.

EU17EC01a 070889



EU17EC02a 070889

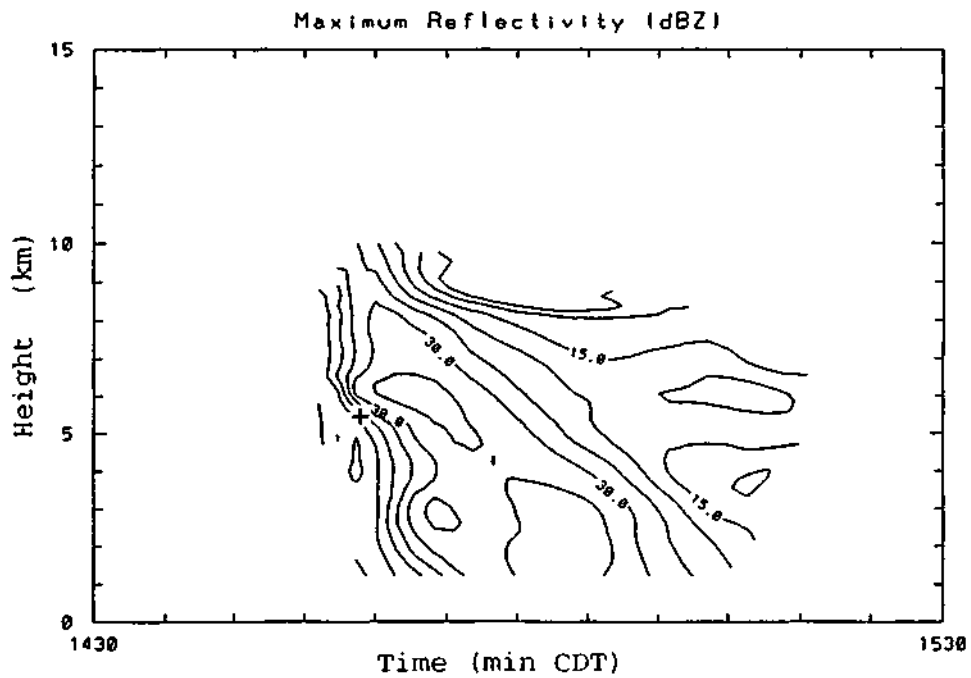
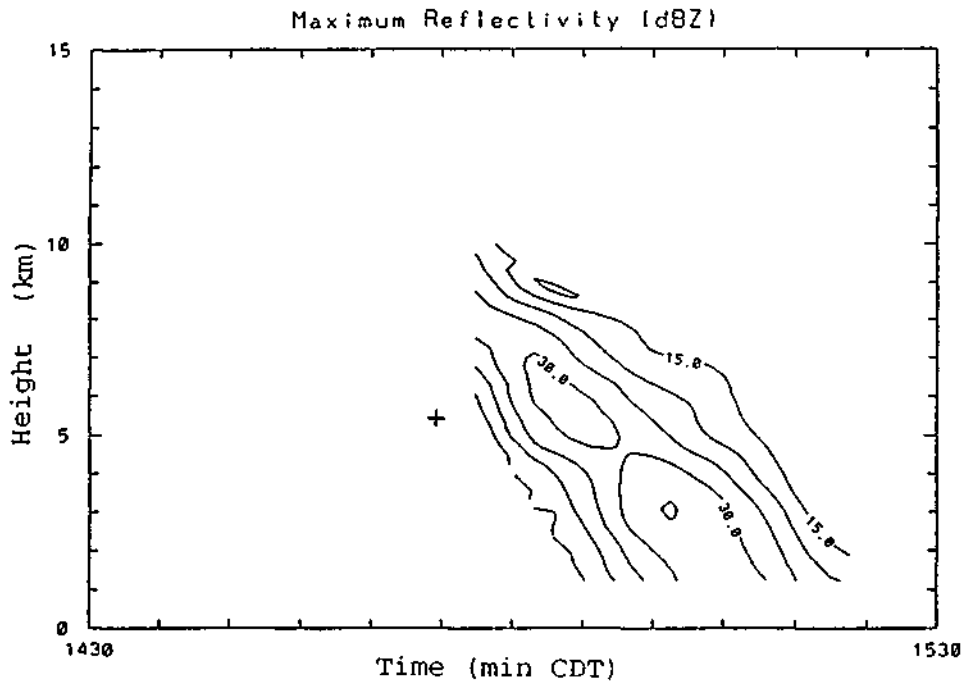


Figure G.22. Time-height histories of the reflectivity cores for clouds EU17EC01a and EU17EC02a in Experimental Unit 17, on July 08, 1989.

EU17EC03a 070889



EU17EC05a 070889

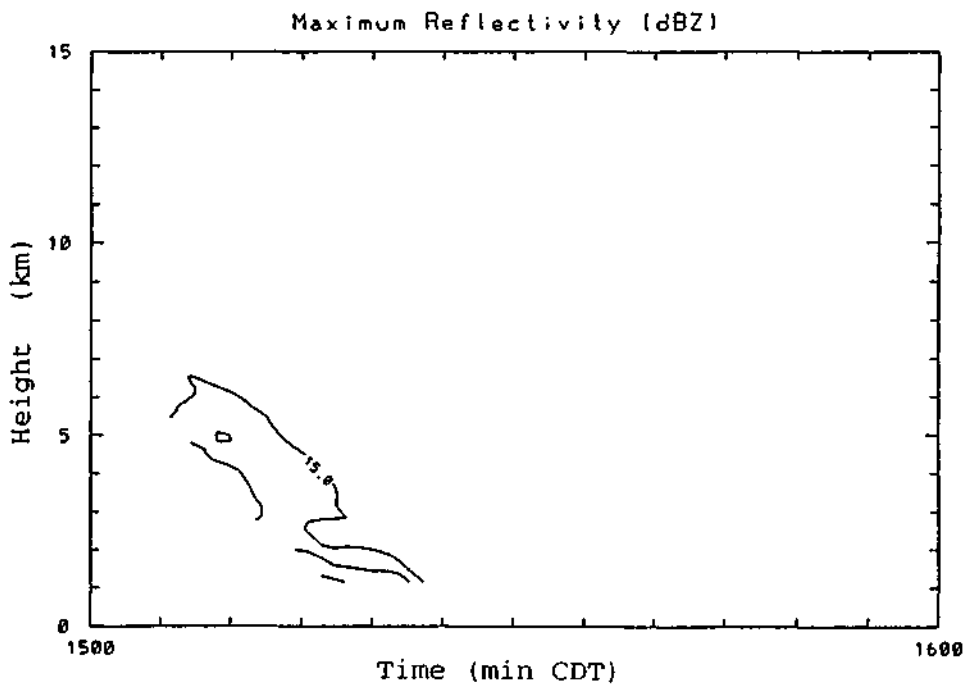


Figure G.23. Time-height histories of the reflectivity cores for clouds EU17EC03a and EU17EC05a in Experimental Unit 17, on July 08, 1989. The cloud pass midtime was 14:58:05 CDT for EU17EC05.

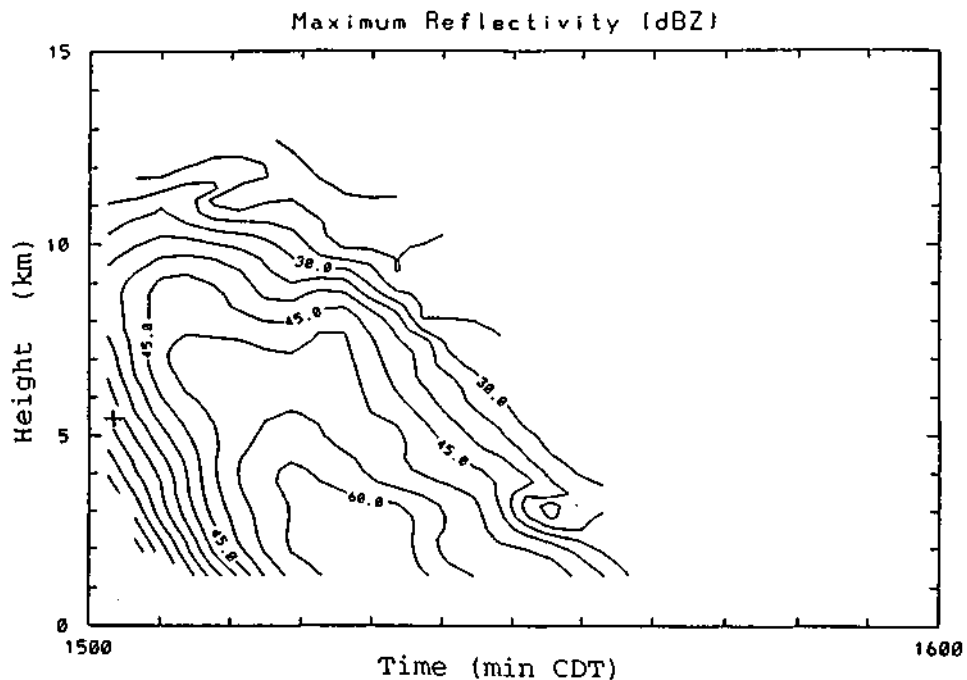


Figure G.24. Time-height histories of the reflectivity cores for clouds EU17EC06a in Experimental Unit 17, on July 08, 1989.

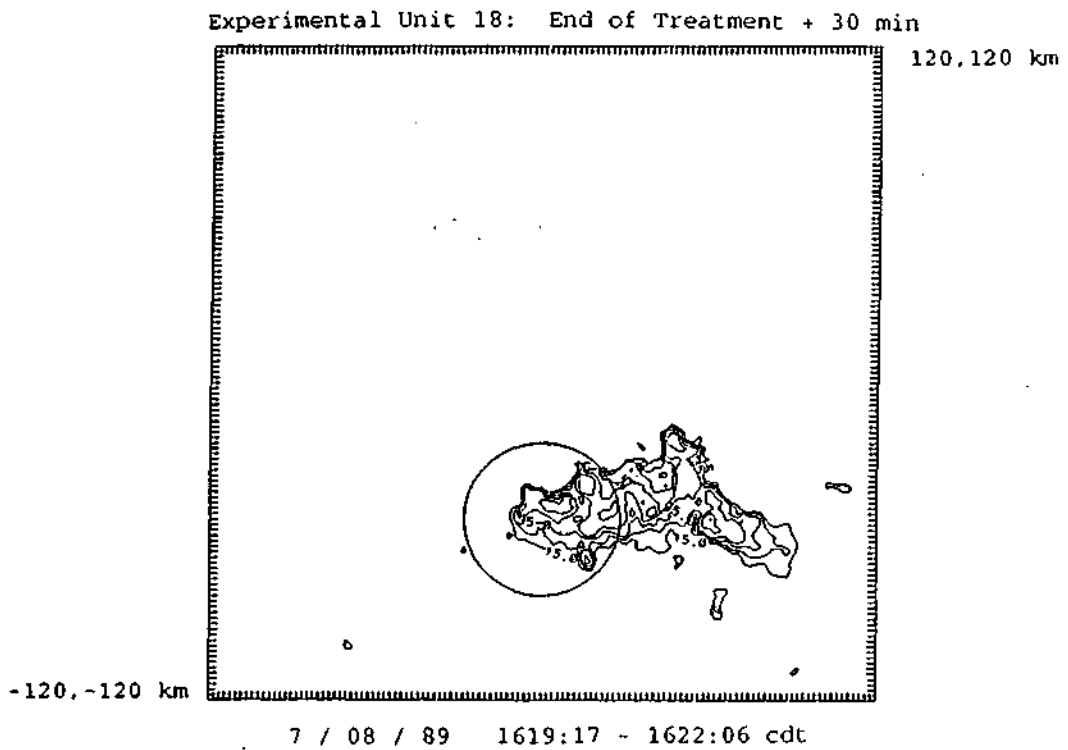
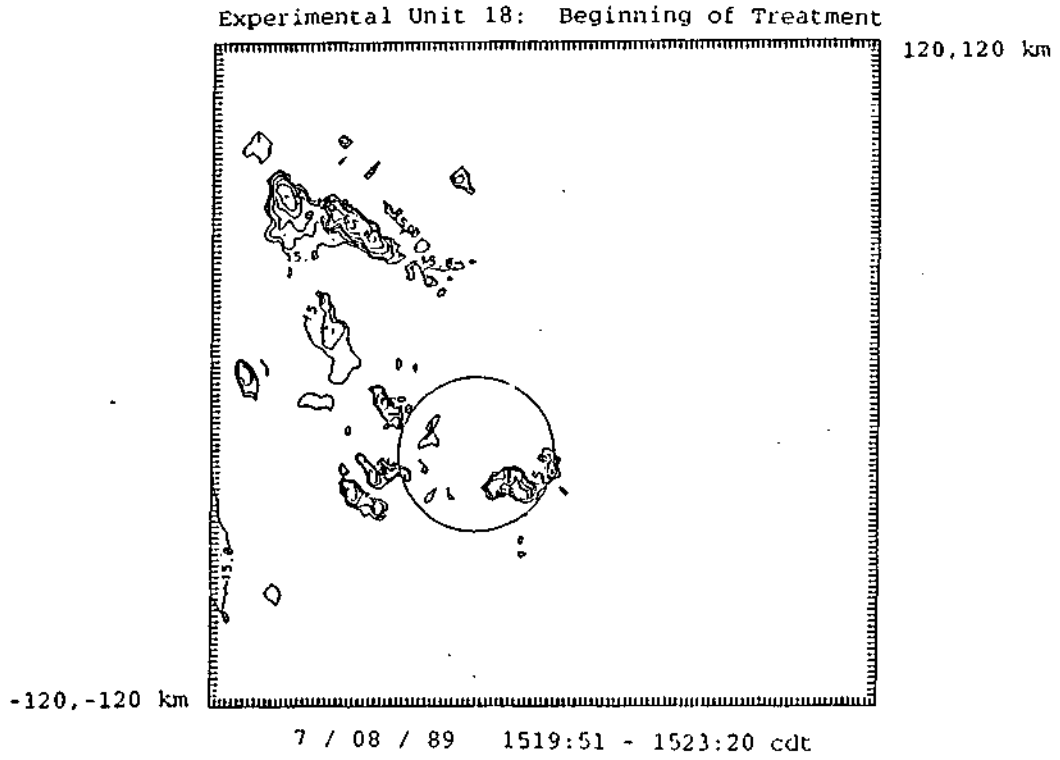


Figure G.25. CAPPIs of radar reflectivity at the 1 km AGL level for Experimental Unit 18, on July 08, 1989.

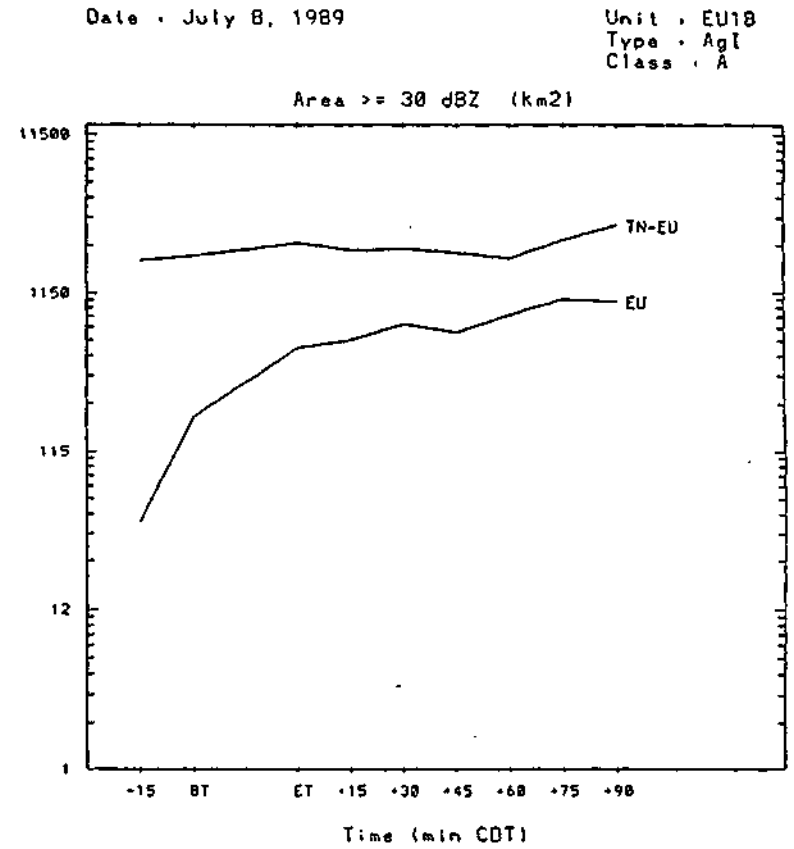
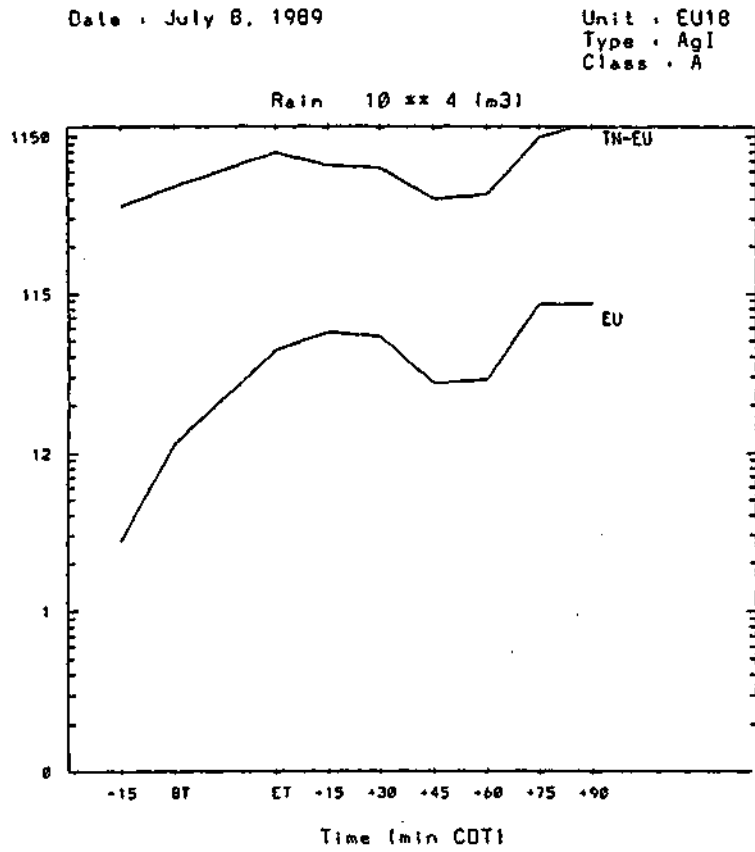
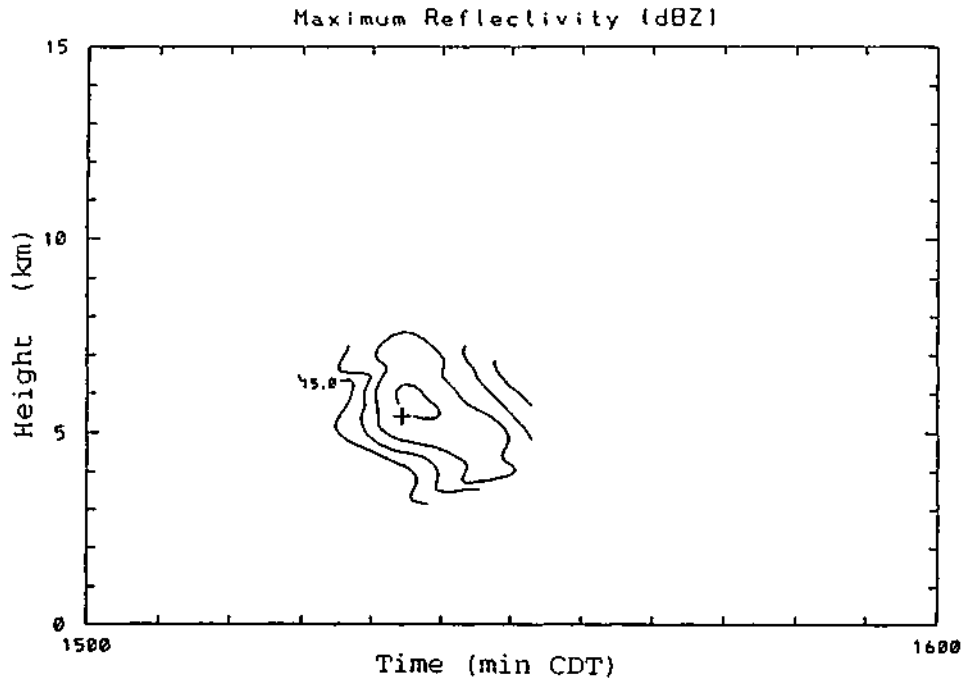


Figure G.26. Time history of radar-estimated rain volume ( $10^4 \text{ m}^3$ ) and echo area for reflectivities  $\geq 30 \text{ dBZ}$  ( $\text{km}^2$ ) in and around Experimental Unit 18, on July 08, 1989.

EU18EC07a 070889



EU18EC11a 070889

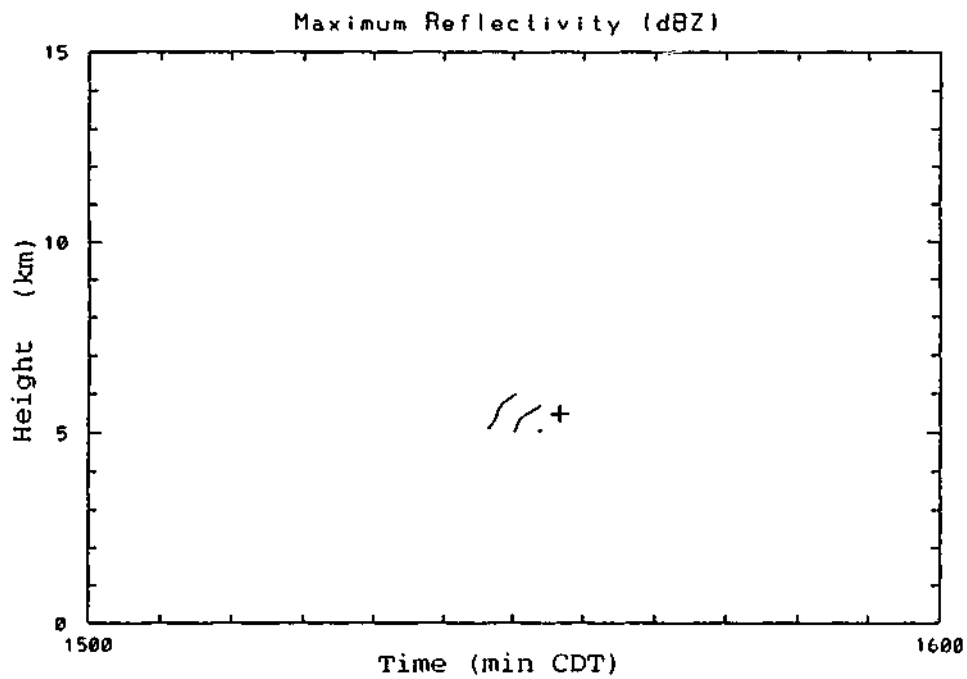
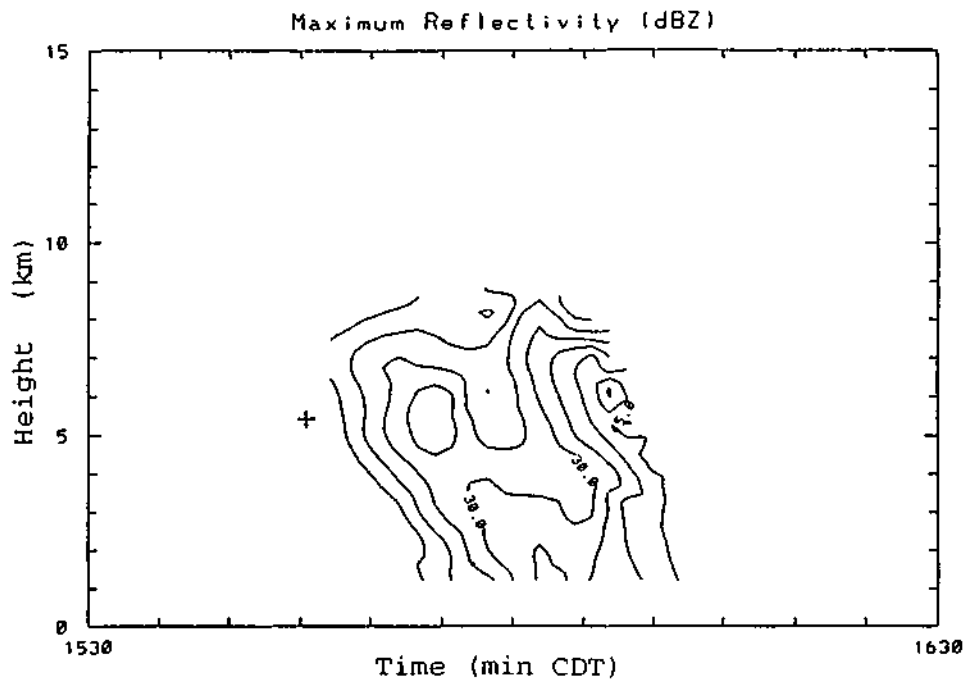


Figure G.27. Time-height histories of the reflectivity cores for clouds EU18EC07a and EU18EC11a in Experimental Unit 18, on July 08, 1989.

EU18EC13a 070889



EU18EC15a 070889

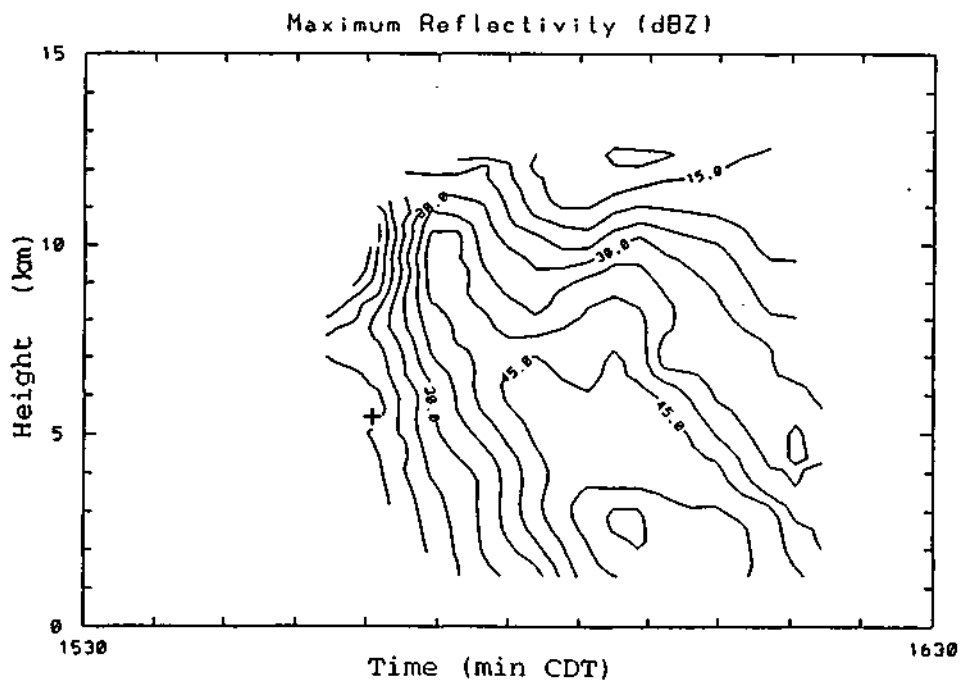


Figure G.28. Time-height histories of the reflectivity cores for clouds EU18EC13a and EU18EC15a in Experimental Unit 18, on July 08, 1989.

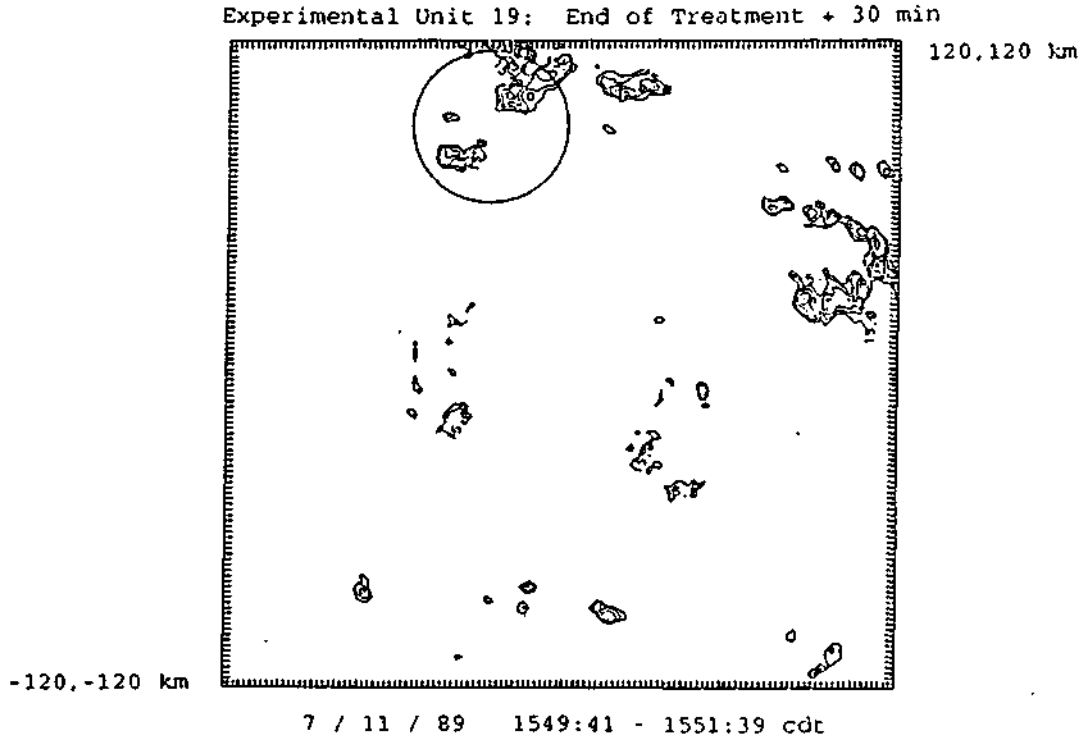
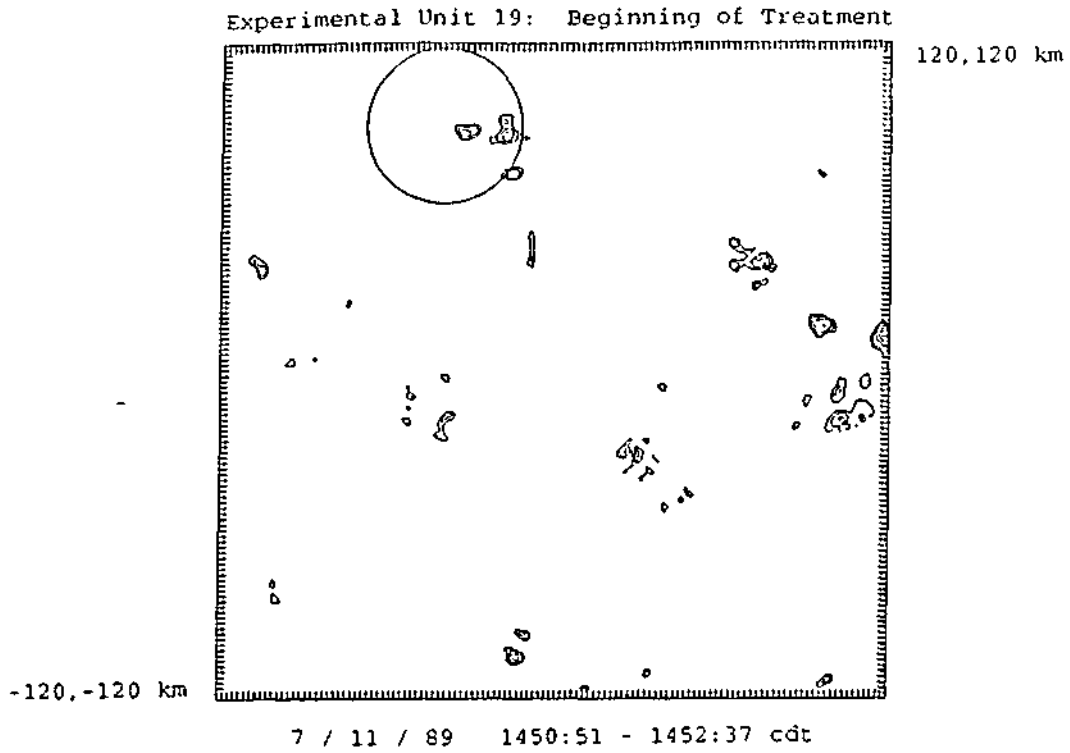


Figure G.29. CAPPIS of radar reflectivity at the 1 km AGL level for Experimental Unit 19 on July 11, 1989.

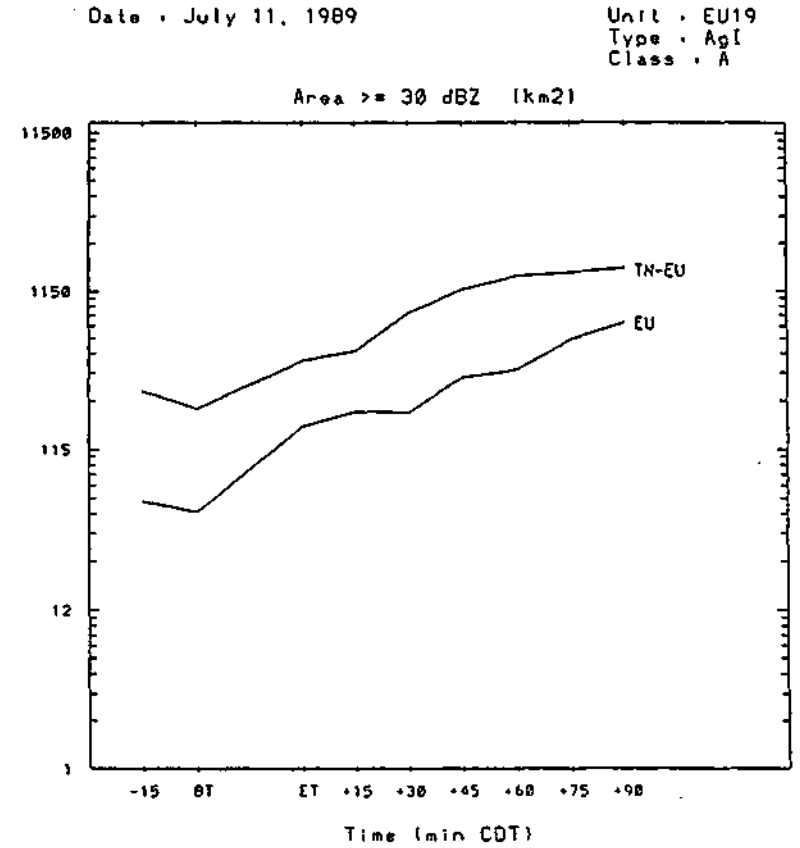
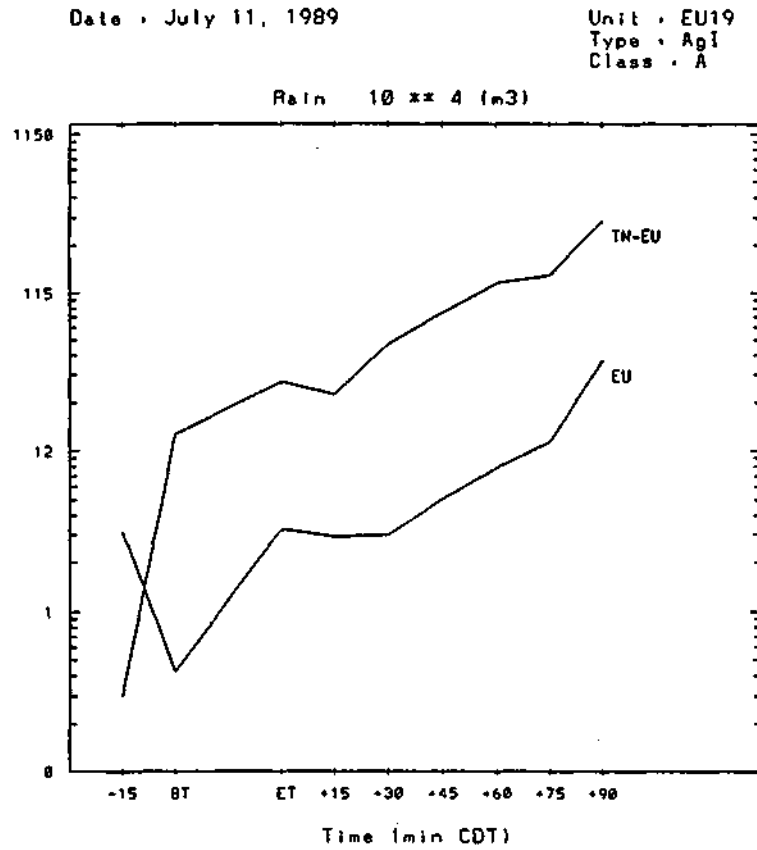
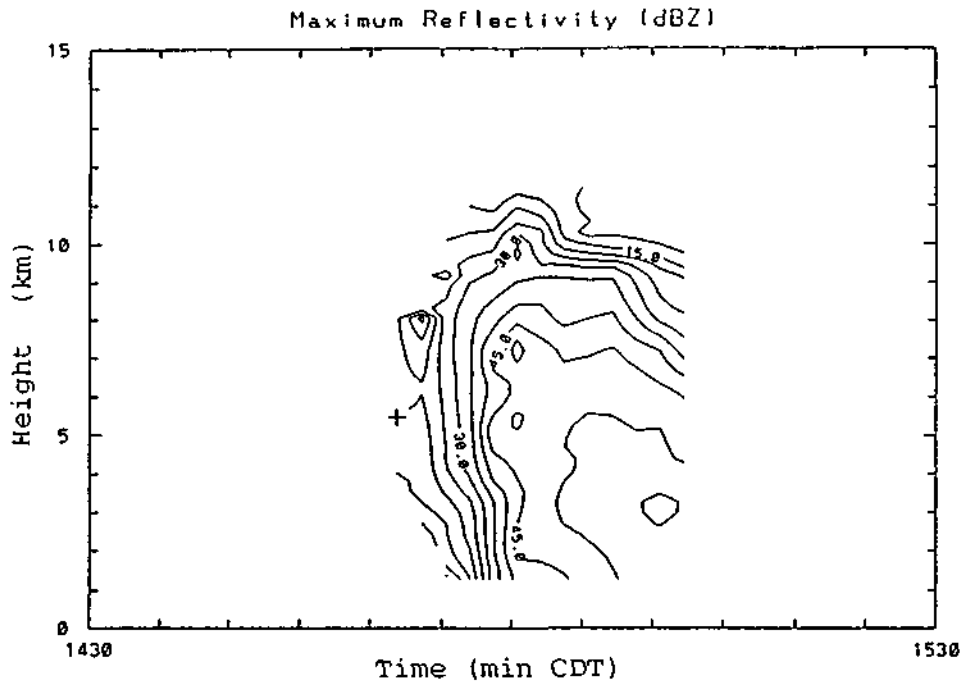


Figure G.30. Time history of radar-estimated rain volume ( $10^4$  m<sup>3</sup>) and echo area for reflectivities  $\geq 30$  dBZ (km<sup>2</sup>) in and around Experimental Unit 19, on July 11, 1989.

EU19EC02a 071189



EU19EC03a 071189

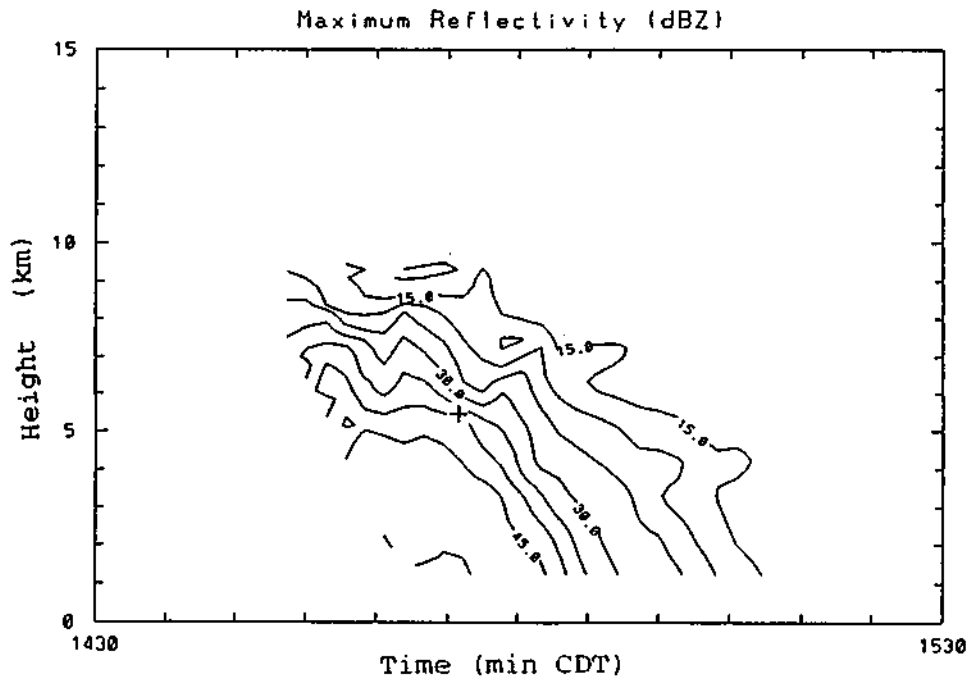
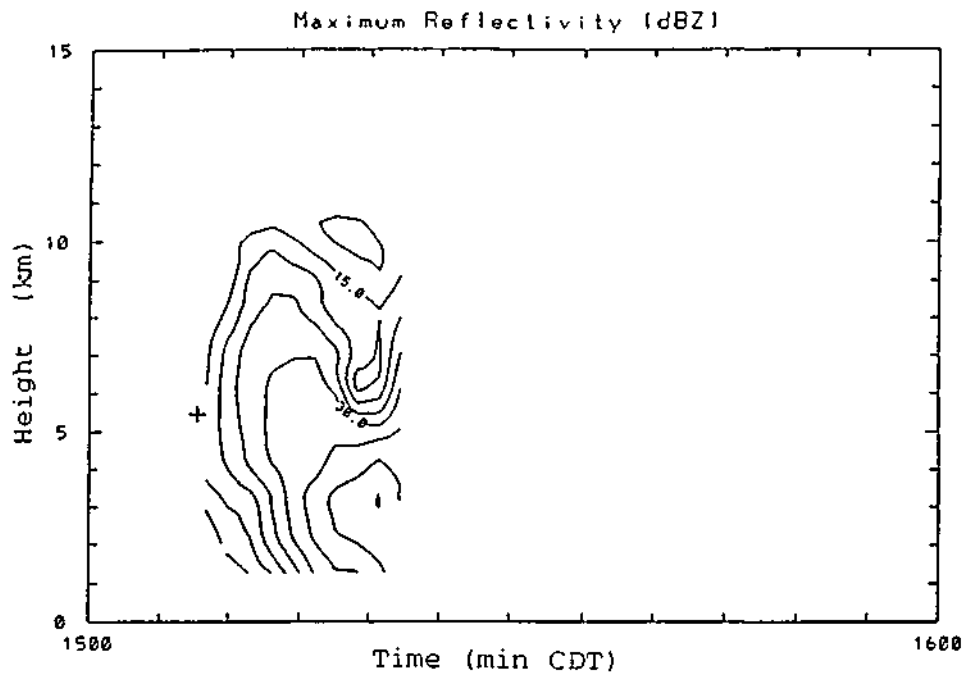


Figure G.31. Time-height histories of the reflectivity cores for clouds EU19EC02a and EU19EC03a in Experimental Unit 19, on July 11, 1989.

EU19EC06a 071189



EU19EC09a 071189

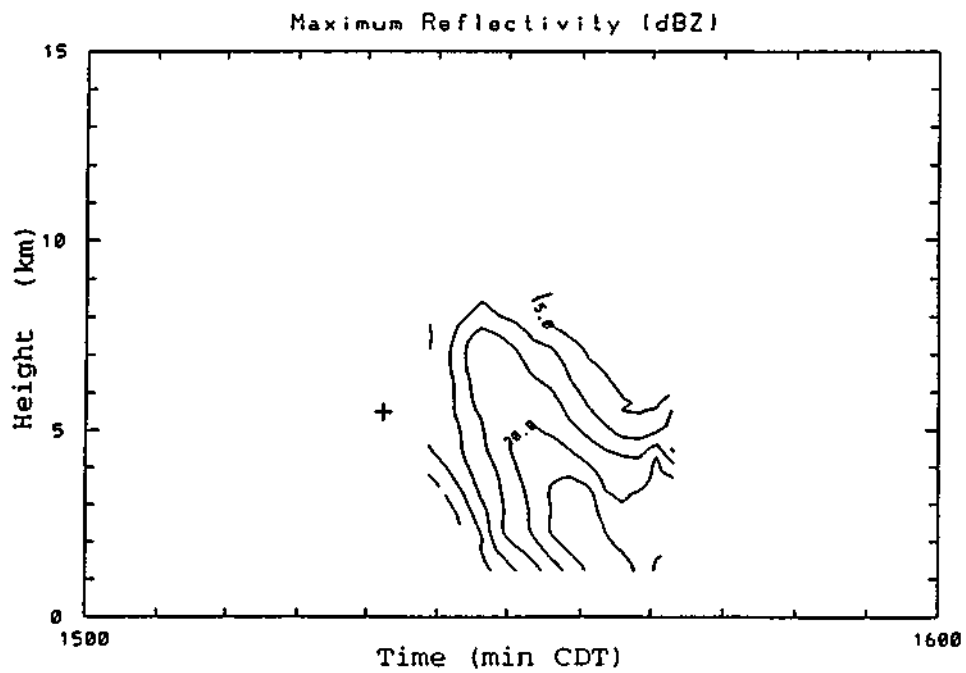


Figure G.32. Time-height histories of the reflectivity cores for clouds EU/9EC06a and EU19EC09a in Experimental Unit 19, on July 11, 1989.

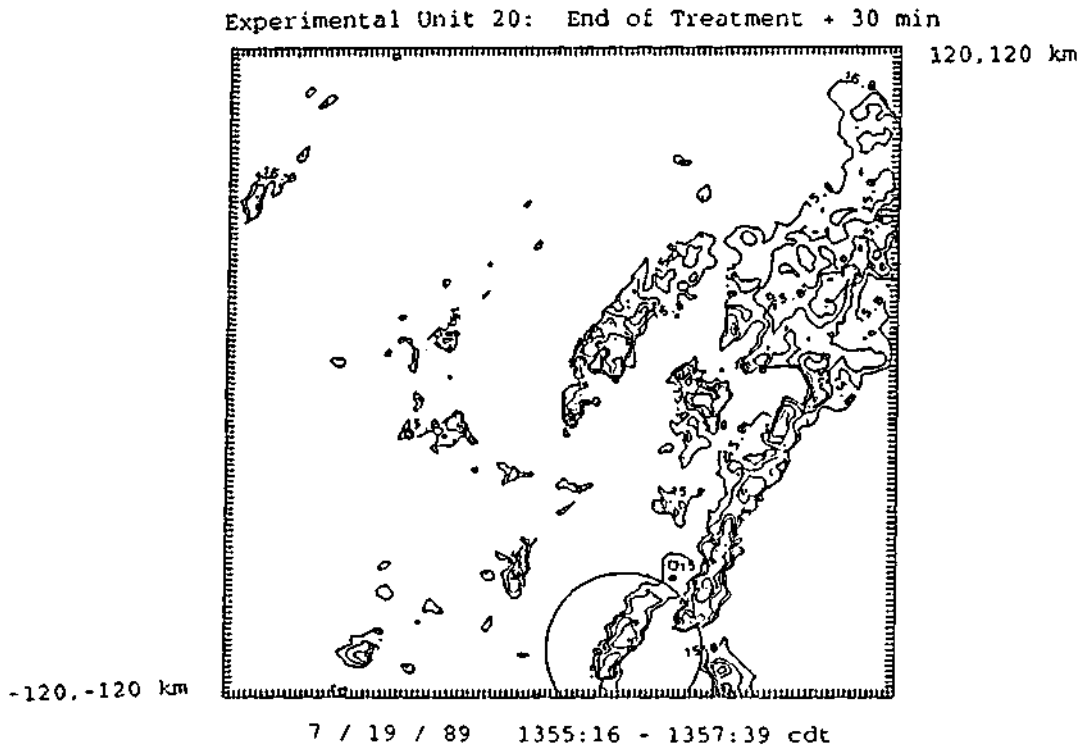
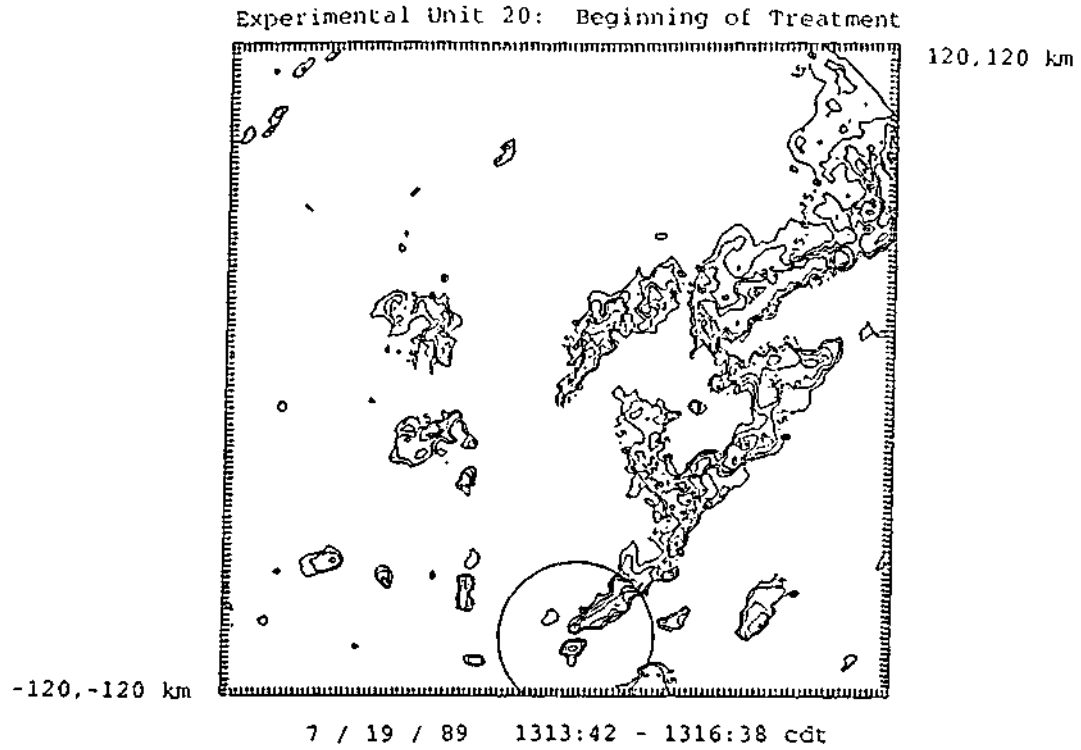


Figure C.33. CAPPi of radar reflectivity at the 1 km AGL level for Experimental Unit 20 on July 19, 1989.

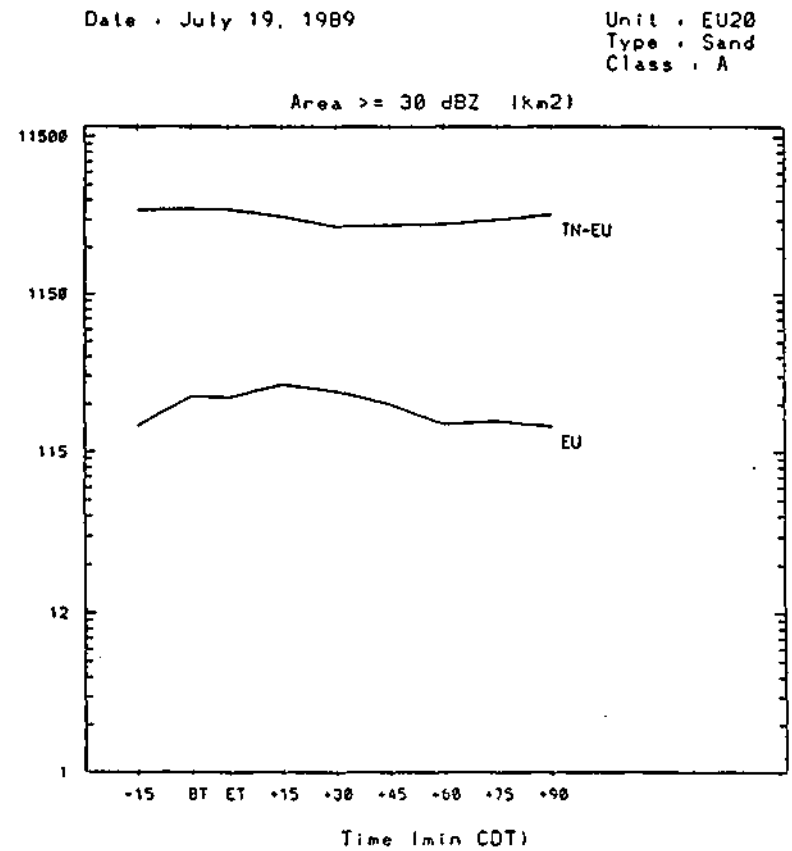
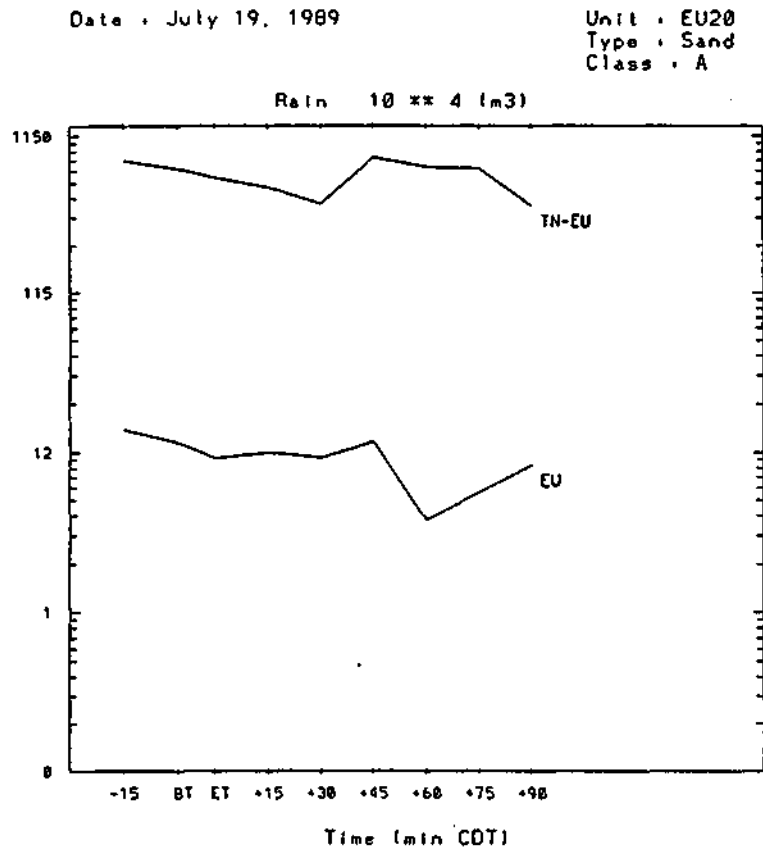
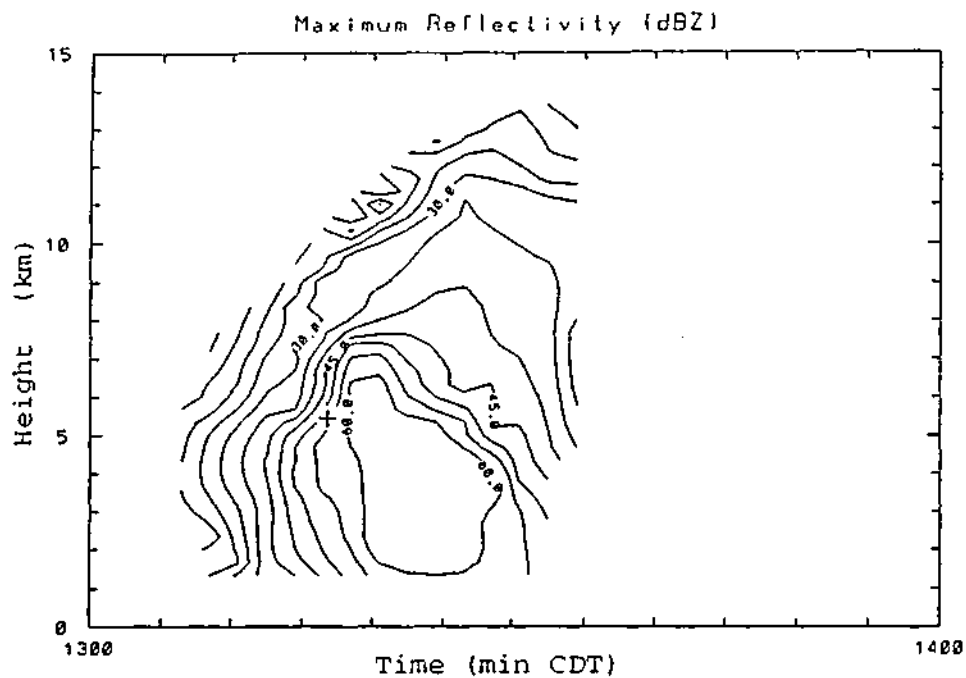


Figure G.34. Time history of radar-estimated rain volume ( $10^{10}$  m<sup>3</sup>) and echo area for reflectivities  $\geq 30$  dBZ (km<sup>2</sup>) in and around Experimental Unit 20, on July 19, 1989.

EU20EC01a 071989



EU20EC02a 071989

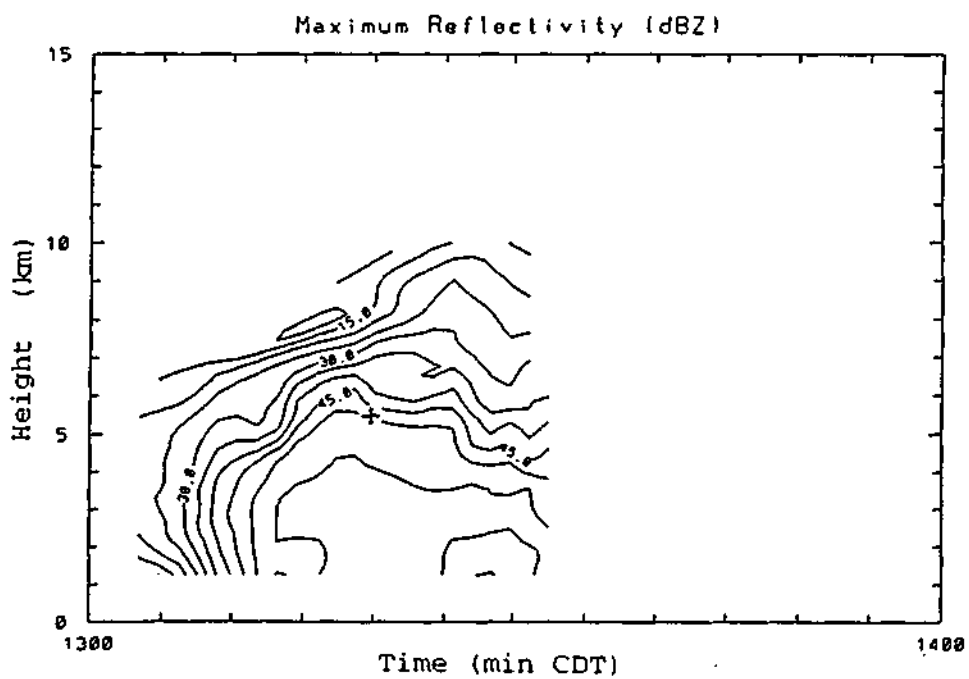


Figure G.35. Time-height histories of the reflectivity cores for clouds EU20EC01a and EU20EC02a in Experimental Unit 20, on July 19, 1989.

EU20EC03a 071989

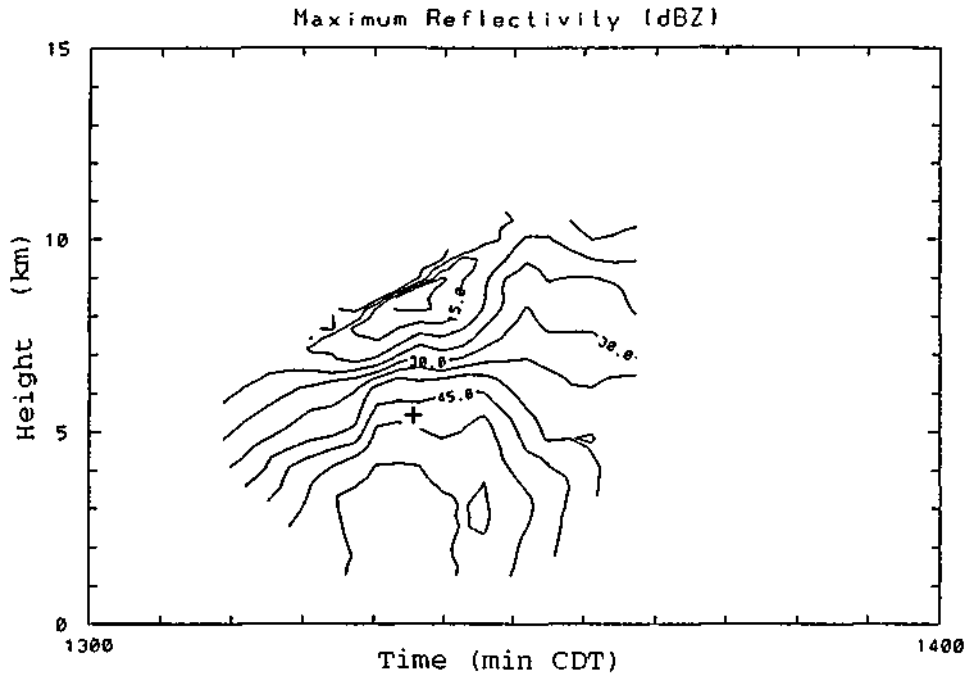


Figure G.36. Time-height histories of the reflectivity cores for clouds EU20EC03a in Experimental Unit 20, on July 19, 1989.

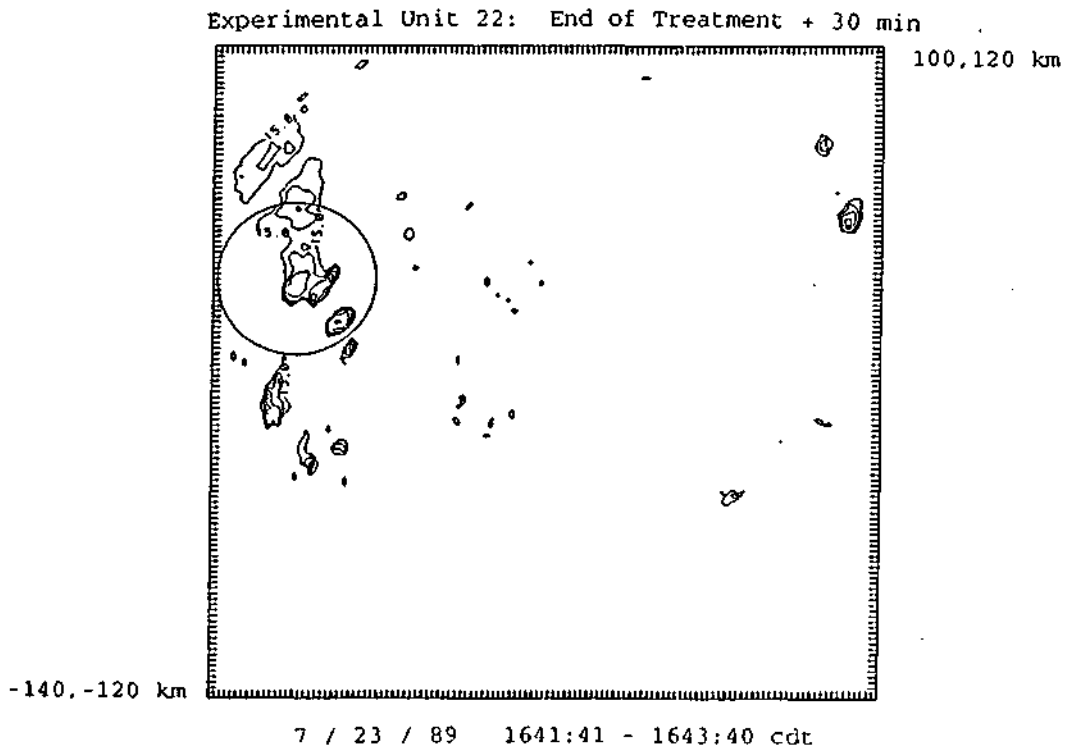
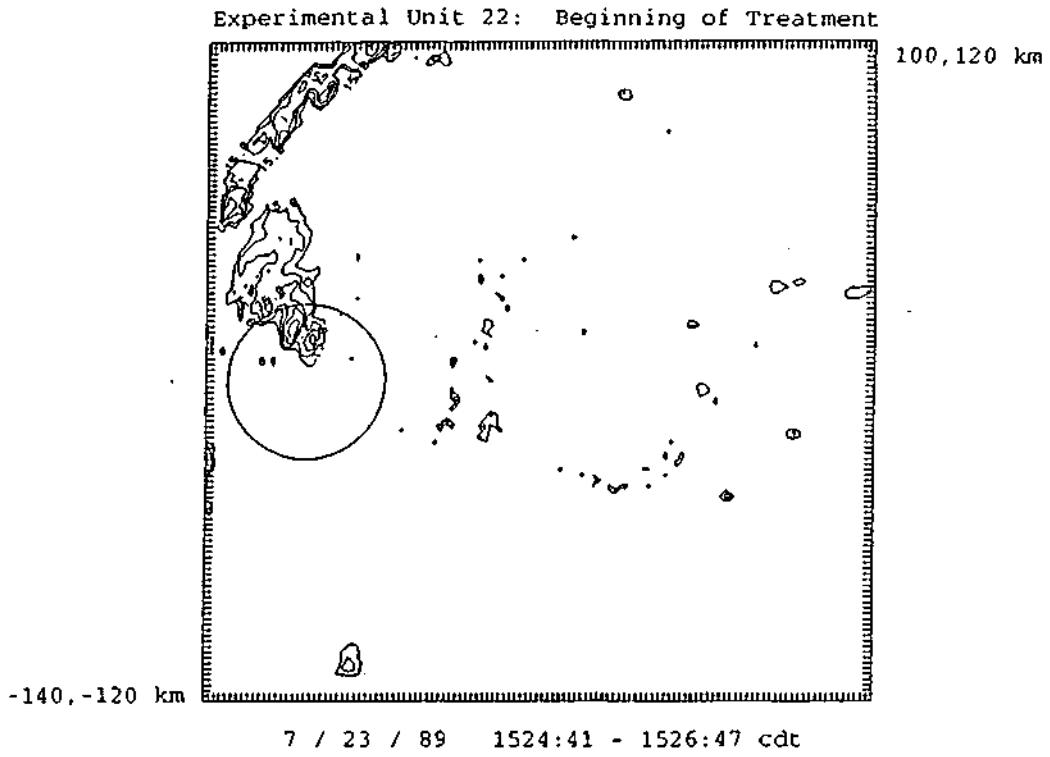


Figure G.37. CAPPIs of radar reflectivity at the 1 km AGL level for Experimental Unit 22 on July 23, 1989.

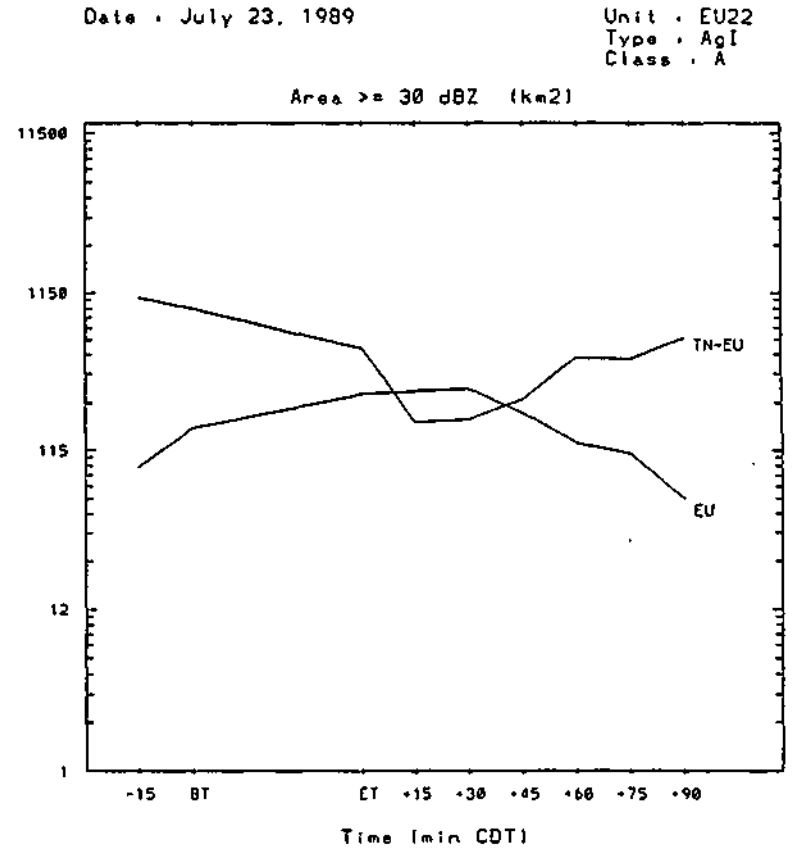
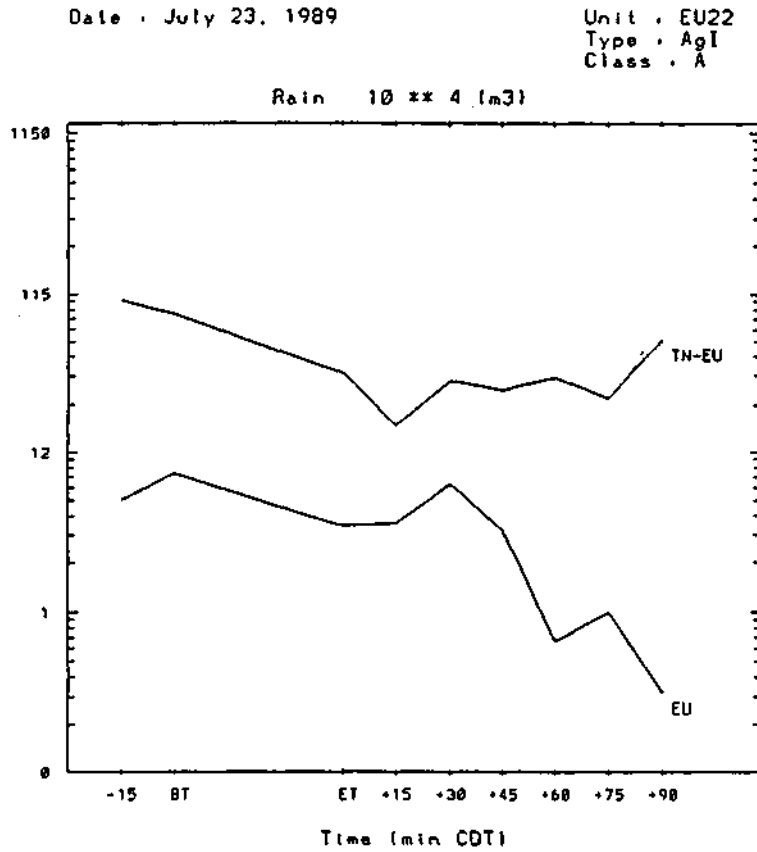


Figure G.38. Time history of radar-estimated rain volume ( $10^{10} \text{ m}^3$ ) and echo area for reflectivities  $\geq 30 \text{ dBZ}$  ( $\text{km}^2$ ) in and around Experimental Unit 22, on July 23, 1989.

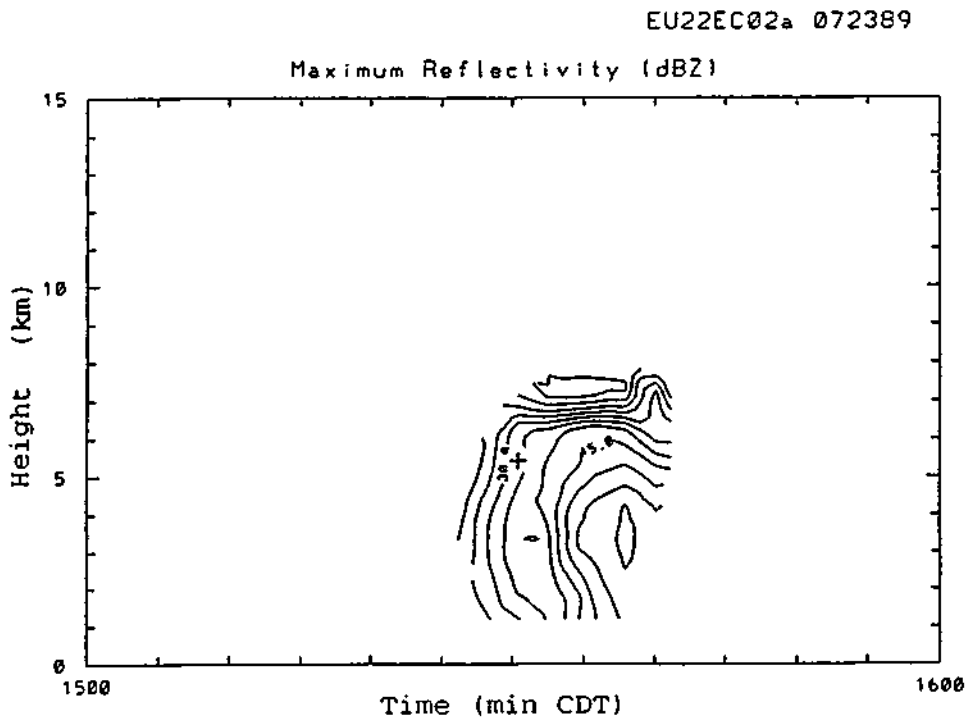
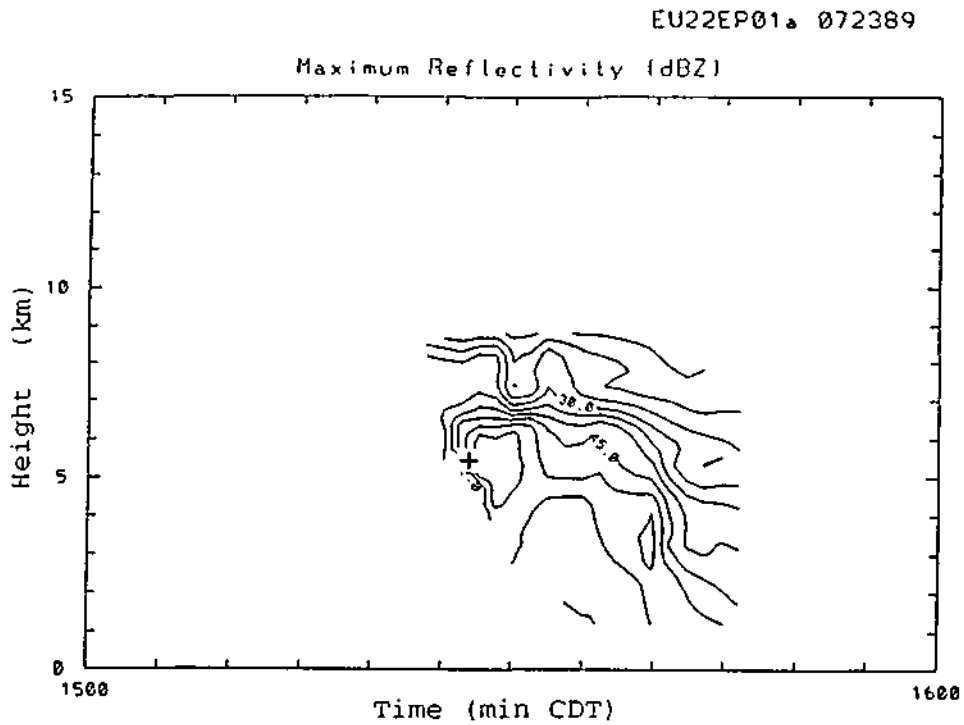


Figure G.39. Time-height histories of the reflectivity cores for clouds EU22EP01a and EU22EC02a in Experimental Unit 22, on July 23, 1989. EU22EP0/a was tracked only through a portion of its history.

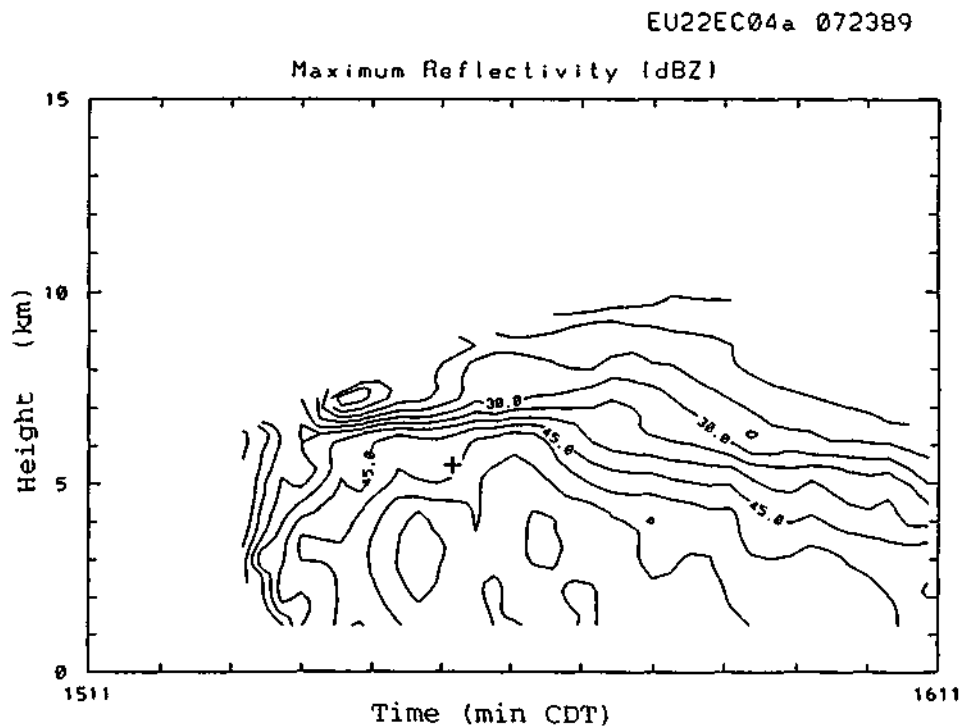
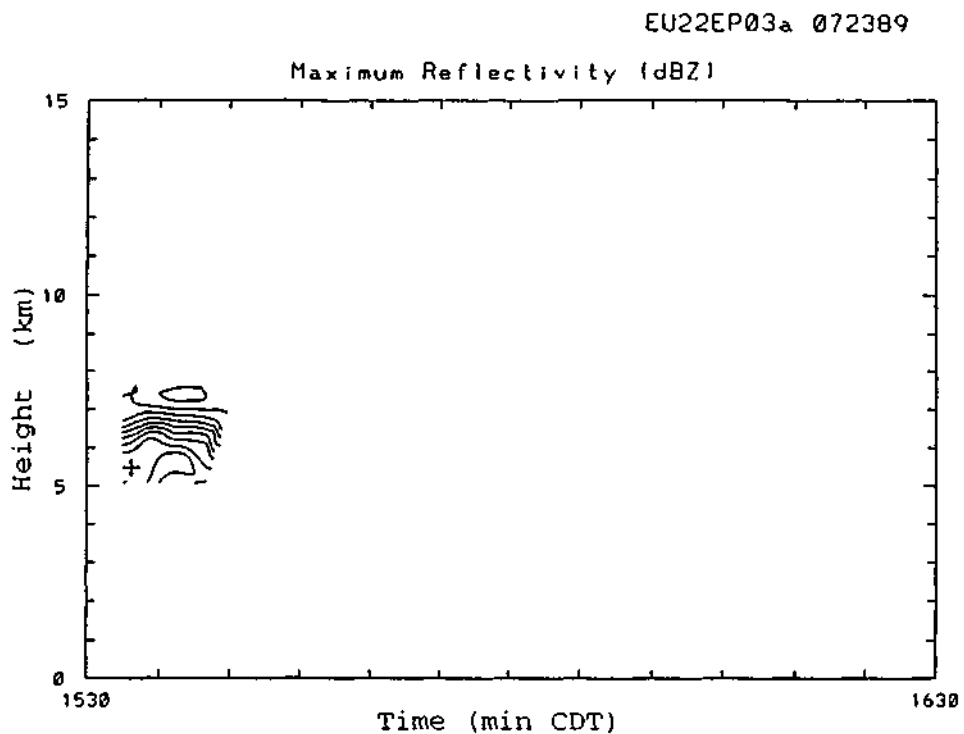
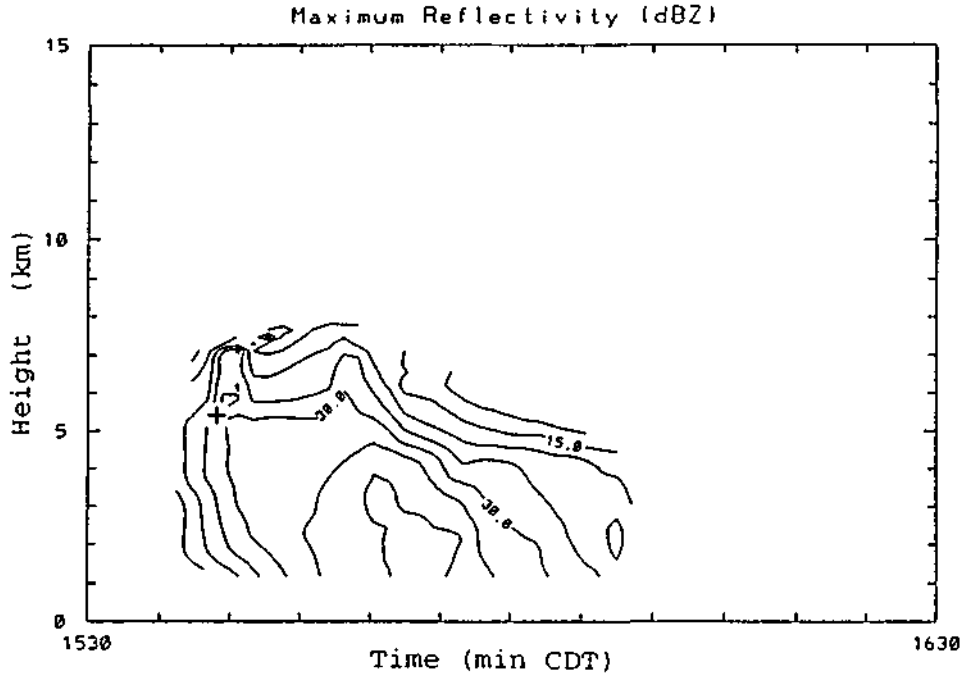


Figure G.40. Time-height histories of the reflectivity cores for clouds EU22EP03a and EU22EC04a in Experimental Unit 22, on July 23, 19S9. EU22EP03a was tracked only through a portion of its history.

EU22EC05a 072389



EU22EC08a 072389

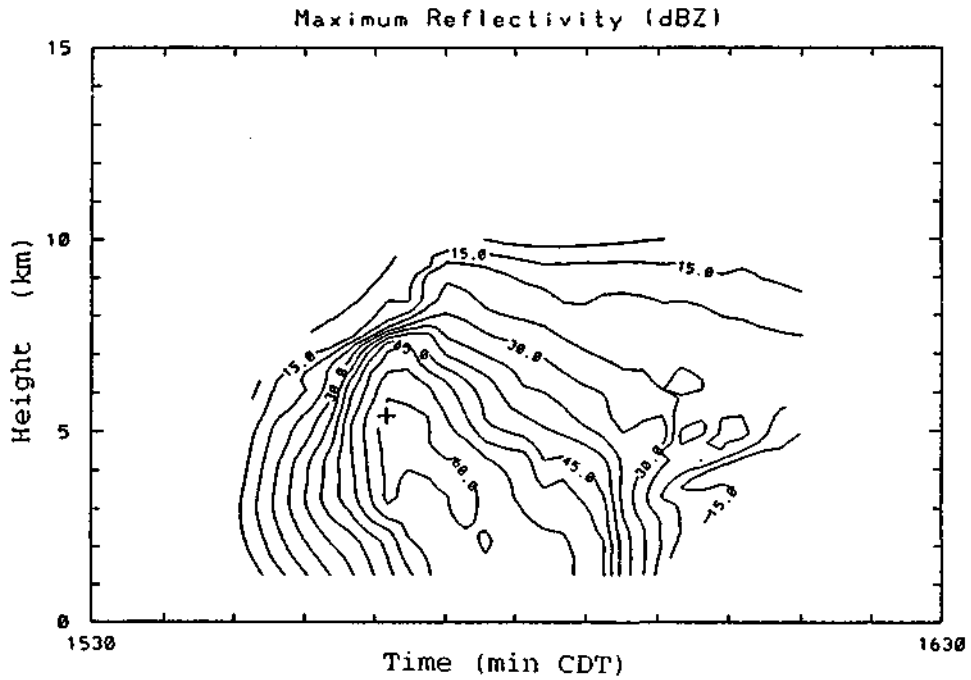
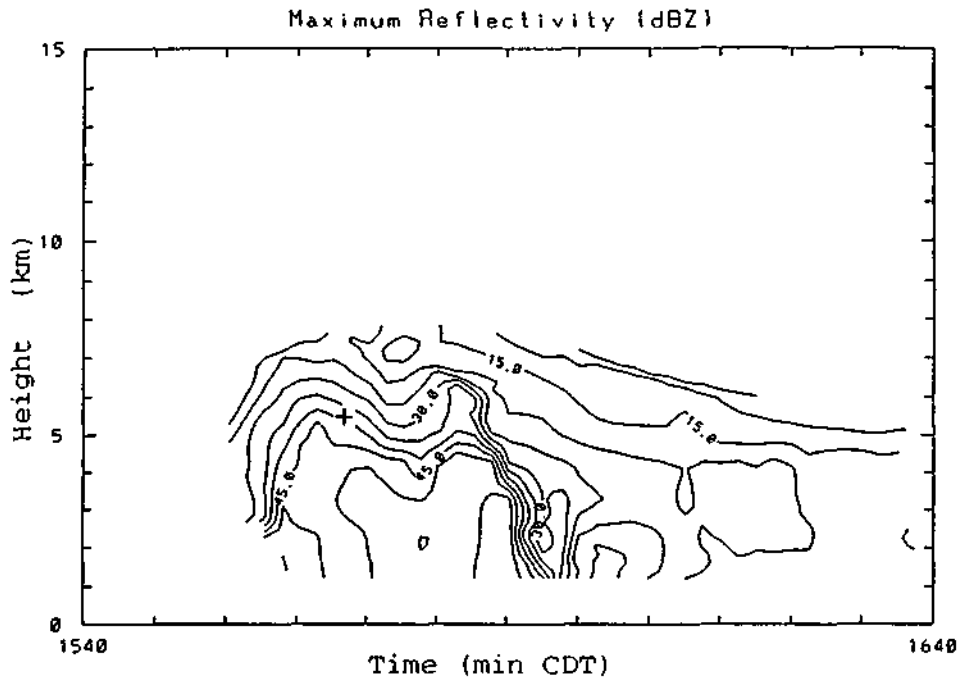


Figure G.41. Time-height histories of the reflectivity cores for clouds EU22EC05a and EU22EC08a in Experimental Unit 22, on July 23, 1989.

EU22EC09a 072389



EU22EC10a 072389

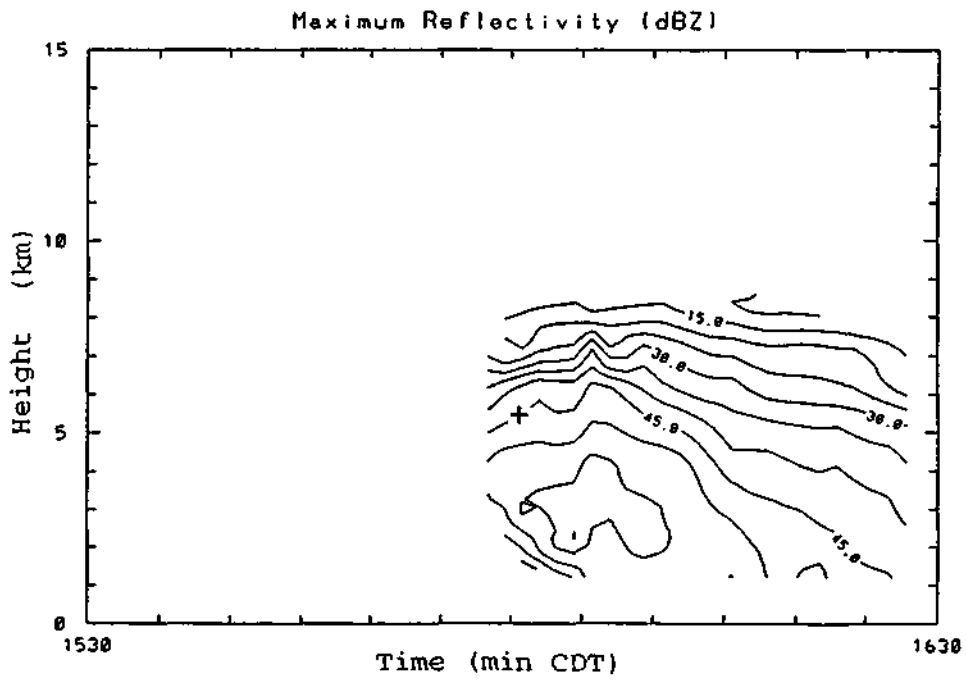
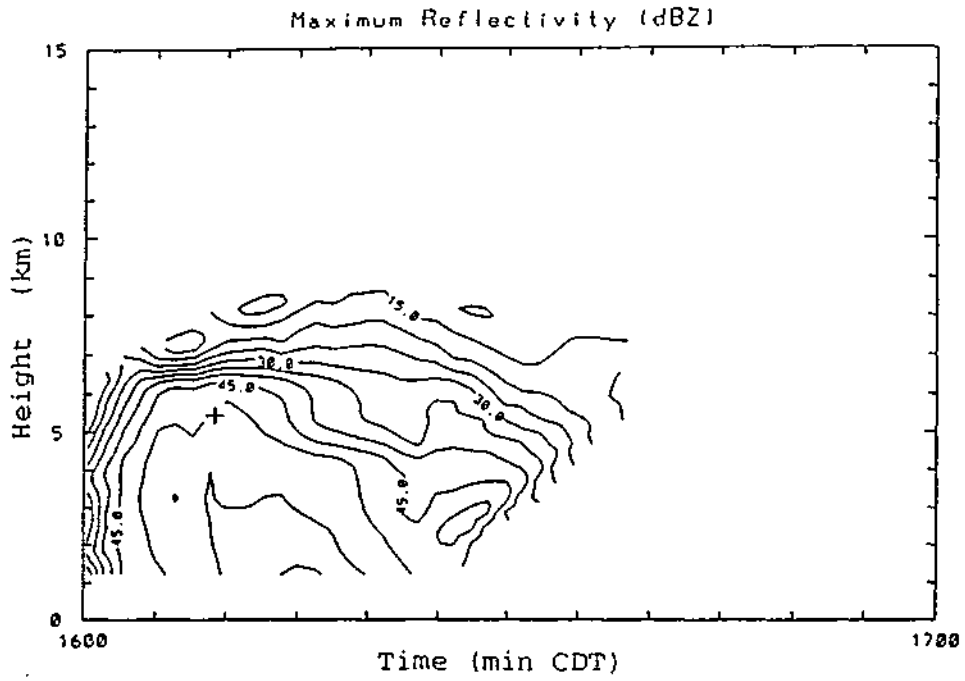


Figure G.42. Time-height histories of the reflectivity cores for clouds EU22EC09a and EU22EC10a in Experimental Unit 22, on July 23, 1989.

EU22EC11a 072369



EU22EC14a 072369

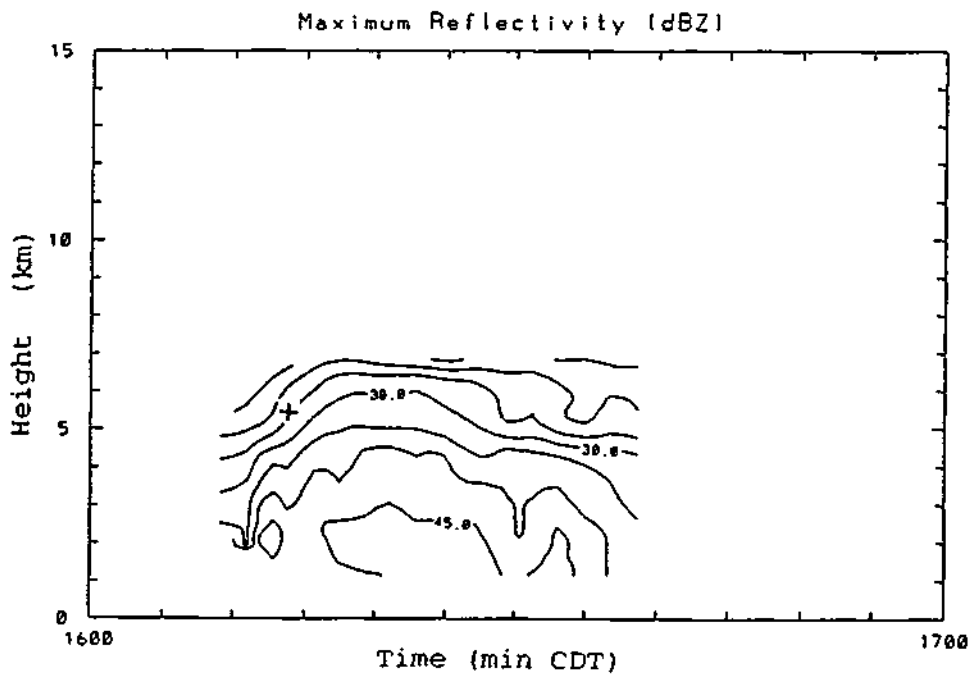


Figure G.43. Time-height histories of the reflectivity cores for clouds EU22EC11a and EU22EC14a in Experimental Unit 22, on July 23, 1989.

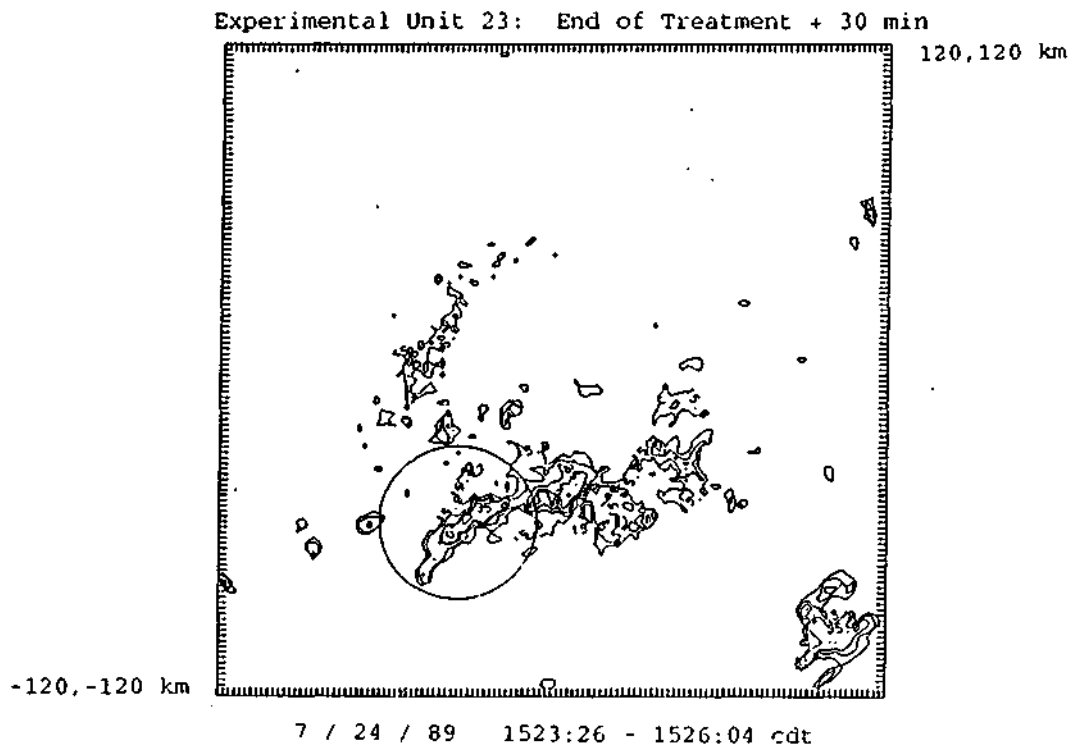
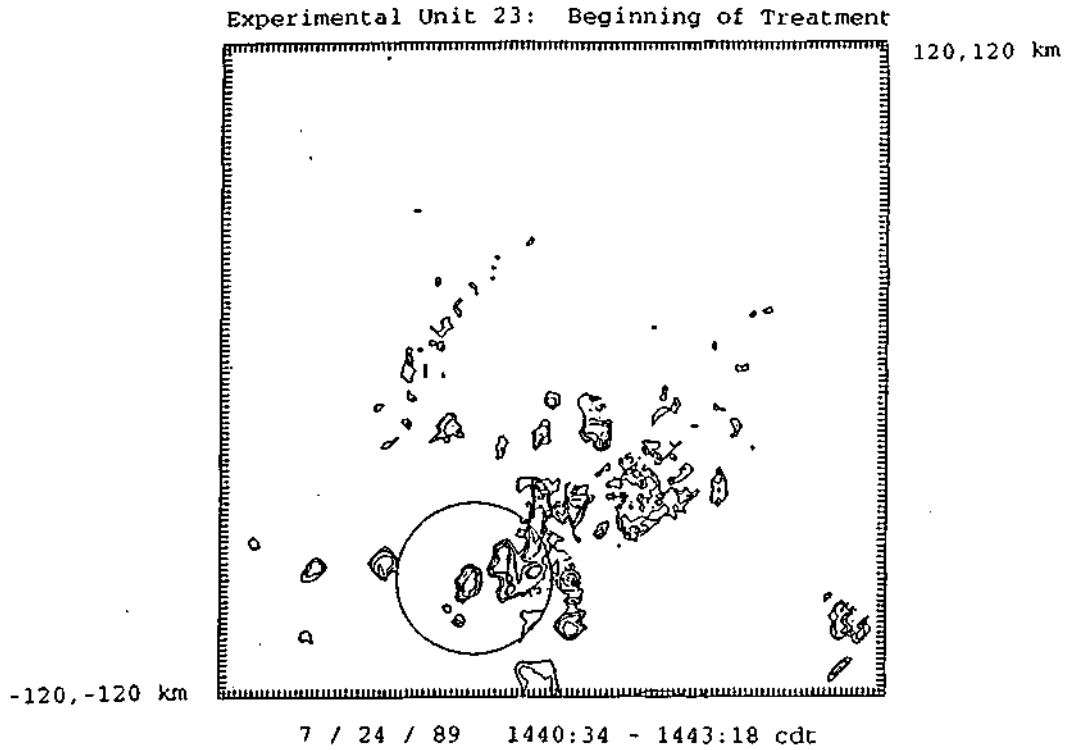


Figure G.44. CAPPIS of radar reflectivity at the 1 km AGL level for Experimental Unit 23, on July 24, 1989.

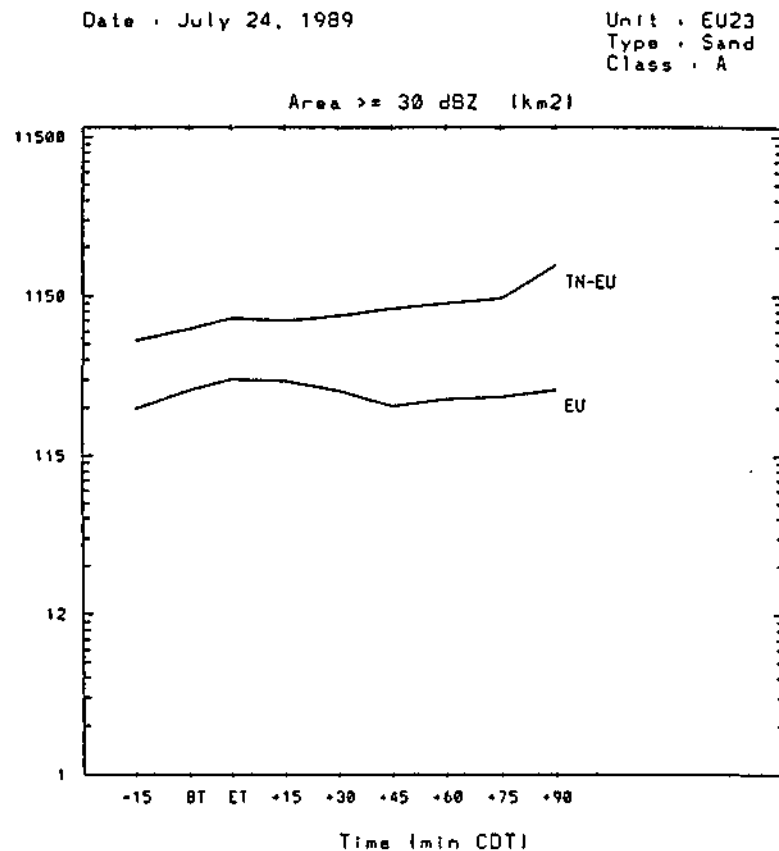
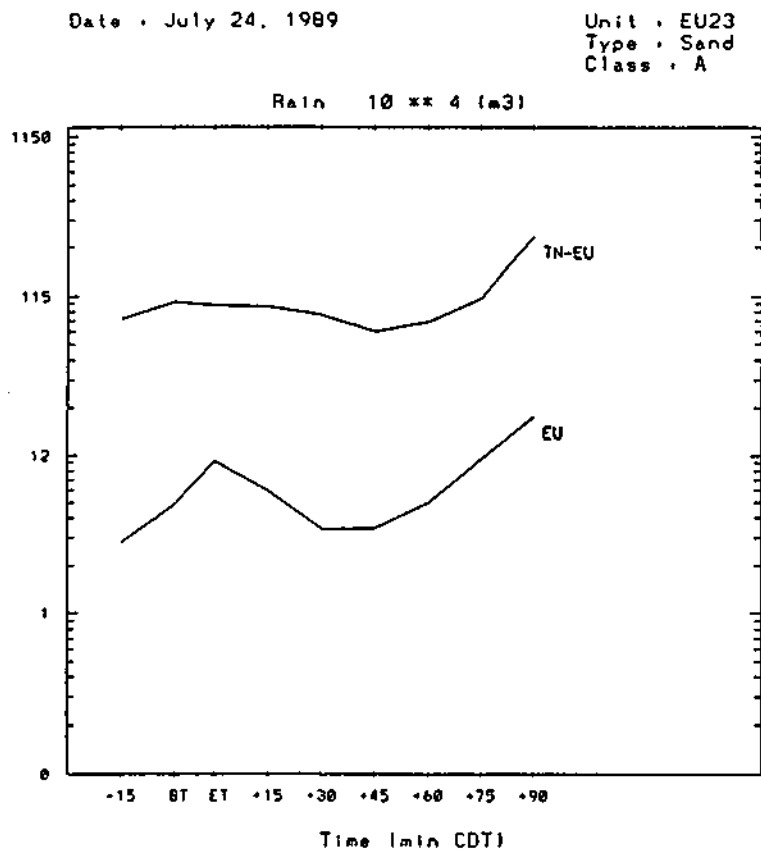
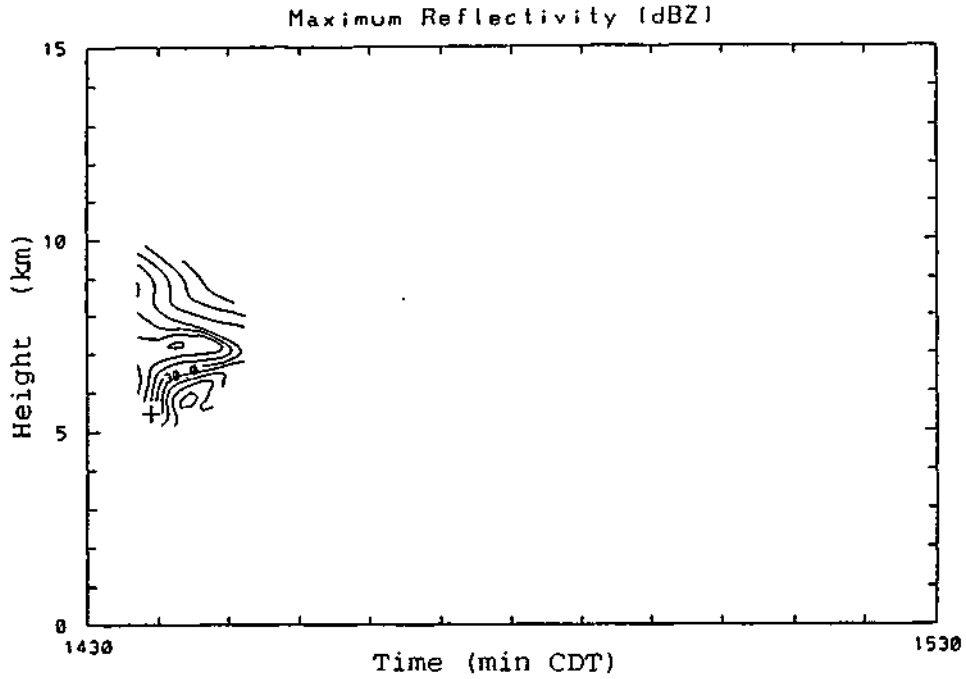


Figure G.45. Time history of radar-estimated rain volume ( $10^4 \text{ m}^3$ ) and echo area for reflectivities  $\geq 30 \text{ dBZ}$  ( $\text{km}^2$ ) in and around Experimental Unit 23, on July 24, 1989.

EU23EP06a 072489



EU23EC07a 072489

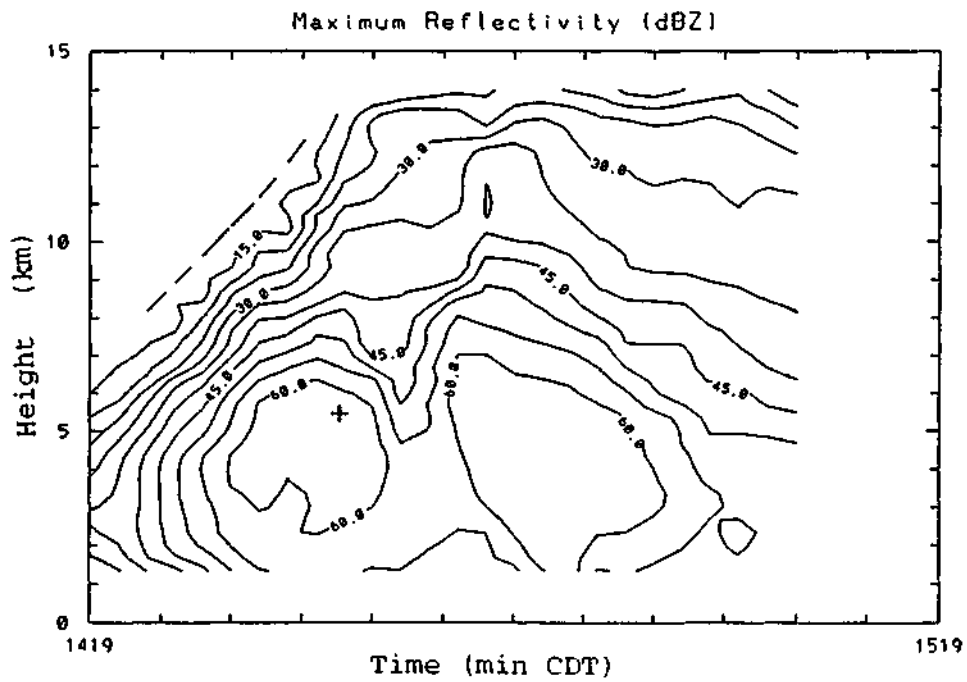
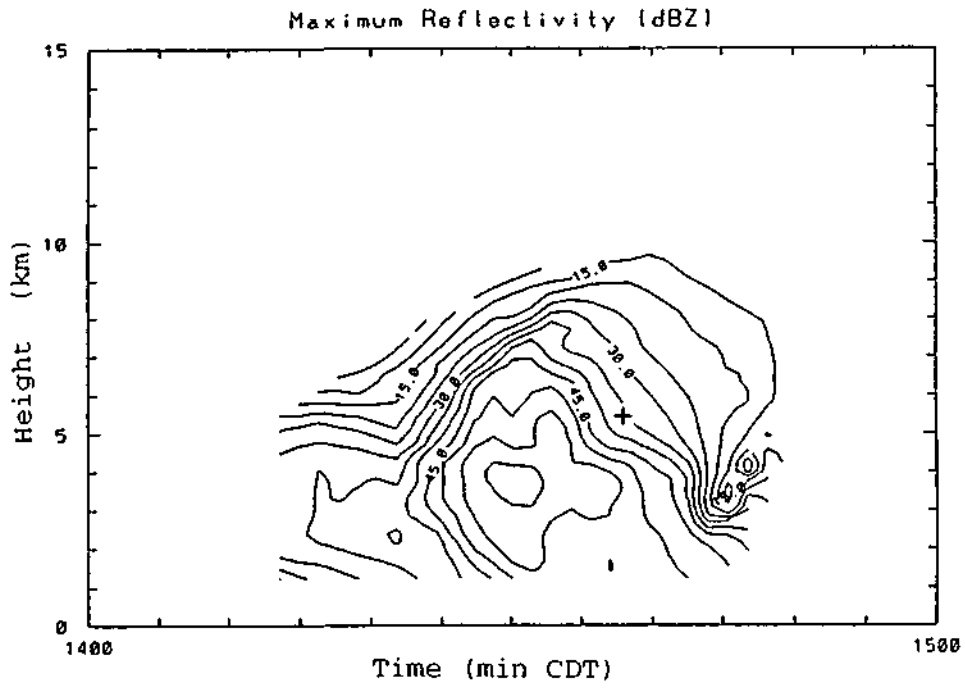


Figure G.46. Time-height histories of the reflectivity cores for clouds EU23EP06a and EU23EC07a in Experimental Unit 23, on July 24, 1989. EU23EP06a was tracked only through a portion of its history.

EU23EC08a 072489



EU23EC09a 072489

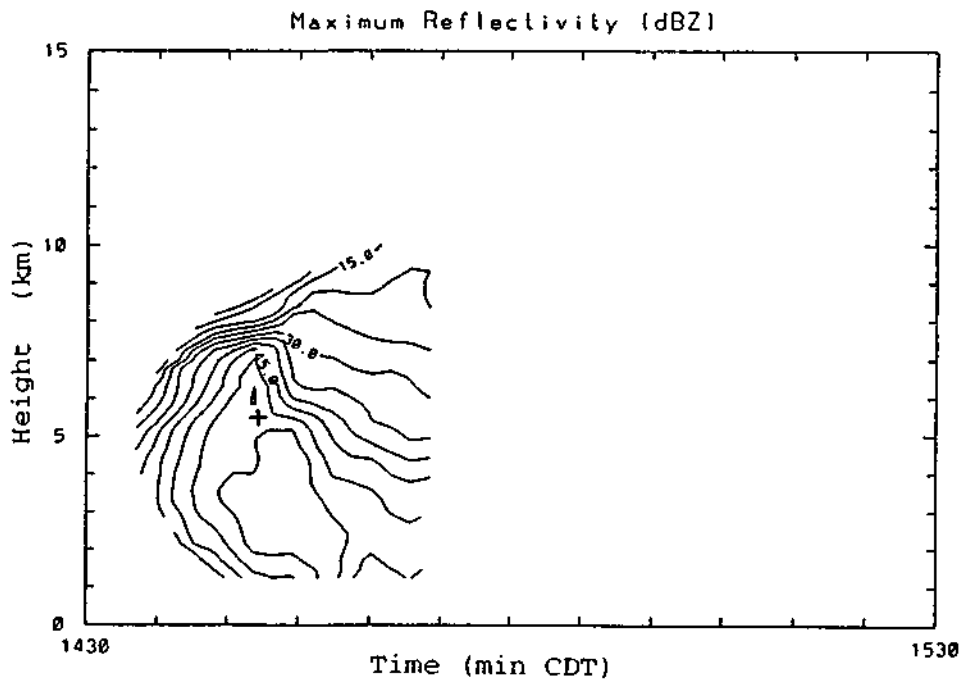


Figure G.47. Time-height histories of the reflectivity cores for clouds EU23EC08a and EU23EC09a in Experimental Unit 23, on July 24, 1989.

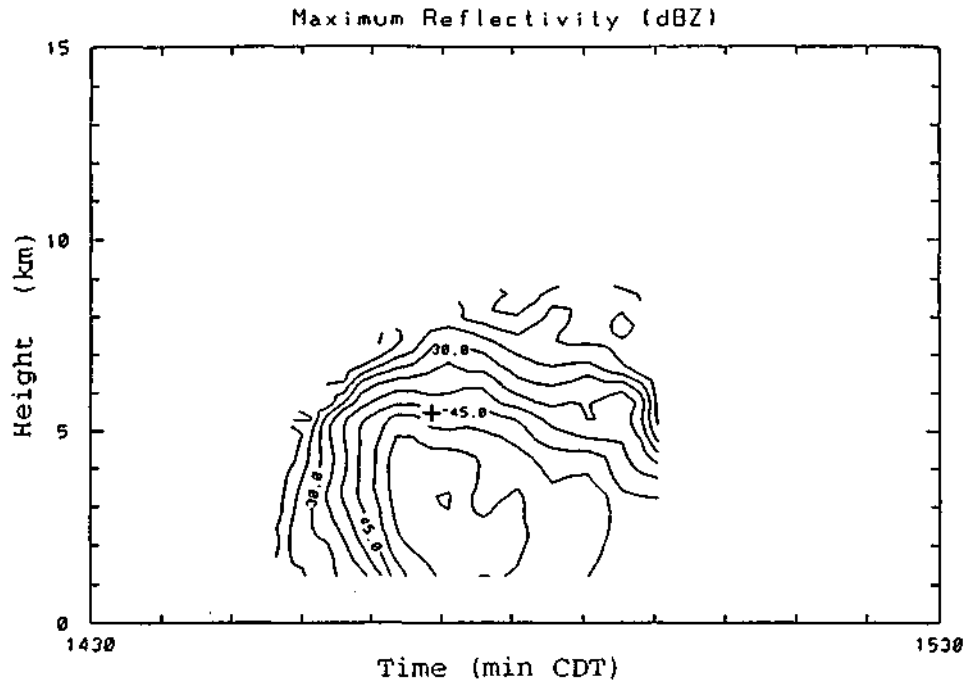


Figure G.48. Time-height histories of the reflectivity cores for clouds EU23EC11a in Experimental Unit 23, on July 24, 1989.

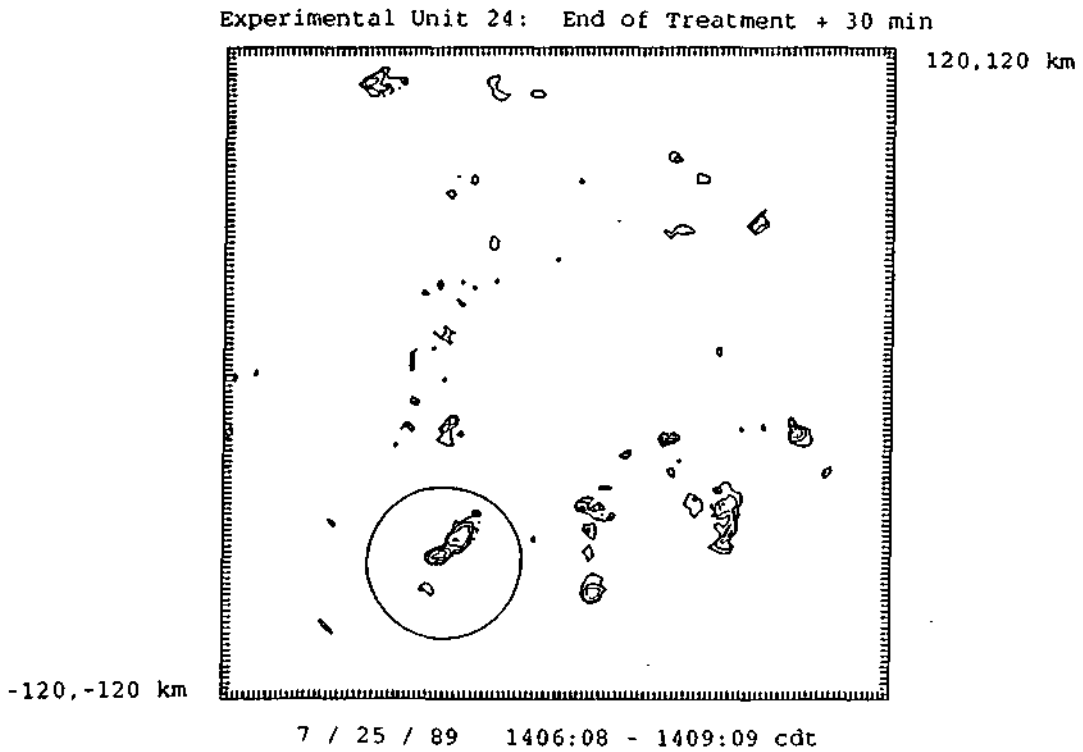
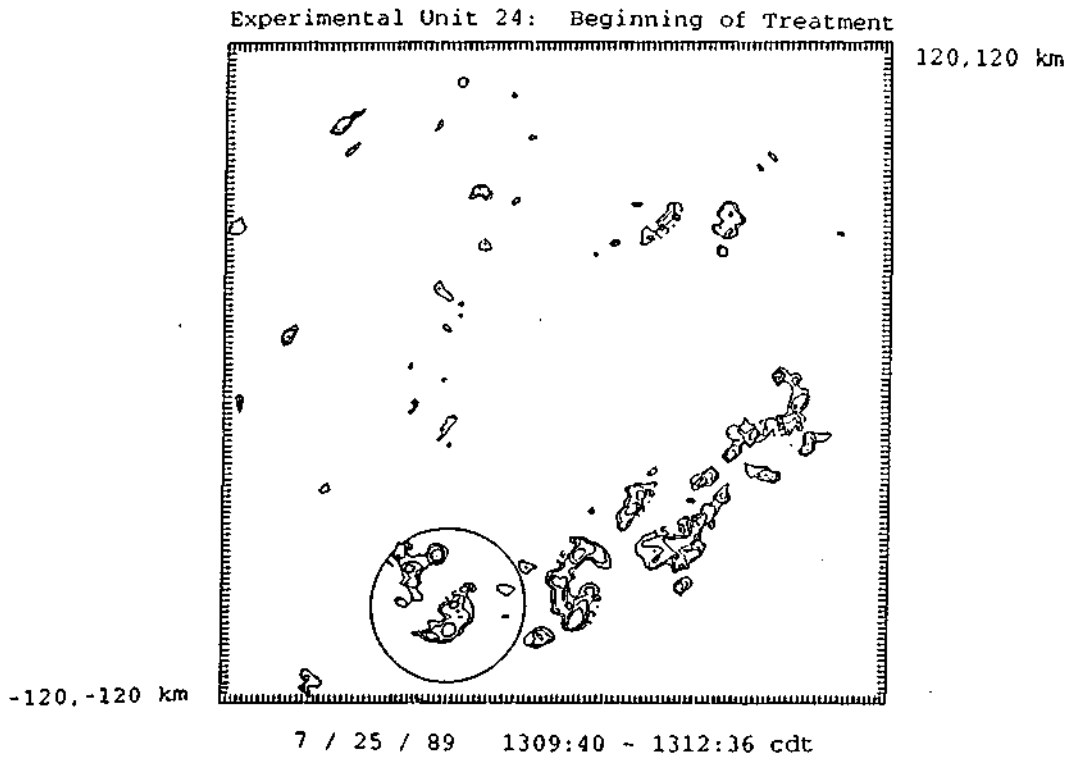


Figure G.49. CAPPIs of radar reflectivity at the 1 km AGL level for Experimental Unit 24, on July 25, 1989.

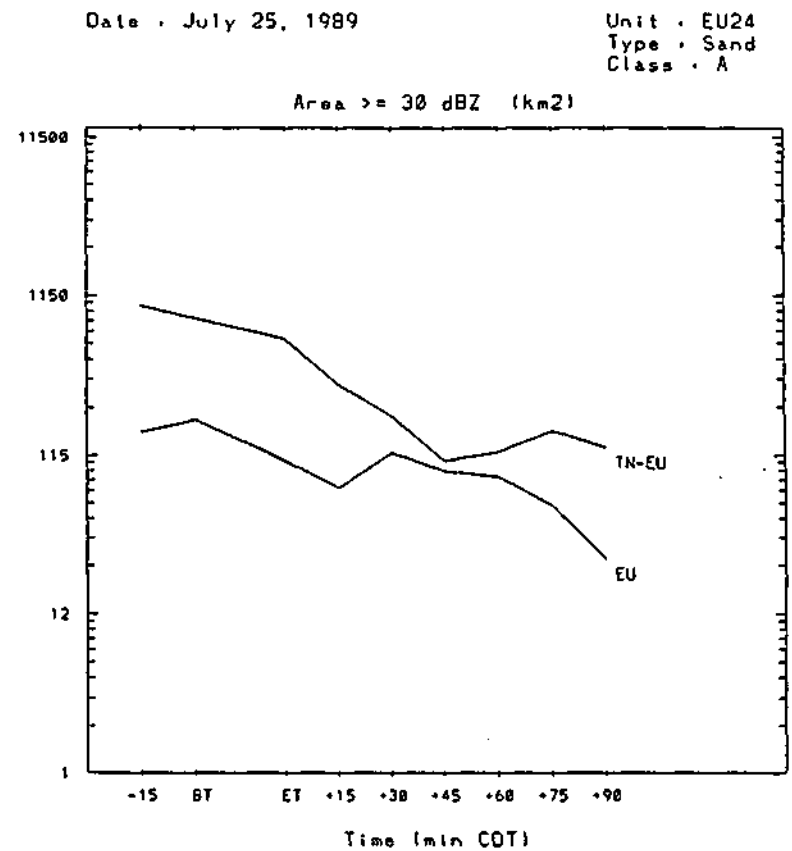
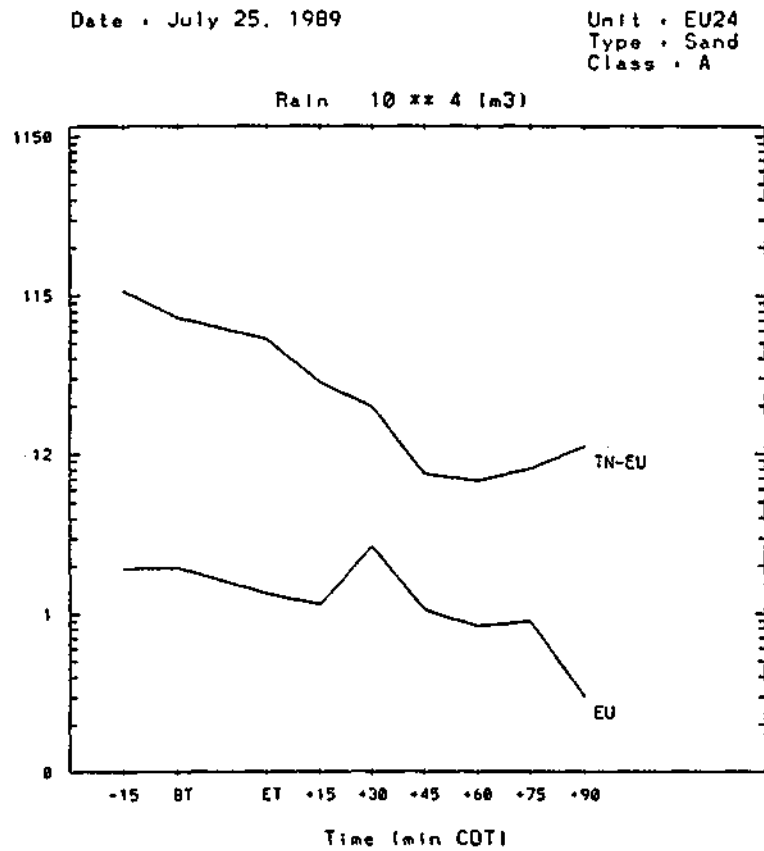
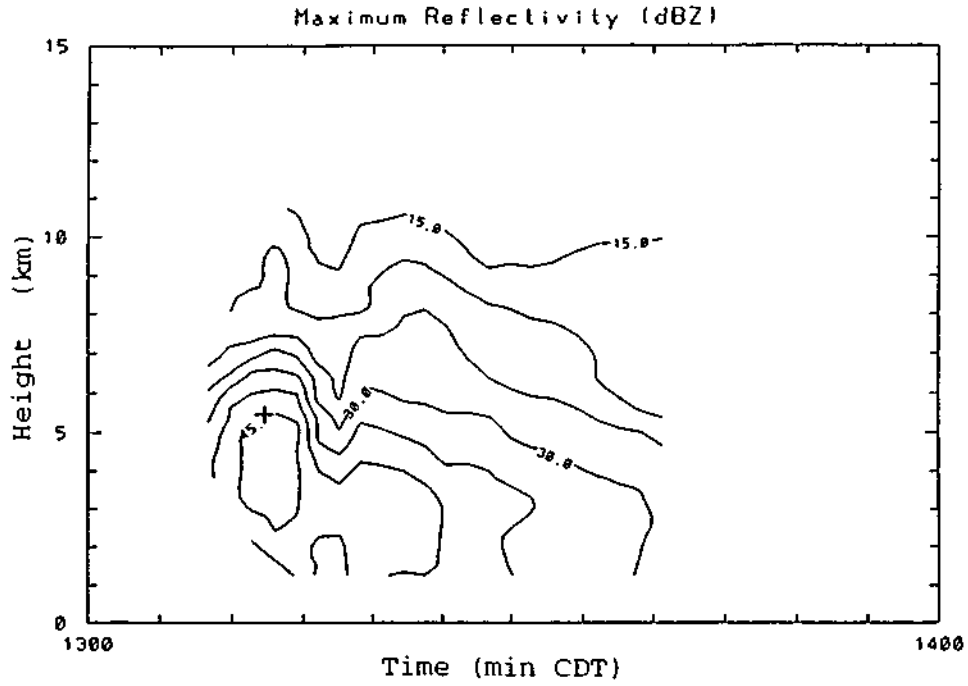


Figure G.50. Time history of radar-estimated rain volume ( $10^4$  m<sup>3</sup>) and echo area for reflectivities  $\geq 30$  dBZ (km<sup>2</sup>) in and around Experimental Unit 24, on July 25, 1989.

EU24EC01a 072589



EU24EC03a

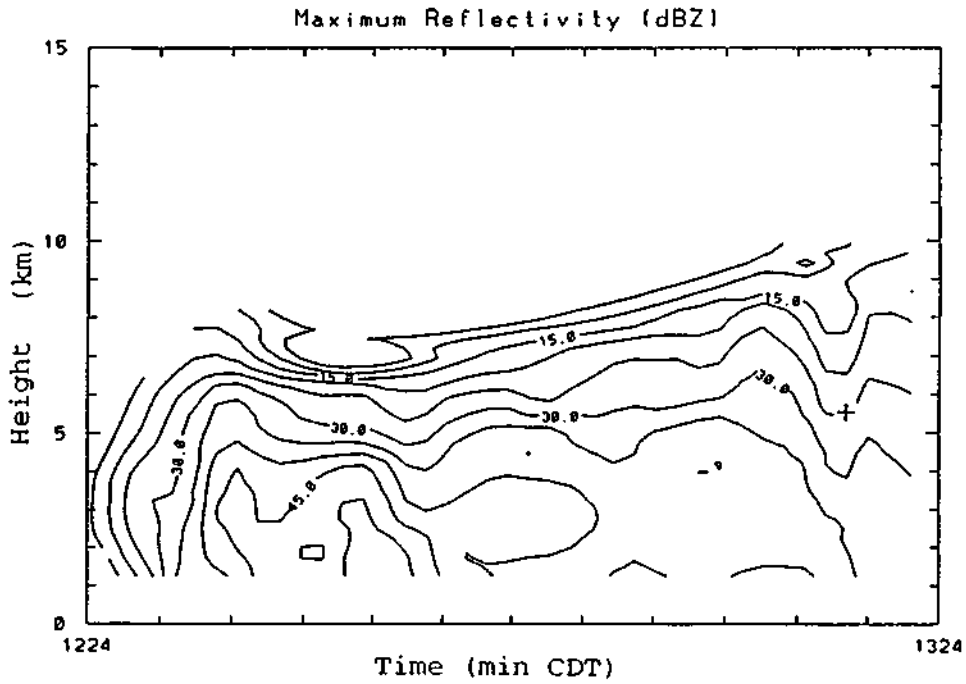
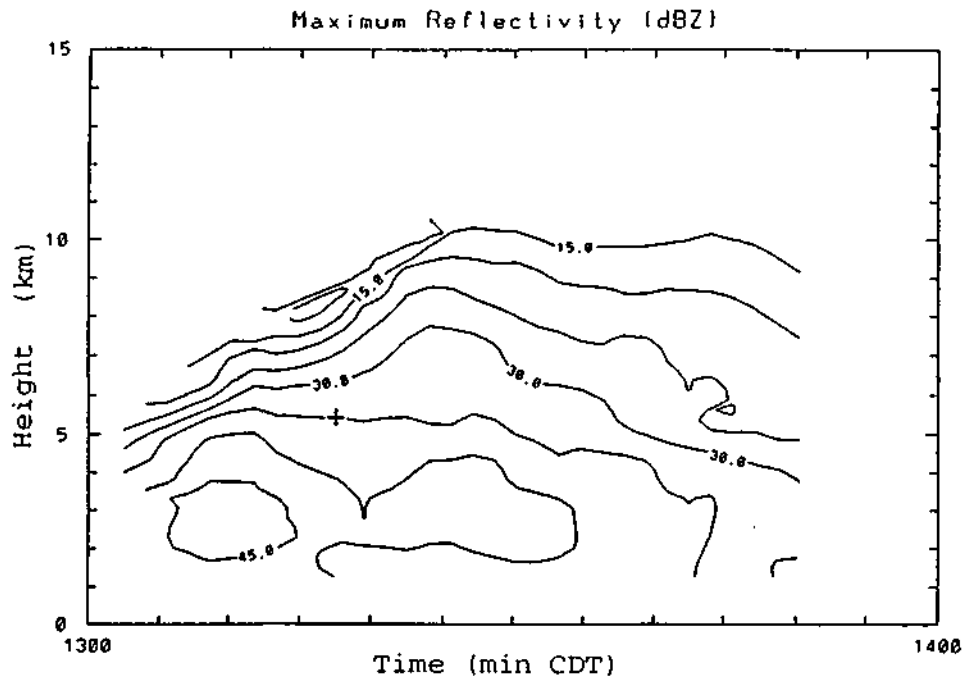


Figure G.51. Time-height histories of the reflectivity cores for clouds EU24EC01a and EU24EC03a in Experimental Unit 24, on July 25, 1989.

EU24EC04a 072589



EU24EC05a 072589

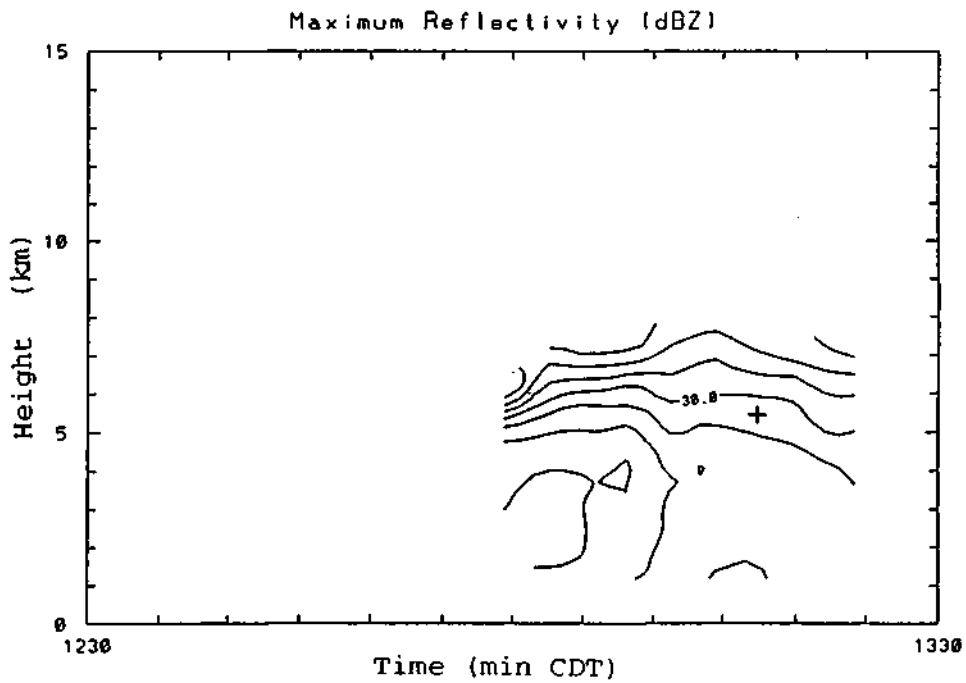
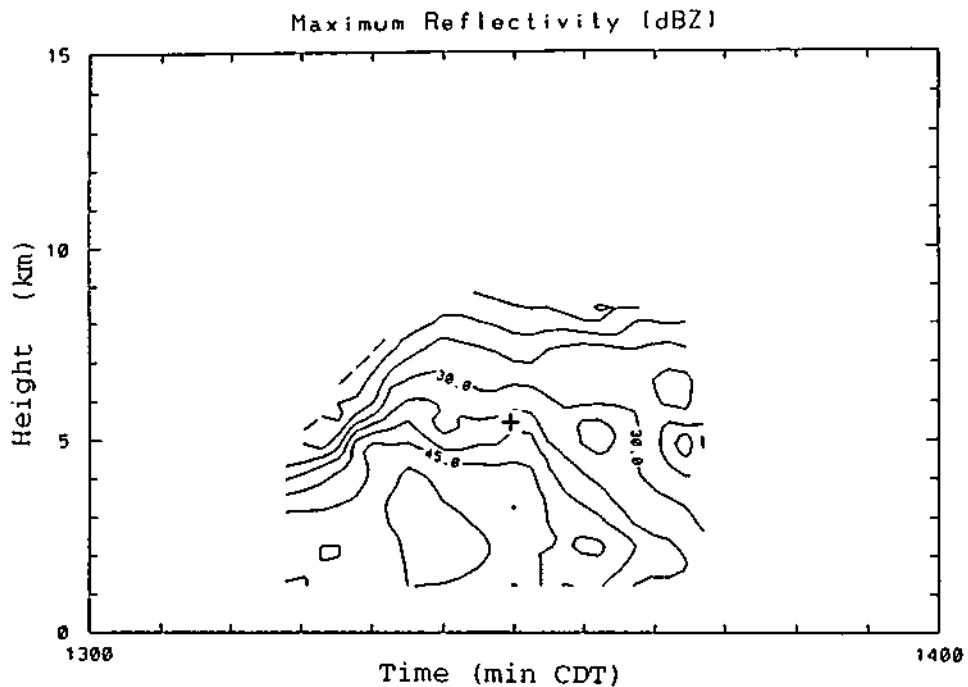


Figure G.52. Time-height histories of the reflectivity cores for clouds EU24EC04a and EU24EC05a in Experimental Unit 24, on July 25, 1989.

EU24EC06a 072589



EU24EC07a 072589

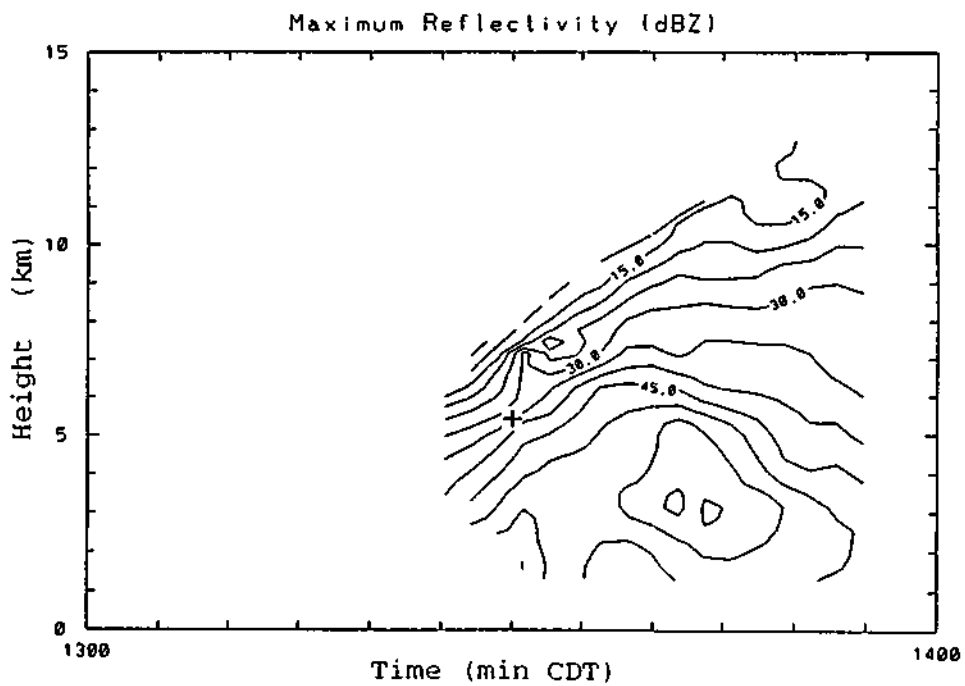
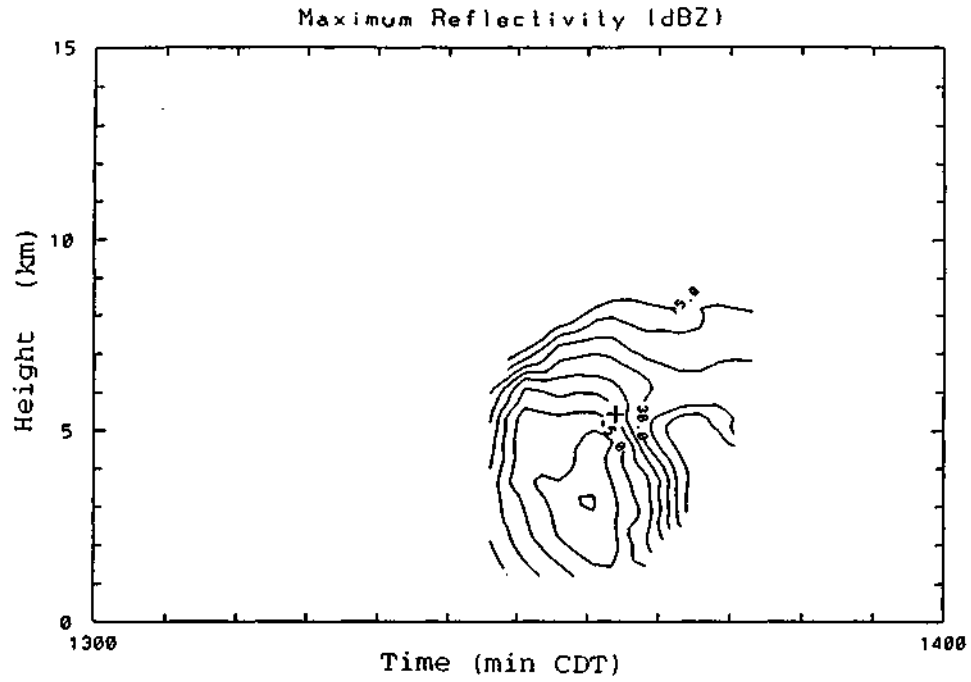


Figure G.53. Time-height histories of the reflectivity cores for clouds EU24EC06a and EU24EC07a in Experimental Unit 24, on July 25, 1989.

EU24EC08a 072589



EU24EC09a

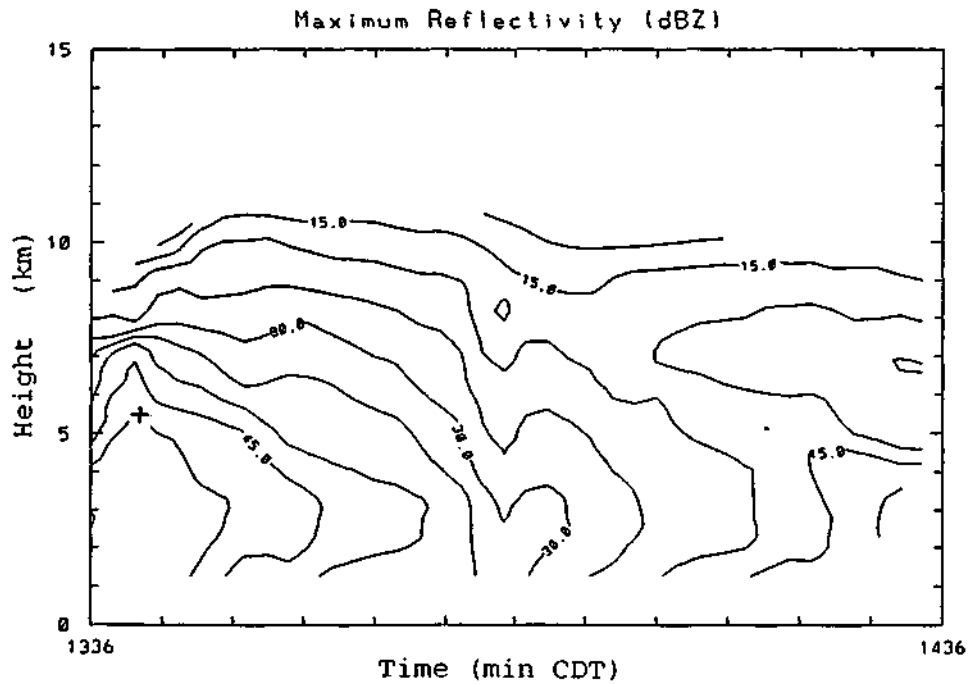


Figure G.54. Time-height histories of the reflectivity cores for clouds EU24EC08a and EU24EC09a in Experimental Unit 24, on July 25, 1989.

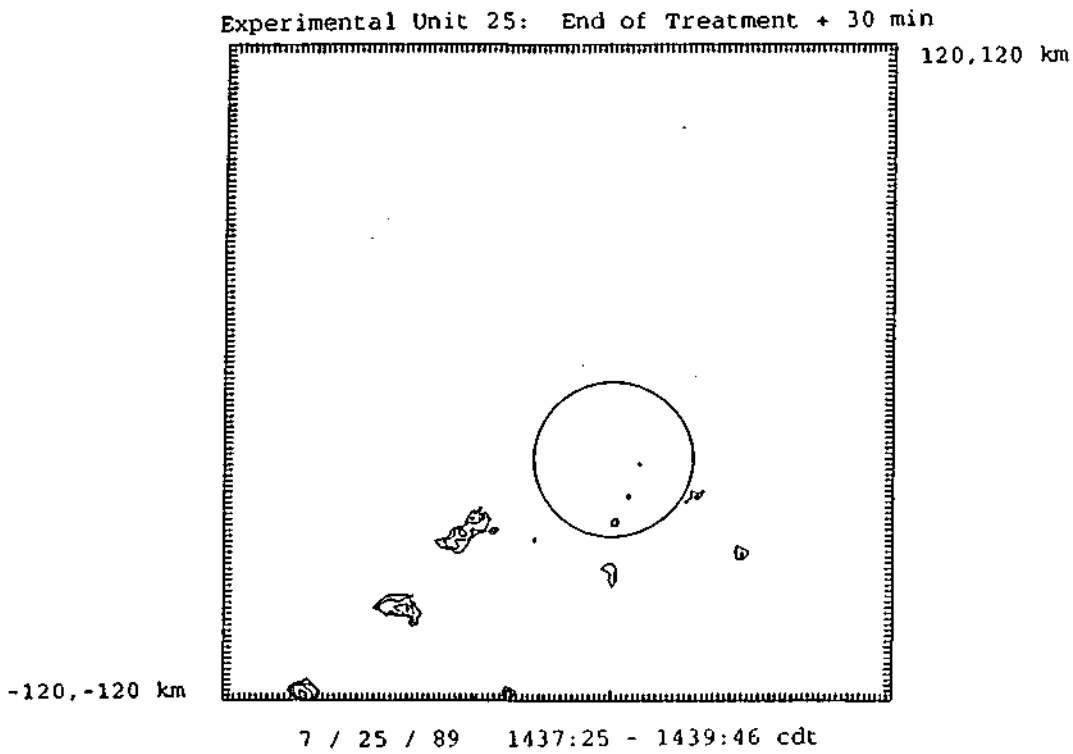
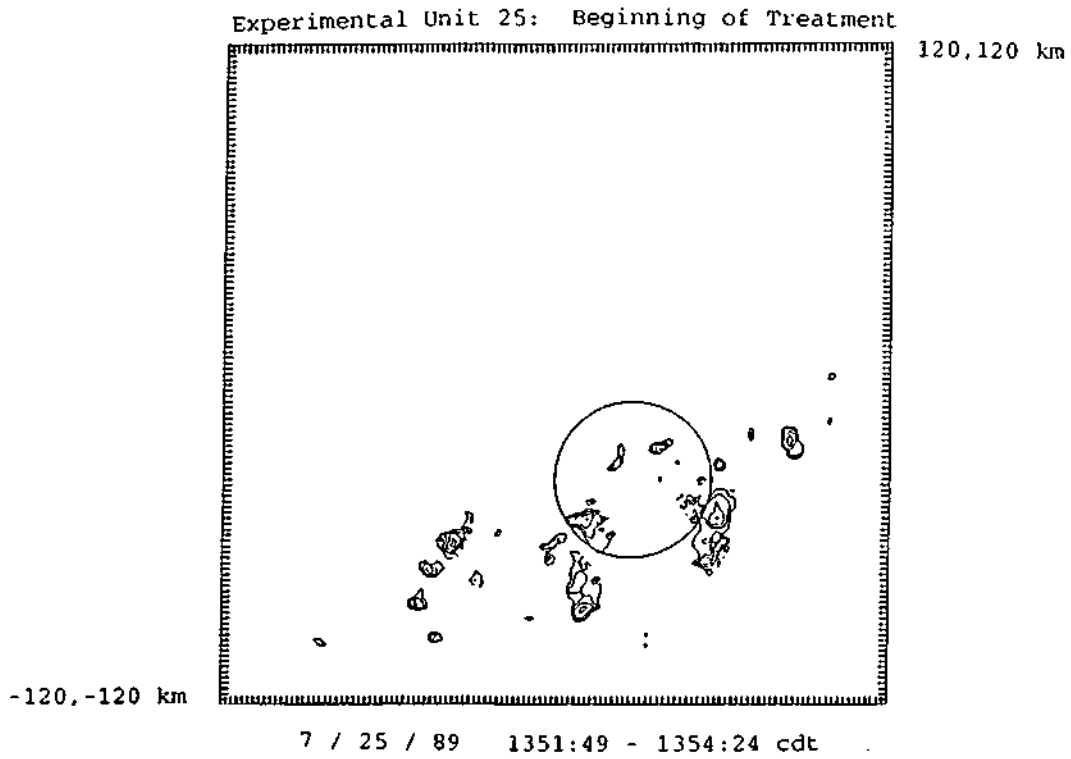


Figure G.55. CAPPi of radar reflectivity at the 1 km AGL level for Experimental Unit 25, on July 25, 1989.

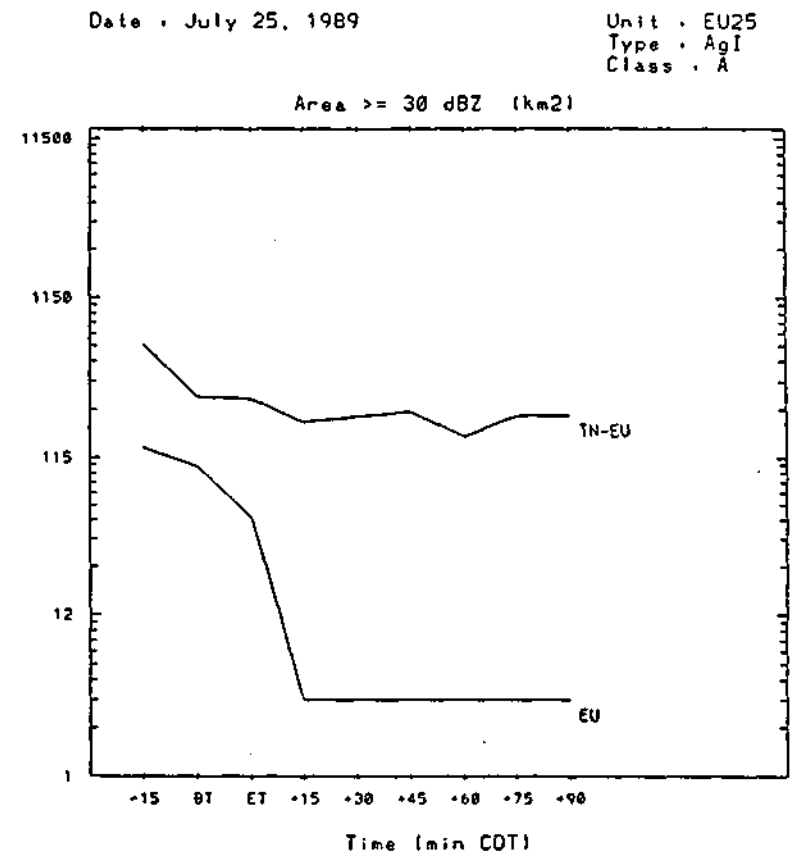
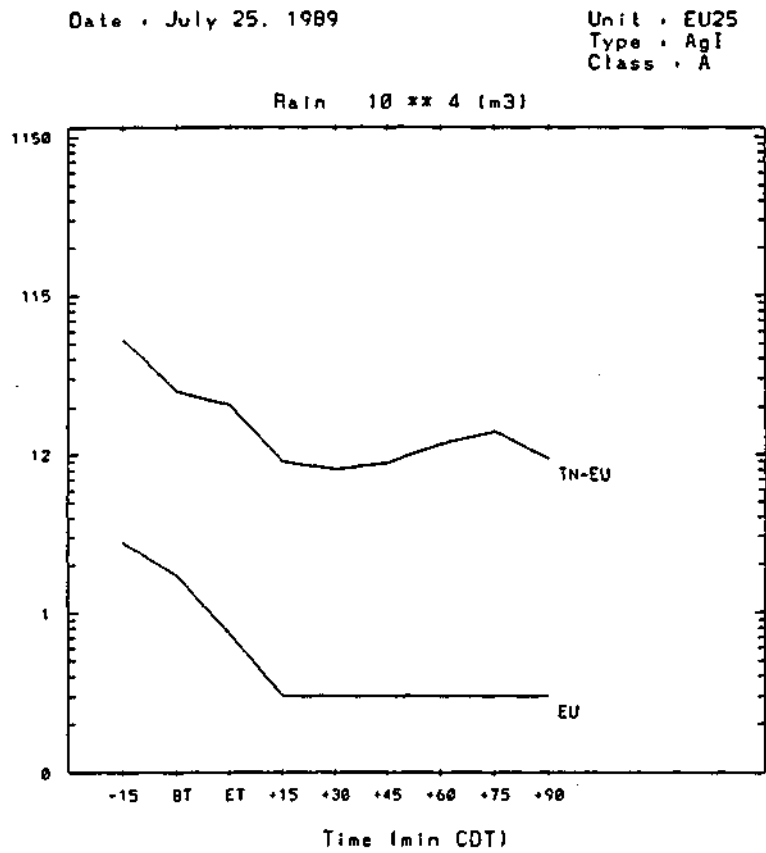


Figure G.56. Time history of radar-estimated rain volume ( $10^4 \text{ m}^3$ ) and echo area for reflectivities  $\geq 30 \text{ dBZ}$  ( $\text{km}^2$ ) in and around Experimental Unit 25, on July 25, 1989.

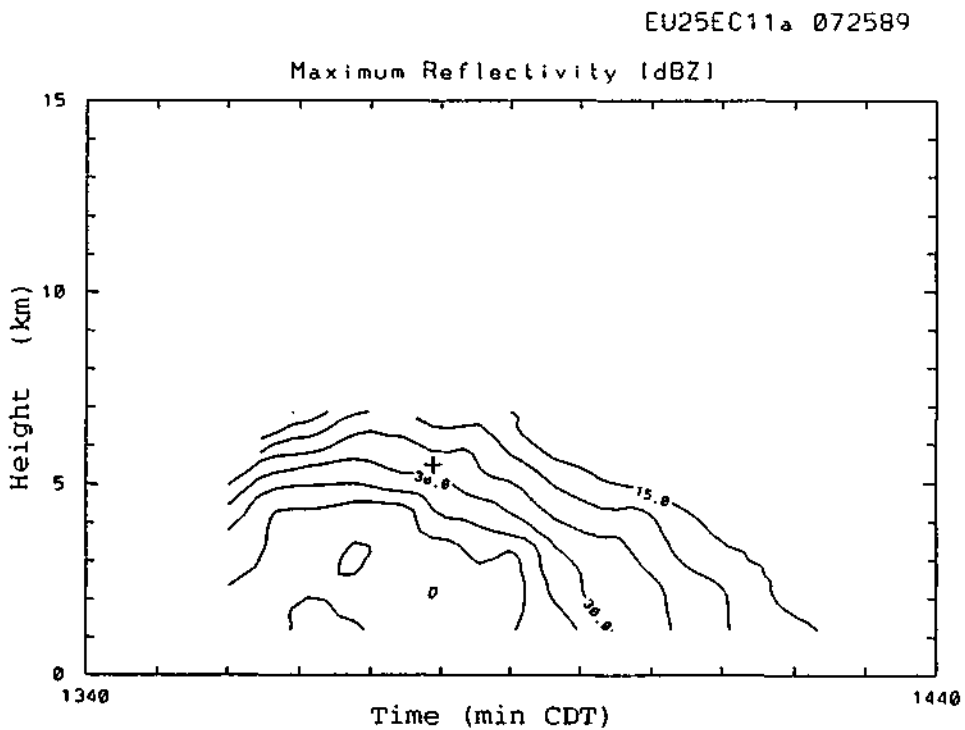
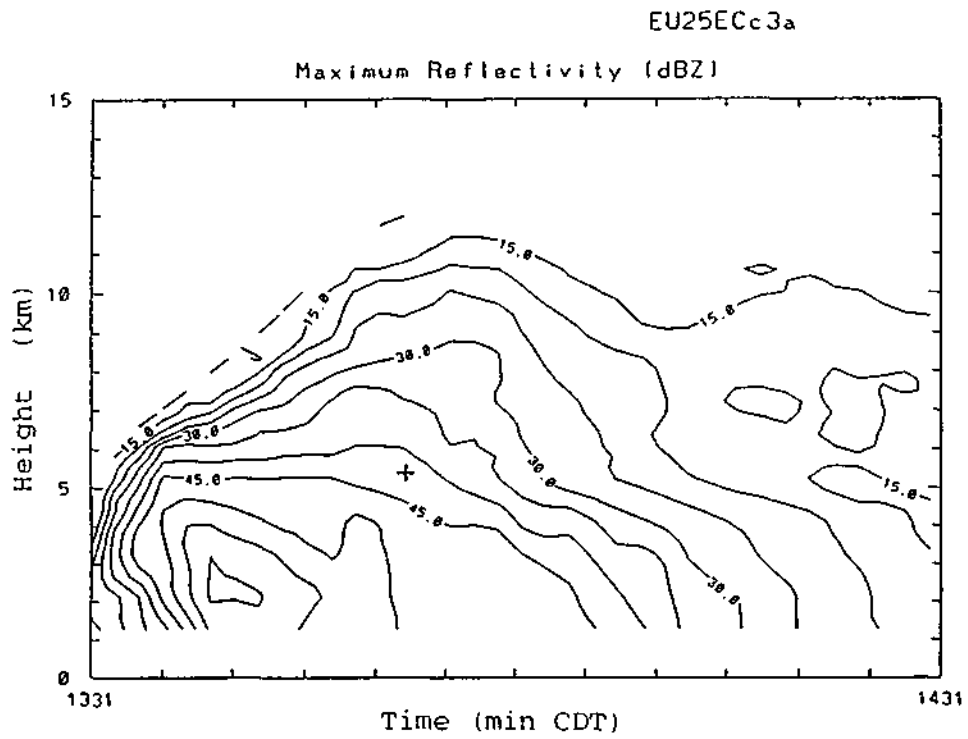


Figure G.57. Time-height histories of the reflectivity cores for clouds EU25ECc3a and EU25EC11a in Experimental Unit 25, on July 25, 1989.

EU25EC12a 072589

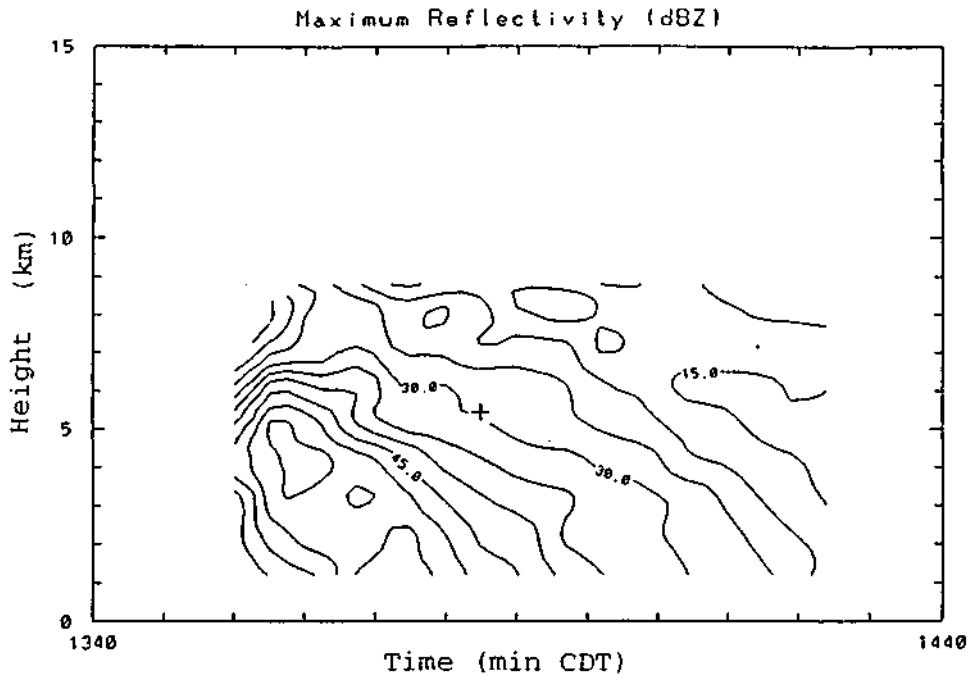


Figure G.58. Time-height histories of the reflectivity cores for clouds EU25EC12a and in Experimental Unit 25, on July 25, 1989.

## **Part H**

### **Daily Synoptic and Mesoscale Charts**

This Part contains synoptic and mesoscale information available daily to the PACE staff from the forecasting/nowcasting system. A host of parameters were extracted/calculated from sounding data, using both the 0700 CDT sounding from Peoria (PIA), Illinois and, when available, the near mid-day sounding from the CLASS sounding system located at Champaign (CMI). These data are displayed in Tables H.1 and H.2; variable definitions can be found in Part A.

A large series of weather charts were provided to the staff, including not only in-house computer-generated maps, but also charts originating from outside the Illinois State Water Survey. The figures provided here are for each of the nine days on which experimental units occurred, and are in groups of four:

1. Synoptic charts -- Standard weather charts produced by the National Meteorological Center were available via Zephyr Weather Service. In this document, the 1200 GMT surface charts, the 500-mb heights maps, the maximum/minimum temperature charts, and 24-hour precipitation maps from NOAA's Daily Weather Map Series are provided. Shading on the surface chart represents areas of precipitation at the time of observation.
2. Skew-T/Log-P thermodynamic charts -- Sounding traces were available for surrounding NWS rawinsonde sites, plus the CLASS system located at CMI (when available). The heavy solid line in each figure represents the temperature trace; the heavy dashed line shows the dewpoint temperature trend.
3. Synoptic scale upper air objective analysis -- Various field parameters were produced over the eastern U.S. and overlaid on a height analysis at user selected mandatory levels. A frequent selection by the forecaster was a height/vorticity analysis at the 700 mb level shown with wind barbs at each rawinsonde site. These figures are shown here. Each full wind barb is  $5 \text{ ms}^{-1}$ .
4. Regional scale surface analyses -- Several parameters were available for objective analysis display at the surface. Shown here are divergence (heavy solid line) and streamlines (light solid line), both superimposed on a simple station model of NWS and FAA reporting sites at a time during treatment flights. Temperature and dewpoint temperature ( $^{\circ}\text{F}$ ), along with wind barbs (each full barb =  $5 \text{ ms}^{-1}$ ) are shown at each site where available. Divergence values are  $10^{-5} \text{ s}^{-1}$ .

Table H. 1. Forecasting/nowcasting parameters at PIA during PACE 1989.

date yyymmddhh	max top		surface			100mb surface average							at 0°C		at -10°C		dh38 (m)	pw (m)
	l00 (kft)	R0 (kft)	temp (°C)	dpt (°C)	ct (°C)	dlbar (°C)	plcl (mb)	dcl (°C)	hlcl (m)	pecl (mb)	tecl (°C)	hecl (m)	pres (mb)	hgt (m)	pres (mb)	hgt (m)		
89051907	43	34	18.6	15.9	22.4	14.1	908	13.6	907	882	13.2	1148	666	3470	529	5277	875	3.3
89060107	53	53	21.2	20.0	28.1	19.0	912	18.6	929	880	18.0	1235	617	4192	540	5691	652	4.4
89062307	55	55	20.4	20.4	31.8	17.9	898	17.2	1073	822	15.8	1829	605	4353	488	6058	833	3.1
89070807	53	53	22.4	15.4	28.9	17.3	857	16.0	1496	741	13.8	2748	594	4556	497	5957	552	3.8
89071107	58	58	23.6	22.7	34.1	19.9	878	18.9	1293	822	17.9	1860	580	4726	480	6237	704	3.9
89071907	40	40	18.0	18.0	22.8	16.3	921	16.1	757	903	15.8	919	645	3712	517	5448	850	3.7
89072307	35	35	17.8	17.5	28.3	17.6	913	17.0	992	867	16.2	1436	626	4119	500	5890	883	3.1
89072407	52	49	20.4	20.4	27.6	19.2	929	18.8	853	897	18.3	1156	608	4378	484	6166	717	4.1
89072507	45	45	20.6	20.1	28.2	19.6	928	19.3	854	895	18.7	1173	597	4547	474	6363	873	4.8

286

Table H.1 (cont). Forecasting/nowcasting parameters at PIA during PACE 1989.

date yyymmddhh	850 winds		500 winds		indices													
	dir (°)	spd (ms <sup>-1</sup> )	dir (°)	spd (ms <sup>-1</sup> )	L (°C)	epe (%)	pb (°C)	li (°C)	ki (°C)	mki (°C)	jef (°C)	msh (°C)	swt (°C)	ptop (mb)	CAPE	vshr	Ri	
89051907	190	15.9	180	23.1	-3.2	50.7	0.8	0.3	33.8	40.1	32.9	8.5	180.9	478	56	51.9	1.1	
89060107	255	11.3	230	20.1	1.6	-25.5	6.4	-5.2	38.1	43.3	37.2	5.3	298.7	390	758	17.2	44.1	
89062307	230	8.7	205	12.3	1.1	-17.5	4.8	-2.1	24.8	30.8	32.9	10.7	166.5	188	772	22.1	35.0	
89070807	285	5.1	340	14.4	8.9	-141.5	8.2	-3.7	30.6	31.6	39.3	8.1	356.6	166	1031	25.0	41.3	
89071107	260	7.2	230	8.7	3.1	-48.9	7.2	-5.4	30.8	36.8	36.0	9.1	237.5	194	867	2.3	382.3	
89071907	270	3.1	265	7.7	-3.2	51.4	2.3	-1.6	35.5	41.2	33.6	7.8	151.9	426	163	13.9	11.7	
89072307	165	5.7	175	12.3	-1.5	24.0	3.5	-1.9	28.0	34.2	30.0	11.6	119.7	252	474	2.6	180.5	
89072407	185	3.1	190	11.3	-3.8	61.0	3.4	-2.2	30.2	36.3	33.1	10.4	180.7	229	420	8.5	49.3	
89072507	170	2.6	165	4.1	-4.0	42.8	3.6	-2.4	36.4	41.6	33.9	6.5	184.5	217	431	1.5	283.8	

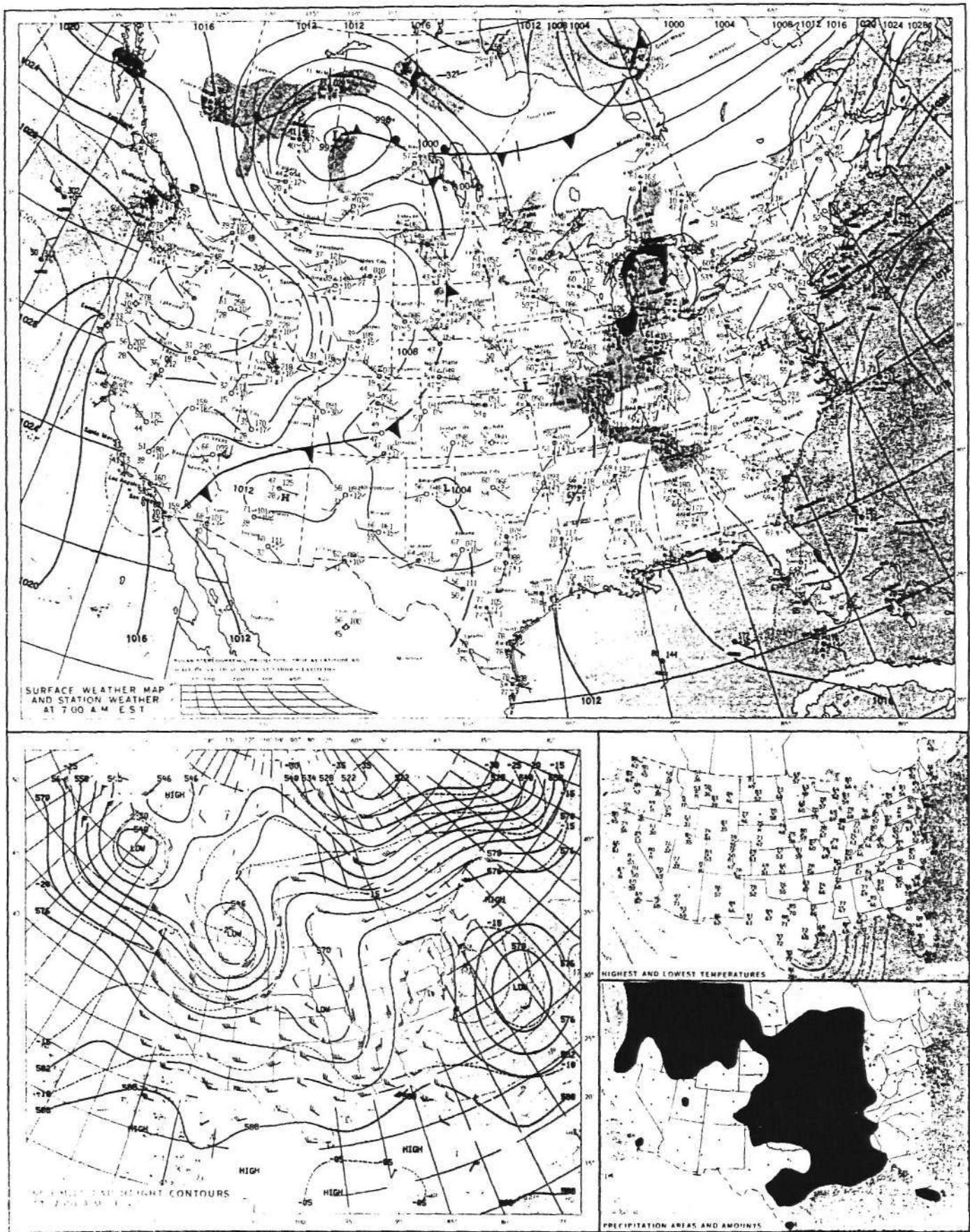
Table H.2. Forecasting/nowcasting parameters at CMI during PACE 1989.

date yyymmddhh	max top		surface			10hmb surface average							at 10°C		at -10°C		dh38 (m)	pw (m)
	100 (kft)	80 (kft)	temp (°C)	dpt (°C)	ct (°C)	dbar (°C)	plcl (mb)	tlcl (°C)	hlcl (m)	pecl (mb)	tecl (°C)	becl (m)	pees (mb)	hgt (m)	pees (mb)	hgt (m)		
89060112	53	53	29.2	19.7	30.5	17.6	866	16.5	1383	833	15.9	1720	612	4262	485	6084	978	3.3
89062312	55	55	29.7	16.3	32.6	15.2	804	13.3	1988	779	12.8	2248	600	4394	476	6213	1018	3.4
89070813	53	53	34.6	22.2	33.9	18.5	820	16.8	1872	807	16.5	2015	604	4409	499	5902	676	4.7
89071113	58	58	33.9	20.9	34.8	18.5	819	16.8	1847	793	16.3	2117	569	4849	461	6505	980	3.7
89071912	40	40	25.7	17.3	25.5	14.9	869	14.1	1206	846	13.7	1435	629	3878	500	5682	1018	3.4
89071917	40	40	23.2	18.4	24.5	16.3	905	15.8	948	884	15.4	1152	623	4034	506	5675	737	4.0

287

Table H.2 (cont). Forecasting/nowcasting parameters at CMI during PACE 1989.

date yyymmddhh	850 winds		500 winds		indices													
	dir (°)	spd (ms <sup>-1</sup> )	dir (°)	spd (ms <sup>-1</sup> )	L (°C)	cpe (%)	pb (°C)	li (°C)	ki (°C)	mki (°C)	jef (°C)	msh (°C)	swt (°C)	ptop (mb)	CAPE	vshr	Ri	
89060112	252	9.3	244	29.2	0.0	-0.6	4.2	-3.0	29.7	39.8	33.0	11.6	189.4	195	552	38.1	14.5	
89062312	202	5.5	238	11.7	-0.5	7.3	2.2	-1.2	32.7	39.8	33.9	10.1	185.9	225	304	11.1	27.4	
89070813	248	5.9	331	12.8	5.2	-82.2	7.6	-7.2	42.7	52.8	39.7	2.5	375.0	185	1068	16.8	63.6	
89071113	259	6.8	287	9.6	0.6	-10.2	4.9	-4.0	31.1	40.9	34.5	10.2	194.8	200	655	2.5	256.9	
89071912	261	5.7	249	6.3	-3.1	49.0	1.1	-0.2	31.5	40.5	31.8	9.2	152.1	490	82	4.1	19.9	
89071917	358	5.4	250	6.3	-3.7	58.9	1.8	-0.9	35.3	43.1	33.0	7.0	162.3	455	108	0.3	323.2	



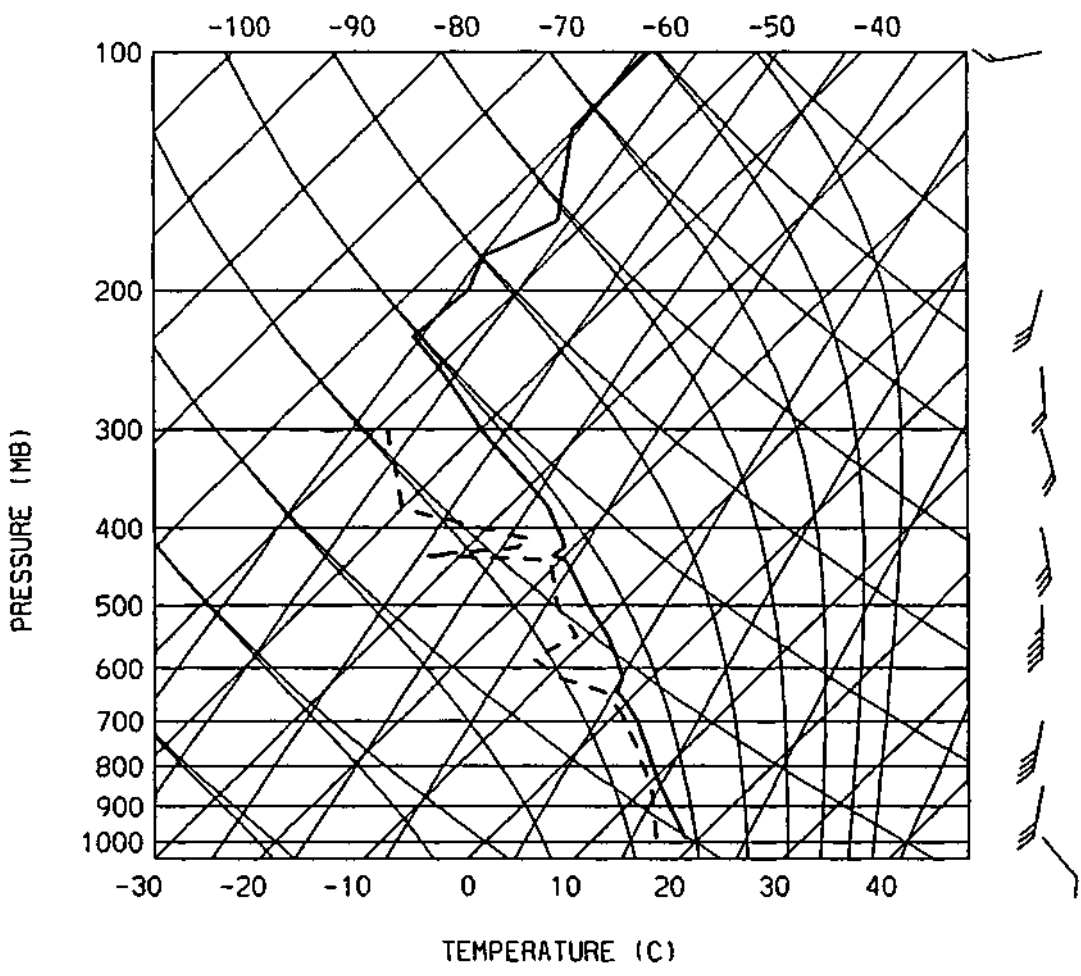
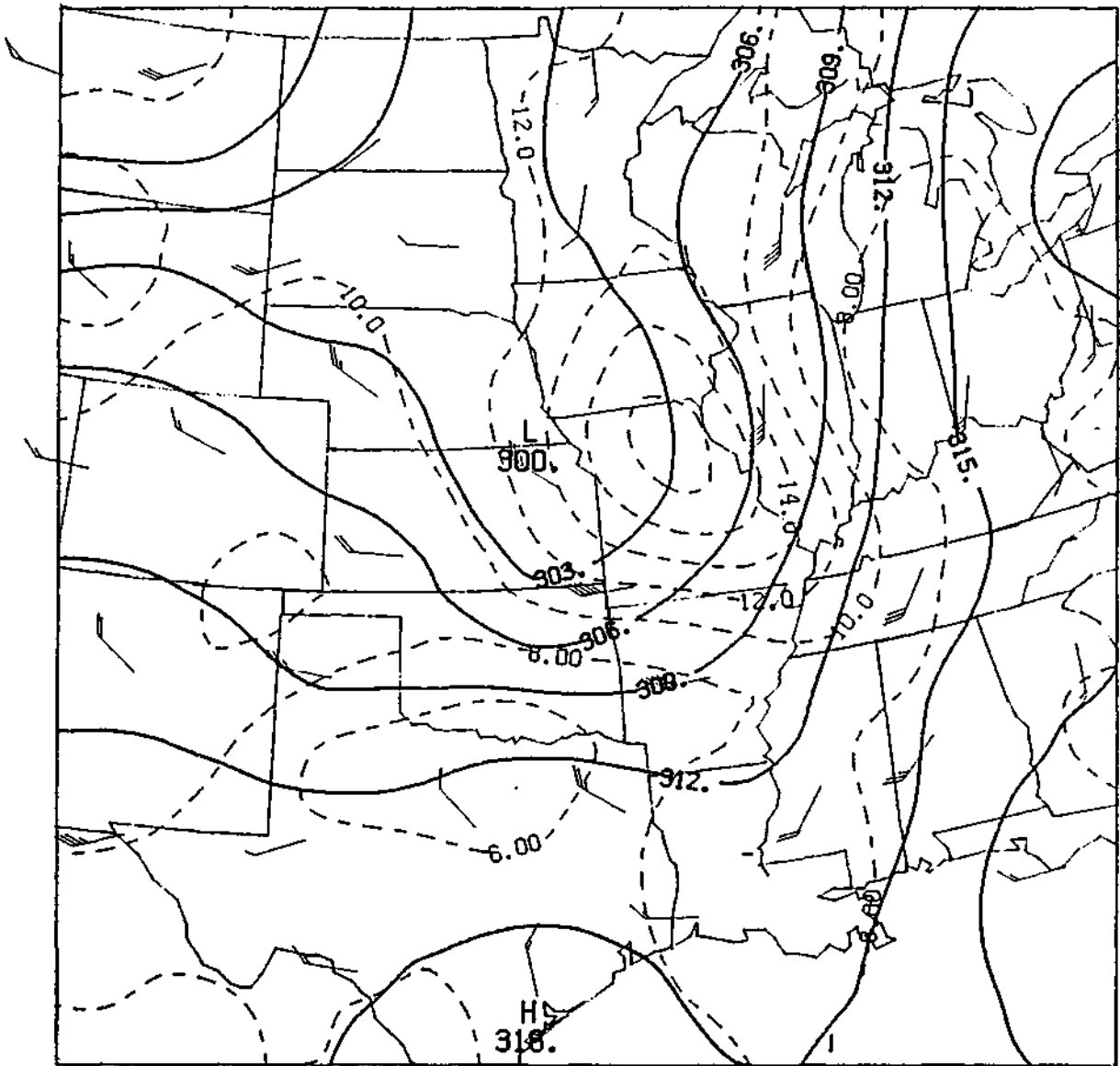


Figure H.2. Skew-T/Log-P chart at PIA for 0700 CDT on 19 May 1989.



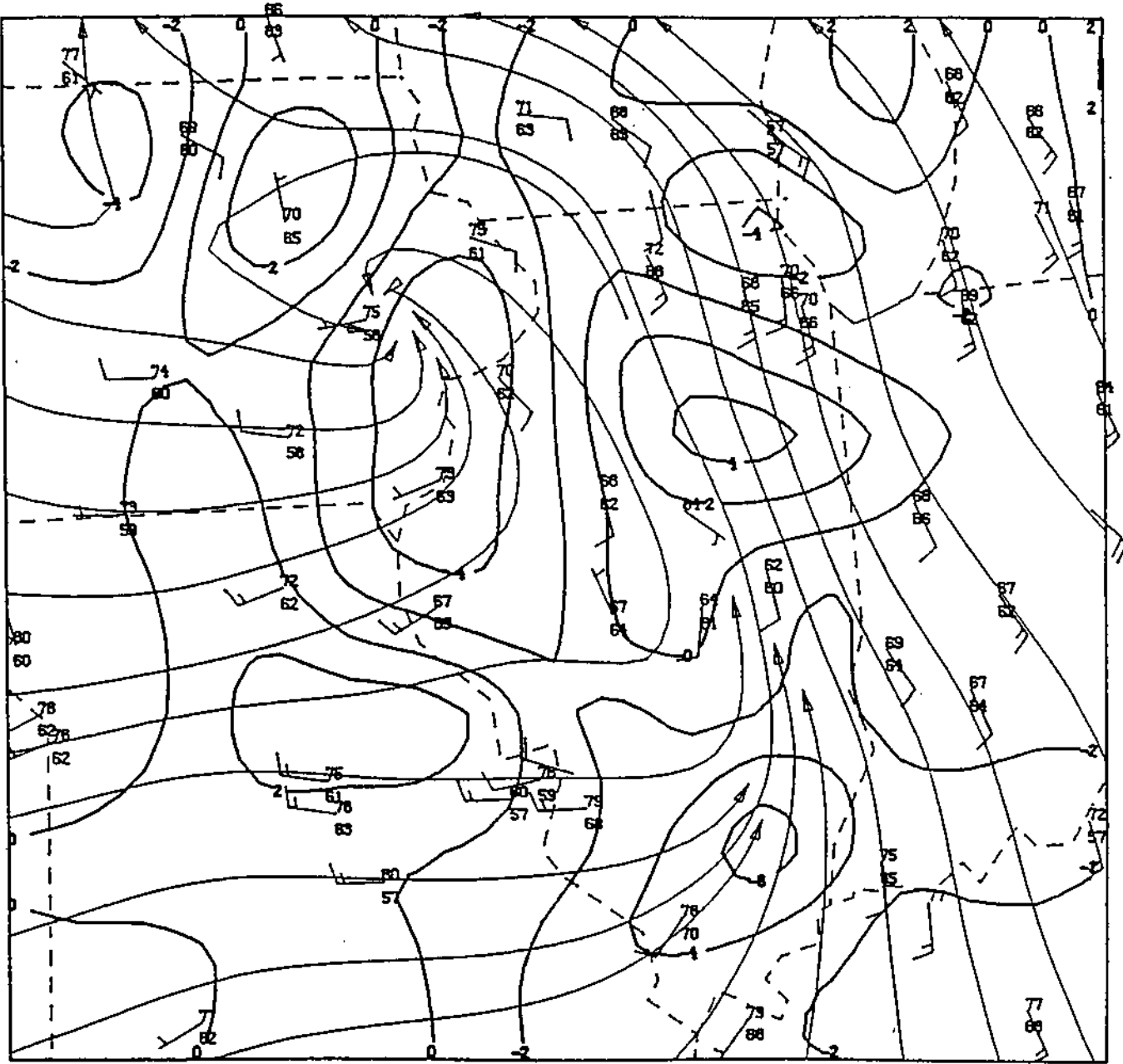


Figure H.4. Regional scale analysis for 1600 CDT on 19 May 1989.

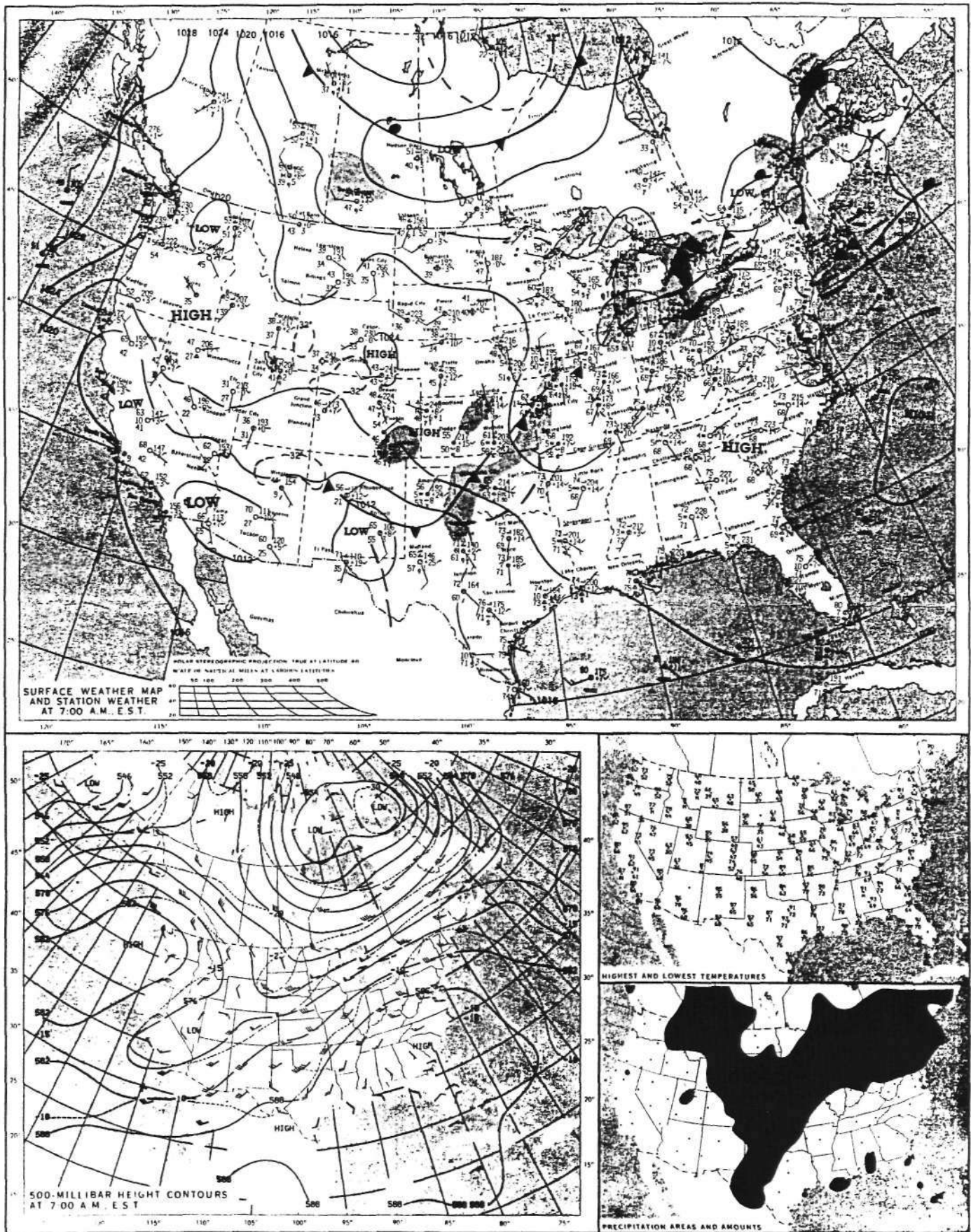


Figure H.5. Synoptic scale weather charts for 0700 CDT on 1 June 1989.

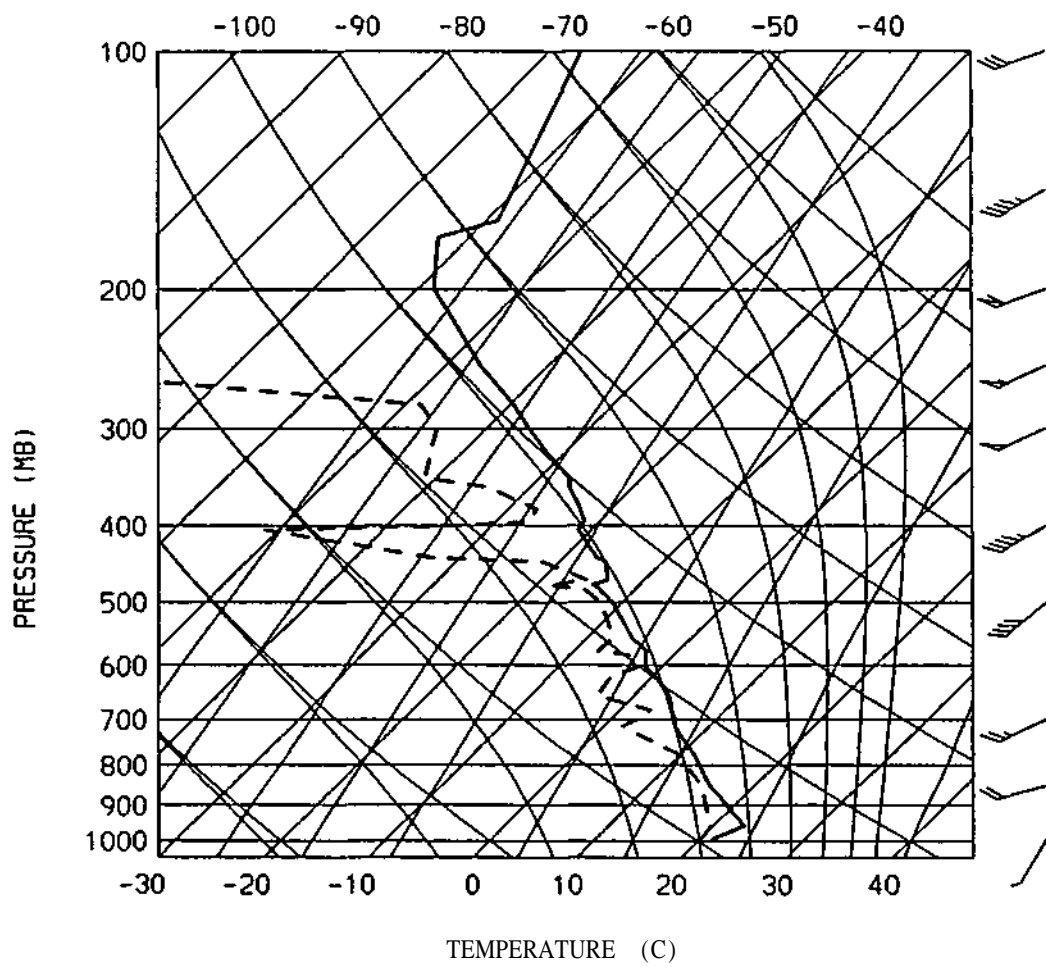


Figure H.6. Skew-T/Log-P chart at PIA for 0700 CDT on 1 June 1989.

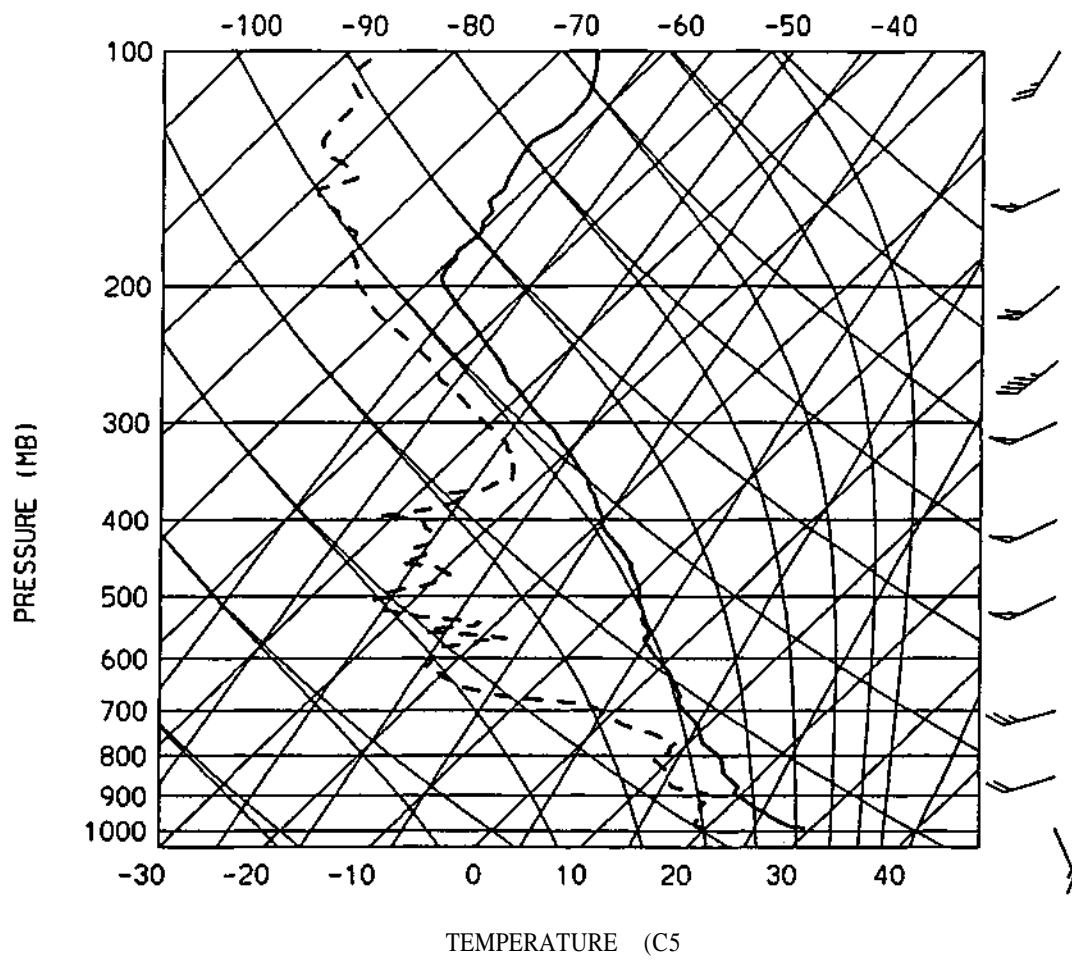


Figure H. 7. Skew-T/Log-P chart at CMI for 1200 CDT on 1 June 1989.

[Missing]

*Figure H.8. Height/vorticity chart at 700 mb for 0700 CDT on 1 June 1989.*

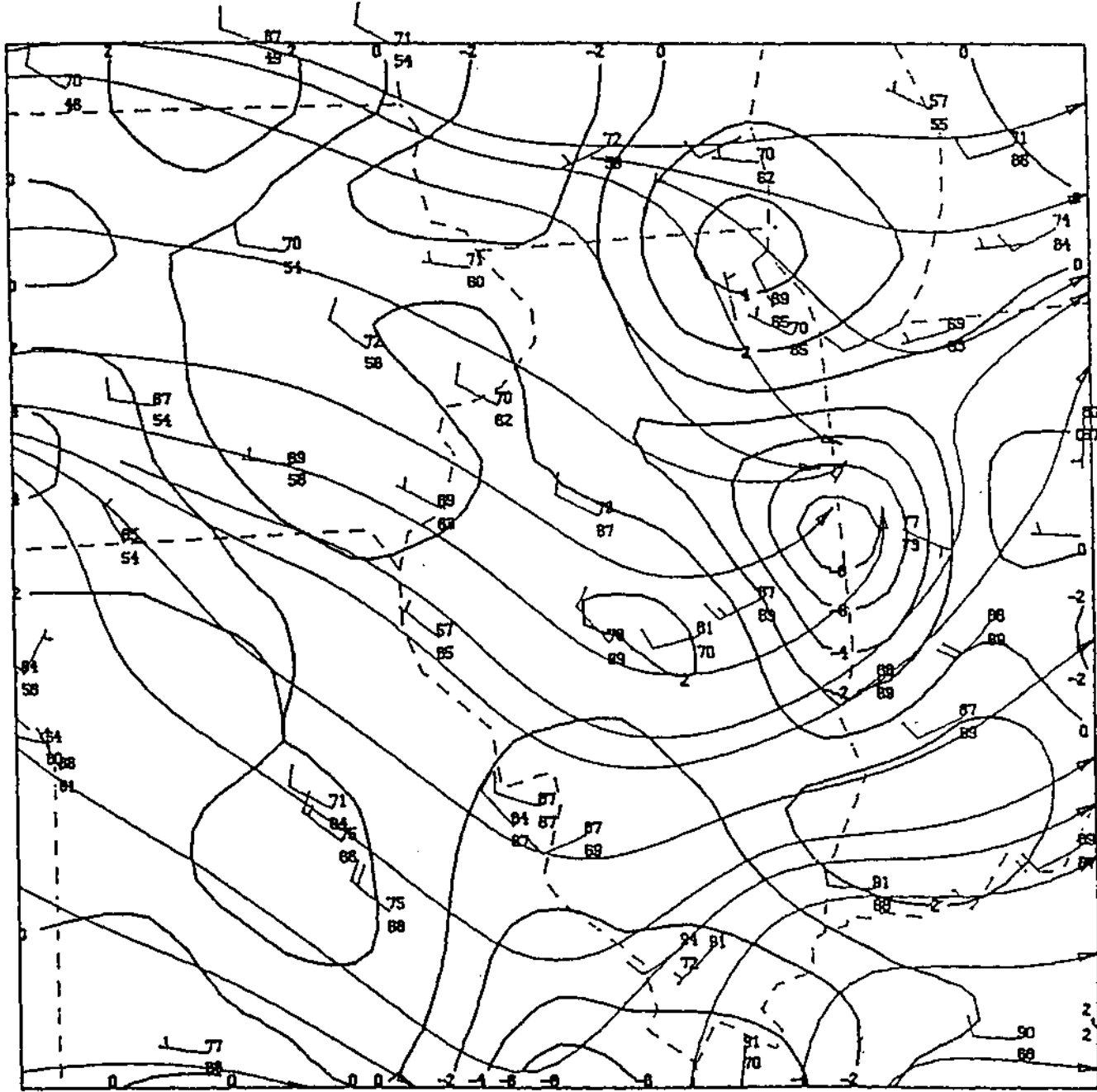


Figure H.9. Regional scale analysis for 1400 CDT on 1 June 1989.

FRIDAY, JUNE 23, 1989

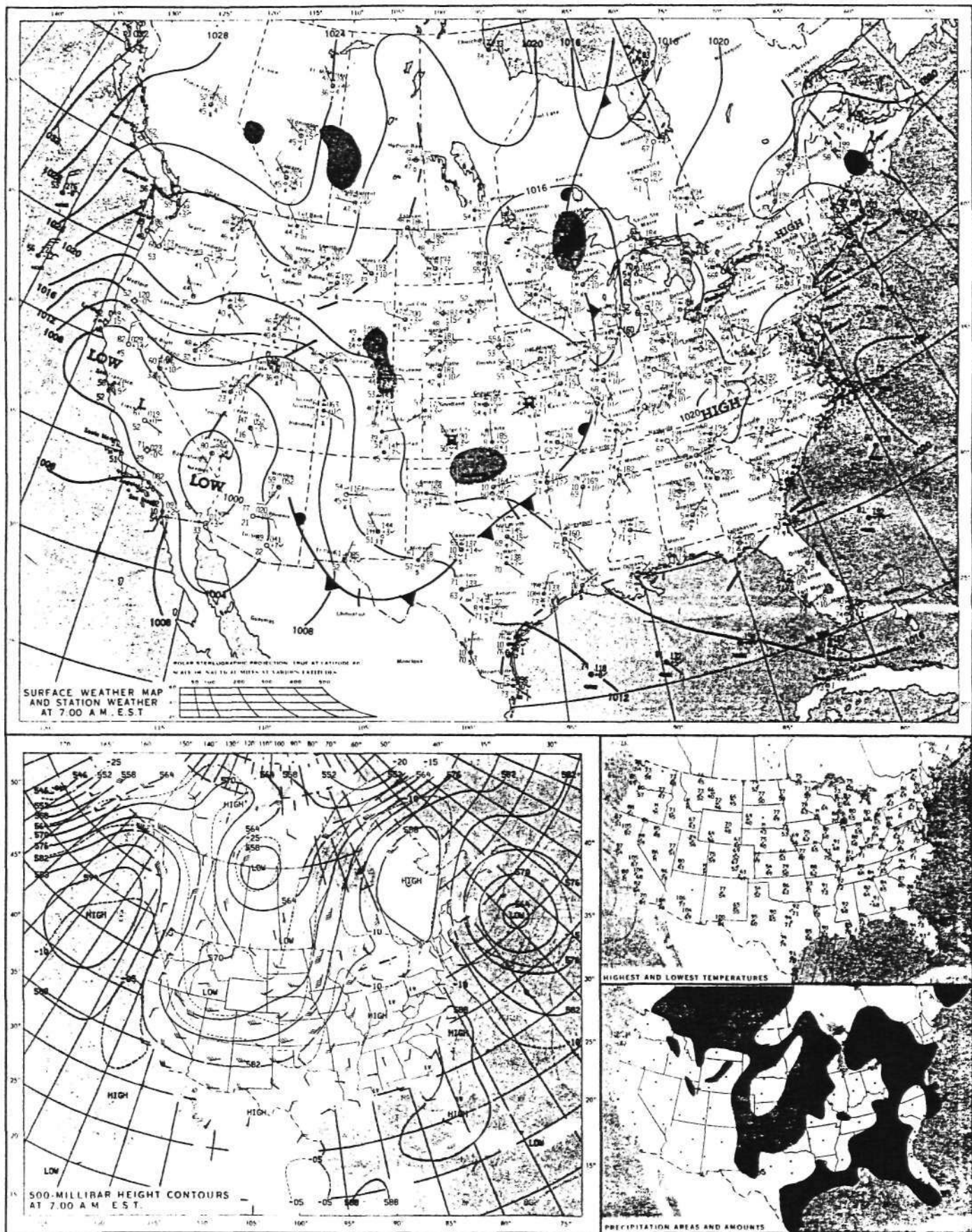


Figure H.10. Synoptic scale weather charts for 0700 CUT on 23 June 1989.

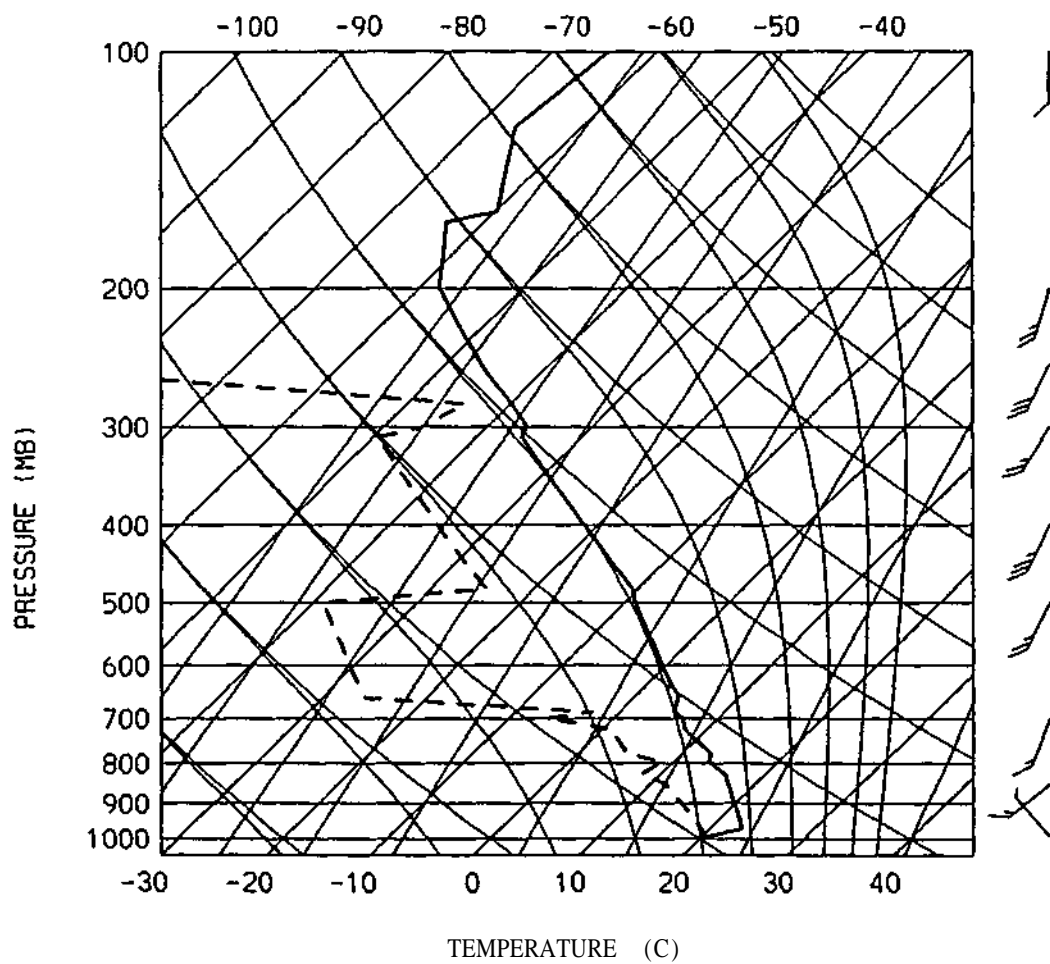


Figure H.11. Skew-T/Log-P chart at PIA for 0700 CDT on 23 June 1989.

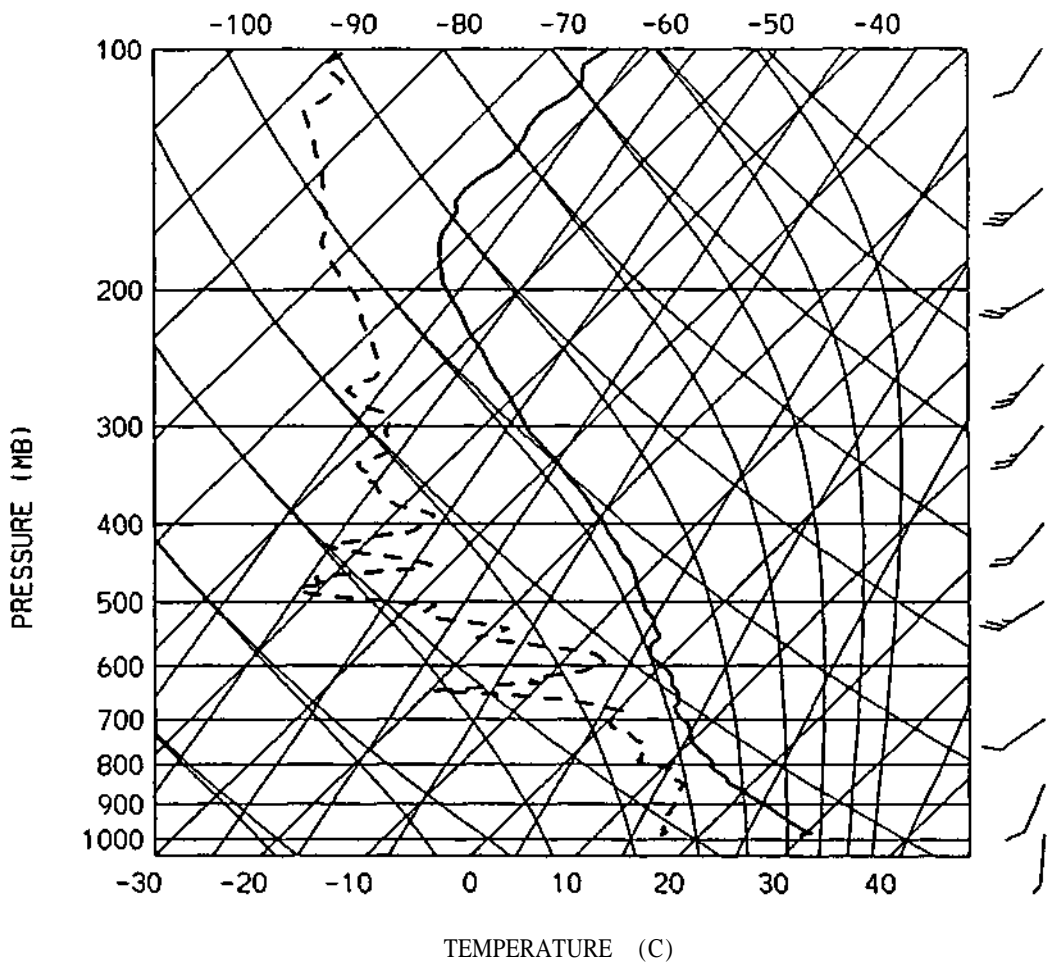


Figure H.12. Skew-T/Log-P chart at CMI for 1200 CDT on 23 June 1989.

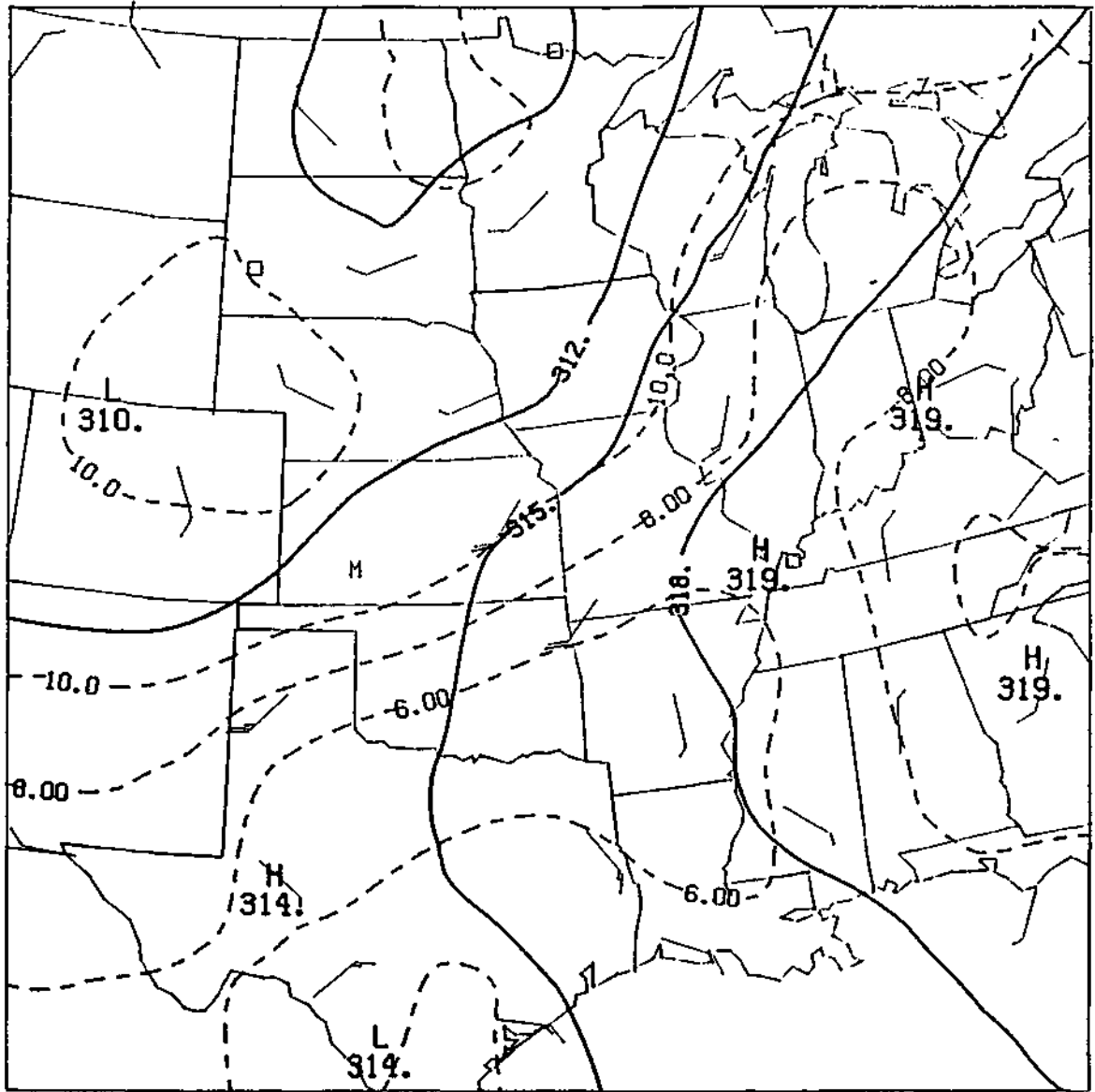


Figure H. 13. Height/vorticity chart at 700 mb for 0700 CDT on 23 June 1989.

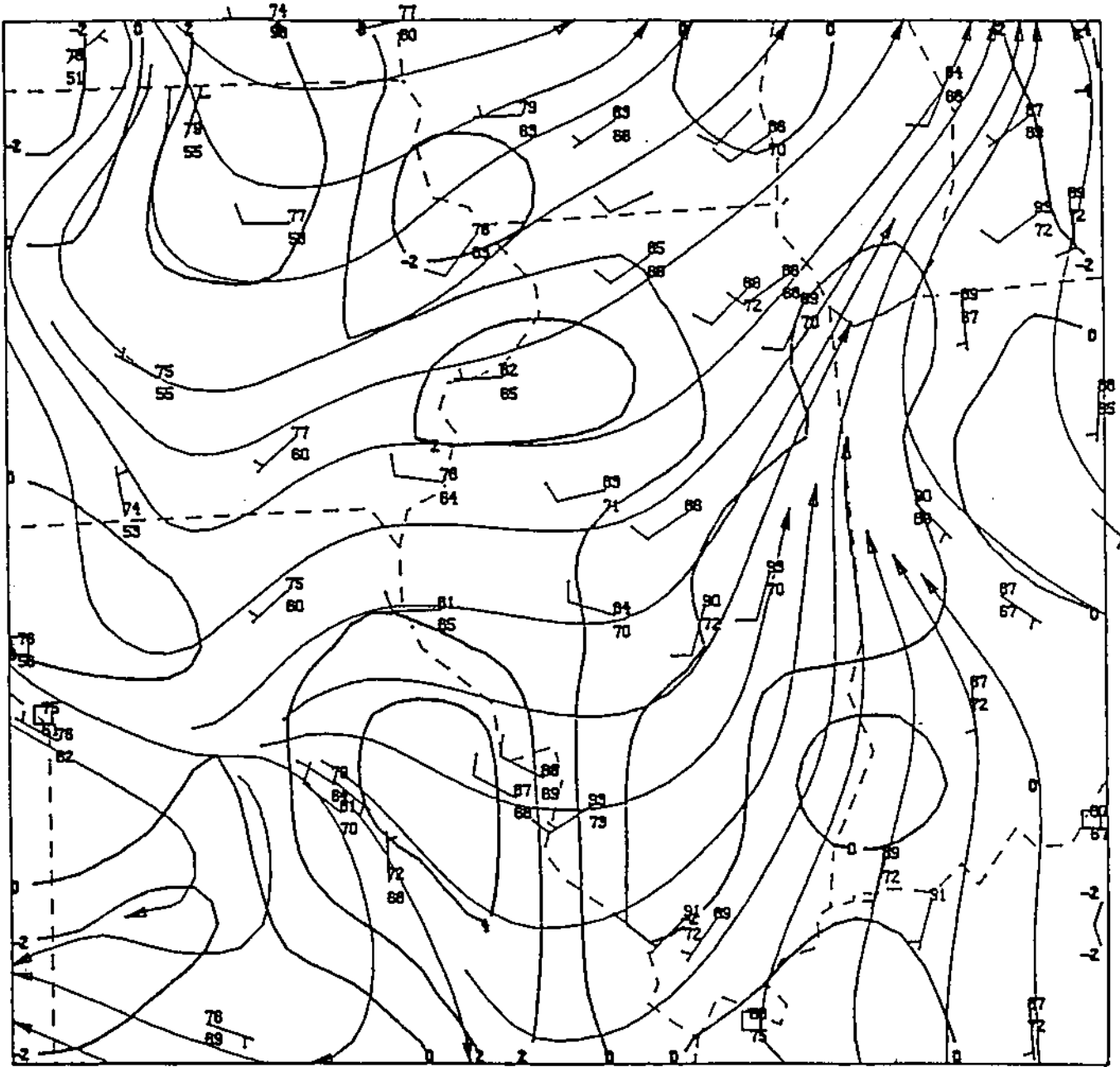


Figure H.14. Regional scale analysis for 1300 CDT on 23 June 1989.

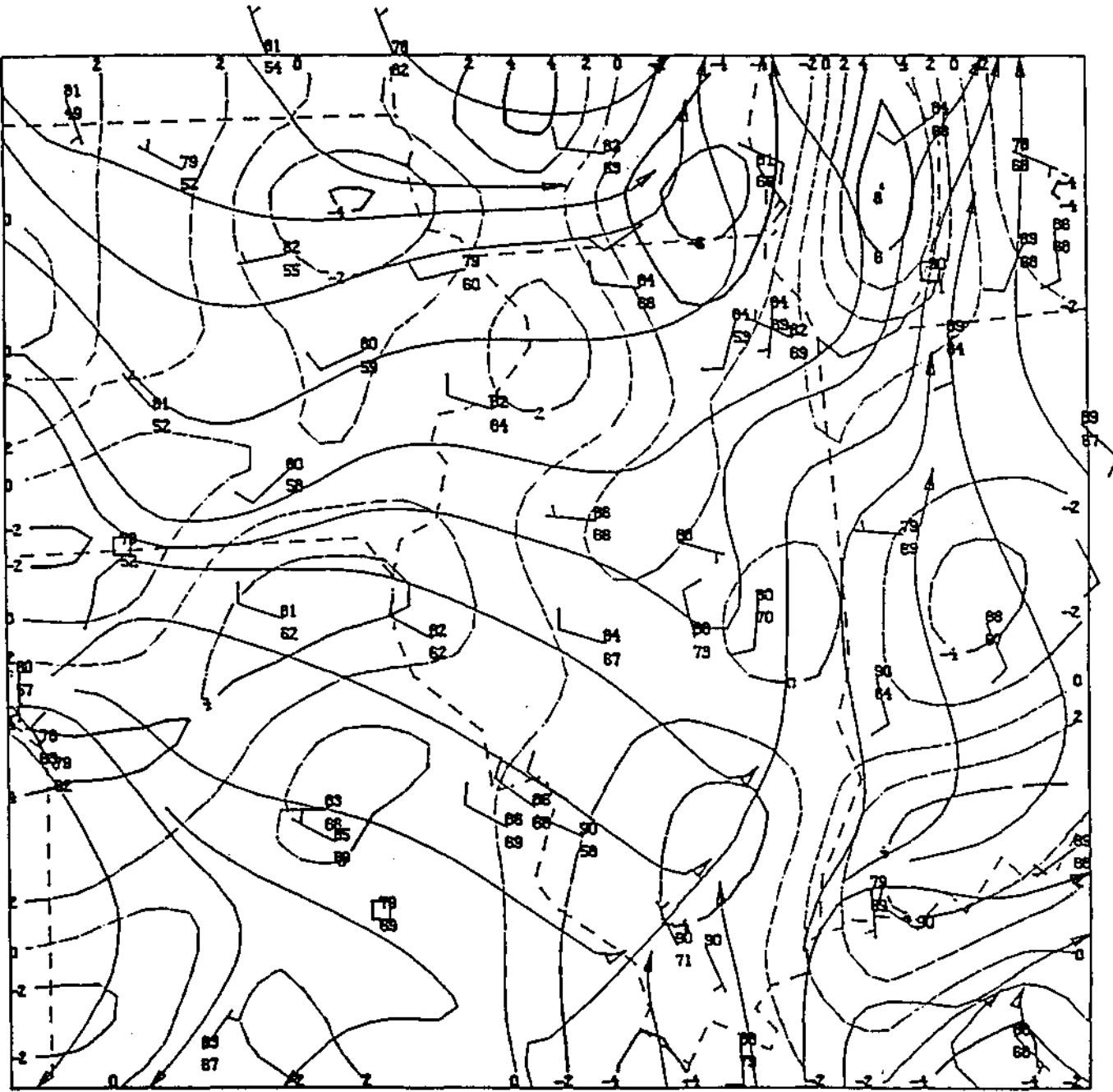


Figure H.15. Regional scale analysis for 1700 CDT on 23 June 1989.

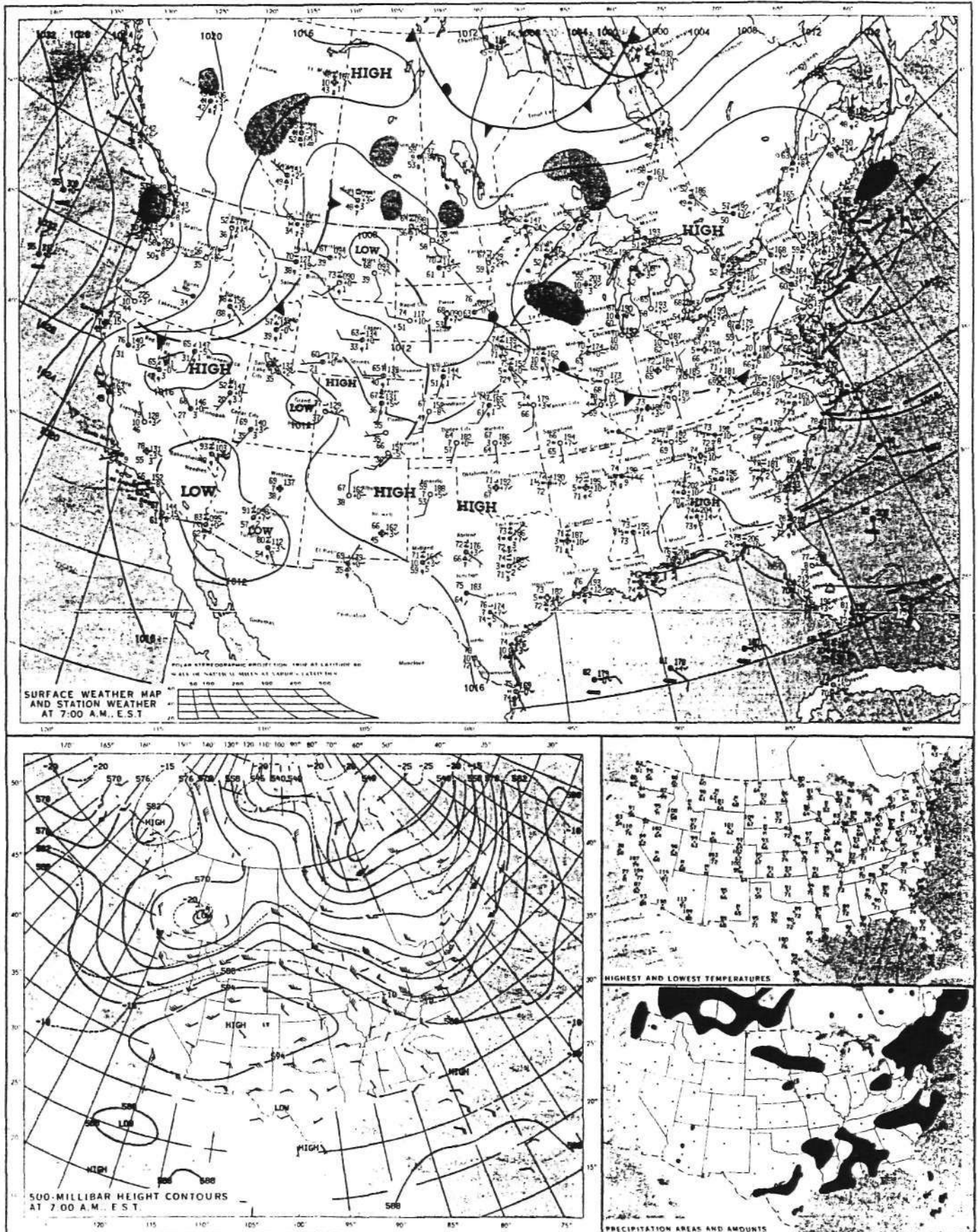


Figure H. 16. Synoptic scale weather charts for 0700 CDT on 8 July 1989.

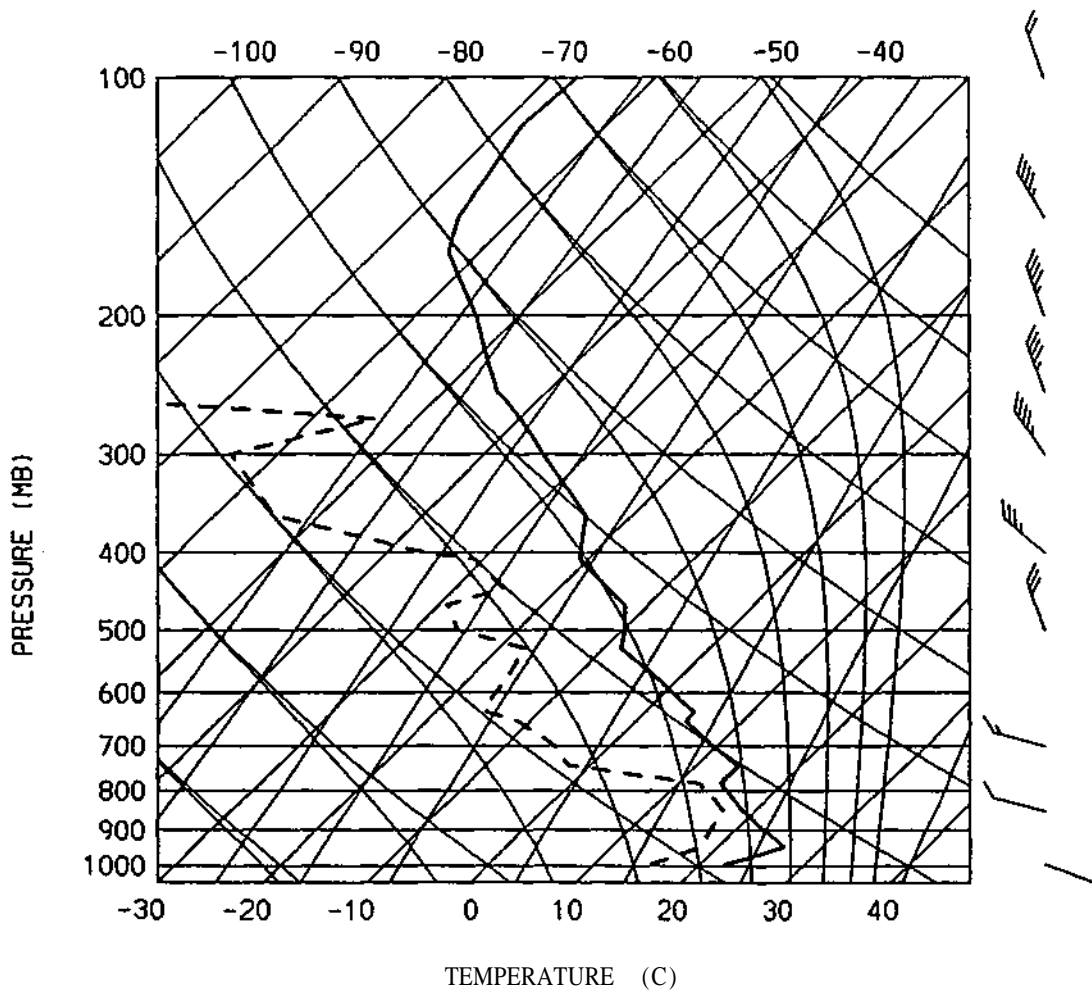


Figure H.17. Skew-T/Log-P chart at PIA for 0700 CDT on 8 July 1989.

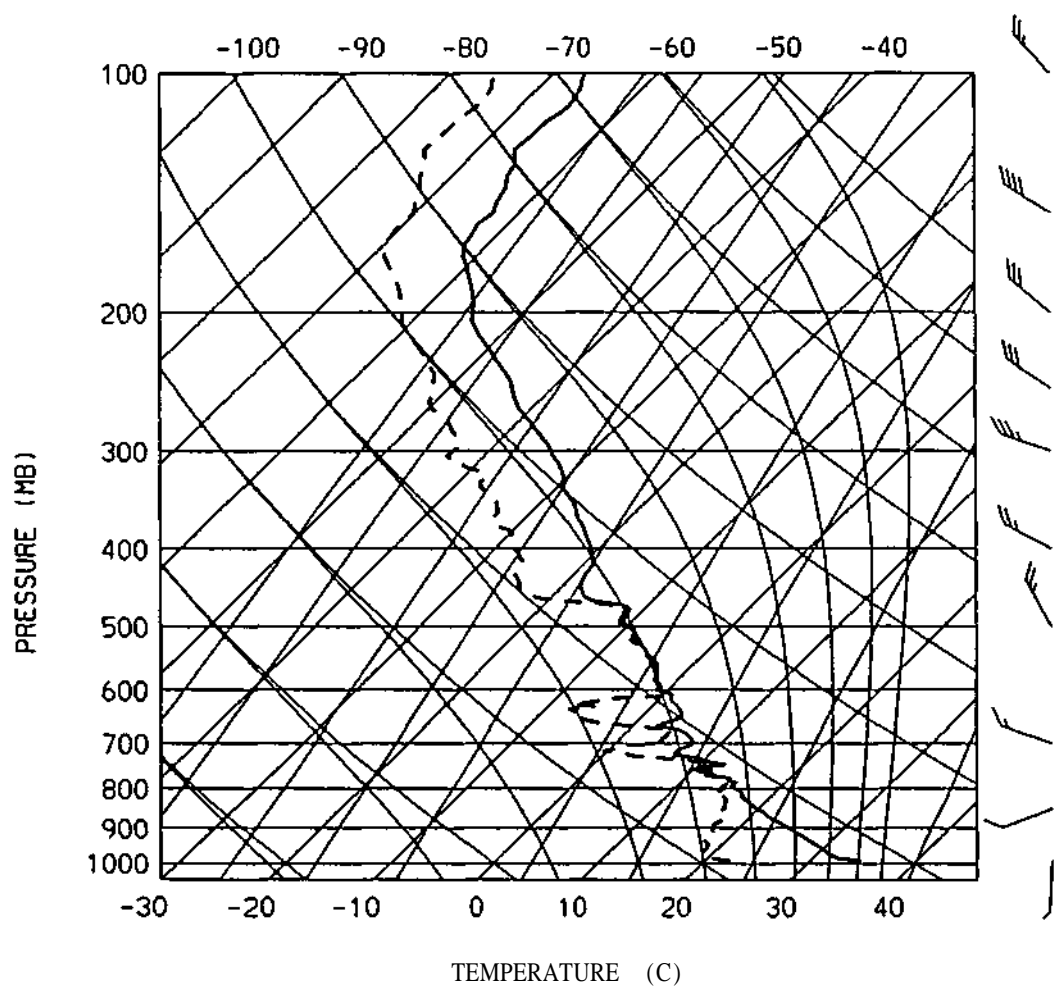


Figure H. 18. Skew-T/Log-P chart at CMI for 1300 CDT on 8 July 1989.

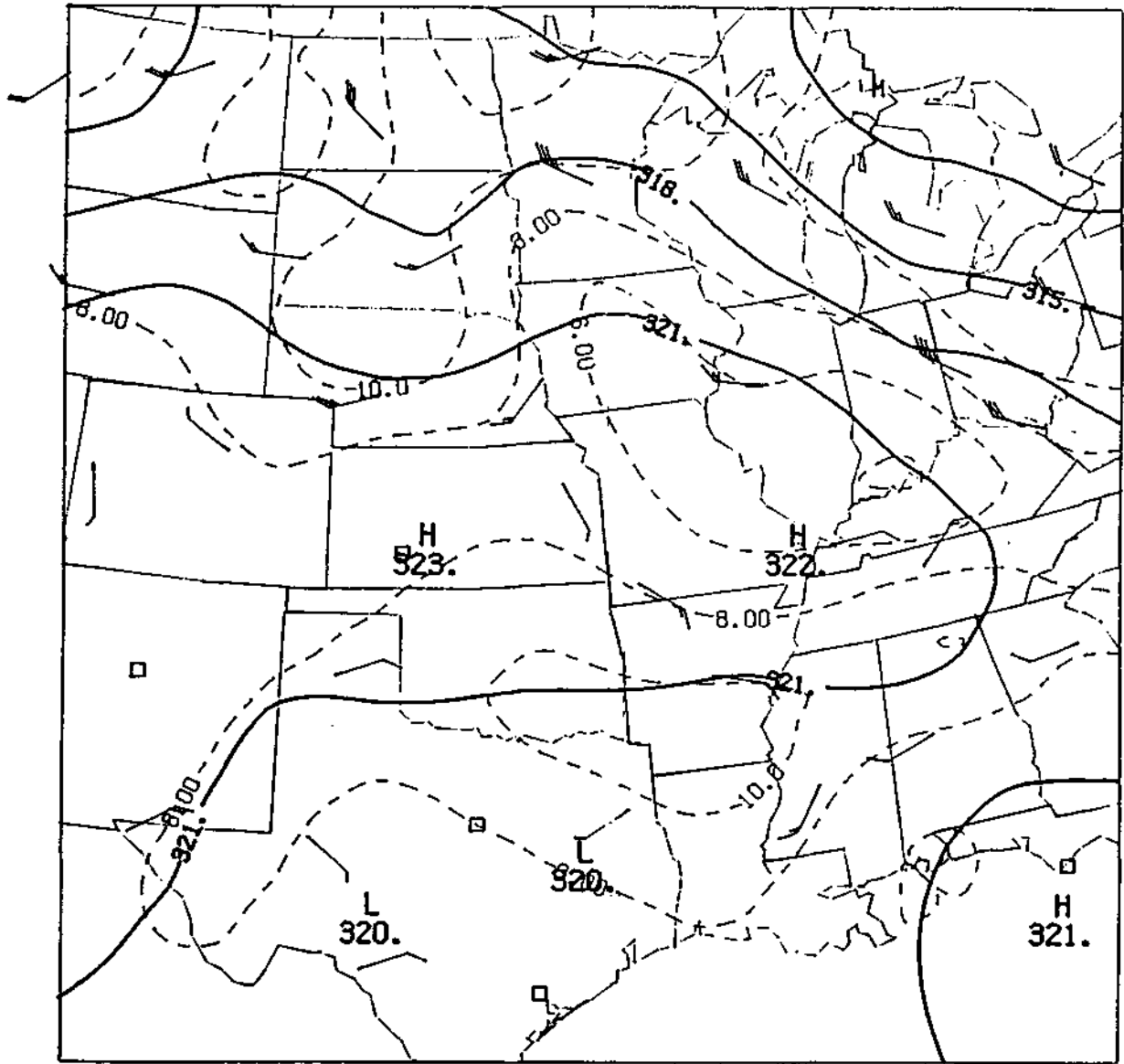


Figure H.19. Height/vorticity chart at 700 mb for 0700 CDT on 8 July 1989.

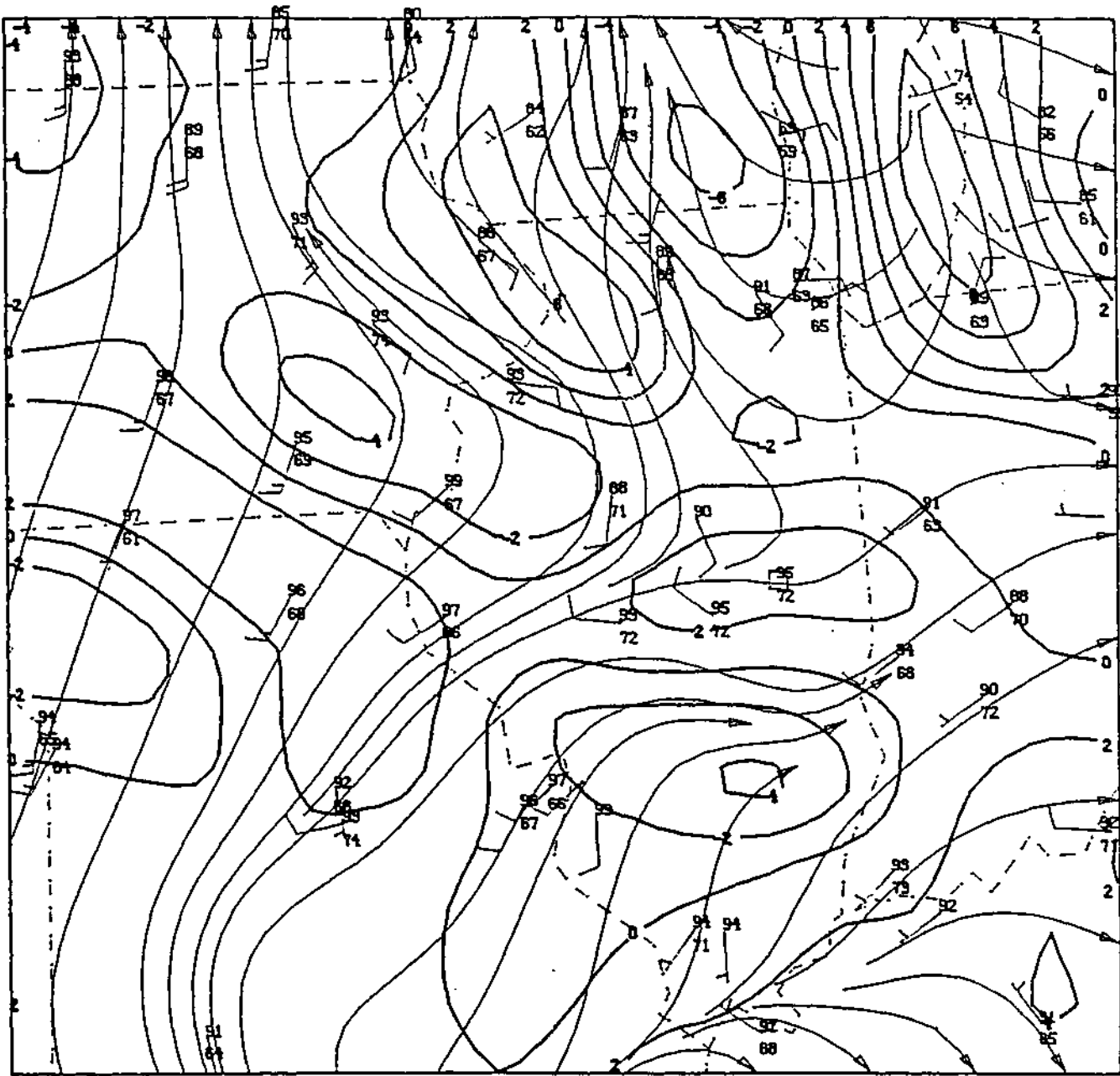


Figure H.20. Regional scale analysis for 1500 CDT on 8 July 1989.

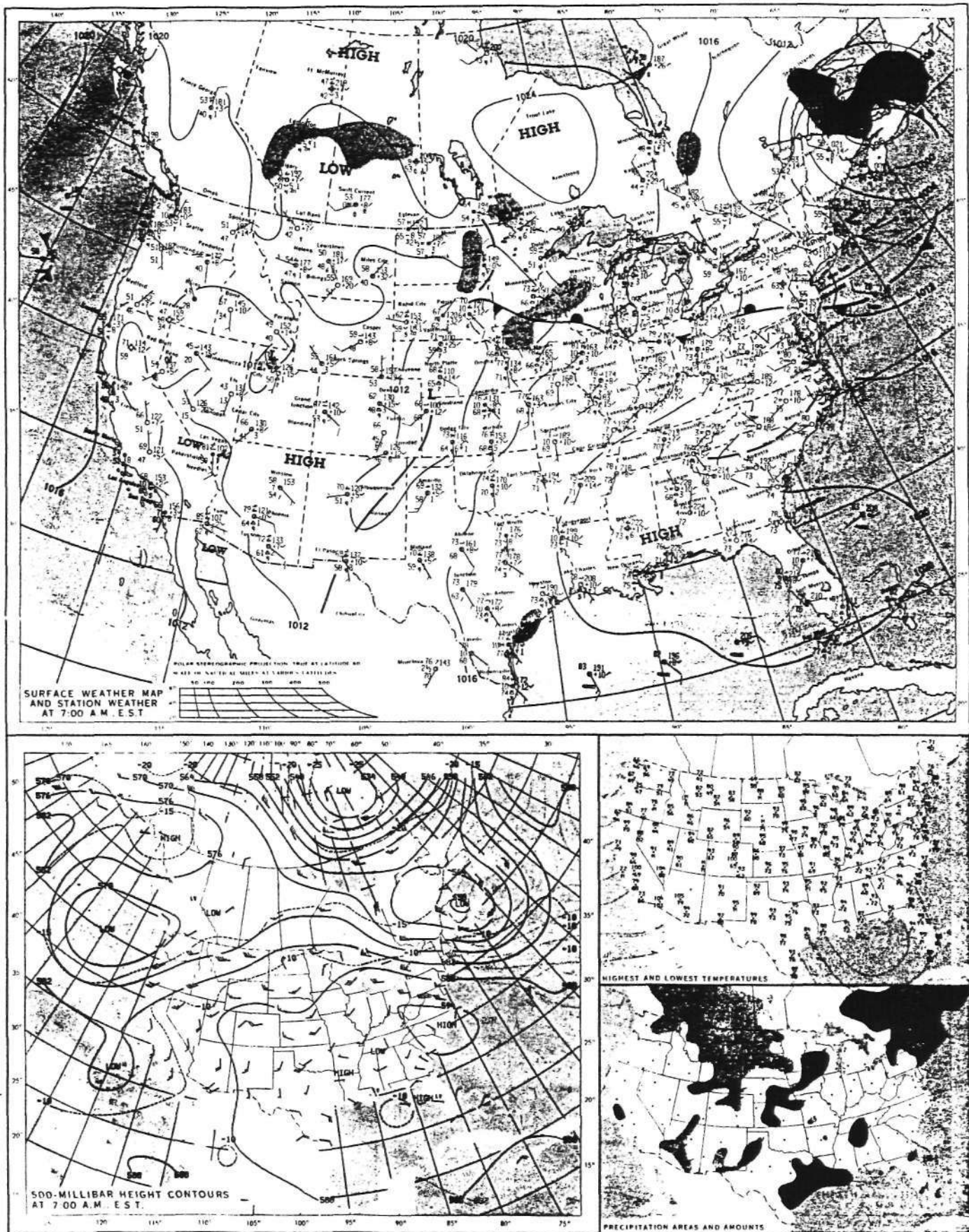


Figure H.21. Synoptic scale weather charts for 0700 CDT on 11 July 1989.

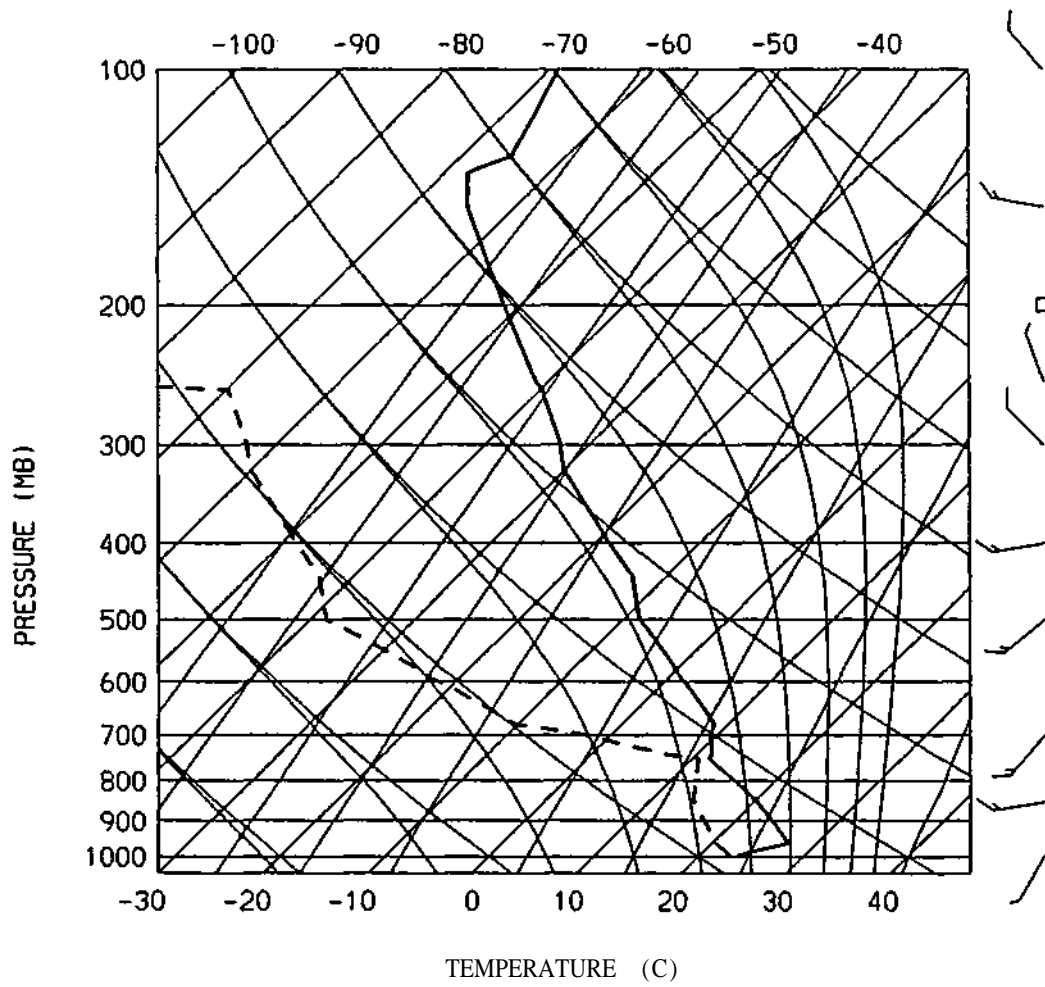


Figure H.22. Skew-T/Log-P chart at PIA for 0700 CDT on 11 July 1989.

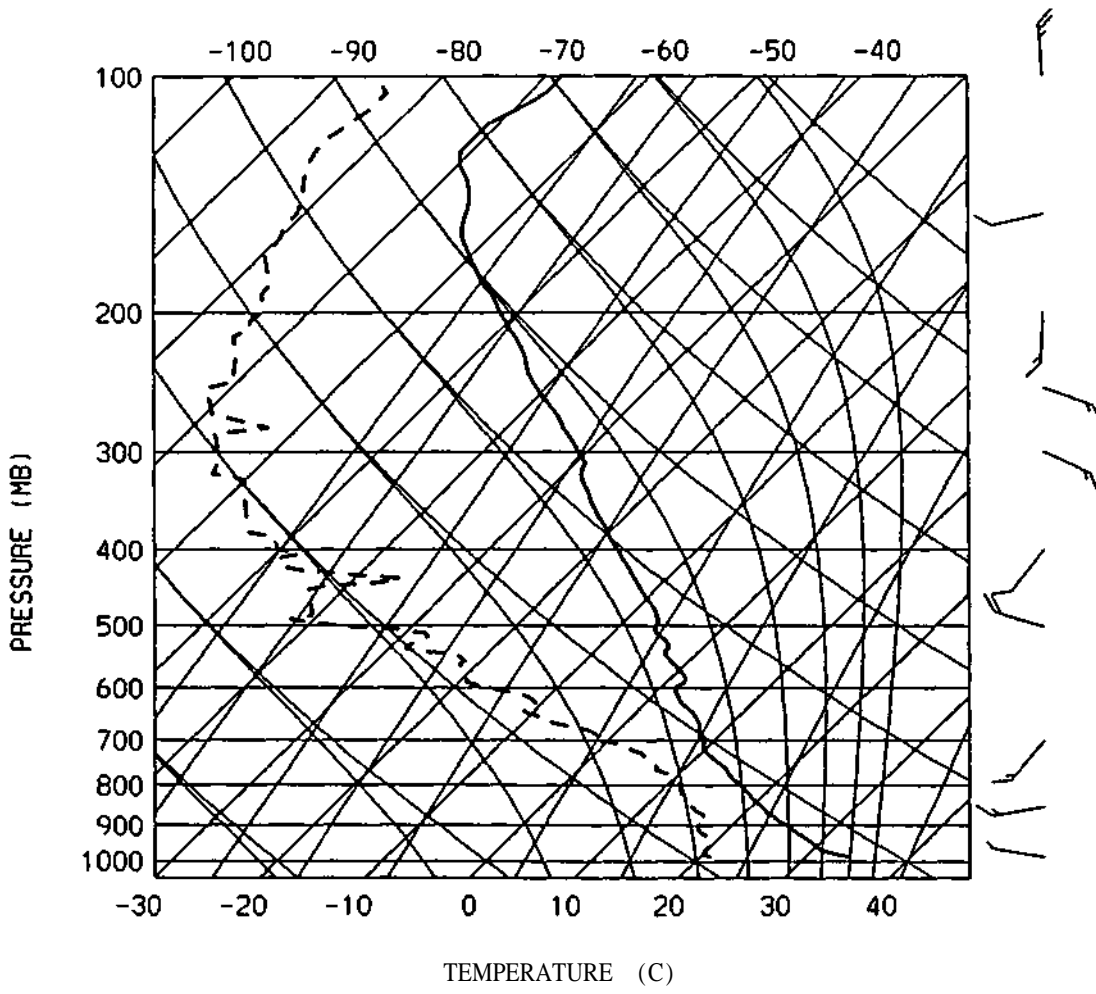


Figure H.23. Skew-T/Log-P chart at CMI for 1300 CDT on 11 July 1989.

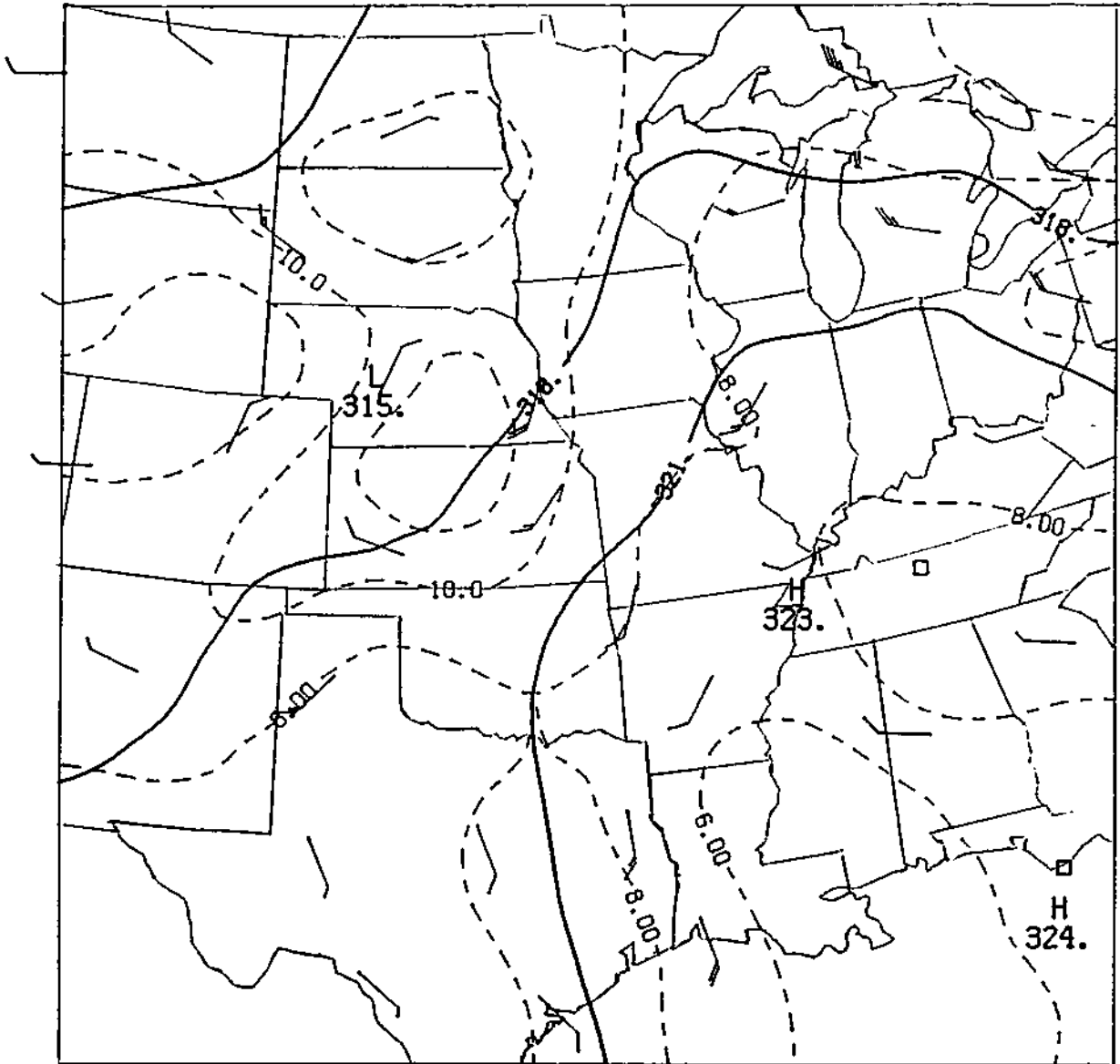


Figure H.24. Height/vorticity chart at 700 mb for 0700 CDT on 11 July 1989.

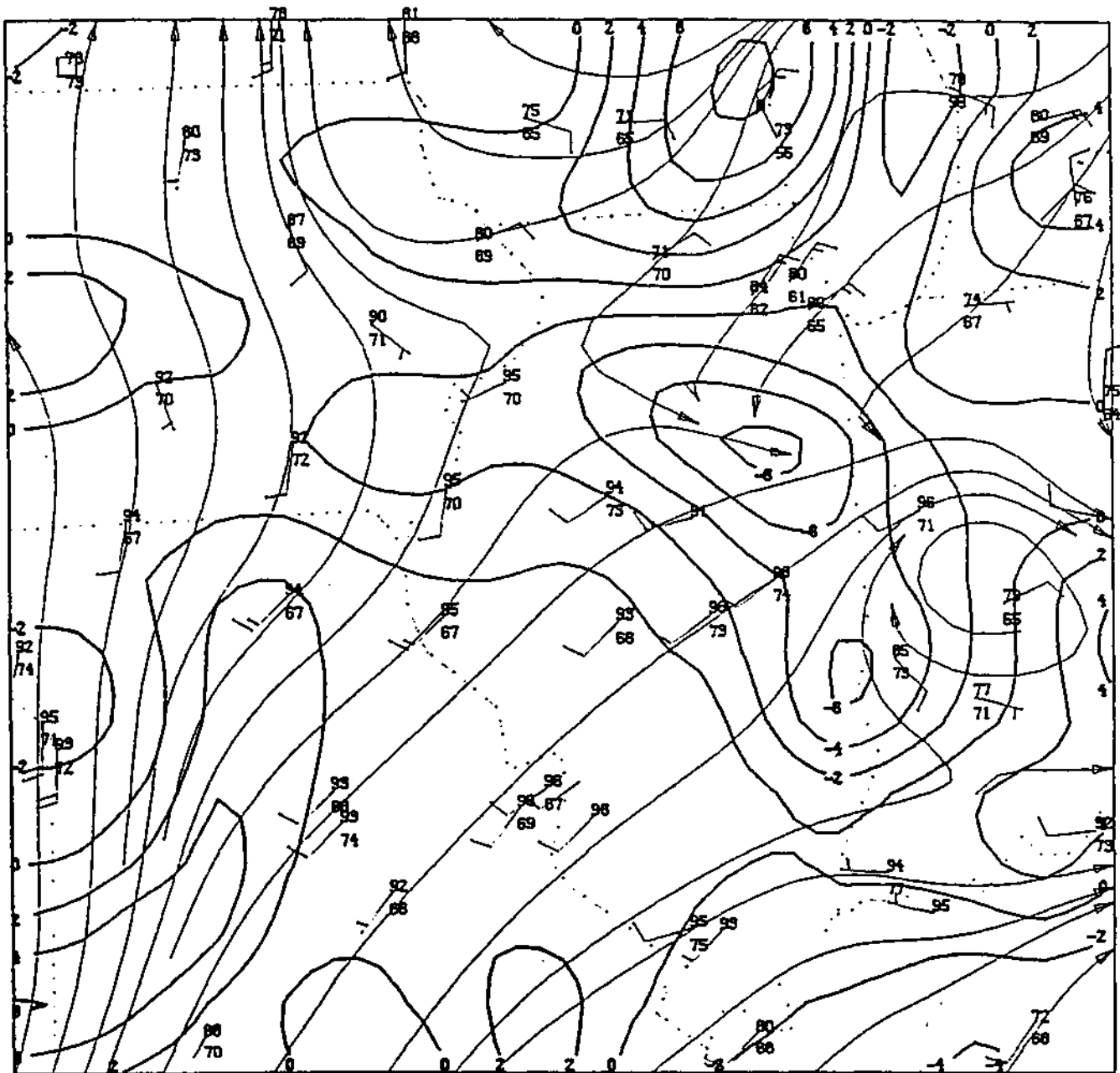


Figure H.25. Regional scale analysis for 1500 CDT on 11 July 1989.

WEDNESDAY, JULY 19, 1989

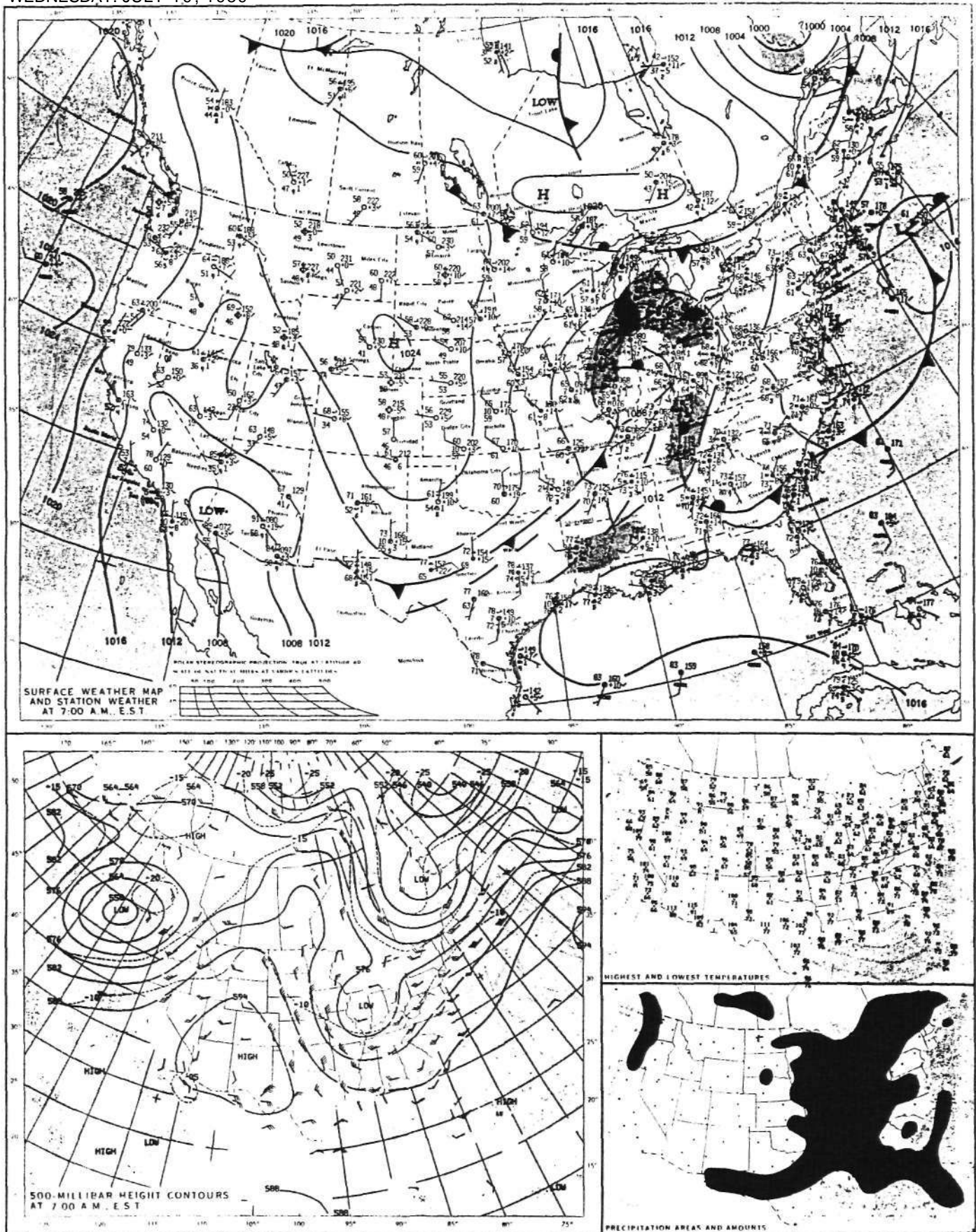


Figure H.26. Synoptic scale weather charts for 0700 CDT on 19 July 1989.

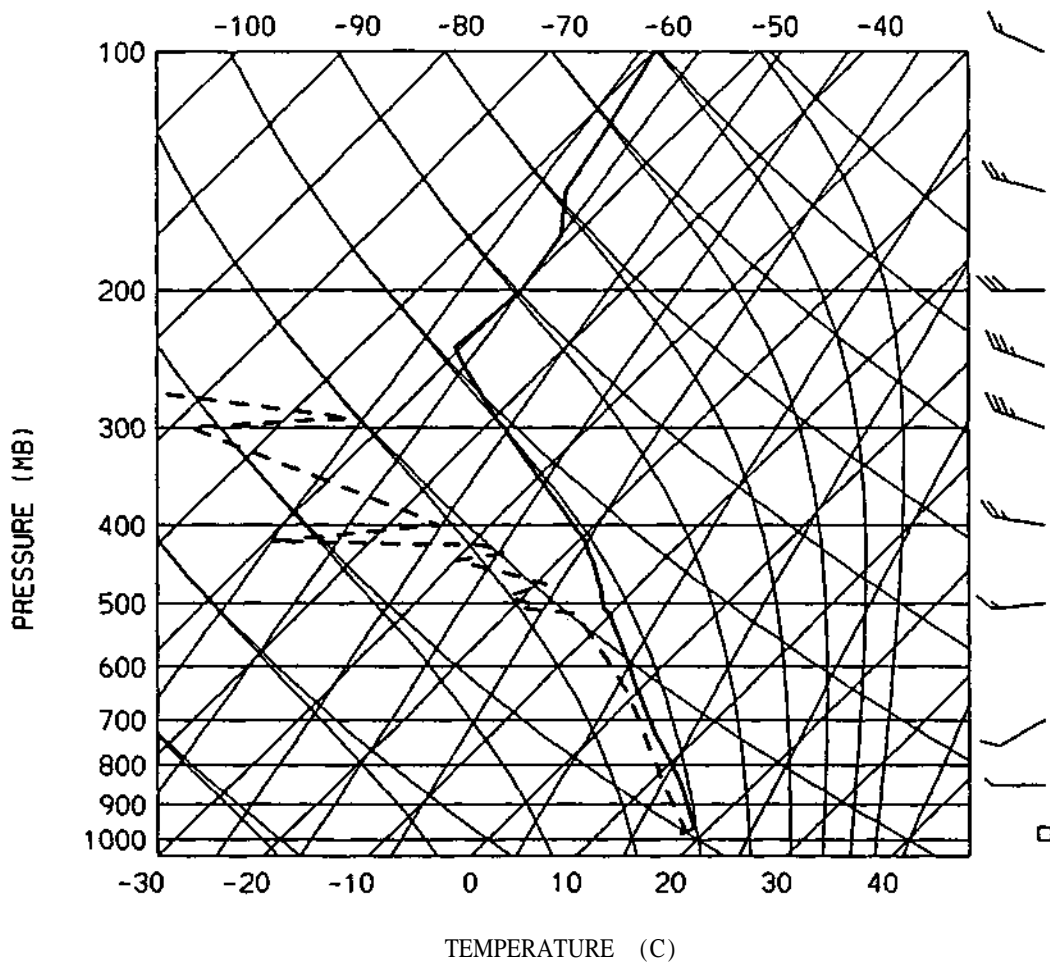


Figure H.27. Skew-T/Log-P chart at PIA for 0700 CDT on 19 July 1989.

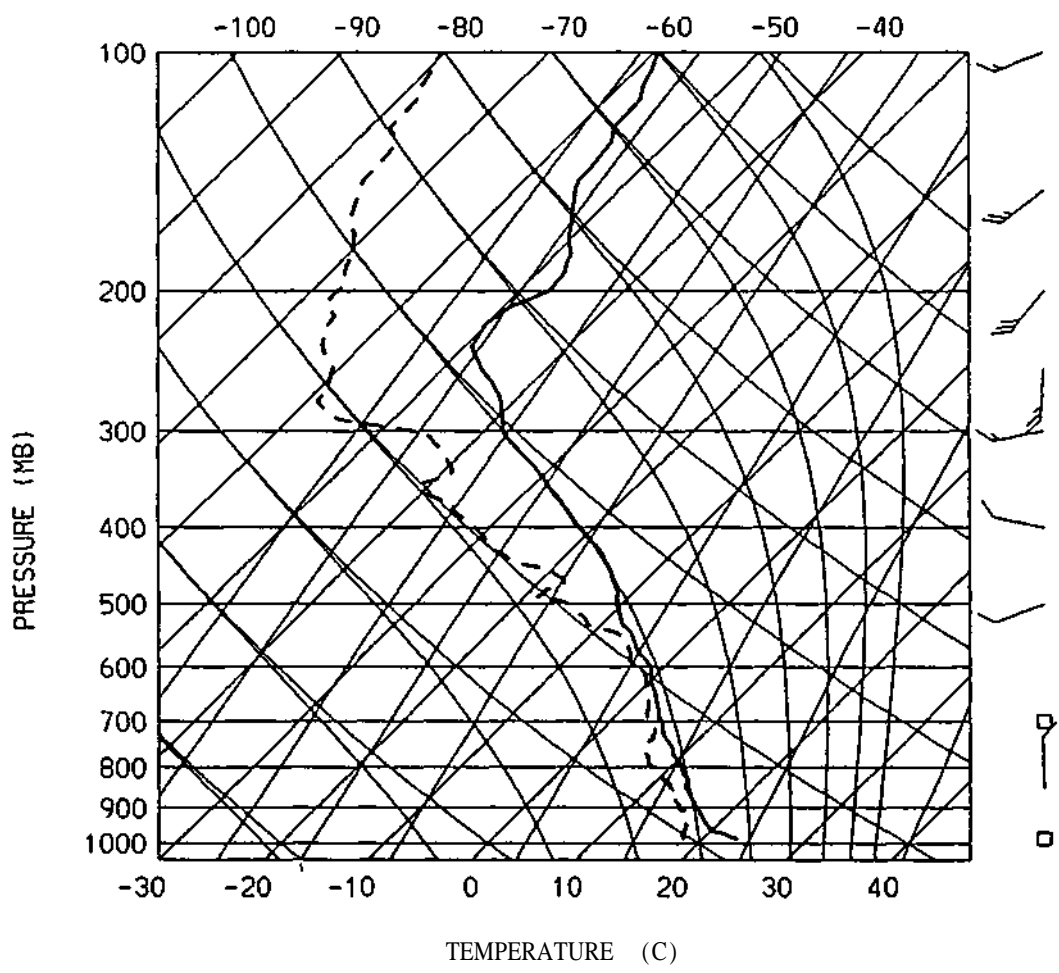


Figure H.28. Skew-T/Log-P chart at CMI for 1200 CDT on 19 July 1989.

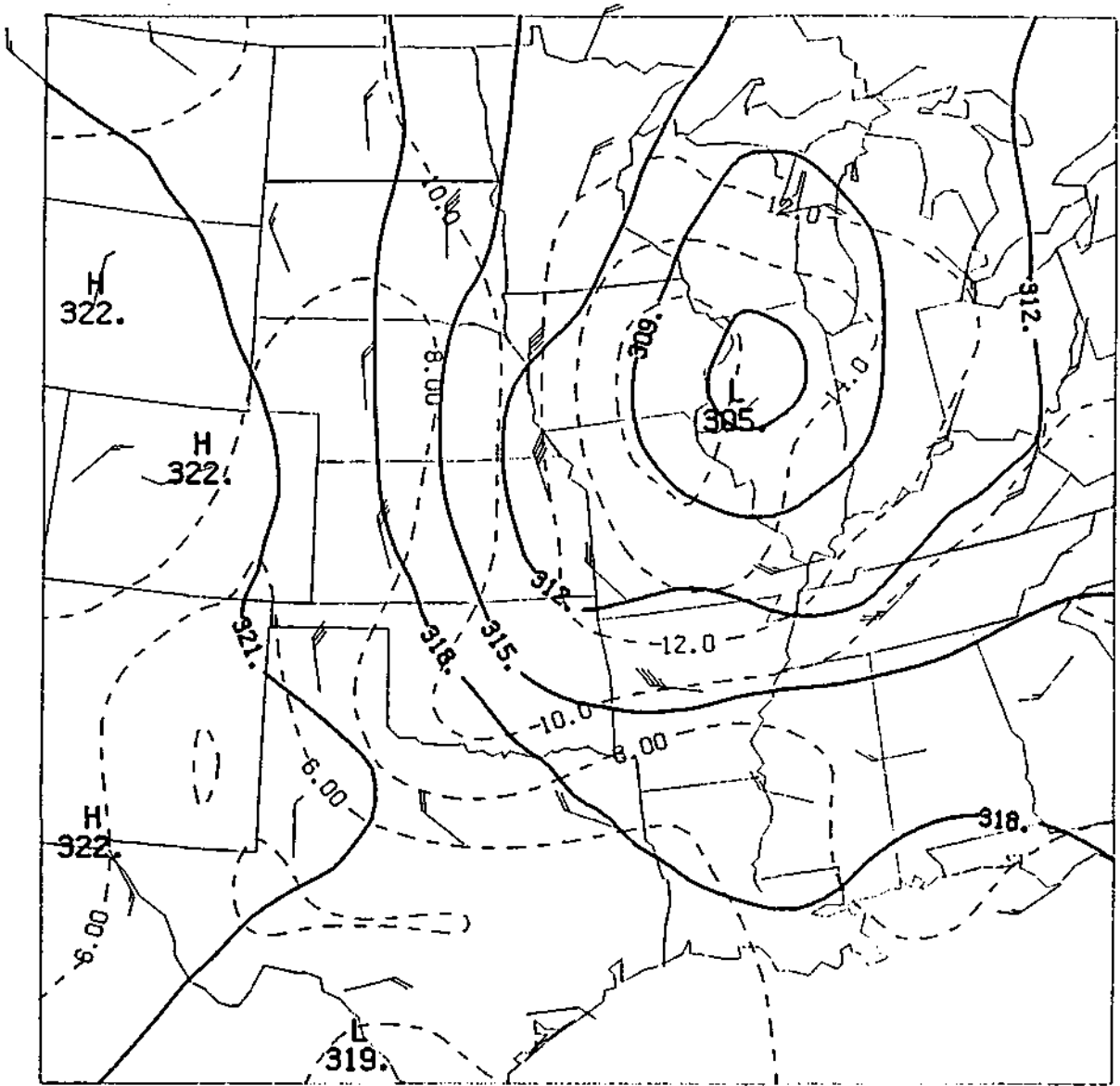


Figure H.29. Height/vorticity chart at 700 mb for 0700 CDT on 19 July 1989.

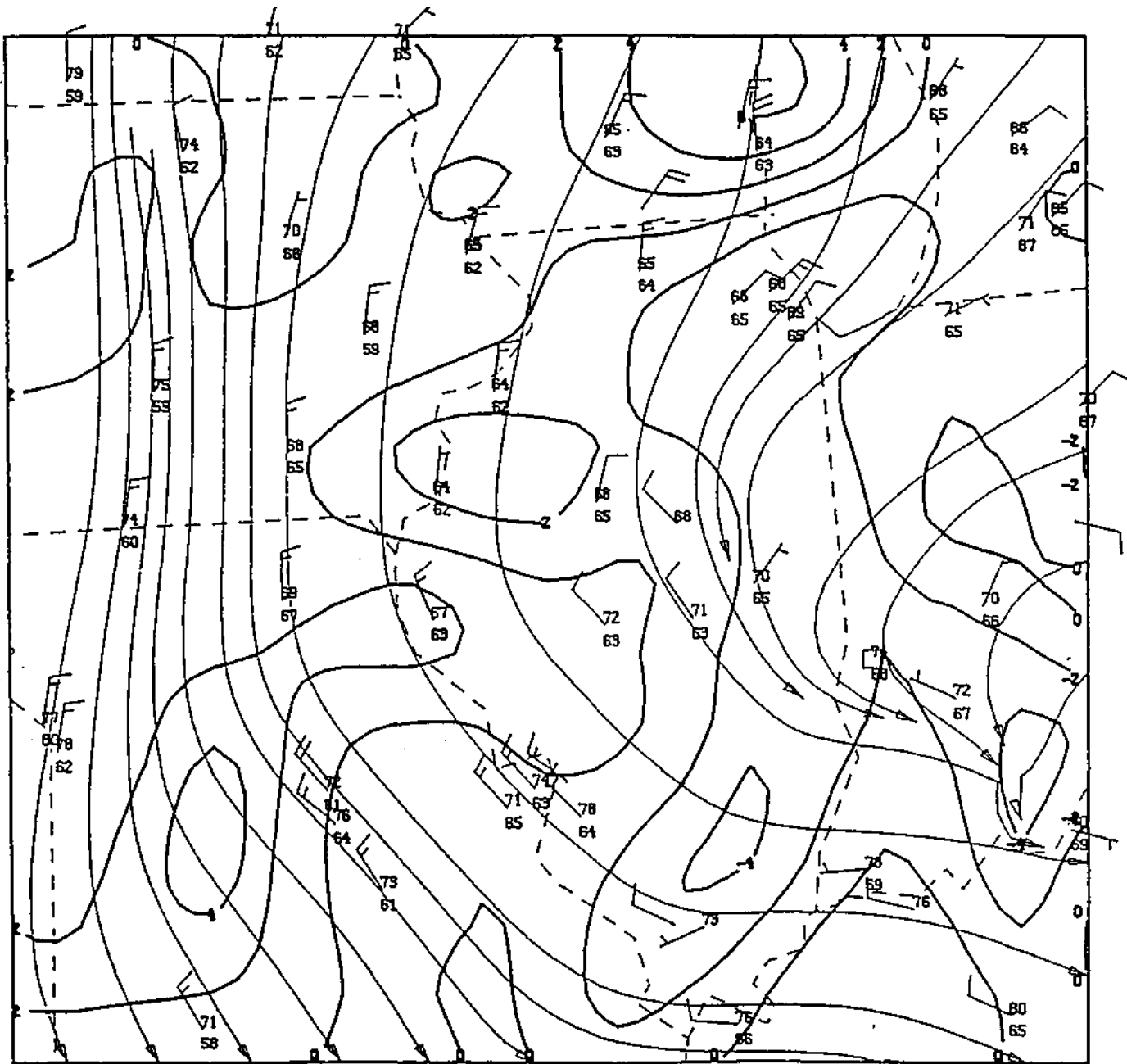


Figure H.30. Regional scale analysis for 1900 CDT on 19 July 1989.

SUNDAY, JULY 23, 1989

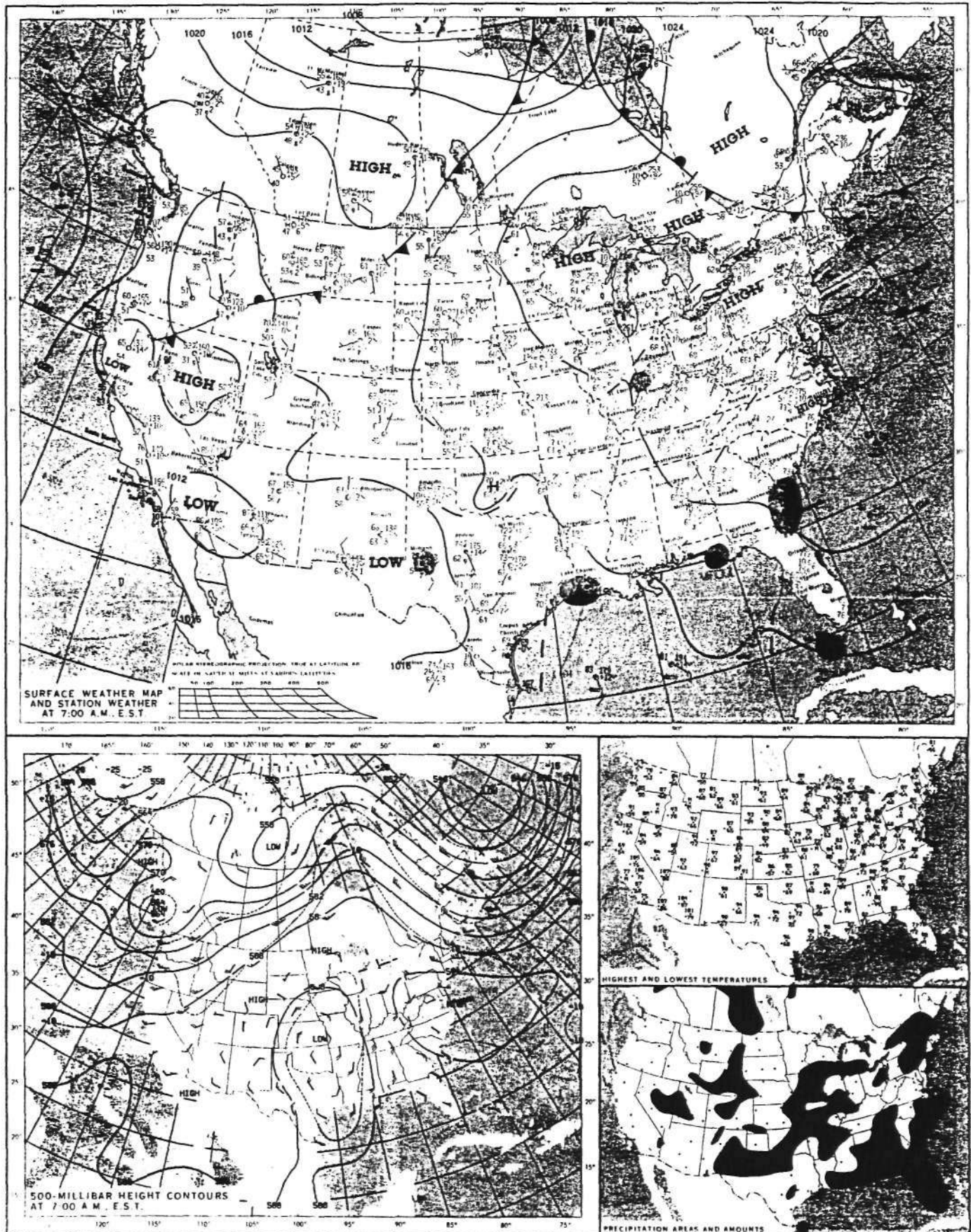


Figure H.31. Synoptic scale weather charts for 0700 CDT on 23 July 1989.

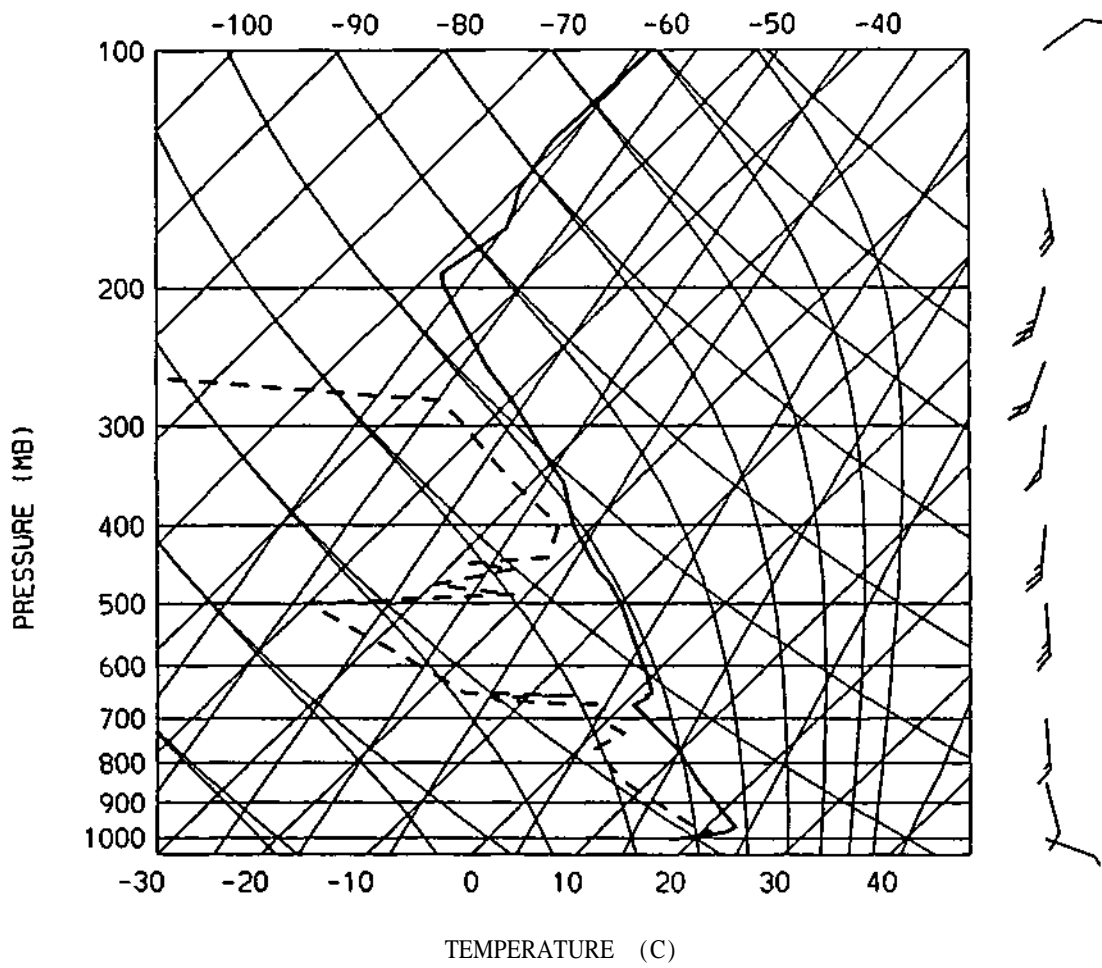


Figure H.32. Skew-T/Log-P chart at PIA for 0700 CDT on 23 July 1989.

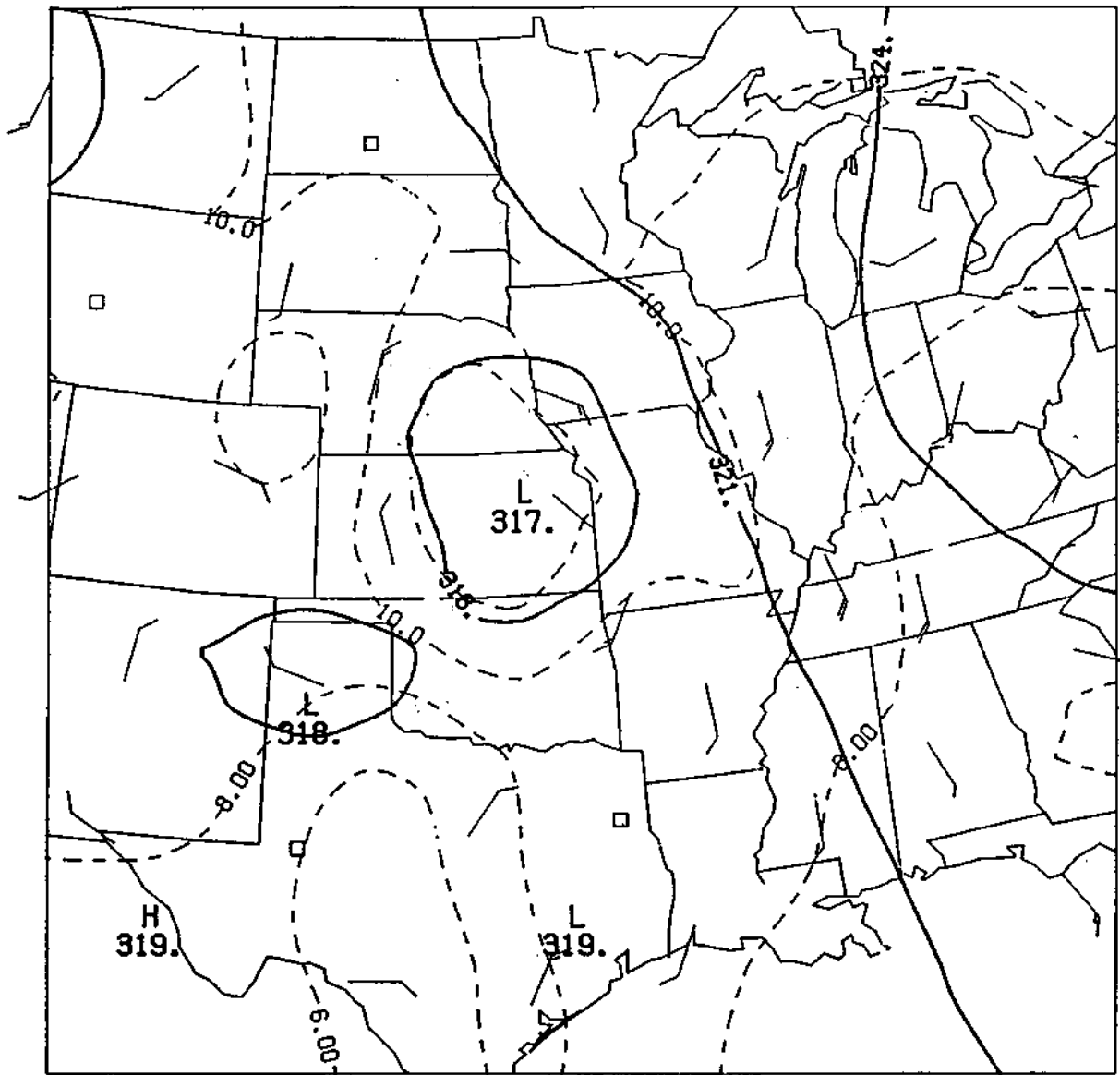


Figure H.33. Height/vorticity chart at 700 mb for 0700 CDT on 23 July 1989.

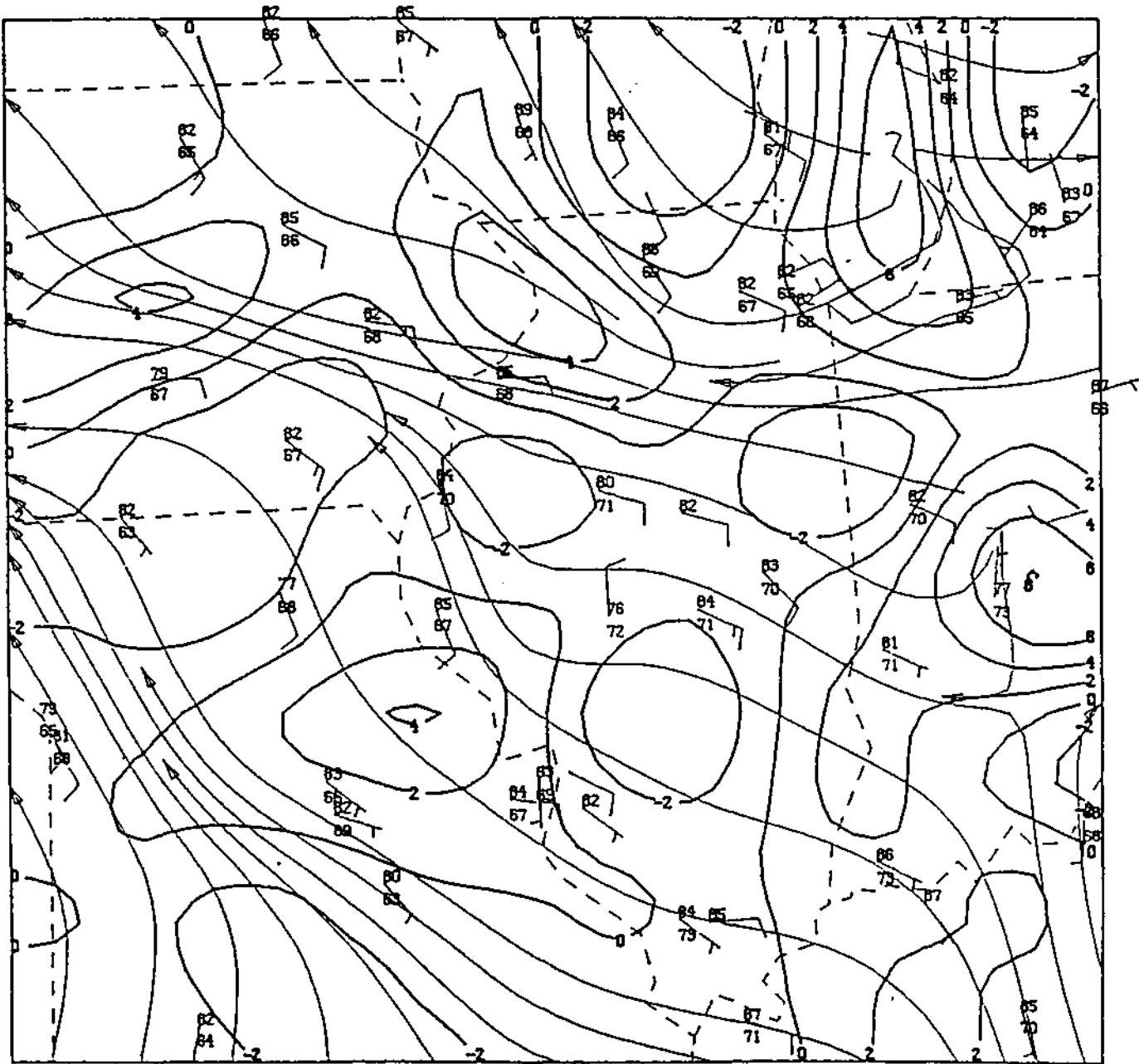


Figure H.34. Regional scale analysis for 1500 CDT on 23 July 1989.

MONDAY, JULY 24, 1989

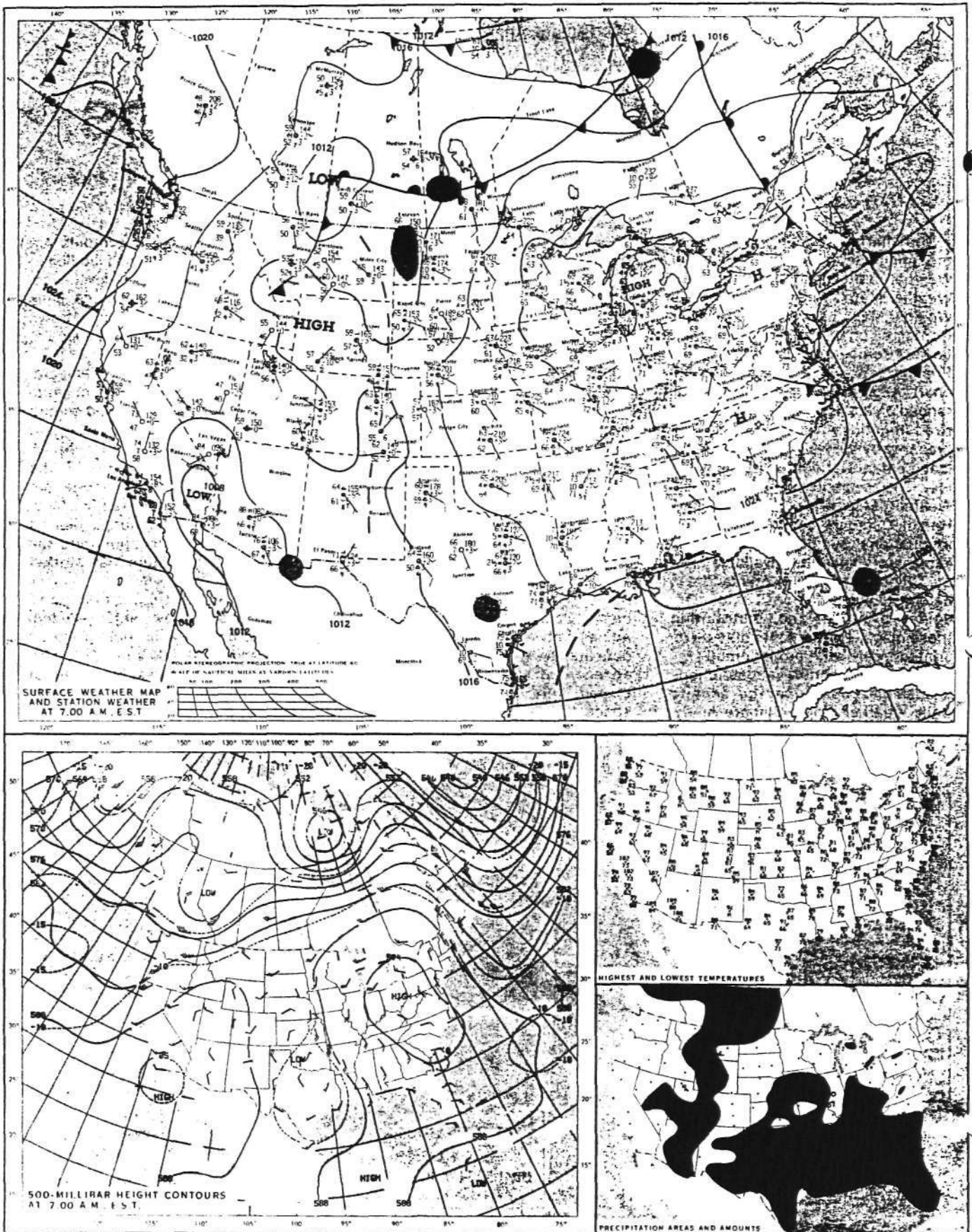


Figure H.35. Synoptic scale weather charts for 0700 CDT on 24 July 1989.

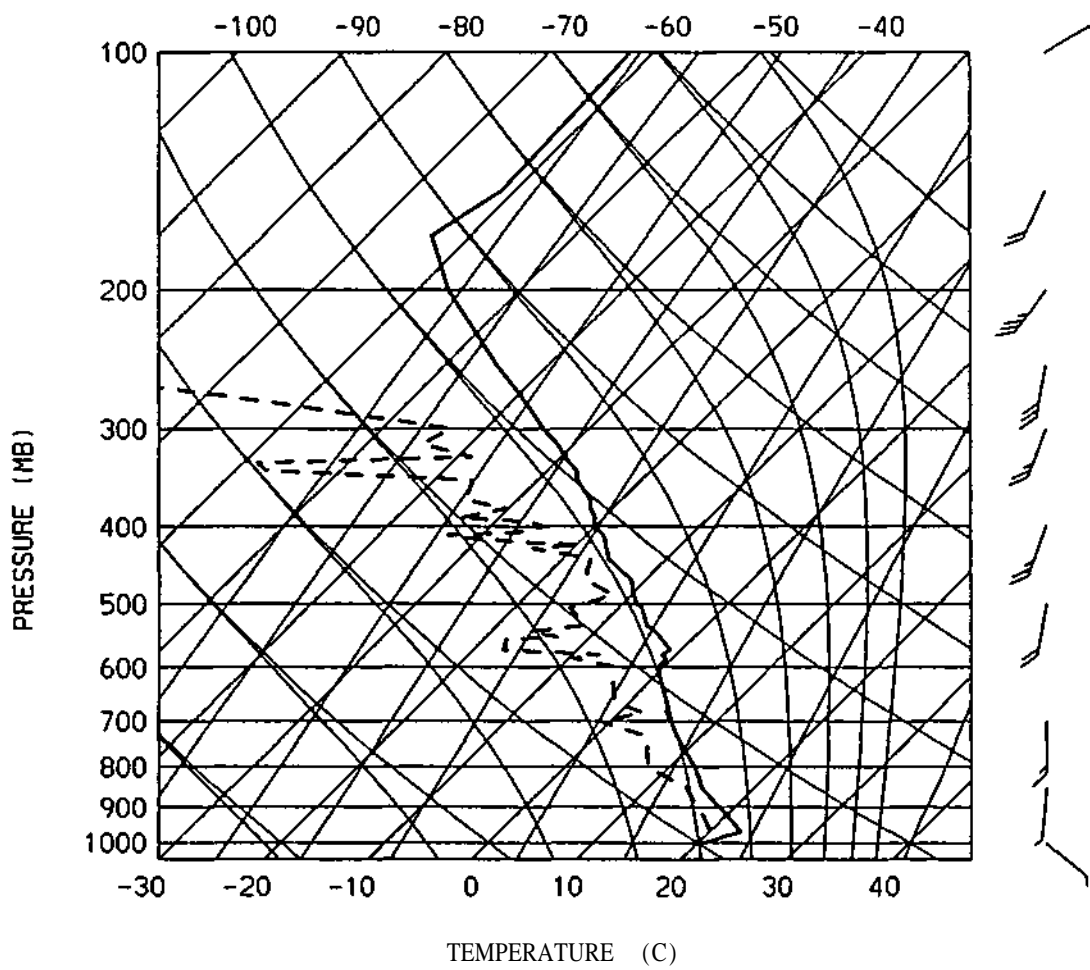


Figure H.36. Skew-T/Log-P chart at PIA for 0700 CDT on 24 July 1989.

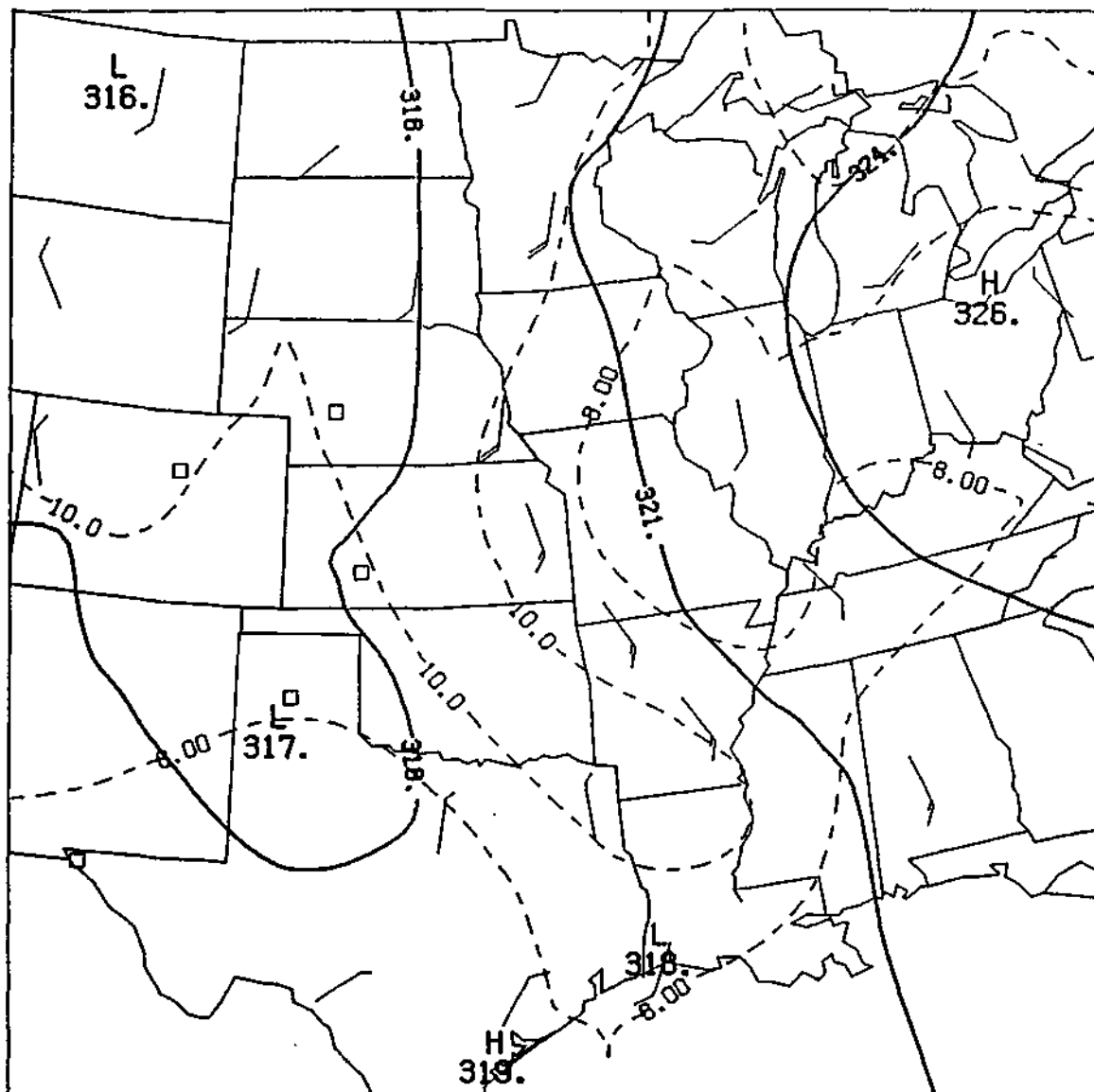


Figure H.37. Height/vorticity chart at 700 mb for 0700 CDT on 24 July 1989.

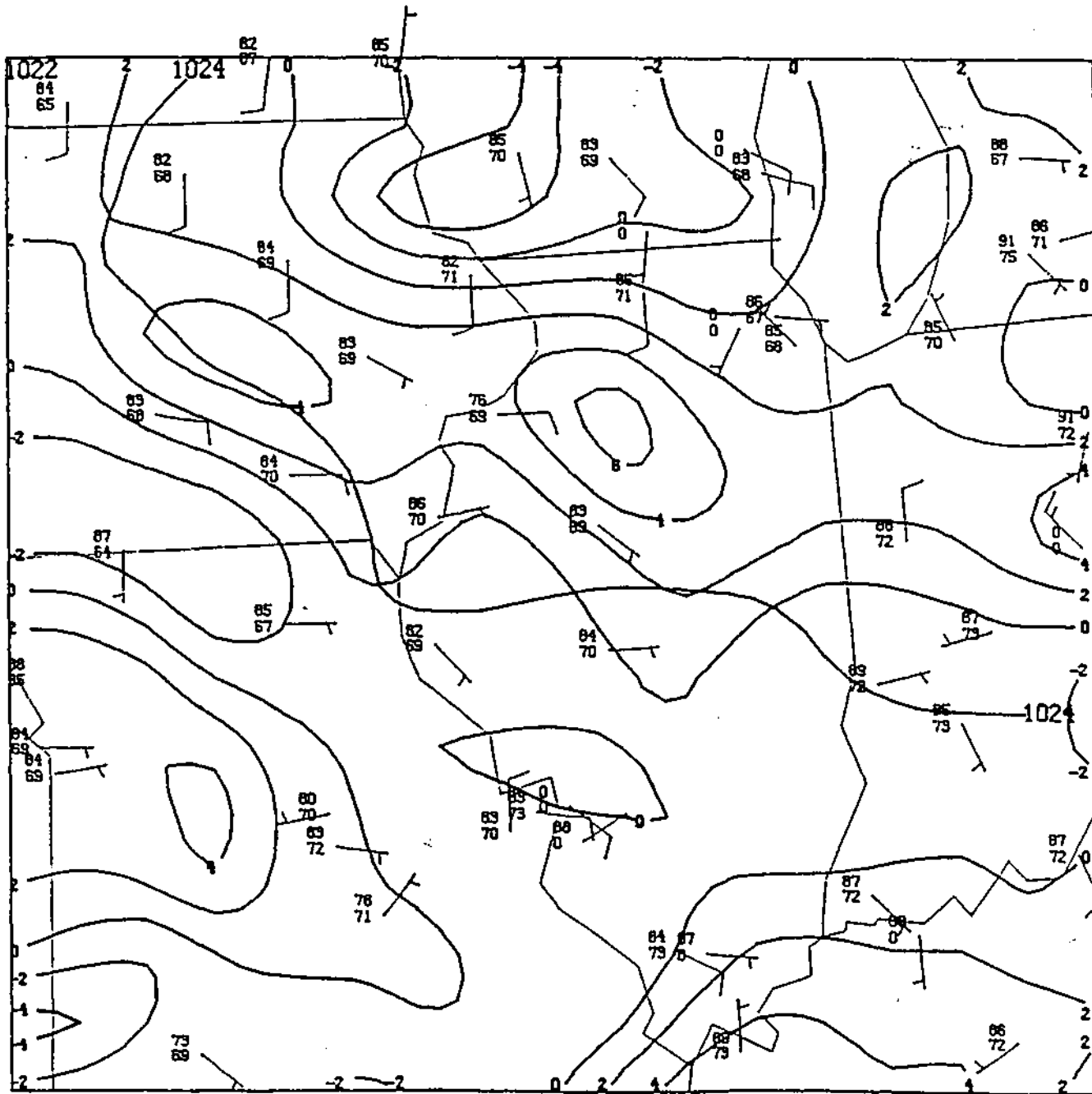


Figure H.38. Regional scale analysis for 1400 CDT on 24 July 1989.

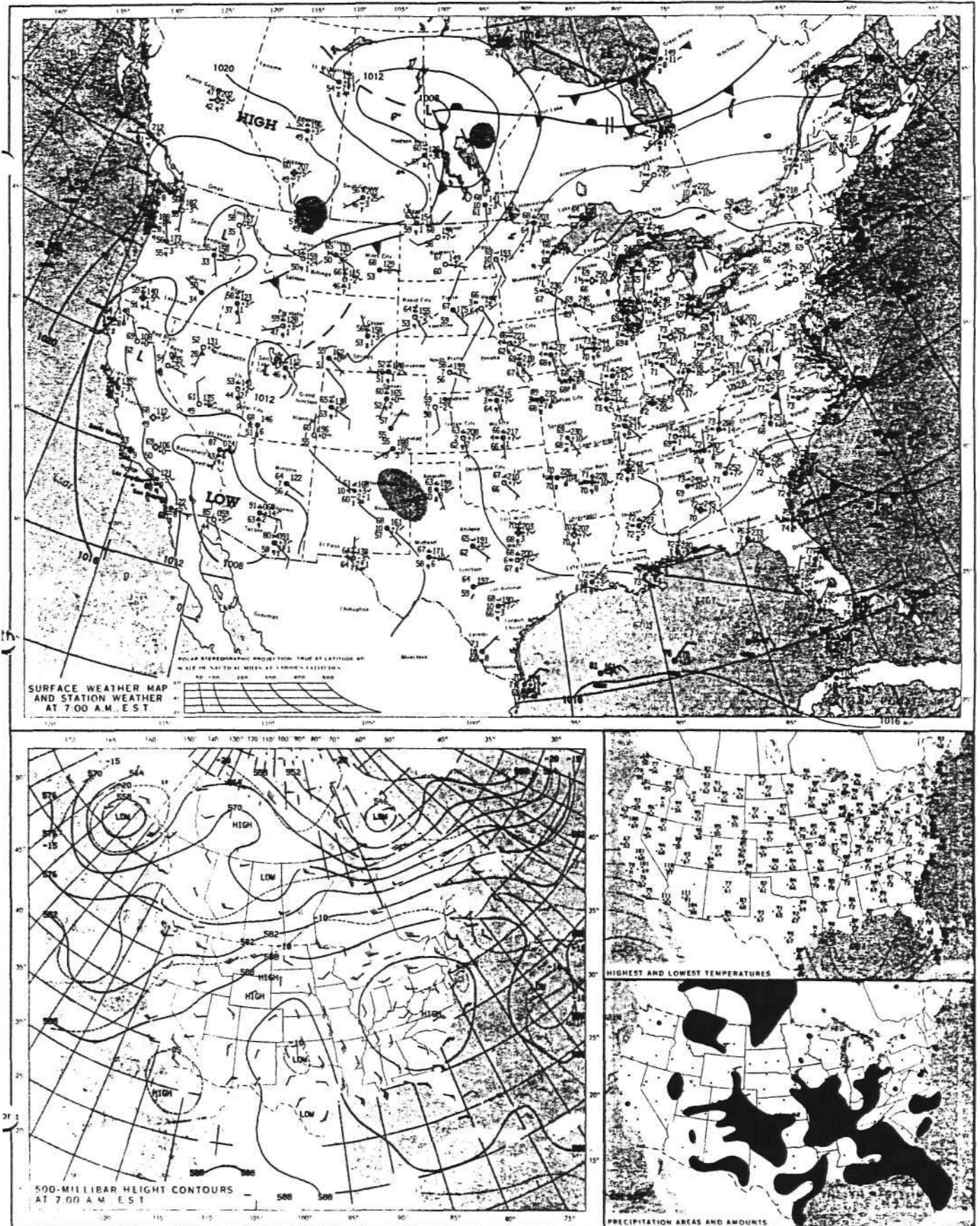


Figure H.39. Synoptic scale weather charts for 0700 CDT on 25 July 1989.